FORM, FUNCTION, AND ANATOMY OF *DORUDON ATROX* (MAMMALIA, CETACEA): AN ARCHAEOCETE FROM THE MIDDLE TO LATE EOCENE OF EGYPT

PAPERS ON PALEONTOLOGY — RECENT NUMBERS

26. The Clarkforkian Land-Mammal Age and Mammalian Faunal Composition across the Paleocene-Eocene Boundary *by Kenneth D. Rose* (1981)

27. The Evolutionary History of Microsyopoidea (Mammalia, ?Primates) and the Relationship between Plesiadapiformes and Primates *by Gregg F. Gunnell* (1989)

28. New Earliest Wasatchian Mammalian Fauna from the Eocene of Northwestern Wyoming: Composition and Diversity in a Rarely Sampled High-Floodplain Assemblage *by Philip D. Gingerich* (1989)

29. Evolution of Paleocene and Eocene Phenacodontidae (Mammalia, Condylarthra) *by J. G. M. Thewissen* (1990)

30. Marine Mammals (Cetacea and Sirenia) from the Eocene of Gebel Mokattam and Fayum, Egypt: Stratigraphy, Age, and Paleoenvironments *by Philip D. Gingerich* (1992)

31. Terrestrial Mesonychia to Aquatic Cetacea: Transformation of the Basicranium and Evolution of Hearing in Whales *by Zhexi Lou and Philip D. Gingerich* (1999)

32. Fishes of the Mio-Pliocene Ringold Formation, Washington: Pliocene Capture of the Snake River by the Columbia River *by Gerald R. Smith, Neil Morgan, and Eric Gustafson* (2000)

33. Paleocene-Eocene Stratigraphy and Biotic Change in the Bighorn and Clarks Fork Basins, Wyoming *by Philip D. Gingerich (ed.) and others* (2001)

34. Form, Function, and Anatomy of *Dorudon atrox* (Mammalia, Cetacea): An Archaeocete from the Middle to Late Eocene of Egypt *by Mark D. Uhen* (2003)

Museum of Paleontology
The University of Michigan
Ann Arbor, Michigan 48109-1079

FORM, FUNCTION, AND ANATOMY OF *DORUDON ATROX* (MAMMALIA, CETACEA): AN ARCHAEOCETE FROM THE MIDDLE TO LATE EOCENE OF EGYPT

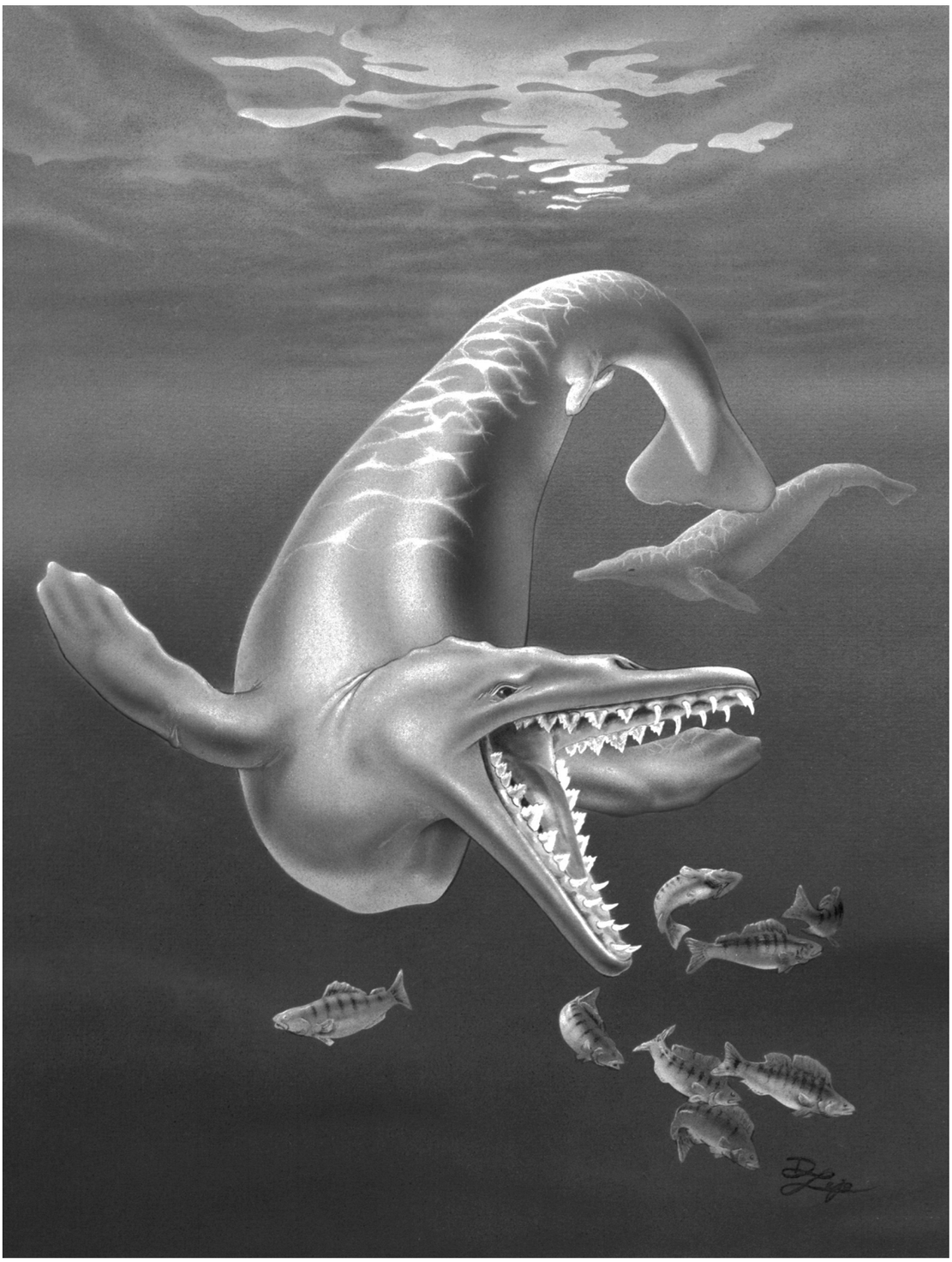

Frontispiece: Life restoration of *Dorudon atrox* in the shallow, nearshore waters of the Tethys Sea during the late middle Eocene in what is today northeastern Egypt. Restoration by Darryl Leja in cooperation with the author.

FORM, FUNCTION, AND ANATOMY OF *DORUDON ATROX* (MAMMALIA, CETACEA): AN ARCHAEOCETE FROM THE MIDDLE TO LATE EOCENE OF EGYPT

Mark D. Uhen

Cranbrook Institute of Science
39221 Woodward Avenue
Bloomfield Hills, Michigan 48303-0801

UNIVERSITY OF MICHIGAN
PAPERS ON PALEONTOLOGY NO. 34

2004

Papers on Paleontology No. 34

Museum of Paleontology
The University of Michigan
Ann Arbor, Michigan 48109-1079

Philip D. Gingerich, Director

Published January 30, 2004

TABLE OF CONTENTS

TABLE OF CONTENTS (cont.)

LIST OF FIGURES

LIST OF FIGURES (cont.)

LIST OF FIGURES (cont.)

LIST OF TABLES

LIST OF APPENDICES

ABSTRACT

Dorudon atrox is a medium-sized archaeocete cetacean, around five meters in length from snout to tail in life, and is known from the Birket Qarun and Gehannam Formations of Fayum, Egypt. These formations are primarily Bartonian, but probably straddle the Bartonian-Priabonian boundary. The Bartonian is the last European marine stage in the middle Eocene, while the Priabonian is the first marine stage in the late Eocene, and the formations from which *D. atrox* are recovered are around 41 to 40 million years old. Anatomical features found in *D. atrox* and its close relatives (Family Basilosauridae), indicate that these animals were the first fully aquatic cetaceans.

The skull of *D. atrox* shows that the bones are arranged in a normal mammalian pattern and the skull lacks the cranial telescoping of either mysticetes or odontocetes. The external nares of *D. atrox* is retracted farther from the tip of the rostrum than in any known protocetid, but it is much farther forward than in any known neocetan. The cheek teeth of *D. atrox* (like those of all basilosaurids) bear multiple accessory denticles, a feature shared with both early mysticetes and early odontocetes.

The vertebral column of *D. atrox* shows numerous adaptations to a fully aquatic existence including: compressed cervical vertebrae, non-revolute zygapophyses, relatively uniform size of posterior thoracics through anterior caudals, and dorso-ventrally flattened posterior caudal vertebrae. *D. atrox*, and fellow members of the Family Basilosauridae are the earliest cetaceans to show a dramatic increase in the length of the lumbar region due to the increase in the number of lumbar vertebrae. The full vertebral count for *D. atrox* is 7 cervicals, 17 thoracics, 20 lumbars, no sacrals, and 21 caudals. The shapes of the caudal vertebrae indicate that although *D. atrox* had a fluke, it lacked a caudal peduncle like those seen in modern cetaceans.

The forelimbs of *D. atrox* are modified into flippers. Movement at the elbow joint is restricted to the antero-posterior plane and pronation and supination at the elbow is not possible. The carpals lack saddle-shaped articular surfaces and are only capable of limited movement between adjacent bones. The hindlimbs of *D. atrox* are similar to those of *Basilosaurus* in that they are very reduced and could not support the body on land.

Reconstructions of the soft anatomy of *Dorudon atrox*, along with analyses of functional morphology show that *D. atrox* was a caudally propelled swimmer, much like modern cetaceans. Based on comparisons with modern cetaceans, *D. atrox* was a relatively slow sprint swimmer, with an estimated speed of around 2.4 body lengths or 12 meters per second. Estimates of the body mass of *D. atrox*, based on the total skeletal length show that *D. atrox* weighted around 2240 kg, slightly smaller than modern *Ziphius cavirostris*. The jaws and teeth, as well as some preserved stomach contents of *D. atrox* indicate that they captured individual prey items (fish, and possibly squid) with their anterior teeth, and then moved the prey items to the cheek teeth for oral processing. The brain mass of adult *D. atrox* was measured to be about 976 g, after correcting for possible overestimation of brain size due to the presence of a large vascular *rete mirabile* in the endocranial space. Using the estimated body mass and brain mass for *D. atrox*, an encephalization quotient of 0.425 was calculated. This indicates that *D. atrox* has a relatively small brain when compared to modern cetaceans of similar body size. Morphology of the lower jaw and ear region indicates that *D. atrox*, like most other archaeocetes could hear directionally under water. The anatomy of the periotic indicates that *D. atrox* could hear only low and mid range frequencies similar to those heard by modern mysticetes, and almost certainly lacked any echolocation capabilities like those of modern odontocetes.

Phylogenetic analysis of *Dorudon atrox*, other archaeocetes, and early mysticetes and odontocetes indicates that *D. atrox* is close to the ancestry of modern cetaceans from the archaeocetes. Basilosaurids as a group share many features with early mysticetes and odontocetes including: accessory cusps on the teeth, greatly reduced hindlimbs, and an increase in the number of trunk vertebrae. *D. atrox* and its close relatives (Subfamily Dorudontinae) share all of these features with mysticetes and odontocetes while lacking the elongate trunk vertebrae of *Basilosaurus*, making them more likely to be the ancestors of modern cetaceans.

I

INTRODUCTION

Cetacea is one of the most ecologically and morphologically divergent orders of living mammals. Cetaceans (whales and dolphins) are completely aquatic, a condition only achieved by one other order, Sirenia (manatees and dugongs). Cetaceans have completely lost external hind limbs and have adopted a form of tail-based locomotion convergently shared with the Sirenia. Lest one think that these two groups have all of the same characteristics, cetaceans are carnivores and planktivores, while sirenians are completely herbivorous. The fundamental change of Cetacea from a terrestrial to a fully aquatic existence represents a shift in adaptive zone (*sensu* Simpson, 1953), with a corresponding dramatic change in morphology. The nature and pace of this transition are two of the main reasons that the study of fossil Cetacea is so worthwhile and interesting.

The transition from a terrestrial to an aquatic habitat in cetaceans can only be documented with fossils. The recognition of cetaceans as mammals and the fact that mammals are primitively terrestrial, along with the acceptance of evolution, created the realization that cetaceans must have arisen from terrestrial ancestors.

Identification of rudimentary structures of the hind limb in the body wall of cetaceans provides additional evidence that the ancestors of cetaceans once walked on land (Arvy, 1979, and references therein). Despite these observations from modern cetaceans, the transition from terrestrial to aquatic habitats happened in the past and can only be documented with fossils. Fossils provide direct evidence of the morphology of organisms at particular times in the geologic past, and document the order of appearance of cetacean characters in the past. The study of fossils along with a phylogenetic analysis to determine the interrelationships of cetaceans is the only way to study the order of appearance of characters and the rates of transition from primitive terrestrial forms to derived aquatic forms. To this end, a study of fossil cetaceans is in order.

In addition to the modern suborders of cetaceans (Mysticeti and Odontoceti), a third suborder of early cetaceans known as Archaeoceti, the "ancient whales" has also been recognized. Archaeocetes, known only as fossils, are characterized by the retention of a differentiated dentition, anteriorly placed external nares (relative to odontocetes and mysticetes), external hind limbs (although some could not support terrestrial locomotion), and the lack of telescoping of the skull seen in odontocetes and mysticetes. The last broad treatment of the suborder Archaeoceti was published in 1936 by Remington Kellogg.

PURPOSE OF STUDY

Today, a complete review of the Archaeoceti would be a daunting task for any one individual. Rather, I have undertaken a complete description and redescription of the single best known archaeocete species: *Dorudon atrox*. The numerous new specimens now referable to *Dorudon atrox* include almost every portion of the skeleton: virtually complete skulls, including the ear ossicles, hyoid apparatus, complete thorax including a sternum with ossified intersternebral cartilages, nearly complete articulated forelimbs, complete lumbar region, nearly complete articulated caudal region with posterior chevron bones, and portions of a hind limb. This abundance of material is described here for the first time to completely characterize the skeleton of *Dorudon atrox*. Several well-preserved endocranial casts of *D. atrox* are also known. These cranial endocasts show the shape of the brain, blood vessels, and paths of many of the cranial nerves.

The skeletal anatomy and the reconstructed soft anatomy along with other evidence is used to reconstruct the life habits and life history of *Dorudon atrox*. One of the main goals of this study is to generate a picture of living *D. atrox*. Using the skeletal anatomy as data, one can place functional constraints on the abilities of fossil mammals. In this case, the structure of the vertebral column, the nature of the elbow and wrist joints, along with the size and form of the hindlimb, suggest that *D. atrox* was incapable of supporting itself on land. In addition, many details of the structure of the forelimb and caudal vertebrae are found only in modern cetaceans and sirenians, further suggesting that *D. atrox* was fully aquatic.

Lastly, an analysis of the phylogenetic position of *Dorudon atrox* relative to other archaeocetes and the modern suborders of Cetacea, Mysticeti and Odontoceti, has been performed. *D. atrox* and its close relatives, all placed in the subfamily Dorudontinae, have long been suggested as the ancestors of

the modern cetaceans (Fordyce and Barnes, 1994; Uhen, 1998). The phylogenetic analysis in this study is designed to assess the hypothesis that dorudontines give rise to modern cetaceans and to determine whether any particular dorudontine, such as *D. atrox*, is more closely related to modern cetaceans than any other dorudontine. This study utilizes a method of phylogenetic analysis called stratocladistics (Fisher, 1992) that can be used to assess not only relative recency of common ancestry, but also ancestor-descendant relationships. Thus the phylogenetic analysis will determine whether any known dorudontine is directly ancestral to modern cetaceans as well.

In short, the purpose of this study is to completely characterize one species, *Dorudon atrox*, out of the diversity of advanced archaeocete cetaceans. The complete description of the skeletal anatomy of *D. atrox* facilitates an analysis of the functional morphology and characterization of the behavior of *D. atrox*, as well as a phylogenetic analysis of *D. atrox* relative to other archaeocetes and to the modern suborders of Cetacea.

GEOLOGY OF FAYUM

The geology of the Fayum, northeastern Egypt has been studied by a long list of geologists from the late nineteenth century to the present. The area of interest, Zeuglodon Valley (Wadi Hitan), is located to the northwest of Lake Birket Qarun, which is northwest of Fayum.

Gingerich (1992) presented a thorough review of previous geologic studies in the Fayum area, as well as new observations and an interpretation of the depositional environments from the middle Eocene to early Oligocene. Three middle to late Eocene (Bartonian and Priabonian) formations in the Fayum have produced specimens of *Dorudon atrox*. A brief review of the lithology and interpretation of the depositional environments of the formations is presented here, taken from Gingerich (1992).

Gehannam Formation

The Gehannam Formation is generally composed of shale that varies in color from gray and green to dark and light brown. Some shale layers are rich in gypsum. Other beds are very sandy, with varying degrees of calcium carbonate cement. The Gehannam also includes marl layers, some of which include abundant calcareous invertebrates. These beds can sometimes form discontinuous layers and other times they can be traced for kilometers. The Gehannam Formation is capped by a hard white marl, the Camp White Layer, that includes abundant mangrove pneumatophores in places.

Birket Qarun Formation

The Birket Qarun Formation discontinuously overlies the Gehannam Formation. It is a massive yellow sandstone punctuated by a few rare beds of differing lithology. These additional beds include a green to gray to black shale (the "Black Layer"), beds of transported *Carolia* (a pelecypod) shells, oyster beds, clay beds (some with abundant gypsum), and sand beds that are well-cemented with calcium carbonate.

Qasr el-Sagha Formation

The Qasr el-Sagha Formation overlies the Birket Qarun Formation. The Qasr el-Sagha Formation is dominated by claystones of varying colors and textures. Some contain abundant gypsum and/or calcium carbonate. The claystones are interrupted by limestone beds containing calcareous invertebrates including: corals, nummulites, gastropods, and pelecypods. Other beds are hard, well-cemented sandstones and crossbedded sandstones.

ENVIRONMENTS OF DEPOSITION

Each of the three formations is interpreted to represent a different environment of deposition within a single large scale sedimentary system. The Gehannam Formation was deposited farthest from the paleoshoreline, while the Qasr el-Sagha Formation was the closest. The Gehannam Formation is thought to represent a shallow, open marine environment. The fauna from the Gehannam includes invertebrates, a diversity of sharks, large sea turtles, sirenians, and archaeocete whales. The Gehannam Formation is capped by a layer of mangrove fossils that represent a low sea stand marker.

The Birket Qarun Formation represents a mostly submerged barrier bar complex. Its long, narrow outcrop area suggests this kind of depositional system parallel to the paleoshoreline. The Birket Qarun Formation includes similar fossils to the Gehannam Formation, including archaeocete whales. The Birket Qarun barrier bar complex is thought to have been flooded and rapidly buried during a subsequent transgression.

The Qasr el-Sagha Formation represents lagoonal deposits that were deposited shoreward of the offshore barrier bar complex of the Birket Qarun. The depositional setting of the Qasr el-Sagha has been divided into a number of different subenvironments discussed by Gingerich (1992) in some detail. The Qasr el-Sagha Formation has produced numerous sirenians and archaeocete whales (including *Saghacetus osiris*, which is not known from the other formations). The only specimen of *Dorudon atrox* possibly from this unit is the now-lost holotype of *Prozeuglodon stromeri*. This specimen has been destroyed, so any indication of the provenance of the specimen, such as adhering sediment, is also gone.

TAPHONOMY OF *DORUDON ATROX* SPECIMENS

Numerous specimens of *Dorudon atrox* have been recovered from both the Gehannam Formation and the Birket Qarun Formation. Specimen numbers of University of Michigan and Cairo Geological Museum specimens of *D. atrox* are shown in Figure 1 at the localities where they were collected in Zeuglodon Valley. Preservation of the specimens varies with the lithology from which they were collected. Specimens or portions of speci-

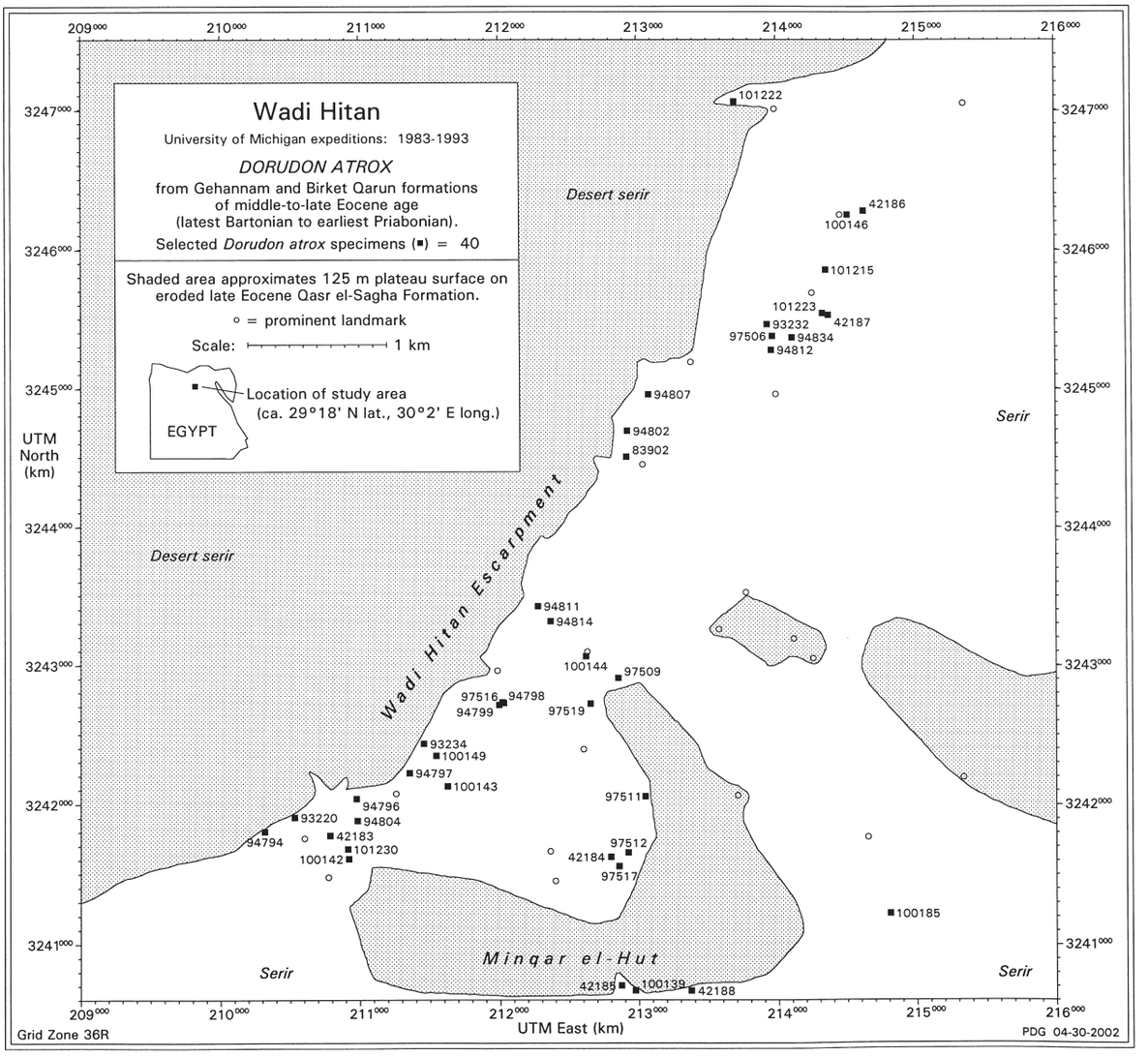

FIGURE 1 — Map of Wadi Hitan (Zeuglodon Valley) showing the localities of University of Michigan Museum of Paleontology and some Cairo Geological Museum specimens of *Dorudon atrox*. Most of the white area represents the Gehannam Formation. The Birket Qarun Formation forms escarpments around the edges of the islands of Qasr el-Sagha Formation in the bottom right corner of the map. The Birket Qarun Formation thins toward the north and eventually wedges out.

mens from both formations that have been subaerially exposed turned white and have become very friable. Colors in the following section are designated in parentheses in standard Munsell color notation.

Specimens from the Gehannam Formation vary more because the Gehannam contains more distinctly different lithologies that have produced *D. atrox* specimens. Some specimens are covered with a thin coating of dark red iron oxide (2.5 YR 3/6). When the bone is cleaned of the coating it is reddish yellow (7.5 YR 6/6) on the outside with the interior of the bone being dark reddish brown (5 YR 3/4). Other specimens from the Gehannam Formation are very pale brown (10 YR 7/4) on the surface, but reddish brown (5 YR 4/4) on the interior of bones. Crowns of teeth of specimens from the Gehannam Formation are usually very dark gray (10 YR 3/1), although some are dark yellowish brown (10 YR 4/4). Most specimens from the Birket Qarun Formation are pinkish gray (7.5 YR 7/2) on the surface and strong brown (7.5 YR 5/6) on the interior of the bone. Teeth are generally brownish yellow (10 Y 6/6) on the crowns, with light colored roots.


A


B

TABLE 1 — Specimens of *Dorudon atrox* at least 25% complete. Note that all of the relatively complete specimens from the Birket Qarun Formation are highly articulated while only one of the specimens from the Gehannam Formation is similarly articulated. The entire skeleton of UM 100185 was not collected, so its completeness and articulation could not be calculated, but field notes indicate that it includes much of a vertebral column with the vertebrae articulated with each other. Articulated specimens have never been recovered from beds that were not dominated by sand.

Locality	Specimen #	Formation	Lithology	Completeness	Articulation
ZV-001	CGM 42183	Birket Qarun	quartz sand	49%	85%
ZV-002	UM 93220	Birket Qarun	quartz sand	63%	86%
ZV-099	UM 97512	Birket Qarun	limey sand	73%	76%
ZV-176	UM 100143	Birket Qarun	quartz sand	34%	100%
ZV-224	UM 101222	Birket Qarun	quartz sand	55%	90%
ZV-139	UM 100185	Gehannam	limey sand	unknown	articulated
ZV-197	UM 100146	Gehannam	Fe rich sand	28%	0%
ZV-210	UM 101215	Gehannam	silty sand	71%	0%
ZV-226	UM 101223	Gehannam	Fe rich shale	25%	0%

Some very complete specimens from the Gehannam Formation are disarticulated. The specimen shown in Figure 2, from the Gehannam Formation, is relatively complete but disarticulated. A single specimen (UM 100146) from Zeuglodon Valley locality ZV-197 has an encrustation of barnacles on the condyle of the mandible. This indicates that this specimen spent some time exposed on the sea floor before it was buried. The sediment adhering to the specimen is an iron rich sand, with a thin coating of iron oxide on some bones, and a calcite crust on some of the others.

Specimens vary in completeness from an isolated bone or tooth, to virtually complete articulated skeletons. Specimens were assessed for completeness by computing the percent of the bones of the entire skeleton represented in the specimen. Specimens from both the Gehannam and Birket Qarun Formations ranged from less than 1% to over 70% complete. A higher proportion of the specimens recovered from the Birket Qarun Formation are at least 25% complete when compared to those of the Gehannam Formation.

Those specimens that were 25% or more complete were also assessed for degree of articulation. Data for these specimens are shown in Table 1. Articulation was calculated by counting the number of joints found articulated in the field and dividing it by the number of joints represented in the specimen (both adjacent bones of a joint present). Multiplying by 100 yields the percent of joints found articulated. Many of the specimens not listed in the table are from different (more shaley) lithologies. It appears that relatively complete specimens are always found in beds that are dominated by sandy lithologies. The distribution of relatively complete specimens among the Gehannam and Birket Qarun lithologies is shown in Figure 3. It is no surprise then that the Birket Qarun Formation contains a high proportion of complete and well-articulated specimens, since it is dominated by sandstone.

This distribution of complete and well-articulated specimens suggests that the beds dominated by sandy lithologies, particularly the Birket Qarun Formation, were deposited rapidly. The specimens that are well-articulated, like UM 100143 and UM 101222, have all of the ribs articulated with the thoracic vertebrae. Figure 4 includes close up views of the skull, caudal vertebrae, and thorax that show the degree of articulation of this individual. UM 101222 also has both forelimbs articulated down to the first row of phalanges. These individuals must have at least become stabilized by sediment before decay had proceeded to degrade the joint capsules. This indicates very rapid burial. Other specimens, like UM 101215, which is

FIGURE 2 — Specimen UM 101215 at locality ZV-210. A, view looking southwest; B, excavation in progress. Latter shows disarticulated lumbar vertebrae and ribs. Individual was found disarticulated, but was relatively complete. This suggests that the specimen experienced little or no post-mortem transport, but probably decomposed in place. There is no direct evidence that this individual was scavenged, but the hind limbs and distal elements of the forelimbs were not recovered, suggesting that scavengers removed them. Photographs by P. Gingerich.

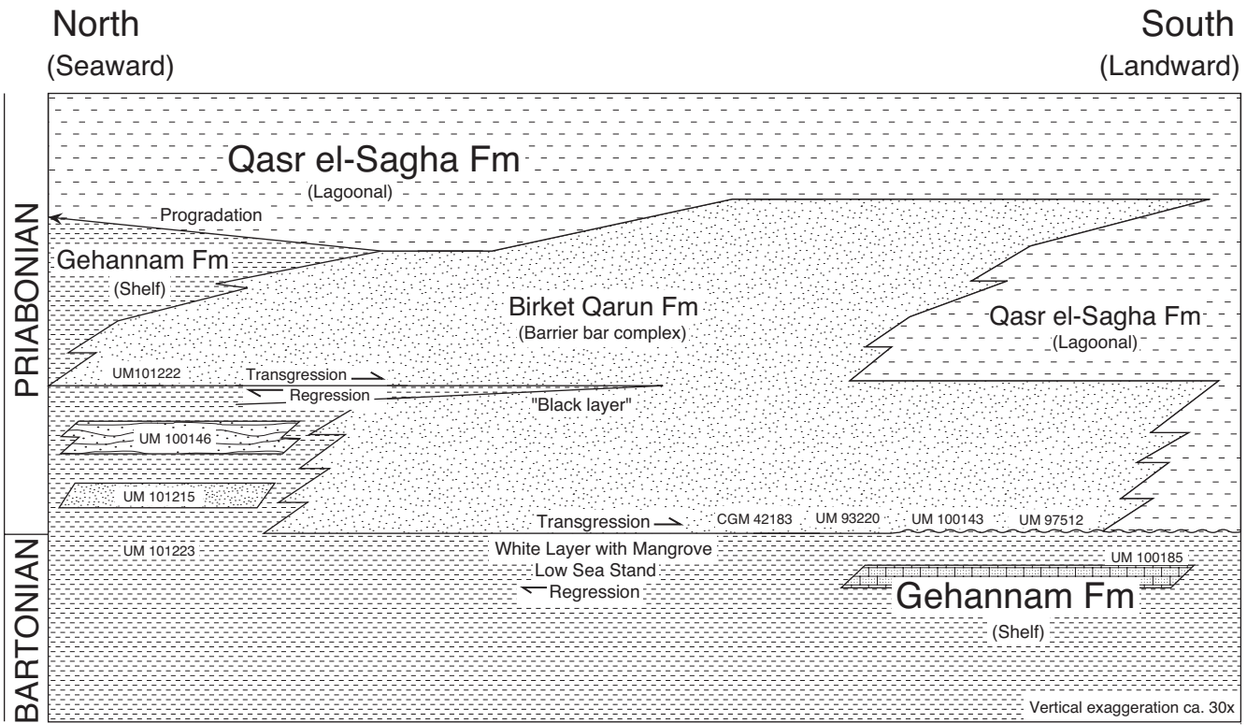

FIGURE 3 — Interpretative cross-section of the stratigraphy of Wadi Hitan (Zeuglodon Valley) showing relationships among different formations and the environments of deposition that they represent. Specimens of *Dorudon atrox* that are more than 25% complete are shown in the stratigraphic context in which they were found. Note that all of the articulated specimens are from sand bodies, and most are from the Birket Qarun Formation. Figure modified from Gingerich (1992).

very complete but totally disarticulated, probably spent more time on the sea floor before being buried. Since most of the bones of this specimen were found in a small area, yet none were articulated, it must have been in a relatively quiet environment to keep the bones close together.

Modern cetaceans that die in shallow water usually sink upon death, but then float to the surface as decomposition gasses fill the peritoneal cavity and decrease the density of the carcass (but see Allison et al., 1991 for a discussion of cetacean carcasses in deep water). These carcasses float on the surface and distal portions of the skeleton drop off into the water. These include (from earliest-to-fall to latest-to-fall): dentaries, distal phalanges, tail stock, and head. At some point the gas pressure in the carcass ruptures the body cavity and the rest of the carcass sinks (Schäfer, 1972). The articulated individuals may represent the carcasses of specimens that underwent this bloat and float process.

Lancaster (1986) described the taphonomy of an individual specimen of *Basilosaurus cetoides* that was found semi-articulated. Some of the bones had become disarticulated by a meter or two at most. Lancaster suggested that animals scavenging the carcass could have moved the bones from their original positions. While this is possible, even likely, for the disarticulated yet complete specimens of *Dorudon atrox*, there is no direct evidence of any scavenging behavior. Lancaster (1986) noted that a diversity of shark teeth had been found in the same deposits as the specimen of *B. cetoides*, but no shark bites were found on the specimen. The same is true of specimens of *D. atrox*. Shark teeth are abundant in both the Gehannam and Birket Qarun formations, but no unequivocal shark tooth marks have been found on any bones of *D. atrox*. Thus, it is unclear what role, if any, scavengers played in distributing bones of *D. atrox*.

FIGURE 4 — Specimen UM 101222 in place at locality ZV-224. A, rostrum in ventral view, and right dentary. Beneath and to the right of the rostrum are the articulated caudal vertebrae. The specimen was preserved fully-curled in a circle with the tail beneath the snout. Some mid-trunk vertebrae were carried down-slope by erosion. B, articulated thorax. Note that the ribs were found articulated with the vertebrae, and sternebrae were preserved in articulation. Photographs by P. Gingerich.


A

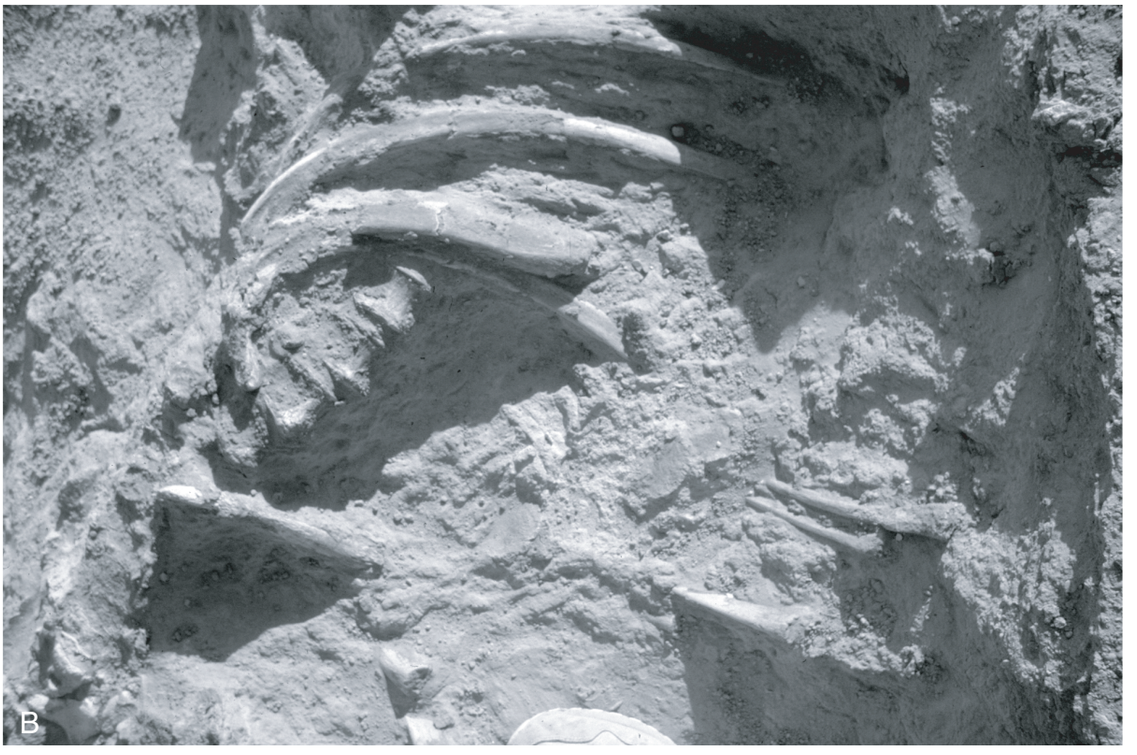
B

INSTITUTIONAL ABBREVIATIONS

The following institutional abbreviations are used throughout this work:

CGM — Cairo Geological Museum, Cairo, Egypt
MCZ — Museum of Comparative Zoology, Harvard University, Cambridge, Massachusetts
BMNH — Natural History Museum, London
NSFM — Naturmuseum Senckenberg, Frankfurt am Main
SMNS — Staatliches Museum für Naturkunde, Stuttgart
UFPM — University of Florence Paleontology Museum, Florence
UM — University of Michigan Museum of Paleontology, Ann Arbor, Michigan

ANATOMICAL ABBREVIATIONS

The following anatomical abbreviations are used throughout this work:

A astragalus
ab auditory bulla
ac acromion process
af arterial foramen
an angle
ang angular process
app anterior process of the periotic
arc articular circumference of the radius
AS alisphenoid
b body
bg bicipital groove
BHy basihyoid
BO basioccipital
boc basioccipital crest
BS basisphenoid
C# cervical vertebra
$C^{\#}_{\#}$ canine
Ca# caudal vertebra
cab caudal border of the scapula
cae caudal epiphysis
cap capitulum
cas caudal articular surface
cbi crus breve of the incus
cbl cerebellum
cbr cerebrum
caf cranial articular fovea
cd mandibular condyle
cdf caudal articular fovea
ch cochlea
cin caudal intervertebral notch
cli crus longum of the incus
clm column of the malleus
cnp coronoid process of the ulna
cop conical process of the auditory bulla
cp coracoid process
cpd coronoid process of the dentary
cpt capitulum of the distal humerus
Cr. # cranial nerve
crb cranial border of the scapula
cre cranial epiphysis
crm cranial rete mirabile
Cun cuneiform
Cv# chevron
d deciduous
D dentary
den dens
doc dorsal orbital crest
dpc deltopectoral crest
dss dorsal sagittal sinus
E ethmoid
eam external auditory meatus
en external nares
EO exoccipital
eoc external occipital crest
ep embrasure pit
etl ethmoidal labyrinth
F frontal
Fe femur
feo fenestra ovalis
fer fenestra rotunda
fhm fossa for the head of the malleus
fm foramen magnum
fo foramen ovale
fpo foramen pseudo-ovale
fps falciform process of the squamosal
frc fovea for rib capitulum
frs frontal shield
fr sn frontal sinuses
frt fovea for rib tuberculum
gc glenoid cavity
gf glenoid fossa
gpr gonial process of the malleus
gt greater tubercle of the humerus
h head of the humerus
H humerus
hf hypophyseal fossa
hm head of the malleus
hp hemal process
hyp hypophysis
$I^{\#}_{\#}$ incisor

iam internal auditory meatus
inf internal maxillary foramen
In incus
inv involucrum of the auditory bulla
iof infraorbital foramen
ipp internal pedicle of the posterior process of the auditory bulla
isc intersternebral cartilages
isf infraspinous fossa
ivf intervertebral foramen
J jugal
jn jugular notch
l lamina
L# lumbar vertebra
La lacrimal
lc lacrimal canal
lpi lenticular process of the incus
lpt lateral lamina of the pterygoid
lt lesser tubercle of the humerus
Lun lunate
lvf lateral vertebral foramen
m metapophysis
M#$_{\#}$ molar
Ma malleus
mc mandibular canal
Mc# metacarpal
mdf mandibular foramen
mf mental foramen
mlp medial lamina of the pterygoid
mo medulla oblongata
MS manubrium sterni
Mx maxilla
n neck
N nasal
na neural arch
nc neural canal
ncr nuchal crest
ns neural spine
ob olfactory bulb
oc occipital condyles
of olecranon fossa
op olecranon process
opf optic foramen
orf orbital fissure
OS orbitosphenoid
p pedicle
P patella
P#$_{\#}$ premolar
Pa parietal
Pal palatine
papr paroccipital process
pcl posterior cleft of the auditory bulla
pcp pars cochlearis of the periotic
Per periotic
pgp postglenoid process
Ph phalanx
Pis pisiform
plf posterior lacerate foramen
PMx premaxilla
po pons
pop postorbital process of the frontal
poz postzygapophysis
ppb posterior process of the auditory bulla
ppf posterior palatine foramen
ppp posterior process of the periotic
prop preorbital process of the frontal
prz prezygapophysis
PS presphenoid
Pt pterygoid
pt sn pterygoid sinus
R# rib
Rd radius
rdn radial neck
rf radial facet
rh radial head
ric radial interosseous crest
rn radial notch
rt radial tubercle
s spine of the scapula
S stapes
sbsf subscapular fossa
sc sagittal crest
Sc scapula
Sca scaphoid
scc semicircular canals
sct scapular tuberosity
sf scaphoid facet
sh shaft of the humerus
SHy stylohyoid
SO supraoccipital
sof sphenorbital fissure
sp sigmoid process of the auditory bulla
spn septal process of the nasals
spp superior process of the periotic
spsf supraspinous fossa
Sq squamosal
St sternebra
stf stapedial foramen
stp styloid process of the ulna
stt stapedial tubercle
sym mandibular symphysis
t transverse process
tc tympanic cavity
tf teres fossa of the scapula
tfa tibial face of the astragalus
THy thyrohyoid
tn trochlear notch
tr trochlea
Trd trapezoid
tsf tractus spiralus foraminosus
tub tuberculum
Tzm trapezium

U ulna
uic ulnar interosseous crest
Unc unciform
ut ulnar tubercle
V vomer
va ventral arch
vb vertebral border of the scapula
vac vertebrarterial canal
vk ventral keel
voc ventral orbital crest
vst vestibule
vt ventral tubercle
X xiphisternum
z zygomatic process of the squamosal

ACKNOWLEDGMENTS

My first thanks go to Philip D. Gingerich for advising me on this project. His work in recent years has produced one of the best archaeocete whale collections in the United States, if not the world, at the University of Michigan Museum of Paleontology. Without his diligent collecting this project would not have been possible. His advice on all aspects of this project is deeply appreciated. I would also like to thank the other members of my doctoral committee: Daniel C. Fisher, Philip D. Myers, Gregg F. Gunnell, and P. David Polly. Their support and advice on all aspects of this project are greatly appreciated. Mike Foote was on my doctoral committee before leaving the University of Michigan.

University of Michigan specimens used in this study were prepared by William J. Sanders. His expertise has helped bring the wonderful material of *Dorudon atrox* to light and helped to preserve it for a long time to come. Jennifer T. Moerman and her staff and volunteers who cast and mounted a complete skeleton of *Dorudon atrox* for the University of Michigan Exhibit Museum were also a great help preparing many of the fossils for me to study before they were molded and cast. John Klausmeyer of the Exhibit Museum was a driving force behind the project to mount *Dorudon atrox*. He helped reconstruct the musculature. Bonnie J. Miljour provided much needed advice on photography and illustration. In addition, she drew Figure 5, and together with Brenner C. Fishman, drew Figures 6 and 7. I thank them both for their wonderful work.

Many thanks as well to Caroline E. Blane, Michael DiPietro, Kerry L. Schwartz, and the Department of Pediatric Radiology at Mott Hospital, the University of Michigan. Their willingness to donate time, expertise, and resources for computed tomography scans of *Dorudon atrox* material has illuminated many aspects of cranial anatomy that would have been difficult to study without their help.

I also want to thank James G. Mead at the United States National Museum of Natural History (USNM). His advice and knowledge of modern cetaceans was greatly appreciated during my tenure as a Predoctoral Fellow at the USNM during the summer of 1994. I thank Charles W. Potter at the USNM for helping me find my way through the marine mammals collections. Clayton E. Ray, Frank C. Whitmore, and David J. Bohaska have all been very helpful in facilitating study of archaeocetes at the USNM. In addition, their discussions about aspects of archaeocete whale anatomy have been most enlightening.

C. Schaff and F. A. Jenkins at the Museum of Comparative Zoology, Harvard University loaned the type specimen of *Dorudon serratus* to Philip Gingerich at the University of Michigan, which I was thus able to study.

A trip to Europe to study archaeocete specimens in Germany and England was made possible by a Graduate Fellowship from the Society of Vertebrate Paleontology. G. Plodowski facilitated my work at the Naturmuseum Senckenberg, Frankfurt am Main, as did Elmar J. Heizmann at the Staatliches Museum für Naturkunde, Stuttgart, and Jeremy J. Hooker at the Natural History Museum, London. I thank them all for the assistance.

This work has benefited from numerous discussions with many other people at the University of Michigan on any number of topics from the nature of phylogeny reconstruction to dental wear and functional morphology. This group includes Jonathan I. Bloch, Brian E. Bodenbender, Robyn J. Burnham, Robert K. Carr, William C. Clyde, David L. Fox, Tracy D. Frank, Robert L. Klein, Daniel W. McShea, B. Holly Smith, Gerald R. Smith, and Xiaoyuan Zhou. These individuals have provided much intellectual stimulation as well as moral support during work on this dissertation.

Support for work toward this dissertation was provided by a Scott Turner Grant from the Department of Geological Sciences at the University of Michigan, a Smithsonian Predoctoral Fellowship from the U. S. National Museum of Natural History, and a Research Partnership (with Philip D. Gingerich) from the Rackham School of Graduate Studies at the University of Michigan.

Most of the University of Michigan and Cairo Geological Museum specimens discussed in this study were collected by Philip D. Gingerich, William J. Sanders, B. Holly Smith, and William C. Clyde, working in Egypt in cooperation with Elwyn L. Simons and Prithijit Chatrath of Duke University. Field work was funded by the Committee for Research and Exploration of the National Geographic Society (grants numbered 3424-86, 4154-89, 4624-91, and 5072-93 to PDG and ELS). Publication has been supported by National Science Foundation grant EAR 9714923 (PDG).

II

DORUDON TAXONOMY

Harlan (1834) named a new genus of Tertiary vertebrate from rocks in Louisiana. Harlan originally thought that it was a large sea reptile of some sort, so he named it *Basilosaurus* or "king lizard." Owen (1842a, b) changed the genus name to *Zeuglodon*, since he felt that the name *Basilosaurus* was inappropriate. Owen suggested the name *Zeuglodon* (yoke tooth) in reference to the yoke-shaped teeth of the animal. He also added the specific epithet *cetoides* to indicate that it was a cetacean. Despite its inappropriateness, the generic name *Basilosaurus* has priority over *Zeuglodon*. This has been recognized for some time (Kellogg, 1936) and was supported by Gingerich et al. (1990) and Uhen (1998).

When Andrews (1904) first named *Zeuglodon isis*, he attributed the species to Beadnell (MS). Andrews specifically stated that Beadnell would refer to *Zeuglodon isis* in his "memoir on the geology of the district, which will be published shortly, as *Zeuglodon isis*." This work was indeed published in 1905 (Beadnell, 1905), but without any diagnosis or description of *Zeuglodon isis*. In addition, Andrews (1904) gives an apt description and diagnosis of the species, and even identifies a type specimen. This specimen is figured in Andrews (1906: p. 241, fig. 78). The problem with Andrews' naming of *Zeuglodon isis*, is that the genus name *Zeuglodon* is a junior subjective synonym of *Basilosaurus* (Harlan, 1834) according to Kellogg (1936).

In addition to this problem, when Andrews (1906) named *Prozeuglodon atrox*, also from Egypt, he did not realize that the type specimen he designated was the skull and lower jaw of a juvenile individual. This was recognized by Kellogg (1936), who thought that the type specimen of *Prozeuglodon atrox* was a juvenile of Andrews' *Zeuglodon isis*. Since Kellogg recognized that the generic name *Zeuglodon* was invalid, he used the generic name *Prozeuglodon* along with the specific epithet for what Andrews had originally called *Zeuglodon isis* creating the new combination, *Prozeuglodon isis*. Since that time, many more specimens attributable to *Prozeuglodon atrox* have been found that show it is not a juvenile of *Zeuglodon isis*. The taxonomic outline below shows the current status and scope of each of these species.

Mammalia
Cetartiodactyla
Cetacea
Archaeoceti

Family Basilosauridae Cope, 1868

Zeuglodontidae Bonaparte, 1849, p. 618.
Hydrarchidae Bonaparte, 1850, p. 1.
Basilosauridae Cope, 1868, p. 144. Barnes and Mitchell, 1978, p. 582.
Stegorhinidae Brandt, 1873, p. 334.
Prozeuglodontidae Moustafa, 1954, p. 87.

Type genus.— *Basilosaurus* Harlan, 1834.

Included subfamilies.— Basilosaurinae Cope, 1868. Dorudontinae (Miller), 1923.

Age and distribution.— Early Bartonian (late middle Eocene) through Priabonian (late Eocene) of Asia (Gingerich et al., 1997), North America (Uhen, 1998), Egypt (Gingerich, 1992), Europe (Kellogg, 1936), and New Zealand (Köhler and Fordyce, 1997).

Diagnosis.— Members of the Basilosauridae lack M^3 and distinct sacral vertebrae. Basilosaurids have accessory denticles on their adult premolars and molars, and have a very reduced hindlimb. Members of the other families of archaeocetes, Protocetidae, Remingtonocetidae, Ambulocetidae, and Pakicetidae, retain M^3, have sacral vertebrae, and have large hind limbs. They also lack accessory denticles on their adult cheek teeth.

Discussion.— The name Basilosauridae is used here rather than Zeuglodontidae because Basilosauridae has been in common use at least since the publication of Kellogg (1936), and it is based on the generic name *Basilosaurus* rather than *Zeuglodon*, which is not currently in use.

Bonaparte (1850) included the Hydrarchidae in the Pinnipedia rather than Cete (Cetacea). Although he does not specify what genera or species are included in the Hydrarchidae, it is almost certain he meant the archaeocetes known at that time and based the family name on the genus *Hydrarchus*, a

TABLE 2 — Species of Basilosauridae currently regarded as distinct.

Basilosaurinae (Cope 1868)
- *Basilosaurus* Harlan 1834
  - *B. cetoides* (Owen 1839)
  - *B. isis* (Andrews 1904)
  - *B. drazindai* (Gingerich, Arif, Bhatti, Anwar, and Sanders 1997)
- *Basiloterus* (Gingerich, Arif, Bhatti, Anwar, and Sanders 1997)
  - *B. hussaini* (Gingerich, Arif, Bhatti, Anwar, and Sanders 1997)

Dorudontinae (Miller 1923)
- *Dorudon* Gibbes 1845
  - *D. serratus* Gibbes 1845
  - *D. atrox* (Andrews 1906)
- *Pontogeneus* Leidy 1852
  - *Pontogeneus brachyspondylus* (Müller 1851)
- *Zygorhiza* True 1908
  - *Z. kochii* (Reichenbach 1847)
  - *Z.* sp. Köhler and Fordyce (1997)
- *Saghacetus* Gingerich 1992
  - *Saghacetus osiris* (Dames 1894)
- *Ancalecetus* Gingerich and Uhen 1996
  - *Ancalecetus simonsi* Gingerich and Uhen 1996
- *Chrysocetus* Uhen and Gingerich, 2001
  - *Chrysocetus healyorum* Uhen and Gingerich, 2001

junior synonym of *Basilosaurus*. Since Basilosauridae has been in common use, at least since the time of publication of Kellogg's monograph on Archaeoceti, it is used here rather than Hydrarchidae.

Subfamily Basilosaurinae (Cope), 1868

Basilosauridae Cope, 1868, p. 144.
Zeuglodontinae Slijper, 1936, p. 540.
Basilosaurinae Barnes and Mitchell, 1978, p. 590.

Type genus.— *Basilosaurus* Harlan, 1834.

Included genera.— *Basilosaurus* Harlan, 1834; *Basiloterus*, Gingerich et al., 1997.

Age and distribution.— Bartonian and Priabonian of North America, North Africa, South Asia, and Europe (Gingerich et al., 1997; Uhen, 1998).

Diagnosis.— Basilosaurinae have all of the characters that distinguish Basilosauridae from other archaeocetes and in addition have greatly elongated posterior thoracic, lumbar, and anterior caudal vertebrae.

Discussion.— Previously Kellogg (1936) included the genus *Prozeuglodon* in the family Basilosauridae (here equivalent to Basilosaurinae). *Prozeuglodon* has been synonomized with the genus *Dorudon*, as discussed below, and it is thus in the subfamily Dorudontinae rather than the Basilosaurinae.

Subfamily Dorudontinae (Miller), 1923

Dorudontidae Miller, 1923, p. 13. Kellogg, 1936, p. 100.
Dorudontinae Slijper, 1936, p. 540. Barnes and Mitchell, 1978, p. 588.

Type genus.— *Dorudon* Gibbes, 1845.

Included genera.— *Dorudon* Gibbes, 1845; *Pontogeneus* Leidy, 1852; *Zygorhiza* True, 1908; *Saghacetus* Gingerich, 1992; *Ancalecetus* Gingerich and Uhen 1996; *Chrysocetus* Uhen and Gingerich, 2001. The type specimens of all species in Basilosauridae are listed in Table 2. The history of each specimen and its current taxonomic status are also listed.

Age and distribution.— Early Bartonian through Priabonian of North America, Egypt, Europe, and New Zealand (Köhler and Fordyce, 1997; Gingerich et al., 1997).

Diagnosis.— Dorudontines have all of the characters of the Basilosauridae listed above, but lack the elongated posterior thoracic, lumbar, and anterior caudal vertebrae of the Basilosaurinae. Most dorudontines are much smaller than basilosaurines, with the exception of the members of the genus *Pontogeneus*, which are thought to be only slightly smaller than members of the genus *Basilosaurus* in most dimensions (Uhen, 1997).

Discussion.— Miller (1923) originally proposed a division of the Archaeoceti into three groups of equal (familial) rank based on his own work and the usage of these terms by previous authors. Miller distinguished the first group, Protocetidae, from Dorudontidae and Basilosauridae by the presence of remnants of lingual extensions of cheek tooth crowns in the included taxa. He also distinguished the Basilosauridae from the Dorudontidae by the presence of elongated vertebrae.

Slijper (1936) and Barnes and Mitchell (1978) placed the families Basilosauridae and Dorudontidae of Miller at the subfamilial level within the families Zeuglodontidae and Basilosauridae, respectively, because they recognized a large suite of characters, especially in the skull and teeth, that these two groups share and that members of the Protocetidae lack.

The subfamilial structure is recognized here since it emphasizes the phylogenetic relationships among the subgroups of archaeocetes. Likewise, Dorudontinae is also likely to be paraphyletic, with Basilosauridae, and probably the modern suborders (Odontoceti and Mysticeti) being derived from within Dorudontinae.

Genus *Dorudon* Gibbes, 1845

Dorudon Gibbes, 1845, p. 255.
Basilosaurus (in part), Gibbes, 1847, p. 5.
Doryodon, Cope, 1868, p. 156 (lapsus).
Durodon, Gill, 1872, p. 93 (lapsus).
Prozeuglodon Andrews, 1906, p. 243. Kellogg, 1928, p. 40.
Zeuglodon (in part), Abel, 1914, p. 204.

Type species.— *Dorudon serratus* Gibbes, 1845.

Included species.— *Dorudon serratus* Gibbes, 1845; *Dorudon atrox* (Andrews), 1906.

Age and distribution.— Same as for the subfamily Dorudontinae.

Diagnosis.— Members of the genus *Dorudon* can be distinguished from other archaeocetes based on overall size, and other morphological characteristics. Members of the genus *Dorudon* are considerably larger than *Saghacetus*, and much smaller than members of the genus *Pontogeneus*. *Saghacetus* lacks the long narial process of the frontals that is characteristic of the genus *Dorudon*. Members of the genus *Dorudon* can be distinguished from members of the genus *Zygorhiza* based on the lingual cingula on P^{2-3}. While members of both genera have cingula on the mesial and distal ends of P^{2-3}, those of *Zygorhiza* are much better developed and more highly ornamented. *Zygorhiza* is slightly smaller than *Dorudon atrox* and has slightly more gracile forelimbs. *Zygorhiza* has a large narial process of the frontals like *Dorudon atrox*, but the medial maxillae of *Zygorhiza* touch both the nasals and the frontals. The posterior medial maxillae of members of the genus *Dorudon* contact only the nasals.

Discussion.— The genus *Dorudon* has had an odd history since it was first diagnosed by Gibbes (1845). First, Gibbes (1847) referred additional specimens to the species, including a pair of fragmentary premaxillae with I^3 (his plate III: figs. 1 and 3), a canine (his plate I: fig. 2) and twelve caudal vertebrae (his plate II: fig. 8). At the same time, he questioned his placement of the species in a separate genus from the previously described *Basilosaurus*, and he later placed both *Dorudon serratus* and a squalodont in *Basilosaurus* (Gibbes, 1847). Cope (1868) listed *Dorudon serratus* in a brief review of fossil Cetacea of the United States, but misspelled the name, calling it *Doryodon serratus*.

After the discovery of archaeocete whales in Egypt, many new species were described that were placed in the genus *Zeuglodon*. These new species include *Z. osiris* (Dames, 1894), *Z. zitteli* (Stromer, 1903), and three species described by Dart (*Z. elliotsmithii*, *Z. sensitivius*, and *Z. intermedius*), which he described in a paper on the brain of archaeocetes (1923). Kellogg (1936) placed all of these species in the genus *Dorudon*, along with a species he previously described as *Prozeuglodon stromeri* (Kellogg, 1928).

Since Kellogg's time, *D. osiris*, *D. zitteli*, *D. elliotsmithii*, and *D. sensitivius* have all been removed from *Dorudon*, synonymized, and placed in a new genus *Saghacetus*, as, *Saghacetus osiris* by Gingerich (1992). In addition Gingerich (1992) referred *Dorudon intermedius* to *Prozeuglodon atrox*, leaving only the type species *D. serratus* and *D. stromeri* in the genus *Dorudon*. Presently, the species *Prozeuglodon atrox* is referred to the genus *Dorudon* based on the observations discussed below.

Dorudon serratus Gibbes, 1845

Dorudon serratus Gibbes, 1845, p. 255.
Basilosaurus serratus, Gibbes, 1847, p. 5.
Doryodon serratus, Cope, 1868, p. 144 (lapsus).
Zeuglodon serratum, Abel, 1914, p. 204.

Type specimen.— MCZ 8763. Right maxilla with dP^2 to dP^4, left maxilla with dP^2?, dI^2?, as originally described by Gibbes (1845). Additional materials collected by Gibbes at the same site include portions of the left and right premaxillae, various cranial fragments, and twelve caudal vertebrae. These were believed to be from the same individual and were added to the type specimen (Gibbes, 1847). True (1908) referred some additional cranial material, a right mandible, an atlas, and some ribs to *Dorudon serratus* that had been collected by Gibbes but not described. The premaxilla pieces and a few of the cranial fragments are still with the type specimen, but some of the cranial fragments and the caudal vertebrae have been lost.

Type locality.— The type locality of *D. serratus* is given by Gibbes as "in a bed of Green sand near Santee Canal, in South Carolina on the plantation of R. W. Mazyck, Esq., about three miles from the entrance of the canal from the head waters of Cooper river" (1845). The sediments from which the type specimen was recovered are almost certainly those of the Harleyville Formation.

Age and distribution.— The description given by Gibbes (1845) and the sediment adhering to the specimen match the lithology of the Harleyville Formation well. Hazel et al. (1977) and Zullo and Harris (1987) list the age of the Harleyville Formation as Priabonian (nannoplankton zone 19/20). Nannoplankton zones 19 and 20 are Priabonian in age according to Berggren et al. (1995). The type locality of *D. serratus* is currently under the waters of Lake Moultrie, an artificial reservoir (see below). A single tooth from the Castle Hayne Formation of North Carolina has been referred to *D. serratus* by Kellogg (1936). Kellogg (1936, p. 178) listed this tooth as USNM 2335. It is actually USNM 2333. This tooth should be considered Dorudontinae *incertae sedis*. This locality (Kellum, 1926) is Bartonian or Priabonian in age.

Diagnosis.— *Dorudon serratus* is difficult to diagnose since there is very little material included in the type specimen and the individual that the material is from is a juvenile. It appears that the posterior upper deciduous premolars of *Zygorhiza kochii*

have a well-developed distal cingulum that is not highly ornamented, which the upper deciduous premolars of members of the genus *Dorudon* lack. Differences that distinguish *D. serratus* from *Dorudon atrox* include: the presence of three vs. two mesial accessory denticles on dP^2; weaker mesial and distal cingula on the upper premolars; stronger vertical rib ornamentation on the upper premolars; and a weaker lingual projection (Andrew's "posterointernal buttress" of *D. atrox*) on dP^3 and dP^4.

Discussion.— The type locality is now under water (Domning et al., 1982). A dam has been built forming a reservoir, Lake Moultrie, at approximately three miles from the Cooper River along the old Santee Canal route. Kellogg (1936) states that at the time he was writing the Mazyck plantation was known as Fair Spring, located one mile west of Macbeth, South Carolina and five and three quarters of a mile north of Moncks Corner, South Carolina, which would place it directly under Lake Moultrie. This conclusion was also reached by Sanders (1974).

Dorudon atrox (Andrews), 1906

Prozeuglodon atrox Andrews, 1906, p. 243. Gingerich, 1992, p. 73.
Dorudon intermedius Dart, 1923, p. 629.
Prozeuglodon stromeri Kellogg, 1928, p. 40.
Prozeuglodon isis, Kellogg, 1936, p. 75 (in part).
Dorudon stromeri, Kellogg, 1936, p. 203. Gingerich, 1992, p. 73.
?*Protocetus isis*, Trofimov and Gromova, 1968, p. 225.
Dorudon osiris, Pilleri, 1985, p. 35.
Dorudon atrox, Uhen, 1996, p. 403; 1998, p. 36.

Type specimen.— CGM 9319, cranium with right ramus of the lower jaw. (NHML 21896 is a cast of CGM 9319)

Type locality.— Andrews (1906) states that the type locality is in the "Birket-el-Qurun beds (Middle Eocene): a valley about 12 kilometres W.S.W. of the hill called Gar-el-Gehannem." Gingerich (1992) notes that this places the locality in Wadi Hitan (Zeuglodon Valley) where both the Gehannam and Birket Qarun Formations are exposed and both produce *Dorudon atrox* specimens. Despite the fact that Andrews indicates that the specimen came from the Birket Qarun Formation it remains unclear which formation produced the type specimen, since Beadnell did not always distinguish between the Gehannam and Birket Qarun Formations (Beadnell, 1905; Gingerich, 1992).

Age and distribution.— Bartonian to early Priabonian. Specimens of *Dorudon atrox* have been recovered from the Gehannam and Birket Qarun Formations of the Fayum. The type specimen of *Dorudon stromeri*, now placed in *Dorudon atrox*, is possibly from the Qasr el-Sagha Formation. The Birket Qarun Formation is interpreted as very shallow marine deposits that mark the lowstand between the Tejas 4 and Tejas 5 sequence tracts. This boundary has also been identified as the Bartonian-Priabonian boundary (Gingerich, 1992).

Diagnosis.— *Dorudon atrox* can be distinguished from all other archaeocetes by its unique conformation of cranial bones in the posterior narial region (see Figure 2.28). In *D. atrox*, the posterior nasals are separated by a long, thin process of the frontals. In addition, the medial edges of the posterior maxillae contact the lateral edges of the nasals. Both species of *Basilosaurus* have small narial processes of the frontals and the medial maxillae touch the nasals only. *D. atrox* is here placed in the genus *Dorudon* due to the similar size and morphology of the type specimen of *Dorudon serratus* to comparable specimens of *D. atrox*. Differences that distinguish *D. atrox* from *Dorudon serratus* include: the presence of three vs. two mesial accessory denticles on dP^2; weaker mesial and distal cingula on the upper premolars; stronger vertical rib ornamentation on the upper premolars; and a weaker lingual projection (Andrew's "postero-internal buttress" of *D. atrox*) and dP^3 and dP^4.

Discussion.— In 1906 Andrews described a new genus and species that he called *Prozeuglodon atrox* and designated the type specimen as CGM 9319. Andrews clearly distinguished it from *Zeuglodon isis* and other Egyptian archaeocetes. The main point that Andrews used to differentiate *P. atrox* from *Z. isis* is the presence of a "posterointernal buttress" on the two posterior premolars (his P^3 and P^4). He failed to recognize that the type specimen of *P. atrox* is a juvenile individual, and the teeth in question are deciduous premolars (dP^3 and dP^4). The "posterointernal buttress" is a feature of basilosaurid deciduous teeth, not of *P. atrox* in particular.

Kellogg added another species to the genus *Prozeuglodon*, *Prozeuglodon stromeri*, from the Qasr el-Sagha Formation, Fayum, Egypt (Kellogg, 1928). In 1936 Kellogg listed the generic name *Zeuglodon* as a junior subjective synonym of the genus *Basilosaurus*. Numerous species from Egypt and Europe had been found since the name *Zeuglodon* was proposed by Owen (1842a) for *Basilosaurus*, most of which were placed in *Zeuglodon*. Kellogg restricted the genus *Basilosaurus* to include only the type species, *Basilosaurus cetoides* from the southeastern United States. He placed most of the other species in the genus *Dorudon*.

Kellogg noted that the character Andrews used to distinguish *P. atrox* from *Zeuglodon isis*, the presence of a lingual expansion on the posterior premolars, was a character emphasized in the deciduous teeth of archaeocetes, not adult teeth and realized that the type specimen of *P. atrox* was a juvenile individual. In addition, three vertebrae (C1-C3; CGM 9329, 9230, 9332 respectively) that had been referred to *P. atrox* were similar to those of *Z. isis*, only smaller. Since the type specimen of *P. atrox* was clearly a juvenile based on the dentition, and it was quite similar to *Z. isis*, only smaller, Kellogg combined the two into a single species that he called *Prozeuglodon isis*, effectively separating it from *Basilosaurus* and emphasizing that he felt the larger individuals (former *Z. isis* individuals) were the proper adult form of the juvenile represented by the type specimen of *Prozeuglodon atrox*.

Gingerich et al. again separated *Prozeuglodon isis* into two species in 1990. These authors referred the type specimen and other smaller archaeocete specimens like the type back to *Prozeuglodon atrox*, and placed the large specimens (including the type specimen of *Zeuglodon isis*) with elongated poste-

rior thoracic and lumbar vertebrae in *Basilosaurus isis*. Gingerich et al. (1990) also noted that numerous specimens of immature skulls like that of the type specimen of *P. atrox* have been found associated with dorudontine vertebral columns, while none have been found with basilosaurine vertebral columns, further supporting their distinction between the two species. This observation also supports the placement of *Zeuglodon isis* in the genus *Basilosaurus* since it shares the elongated vertebrae and large size with *B. cetoides*.

Gingerich (1992) synonomized *Dorudon intermedius* with *Prozeuglodon atrox*, noting the similarities in brain size, skull length, and stratigraphic position of the type specimen of *D. intermedius* and *P. atrox*. Additional observations and detailed measurements of the type specimen of *D. intermedius* show that it is well within the range of variation of *P. atrox*.

Since that time, more specimens of *Prozeuglodon atrox* have been collected and studied (Uhen, 1996; 1998). These specimens include juveniles and adults with varying completeness of the skeleton and are now placed in the genus *Dorudon*, making the species *Dorudon atrox*. The type specimen of *Dorudon serratus* consists mainly of three upper right deciduous premolars ($dP^{2\text{-}4}$) and a lower deciduous premolar (dP_3?). These teeth are virtually indistinguishable from those of *D. atrox*. In addition, Gibbes (1847) referred a series of twelve anterior caudal vertebrae to *Dorudon serratus* that are again indistinguishable from those of *D. atrox* in size and morphology. These features support the placement of *P. atrox* in the genus *Dorudon*.

Prozeuglodon stromeri (Kellogg, 1928) is also considered to be a junior synonym of *Dorudon atrox*. Although the type specimen has been destroyed (Gingerich, 1992), it was well described and well figured (Kellogg, 1928; Kellogg, 1936 plates 24 & 25). The description and measurements of the type specimen are fully consistent with assignment to *D. atrox*.

Kellogg (1936, p. 76) listed all of the specimens that he included in *Prozeuglodon isis*. Since this list is a mixture of at least two, possibly three species, those specimens that do not pertain to *Dorudon atrox* are briefly listed here. CGM 10019 (posterior lumbar and anterior caudal vertebrae), SMNS 11787 (skull and much of a skeleton), Munich 1904 XII 135 (broken right mandible, destroyed), Munich 1904 XXI 135a (portions of right and left premaxillae and the left maxilla, destroyed), Munich 1904 XII 135b, (right and left dentaries, destroyed), and AMNH 14381 (incomplete skull), are all referable to *Basilosaurus isis*. SMNS 11413 (fragmentary skull) and SMNS 11414 (atlas, an axis, and numerous trunk vertebrae), are both part of the same individual and are probably referable to *Pontogeneus brachyspondylus*.

Kellogg (1936) stated that SMNS 11417 consists of right and left mandibles (dentaries). Kellogg (1936, p. 185) also listed this specimen under *Dorudon* (*Saghacetus*) *osiris*, and noted the left and right dentaries were different in size and probably from two different species. The smaller right dentary, now cataloged under the specimen number 11417a, is clearly too large to be referred to *Saghacetus osiris*, and is almost certainly from *Dorudon atrox*. The left dentary, now cataloged under the specimen number 11417b, is from *Basilosaurus isis*. Kellogg (1936) lists an isolated humerus and crushed ulna under SMNS 11417a (St. 15 of Stromer, 1908). No specimen matching the description of St. 15, nor one bearing a tag with St. 15 on it could be located. Another specimen, SMNS 11417b, consisting of a right and a left humerus was also located. The tags on this specimen state that it is St. 12 of Stromer. This was confirmed with measurements taken of the specimens that match those of Stromer (1908, p. 35, table IV). Currently, both the left dentary of *Basilosaurus isis* described above and St. 12 humeri bear the same specimen number, SMNS 11417b.

III

DENTAL AND SKELETAL ANATOMY

The only specimens of *Dorudon atrox* described previously are the holotype skull and lower jaws, and several referred cervical vertebrae reported by Andrews (1906). Some sixty cataloged specimens of *Dorudon atrox* are now known. Almost every portion of the skeleton is represented including: complete skulls with ear ossicles, hyoid apparatus, thorax with ribs and sternum, articulated forelimbs, lumbar region, articulated caudal region with posterior chevron bones, and portions of a hind limb. This abundance of material has facilitated a complete characterization of the *D. atrox* skeleton (Fig. 5) and skull (Figs. 6 and 7). Specimens are listed in Appendix I.

The anatomy of *Dorudon atrox* is described regionally in this chapter. The description begins with the dentition and continues with the skull, postcranial axial skeleton, and appendicular skeleton. Anatomical terminology is primarily derived from Flower (1876), Rommel (1990), and Evans (1993). A reconstruction of the skeleton of *Rodhocetus kasrani* (Gingerich et al., 2001), a protocetid, is provided in Figure 8 for comparison with the more derived basilosaurid *D. atrox*.

DENTAL ANATOMY

Archaeocetes, including *Dorudon atrox*, are diphyodont and retain the primitive mammalian pattern of dental differentiation. All of the teeth have better developed ornamentation on the lingual side than on the buccal side. The incisors and canines are relatively simple conical teeth. Archaeocete premolars and molars are more complex, having multiple cusps and multiple roots. *Dorudon atrox* is unusual among mammals in that it replaces both upper and lower first premolars. The evidence for the replacement of the first premolars is discussed below with the description of P_1. Measurements taken on the teeth of *D. atrox* are shown in Figure 9.

The premolars and molars of *Dorudon atrox* are much more complex than the anterior dentition. These teeth are buccolingually flattened blades that are mesiodistally elongated. They have a central main cusp with numerous accessory denticles along the mesial and distal edges of the triangularly shaped crowns and have two roots. The only exceptions to this general description are the lower molars, each of which has a groove down its mesial face, rather than denticles. It is thought that the central cusp is the paracone on the upper cheek teeth and the protoconid on the lower cheek teeth, based on comparisons with other archaeocetes and other mammals (Gingerich and Russell, 1990), and that the accessory denticles are neomorphs of basilosaurid archaeocetes, at least in the permanent teeth.

Deciduous dentition

There are three deciduous incisors, one canine, and four deciduous premolars in each dental quadrant of *Dorudon atrox* yielding a deciduous dental formula of 3.1.4/3.1.4. The anterior teeth are arranged in a line parallel with the deciduous canine and premolars. Summary statistics for the measurements of *D. atrox* deciduous upper teeth are shown in Table 3 and those for the lower deciduous teeth are shown in Table 4.

Deciduous upper incisors

The deciduous upper incisors are similar to each other, but change slightly in size and morphology from dI^1 to dI^3 (Fig. 10). All of the deciduous upper incisors are single-rooted. Crowns are conical and slightly flattened buccolingually. There are no well-developed cingula on the deciduous upper incisors. The crowns are also slightly curved both buccally and distally**.**

The deciduous upper first incisor [**dI^1**, Fig. 10] is the smallest of the deciduous upper incisors. It is not nearly as small as dI_1 (discussed below), so it is easy to distinguish it from dI_1. The crown of dI^1 is similar to the crowns of the other deciduous upper incisors. It is in the shape of a cone that is curved distally. The root of dI^1 gently tapers from the base of the crown to its tip.

The deciduous upper second incisor [**dI^2**, Fig. 10] is larger than either dI^1 or dI^3. It is longer, higher, and wider than any of the other deciduous upper incisors. The root of dI^2 is noticeably inflated just proximal to the base of the crown. This makes the alveolus for dI^2 much larger than those for dI^1 and dI^3.

The deciduous upper third incisor [**dI^3**, Fig. 10] is larger than dI^1, but slightly smaller than dI^2. A mesiodistal midline ridge is best developed on dI^3, where it is very distinct and sharp. In addition, small serrations are present on the ridge at the base of the crown on both the mesial and distal edges. The serrations are tiny on the mesial edge, but larger on the distal edge, where they also extend farther up the crown. The serrations decrease in size from the base of the crown up the ridge.

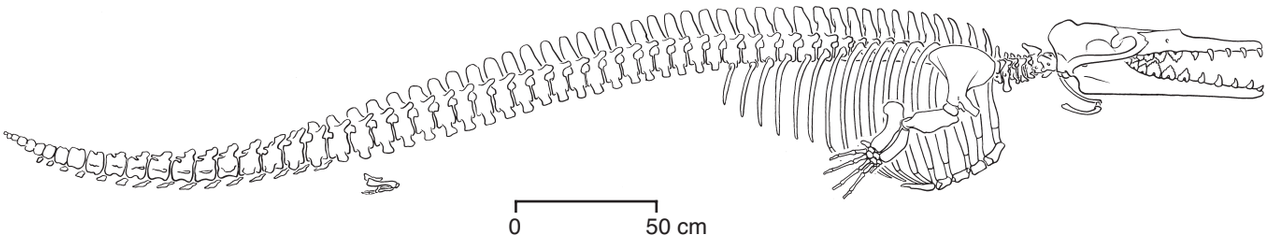

FIGURE 5 — *Dorudon atrox* skeletal restoration. This restoration is a composite based mainly on UM 101215 and 101222. The innominate and pes are not known from *D. atrox*, but the proximal femur, patella, and astragalus of *D. atrox* are similar to those of *Basilosaurus isis* (Gingerich et al, 1990). The innominate here is restored from closely related *Chrysocetus healyorum* (Uhen and Gingerich, 2001), and the pes is restored from *B. isis*. Length of skeleton is 4.85 meters.

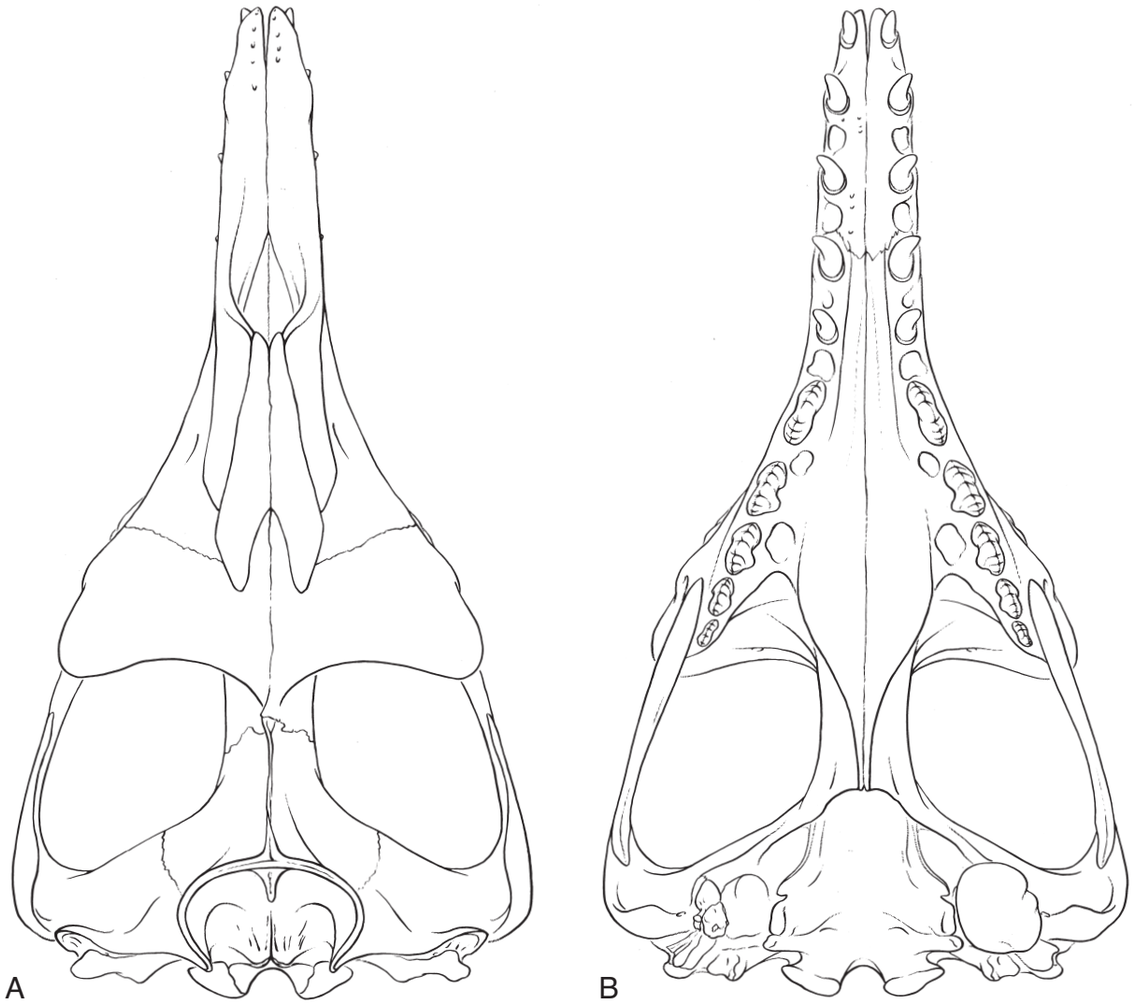

FIGURE 6 — *Dorudon atrox* skull restoration. This restoration is a composite based mainly on UM 100139, 93220, and 101222. A, dorsal view. B, ventral view. Length of skull is about 95 cm.

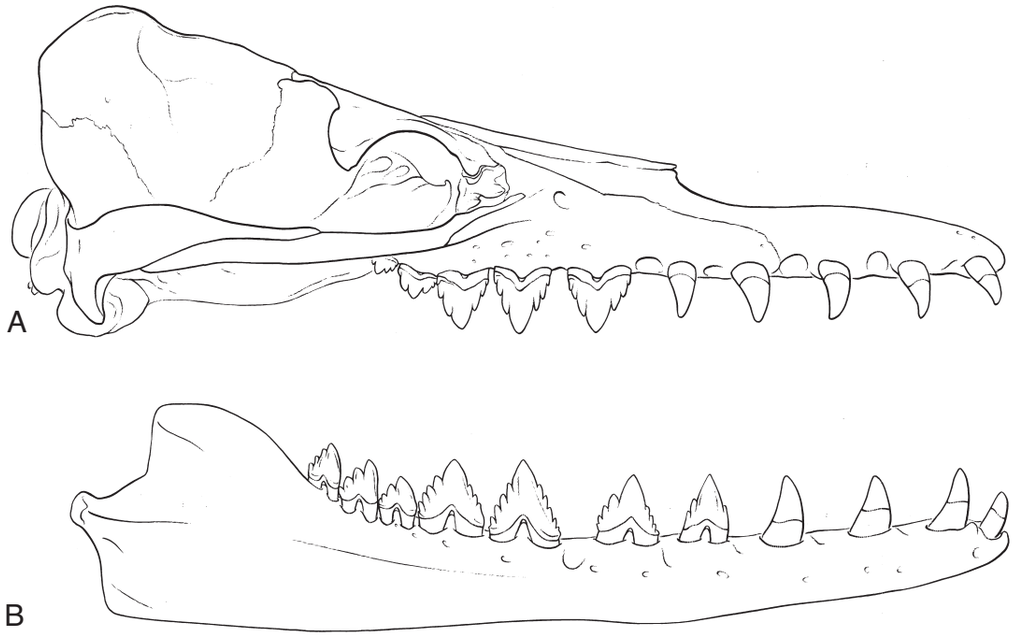

FIGURE 7 — *Dorudon atrox* skull (A) and dentary (B) restoration, in right lateral view. Restoration is a composite, based mainly on NSFM 4451, and UM 93220, 100139, and 101222. The dentary is shown disarticulated from the skull. Length of skull is about 95 cm.

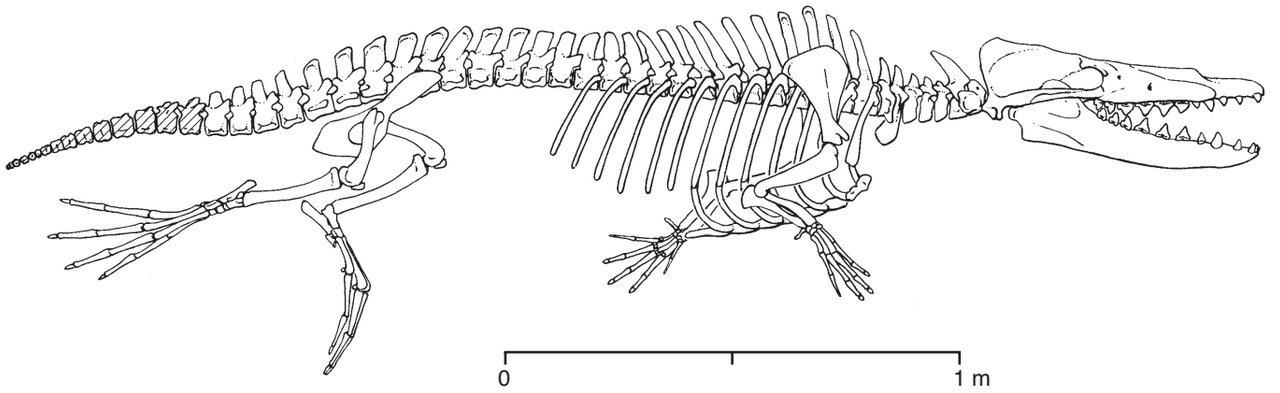

FIGURE 8 — Composite restoration of the skeleton of *Rodhocetus kasranii* in a paddling pose for comparison with the skeleton of *Dorudon atrox* (Figure 5). Terminal vertebrae of the tail (hatched) are conjectural, and the tail was probably longer than shown (Gingerich et al., 2001). Note the smaller number of trunk vertebrae in *Rodhocetus* and the large hind limbs when compared with *D. atrox*. Illustration by Doug Boyer, used by permission, ©2001, AAAS.

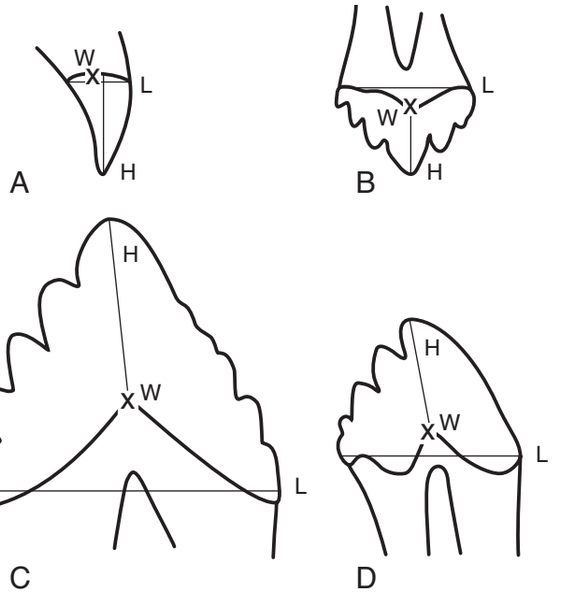

FIGURE 9 — Tooth measurements for *Dorudon atrox*. All teeth are shown in right lateral view. A, upper incisor; all incisors and canines were measured in this fashion. B, upper molar. C, lower premolar; all premolars were measured in this fashion. D, lower molar. Abbreviations: *H*, crown height from the cingulum to the tip of the apical cusp on multi-cusped teeth; *L*, length along the tooth row; *W*, buccolingual width taken at the X symbol. Measurement values for deciduous teeth of *D. atrox* are listed in Appendix II. Measurement values for permanent teeth of *D. atrox* are listed in Appendix III.

The root of dI^3 is not inflated like that of dI^2, but rather tapers gently from the base of the crown to the tip.

Deciduous upper canine

The deciduous upper canine [**dC^1**, Fig. 10] is larger than any of the upper incisors. It projects more mesially than the upper incisors, and it is also less curved distally. The midline ridge of dC^1 is very strong and shows the development of tiny serrations on both the mesial and distal ridges in some individuals. The single root of the upper canine carries shallow grooves on both its buccal and lingual sides.

Deciduous upper premolars

Dorudon atrox, unlike most mammals that have first premolars, replaces its first premolar rather than retaining the deciduous P^1 [**dP^1**, Fig. 11]. The evidence for replacement of dP^1 is similar to that for dP_1, as discussed by Uhen (2000). The deciduous first premolar has a single mesiodistally elongated root and is multicusped. It has a large apical cusp and a strong midline ridge. The mesial edge has a variable number of small accessory denticles, usually 2-4, and the distal edge has 2-3 large accessory denticles and a variable number of smaller ones that are similar in size to the mesial accessory denticles.

The deciduous second upper premolar [**dP^2**, Fig. 12] is buccolingually compressed and double rooted. The mesial and distal roots are subequal in size. The crown is dominated by a very large central cusp. It is about twice as high and twice as long as the central cusp of dP^3. There are two accessory denticles on the mesial edge, along with a moderately developed mesial cingulum. There are three accessory denticles on the distal edge, with the last denticle arising from the moderately developed distal cingulum. The distal edge of dP^2 is just below the anterior border of the infraorbital foramen in the maxilla.

The deciduous third upper premolar [**dP^3**, Fig. 12] has three to four accessory denticles on the mesial edge. The mesial denticles increase in size from mesial to distal. The basal mesial accessory denticle arises from the mesial cingulum. There are variably-developed cuspules on the lingual extension of the mesial cingulum. There are four accessory denticles on the distal margin of the crown. A weak buccal cingulum is present, and a moderately-developed lingual cingulum is present on the crown below the mesial root. There is a very strong lingual projection of the crown below the mesial edge of the distal root. Andrews (1906) termed this feature a "posterointernal buttress", and identified it as a third root. It is unclear from direct observation, radiographs, or CT scanning whether dP^3 and dP^4 actually have a third root or whether they have expanded distal roots covered by the lingual projection of the crown. Even if the distal root is undivided near the crown, it may be divided at its tip.

The deciduous fourth upper premolar [**dP^4**, Fig. 12] has three to four accessory denticles on the mesial edge. The first denticle arises from the well-developed mesial cingulum. There are four to five accessory denticles on the distal edge. The last denticle arises from the distal cingulum. The profile of the crown is more rounded than triangular as in dP^{2-3}. A weak buccal cingulum is present. There is a strong lingual cingulum on the crown above the mesial root and a weak lingual cingulum on the crown above the distal root. There is a lingual projection of the crown above the mesial edge of the distal root, but it is not as strong as that seen in dP^3.

Deciduous lower incisors

Dorudon atrox has three deciduous lower incisors arranged in a row. These deciduous lower incisors are similar to one another, but change slightly in size and morphology from dI_1 to dI_3 (Fig. 13). All of the deciduous lower incisors are single rooted. The crowns of the teeth are conical and slightly flattened buccolingually. There are no well-developed cingula on the deciduous lower incisors. The crowns have vertical crenulations on the lingual side, extending from the base to two-thirds of the way up the crown. There is a mesiodistal midline ridge on each of the teeth. The crowns are also slightly curved distally. Each of the roots is generally oval in cross-section,

TABLE 3 — Summary statistics for deciduous upper teeth of *Dorudon atrox*. All measurements are in millimeters. L, length along the tooth row; H, height of the crown measured from the cingulum to the apical cusp for premolars; W, maximum buccolingual width for anterior teeth and measured below the apical cusp for premolars. N, sample size; SD, standard deviation; CV, ratio of the standard deviation to the mean (in percent). Measurements are shown in Figure 9 and are listed in Appendix IIA.

Tooth	Dimension	N	Minimum	Maximum	Mean	SD	CV
dI^1	L	2	14.0	15.0	14.5	0.7	4.9
	W	2	10.3	12.0	11.2	1.2	10.8
	H	0	—	—	—	—	—
dI^2	L	2	20.1	20.2	20.2	0.1	0.4
	W	2	12.6	13.0	12.8	0.3	2.2
	H	1	32.3	32.3	32.3	—	—
dI^3	L	6	14.2	19.9	16.1	2.1	13.0
	W	6	9.5	15.6	11.0	2.3	21.1
	H	3	21.0	24.2	22.5	1.6	7.2
dC^1	L	2	21.4	26.0	23.7	3.3	13.7
	W	2	13.2	14.0	13.6	0.6	4.2
	H	0	—	—	—	—	—
dP^1	L	1	31.7	31.7	31.7	—	—
	W	1	16.0	16.0	16.0	—	—
	H	0	—	—	—	—	—
dP^2	L	7	43.0	48.2	45.7	2.0	4.3
	W	3	11.2	12.1	11.7	0.5	3.9
	H	2	23.9	26.0	25.0	1.5	6.0
dP^3	L	10	42.0	49.0	46.7	2.1	4.5
	W	4	11.3	12.4	12.0	0.5	4.0
	H	1	24.3	24.3	24.3	—	—
dP^4	L	9	40.1	45.8	43.0	1.6	3.8
	W	5	10.8	12.8	11.6	0.7	6.5
	H	3	17.5	18.3	18.0	0.4	2.3

and each has a shallow groove running down the root on the lingual side**.**

The first deciduous lower incisor [**dI_1**, Fig. 13] is the smallest deciduous incisor. It has the shortest crown and the most gracile root. A single first deciduous lower incisor is known from one specimen, UM 94814. It would be difficult to confuse dI_1 with any other incisor based on its size. Another specimen, UM 101223, preserves the alveolus for dI_1 in the left dentary. It is very small and very close to the midline and to the alveolus for dI_2. This conformation is similar to that of the adult I_1 and I_2 alveoli.

The second deciduous lower incisor [**dI_2**, Fig. 13] is much larger than dI_1, but it is otherwise similar in morphology. The root of dI_2 is slightly expanded just proximal to the base of the crown, making the alveolus for dI_2 slightly larger than that for dI_3. In addition, the roots of dI_2 are slightly longer than those of dI_3 and are more curved.

The third deciduous lower incisor [**dI_3**, Fig. 13] is similar in size to dI_2, but it does not have the expanded root of dI_2. The third deciduous lower incisors have shallow grooves on both the lingual and buccal sides of their roots, which may make them a bit harder to distinguish from deciduous lower canines (see below). The third deciduous lower incisor can be distinguished from the deciduous canine, since the deciduous canine is much larger than dI_3.

Deciduous lower canine

The deciduous lower canine [**dC_1**, Fig. 13] is similar to the deciduous lower incisors, but it differs in some significant ways. The first is that the tooth is considerably larger. The conical crown is both taller and longer at the base than any incisor. The crown also has a well-developed midline ridge like that of the incisors, and it has vertical crenulations on the lingual side. The canine lacks any well-developed cingula. The root of the deciduous lower canine is mesiodistally long. It is divided on both the lingual and buccal sides by a groove running down the root.

TABLE 4 — Summary statistics for deciduous lower teeth of *Dorudon atrox*. All measurements are in millimeters. L, length along the tooth row; H, height of the crown measured from the cingulum to the apical cusp for premolars; W, maximum buccolingual width for anterior teeth and measured below the apical cusp for premolars. N, sample size; SD, standard deviation; CV, ratio of the standard deviation to the mean (in percent). Measurements are shown in Figure 9 and are listed in Appendix IIB.

Tooth	Dimension	N	Minimum	Maximum	Mean	SD	CV
dI_1	L	3	9.5	17.0	12.0	4.3	36.1
	W	2	7.6	11.0	9.3	2.4	25.9
	H	1	14.9	14.9	14.9	—	—
dI_2	L	2	15.5	17.3	16.4	1.3	7.8
	W	2	10.6	10.8	10.7	0.1	1.3
	H	2	24.2	25.5	24.9	0.9	3.7
dI_3	L	2	17.0	17.7	17.4	0.5	2.9
	W	3	10.9	12.0	11.3	0.6	5.6
	H	1	25.6	25.6	25.6	—	—
dC_1	L	1	20.3	20.3	20.3	—	—
	W	1	12.2	12.2	12.2	—	—
	H	1	30.9	30.9	30.9	—	—
dP_1	L	4	22.5	28.0	25.5	2.3	8.9
	W	3	11.4	12.9	12.3	0.8	6.6
	H	3	29.2	35.0	31.3	3.2	10.4
dP_2	L	8	33.3	43.5	38.1	3.2	8.3
	W	4	9.5	11.4	10.6	0.8	7.7
	H	2	21.5	22.7	22.1	0.8	3.8
dP_3	L	8	54.3	60.2	57.5	2.3	4.1
	W	3	11.3	11.8	11.5	0.3	2.3
	H	2	26.3	27.2	26.8	0.6	2.4
dP_4	L	9	53.0	61.0	56.6	2.9	5.0
	W	5	10.7	14.0	12.3	1.2	9.9
	H	3	27.0	34.0	29.7	3.7	12.6

Deciduous lower premolars

The deciduous first premolar [**dP_1**, Fig. 14] has a single root, a strong midline ridge, no accessory denticles (or at most very tiny serrations) on the mesial edge, a tall central cusp, and two well-developed accessory denticles on the distal edge.

The deciduous second lower premolar [**dP_2**, Fig. 14] is double rooted and buccolingually compressed. The crown is dominated by a large central cusp that is directly above the division between the mesial and distal roots. The mesiodistal midline ridge is elaborated into a series of cusps. There are small serrations on the mesial and distal edges of the central cusp. There are three very small accessory denticles on the midline ridge, mesial to the central cusp. There are three larger accessory denticles on the ridge distal to the central cusp. In addition, there is a moderately developed distal cingulum.

The deciduous third premolar [**dP_3**, Fig. 14] is much longer than dP_2. It is buccolingually compressed and double rooted. The crown is dominated by a large central cusp directly above the division between the two roots. This cusp has fine serrations like dP_2. There are four accessory denticles on the mesial edge of the tooth. There are five accessory denticles on the distal edge of the tooth that are about twice as large as the mesial accessory denticles. The last distal accessory denticle arises from the well-developed distal cingulum.

The deciduous fourth premolar [**dP_4**, Fig. 14] is slightly smaller than dP_3. It is buccolingually compressed and double rooted. It can be distinguished from dP_3 by its smaller size overall and the smaller size of the central cusp. The central cusp is both shorter mesiodistally and shorter in height. The central cusp is above the division between the two roots. There are four to five accessory denticles on the mesial edge of the tooth. An additional cuspule is present on the buccal side of the mesial cingulum. There are five accessory denticles on the distal edge of the tooth that are larger than the mesial accessory denticles. The last denticle is on the small distal cingulum.

A dentary of *Zygorhiza kochi* with an erupting canine and premolars is shown in Figure 15, supporting the idea that dP_1 is replaced by a permanent tooth at this position (Uhen, 2000).

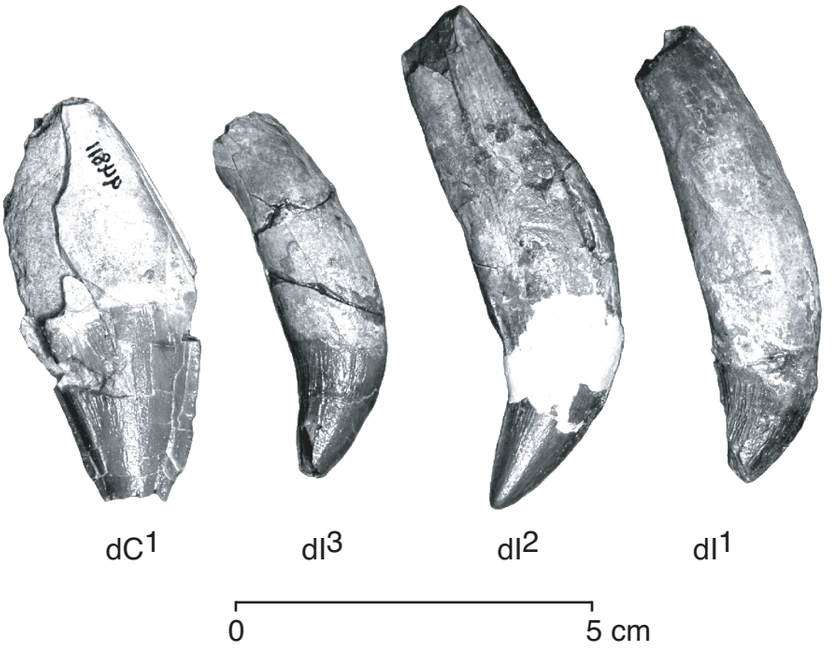

FIGURE 10 — Deciduous upper incisors and canine of *Dorudon atrox*. The series from dI^1 to dC^1 is shown in right lateral view. Note the similarity in size of dI^1 and dI^3, and the inflated root of dI^2 . In addition, the deciduous canine is much larger than the other anterior deciduous upper teeth. dI^1 is from UM 101223. dI^2 and dI^3 are from UM 94814. dC^1 is from UM 94811. Each of these isolated teeth were identified by comparison to teeth in place in other specimens. The image of dC^1 is reversed from the left side.

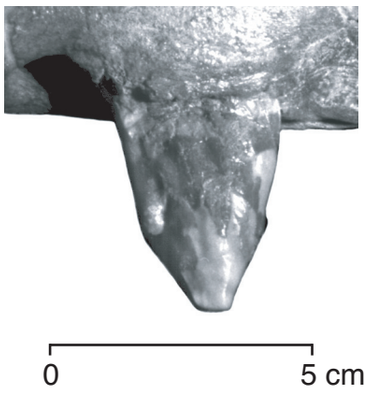

FIGURE 11 — Deciduous first upper premolar of *Dorudon atrox*, UM 93220, in right lateral view.

Permanent dentition

The permanent dental formula of *Dorudon atrox* is 3.1.4.2/3.1.4.3. All of the incisors are in line with the remaining tooth row, rather than in an arch across the anterior of the upper dental arcade, a feature typical of cetaceans. The upper molars extend onto the underside of the zygomatic arch while the lower molars are on the ascending edge of the mandible as it rises to the coronoid process.

Upper incisors

The upper incisors are difficult to distinguish from the lower incisors and from both upper and lower canines when they are recovered as isolated teeth. This problem is compounded by heavy tooth wear that is often present on the anterior teeth. The anterior teeth can be differentiated by slight differences in size and shape, but heavy wear often obscures these features. Most specimens of adult *Dorudon atrox* studied either did not include upper incisors or had upper incisors disarticulated from the skull. One specimen (NSFM 4451) has the anterior dentition preserved in place in almost perfect condition. Another specimen (UM 101222) has the anterior dentition in place, but the teeth are heavily weathered and fractured, preserving essentially only the roots. The description of the upper incisors, canines, and first premolars are based mainly on these two specimens. Summary statistics for the measurements of *D. atrox* permanent upper teeth are shown in Table 5.

The upper incisors are simple conical teeth, curved distally (Fig. 16). There are no accessory denticles on the upper incisors and all are single rooted. The upper incisors project slightly buccally from their alveoli in the premaxillae. The alveoli all open ventrally, but the teeth themselves project mesially to differing degrees. The root of the first upper incisor projects

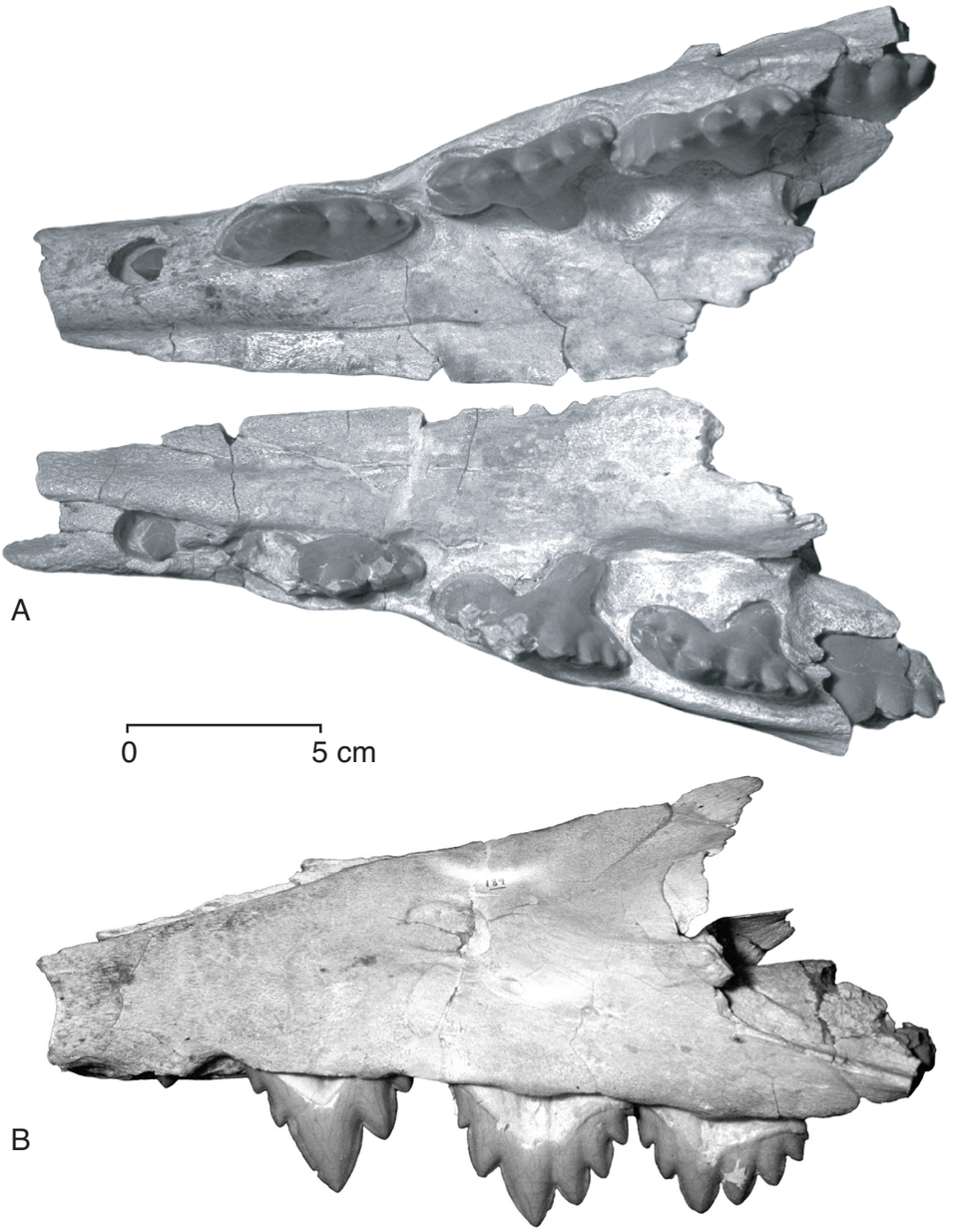

FIGURE 12 — Maxilla of *Dorudon atrox*, UM 100139, showing deciduous upper premolars. A, left and right maxillae in occlusal view. B, left maxilla in lateral (buccal) view. Note that the almost completely formed crown of M^1 is erupting and that dP^1 is also beginning to erupt. An erupted dP^1 can be seen in palatal view in Figure 25. In addition, note the prominent "posterointernal buttress," which is the remnant of a third root on the lingual side of dP^3 and dP^4.

strongly mesially, but the tooth is curved distally, with most of the curvature concentrated at the base of the crown. I^2 and I^3 project mesially progressively less than I^1. The upper incisors are separated from one another by diastemata that contain embrasure pits that accept the lower incisors and are described with the premaxilla and maxilla below.

The first upper incisor [**I^1**, Fig. 16] is the smallest of the upper incisors. It has a single gently tapering root. The crown

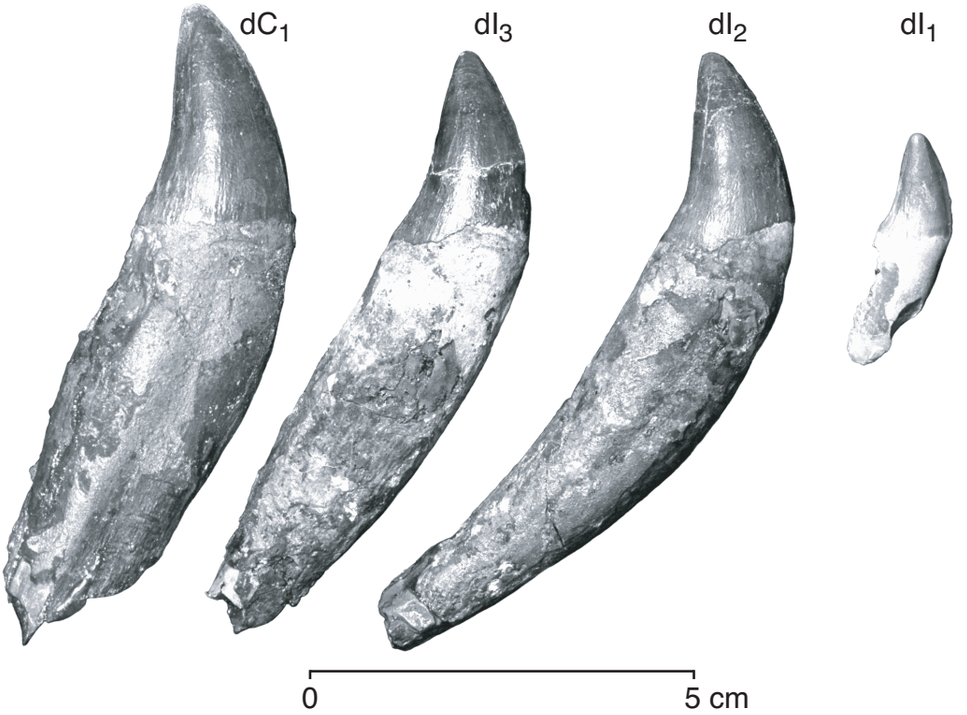

FIGURE 13 — Deciduous lower incisors and canine of *Dorudon atrox*. The series from dI_1 to dC_1 is shown in right lateral (buccal) view. Note the similarity in size between dI_2 and dI_3, and the decidedly smaller dI_1. The deciduous canine is easily distinguished from the deciduous incisors by its larger size. dI_1 is from UM 94814. dI_2 to dC_1 are from UM 101223. dI_1 was identified as such by its very small size relative to the other deciduous teeth, and a similar size relationship between permanent I_1 and the other permanent incisors. dI_2 to dC_1 were identified based on comparison with other teeth in place.

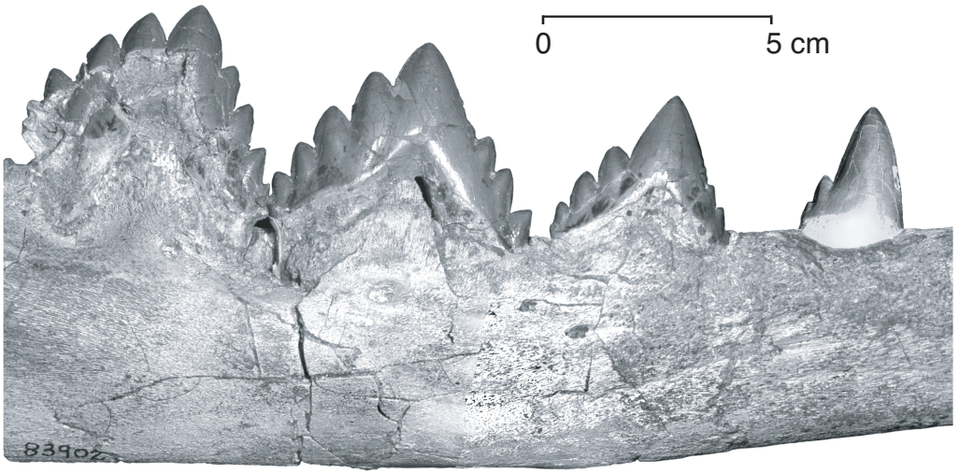

FIGURE 14 — Deciduous lower premolars of *Dorudon atrox* in right lateral (buccal) view. The image of dP_2 is reversed from the left side of the same specimen as dP_3 and dP_4 (UM 83902), while dP_1 is from another specimen (UM 93220). dP_4 is somewhat crushed. Note that dP_1 is single rooted.

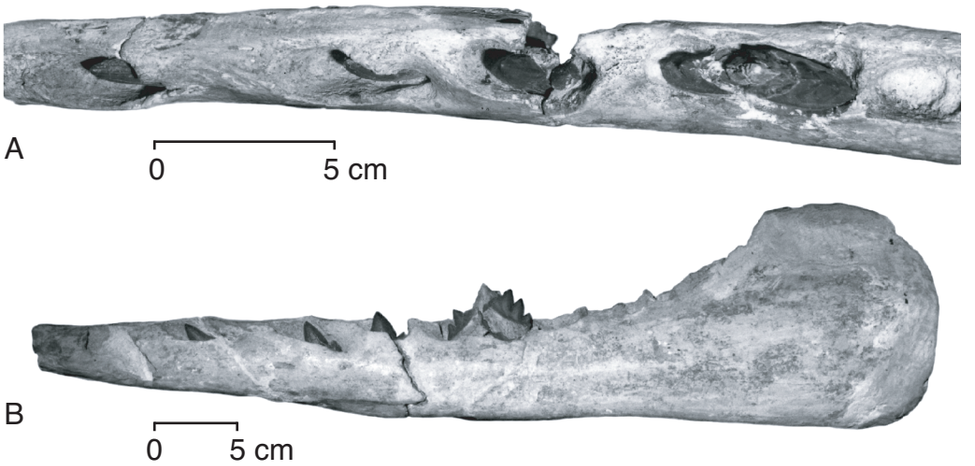

FIGURE 15 — Erupting adult teeth of *Zygorhiza kochii* (USNM 16639). A, occlusal view of C_1 to P_3, with the alveolus for the anterior root of P_4. B, lateral view of entire dentary. P_3 is almost entirely erupted. P_2 is the next highest tooth, followed by P_1 and C_1. Specimens of *Dorudon atrox* that have dP_2-dP_4 in place also have a fully erupted tooth in the P_1 position. This suggests that P_1 is replaced in dorudontine archaeocetes.

of I^1 is a simple cone that is curved both distally and buccally. There is a small but distinct midline ridge on the mesial and distal surfaces of the crown. The enamel has weak crenulations near the base that are concentrated on the buccal surface.

The second upper incisor [**I^2** , Fig. 16] can be distinguished from I^1 and I^3 by its bulbous, inflated root. The root is very expanded proximal to the base of the crown, just where the tooth emerges from the alveolus. The crown is similar in size and shape to that of I^1, being slightly curved buccally and caudally. It too has crenulations near the base of the crown concentrated on the buccal surface.

The third upper incisor [**I^3** , Fig. 16] is larger than I^1 or I^2 . Its root is about the same size as I^2 , but it has a larger crown, thus the root does not give the impression of being expanded like that of I^2 . The crown is larger in all dimensions when compared with I^1 or I^2. The enamel of the crown is crenulated near the base and the crenulations are concentrated on the buccal surface.

Upper canine

The upper canine [**C^1**, Fig. 16] projects slightly buccally and mesially from its alveolus just behind the premaxillomaxillary suture. There are no accessory denticles on the upper canine. The canine is somewhat larger than the upper incisors in every dimension. The crown is conical and it curves slightly buccally and distally. There is a midline ridge that runs up the mesial and down the distal surface of the crown. The enamel is moderately rugose near the base of the crown and the rugosity is concentrated on the buccal surface. The upper canine is separated from I^3 mesially and P^1 distally by diastemata.

Upper premolars

The first upper premolar [**P^1**, Fig. 17] is only known from a single specimen, NSFM 4451, and the root of P^1 is known from specimen UM 101222. Both first upper premolars are slightly damaged in NSFM 4451, but both apparently have no accessory denticles on the mesial edge or the distal edge. The teeth are rather small and peg-like, without any apparent curvature. The crowns are conical with a single root. The root of the first premolar in specimen UM 101222 is smaller than the root of the upper incisor or the canine, and this is also the case in NSFM 4451. The first premolar is separated from C^1 mesially and P^1 distally by diastemata.

The second upper premolar [**P^2**, Fig. 17] is the most mesial upper tooth with large accessory denticles. It is also the largest tooth in the upper cheek tooth series. It is buccolingually compressed and double rooted. The mesial and distal roots are similar in size and shape. The central cusp is the largest cusp on P^2. It is located directly below the division between the two roots. There are three to four accessory denticles on the mesial edge of the tooth. The most basal denticle is separate from the short, but well-defined mesial cingulum. This cingulum is best developed on the lingual side of the tooth. The mesial denticles are much smaller than the distal denticles. There are three distal accessory denticles. They decrease in size from mesial to distal. The last denticle arises from the short but well-defined distal cingulum. There are well-developed rugosities on the enamel near the base of the crown on both the buccal and lingual sides of the tooth. The second upper premolar is separated from P^1 mesially and P^3 distally by large diastemata.

The third upper premolar [**P^3**, Fig. 17] is the second largest tooth in the upper cheek tooth series, being slightly smaller

TABLE 5 — Summary statistics for permanent upper tooth measurements of *Dorudon atrox*. All measurements are in millimeters. L, length along the tooth row; H, height of the crown measured from the cingulum to the apical cusp for premolars; W, maximum buccolingual width for anterior teeth and measured below the apical cusp for premolars. N, sample size; SD, standard deviation; CV, ratio of the standard deviation to the mean (in percent). Measurements are shown in Figure 9, and are listed in Appendix IIIA.

Tooth	Dimension	N	Minimum	Maximum	Mean	SD	CV
I^1	L	2	21.5	22.0	21.8	0.4	1.6
	W	2	15.1	15.3	15.2	0.1	0.9
	H	0	—	—	—	—	—
I^2	L	1	22.9	22.9	22.9	—	—
	W	1	14.2	14.2	14.2	—	—
	H	1	30.2	30.2	30.2	—	—
I^3	L	2	25.3	25.7	25.5	0.3	1.1
	W	2	14.4	17.0	15.7	1.8	11.7
	H	2	36.6	36.9	36.8	0.2	0.6
C^1	L	4	28.6	33.2	31.0	2.1	6.9
	W	4	17.4	19.4	18.3	1.0	5.2
	H	3	34.5	39.1	36.7	2.3	6.3
P^1	L	3	21.7	27.0	23.6	3.0	12.5
	W	0	—	—	—	—	—
	H	1	9.3	9.3	9.3	—	—
P^2	L	3	51.7	56.2	53.2	2.6	4.9
	W	3	13.5	20.0	15.9	3.6	22.6
	H	2	27.7	32.5	30.1	3.4	11.3
P^3	L	4	42.6	53.6	49.1	4.9	10.1
	W	4	13.4	17.0	14.8	1.6	10.8
	H	3	11.8	31.6	21.9	9.9	45.2
P^4	L	4	43.0	54.6	47.3	5.4	11.5
	W	4	13.6	15.8	14.6	1.1	7.3
	H	4	24.7	28.0	26.7	1.5	5.6
M^1	L	9	29.6	34.0	31.4	1.6	5.0
	W	7	9.6	13.9	11.4	1.5	12.9
	H	6	11.0	18.7	15.3	3.1	20.1
M^2	L	3	25.7	30.2	28.3	2.3	8.2
	W	3	10.0	11.7	10.7	0.9	8.3
	H	2	12.0	14.7	13.4	1.9	14.3

than P^2. It is buccolingually compressed and double rooted. The distal root is buccolingually much wider than the mesial root. There is a lingual projection of the distal root that is the remnant of the third root. The crown has a lingual projection over this root. The central cusp is the largest cusp on P^3 . It is located directly below the division between the two roots. There are four accessory denticles on the mesial edge of the tooth. The first denticle is separate from the short, but well-defined mesial cingulum. The fourth denticle does not project very far from the crown and is almost worn away in all specimens. There are three distal accessory denticles. They decrease in size from mesial to distal. The last denticle arises from the short but well-defined distal cingulum. The third upper premolar is separated from P^2 by a wide diastema and is adjacent to P^4, with no significant diastema.

The fourth upper premolar [**P^4**, Fig. 17] is slightly smaller than P^3. It is buccolingually compressed and double rooted. The distal root is much wider than the mesial root and is formed from the fusion of two roots. The crown has a lingual projection over the expanded distal root. The central cusp is the largest

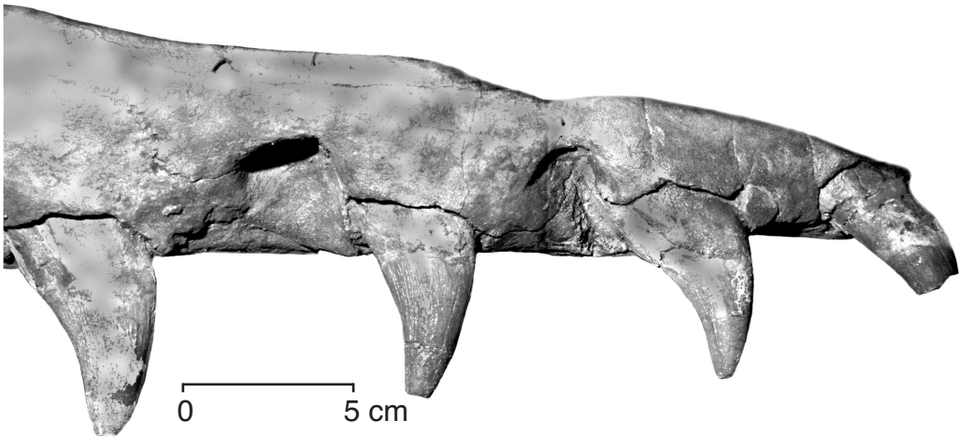

FIGURE 16 — Upper incisors and canine of *Dorudon atrox*, right lateral (buccal) view, NSFM 4451. Note that I^1 angles much more anteriorly from its alveolus than the other incisors or canine.

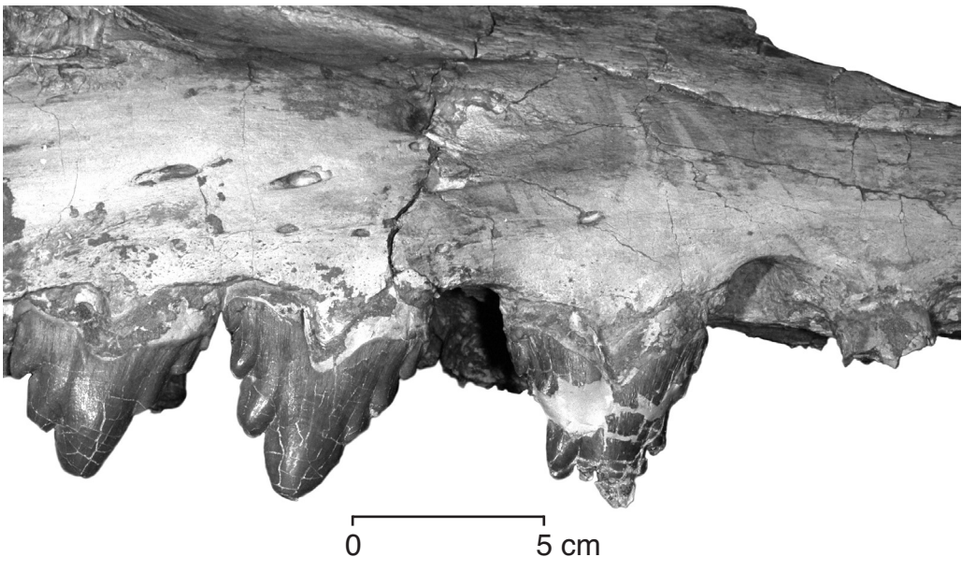

FIGURE 17 — Upper premolars of *Dorudon atrox* (UM 101222), right lateral (buccal) view. Only the root of P^1 is preserved. Note that P^1 is much smaller than all of the other upper premolars, that P^2 is the largest, and that P^3 and P^4 are progressively slightly smaller. The embrasure pit between P^1 and P^2 is the most posterior embrasure pit visible on the lateral side of the skull. Posterior embrasure pits are visible only in a palatal view (see Figure 24).

on the tooth. There are two accessory denticles on the mesial edge of P^4 . There is a well-developed mesial cingulum that is clearly separated from the most mesial accessory denticle. There are two large accessory denticles on the distal edge of the tooth. In addition, there is a well-developed distal cingulum that forms a small denticle. The fourth upper premolar is separated from P^3 mesially by a short diastema and there is no significant separation between P^4 and M^1 distally.

Upper molars

The first upper molar [**M^1**, Fig. 18A-B] is much smaller than the preceding premolars. The lateral-view profile of M^1 is much more rounded than that of the premolars, which are distinctly triangular. M^1 is buccolingually compressed and generally mesiodistally symmetrical. The distal root has a lingual expansion and a midline groove on its distal margin. The crown also has a lingual projection over this root. The distal root appears

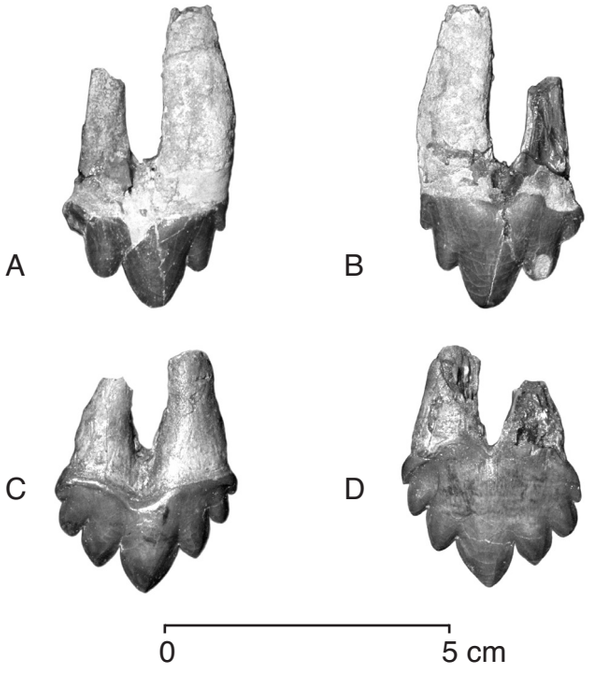

FIGURE 18 — Upper molars of *Dorudon atrox*. Both teeth are from the left side. A-B, M1 of UM 101215. C-D, M2 of UM 94814. A and C are in buccal view. B and D are in lingual view. Note that the posterior accessory denticles are slightly larger than the anterior accessory denticles, but the size difference is not nearly as dramatic as it is on upper premolars. Note also that the crowns of the upper molars extend much farther up the surface of the roots on the lingual side than on buccal side.

to have developed from the fusion of two separate roots. The crown projects farther up onto the roots on the lingual side than on the buccal side. The crown is deflected away from the division between the roots on both the buccal and lingual sides. The central cusp of M1, the paracone, is located directly below the division between the mesial and distal roots. There are three accessory denticles on the mesial edge of the crown. The denticles increase in size from mesial to distal. The first denticle is on the well-developed mesial cingulum. There are also three accessory denticles on the distal edge of the crown. The denticles decrease in size from mesial to distal. The last denticle joins with the well-developed distal cingulum. There are no diastema mesial or distal to M1.

The second upper molar [**M2**, Fig. 18C-D] is located on a projection of the maxilla onto the zygomatic arch. M2 is subequal in size to M1 It too has a rounded rather than triangular profile. M2 is buccolingually compressed, and has two roots. The distal root is lingually expanded and has a midline groove on its distal margin. The crown of M2 projects farther up onto the roots on the lingual side than on the buccal side. The crown is deflected down away from the division between the roots on both the buccal and lingual sides, just like M1. The central cusp of M2, the paracone, is located directly below the division between the two roots. There are two accessory denticles on the mesial edge of the tooth. They increase in size from mesial to distal. The first denticle is on the well-developed mesial cingulum. There are three accessory denticles on the distal edge of the tooth. The denticles decrease in size from mesial to distal. The last denticle is on the well-developed distal cingulum. There is no diastema mesial to M2.

Lower incisors

The lower incisors are relatively simple conical teeth that are curved distally. All of the incisors are in line with the canine and cheek teeth. There are no accessory denticles on the lower incisors. The lower incisors are separated from each other and from the lower canine by diastemata of varying sizes. Summary statistics for the measurements of *D. atrox* permanent lower teeth are shown in Table 6.

The lower first incisor [**I_1**, Fig. 19] is the smallest tooth in *Dorudon atrox*. The alveolus for I_1 is found just proximal to the anteriormost tip of the dentary. The lingual wall of the alveolus is not completely formed along its dorsal margin, leaving the alveolus partly open along the mandibular symphysis. The tooth projects mesially and slightly buccally from the alveolus. No crown is known from I_1, since the tooth itself is so small, and the anterior tip of the dentary is so gracile, both are easily broken and lost. Specimen UM 97512 preserves an intact anterior right dentary with the root of I_1 in place. The root is similar to the roots of the other lower incisors, flaring out a bit from the base of the crown, then tapering as it enters the alveolus. The distal end of I_1 is very close to the mesial edge of the alveolus for I_2.

The second lower incisor [**I_2**, Fig. 19] is much larger than I_1, and slightly smaller than I_3. The alveolus for I_2 has a large lip on its mesiobuccal side, and it is very close to I_1. The second lower incisor projects mesially and slightly buccally from the alveolus. The crown of I_2 is conical and curved distally. There is a midline ridge running up the mesial face and down the distal face of the crown. The enamel on the base of the crown is slightly rugose, with the rugosity better developed on the lingual side. A large diastema separates I_2 from I_3.

The third lower incisor [**I_3**, Fig. 19] is much larger than I_1, and slightly larger than I_2. The alveolus for I_3 has a moderately developed lip on its mesiobuccal side. The third lower incisor projects almost directly mesially from the alveolus. The crown of I_3 is conical and curved distally. There is a midline ridge running up the mesial face and down the distal face of the crown. The enamel on the base of the crown is slightly rugose, with the rugosity better developed on the lingual side. I_3 can be difficult to distinguish from I_2 and C_1 when the teeth are separated from the jaw, as all of these teeth are similar in shape. I_3 is slightly larger than I_2 , but it is very close in size to C_1. All known specimens of lower incisors lack any tiny serrations on the midline ridge that some canines develop. A large diastema separates I_3 from I_2 mesially and from C_1 distally.

TABLE 6 — Summary statistics for permanent lower tooth measurements of *Dorudon atrox*. All measurements are in millimeters. L, length along the tooth row; H, height of the crown measured from the cingulum to the apical cusp for premolars; W, maximum buccolingual width for anterior teeth and measured below the apical cusp for premolars. N, sample size; SD, standard deviation; CV, ratio of the standard deviation to the mean (in percent). Measurements are shown in Figure 9 and are listed in Appendix IIIB.

Tooth	Dimension	N	Minimum	Maximum	Mean	SD	CV
I_1	L	1	17.6	17.6	17.6	—	—
	W	1	12.2	12.2	12.2	—	—
	H	0	—	—	—	—	—
I_2	L	1	21.3	21.3	21.3	—	—
	W	1	15.2	15.2	15.2	—	—
	H	0	0.0	0.0	—	—	—
I_3	L	1	26.4	26.4	26.4	—	—
	W	1	16.4	16.4	16.4	—	—
	H	0	—	—	—	—	—
C_1	L	3	26.3	30.0	27.6	2.1	7.4
	W	1	18.0	18.0	18.0	—	—
	H	1	28.5	28.5	28.5	—	—
P_1	L	3	31.7	38.0	34.7	3.2	9.1
	W	2	11.5	14.4	13.0	2.1	15.8
	H	2	24.1	26.2	25.2	1.5	5.9
P_2	L	0	—	—	—	—	—
	W	1	13.7	13.7	13.7	—	—
	H	1	15.4	15.4	15.4	—	—
P_3	L	2	60.2	63.9	62.1	2.6	4.2
	W	2	17.5	18.8	18.2	0.9	5.1
	H	1	38.2	38.2	38.2	—	—
P_4	L	3	56.0	61.4	58.5	2.7	4.7
	W	2	13.9	18.6	16.3	3.3	20.5
	H	2	36.0	36.4	36.2	0.3	0.8
M_1	L	9	36.0	45.9	41.1	3.2	7.8
	W	6	12.3	17.0	14.7	1.6	10.8
	H	7	22.7	31.6	29.0	3.2	10.9
M_1	L	6	34.0	40.6	37.5	3.1	8.2
	W	7	10.3	15.4	13.9	1.8	12.8
	H	7	27.5	38.0	34.0	3.8	11.1
M_1	L	4	32.2	40.0	35.5	3.4	9.5
	W	2	10.3	13.9	12.1	2.5	21.0
	H	4	25.8	30.0	28.7	2.0	6.9

Lower canine

The lower canine [**C_1** , Fig. 19] is a simple conical tooth that is slightly curved distally. It angles slightly mesially from its alveolus in the dentary. It is single rooted, and the root tapers gently from the base of the crown to its tip. The crown tapers from its base to the tip and it has no accessory denticles. There is a midline ridge running up the mesial face of the tooth and down the distal face of the tooth. Some canines show the development of tiny serrations on the midline ridge. There are no cingula at the base of the crown. The enamel is rugose at the base of the crown, and the rugosity is much better developed on the lingual side of the tooth. The lower canine is larger than the lower incisors in all dimensions. It is separated from I_3 mesially and P_1 distally by wide diastemata.

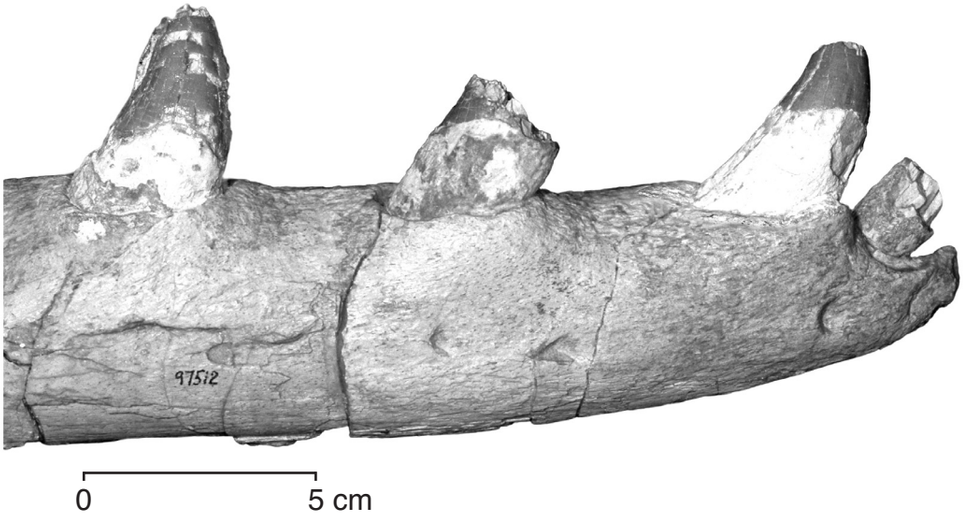

FIGURE 19 — Lower incisors and canine of *Dorudon atrox* in right lateral (buccal) view. The mandible, I_1, and I_3, are from the right side of specimen UM 97512, while the images of I_2 and C_1 are reversed from the left side of the same specimen. The crowns of both I_1 and I_3 are damaged. Note how small I_1 is relative to the other incisors and canine. Note also its proximity to I_2 in comparison to the long diastemata between other anterior teeth.

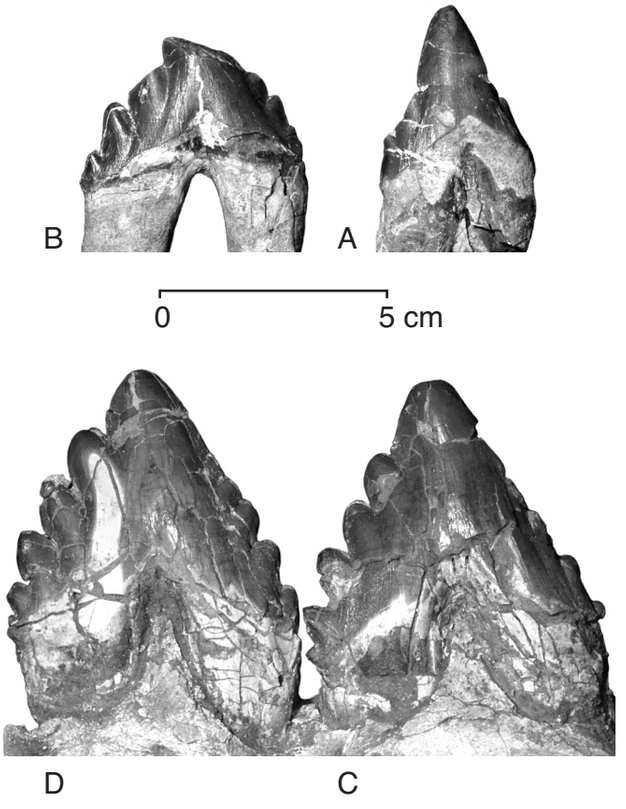

Lower premolars

The first lower premolar [**P_1**, Fig. 20A] is buccolingually compressed and double rooted. The distal root is slightly larger than the mesial root. The roots meet just below the crown. The first lower premolar is the most mesial lower tooth that has accessory denticles. The crown is dominated by a large central cusp. The mesial edge of the tooth has one small accessory denticle and some additional fine serrations near the base of the crown. There is also a midline ridge running up the mesial face of the central cusp. The midline ridge continues down the distal edge of the central cusp and is finely serrated near the distal accessory denticles. There are two accessory denticles on the distal edge of the tooth, in addition to a moderately developed distal cingulum. The first lower premolar is separated from C_1 mesially and P_2 distally by large diastemata.

The second lower premolar [**P_2**, Fig. 20B] is slightly smaller than P_3. It is double rooted and buccolingually compressed. The mesial and distal roots are subequal in size. The crown is

FIGURE 20 — Lower premolars of *Dorudon atrox* in right lateral (buccal) view. P_1 and P_2 from specimen UM 101215 are in the top row, and P_3 and P_4 from specimen UM 101222 are in the bottom row. Note that P_1 has two roots, in contrast to the deciduous P_1 in Figure 14. P_2 shows heavy apical wear, with the apical cusp almost entirely worn away. P_3 and P_4 show moderate lateral wear and light to moderate apical wear. Note how much larger the posterior accessory denticles are when compared to the anterior accessory denticles.

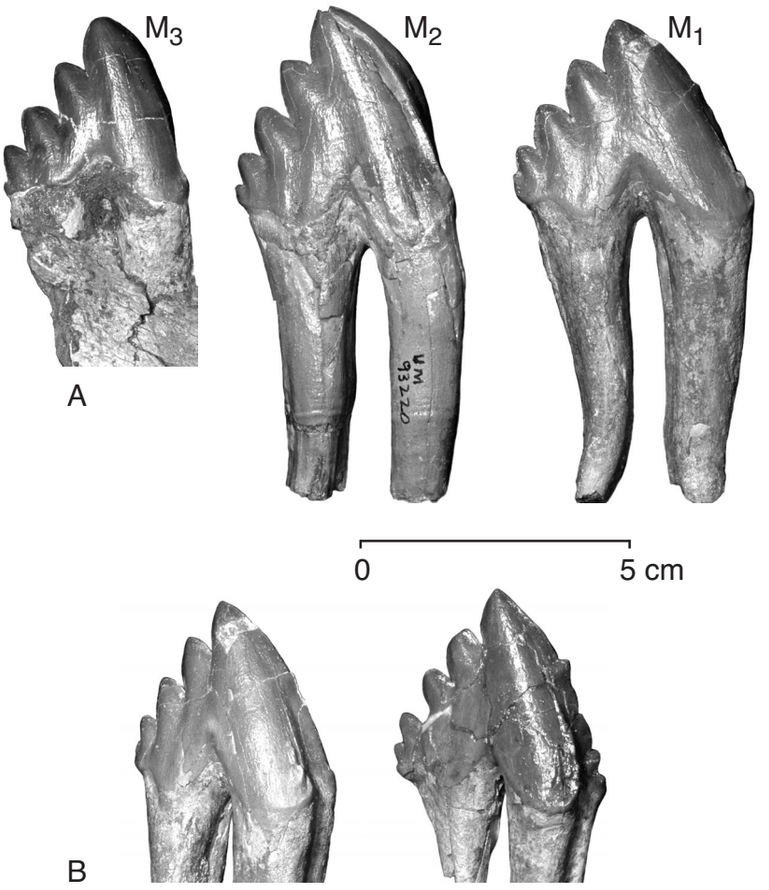

FIGURE 21 — Lower molars of *Dorudon atrox*. A, lower molars in right lateral (buccal) view. M_1 and M_2 are from specimen UM 93220, and M_3 is from UM 100146. UM 100146 is a slightly smaller individual than UM 93220, so the M_3 has been enlarged such that the M_2 of UM 100146 is the same size as the M_2 of UM 93220. Note the distinctly different shape of the crown of M_1 when compared to M_2 and M_3 . Note also the thin, curved, posterior root of M_1, which both M_2 and M_3 lack. B, lower first molars in right anterolateral view. The M_1 on the left is from specimen UM 93220, and is the same tooth as that in part A of this figure. M_1 on the right is from specimen UM 94814. Note the deep reentrant groove and sharp lingual ridge on both lower teeth. Note also the lack of any accessory denticles on UM 93220 and the well-developed accessory denticles on UM 94811.

triangular in lateral view and dominated by a large central cusp directly above the division between the mesial and distal roots. The mesial edge of the tooth has three to four accessory denticles. The mesial accessory denticles are smaller than the distal accessory denticles. The denticles nearest the crown base are very small and variable in shape and size. There is no distinct mesial cingulum. The central cusp is considerably larger than all of the accessory denticles. There are three accessory denticles on the distal edge of the tooth. These denticles project somewhat distally and are larger than the mesial accessory denticles. There is a small distal cingulum. The second lower premolar is separated from P_1 mesially and P_3 distally by large diastemata.

The third lower premolar [**P_3**, Fig. 20C] is the second largest cheek tooth. P_3 is not as tall as P_4, but they are subequal in length along the tooth row. It is double rooted and buccolingually compressed. The mesial and distal roots are subequal in size. The crown is triangular in lateral view and dominated by a large central cusp directly above the division between the mesial and distal roots. The mesial edge of the tooth has four accessory denticles. The mesial accessory denticles are smaller than the distal accessory denticles. The denticles project somewhat mesially, rather than straight up. The first denticle is on the edge of the crown just above the root. The central cusp is the considerably larger than all of the accessory denticles. There are four accessory denticles on the distal edge of the tooth. These denticles project somewhat distally and are larger than the mesial denticles. The third lower premolar is separated from P_2 mesially and P_4 distally by di-

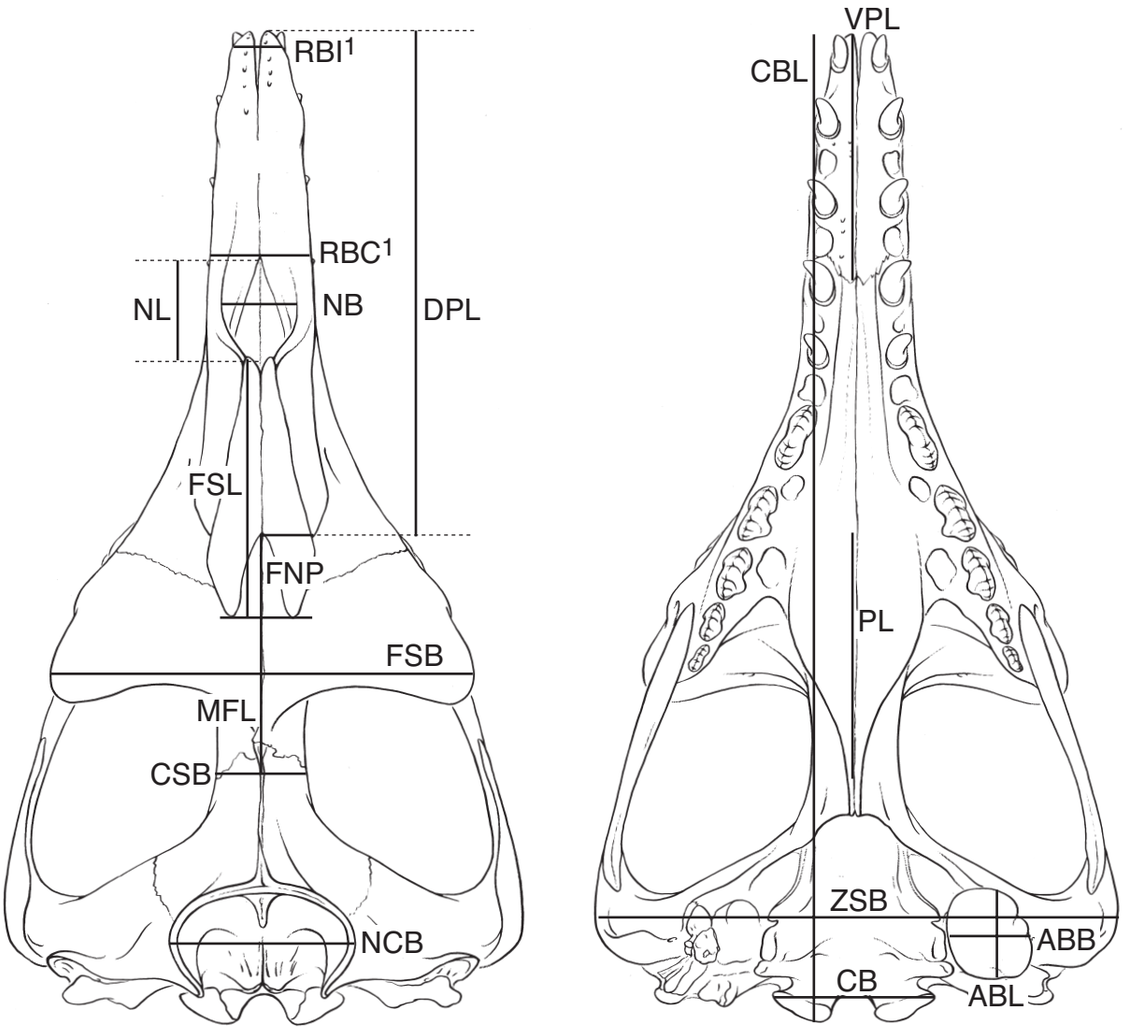

FIGURE 22 — Skull measurements of *Dorudon atrox* in dorsal and ventral views. Measurement values are listed in Appendix IV. Abbreviations: *CBL*, condylobasal length; *RBI¹*, rostrum breadth at I^1; *RBC¹*, rostrum breadth at C^1; *DPL*, dorsal premaxilla length; *NL*, narial length; *NB*, narial breadth; *NSL*, nasal length; *FNP*, frontal-nasal projection length; *FSB*, frontal shield breadth; *MFL*, maximum frontal length; *CSB*, central skull breadth; *NCB*, nuchal crest breadth; *VPL*, ventral premaxilla length; *PL*, palatine length; *ABL*, auditory bulla length; *ABB*, auditory bulla breadth; *CB*, condylar breadth; and *ZSB*, zygomatic skull breadth.

astemata. The diastema between P_3 and P_4 is much smaller than the diastema between P_2 and P_3.

The fourth lower premolar [**P_4**, Fig. 20D] is the largest cheek tooth. It is very similar to P_3. The tooth is double rooted and buccolingually compressed. The mesial and distal roots are subequal in size. The crown is triangular in lateral view and dominated by a large central cusp directly above the division between the mesial and distal roots. The mesial edge of the tooth has four accessory denticles. The mesial accessory denticles are smaller than the distal accessory denticles. The denticles project somewhat mesially, rather than straight up. The first denticle arises from the very short but well-developed mesial cingulum on the edge of the crown just above the root. The central cusp is considerably larger than all of the accessory denticles. There are four accessory denticles on the distal edge of the tooth. These denticles project somewhat distally and are larger than the mesial denticles. The last distal denticle arises from the short but well-developed distal cingulum. The fourth lower premolar is separated from P_3 mesially by a short diastema. Its distal end rests in the mesial reentrant groove of M_1.

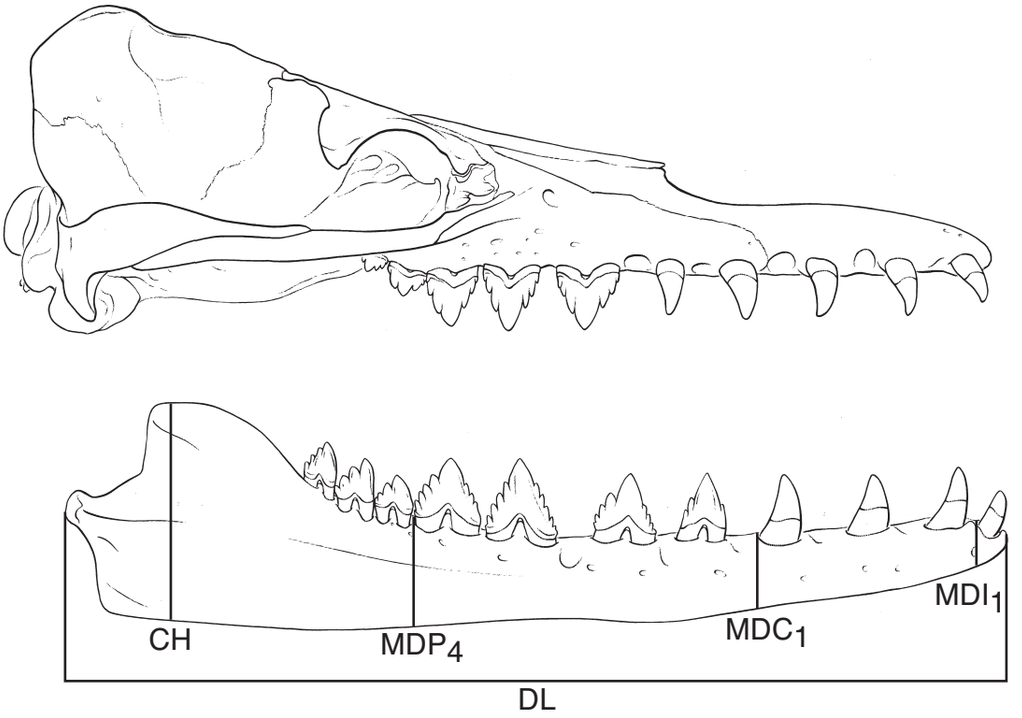

FIGURE 23 — Dentary measurements of *Dorudon atrox* in lateral view. Measurement values are listed in Appendix IV. *DL*, dentary length; *MDI1*, mandibular depth at I_1; *MDC1*, mandibular depth at C_1; *MDP4*, mandibular depth at P_4; and *CH*, coronoid height.

Lower molars

Unlike the premolars, the lower molars have mesial and distal edges that are very different from one another. The mesial edges of the lower molars lack large accessory denticles, although some individuals have small, irregularly placed denticles. The mesial edge of the crown rises steeply to the apical cusp. The apical cusp is the primitive protoconid. The distal accessory denticles decrease in size from the apical cusp to the last accessory denticle.

The lower molars have a deep groove on their mesial margins. This groove extends from the base of the mesial root to about two thirds of the way up the crown. A similar groove found in hapalodectine mesonychids is termed the reentrant groove (Szalay, 1969) and this term is adopted here. There is a sharp ridge running up the crown to the protoconid on the lingual side of the groove. This groove accepts the distal projection of the preceding tooth when the teeth are in place in the jaw. The mesial root is also grooved when viewed from the distal side, and it is larger than the distal root. The distal root is grooved on its mesial side as well.

The first lower molar [**M_1**, Fig. 21A] has a much shorter protoconid than either M_2 or M_1, making M_1 appear elongate relative to its height. It also has four accessory denticles on its distal edge in addition to the protoconid. It has a very weak cingulum on all sides. There are serrations on the ridge on the lingual side of the mesial groove that are variably developed. Some individuals have only weakly developed serrations while others have well-developed accessory denticles that are irregularly spaced (Fig. 21B). In addition, the ridge on the buccal side of the groove is variably developed. It is strong in individuals that also have well-developed mesial accessory denticles. It too has variably-present accessory denticles and occasionally some develop just off the ridge.

The second lower molar [**M_2**, Fig. 21A] has four accessory denticles distal to the protoconid. The distal cingulum is better developed in M_2 than in M_1. The ridge on the lingual side of the reentrant groove has a well-developed cuspule at the base of the crown. There is also a ridge on the buccal side of the groove with a cuspule at its base. The mesial root is buccolingually wider in M_2 than in M_1. M_2 is very similar in size and shape to M_3, making them difficult to distinguish when they are found out of place.

The third lower molar [**M_3**, Fig. 21A] is the smallest of three molars. It has four accessory denticles distal to the protoconid. The last denticle is on the moderately developed distal cingulum. There is a well-developed ridge on the lingual side of the reentrant groove. The third lower molar is positioned high on the ascending ramus of the mandible, thus its cusps project higher than any other cheek teeth.

TABLE 7 — Summary statistics for dorsal-view cranial measurements of adult *Dorudon atrox*. Measurements are shown in Figure 22 and are listed in Appendix IVA. CBL, condylobasal length; RBI^1, rostrum breadth at I^1; RBC^1, rostrum breadth at C^1; DPL, dorsal premaxilla length; NL, length of the narial opening; NB, breadth of the narial opening; NSL, length of the nasal bone; FNP, length of the projection of frontals between the nasals; FSB, frontal shield breadth; MFL, maximum frontal length; CSB, central skull breadth at the frontal-parietal suture. N, sample size; SD, standard deviation; CV, ratio of the standard deviation to the mean (in percent). All measurements are in millimeters.

Measurement	N	Minimum	Maximum	Mean	SD	CV
CBL	3	940.0	944.0	941.3	2.3	0.2
RBI^1	3	45.8	53.9	48.6	4.6	9.4
RBC^1	2	82.0	91.8	86.9	6.9	8.0
DPL	2	487.0	503.0	495.0	11.3	2.3
NL	1	126.8	126.8	126.8	—	—
NB	2	51.7	55.8	53.8	2.9	5.4
NSL	2	240.0	240.5	240.3	0.4	0.1
FNP	2	76.3	87.0	81.7	7.6	9.3
FSB	3	342.0	356.0	351.0	7.8	2.2
MFL	2	179.8	195.0	187.4	10.7	5.7
CSB	2	50.0	57.3	53.7	5.2	9.6

CRANIAL ANATOMY

Face and Palate

Measurements of the bones of the skull of *Dorudon atrox* were taken as shown in Figures 22 and 23. Summary statistics for measurements of the skull of *D. atrox* are shown in Tables 7 and 8.

Premaxilla

Left and right premaxillae [**PMx**, Fig. 24] are long paired bones that form the anterior portion of the skull as well as much of the side of the face and anterior extension of the palate. The premaxillae in *Dorudon* are approximately half as long as the entire skull. The anteriormost extensions of the left and right premaxillae are separated along the midline by less than half a centimeter, but the two sides meet above the posterior edge of the alveolus for I^1, and are joined, but unfused back as far as the canine teeth.

The anterior portion of each premaxilla contains alveoli for the three upper incisors. Each incisor projects anteriorly and slightly buccally. The roots of the incisors are deep and extend well into the body of the premaxilla. The premaxilla contains deeply excavated embrasure pits [**ep**] between the incisors where the crowns of the lower incisors rested in life when the jaw was closed. The embrasure pits are open laterally. The embrasure pit between I^1 and I^2 is not nearly as deep as those between I^2 and I^3, and between I^3 and C^1. The palatal presentation of the premaxilla is narrower toward the midline at the anterior edge of the alveolus for C^1, where the premaxillae meets the maxillae. The medial edges of the premaxilla meet to form a narrow ridge along the midline that projects back along the palate to the anterior edge of the alveolus for P^2. The lateral border of the premaxilla extends up the side of the face from the palate through the embrasure pit between I^3 and C^1. The distal projection of the premaxilla on the side of the face extends up around the nares, where it forms the lateral border of the nares. Just posterior to this, the medial border of the premaxilla meets the lateral border of the nasal. The premaxilla extends about half the length of the nasal where the posterior end of the premaxilla meets the frontal. The lateral border of the premaxilla follows the same path, roughly parallel with the medial border.

Just lateral to the midline on the dorsal surface of each premaxilla is a row of foramina running from the anterior border of the premaxilla to above the middle of the alveolus for I^2. The foramina vary in number: there are generally around ten, and vary in size, with the left and right sides not necessarily being identical. These foramina are connected to the incisivomaxillary canal, which is connected in turn to the maxillary canal through a foramen in the premaxillomaxillary suture. The latter foramen can be seen in juvenile individuals that have

TABLE 8 — Summary statistics for ventral and posterior view cranial measurements of adult *Dorudon atrox*. Measurements are shown in Figure 22 and the data are in Appendix IVB. VPL is ventral premaxilla length. ABL is auditory bulla length. ABB is auditory bulla breadth. NCB is nuchal crest breadth. NCH is nuchal crest height. FMH is foramen magnum height. FMB is foramen magnum breadth. CB is condylar breadth. OB is occipital breadth. ZSB is breadth of the skull across the zygomatic arches. N, sample size; SD, standard deviation; CV, ratio of the standard deviation to the mean (in percent). All measurements are in millimeters.

Measurement	N	Minimum	Maximum	Mean	SD	CV
VPL	2	353.0	362.0	357.5	6.4	1.8
ABL	3	79.9	86.1	83.0	3.1	3.7
ABB	3	53.0	59.1	56.0	3.1	5.4
NCB	3	115.0	152.1	135.5	18.9	13.9
NCH	2	144.0	184.0	164.0	28.3	17.2
FMH	1	35.0	35.0	35.0	—	—
FMB	1	46.0	46.0	46.0	—	—
CB	3	121.0	126.0	122.9	2.7	2.2
OB	4	300.0	353.0	316.8	24.5	7.7
ZSB	2	416.0	500.0	458.0	59.4	13.0

the premaxilla and maxilla unfused. The incisivomaxillary canal carried the maxillary branch of the trigeminal nerve (V_2), and associated blood vessels to the premaxillary foramina and also to the teeth.

It is unclear what structure present in *Dorudon atrox*, if any, is homologous with the anterior palatine foramina in other mammals. Numerous small foramina are present on the palatal presentation of the premaxilla near the midline of the skull. These foramina are variable in number and size from side to side and from individual to individual. Any or all of these structures could be homologous with the anterior palatine foramina and could have transmitted the naso-palatine nerve (part of cranial nerve V_2) to the palate.

Maxilla

The maxilla [**Mx**] makes up a large portion of the lateral posterior face of *Dorudon atrox* (Figs. 6 and 24). The anteriormost extension of the maxilla lies in the posterior portion of the embrasure pit on the lateral side of the face, posterior to I^3 and anterior to C^1. The premaxillomaxillary suture continues onto the palate just anterior to the alveolus for C^1. The left and right premaxillae meet along the midline of the palate and form the surface of the palate to the posterior edge of C^1. Posterior to this, the medial edges of the premaxillae form a ridge along the midline of the palate that separates the two medial edges of the maxillae back to the anterior edge of the alveolus for P^2. Posterior to this point, the medial edges of the maxillae meet along the midline of the palate and continue posteriorly to a point approximately even with the anterior edge of the posterior root of P^4, where the maxillae meet the palatines (Fig. 25). The palatomaxillary suture projects anteriorly as it progresses laterally from the midline, and then shifts dramatically posteriorly and dorsally. The lateral edge of the maxilla projects far posteriorly, with the first upper molar directly below the anterior edge of the orbit, and the second upper molar directly beneath the orbit on the maxillary tuberosity.

The infraorbital foramen [**iof**] is present on the lateral presentation of the maxilla above the diastema between P^2 and P^3. The foramen is quite variable in form among individuals. In some, the foramen is large and opens obliquely on the side of the face, deepening posteriorly. A small accessory infraorbital foramen is often present slightly posterior and ventral to the main foramen. In other individuals there are two foramina, one more anterior and the other more posterior, subequal in size. Double foramina of this sort are smaller than a single foramen of the first type. The infraorbital foramen is the anterior opening of the infraorbital canal, which transmitted cranial nerve V_2 from the orbit to the face and lips. The proximal opening of the infraorbital canal in the anterior orbit is called the internal maxillary foramen.

The posterior and posterodorsal extensions of the maxilla have complex articulations with the jugal, lacrimal, and frontal bones (see Fig. 26). The dorsolateral surface of the maxillary tuberosity articulates with the ventral surface of the jugal, and the body of the maxillary tuberosity contains the alveoli for M^1 and M^2. The articulation with the jugal extends as far anteriorly as P^4. Medi-

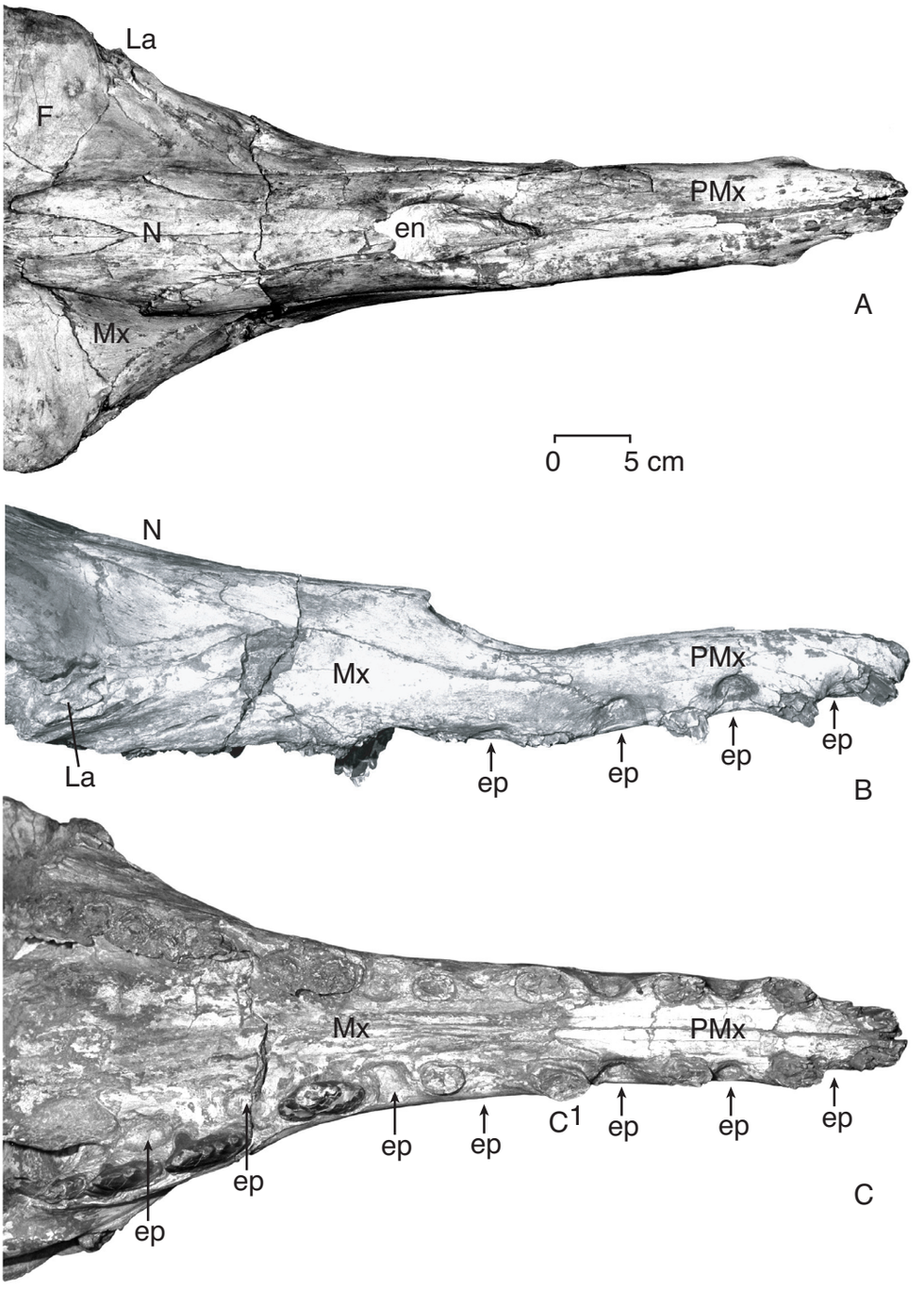

FIGURE 24 — Rostrum of *Dorudon atrox* (UM 101222) in A, dorsal; B, right lateral; and C, ventral (palatal) view. Note the conformation of the posterior nasals, the position of the external nares, and the positions of the embrasure pits (*ep*). The premaxillae are artificially deformed dorsally at the maxilla-premaxilla suture.

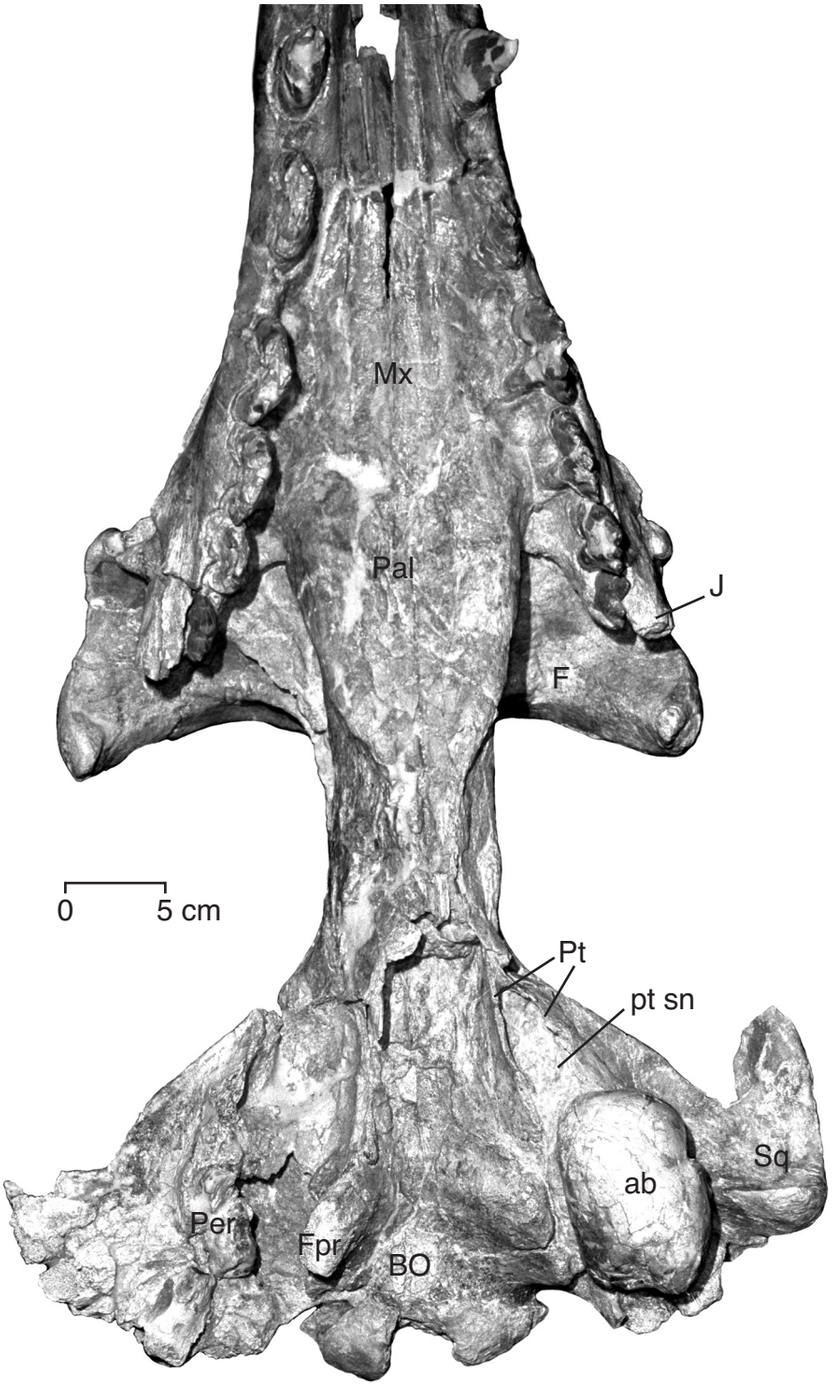

FIGURE 25 — Posterior palate and basicranium of a juvenile *Dorudon atrox* (UM 97506). Note how the upper molars and maxilla extend posteriorly underneath the jugal out on to the zygomatic arch. The palate narrows posteriorly where the palatines meet the pterygoids. The internal nares are a bit damaged, but at this point the pterygoid splits into its medial and lateral laminae which enclose the pterygoid sinuses.

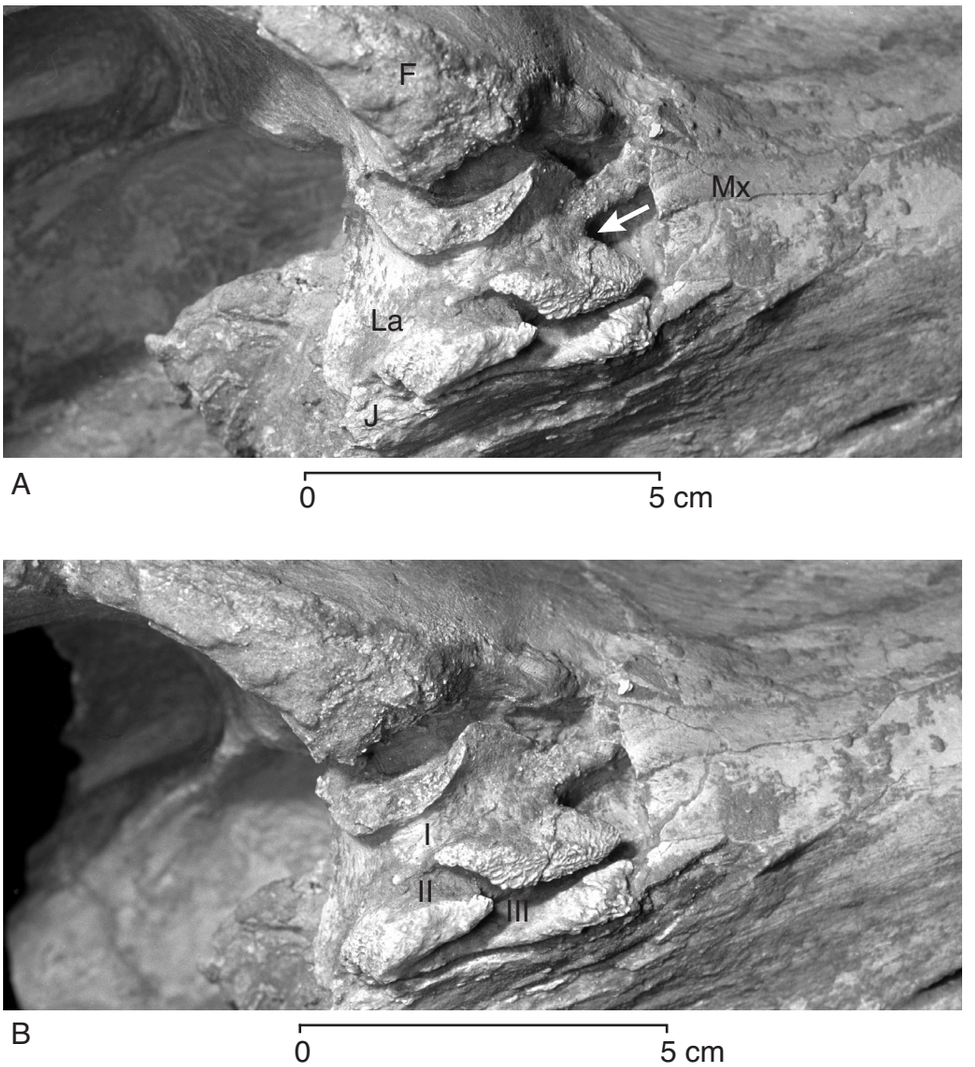

FIGURE 26 — Lacrimal of *Dorudon atrox* (UM 101222) in A, right lateral, and B, right anterolateral view. Note that the dorsal edge of the lacrimal has separated from the frontal due to deformation. In addition, the jugal has been pushed toward the midline of the skull due to deformation. Roman numerals refer to the three channels in the lacrimal leading to the lacrimal canal, numbered from ventral to dorsal. The arrow indicates the opening to the lacrimal canal.

ally, the maxilla forms part of the floor of the orbit. Just dorsal to the articulation with the jugal is a low ridge on the maxilla. This ridge projects posteriorly from the generally smoothly convex dorsal surface of the maxilla, and anteriorly to the edge of the lacrimal. This portion of the maxilla articulates with the anterior end of the lacrimal and forms the roof over the lacrimal canal. The lacrimomaxillary suture continues medially along the convex surface of the maxilla. Medially, the frontal process of the maxilla articulates with the frontal.

Palatine

The paired left and right palatines [**Pal**] form the posterior portion of the palate and extend posteriorly to the basicranium (Figs. 25 and 27). These articulate anteriorly with the maxillae. The posterior palatine foramina [**ppf**] are present in the palatomaxillary suture, about midway between the midline and the lateral edges of the palate. The palatomaxillary suture extends laterally and caudally from the midline. The suture also extends somewhat dorsally, where the perpendicular lamina of

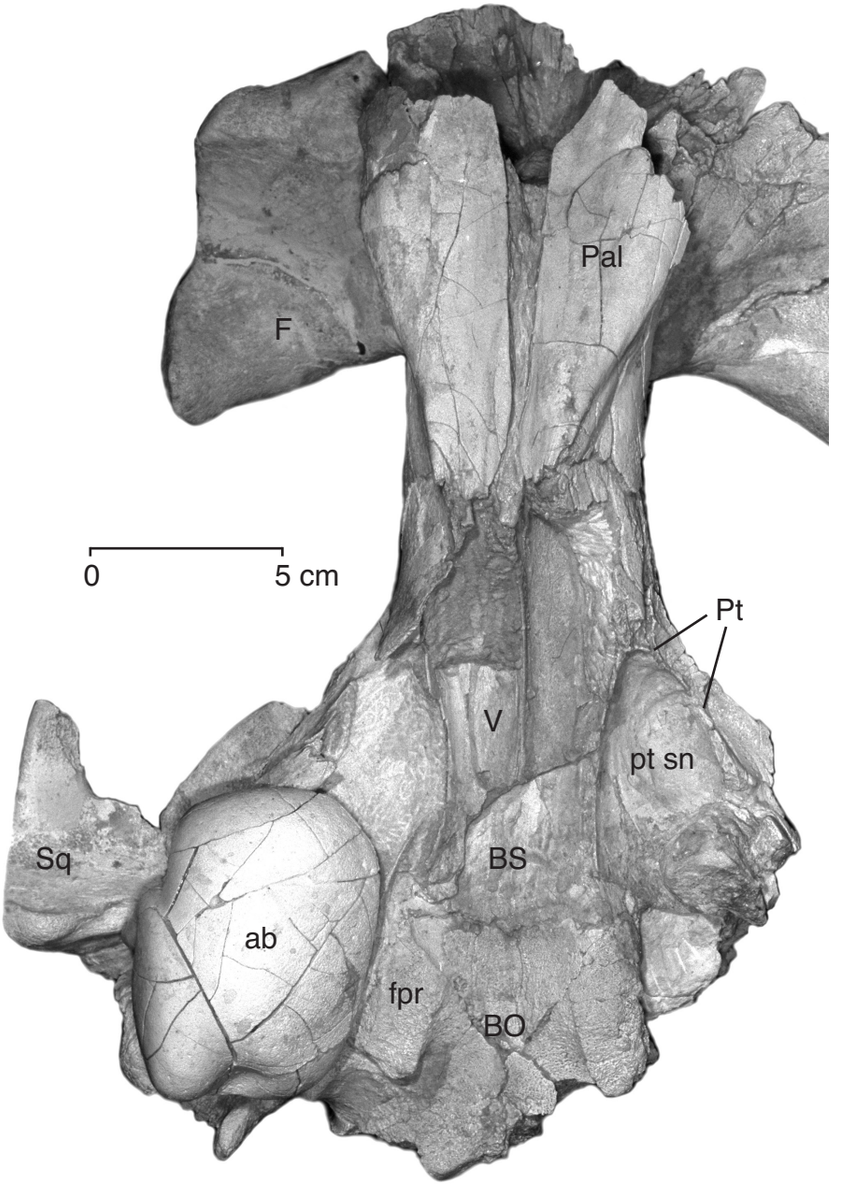

FIGURE 27 — Basicranium of juvenile *Dorudon atrox*, specimen UM 100139. Note the well-developed pterygoid sinus that is confluent with the tympanic cavity under the auditory bulla. Note also the broken edges of the posterior vomer and pterygoids, which normally cover the ventral surface of the basisphenoid.

the palatine forms part of the embrasure pit posterior to P^4. The palatofrontal suture continues onto the side of the skull medial to the orbit.

The ventral surface of the horizontal lamina of the palatine forms the posterior portion of the hard palate. It extends posteriorly to form a point just anterior to the opening of the internal nares into the oropharynx. The dorsal surface of the horizontal lamina of the palatine forms the ventral surface of the narial passage.

The perpendicular lamina of the palatine extends dorsally from the lateral edge of the horizontal lamina. Anteriorly, the perpendicular lamina forms part of the embrasure pit posterior to P^4. The perpendicular lamina of the palatine also forms part of the medial wall and floor of the orbit. Posterior to the orbit,

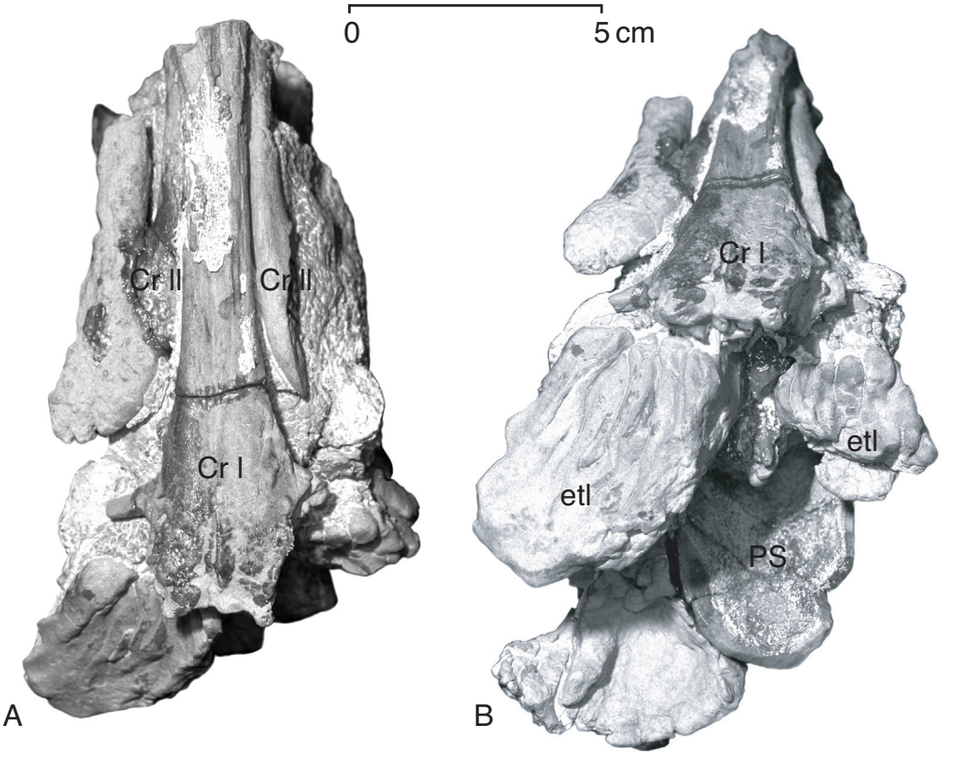

FIGURE 28 — Cast of the posterior narial region of a juvenile *Dorudon atrox* (UM 97516) in A, dorsal, and, B, anterodorsal view. Both views show the olfactory nerve (*Cr. I*) along the midline and the left and right optic nerves (*Cr. II*) lateral to the olfactory nerve. The anterior end of the cast of the right optic nerve (on the left of the photos) is attached to a mass of sediment. This is a cast of the orbit, and it shows where the optic nerves open into the orbit. The olfactory nerve continued farther anteriorly to enter the frontal sinuses, which are confluent with the posterior narial passages. Very thin scrolls of bone (*etl*) can be seen in the sediment cast of the posterior narial region. In B, one can see the heavily weathered presphenoid (*PS*) along the midline ventral to the sinuses. In addition, a cast of the right narial passage is visible in the lower left corner of the photograph.

the lateral surface of the perpendicular lamina forms the medial wall of the pterygopalatine fossa. The medial surface of the horizontal lamina of the palatine forms the lateral wall of the nasal passage. These areas are probably covered over internally by the thin vomer. It is difficult to assess the extent of the vomer in this area since it is entirely internal and the vomer is extremely thin, thus making it difficult to see in computed tomography scans.

Pterygoid

The pterygoid [**Pt**] is one of the most complex bones of the cetacean basicranium. Paired left and right pterygoids articulate anteriorly with the posterior palatines (Fig. 27). The ventral portions of the pterygoids meet along the midline to form the posterior extension of the ventral and lateral walls of the internal narial passages.

The pterygoid has numerous surfaces that project in many different directions. One of these projections is contiguous with the ventral portions of the palatines described above. This is the lateral lamina of the pterygoid [**lpt**]. The posterior border of the lateral lamina angles away from the midline laterally and posteriorly. The lateral presentation of the lateral lamina forms the side of the skull and the lateral wall of the pterygoid sinus [**pt sn**]. The dorsal border of the lateral lamina of the pterygoid meets the squamosal. The pterygosquamosal suture proceeds dorsally and then turns sharply anteriorly, where the squamosal meets the alisphenoid. The pterygoid makes a short dorsal contact with the alisphenoid. The suture turns ventrally where the pterygoid meets the posterior palatine. The pterygopalatine suture then angles ventrally and anteriorly to the midline where the two palatines meet.

Another surface of the pterygoid forms the medial wall of the pterygoid sinus. This is the medial lamina of the pterygoid [**mlp**]. The medial lamina is roughly parallel to the midline and contacts the lateral lamina of the pterygoid dorsal to the ventral border of the lateral lamina. The medial lamina projects ventrally and is nearly vertical on its anterior end, and angles laterally at its posterior end. The medial lamina of the pterygoid

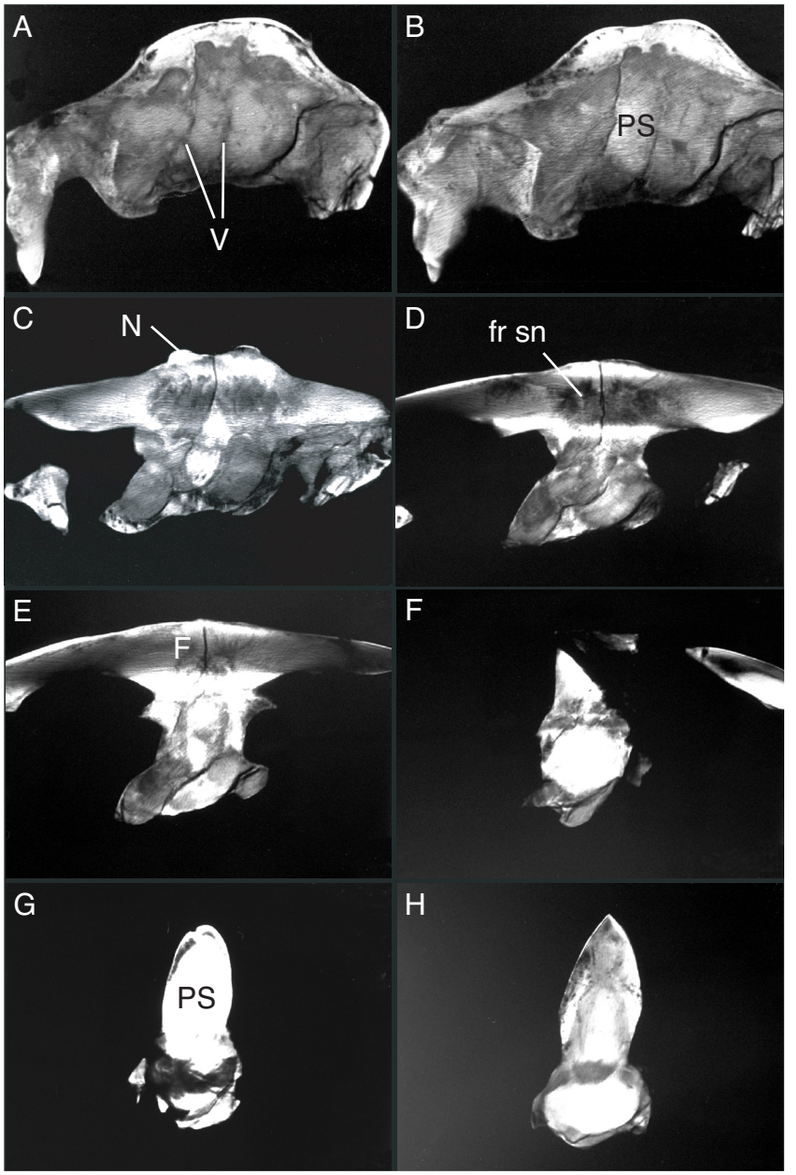

FIGURE 29 — Computed tomography (CT) scans of a skull of *Dorudon atrox* (UM 101222). Images A-H go from anterior to posterior, spaced three centimeters apart. Images A and B are anterior to the orbit. The two dark lines around the midline of image A are the laminae of the vomer. The cartilaginous nasal septum would have been between them in life. The large, bright midline structure visible in image B that is not present in image A is the anterior presphenoid. Image C is through the orbit, and image D is posterior to the orbit. Bumps on the dorsal surface are the posterior nasals that lie on top of the frontals. The dark spaces below the bumps are the frontal sinuses. The piece of bone that appears to be floating in the bottom left corner is the anterior zygomatic arch. Narial passages are the dark gray ovals visible in images C and D, lateral and ventral to the anterior presphenoid in image C. Images E and F show the posterior end of the frontal shield. Note that the frontal sinuses are almost gone in image E. The dark areas that appear to be missing in image F are due to a crack in the specimen that was not completely joined. The bright circular bone in the ventral portion of image F is the posterior presphenoid. Images G and H show the parietals dorsally, and the presphenoid ventrally. The dark areas in between the parietals and presphenoid, visible in image H, are the nerve tracts for the olfactory and optic nerves along the midline, and the ophthalmic and maxillary divisions of the trigeminal laterally.

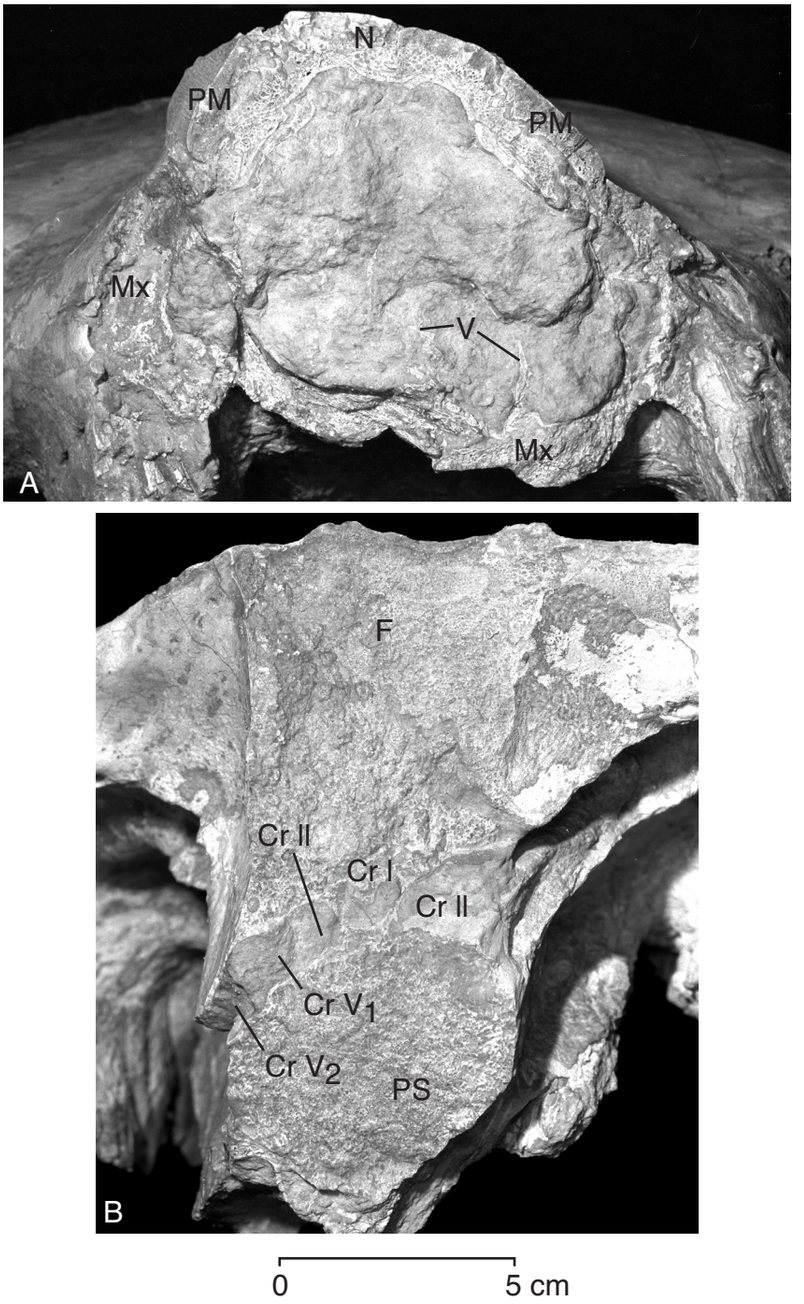

FIGURE 30 — Natural cross sections of the skull of *Dorudon atrox* (UM101222). A, anterior to the orbit, and B, posterior to the orbit. A shows the two laminae of the vomer as thin stringers of bone extending up from the palate. B shows the sediment casts of the cranial nerves. The olfactory (*Cr. I*) and optic (*Cr. II*) nerves are near the midline. The ophthalmic and maxillary divisions of the trigeminal nerve (*Cr. V_1* and *Cr. V_2*, respectively) are entering the orbit through the orbital fissure.

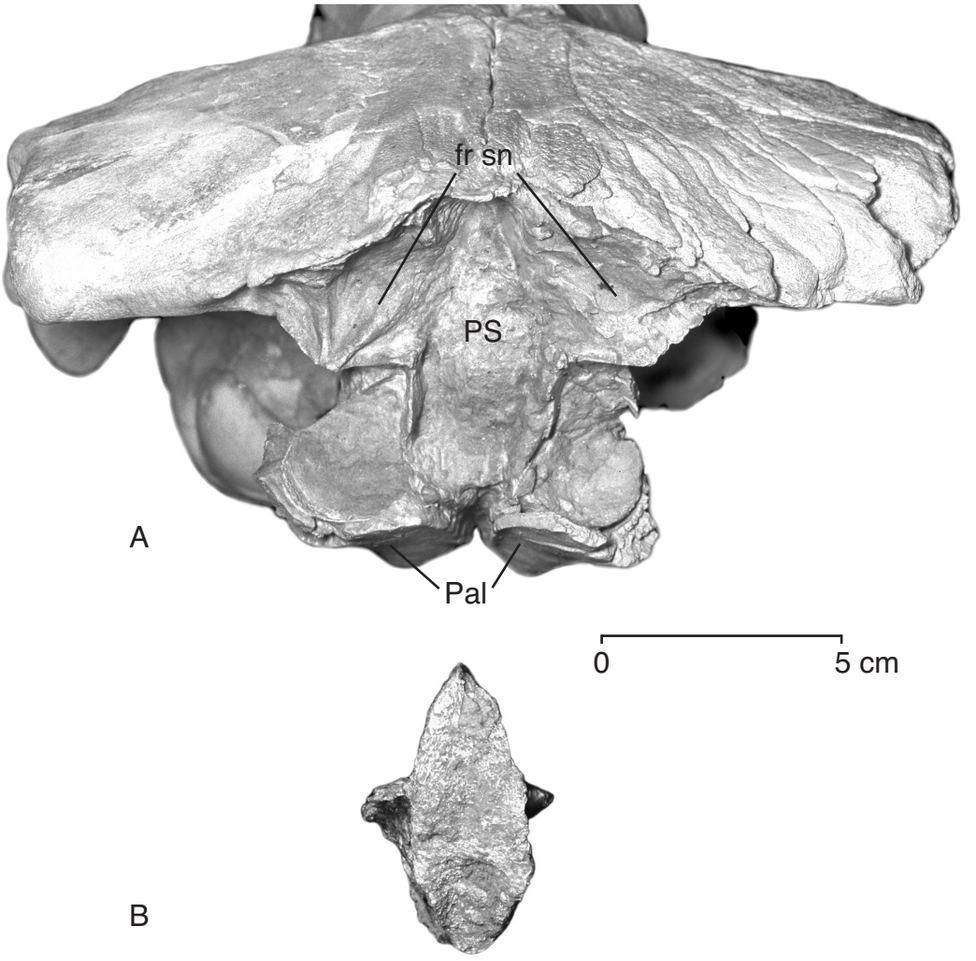

FIGURE 31 — Anterior presphenoid of *Dorudon atrox*. A, anterior presphenoid of UM 100139 in place relative to the frontal sinuses and narial passages. B, anterior presphenoid of UM 97512 separated from the rest of the skull. The anterior presphenoid has a roughly-textured anterior surface, indicating that it articulated with cartilage, in this case the cartilaginous nasal septum.

forms a thin covering of the basisphenoid. The posterior border of the medial lamina makes contact with the anterior border of the basioccipital crest just posterior to the basioccipital-basisphenoid suture.

The medial border of the medial lamina of the pterygoid contacts the lateral edge of the vomer. As stated above, the lateral and medial laminae of the pterygoid form a large space known as the pterygoid sinus. This sinus is confluent with the tympanic cavity posteriorly, is open ventrally, and is enclosed anteriorly by the pterygoid.

Nasus

Nasal

The nasals [**N**] of *Dorudon atrox* are long, relatively narrow bones that form the roof of the nasal cavity (Fig. 24). They are elongated parallel to the long axis of the skull, and their medial edges contact each other along the midline. The pointed anterior ends of the nasals form the posterodorsal margin of the external nares. Thus, there is a **V**-shaped notch formed between the nasals in the posterodorsal margin of the external nares, with the apex of the **V**-shaped notch pointing posteriorly. Left and right nasals are separated posteriorly by a very narrow, triangular projection of the frontals. The nasals are widest just anterior to the midline projection of the frontal and taper anteriorly. Laterally, the nasals articulate with the medial borders of the premaxillae along the anterior two thirds of their length. Posterior to the premaxillae, the nasals articulate with the posteromedial borders of the maxillae. The posteriormost tips of the nasals are completely surrounded by the frontals laterally, medially, and posteriorly. The posterior nasals overlap onto the dorsal surface of the frontals.

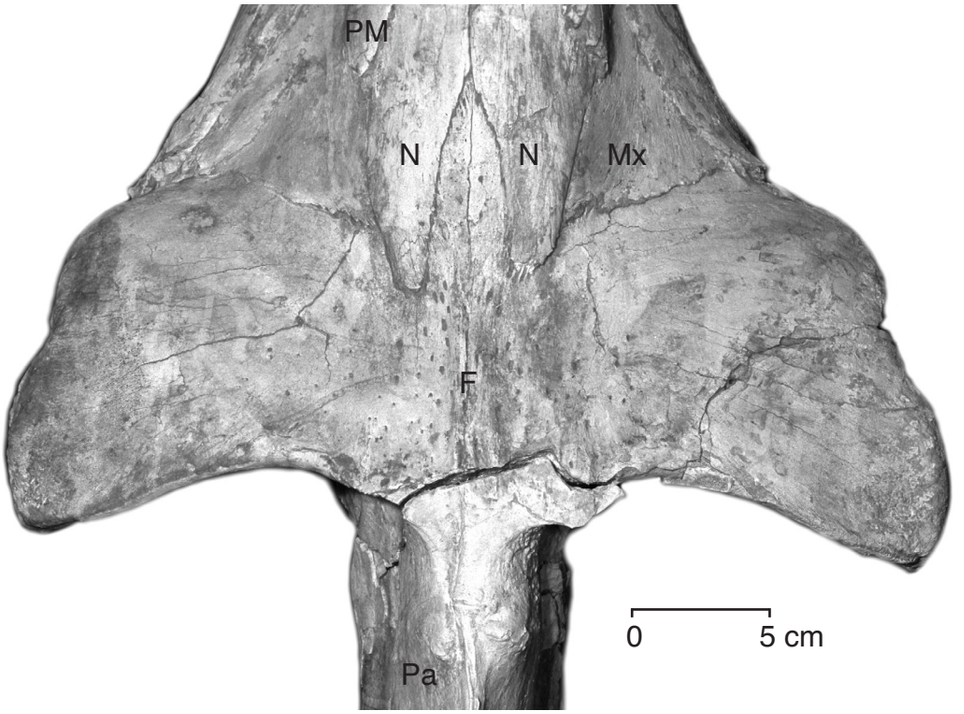

FIGURE 32 — Frontal shield of *Dorudon atrox* (UM 101222). Note the large process of the frontals extending anteriorly between the posterior nasals. Note also that the medial maxilla contacts the lateral nasals. Both lap posteriorly onto the frontals. The posterior premaxillae are visible at the top of the photograph, lateral to the nasals.

Opening of the external nares

The external nares [**en**] are confluent, with a single opening that has migrated posteriorly along the dorsal surface of the skull relative to its position in earlier archaeocetes. The opening of the external nares faces anterodorsally and is located dorsal to P^1. Viewed dorsally (Fig. 24), the narial opening is teardrop-shaped in outline, with the apex of the teardrop pointing anteriorly. The anterior and lateral borders of the nares are formed by the premaxillae, while the posterodorsal margin is formed by the nasals. The posterior border of the nares is above the diastema between P^1 and P^2. The ventral surface of the nasal cavity is rather complex, and it is formed from three different bones. The premaxillae slope down from the lateral borders of the nares to form the lateral margins of the ventral surface of the nasal cavity. Medial and ventral (i.e., toward the palate) to the medial borders of the premaxillae, the maxillae form shelves that project medially from their contact with the premaxillae. These horizontal shelves terminate away from the midline and the maxillae slope down from the edges to form a deep groove along the midline and meet at the bottom of the groove. Much of the ventral surface of the narial cavity is formed by the maxilla, with the vomer contributing to the ventral surface, along the midline, posterior to the opening of the external nares.

The roof of the nasal cavity is formed by the nasals themselves. The paired nasals meet along the midline and form a small projection down into the nasal cavity. This process can be seen in CT scans and in specimens fractured through this area. This is the septal process of the nasals [**spn**]. The septal process forms the dorsal attachment of the cartilaginous nasal septum.

Ethmoid

The ethmoid [**E**] is a complex, unpaired midline bone of the skull that forms the posterior narial region. It has no surficial presentation on the skull, and it is bounded by many other bones. The anterior end of the ethmoid is the only surface that is not bounded by bone. It is open to the anterior narial cavity and presumably had a cartilaginous extension during life. The dorsal ethmoid is roofed over anteriorly by the nasals and posteriorly by the frontals. The posterior ethmoid abuts against the anterior presphenoid. Lastly, the ventral ethmoid meets the unpaired midline vomer along its entire extent. The portions of the ethmoid are most easily described from posterior to anterior.

The cribriform plate of the ethmoid usually forms the division between the endocranial space and the posterior narial

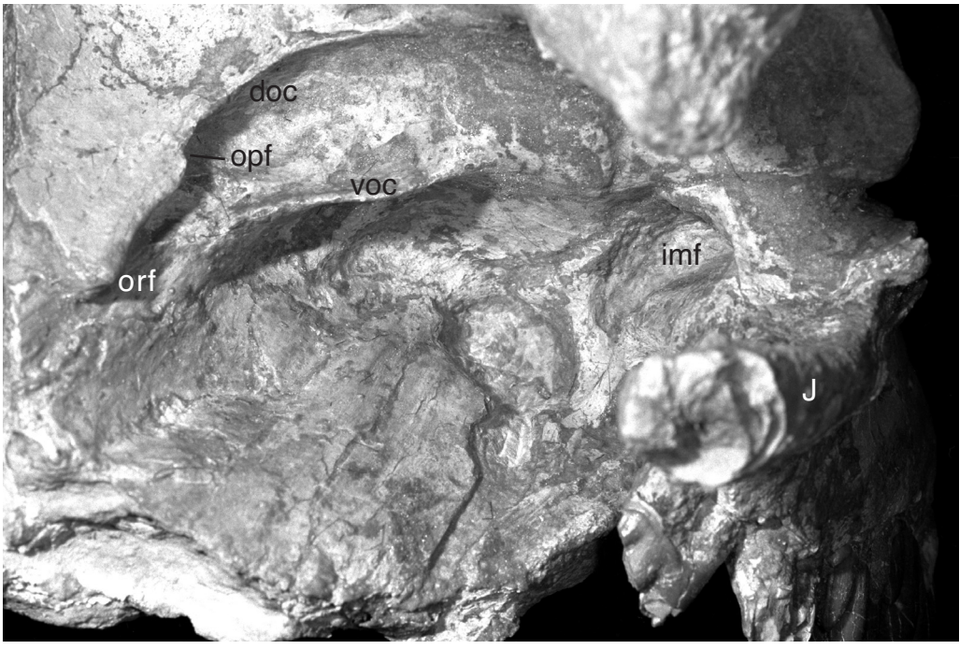

FIGURE 33 — Orbit of *Dorudon atrox* (UM 101222) in posterolateral view. The postorbital process of the frontal is the object out of focus in the upper right of the photograph. The broken zygomatic arch is visible above the tooth row in the bottom right of the photograph. The superior and inferior orbital ridges are seen in the upper left of the photograph. Details of anatomy are reviewed in the text.

cavity in mammals. The cribriform plate is much reduced in modern cetaceans, but it is present and substantial in *Dorudon atrox*. In archaeocetes, the posterior narial cavity is far anterior to the endocranial cavity, so the cribriform plate simply forms the division between the nerve tract for the olfactory nerve (Cr. I) and the posterior narial cavity. Natural casts of the posterior narial region show that the olfactory nerve enters the posterior narial cavity and distributes through perforations in the cribriform plate slightly anterior to the opening of the optic nerve tract into the orbit (Fig. 28).

The ethmoid forms a complex ethmoidal labyrinth [**etl**] in *Dorudon atrox*, but it is difficult to separate the labyrinth into separate scrolls (Fig. 29). The turbinates extend as far anterior as the mesethmoid that supports them medially. The turbinals extend laterally to fill the dorsal narial passages, but most of the ventral portion of the narial passages is free from turbinals. The turbinals extend anteriorly from the cribriform plate.

Vomer

The vomer [**V**] divides the nasopharynx into two separate internal nares at the posterior end of the nasopharynx (Fig. 27). The vomer is usually a single midline element in most mammals, but the posterior extension of the vomer is divided along the midline in juvenile *Dorudon atrox*. It is unclear whether the posterior halves of the vomer fused in adult individuals. The posteriormost extensions of the vomer is ventral to the basisphenoid, just anterior to its articulation with the basioccipital. The left and right portions of the vomer are separated by a thin gap along the midline. The lateral edges of the vomer expand laterally as they extend anteriorly. The medial edges of the separate posterior projections of the vomer form a thin sharp ridge along the midline that extends ventrally from the basicranium and forms the septum between the paired narial passages. The two separate posterior portions of the vomer meet about half way along the rise of the ridge to fuse into a single midline element. At the level of the palate, the midline ridge expands laterally to form a small wedge-shape that rests in between the posterior palatines.

Anteriorly, the vomer expands laterally to cover some of the dorsal side of the palatines, forming the floor of the narial cavity. Anterior to the presphenoid, the lateral edges of the vomer turn dorsally and project up into the narial passages forming a tall, **V**-shaped structure The arms of the **V** are very thin and sub-parallel to the lateral sides of the anterior presphenoid (Figs. 29 and 30). The valley of the **V** would have accepted the cartilaginous nasal septum projecting ventrally from the nasal bones that roof the narial passages during life. The arms of the **V** become shorter near the anterior extension of the vomer. The vomer also covers the medial maxillae, covering the floor of the narial cavity anterior to the palatomaxillary suture. The anterior vomer terminates at a point approximately where the anterior nasals begin to cover the narial cavity.

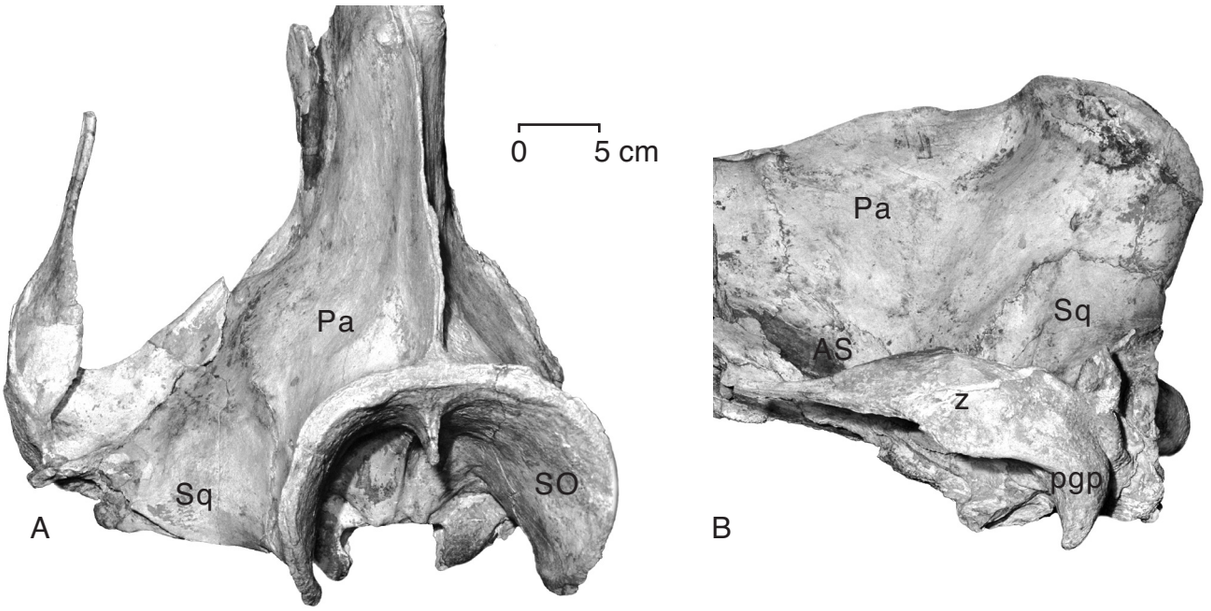

FIGURE 34 — Parietal and squamosal of *Dorudon atrox* (UM 101222) in, A, dorsal, and B, lateral view. A shows the left side of the skull. The view is slightly distorted due to parallax to maximize the view of the left side of the skull. The parietal-squamosal suture is visible running diagonally toward the nuchal crest from the medial side of the skull. The zygomatic process of the squamosal is broken anteriorly. Note the extremely tall and sharp sagittal crest. B shows a lateral view of the left side of the skull. The postglenoid process of the squamosal is in the foreground at the posterior end of the zygomatic process of the squamosal. The post parietal foramen is visible just dorsal to the parietal squamosal suture.

Presphenoid

The presphenoid [**Ps**, Figs. 29-31] is a semi-cylindrical bone that has no surficial presentation on the skull of *Dorudon atrox*. The presphenoid articulates anteriorly with the cartilaginous nasal septum. The presphenoid meets the nasal septum anterior to the point where the optic foramen opens into the orbit and posterior to the anteriormost edge of the frontal.

The anterior presphenoid (Fig. 31) is a large, midline bone just anterior to the cribriform plate. The mesethmoid contacts the frontals dorsally along the midline, and contacts the vomer ventrally. The anterior presphenoid is somewhat ovate in cross section, tapering to a thin partition between the left and right narial passages where the mesethmoid meets the frontals. The anterior end of the presphenoid would have articulated with a cartilaginous nasal septum in life, but this is not preserved in any specimens of *Dorudon atrox*.

The presphenoid undergoes a dramatic shape transformation approximately at the anterior end of the orbit. While the anterior presphenoid is in the shape of a pointed oval as described above, the posterior presphenoid is much more cylindrical. The lateral sides of the cylindrical presphenoid are covered by a thin layer of the frontal bone, which in turn forms the medial wall of the orbital fissure [**orf**]. The ventrolateral wall of the orbital fissure is formed by the thin palatine in the region of the orbit. Throughout its entire extent, the ventral surface of the presphenoid is covered by the vomer, which lines the floor of the narial passages. Posterior to the orbit, the presphenoid is surrounded by numerous bones. The dorsal and dorsolateral surfaces are covered by the frontal. The lateral surfaces form the medial wall of the canal for the ophthalmic (Cr. V_1) and maxillary (Cr. V_2) divisions of the trigeminal nerve. The lateral wall of the nerve tract is covered by the palatines. Posterior to the frontoparietal suture, the presphenoid is covered dorsally by the parietals, and the lateral wall of the nerve tract is covered by the alisphenoids. The posterior end of the presphenoid articulates with the basisphenoid along a flat surface.

Mesocranium

Frontal

The frontals [**F**] form the large frontal shield over the orbits typical of archaeocete whales (Fig. 32). The frontal shield is a broad flat area that forms the roof of the posterior nasal cavity and orbits. The frontals fuse early in ontogeny and articulate anteriorly with the nasals along the midline. The paired frontals extend far anterior in a wedge-shaped projection along the midline between the nasals, but most of the anterior border of the frontal contacts the maxilla. The frontomaxillary suture extends slightly anteriorly and laterally, over the dorsal surface of the skull. The frontomaxillary suture continues laterally until it contacts the lacrimal.

FIGURE 35 — Right zygomatic arch of *Dorudon atrox* (UM 101222). The zygomatic process of the squamosal is dorsal to the jugal on the left side of the image. The zygomatic process of the squamosal is broken near where it meets the postglenoid process. The anteriormost tip of the squamosal is broken, but the broken piece is present, slightly displaced from its original position, and adhering to the jugal via sediment. The jugal is broken at its base where it articulates with the lacrimal and maxilla anteriorly. The posteriormost tip of the jugal is also missing.

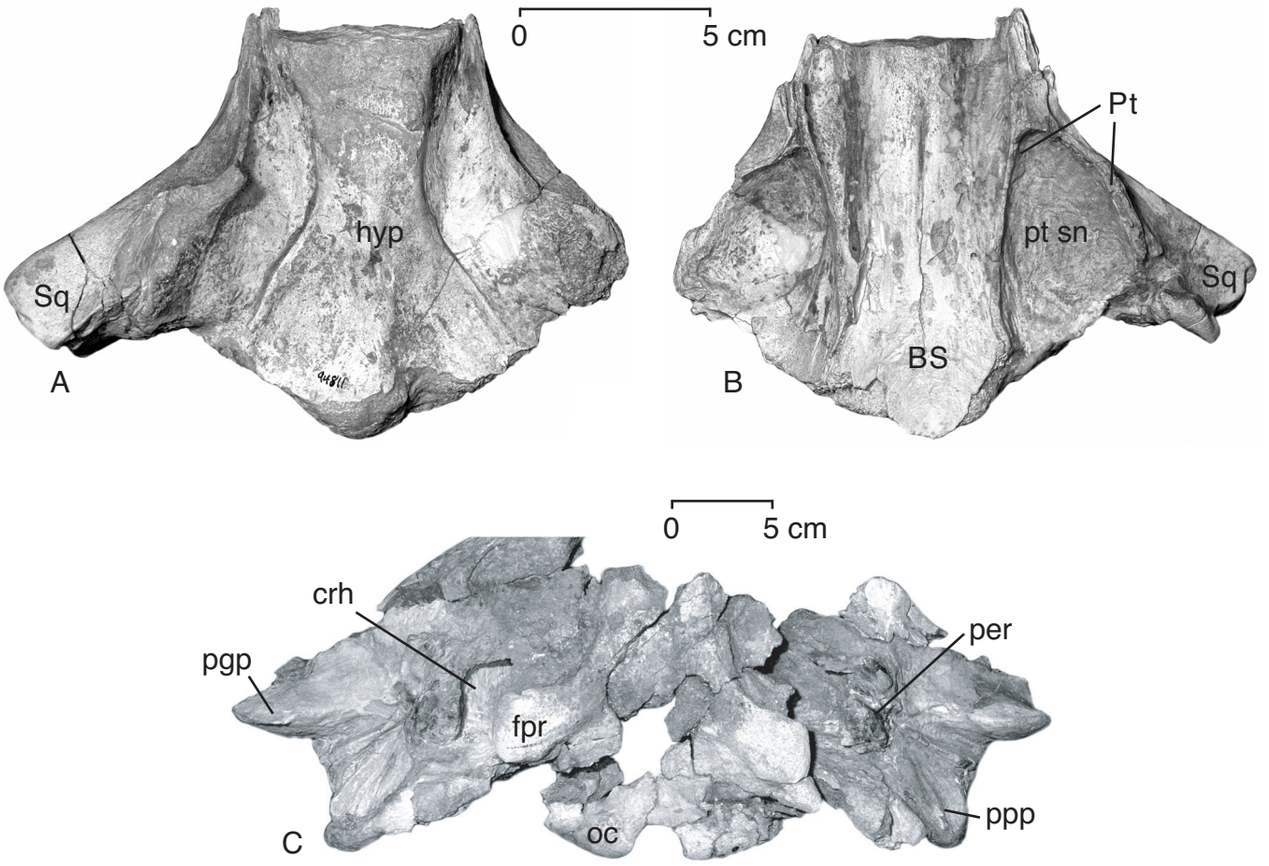

FIGURE 36 — Basisphenoid and basioccipital of *Dorudon atrox*. A and B, basisphenoid of UM 94811, in dorsal (endocranial) and ventral views, respectively. The hypophyseal fossa is visible along the midline of A just posterior to the constriction of the hourglass shape. Portions of the squamosal and pterygoids are attached to the basisphenoid. The pterygoid sinuses are visible in B lateral to the midline basisphenoid. Normally the basisphenoid is covered by the vomer and pterygoids which are broken off in this specimen. C, basicranium of UM 101223. The basioccipital is the midline structure with the large, dorsolateral projections on the posterior end. These are the falcate processes of the basioccipital. Note that there is a distinctly separate portion of this process on the left side of the skull (right side of the photograph) that is broken from the right side. This is the exoccipital contribution to the falcate process. The large gap in the center of the basioccipital is a broken and missing piece. The large space between the falcate process and the periotic (farther laterally), most clearly seen on the right side of the skull, is the cranial hiatus.

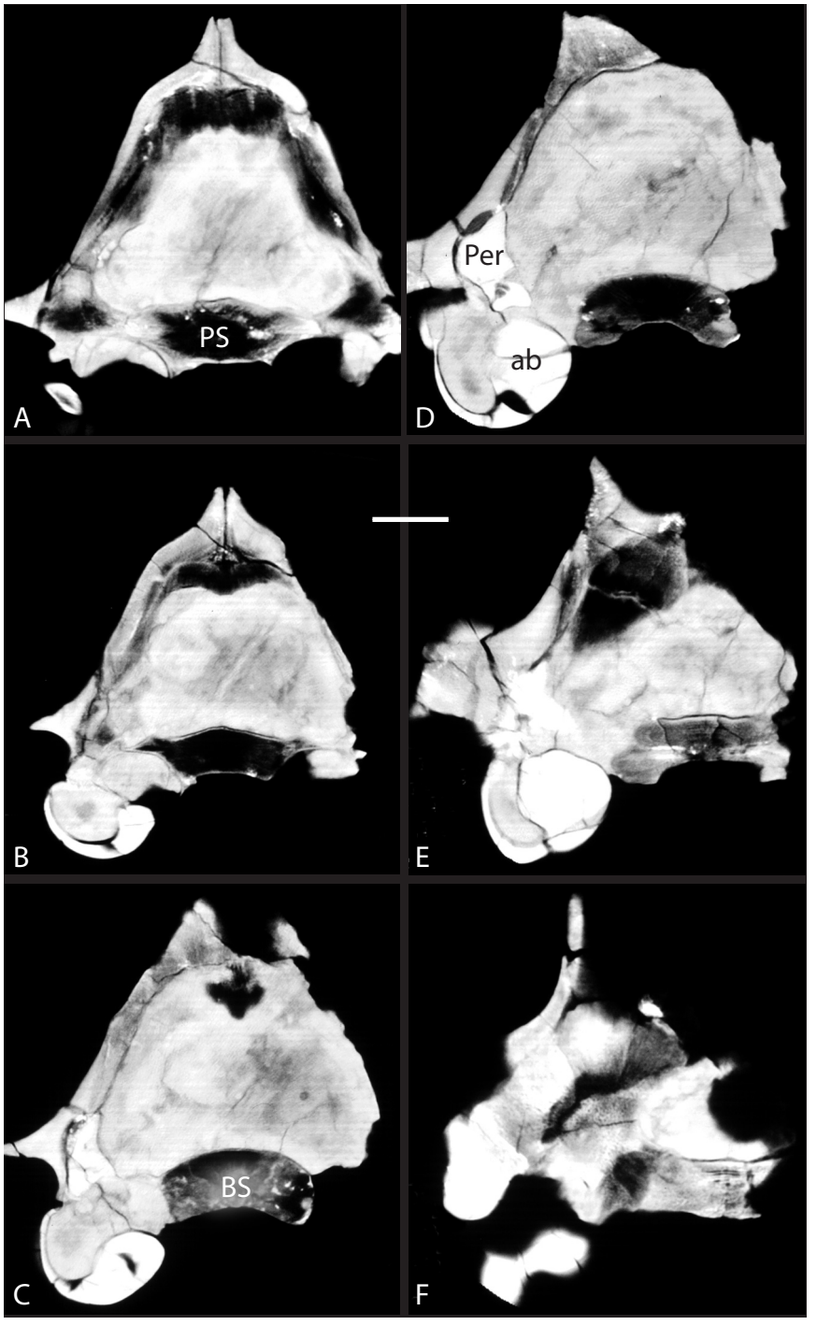

FIGURE 37 — Computed tomography scans of a skull of a juvenile *Dorudon atrox* (UM 100139). Images A-F are from anterior to posterior, spaced 1.5 cm apart. This skull is also shown in Figure 27. The large gray area in the center of each of the images is the endocranial space. The endocranial space is floored by the basisphenoid in images A and B, and by the basioccipital in images C-F. The lower left hand corner of the images shows the otic region. The large curved structure is the tympanic bulla. Note that its medial side is very thick and dense. This is the involucrum of the bulla. The smaller curved structure in image D to the left and dorsal to the bulla is the sigmoid process of the bulla. Medial to its dorsomedial end is the malleus. The bone dorsal to the bulla that is similarly dense is the periotic. Image D shows a small, coiled space inside the periotic. This is the cochlea. More detailed and larger images of this region are shown in Figure 42.

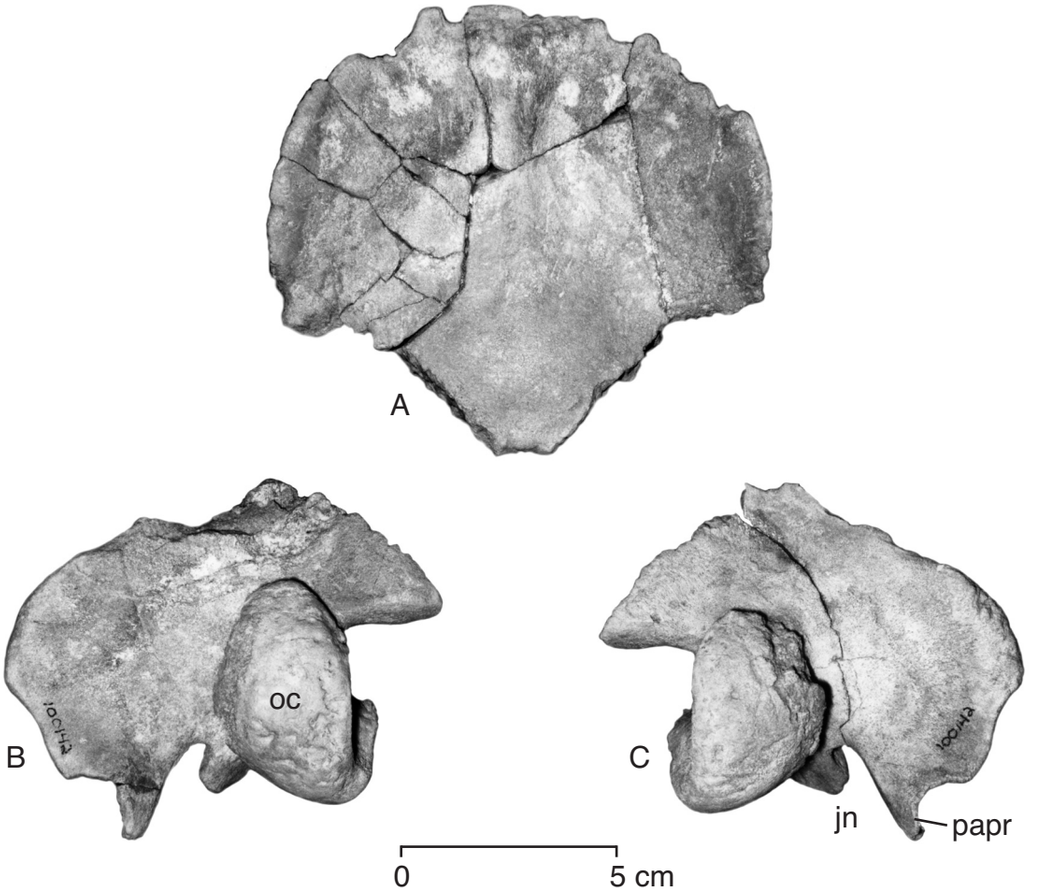

FIGURE 38 — Supraoccipital and exoccipitals of a juvenile *Dorudon atrox* (UM 100142). The supraoccipital is not fused to the exoccipitals in this very young individual. Note the shape of the supraoccipital and the small size of the nuchal crest. Compare this to the supraoccipital of an adult *D. atrox* in Figure 39. The juvenile lacks the very dramatic curvature of the nuchal crest, midline ridge, and bosses just above the foramen magnum. The exoccipitals are not fused to the squamosals or periotics in UM 100142. Note the prominent jugular notches and paroccipital processes.

The frontolacrimal contact extends caudally into the orbit. The lacrimal and frontal are never fused, even in old adults. The orbital portion of the frontal forms most of the anterior and medial aspects of the orbit. Within the orbit, the frontal contacts the palatine along its ventral border. The frontopalatine suture continues posteriorly and slopes slightly dorsally toward the orbital fissure. At the orbital fissure, the suture continues medial to the ophthalmic and maxillary nerve tract, to where the palatine and frontals end, just anterior to the presphenoid-basisphenoid suture. In addition, the surficial frontal and palatine meet to cover the lateral side of the ophthalmic and maxillary nerve tract. This suture continues posteriorly until the frontal and palatine meet the parietal.

The frontals articulate posteriorly with the parietals. The frontoparietal suture is just posterior to the point where the frontal shield meets the midline of the skull. The frontal extends posteriorly along the midline, but the suture is farther anterior, just lateral to the midline on the dorsal surface of the skull. The suture sweeps posteriorly down the lateral side of the cranium, and then turns ventrally. The suture continues until it meets the alisphenoid, where it angles slightly cranially as it continues down the lateral wall of the skull. The sphenofrontal suture extends horizontally in a cranial direction for a short distance, where it meets the posteriormost extension of the optic fissure and the dorsal margin of the palatine.

In this region of the orbit, the palatine forms a very thin covering over the presphenoid. As the frontopalatine suture continues anteriorly, the optic fissure opens into the posteromedial wall of the orbit. The fissure is bounded by two prominent ridges of bone, the dorsal orbital crest [**doc**] and the

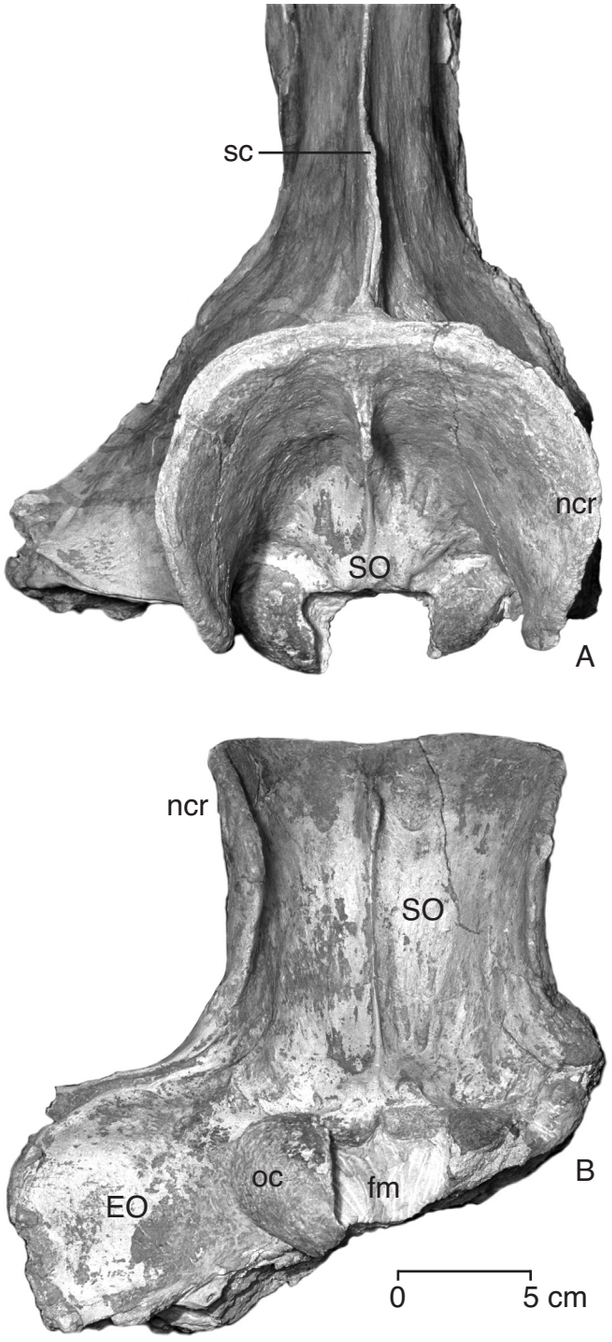

FIGURE 39 — Nuchal crest and occiput of *Dorudon atrox* (UM 101222) in A, dorsal, and B, caudal view. Note the dramatically different shape between the juvenile *D. atrox* in Figure 38 and the adult here. The shape of the overlap between the lateral exoccipitals and the squamosal is quite variable.

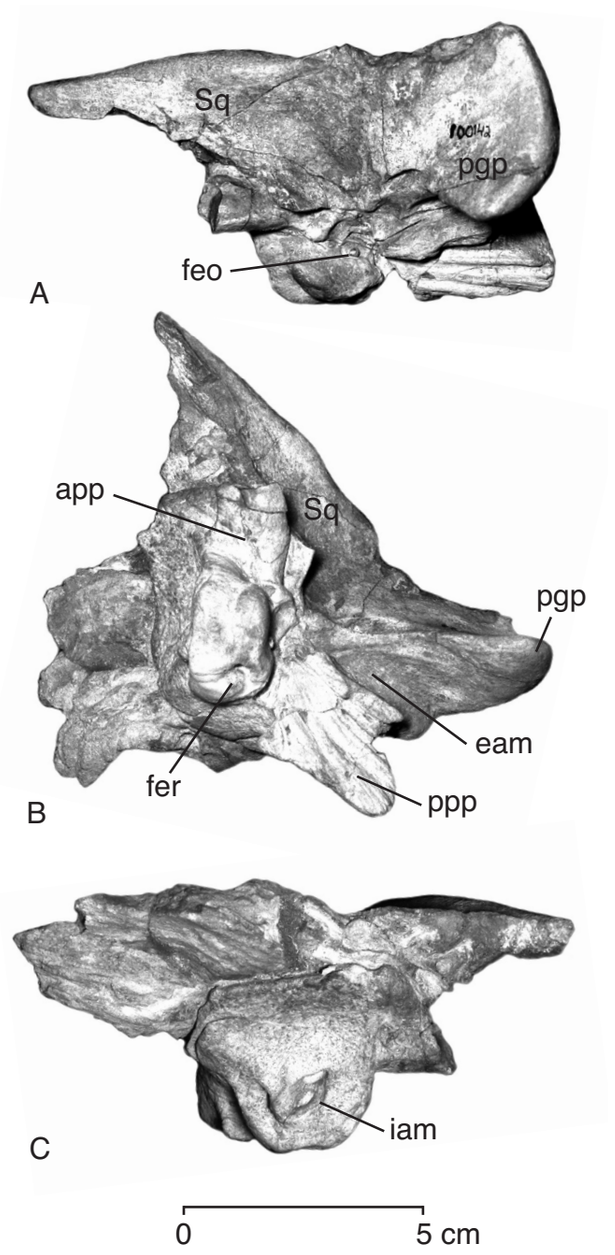

FIGURE 40 — Periotic and part of the squamosal of *Dorudon atrox* (UM 100142) in A, lateral, B, ventral, and C, medial view. The complex anatomy of the periotic and its relationships to the surrounding bones are discussed in the text.

ventral orbital crest [**voc**] (Fig. 33). Both ridges continue laterally along the posterior edge of the ventral surface of the frontal shield for a short distance. At the posterior end of the inferior orbital ridge, the frontal becomes a thin, flat covering over the surface of the midline presphenoid. This covering

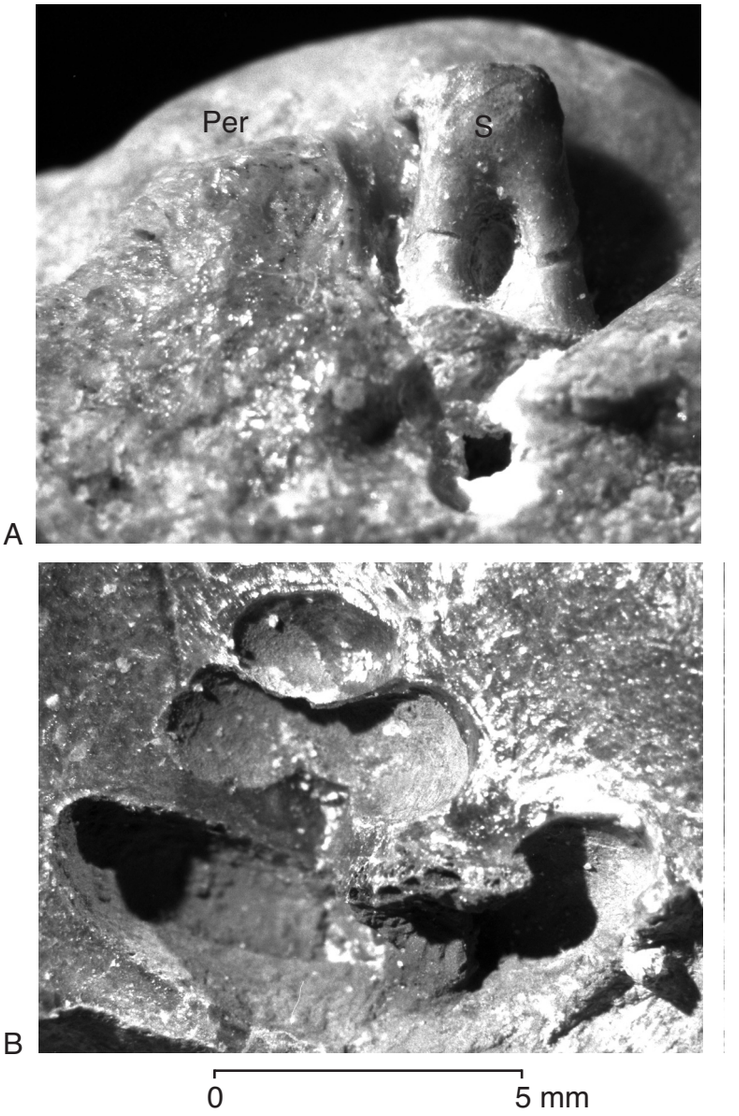

FIGURE 41 — Articulated periotic and stapes of *Dorudon atrox* (A, UM 93232), and cochlea of *Dorudon atrox* (B, UM 101223). The periotic is broken in A, showing the space below the stapes. This space is the vestibule, partially filled with calcite. The cochlea in B is partially filled with hematite. The plane of section does not include the axis of the cochlea.

forms the medial wall of the ophthalmic and maxillary nerve tract near the orbital fissure. The presphenoid is not exposed in the orbit or the orbital fissure.

Between the dorsal and ventral orbital crests are a series of openings that conduct structures into the orbit. The most posterior of these is the orbital fissure, which opens anteriorly into the orbital space. Anterior to the orbital fissure is the optic foramen. Anterior and slightly ventral to the optic foramen is a smaller foramen for the ophthalmic artery. The orbit is discussed in more detail below.

The frontals extend laterally from the midline out over the orbit forming the frontal shield [**frs**]. The lateral edge of the ventral surface of each side of the frontal shield has a slight ventral extension on its anterior margin which is the preorbital process of the frontal [**prop**]. A larger ventral extension on the posterior end of the lateral edge of each frontal shield is the postorbital process [**pop**]. These two processes define the anterior and posterior edges of the bony orbit respectively. The lateral edge of the frontal shield in between the two processes is concave on the ventral surface, forming a hemispherical recess

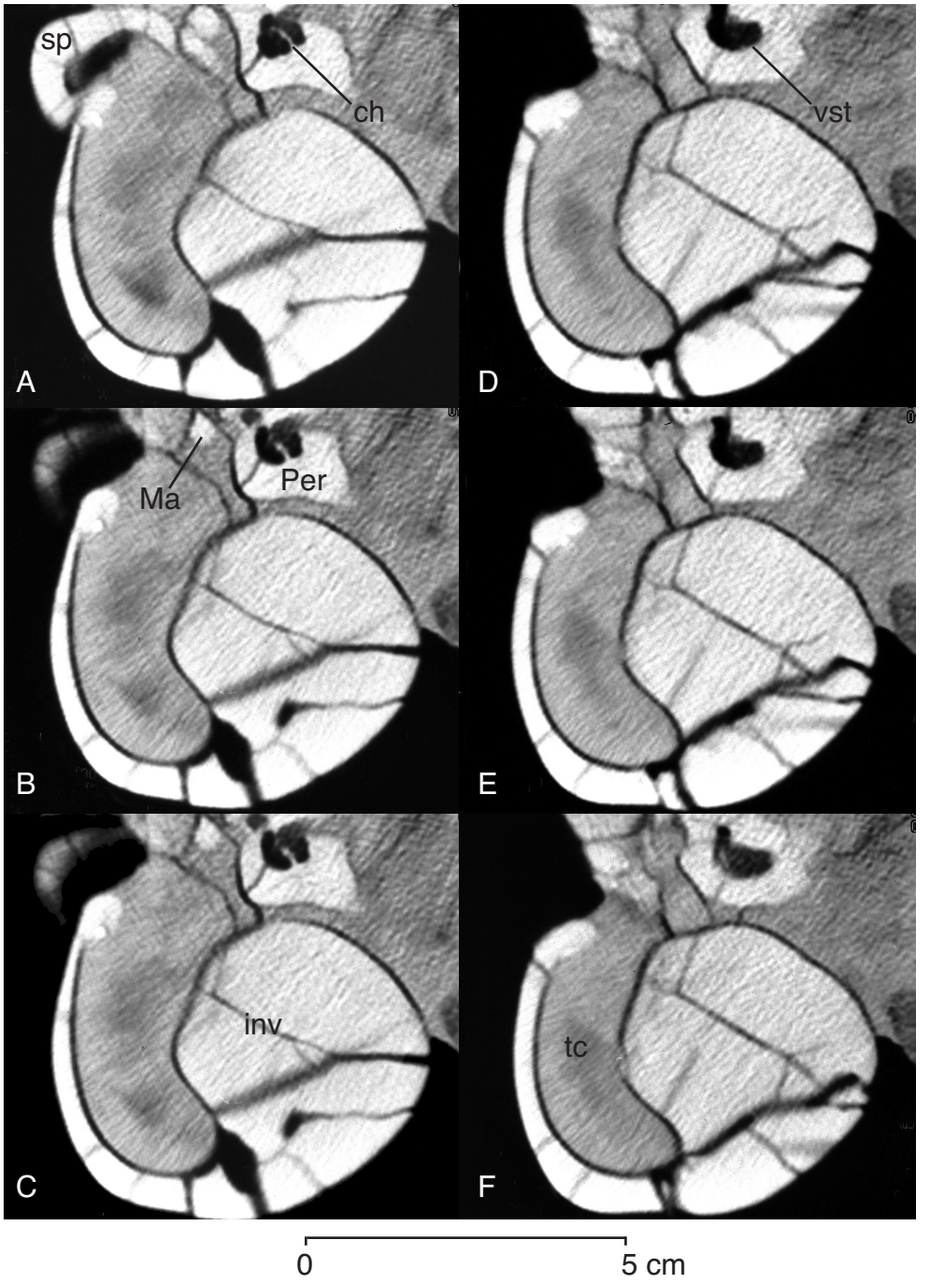

FIGURE 42 — Computed tomography images of the periotic and bulla of *Dorudon atrox* (UM 100139). Images A-F are from anterior to posterior, spaced 1.5 millimeters apart. The tympanic bulla is the bright curved object filling most of the image. The large round portion of dense bone filling the bottom right quadrant of each image is the involucrum of the bulla. The small curved object in the upper left of images A and B is the sigmoid process of the bulla. The small, dense bone in center of the top of each image is the periotic. The small bone between the sigmoid process in images A and B is probably the malleus. The similar object in image C may be the malleus or the incus. The spaces in the periotic are the vestibule and cochlea.

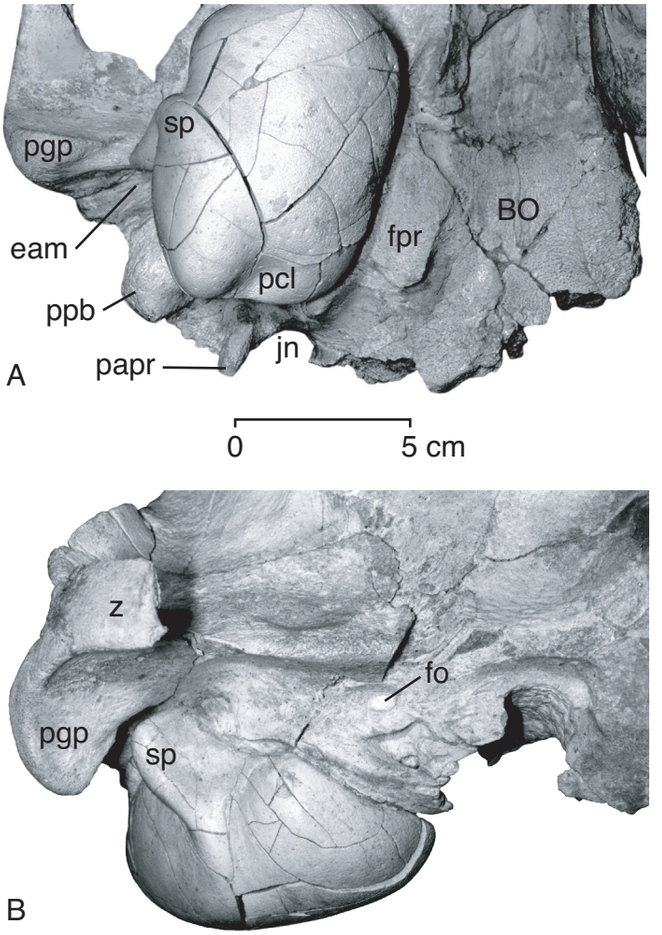

FIGURE 43 — Tympanic bulla of *Dorudon atrox* (UM 100139) in articulation with the skull in A, ventral, and B, anterolateral view. Note the position of the bulla relative to the falcate process (fpr), the paroccipital process (papr), external auditory meatus (eam), and the postglenoid process of the squamosal (pgp).

for the eye. A small frontal foramen is located on the posteroventral margin of the frontal shield.

The frontals enclose a pair of frontal sinuses [**fr sn**, Figs. 29 and 31]. These sinuses are found medial to the orbit along the midline of the frontal shield. The left and right sinuses are separated by the medial edges of the frontal bones along the midline. The sinuses narrow to a rounded point just anterior to the caudal edge of the frontal shield. The anterior ends of the frontal sinuses are bounded by the posterior maxillae, rather than portions of the frontal bones. Multiple small foramina that open anterodorsally are scattered on the dorsal surfaces of the frontals.

Parietal

The parietals [**Pa**] cover the lateral sides of the posterior portion of the skull (Fig. 34). Anteriorly, the parietals fuse with the frontals just posterior to the posterior border of the frontal shield. The suture is often complexly interdigitated and bulges laterally. The suture continues down the side of the skull, sloping slightly posteriorly, until it meets the alisphenoid. The sphenoparietal suture turns posteriorly, and somewhat ventrally. It continues until it meets the squamosal, near the anterior end of the squamosal. The sphenoparietal suture turns dramatically dorsally, while continuing in a caudal direction as well. Approximately half the way to the dorsal border of the nuchal crest, the sphenoparietal suture turns directly posteriorly, and intersects the nuchal crest [**ncr**].

At the point where the suture meets it, the nuchal crest is almost vertical. The anterolateral face of the nuchal crest is formed from the parietal, while the posteromedial face is formed from the supraoccipital. The nuchal crest curves in toward the midline of the skull. At the point where the two sides of the

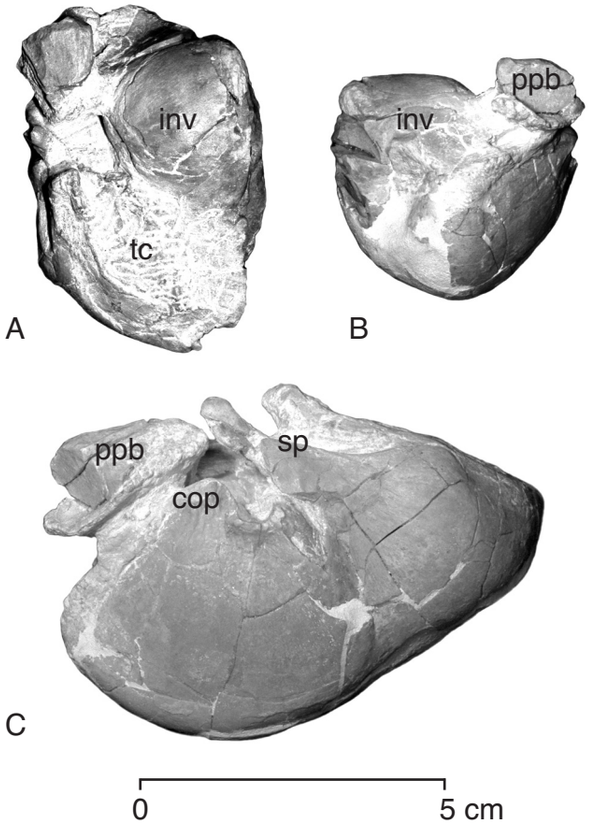

FIGURE 44 — Tympanic bulla of *Dorudon atrox* (UM 97512) in A, dorsal, B, posterior, and C, lateral view. The tympanic cavity is filled with sediment. Note that much of the sigmoid process is missing, and that small pieces of all of the processes are missing.

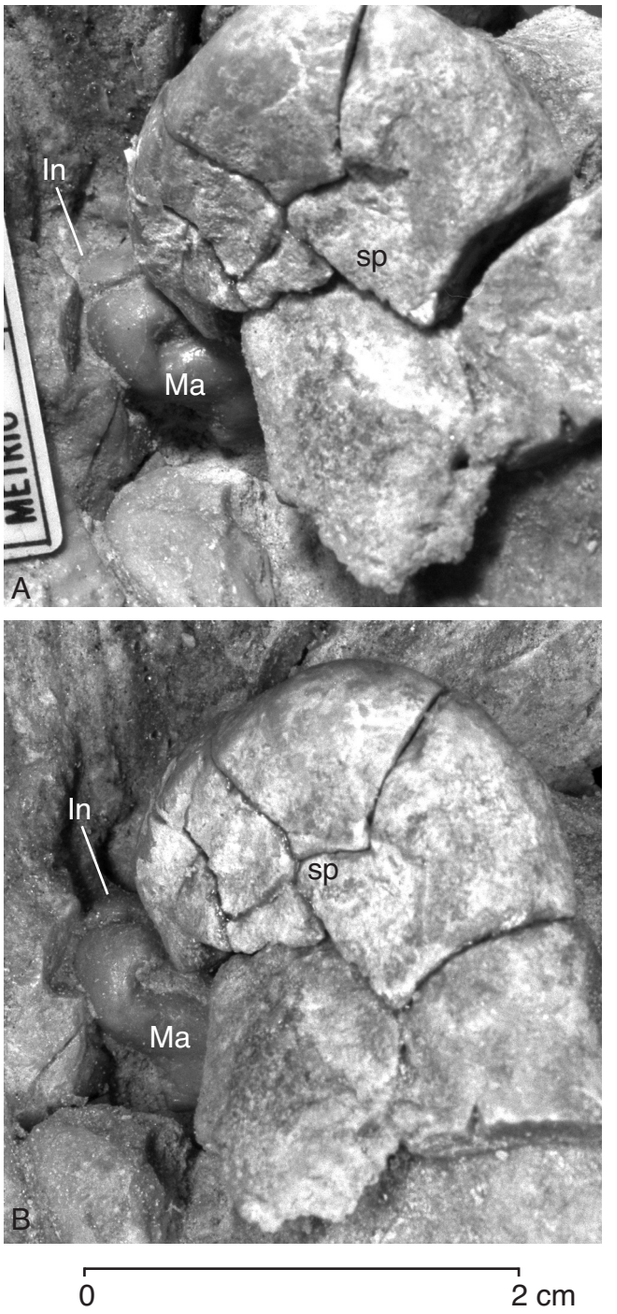

FIGURE 45 — Articulation of the sigmoid process and malleus of *Dorudon atrox* (UM 101222). A, view with ventral up and slightly to the left. B, view with ventral almost directly up. Anterior is to the left in each view. It is unclear if the malleus articulated with the sigmoid process or was fused to it.

nuchal crest meet, the parietals turn anteriorly. The back to back parietals continue anteriorly, forming a sharp sagittal crest [**sc**] until they meet with the frontals along the midline, just posterior to the frontal shield. No bony falx cerebri is known in any specimen of *Dorudon atrox*. In addition, no sylvian ridge is known from any specimen of *D. atrox*.

Interparietal

There is no interparietal known from *Dorudon atrox* or any other archaeocetes. This bone is found along the midline of the skull dorsal to the supraoccipital between the paired parietals in modern cetaceans (Rommel, 1990).

Orbital Region

Lacrimal

The lacrimal [**La**] forms the anterior portion of the orbit. Figure 26 shows the lacrimal in articulation with other bones

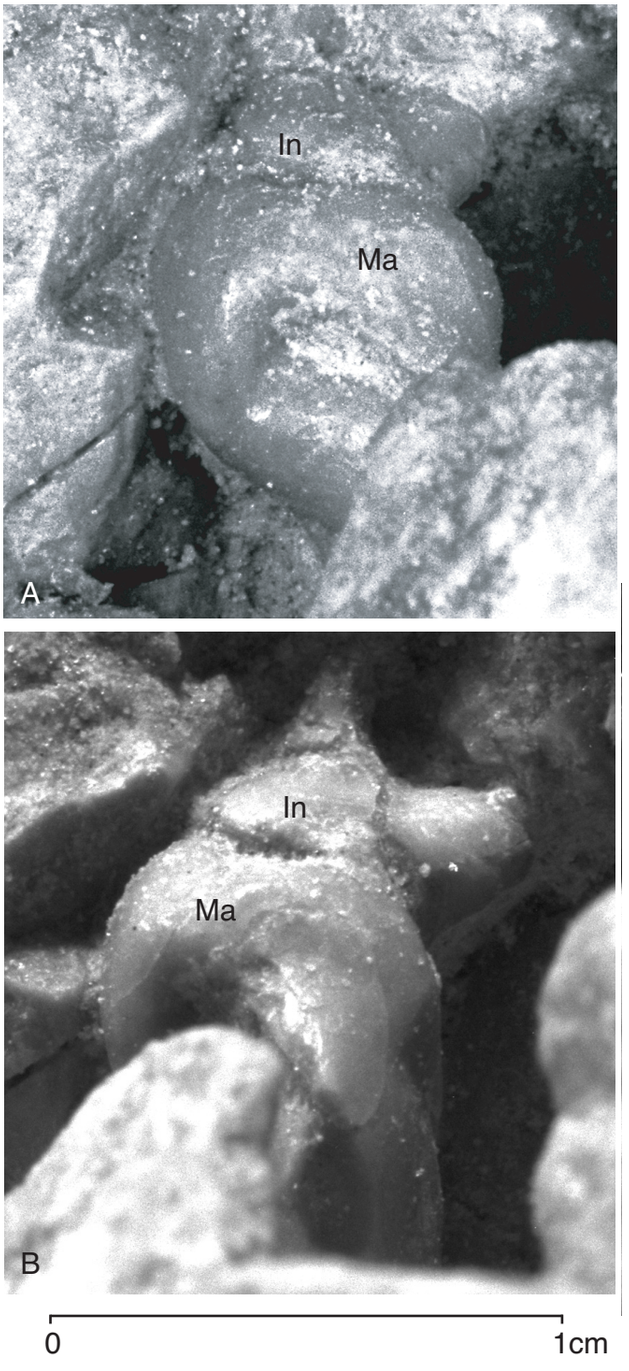

FIGURE 46 — Malleus and incus of *Dorudon atrox* (UM 101222) in place in the skull with the sigmoid process removed. The base of the sigmoid process is at the bottom right of the upper photo and the bottom left of the lower photo. The incus is broken and disarticulated from the malleus. The incus articulates with the stapes medially.

of the posterior face. The lacrimal has a complex three dimensional shape and articulation with adjacent bones of the skull. The posterior surface of the lacrimal forms part of the anterior wall of the orbit. The lateral surface contains three channels that are visible on the side of the skull in lateral view and described in detail below. The medial surface of the lacrimal forms the posterior end of the lateral wall of the internal maxillary foramen. A long process of the lacrimal articulates with the anterolateral border of the frontal. This process is not visible on intact skulls, but has been observed in disarticulated lacrimals. The anteromedial surface of the lacrimal articulates with the maxilla. The ventral surface of the lacrimal articulates with the dorsal surface of the anterior end of the jugal.

There appear to be three separate channels that feed into a single lacrimal canal, which empties into the nasal cavity. The two more ventral channels are somewhat smaller than the larger dorsal channel. The channels are numbered I to III from ventral to dorsal (Figure 26). Channel I connects the ventral edge of the anterior orbit to the lacrimal canal, running roughly parallel to the ventral edge of the lacrimal. Channel II meets the orbit just dorsal to channel I and angles ventrally to meet channel I proximal to the opening of the lacrimal canal. Channel III is much broader than channels I and II and its opening to the orbit is confluent with channel II. Channel III meets with the confluent channels I and II at the anterior edge of the lacrimal, where they enter the lacrimal canal beneath the posterior maxilla.

Jugal

The jugal [**J**, Fig. 35] forms the ventrolateral border of the orbit and much of the zygomatic arch. Anteriorly, it is wedged into the anterior wall of the orbit between the lacrimal on its dorsal surface and the zygomatic process of the maxilla on its ventral surface. The jugal then extends posteriorly, forming the ventral border of the orbit on its dorsal side, and continuing its articulation with the maxilla on its ventral side. At approximately mid-orbit, the maxilla ends and the jugal continues posteriorly. There is an elongate contact between the dorsal surface of the posterior jugal and the ventral surface of the anterior end of the zygomatic process of the squamosal.

The jugal is thickest at its anterior end and it becomes dorsoventrally flattened posterior to its contact with the maxilla. Posteriorly the jugal becomes mediolaterally flat. The posterior end of the jugal becomes dorsoventrally thinner along the articulation with the zygomatic process of the squamosal. Just anterior to the glenoid fossa the jugal comes to a point and ends.

Orbitosphenoid

The orbitosphenoid [**OS**, Fig. 33; also see Andrews, 1906, Plate XXI] is visible in a lateral view of the skull anterior to the optic foramen, ventral and medial to the ventral border of the frontal, and dorsal and medial to the dorsal border of the palatine. The orbitosphenoid forms the medial wall of the groove between the dorsal and ventral orbital crests just described.

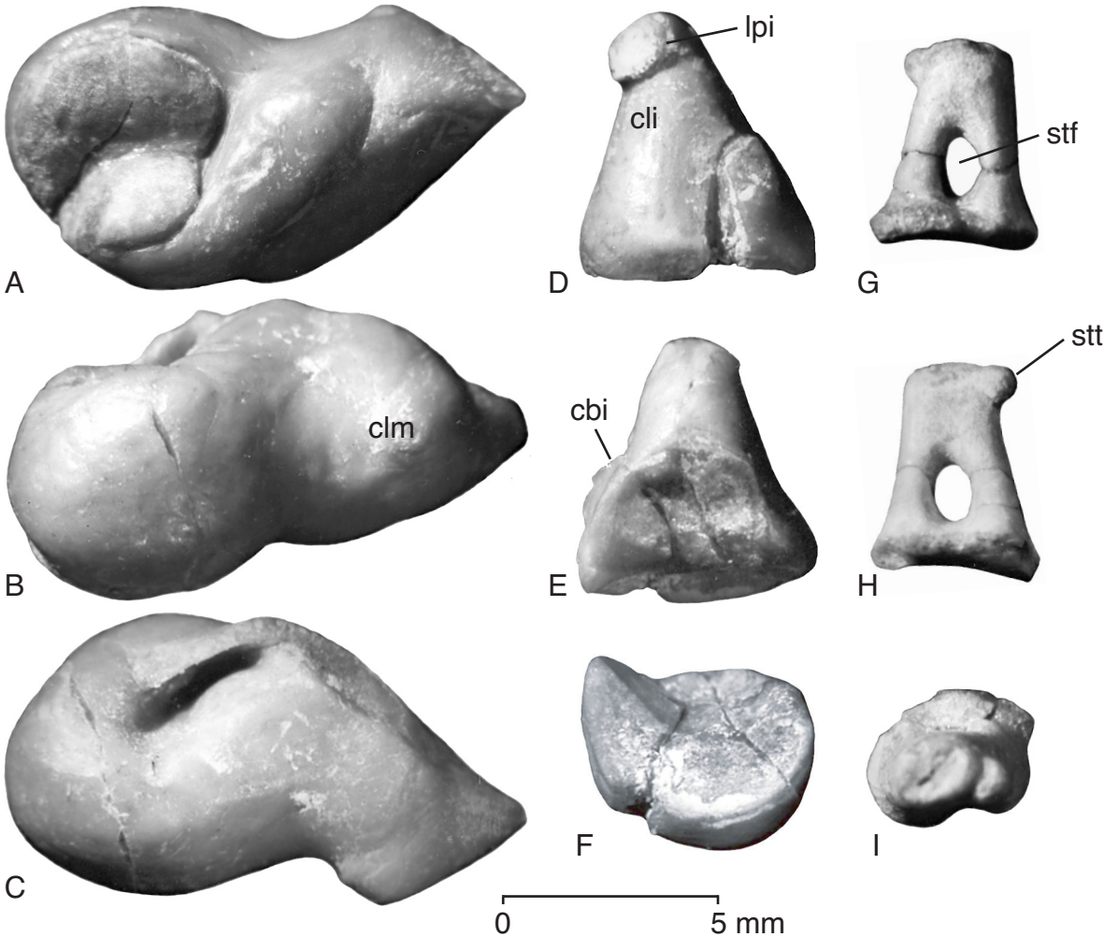

FIGURE 47 — Auditory ossicles of *Dorudon atrox*. A-C, malleus, and D-F, incus, of UM 101222. G-I, stapes of UM 93232. The malleus is shown in A, posteromedial, B, anterior, and C, anterolateral view. The incus is shown in D, dorsolateral, E, ventromedial, and F, malleal articular views. The stapes is shown in G, anterior, H, posterior, and I, incal articular views. The crus breve of the incus is broken and missing.

Orbital region as a whole

Descriptions of the bones that form the orbital region are scattered throughout this section on the skull, since most of the bones are major contributors to other cranial regions, and have only small orbital contributions. Since this region contains many important structures, it is described here in detail as an integrated whole. The bones that significantly contribute to the orbit are: frontal, lacrimal, palatine, jugal, orbitosphenoid and alisphenoid. The orbit is shown in a posterolateral view in Figure 33.

The frontal is broadly expanded over the orbital region into the frontal shield. The lateral edges of the frontal shield form the orbit proper. The anterior edge of the orbit is delimited by the small preorbital process of the frontal, a slightly thickened area along the anterolateral margin of the frontal shield. The posterior edge of the orbit is delimited by the much larger postorbital process of the frontal. The postorbital process is a greatly thickened region of the frontal that projects ventrally from the frontal shield. The area between the preorbital and postorbital processes is much thinner, and arched dorsally.

The anterior margin of the orbit is formed by the lacrimal. The lacrimal has multiple grooves leading from the orbit to the lacrimal canal. The ventral margin of the orbit is formed by the jugal. The jugal articulates with the ventral margin of the lacrimal, and the maxilla extends posteriorly underneath the orbit, ventral to the jugal. The jugal continues posteriorly, beyond the orbital region.

The more medial portion of the orbital region is much more complex. The frontal forms two ridges in the medial orbital region. These are here termed the dorsal orbital crest [**doc**]

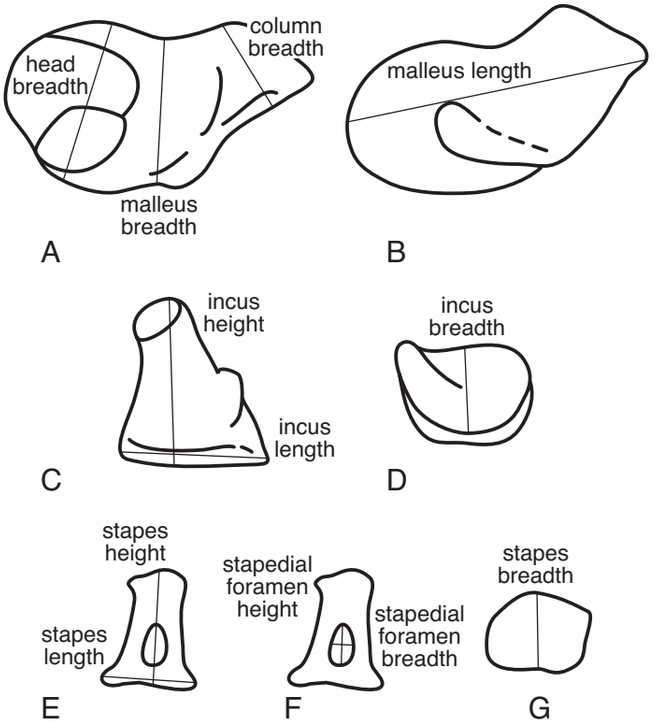

FIGURE 48 — Measurements of auditory ossicles of *Dorudon atrox*. A-B, malleus. C-D, incus. E-G, stapes. Measurement values for the ear ossicles are listed in Table 9.

and ventral orbital crest [**voc**] for ease of reference. The two ridges delimit a space between them that contains a number of important structures, described below from posterior to anterior.

The orbital fissure [**orf**] opens into the posterior orbital region. Posterior to the orbital region the canal which opens at the orbital fissure is covered over by the alisphenoid. The dorsal margin of the orbital fissure is formed by the dorsal orbital crest of the frontal, while the ventral margin of the orbital fissure is formed by the ventral orbital crest. In addition to the optic ridges of the frontal delimiting the dorsal and ventral margins of the orbital fissure, the frontal forms the medial wall of the fissure. This portion of the frontal is a thin layer of bone covering the lateral surface of the presphenoid. The orbital fissure transmitted the ophthalmic nerve (Cr. V_1) to the orbital space.

Anterior to the orbital fissure, the optic foramen [**opf**] opens into the orbit from within the frontal. The optic foramen is a large elongate oval foramen that transmits the optic nerve. The superior and ventral orbital crests continue for a short distance out onto the ventral side of the frontal shield, forming a shallow sulcus for the optic nerve to follow to the orbit proper, to provide special sensory innervation to the eye. Anterior to the optic foramen and close to the ventral orbital crest is another smaller opening, the foramen for the ophthalmic artery. This foramen also opens laterally, and conducts the ophthalmic artery to the eye.

Ventral to the orbital fissure is the foramen rotundum or sphenorbital fissure [**sof**]. This structure is bounded ventrally by the ventral orbital crest. The sphenorbital fissure transmits the maxillary nerve (Cr. V_2), and probably the oculomotor (Cr. III), trochlear (Cr. IV), and abducens (Cr. VI) into the orbital space. The ventral part of the posterior orbital region is formed by the palatine, which reaches far dorsally from the palate. Anteriorly, the palatine meets the frontal. The frontal forms the entire anterior aspect of the orbital region. There is a large foramen in the anterior surface of the orbital region, the internal maxillary foramen [**imf**]. This foramen conducts the maxillary nerve from the orbit to the maxillary canal.

Basicranium

Basioccipital

The basioccipital [**BO**] forms the posterior basicranium (Figs. 36 and 37). The basioccipital articulates anteriorly with the posterior basisphenoid, which is superficially covered by the pterygoids and vomer. The posterior corner of the basioccipital articulates with the exoccipital. This suture is difficult

TABLE 9 — Measurements of auditory ossicles of *Dorudon atrox*. Measurements of the malleus and incus are from UM 101222. Measurements of the stapes are from UM 101223. All measurements are in millimeters. Measurements are shown in Figure 48.

Feature	Length	Breadth	Height
Malleus	11.77	6.42	—
Malleus column	—	4.09	—
Malleus head	—	4.91	—
Incus	5.19	3.74	5.61
Stapes	3.77	—	4.45
Stapedial foramen	—	1.40	2.10

to distinguish in older juveniles and adults, but is readily apparent in very young individuals. The caudalmost projection of the basioccipital extends between the occipital condyles (exoccipitals) and forms the ventral floor of the foramen magnum [**fm**]. The intercondyloid notch is shallow. Internally, the basioccipital forms the floor of the braincase.

The main body of the basioccipital is saddle-shaped. There is a broad trough along the midline formed by the ventrally projecting lateral edges. On the lateral edges are large crests that project ventrally from the basioccipital. These crests are referred to as the lateral process of the basioccipital by Kellogg (1936). Other authors refer to the ventrally flaring lateral edges of the basioccipital in cetaceans as the falcate processes of the basioccipital [**fpr**], or basioccipital crests. Observations on recent and fossil odontocetes support the identification of these structures as primarily basioccipital in origin, but also indicate that the basioccipital crest is formed both from the basioccipital and from a small portion of the exoccipital (Fordyce, 1994).

Juvenile individuals of *Dorudon atrox* show that the jugular notch identified by Kellogg as being between the paroccipital process (of the exoccipital) and the basioccipital crest is entirely contained within the exoccipital. Exoccipitals from individuals that died prior to fusion of the exoccipitals to the basioccipitals and supraoccipital clearly show that both the lateral and medial margins of the jugular notch are formed by the exoccipital.

The endocranial-lateral face of the basioccipital crest forms the medial margin of the posterior lacerate foramen (Fraser and Purves, 1960). The posterior lacerate foramen [**plf**] is a large space delimited by the basioccipital, alisphenoid, pterygoid, periotic, squamosal, and exoccipital. In modern cetaceans, the carotid canal is found in the lateral face of the basioccipital crest (McFarland et al., 1979). There are two grooves in the lateral face of the basioccipital crest in *Dorudon atrox*. The more anterior groove is almost in the form of a canal, but even in the oldest individual known (UM 101215) it is still open. This groove is probably for the carotid artery. Thus, the carotid foramen is also merged with the posterior lacerate foramen.

Basisphenoid

The basisphenoid [**BS**] has no surficial presentation on the basicranium. The shape and contacts of the basisphenoid are described from broken specimens. The basisphenoid is virtually completely covered by the pterygoids and vomer (Fig. 27). The posterior end of the basisphenoid is rather flat like the basioccipital (Fig. 37), while the anterior extension of the basisphenoid is sub-cylindrical (Fig. 36). Its ventral surface is convex on the anterior end, but somewhat narrower than its dorsal surface. The dorsal surface is slightly less convex on the anterior end, and somewhat flattened. The ventral surface is hourglass-shaped in outline. It is broad anteriorly, narrow at the widest extent of the pterygoid sinuses, and broad again posteriorly. The basisphenoid is dorsoventrally thickest at its anteriormost extent and it thins posteriorly. The ventral surface changes from being convex to concave at the widest extent of the pterygoid sinuses. The posterior end of the ventral surface is turned ventrally on its lateral edges, with a broad depression along the midline.

The dorsal surface (endocranial presentation) of the basisphenoid is also hourglass-shaped in outline. The dorsal surface is convex on its anterior half and becomes complexly shaped in the more posterior half. A midline ridge extending dorsally continues from the anterior half to its posteriormost extent. The midline ridge is interrupted at the most constricted point of the hourglass shape by a small depression. This depression is the hypophyseal fossa [**hf**] (= sella turcica) of the basisphenoid. The depression received the ventrally projecting pituitary gland that rests ventral to the brain. Lateral to the midline ridge the dorsal surface is concave on both sides. The lateral edges of the basisphenoid articulate with the squamosal.

The anterior surface is relatively flat and articulates with the presphenoid. The suture between the basisphenoid and presphenoid is almost vertical in orientation. The posterior surface articulates with the basioccipital. The basisphenoid-basioccipital suture is also almost vertical.

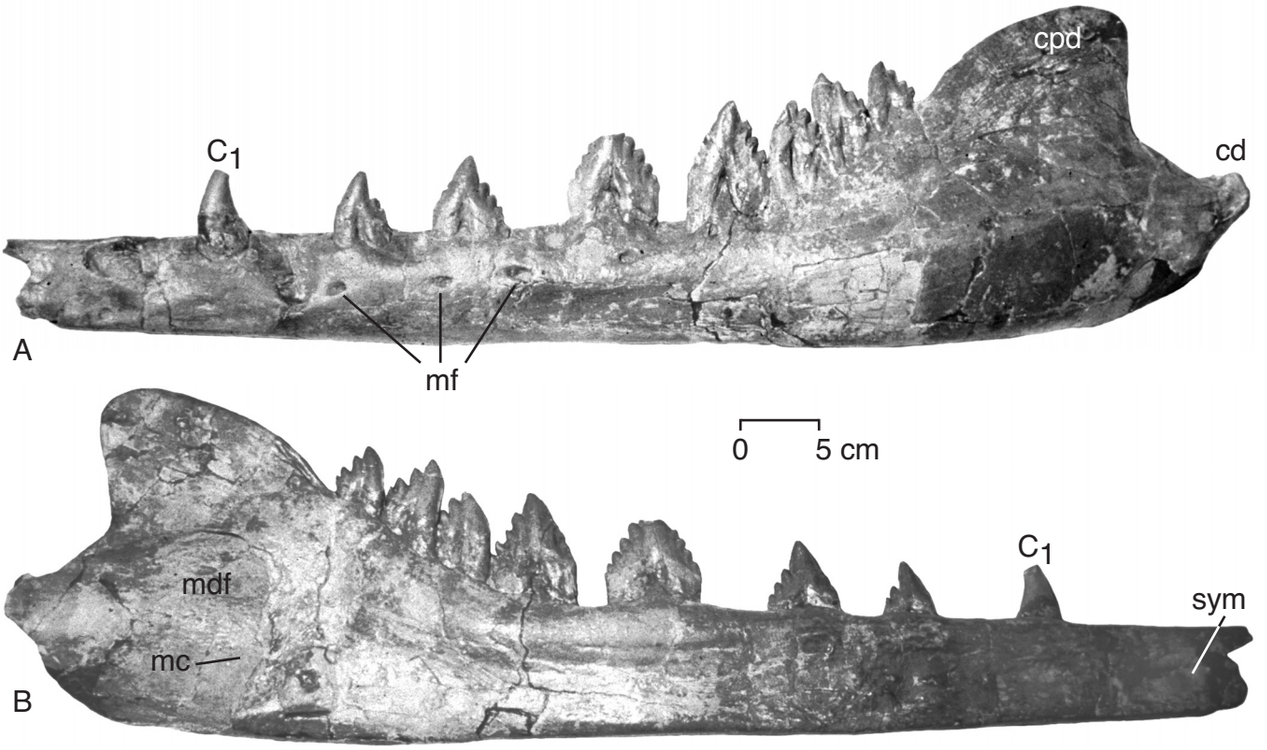

FIGURE 49 — Left dentary of *Dorudon atrox* (NSFM 4451) in A, lateral, and B, medial view. The anterior tip of the dentary is missing and some of the angle is broken. Note the multiple mental foramina on the lateral side and the large mandibular foramen on the medial side of the dentary. Note also the position of the molars on the ascending portion of the dentary.

Supraoccipital

The supraoccipital [**SO**] is a singular midline bone that forms the posterior portion of the braincase and the posterior of the skull (Figs. 38 and 39). The supraoccipital articulates anteriorly with the parietals. The parietal-supraoccipital sutures parallel the nuchal crests, with the parietals forming the anterior face of the crests and the supraoccipitals forming the posterior face of the crests. The supraoccipital articulates ventrolaterally with the exoccipitals. The suture runs diagonally from the foramen magnum to the ventral borders of the nuchal crests. The sutures between the supraoccipital and the basioccipital, as well as that of the supraoccipital and the exoccipitals, are described from juvenile specimens in which the sutures are still open. These sutures are not visible in adult specimens. The ventralmost projection of the supraoccipital forms the dorsal border of the foramen magnum.

The posterior surface of the supraoccipital is extremely concave, with the lateral edges flaring out to form the nuchal crests. In addition, the ventral extension flares out from the center to the edge of the foramen magnum. A pair of nuchal tuberosities are present on the ventralmost supraoccipital dorsal to the foramen magnum. The external occipital crest [**eoc**] arises from the dorsal border of the supraoccipital and continues toward the foramen magnum along the midline about two thirds of the way down the supraoccipital. The crest is highest near the dorsal border, and gradually decreases in height ventrally.

Exoccipital

The exoccipitals [**EO**] are a pair of bones that form the ventral posterior skull and the articulation with the vertebral column (Fig. 38 and 39). The exoccipitals articulate anterolaterally with the squamosal and anteromedially with the parietals. The periotic has a thin wedge-shaped flange connected to the posterior process that extends dorsally between the squamosal and the exoccipital on the lateral extent of the anterior articulation of the exoccipital that is visible posterolaterally. The exoccipitals articulate medioventrally with the basioccipital.

The occipital condyles [**oc**] arise from the medial edges of the exoccipitals. They extend ventrally to the suture with the basioccipital. The occipital condyles surround the foramen magnum and form the articulation with the vertebral column

TABLE 10 — Summary statistics of dentary measurements for adult *Dorudon atrox*. Measurements are shown in Figure 23 and data are listed in Appendix IVC. DL is dentary length. MDI_1 is the mandible depth posterior to I_1. MDC_1 is the mandible depth posterior to C_1. MDP_4 is the mandible depth posterior to P_4. CH is the coronoid height. N, sample size; SD, standard deviation; CV, ratio of the standard deviation to the mean (in percent). All measurements are in millimeters.

Measurement	N	Minimum	Maximum	Mean	SD	CV
DL	1	850.0	850.0	850.0	—	—
MDI_1	1	32.7	32.7	32.7	—	—
MDC_1	5	53.0	68.8	58.7	6.4	10.9
MDP_4	4	79.3	92.5	85.4	6.4	7.5
CH	1	218.0	218.0	218.0	—	—

via the atlas. Lateral and ventral to the occipital condyles, two processes of the exoccipital form the borders of the jugular notch [**jn**], which is between them. The more medial process is the posterior (exoccipital) portion of the basioccipital crest. The more lateral process is the paroccipital process [**papr**]. Just lateral to the paroccipital process is a posterior flare of the exoccipital that forms a small arch of bone with a depression on its ventral surface for articulation with the stylohyal. The anterior face of the paroccipital process contains a fossa that is an extension of the pterygoid sinus.

The lateral portions of the exoccipitals form the posterior face of the skull. The lateral edges are broadly scalloped, and they do not extend as far laterally as the squamosals, leaving the posterior faces of the squamosals partially exposed. These scalloped edges may be sites of muscle origins or insertions.

Alisphenoid

The alisphenoid [**AS**] forms the ventral portion of the lateral wall of the mesocranium. The alisphenoid is lateral to the tracts for the ophthalmic and maxillary divisions of the trigeminal nerve (V_1 and V_2). The alisphenoid is visible in the lateral view of the skull where it forms the medial wall of the temporal fossa. The alisphenoid forms the anterior third of the lateral border and the roof of the pterygoid sinus fossa. The alisphenoid is excluded from the border of the foramen pseudo-ovale and does not contribute to the border of the foramen ovale proper.

The dorsal border of the alisphenoid fuses with the frontal anteriorly and the parietal posteriorly. The sphenoparietal suture slopes posteriorly and ventrally, to the anterior end of the subtemporal crest. This complex suture continues down the lateral side of the skull and turns anteriorly, where the squamosal meets the pterygoid. The pterygosphenoid suture trends anteriorly. Just ventral to the pterygosphenoid suture, and just anterior and dorsal to the end of the subtemporal crest, there is an elongated, roughly-oval depression in the surface of the alisphenoid. The pterygosphenoid suture continues anteriorly until the pterygoid meets the palatine. Here the pterygosphenoid suture arches dorsally until the suture meets the orbital fissure and ends.

Squamosal

The squamosal [**Sq**] forms the posterolateral wall of the side of the skull (Fig. 34 and 37). The squamosal articulates anteriorly with the parietal on the dorsal side and meets the alisphenoid on the ventral side as described above. On its ventral side, the squamosal has a complex relationship with the periotic described below. The posterior face of the squamosal is plane-sutured to the anterior face of the exoccipital. Together these bones form the lateral portion of the nuchal crest. The occipitosquamous suture is in a groove between these bones that extends up the middle of the nuchal crest. The crest and the suture continue medially and then turn abruptly dorsally where the squamosal meets the parietal. The squamous suture turns anteriorly across the anterolateral face of the nuchal crest and then turns ventrally to meet the alisphenoid. The squamosal is expanded into the subtemporal crest, which flows into the glenoid fossa posteriorly and decreases in prominence anteriorly. The squamosal meets the alisphenoid at the anterior end of the crest. Just ventral to the crest and approximately in line with the anterior end of the auditory bulla is the foramen pseudo-ovale [**fpo**] where the mandibular nerve (Cr. V_3) exited the skull.

The squamosal projects laterally from the side of the skull forming the zygomatic process of the squamosal [**z**]. The zygomatic process turns anteriorly and becomes laterally flattened. The zygomatic process is dorsoventrally thickest just anterior to the glenoid fossa. The zygomatic process becomes dorsoventrally thinner more anteriorly. Just anterior to the glenoid fossa, it begins its articulation with the jugal. The jugal articulates with the ventral side of the zygomatic process, but the two bones remain free along their entire articular surface. The zygomatic process thins dorsoventrally farther anteriorly and terminates approximately half way down the length of the jugal.

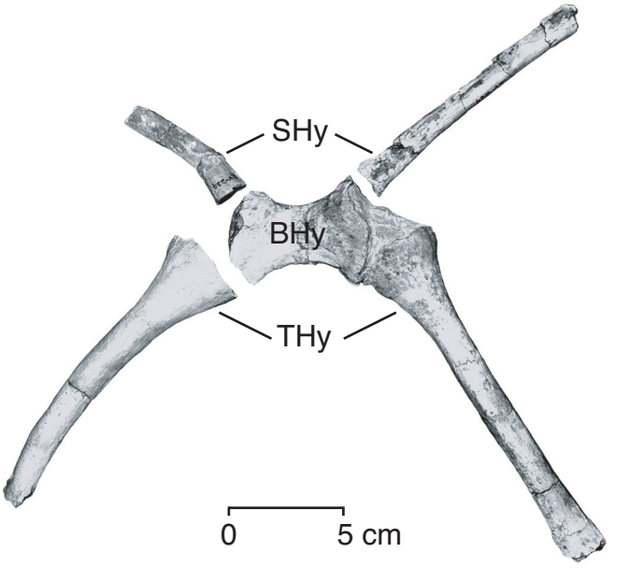

FIGURE 50 — Hyoid apparatus of *Dorudon atrox* (UM 101222), in anteroventral view. The thyrohyals were found semi-articulated with the basihyal here, while the stylohyals were found nearby. The hyoid apparatus is shown spread out, but it was probably articulated as shown in the reconstruction in Figure 5. Articular surfaces of the hyoid elements indicate former cartilaginous connections.

The glenoid fossa [**gf**] is found on the posterior end of the zygomatic process of the squamosal, just posterior to where it turns anteriorly. The glenoid fossa is the articular surface for the dentary. The articular surface extends anteriorly along the ventral side of the process to a point just posterior to the end of the jugal. A large vertical postglenoid process [**pgp**] extends ventrally from the zygomatic process.

The falciform process of the squamosal [**fps**] projects anteroventrally from the main body of the squamosal. It is visible on the skull in a lateral view, just anterior to the auditory bulla. The posteroventral surface of the falciform process is closely applied to the anterodorsal surface of the tympanic bulla. Much of the medial surface is in contact with the anterior process of the periotic. The tip of the process is singular and the anterior end touches the posterior end of the pterygoid.

There is no postglenoid foramen in archaeocete cetaceans. Venous drainage is entirely through the jugular and other veins passing out of the cranial cavity via the posterior lacerate foramen. There is a small foramen just medial to the postglenoid process that is inside an ovate depression. This foramen may be homologous with the postglenoid foramen, but it does not continue through the bone. Just posterior to the postglenoid process is the external auditory meatus [**eam**]. There is a groove between the postglenoid process and posterior meatal crest. This crest articulates with the posterior process of the periotic.

Periotic

The periotic [**Per**] forms the portion of the basicranium that surrounds the inner ear and forms the medial boundary of the middle ear (Figs. 37, 40-42). The periotic is usually divided into two portions, the petrosal and the mastoid. The petrosal (anteromedial) portion of the periotic is very dense and houses the inner ear. The mastoid region is much less expansive than the petrosal portion in archaeocetes, so much so that the division into two distinct portions is somewhat arbitrary. The less dense posterior process of the periotic extends posteriorly from the petrosal portion to articulate on its ventral surface with the posterior process of the auditory bulla (described below). In addition, a thin plate-like projection from the dorsum of the posterior process of the periotic is sandwiched between the squamosal anteriorly and the supraoccipital posteriorly. Kellogg (1936) provides a good description of the periotic of *Zygorhiza* for comparison with *Dorudon*, and Luo and Gingerich (1999) provide descriptions of the periotics of many archaeocetes, including *Dorudon*.

A more helpful way to divide the archaeocete periotic for discussion is to divide it into the body and three processes. The processes are anterior, posterior, and superior, described below following a description of the body of the periotic.

Body of the periotic and its foramina

The body is in the center of the periotic and contains the inner ear and the main foramina of the periotic (Fig. 40B). The body projects ventrally from the base of the skull. It is roughly semicircular in outline when viewed from the dorsomedial or ventral sides. Its anterior surface has gently raised dorsomedial and ventral edges, forming a broad sulcus down its midline. The ventral eminence is the pars cochlearis [**pcp**] of the periotic. It covers the bony cochlea within the periotic. The ventral face of the body of the periotic contains a groove running roughly anteroposteriorly. The groove is located at the base of the body, anterior to the fenestra ovalis and medial to the fossa for the head of the malleus. Kellogg (1936) identified this as the groove for the tensor tympani muscle in *Zygorhiza kochii*. Lancaster (1990) stated (incorrectly) that the tensor tympani runs in the same groove as the facial nerve. These structures are clearly separated in *Dorudon atrox*, as well as in Kellogg's (1936, p. 116, fig 35a) figure of the periotic of *Z. kochii*. The foramina of the dorsomedial, ventral, and posterior faces are discussed below.

The body has some accessory structures directly associated with it. The largest of these is the fossa for the head of the malleus [**fhm**], located on the ventral side of the body. The fossa is an almost circular concavity that faces ventrally and slightly posteriorly. It projects from the main portion of the body just anterior to the fenestra ovalis. The head of the malleus rests in the concavity when the malleus is in articulation with the periotic.

The internal auditory meatus [**iam**] is the most prominent structure on the dorsomedial (endocranial) side of the periotic (Fig. 40C). It is a large concavity that houses multiple foramina for the facial nerve (Cr. VII) and the primary branches of the

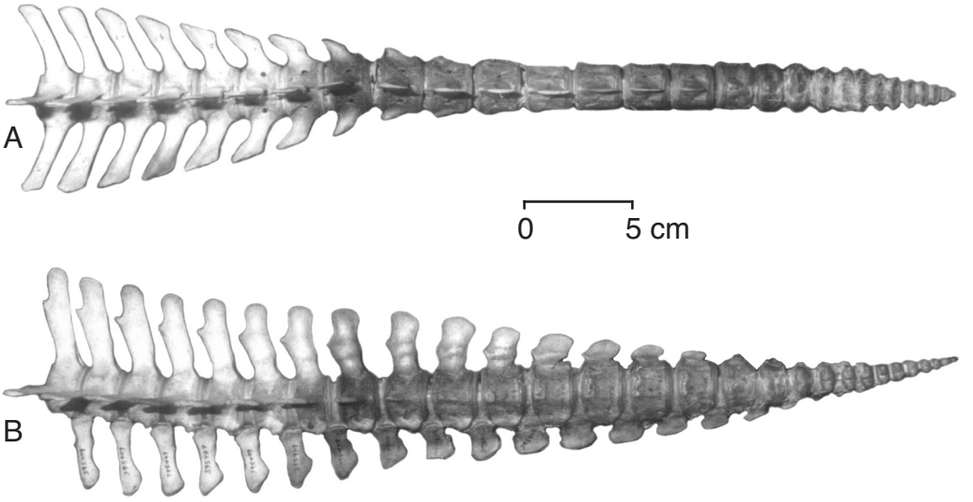

FIGURE 51 — Caudal vertebrae and chevrons of *Stenella attenuata* (USNM 395409) in A, dorsal, and B, lateral view. Caudal vertebrae at the left are very similar to the posterior lumbar vertebrae: these are the anterior caudals. Caudal vertebrae in the middle are very tall relative to their widths: these are the peduncular caudals. Caudal vertebrae at the right are very wide relative to their heights: these are the posterior caudals.

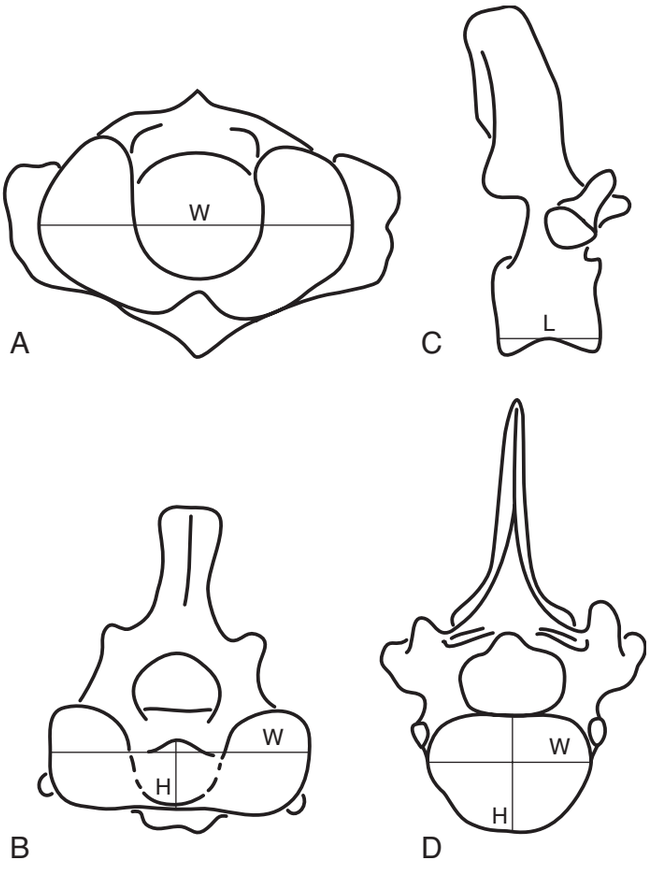

FIGURE 52 — Vertebral measurements of *Dorudon atrox*. A, atlas. B, axis. C, representative thoracic vertebra, in lateral view. D, representative thoracic vertebra, in cranial view. Measurement values for vertebrae of *D. atrox* are listed in Appendix V.

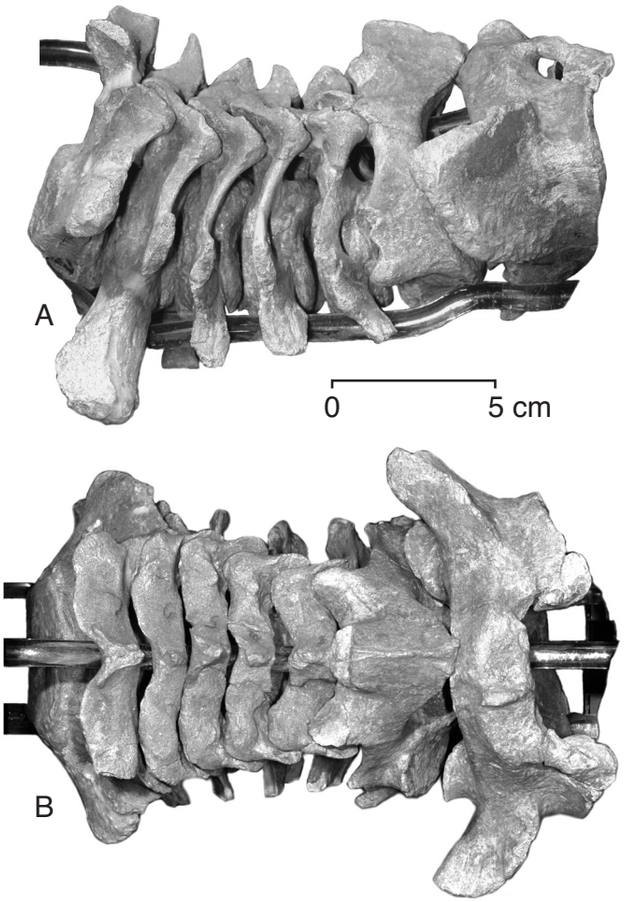

FIGURE 53 — Cervical vertebrae of a juvenile *Dorudon atrox* (UM 93220) in A, lateral, and B, dorsal view. The neural spines of C2 and C7 are both broken. Note the slight curvature of the neck when the vertebrae are articulated, and a broadening of the dorsal surface of the neural arches from C2 to C7.

vestibulocochlear nerve (Cr. VIII). The largest of the foramina is the most posterior, and it is slightly ventral relative to the two smaller foramina. This large foramen is separated from the other foramina by a thin ridge of bone known as the transverse septum. The large foramen is for the cochlear portion of the vestibulocochlear nerve (Cr. VIII, cochlear nerve). Kellogg (1936) called this structure the tractus spiralus foraminosus with a "foramen centrale at its anterior end." Here it is simply identified as the tractus spiralus foraminosus [**tsf**]. Anterior and dorsal to the transverse septum are the facial canal and the canal for the vestibular canal. The more anterior of these foramina is for the facial nerve, while the more posterior is for the vestibular nerve. Kellogg (1936) called the foramen for the facial nerve the "internal aperture of the aqueductus Fallopii", while he called the foramen for the vestibular nerve the foramen singulare in his discussion of the periotic of *Zygorhiza kochii*. The facial canal is slightly larger than the vestibular canal.

Also present on the dorsomedial surface of the body of the periotic are the openings to the perilymphatic duct and endolymphatic duct. Both of these openings are posterior to the internal auditory meatus, with the perilymphatic duct placed ventral to the endolymphatic duct. They are separated from the internal auditory meatus by a moderately sized protuberance that projects medially. The opening to the perilymphatic duct is very small compared to the other foramina on the endocranial surface of the periotic. The opening to the endolymphatic duct is deep within a much larger fossa.

The fenestra ovalis [**feo**] is present on the ventral side of the body of the periotic (Fig. 40A). The fenestra ovalis is the shape of a nearly equant oval, with its long axis angling dorsally on its cranial and ventrally on its caudal end. The fenestra ovalis lodges the footplate of the stapes and forms the entrance to the vestibule of the inner ear cavity. Neither the fenestra ovalis nor the head of the stapes is visible when viewing the periotic down the external auditory meatus. They are both slightly posterior to the proximal end of the external auditory meatus. The margins of the fenestra ovalis are all rounded, and the canal narrows slightly as it extends into the periotic. Three specimens of

TABLE 11 — Summary statistics for cervical vertebra measurements of *Dorudon atrox*. Measurements are shown in Figure 52 and are listed in Appendix V. L is ventral centrum length. W is cranial centrum breadth. H is cranial centrum height. N, sample size; SD, standard deviation; CV, ratio of the standard deviation to the mean (in percent). All measurements are in millimeters.

Vertebra	Dimension	N	Minimum	Maximum	Average	SD	CV
C1	L	1	40.9	40.9	40.9	—	—
	W	2	115.7	137.3	126.5	15.3	12.1
	H	1	22.0	22.0	22.0	—	—
C2	L	2	34.6	39.6	37.1	3.5	9.5
	W	1	110.1	110.1	110.1	—	—
	H	2	32.9	33.4	33.2	0.4	1.1
C3	L	2	25.0	26.9	26.0	1.3	5.2
	W	1	66.7	66.7	66.7	—	—
	H	1	61.6	61.6	61.6	—	—
C4	L	4	23.4	28.0	25.5	2.0	7.7
	W	3	56.7	65.2	61.3	4.3	7.0
	H	3	56.3	59.0	57.4	1.4	2.4
C5	L	5	23.0	30.0	25.5	3.0	11.6
	W	3	59.2	69.2	64.1	5.0	7.8
	H	3	56.4	62.3	58.8	3.1	5.3
C6	L	4	24.6	34.0	29.4	4.0	13.7
	W	2	61.0	71.1	66.1	7.1	10.8
	H	2	61.0	61.5	61.3	0.4	0.6
C7	L	4	25.7	31.0	28.4	2.5	8.8
	W	2	67.9	73.0	70.5	3.6	5.1
	H	1	58.7	58.7	58.7	—	—

Dorudon atrox have the stapes in place in the fenestra ovalis (UM 93232, UM 101222, UM 101223). The fenestra ovalis opens into the vestibule of the inner ear, which in turn communicates with the basal turn of the cochlea.

In addition to the fenestra ovalis, the ventral face of the body of the periotic also contains the ventral opening of the facial canal. Kellogg (1936) calls this structure the "epitympanic orifice of the aqueductus Fallopii." It is a small foramen that is situated between the main portion of the body and the fossa for the head of the malleus. It opens posteriorly into a well-defined groove that runs posteriorly, dorsal to the fenestra ovalis. The path of the facial nerve is completely outlined in the following chapter on reconstructed soft anatomy.

The fenestra rotunda [**fer**] is located on the ventroposterior face of the body of the periotic. The fenestra rotunda has the shape of an elongate and irregular oval, with its long axis oriented roughly anteroposteriorly. The fenestra rotunda communicates between the inner ear cavity and the middle ear cavity. The secondary tympanic membrane covers the fenestra rotunda in life, so no structures are transmitted through this opening.

Internal structures of the periotic

The body of the periotic houses the cochlea, semicircular canals, and the vestibule that connects them. In addition, the body houses the endolymphatic duct system, the facial canal, and the canals for the cochlear and vestibular nerves. The interior structure of the periotic was studied using broken specimens and computed tomography (CT) scans of the otic region.

The bony cochlea [**ch**] is situated slightly medial, anterior, and ventral to the fenestra ovalis, internal to the pars cochlearis of the periotic. The cochlea goes through $2^1/_2$ turns (Figs. 41 and 42). A serially sectioned *Dorudon atrox* (?) periotic shows a cochlea that has slightly less than two turns in the cochlea, which may indicate some variability of this feature (Luo and Gingerich, 1999). The turns of the cochlea appear to be coaxial, rather than offset as in a squalodontid investigated by Luo and Eastman (1995). The primary bony lamina is visible in one specimen (UM 101223). It is found extending out from the axis of coiling. It is thin, and slightly upturned along its inner edge. The secondary bony lamina is also visible in the basal turn of the cochlea. The basal turn of the cochlea (as possibly are the other turns, which are not as easily viewed) is underlain by bone with a spongy texture. It is filled with interconnected cellular spaces separated by bony struts.

The basal turn of the cochlea connects to a large vestibule [**vst**]. The vestibule communicates with the middle ear via the fenestra ovalis. The stapes inserts into the fenestra ovalis when it is properly articulated. Based on the same serially-sectioned

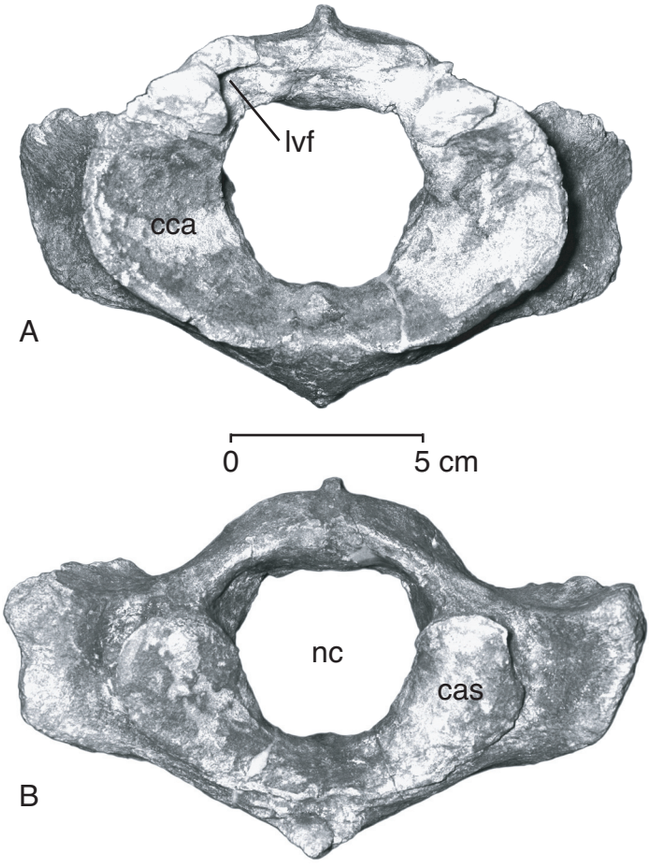

FIGURE 54 — First cervical vertebra (C1) of a juvenile *Dorudon atrox* (UM 93220) in A, cranial, and B, caudal view.

specimen mentioned above, the vestibule and the semicircular canals [**scc**] are very reduced in *Dorudon*, as is true in *Basilosaurus* (Luo and Gingerich, 1999) and modern cetaceans.

Processes of the periotic

The anterior process of the periotic [**app**] extends anteriorly and slightly ventrally from the body. It is a broad plate of dense bone that comes to a rounded apex. The anterior process runs parallel to a process of bone on the squamosal, with a deep cleft remaining between them.

The posterior process of the periotic [**ppp**] mentioned above projects posteriorly and laterally away from the body. Its ventral surface is teardrop- to oval-shaped, with the apex of the teardrop pointing toward the body of the periotic. The ventral surface is covered with series of shallow grooves that are parallel to the long axis of the oval surface. These grooves of varying depth interlock with tongues on the dorsum of the posterior process of the auditory bulla. The anterior side of the proximal end of the posterior process of the periotic meets the posterior edge of the external auditory meatus discussed below. At the ventral surface of the anterior side of the proximal end is a small lip of bone that projects anteriorly into the cavity of the meatus. Kellogg (1936) identified the area dorsal to this overhang as the site of origin of the stapedial muscle. Although this lip is present in most specimens (it is easily broken off, so it is missing in some), it is difficult to determine if this spot is truly a site of muscle attachment. The distal margin of the posterior process of the periotic is visible in the posterolateral wall of the skull.

The third process is the superior process of the periotic [**spp**]. The superior process is a curved plate-like projection from the body of the periotic. It extends somewhat dorsally and curves medially from the body, forming a broad concavity on its endocranial surface. The superior process is dorsal to the internal auditory meatus.

Foramina and structures around the periotic

The external auditory meatus [**eam**, Fig. 40] is a simple groove that is open ventrally. The dorsal margin of the external auditory meatus is formed from the squamosal and meets the dorsal surface of the posterior process of the periotic. The anterior wall and the roof of the external auditory meatus are

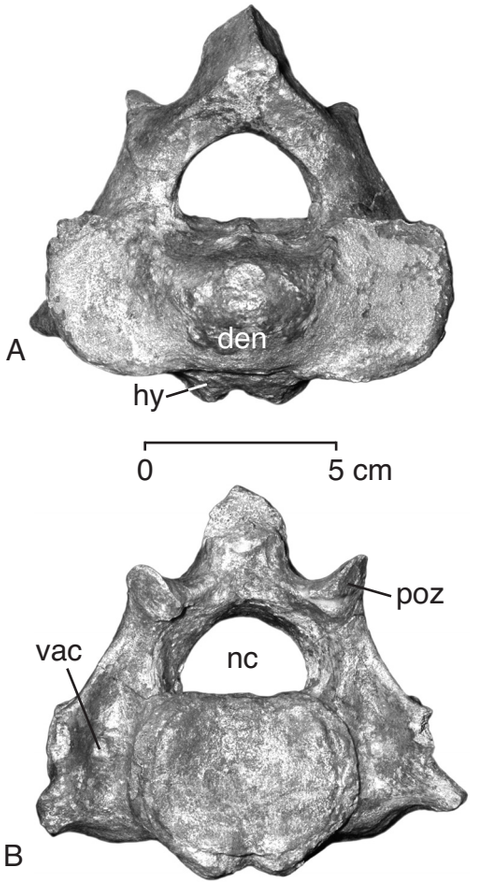

FIGURE 55 — Second cervical vertebra (C2) of a juvenile *Dorudon atrox* (UM 93220) in A, cranial, and B, caudal view. Note that the neural spine is broken in this specimen.

formed from the posterior edge of the postglenoid process of the squamosal. The posterior border of the external auditory meatus is formed by the posterior meatal crest of the squamosal. The posterior border of the crest contacts the anterior border of the posterior process of the periotic.

The posterior lacerate foramen is not separate from the carotid foramen and the foramen ovale. The anterolateral border is formed by the squamosal and alisphenoid, the anteromedial border by the pterygoid, the ventral border by the periotic, and the posterior border by the exoccipital. Thus, the posterior lacerate foramen extends from the posterior edge of the pterygoid sinus (at the posterior border of the basicranial presentation of the squamosal) to the posterior edge of the basicranium at the jugular notch of the exoccipital. The posterior lacerate foramen is partially covered by the medial auditory bulla.

Numerous structures are thought to pass through the posterior lacerate foramen. The facial nerve (Cr. VII) and the vestibulocochlear nerve (Cr. VIII) travel through the posterior lacerate foramen as they extend from the base of the brain to the internal auditory meatus of the periotic. In addition the glossopharyngeal (Cr. IX), vagus (Cr. X), and accessory (Cr. XI) nerves all exit the cranial cavity through the posterior lacerate foramen. The jugular vein leaves the braincase through the posterior end of the posterior lacerate foramen and continues caudally through the jugular notch of the exoccipital.

Ectotympanic

The auditory bulla [**ab**] of *Dorudon atrox* is a very complex and highly derived structure. The auditory bulla is composed of extremely dense compact bone. The bulla is formed from an ossification center that is separate from the basicranium. The auditory bulla of modern cetaceans is usually referred to as a "tympanic bulla" (*e.g.*, Fraser and Purves, 1960), but it is not clear from this term whether the bulla is entotympanic or ectotympanic in origin. Novacek (1977) lists the Cetacea as having ectotympanic bullae according to Van Beneden and Gervais (1880) and Kellogg (1928). (Note that Novacek's table 2, p. 138, which includes Cetacea, is mislabeled as those taxa that have entotympanic rather than ectotympanic bullae.) A clear statement of the homology of the cetacean auditory bulla is made by Ridewood (1923) who studied the fetal development of mysticete skulls "There is no endotympanic [entotympanic]... the structure known as the tympanic bone in the Whale arises solely by the increase in size of the original annulus tympanicus." Odontocetes as well are known to develop the auditory bulla from the ectotympanic based on studies of skull development (Eales, 1950). Based on these studies, the auditory bulla of *D. atrox* is here identified as ectotympanic in origin.

The overall shape of the main body of the auditory bulla is a little like a cowry shell (Figs. 42-44). It is generally ovate, convex, and continuous on the ventral surface, and has a deeply excavated space on its dorsal (cranial) surface. When describing the auditory bulla, the side facing the skull will be referred to as cranial to facilitate orientation relative to the skull.

The smooth convexity of the ventral surface is interrupted by a shallow sulcus originating near the posterior border and shallowing toward the center of the bulla. Just lateral to the sulcus is a low, smoothly rounded eminence. Medial to the sulcus is a large bolus of bone that is the posterior part of the medial wall of the bulla. This medial wall is known as the involucrum [**inv**] of the bulla. The involucrum is much thicker than the lateral wall of the bulla. Since the lateral wall of the bulla is so thin, many specimens have the lateral wall broken off the more robust involucrum and ventral wall of the bulla. The cranial surface of the bulla is divided by the tympanic cavity [**tc**] into the involucrum on the medal side and the lateral wall on the lateral side. The tympanic cavity is an elongate space that houses the middle ear ossicles. The space is widest at the anterior end and narrows toward the posterior end of the bulla.

The lateral wall of the bulla presents three separate processes that will be described from anterior to posterior. The anteriormost process of the auditory bulla is the sigmoid process [**sp**]. The sigmoid process originates on the ventrolateral

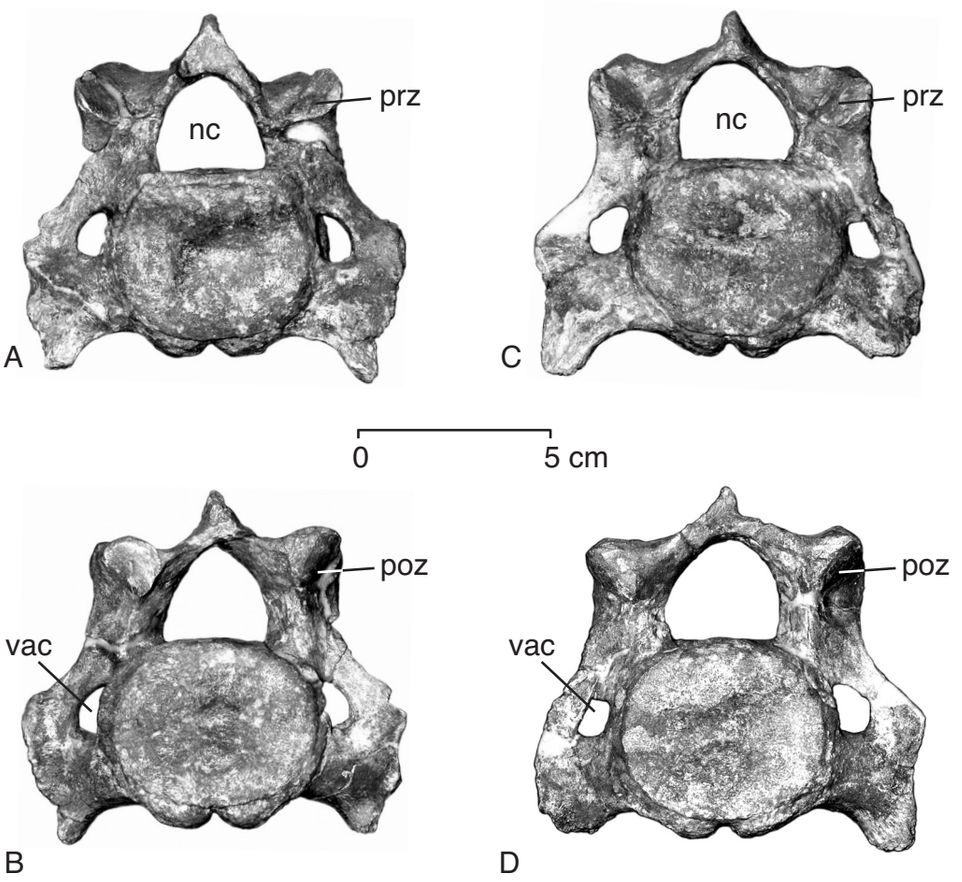

FIGURE 56 — Third and fourth cervical vertebrae (C3 and C4) of a juvenile *Dorudon atrox* (UM 93220). A-B, C3 in cranial and caudal views; C-D, C4 in cranial and caudal views.

side of the bulla, curves posteriorly and projects cranially along the lateral surface of the bulla. The sigmoid process has been identified by Lancaster (1990) as the homologue of the anterior limb of the ancestral U-shaped (ecto-) tympanic. The sigmoid process is large and well-developed in *Dorudon atrox*. The sigmoid process supports the anterior portion of the tympanic membrane. The body of the sigmoid process is very thick along the lateral margin, and very thin over much of its surface and toward the body of the bulla.

The conical process [**cop**] is a small eminence posterior to the sigmoid process. This process has also been called the conical apophysis or the median process (Kellogg, 1936; Lancaster, 1990). The conical process is separated from the body of the sigmoid process by a shallow groove. The conical process itself is very small when compared to any of the other bullar processes. It projects slightly anteriorly and cranially. The conical process supports part of the ventral portion of the tympanic membrane.

The last process on the bulla is the posterior process of the auditory bulla [**ppb**]. The posterior process bridges the posterior cleft. Kasuya (1973) calls this the elliptical foramen in modern cetaceans. The elliptical foramen opens from the posterior surface of the bulla into the tympanic cavity. The posterior process is attached to the medial side of the elliptical foramen by a thin strut of bone termed the internal pedicle of the posterior process [**ipp**]. The posterior process also attaches to the lateral side of the elliptical foramen via the external pedicle of the posterior process. The posterior process of the auditory bulla is a "slipper-shaped" projection of bone that articulates with the posterior process of the periotic. The cranial surface of the posterior process of the auditory bulla has numerous grooves on it running parallel to its long axis. These grooves articulated with similar ridges on the posterior process of the periotic, thus very loosely attaching the bulla to the basicranium.

Malleus

The malleus [**Ma**, Figs. 45-47] is the most lateral bone in the ossicular chain of the middle ear. It is similar in appearance to the malleus of other basilosaurid archaeocetes

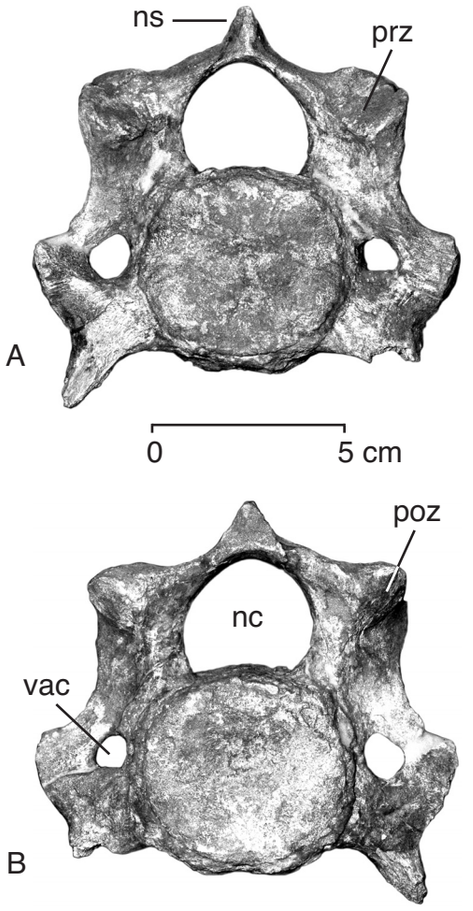

FIGURE 57 — Fifth cervical vertebra (C5) of a juvenile *Dorudon atrox* (UM 93220) in A, cranial, and B, caudal view.

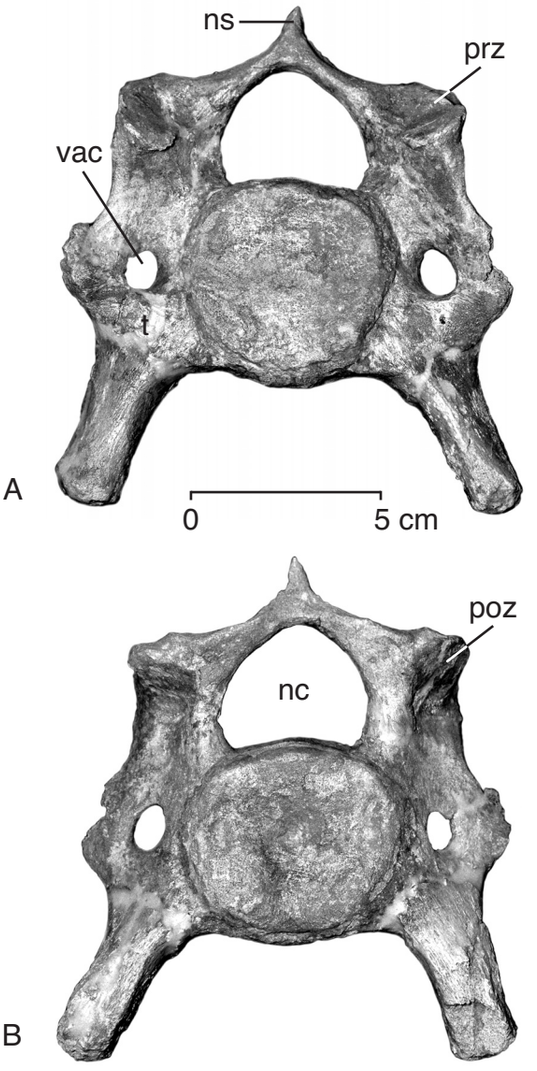

FIGURE 58 — Sixth cervical vertebra (C6) of a juvenile *Dorudon atrox* (UM 93220) in A, cranial, and B, caudal view. Note the very large, ventrally projecting transverse processes when compared to other cervical vertebrae.

(Pompeckj, 1922; Lancaster, 1990). Measurements taken on the auditory ossicles of *Dorudon atrox* are listed in Figure 48. Summary statistics for the measurements of *D. atrox* ossicles are shown in Table 9. The malleus is fused with the sigmoid process of the bulla and it articulates with the periotic. Lancaster (1990) indicates that the malleus of *Zygorhiza kochii* is "firmly attached" to the auditory bulla by the gonial process. Pompeckj (1922) also shows the malleus of *Saghacetus osiris* attached to the bulla. The gonial process is present on the malleus of UM 101222 (Fig. 47A and C), but it may be slightly broken. The nature of the articulation of the malleus and the auditory bulla is not apparent, since the single malleus known of *Dorudon atrox* (UM 101222) was recovered from an individual with most of the auditory bulla, including the sigmoid process damaged. The original association of the malleus and the fragmented and reassembled sigmoid process can be seen in Figure 45. Both the sigmoid process and the ossicular chain appear to be displaced from their life positions, but the gonial process is in contact with the sigmoid process. It is not clear how the malleus and auditory bulla contacted in *D. atrox*. Lancaster (1990) indicates that the gonial process of the malleus of *Zygorhiza kochii* articulates with the auditory bulla just anterior and medial to the sigmoid process. This may also be the case for *D. atrox*.

The malleus of *Dorudon atrox* is similar to those of *Basilosaurus cetoides* and *Zygorhiza kochii*, as illustrated and described by Lancaster (1990). The malleus is divided into two portions, the more lateral head [**hm**], that articulates with the sigmoid process and the fossa for the head of the malleus

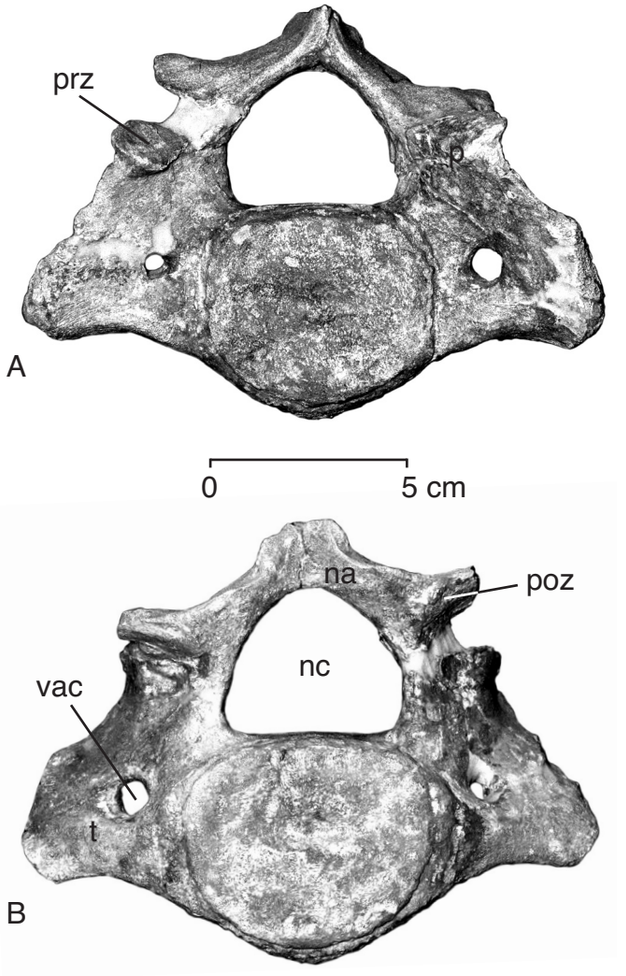

FIGURE 59 — Seventh cervical vertebra (C7) of a juvenile *Dorudon atrox* (UM 93220) in A, cranial, and B, caudal view. Note the broadly expanded transverse processes.

on the periotic, and the more medial column [**clm**], which supports the gonial process. The ventromedial side of the head forms the articular surface for the incus. The articular surface is roughly in two planes oriented perpendicular to one another. Lancaster (1990) described these as two articular surfaces, but there is no break between them. One of the surfaces is kidney-shaped. The other more round and markedly convex.

The column of the malleus extends ventrally and posteriorly from the head. The column has two prominent tubercles. One is directed ventrally, and is the ventralmost point on the malleus. This process attaches to the tympanic conus in modern cetaceans, and has been hypothesized to do so in archaeocetes as well (Lancaster, 1990). The tympanic conus is primitively the center of the tympanic membrane, which is stretched into a cone-shaped structure in modern cetaceans (Fleischer, 1973). The other process is on the anteromedial side of the column. This process projects just anteromedially to the fossa for the head of the malleus when the malleus is in articulation with the periotic. Lancaster (1990) described a pit near this position that is the insertion for the tensor tympani muscle. There is a very small depression just lateral to the anteromedial process that may be the pit for the tensor tympani.

Incus

The incus [**In**, Figs. 45-47] of *Dorudon atrox* is the middle bone in the middle ear ossicular chain. It is generally pyramidal in shape narrowing from the base, where it articulates with the malleus, to the apex, where it articulates with the stapes. The articular surface for the malleus is concave and saddle-shaped. This articular surface is located at the broad end of the pyramidal incus. Lancaster (1990) described two articular surfaces on the incus for articulation with the malleus. Here it appears that there is a single, articular surface that laps onto both the lateral and ventral sides of the incus. One of the surfaces is kidney-shaped, and it articulates with the similarly-shaped surface on the malleus. The other surface is more oval. Both are concave, but the oval surface is much more concave, and it articulates with the convex articular surface on the malleus.

The body of the incus is continuous with the crus longum [**cli**], which extends posteriorly and slightly medially from the base and body. The crus longum ends in a small lenticular process [**lpi**] that supports the articular surface for the stapes. This surface is oval in shape and generally flat. The articular surface for the stapes is twisted medially and posteriorly from the apex of the incus. The crus breve [**cbi**] arises from the body of the incus near the base and projects dorsally. The crus breve is broken off at the base in the only known incus of *Dorudon atrox* (UM 101222), so its shape and length are unknown.

Stapes

The stapes [**S**, Fig. 41 and 47] is the last bone in the ossicular chain. It articulates with the incus and the fenestra ovale of the periotic. The stapes is tall, with an oval-shaped stapedial foramen [**stf**]. The apex articulates with the lenticular process of the incus [**lpi**]. The articular surface is oval in shape. The footplate of the stapes at it base is a much larger oval, and fits into the fenestra ovale. It is flat to slightly concave. The stapedial tubercle [**stt**] is a small, stout tubercle on the posterior side of the apex of the stapes for the insertion of the stapedial muscle (Lancaster, 1990).

Mandible

Dentary

As in all eutherian mammals, the lower jaw of *Dorudon atrox* is composed of a single bone, the dentary [**D**, Fig. 49]. Summary statistics for the measurements of *D. atrox* dentaries are shown in Table 10. The left and right dentaries meet along the medial sides of their anterior ends at the mandibular symphysis [**sym**],

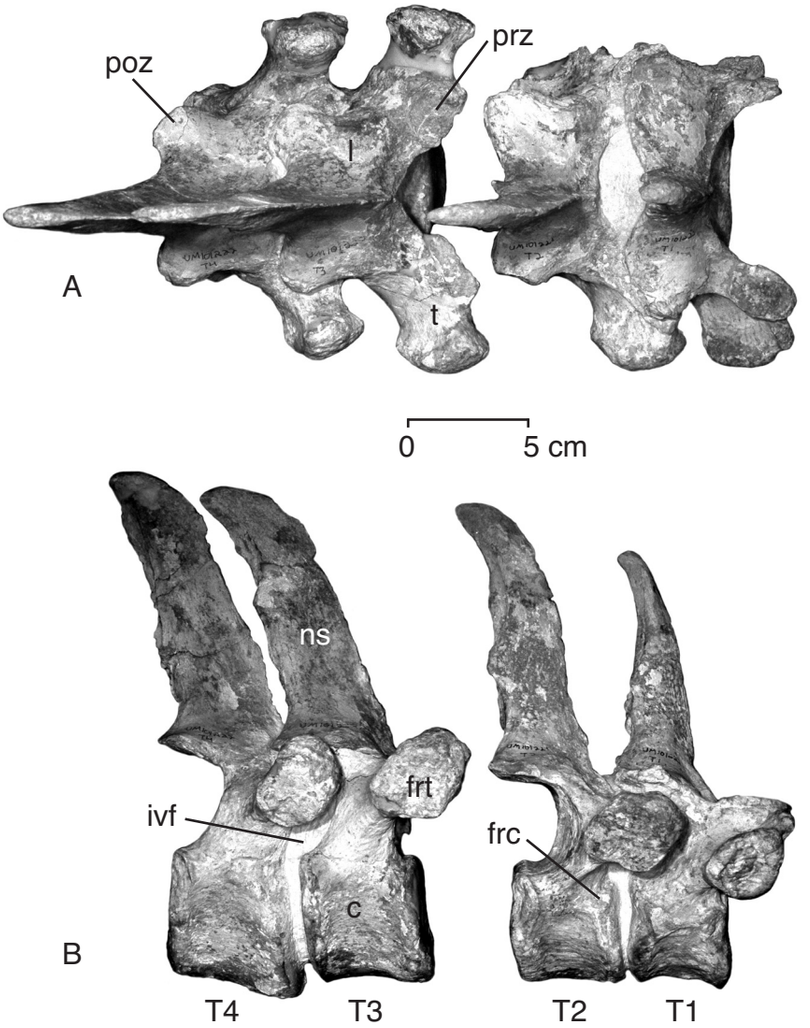

FIGURE 60 — Thoracic vertebrae 1-4 of *Dorudon atrox* (UM 101222) in A, dorsal, and B, right lateral view. T1 and T2 are still held together by sediment, as are T3 and T4. Note the dramatic change in the size and shape of the neural spines, as well as the orientation of the rib articular facets from T1 to T4.

which is unfused in all specimens. The symphysis extends from the anteriormost tip of the dentary back to below the alveolus for P_2. The medial surface of the dentary is flat along the whole articular surface, with this surface of the bone having a roughened texture. Posterior to the mandibular symphysis the dentaries diverge in a gentle curve as far as the posterior end of the molar series, where the medial surfaces of the mandibular rami are again sub-parallel to each other. Posterior to the symphyseal surface the medial surface of the dentary is gently concave. The lateral surface of the dentary is distinctly convex, with the convexity being most pronounced in the posterior one third of its length. The lateral surface of the body of the dentary includes a series of mental foramina [**mf**]. These foramina are near the ventral border of the body on the anterior end and each successive foramen is slightly closer to the alveolar border until finally the last one is near the alveolar border. The last foramen is found below P_3 or just posterior to P_3. There are usually seven or eight mental foramina. These transmitted fibers of cranial nerve V_3 (mandibular nerve) and blood vessels to the lower lip.

The body of dentary is long and relatively shallow, increasing only slightly in depth from the anterior tip to the end of the premolar series. The dentary then increases in depth dramatically such that each more posterior molar is higher on the dentary.

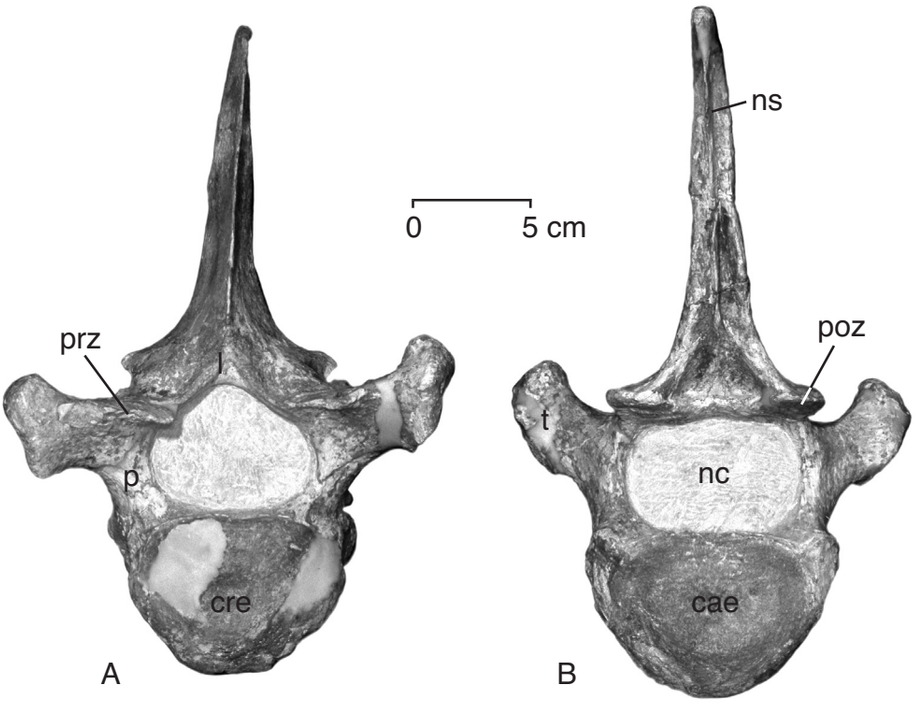

FIGURE 61 — Thoracic vertebrae 3 and 4 *Dorudon atrox* (UM 101222). A, T3 in anterior view, and B, T4 in posterior view. Note the sharp ridge delimiting areas of muscular attachment along the posterior margin of the neural spine, as well as the deep excavations lateral to the base of the ridge.

Posterior to the molars is the non-tooth-bearing portion or ramus. The dorsal surface of the dentary continues to extend upward toward the apex of the coronoid process [**cpd**]. The coronoid process is broad and sweeps up in a gentle arc that peaks just slightly higher than the main cusp of M_3. The edge of the coronoid process turns ventrally again and curves just slightly anteriorly, leaving the coronoid process projecting both dorsally and posteriorly. The coronoid process forms the insertion for the temporalis muscle on its medial side.

The posterior edge of the mandible continues ventrally, forming the mandibular notch, between the coronoid process and the mandibular condyle [**cd**], which is just ventral to the lower border of the coronoid process. The condyle is elongated mediolaterally and placed on a process that is shallowly excavated on the medial side. The articular surface of the condyle is generally subtriangular in dorsal view and its surface is broadly convex. There is a rather large projection on the anterolateral edge of the condyle that extends the articular surface in that direction. The entire articular surface is angled at about 45° to the horizontal ramus, sloping down and back. The condyloid crest arises from the mandibular condyle and extends anteriorly along the lateral face of the dentary to around P_4.

The lateral surface of the ramus of the mandible is divided into sections by three crests. The anterodorsal border of the ramus is formed by the coronoid crest. The condyloid crest forms the apex of the convex surface of the lateral side of the mandible, running from the ramus anteriorly down the body. Another crest is present on the coronoid process which runs anteroventrally from the dorsal edge of the mandibular notch to a point ventral to the posterior edge of the alveolar groove. This crest delimits the posteroventral border of the masseteric fossa.

The angular process [**ang**] is well-preserved in the type specimen. The lateral face of the dentary turns under to form the floor of the mandibular foramen, and then the surface turns laterally to form the angular process. The edge of the dentary points directly medially at the angle of the jaw. Farther anteriorly, the edge of the dentary turns dorsally and extends dorsally to form the anterior margin of the mandibular foramen.

The mandibular canal [**mc**] and its opening on the medial side of the dentary, the mandibular foramen [**mdf**], are very large in *Dorudon atrox*. This feature is shared with many modern and many fossil cetaceans, with the conspicuous exception of pakicetids, which have a small mandibular foramen

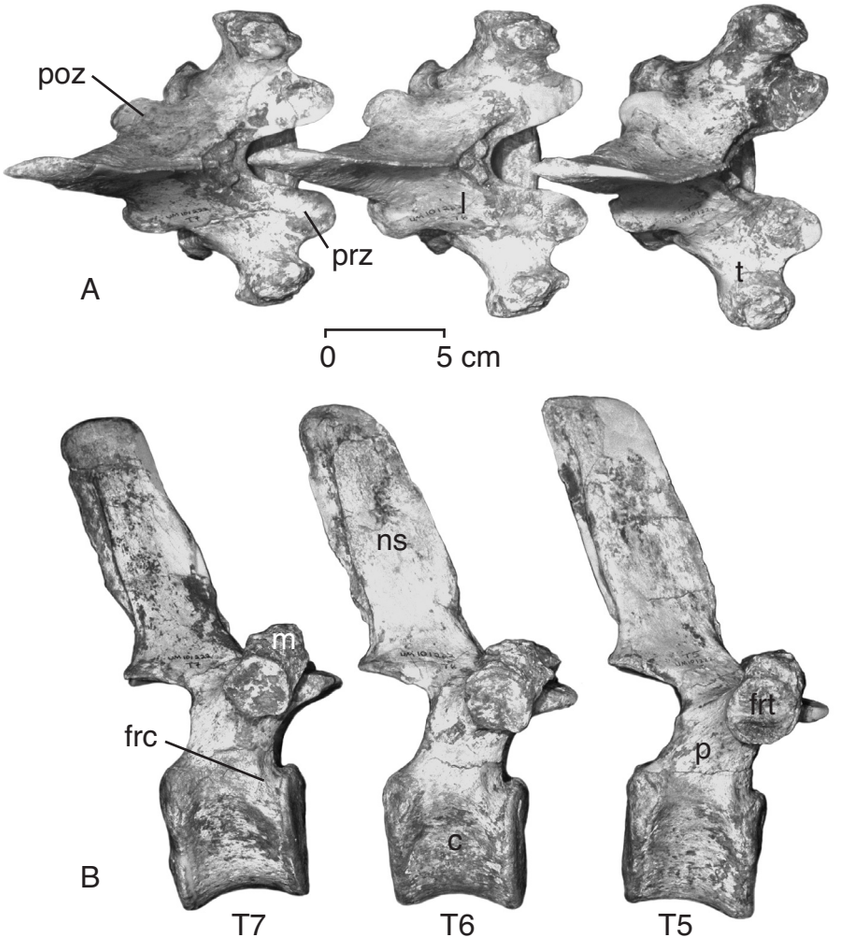

FIGURE 62 — Thoracic vertebrae 5-7 of *Dorudon atrox* (UM 101222) in A, dorsal, and B, right lateral view. Note the large zygapophyses, the size and orientation of the rib articular facets, and the increase in size of the metapophyses from T5 to T7.

(Thewissen and Hussain, 1993). The lateral wall of the dentary is very thin over this portion of the mandible. The mandibular canal also transmits cranial nerve V_3 and blood vessels to the teeth in the lower jaw and to the exterior surface of the lower jaw via the mental foramina.

Hyoid apparatus

The hyoid apparatus of *Dorudon atrox* is composed of five bony elements: the central, unpaired basihyal, paired stylohyals, and paired thyrohyals (Fig. 50). The hyoid apparatus, particularly the stylohyal, articulates with the paroccipital process of the basicranium via the tympanohyal cartilage. The hyoid apparatus, particularly the thyrohyal, also articulates with the thyroid cartilage. Numerous elements of the mammalian hyoid apparatus (ceratohyal, epihyal, tympanohyal) are either fused to other bony elements (stylohyal, periotic, or paroccipital process), represented only by cartilage, or completely absent. Howell (1927) suggested that the stylohyal of *Neophocaena*(= *Neomeris*) *phocaenoides* is formed from the fused stylohyal and tympanohyal.

The paired stylohyals [**SHy**, Fig. 50] are the cranialmost elements of the hyoid apparatus. Kellogg (1936) hypothesized that the long stylohyal in *Basilosaurus* was the fused epihyal and stylohyal. There is no visible evidence of fusion in the stylohyal of *Dorudon atrox*. The proximal end of the stylohyal articulates with the paroccipital process of the exoccipital. The distal end of the stylohyal is expanded where it articulates with

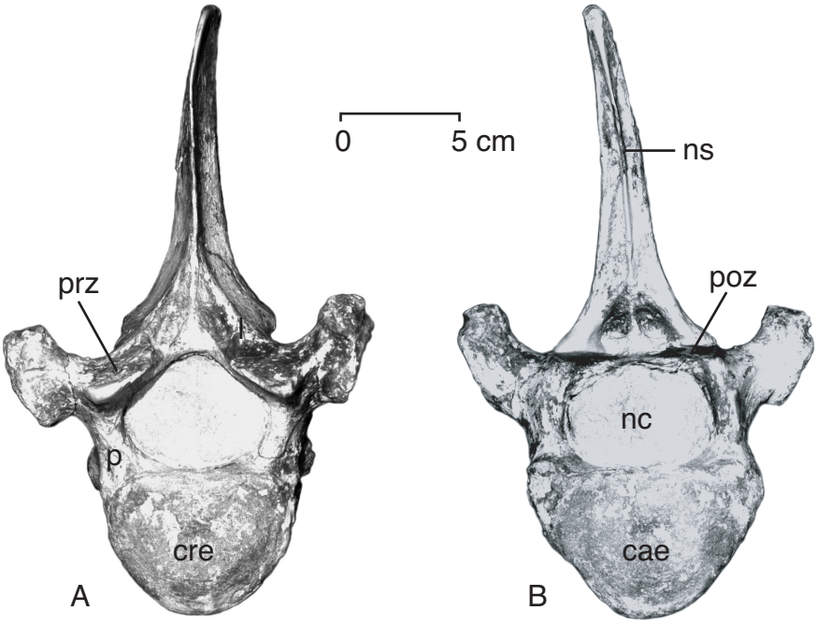

FIGURE 63 — Thoracic vertebra 5 of *Dorudon atrox* (UM 101222) in A, anterior, and B, posterior view. Note the sharp anterior edge of the neural spine, and midline ridge on the posterior edge. The base of the neural spine complex on the anterior face and deeply excavated on the posterior face.

the basihyal. The articulation was probably by an intervening cartilage, since the surface of the basihyal is roughened in the manner of other bones that have cartilaginous extensions (*e.g.*, the sternal elements). The articular surface is cup-shaped and generally smooth, with a raised center. The shaft is long and thin, with the cross section oval in shape. The distal end of the stylohyal is not known from any *D. atrox* specimen.

Problems with Kellogg's reconstruction of the hyoid apparatus should be noted. The reconstructions shown in his figures 8 and 9 (1936, p. 37) show a basihyal that is very different from that of *D. atrox* discussed below. It resembles mesosternal elements of *D. atrox*. Elements that are very similar to the basihyal of *D. atrox* have been found with skeletons of *Basilosaurus cetoides* since Kellogg's time. In addition, the right stylohyal shown in his figure 8 looks conspicuously like a posterior rib and is very different from the left stylohyal in the same figure. Lastly, it should be noted that figure 8 is upside down. The way it is shown, anterior is toward the bottom of the page.

The paired thyrohyals [**THy**, Fig. 50] are much more robust than the thin stylohyals. They are greatly expanded proximally where they articulated with the basihyal. Just distal to the proximal articular surface the shaft is roughly triangular in cross section. The shaft then flattens out and then expands slightly toward the distal tip. The distal ends of all known thyrohyals are broken to some extent, so the morphology remains unknown. There is a small ridge on the ventral surface of the proximal end of the thyrohyals. This ridge is probably the origin of the hyoglossus muscle.

The basihyal [**BHy**, Fig. 50] is the central unpaired element of the hyoid apparatus. It is bow-shaped, with the lateral edges expanded for articulation with the stylohyals and thyrohyals. The articular surfaces on the lateral edges are somewhat irregular, indicating that there was cartilage in between the basihyal and the elements with which it articulates. The main body of the basihyal is rather thin and oval in cross section. The bone is mostly cancellous with a thin cortical layer. There is a pair of raised roughened surfaces on the cranial-ventral surface, most likely for the attachment of the m. geniohyoideus.

AXIAL POSTCRANIAL SKELETON

The axial postcranial skeleton of cetaceans has been of great interest to modern and fossil cetologists alike since it has undergone a major transformation from the terrestrial ancestors

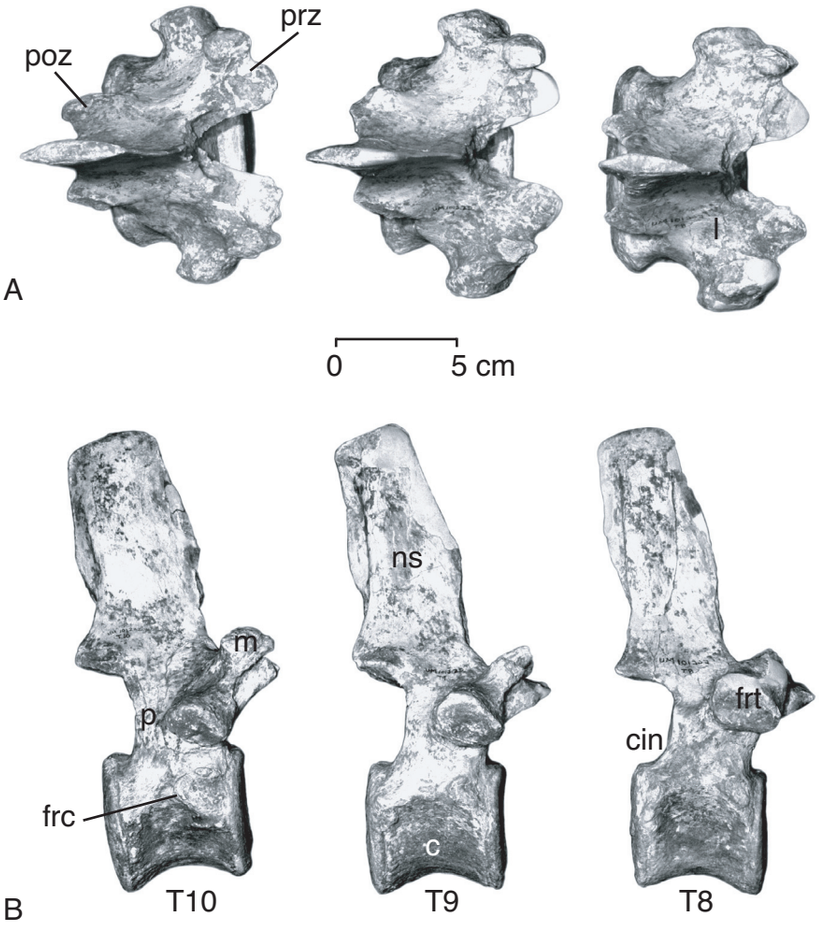

FIGURE 64 — Thoracic vertebrae 8-10 of *Dorudon atrox* (UM 101222) in A, dorsal, and B, right lateral view. Note the increasing distance of the transverse processes ventrally away from the metapophyses from T8 to T10. The fossae for muscle attachment are clearly visible on the posterior ends of the neural spines in lateral view.

of cetaceans, and it is the sole body support for the musculature used for propulsion in modern cetaceans. Most vertebrae in mammalian vertebral columns can be separated into five distinct regions. From anterior to posterior these are: cervical, thoracic (dorsal), lumbar, sacral, and caudal.

Cervical vertebrae are those at the anterior end of the column that are not associated with ribs. The osteological identification of cervical vertebrae agrees with identification based on neurological markers as well, even in taxa with aberrant numbers of cervical vertebrae (Giffin and Gillett, 1995). Thoracic vertebrae are those that are associated with a set of vertebral ribs. Lumbar vertebrae are those posterior to the thoracic series and anterior to the sacrum. There are few lumbar vertebrae in most mammals, relative to the number of thoracic and caudal vertebrae, but the number of lumbars is greatly multiplied in cetaceans. Sacral vertebrae are those that articulate with the innominata or are joined to vertebrae articulating with the innominata. The sacrum may be fused directly to the ilium via a synarthrosis or it may be attached at a distance via ligaments (Flower, 1883). Caudal vertebrae are those that are posterior to the sacrum or last sacral vertebra. Chevron bones may be present on the ventral surface of caudal vertebrae, articulating with hypapophyses on the posteroventral surface of the body and located between adjacent vertebral bodies (Fig. 51).

Buchholtz (1998) points out that the anatomical landmarks used to delimit regions of the vertebral column in terrestrial

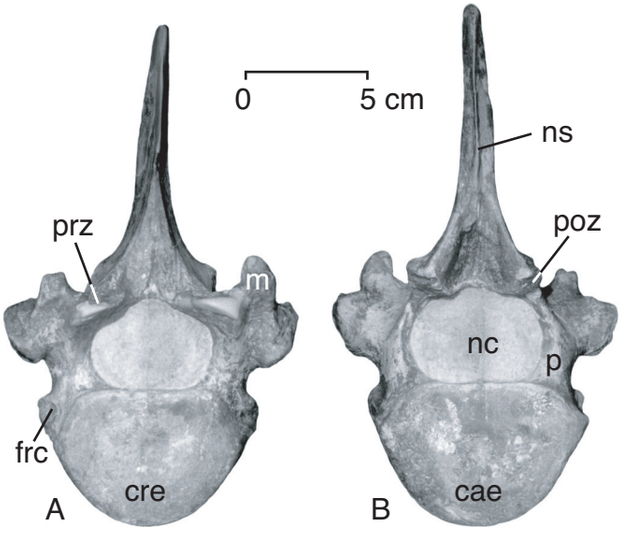

FIGURE 65 — Thoracic vertebra 9 of *Dorudon atrox* (UM 101222) in A, anterior, and B, posterior view. Note the large metapophyses and the deeply excavated base of the neural spine on the posterior face.

mammals have become non-coincident with the functional regions of the cetacean vertebral column. Mainly, this has involved incorporation of vertebrae other than the lumbars into the functional torso. Buchholtz employs a binomial terminology for these vertebrae in which the first term describes the homology of the vertebra and the second term describes the functionality of the vertebra. For instance, the sacral vertebrae of cetaceans have been incorporated into the lumbar region, so these vertebrae are described as sacral lumbars. The vertebrae of *Dorudon atrox* are described here using the conventional anatomical delimitations of the vertebral column, with additional description using Buchholtz's terminology where it is applicable.

Dorudon atrox has 7 cervicals, 17 thoracics, 20 lumbars, no sacrals, and 21 caudals. Measurements taken on the vertebrae of *Dorudon atrox* are shown in Figure 52.

Cervical vertebrae

Numerous cervical regions have been found in articulation, so the number of cervicals and the identity of each cervical vertebra is known with certainty (UM 93220, UM 101222). The bodies of the cervical vertebrae of *D. atrox* are compressed like those of modern cetaceans (Fig. 53), but they remain relatively longer than the cervical vertebrae of most modern cetaceans. There is no cervical fusion known in any specimens of *D. atrox*. Summary statistics for measurements of *D. atrox* cervical vertebrae are shown in Table 11.

Atlas and Axis

The first cervical vertebra or atlas [**C1**, Fig. 54], is the largest of all of the cervical vertebrae. It has a very thin body and forms an oval ring around the foramen magnum. The neural arch [**na**] is robust and is about equal in craniocaudal length to the ventral arch. The ventral arch [**va**] is dorsoventrally thicker than the neural arch and it supports both the cranial articular fovea [**caf**] and the caudal articular fovea [**cdf**] on its cranial and caudal sides, respectively. The ventral surface of the ventral arch is smooth and lacks a hypapophysis. The neural canal [**nc**] is generally round, and is approximately the same size as the foramen magnum. There is a single broad transverse process [**t**] that projects laterally and caudally from the sides of the vertebrae. The transverse process is narrow on its ventral surface and forms a broad, convex shelf on its dorsal surface. The transverse process contains a small foramen that opens into a canal that runs craniocaudally, entering the vertebra lateral to the cranial articular fovea and exiting lateral to the caudal articular fovea. This foramen is very small when compared to the vertebrarterial foramina of the other cervical vertebrae. It is unlikely that this foramen could have transmitted the vertebral artery. It is also quite variable in size from specimen to specimen.

The cranial articular foveae are concave and kidney-shaped. The ventral edges are separated by a narrow space on the ventral arch of the vertebra. The dorsal margins of the foveae are connected to the neural arch by bony bridges that form the lateral vertebral foramina [**lvf**] through which the vertebral arteries passed. The caudal articular foveae project caudally from the posterior surface of the vertebra. The dorsal projections of the foveae are rounded when viewed from the caudal side, but are very thin craniocaudally. The two sides of the foveae are confluent with the fovea of the dens across the ventral arch. The dens of the axis rests in the fovea of the dens. The ventral tubercle of the atlas [**vt**] is a small, rounded, sub-triangular process projecting from the posterior side of the ventral arch that projects under the body of C2, but it does not articulate with C2. When in articulation with the axis, the neural arch of the atlas and the pedicles of the axis form the intervertebral foramen [**ivf**] through which the second spinal nerve passes. The first spinal nerve passes between the atlas and the skull anterior to the dorsal arch of the atlas.

The axis [**C2**, Fig. 55] has the longest body of all of the cervical vertebrae when the dens is included in the measurement. The dens or odontoid process [**den**] projects anteriorly from the body to articulate with the ventral arch of the atlas. The dens is large and roughly conical with a rounded apex on the cranial projection. It is broader than it is tall. On either side of the dens and along the ventral surface of the dens is the cranial articular surface [**crs**], which conforms to the shape of the caudal articular surface of the atlas. The caudal epiphysis [**cae**] is roughly oval in shape when viewed from the caudal direction. The center of the caudal epiphysis is deeply depressed into the body at the notochordal pit.

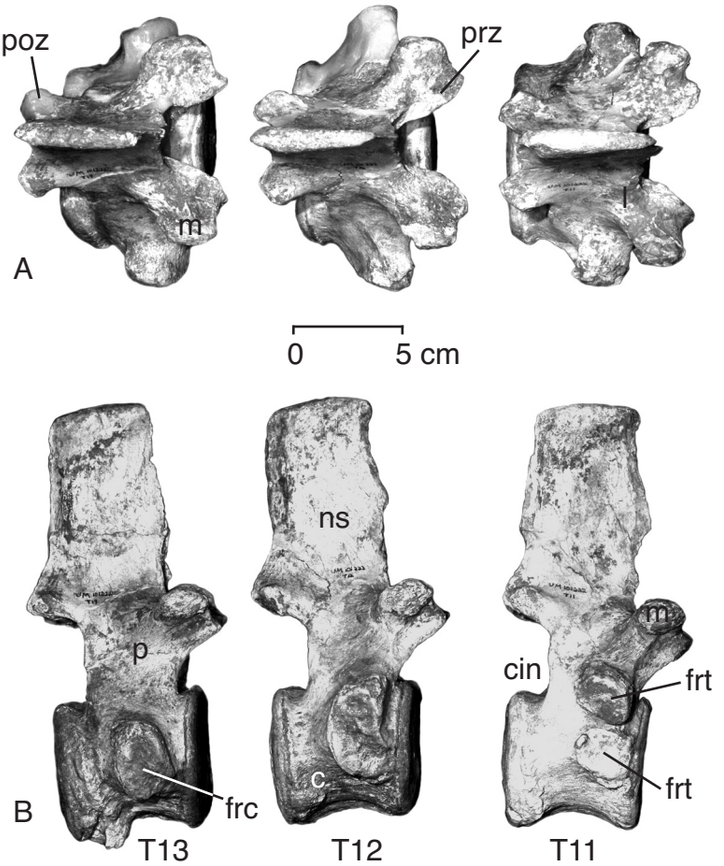

FIGURE 66 — Thoracic vertebrae 11-13 of *Dorudon atrox* (UM 101222) in A, dorsal, and B, right lateral view. Note the increased anteroposterior breadth of the neural spines over those of T8-10. The transverse processes and the processes that support the articular surface for the rib tuberculae are clearly separated in T11, and merged in T12.

The pedicles [**p**] are large and at an angle to the midline of the vertebral column, but these are not nearly as robust as the neural arch of the atlas. The laminae [**l**] are craniocaudally long and dorsoventrally thick relative to the subsequent cervical vertebrae. The pedicles and laminae together form the neural arch on the dorsal surface of the vertebra. The neural arch encloses the neural canal, which is shaped like an upside-down heart when viewed from the cranial side. The neural spine is craniocaudally long at its base on the neural arch. The neural spine becomes craniocaudally flattened dorsal to the base at the neural arch. A ridge is variably present up the midline of the neural spine. It is best developed at the base in all specimens. The neural spine of the axis is the largest neural spine of any of the cervical vertebrae. The postzygapophyses [**poz**] are attached to the laminae and project caudally to articulate with the prezygapophyses of C3. The postzygapophyses are angled such that their articular surfaces face somewhat laterally, caudally, and ventrally. There is no ventral keel, but there is a double hypapophysis [**hy**] on the ventral surface of the body.

There are two separate transverse processes [**t**] projecting laterally from the body. Both are very small but distinct. The upper is the diapophysis and the lower is the parapophysis. The two are not conjoined laterally, and thus do not enclose a vertebrarterial canal. The two processes meet and join the body via a common base. The vertebrarterial canal [**vac**] enters the vertebra from the lateral side, just caudal to the dorsal margin of

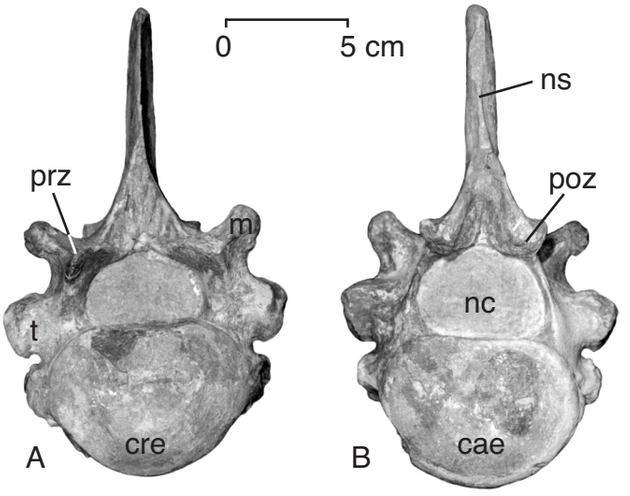

FIGURE 67 — Thoracic vertebra 11 of *Dorudon atrox* (UM 101222) in A, anterior, and B, posterior view. Note the large body and large, dorsally projecting metapophyses.

the cranial articular surface on both sides of the vertebra. The canal turns 90° and exits the vertebra at the base of the transverse processes, lateral to the caudal epiphysis.

Cervical vertebrae 3 to 7

Cervical vertebrae C3-C7 are illustrated in Figures 56-59.

Body.— The bodies [**b**] of C2-C7 are craniocaudally compressed and concave on the cranial and caudal ends. The vertebral bodies decrease in length from C3 to C5 and increase from C5 to C7. The cranial epiphyses [**cre**] are roughly oval in shape, but somewhat flattened along the dorsal and ventral margins. The caudal epiphyses [**cae**] are more nearly oval in shape, especially in younger individuals. Older individuals are less oval because the epiphysis extends onto the double hypapophyses [**hy**] present on the anterior and posterior ends of the ventral surfaces of the bodies. There is a ventrally projecting midline ridge on the ventral surface of each vertebral body. The double hypapophyses of C2-C5 are reduced in C6 and C7.

Neural arch.— The pedicles [**p**] are elongated laterally and rather short craniocaudally. They are not nearly as large as those of the axis. The pedicles become more laterally elongated from C3 to C7. Spaces between pedicles on adjacent vertebrae form the intervertebral foramina [**ivf**] for the passage of spinal nerves. The pedicles on each side of the vertebrae join the laminae [**l**], which together form the neural arches [**na**]. The laminae are flat and both craniocaudally and dorsoventrally thin. The laminae become more craniocaudally narrow from C3 to C6. The laminae of C7 are craniocaudally broader than in C3 to C6. The neural canals [**nc**] are arch-shaped. The area of the neural canal increases from C3 to C7.

Neural spine.— The neural spines [**ns**] are very short and blunt. The neural spines are low on the cranial margin of the neural arch and higher on the posterior margin. The neural spine [**ns**] of C7 is a little more substantial. It has a broader base and is a little taller than the neural spines of C3 to C6.

Zygapophyses.— The prezygapophyses [**prz**] project cranially from the neural arch, and the articular surfaces are angled ventrally and medially. The articular surfaces of C6 are larger than those of C3 to C5. The prezygapophyses of C7 are more nearly flat than those of C3 to C6. The prezygapophyses articulate with the postzygapophyses [**poz**] of the preceding vertebra. The postzygapophyses are angled ventrally and laterally.

Transverse processes.— The transverse processes [**t**] are broad and flattened craniocaudally. They are formed by fusion of the more dorsal diapophyses with the more ventral parapophyses. The parapophyses retain slender processes that project ventrally and cranially from the ventral margin of the transverse processes. These processes become more robust from C3 to C5. The parapophyses are very large and club-shaped in C6. The processes project about as far from the ventral surface of the body as the body is tall. The processes are thickest along their cranial margins and slightly thinner toward their caudal margins. The transverse processes of C7 are broad and flat. They project farther laterally than any other cervical vertebrae. There are no projections from the parapophyseal portion of the transverse process. The transverse processes transmit the vertebrarterial canal [**vac**] through the vertebrarterial foramina. These foramina are large, and perforate the transverse processes just lateral to the body. The vertebrarterial canal transmits the vertebral artery.

Thoracic vertebrae

Two specimens of *Dorudon atrox* were found with articulated thoracic regions (UM 93220, UM 100143), both of which have 17 thoracic vertebrae. Other specimens that include thoracic vertebrae have never been found with more than seventeen thoracic vertebrae or more than seventeen sets of ribs. Thoracic vertebrae are illustrated in Figures 60-69. Summary statistics for the measurements of *Dorudon atrox* thoracic vertebrae are shown in Table 12.

Thoracic vertebrae 1-17

Body.— The bodies [**b**] of the thoracic vertebrae increase in length, height, and breadth from anterior to posterior. The body of T1 is especially wide relative to its height. The body surfaces become more nearly equant (height equaling width) as one proceeds down the column from T1. The bodies are moderately waisted. The degree of waisting decreases from T11 to T13.

The cranial epiphysis [**cre**] of T1 is generally oval in shape, being elongate laterally. The cranial epiphyses become more heart-shaped and then circular as one proceeds down the column. The posterior portion of the fovea for the rib capitula forms a small

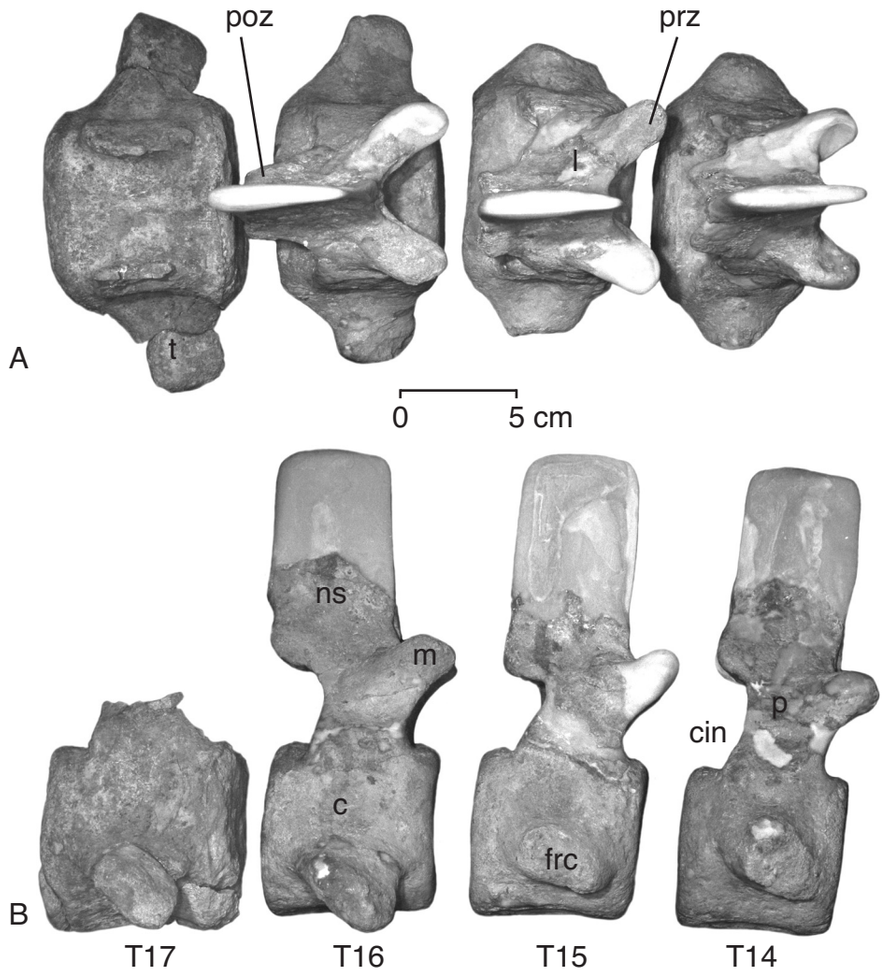

FIGURE 68 — Thoracic vertebrae 14-17 of *Dorudon atrox*. T14-T16 are from UM 101215, with T17 is from UM 97506. A, dorsal, and B, right lateral view. The neural spines of T14-T16 have all been reconstructed, along with some of the pre- and postzygapophyses.

protuberance on the dorsolateral edge of the body. This notch is not covered by the cranial epiphysis. Beginning with T8, the notch is covered by a separate epiphysis. This epiphysis forms the posterior portion of the fovea for the rib capitulum [**frc**] on each of the vertebrae. By thoracic vertebra ten, the rib articular epiphysis is beginning to project laterally from the body. The caudal epiphyses [**cae**] are similar in shape to the cranial epiphyses of the cranially adjacent vertebrae. They differ in that the dorsum of the lateral edges of the caudal epiphyses turn cranially onto the lateral face of the bodies to form the anterior edge of the fovea for the rib capitula. These surfaces project farther laterally than the corresponding surfaces on the cranial epiphyses. The size of the anterior portion of the fovea for the rib capitulum decreases in size from T8 to T10. By T10 or T11 the caudal epiphysis no longer forms the anterior portion of the fovea for the rib capitulum and no longer wraps onto the lateral face of the body.

The ventral side of the body of each vertebra includes a distinct ventral keel [**vk**] along the midline. This ventral keel is flanked by a pair of nutrient foramina, one on each side of the keel. These foramina are variably developed, with one foramen often much better developed than the other, or with one missing altogether. There is also a pair of accessory ridges lateral to the nutrient foramina that parallel the ventral keel.

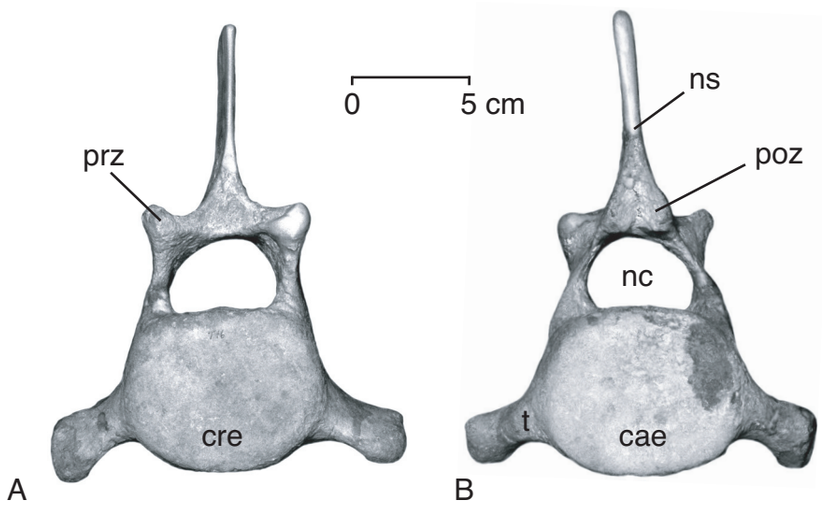

FIGURE 69 — Thoracic vertebra 16 of *Dorudon atrox* (UM 101215) in A, anterior, and B, posterior view. Note the length and orientation of the transverse processes relative to more anterior thoracic vertebrae.

These accessory ridges are always smaller than the midline keel, but are similar in form.

Neural arch.— The pedicles [**p**] of T1 to T4 are very long and robust. The pedicles undergo a dramatic reorientation moving down the column from T1 to T4. The pedicles of the first thoracic vertebra are very long and are oriented mediolaterally. The pedicles of T2 are a bit shorter and at an angle to the midline. The lateral edge of the pedicle is more posterior than in T1, while the medial edge is more anterior. This reorientation of the pedicle from a medial-lateral orientation to a cranial-caudal orientation continues in T3 and is virtually complete in T4. The pedicles become progressively longer from T5 to T10.

The dorsal edges of the pedicles are connected to the laminae [**l**], which together form the neural arch [**na**]. The laminae angle in a dorsal direction from their connections with the pedicles to the point where they join the neural spine along the midline to complete the neural arch. The laminae are broadest at their most lateral point, where they join the pedicles, and narrow toward the midline. This narrowing is most pronounced in T1 and is less pronounced in more posterior vertebrae. The neural arch encloses the neural canal [**nc**] in each of the vertebrae. The canals are large, and each has a relatively flat ventral border along the dorsal surface of the each of the bodies. The dorsal border of each of the canals comes to a rounded point where the laminae join along the midline.

The intervertebral foramen [**ivf**] is found between adjacent vertebrae. For any pair of thoracic vertebrae, the caudal edge of the pedicle of the anterior vertebra is incised to some degree, forming the caudal intervertebral notch [**cin**] and the anterior edge of the intervertebral foramen. The anterior edge of the pedicle of the posterior vertebra forms the posterior edge of the intervertebral foramen. The caudal intervertebral notch is insignificant on T1, but it becomes more deeply incised toward T4. The caudal intervertebral notches [**cin**] become progressively less pronounced from T5 to T7. The caudal intervertebral notch [**cin**] becomes more pronounced from T8 to T10. As the bodies increase in length from T8 to T10, the laminae increase in length as well. The laminae however, do not increase in length at the same pace as the bodies. The portions of the bodies caudal to the laminae become slightly elongated, effectively moving the caudal epiphyses farther from the posterior edge of the laminae. A distinct groove forms in the space between the caudal epiphysis and the caudal edge of the laminae for the passage of spinal nerves out of the neural canal. This groove is not yet present in T8 or T9 and is incipient in T10. There is a well-developed groove in the body between the caudal epiphysis and the caudal border of the pedicles for passage of spinal nerves out of the neural canal in thoracic vertebrae posterior to T10.

Neural spine.— The neural spines [**ns**] are relatively narrow and curved posteriorly. The neural spines change dramatically from T1 to T4. The neural spine of T1 is very narrow from its base to the dorsal tip. The dorsal tip is especially narrow, forming a point. The neural spine of T1 is not as curved as those of T2-T4. The body of the spine is wedge-shaped, coming to a narrow edge at its cranial border, and widening laterally toward its posterior edge. The posterior edge is complex,

TABLE 12 — Summary statistics for thoracic vertebra measurements of *Dorudon atrox*. Measurements are shown in Figure 52 and listed in Appendix V. H, cranial centrum height; L, ventral centrum length; W, cranial centrum breadth. N, sample size; SD, standard deviation; CV, ratio of the standard deviation to the mean (in percent). All measurements are in millimeters.

Vertebra	Dimension	N	Minimum	Maximum	Average	SD	CV
T1	L	1	41.0	41.0	41.0	—	—
	W	3	68.1	75.2	72.1	3.6	5.0
	H	3	49.8	57.1	54.3	3.9	7.2
T2	L	3	45.0	49.0	46.7	2.1	4.4
	W	1	70.0	70.0	70.0	—	—
	H	1	45.1	45.1	45.1	—	—
T3	L	3	46.8	52.8	49.5	3.0	6.1
	W	3	59.0	72.0	66.0	6.6	9.9
	H	2	50.0	52.2	51.1	1.6	3.0
T4	L	3	49.8	56.1	53.3	3.2	6.0
	W	2	72.3	74.0	73.2	1.2	1.6
	H	1	52.7	52.7	52.7	—	—
T5	L	4	48.0	57.6	51.5	4.2	8.2
	W	3	69.7	74.0	71.4	2.3	3.2
	H	2	52.5	53.5	53.0	0.7	1.3
T6	L	4	49.0	57.7	51.4	4.2	8.2
	W	2	68.4	70.1	69.3	1.2	1.7
	H	2	52.3	53.9	53.1	1.1	2.1
T7	L	2	51.2	58.1	54.7	4.9	8.9
	W	2	71.0	76.0	73.5	3.5	4.8
	H	2	55.2	62.0	58.6	4.8	8.2
T8	L	4	52.2	60.2	55.5	3.5	6.3
	W	3	68.3	74.5	72.4	3.6	4.9
	H	4	45.0	56.9	52.1	5.0	9.7
T9	L	3	56.3	63.8	59.7	3.8	6.4
	W	2	69.2	80.3	74.8	7.8	10.5
	H	2	54.3	57.2	55.8	2.1	3.7
T10	L	3	57.0	65.0	60.2	4.2	7.0
	W	2	77.2	80.9	79.1	2.6	3.3
	H	3	56.1	61.2	58.0	2.8	4.8
T11	L	3	57.0	68.7	62.8	5.9	9.3
	W	3	82.1	89.1	84.7	3.8	4.5
	H	3	59.0	65.7	62.7	3.4	5.4
T12	L	4	62.0	70.6	66.3	4.0	6.0
	W	2	79.9	85.2	82.6	3.7	4.5
	H	4	57.1	65.3	62.2	3.6	5.7
T13	L	3	64.0	71.0	66.9	3.6	5.4
	W	1	85.0	85.0	85.0	—	—
	H	2	63.8	66.0	64.9	1.6	2.4
T14	L	2	68.0	68.3	68.2	0.2	0.3
	W	2	84.0	93.0	88.5	6.4	7.2
	H	2	68.6	69.0	68.8	0.3	0.4

TABLE 12 (cont.)

Vertebra	Dimension	N	Minimum	Maximum	Average	SD	CV
T15	L	3	62.0	68.9	65.6	3.5	5.3
	W	3	75.1	93.7	83.9	9.3	11.1
	H	3	61.5	68.1	65.2	3.4	5.2
T16	L	3	70.5	73.0	71.6	1.3	1.8
	W	3	77.6	90.1	82.6	6.6	8.0
	H	3	62.7	73.2	67.6	5.3	7.8
T17	L	1	80.4	80.4	80.4	—	—
	W	1	91.7	91.7	91.7	—	—
	H	1	80.2	80.2	80.2	—	—

with a caudally-projecting midline ridge extending from the top of the neural arch to the dorsal tip of the spine. The lateral edges also flare posteriorly, forming two fossae for muscle attachment in between the lateral edges and the midline ridge. The neural spines of T2-T4 share most of these attributes with T1, but they become progressively wider from the base to the tip. The tips of the neural spines are rounded and dramatically curved posteriorly. The lateral edges of the posterior borders of the neural spines flare posteriorly like those of T1, but those of T2-T4 include an additional posterior projection at about one third of the way up the height of the spine. The body of the neural spine of T1 is almost vertical (except for its curved dorsal tip). The neural spines of T2-T4 are progressively more posteriorly inclined. There is a slight ventral keel on T1 that is entirely absent on T2-T4. No hypapophyses are present on T1 to T4.

The neural spines [**ns**] of T5 to T17 are broader, taller and less curved than those of T1 to T4. Only T5 has a slightly curved tip, while the others lack this feature completely. The dorsal tips of the neural spines do not come to rounded points as in T1 to T4, but rather the tips are flat-topped and have rounded edges cranially and caudally in lateral view. Posterior to T5 the neural spines are generally rectangular when viewed laterally. The anterior edges of the neural spines have a complex form just dorsal to the neural canal. The anterior face of the base of the neural spine is roughly triangular in shape, coming to a point dorsally. The base of the triangular surface is formed by the dorsal edge of the neural arch. A pair of low ridges originates at the base of the triangular space and angle medially to meet at a point. These ridges delimit three fossae. One is triangular along the midline, the others are a pair of broad grooves that meet along the midline. Dorsal to the apex of this complex area, the cranial border of the neural spine is a sharp ridge. The caudal borders of the neural spines are divided into three parts: caudally projecting midline ridges, and paired lateral ridges. All of these ridges are pronounced, but the midline ridges project farther caudally than do the lateral ridges. These ridges define a pair of fossae on each vertebra on either side of the midline ridges for the attachment of epaxial muscles. The caudal projection of the lateral margins of the caudal border of the neural spines decreases from T8 to T10, so that in T10 and more posterior vertebrae the lateral edges terminate in simple thickened margins rather than projecting caudally as ridges.

Zygapophyses.— The prezygapophyses [**prz**] are attached to the neural arch and project anteriorly to articulate with the postzygapophyses of the adjacent anterior vertebra. The prezygapophyses are large and flat, but they decrease in size from T1 to T4. The prezygapophyses are oval shaped and inclined medioanteriorly. The prezygapophyses become more saddle-shaped posterior to T10. There is a small dorsal projection on the dorsum of the transverse process of T4 just lateral to the prezygapophysis. This is a small metapophysis [**m**]. The metapophyses increase in size and rugosity from T5 to T10. The metapophyses are closely associated with both the prezygapophyses and the rib articular surface on the transverse processes, being situated directly between them. The metapophyses form attachment surfaces for epaxial muscles. The metapophyses change from raised rugose surfaces to well-differentiated processes projecting cranially and laterally from the lateral side of the prezygapophyses around T5. The postzygapophyses [**poz**] extend posteriorly from the laminae. They are flat and oval, and those of T1 to T5 are inclined medioanteriorly, while those of more posterior vertebrae are horizontal. The articular surfaces become progressively more triangular in shape from T5 to T7. The postzygapophyses become more convex rather than flat posterior to T10.

Transverse processes.— The transverse processes [**t**] bear the foveae for articulation with rib tubercula [**frt**]. These surfaces are circular to oval in shape, being more circular in T1 and trending toward a more oval shape posteriorly. The transverse processes are mediolaterally very short and project slightly caudally from the top of the pedicles, with which they are joined. In more anterior thoracics the transverse processes arise from the junction between the pedicles and the laminae. Posterior to T8 the transverse processes arise progressively farther down the pedicles toward the bodies. In addition, the transverse processes get mediolaterally longer from T8 to T17,

but as they lengthen they also become dorsoventrally thinner. The articular surfaces for the rib tubercula become smaller and angle farther caudally moving from T8 to T17. The foveae for the rib tubercula on the transverse process become closely approximated with the foveae for the rib capitula on the bodies. The movement of the transverse processes down the pedicles toward the bodies further emphasizes the separation of the metapophyses from surrounding structures, since the transverse processes move away from the metapophyses.

In T12, the two articular surfaces merge into one kidney-shaped fovea. The two articular surfaces of rib 12 are also touching as described in the next section. The transverse process of T12 arises from the base of the pedicle and from the body of the vertebra. Thoracic vertebrae 13 and those more posterior continue this trend.

Sternum and Ribs

The sternum and ribs, along with the thoracic vertebrae, form the bony support and the protective cage that encloses the thoracic region of the body. While all of the ribs of *Dorudon atrox* articulate with thoracic vertebrae, only some of them articulate with the sternum. The anatomical evidence discussed below indicates that the first five ribs were attached directly to the sternum via costal cartilages, with ribs six, seven, eight, nine and ten attached to the sternum indirectly with a common costal cartilage attached to the xiphisternum. Each of the first five ribs attached to the lateral side of the anterior end of the correspondingly numbered sternebra. Another source of evidence about rib attachments comes from specimen UM 101222, which was found partially articulated. None of the ribs were found articulated with the sternum, but some of the ribs were articulated with the thoracic vertebrae. Ribs one to six on the right side were articulated almost in anatomical position relative to the thoracic vertebrae while the more posterior ribs were flattened against the bodies of the thoracic vertebrae. It is possible that the first six ribs remained attached to the sternum for some time after death and into the burial phase and only became detached after they had been sufficiently buried to keep them in anatomical position, while the other ribs were flattened against the vertebrae early in burial. This could indicate that the first six ribs were more firmly attached to the sternum, ribs one to five directly with the costal cartilages, and rib six indirectly with a common costal cartilage. Rib six may have remained more firmly attached to the sternum since it is the closest to the sternum of those attached with a common costal cartilage.

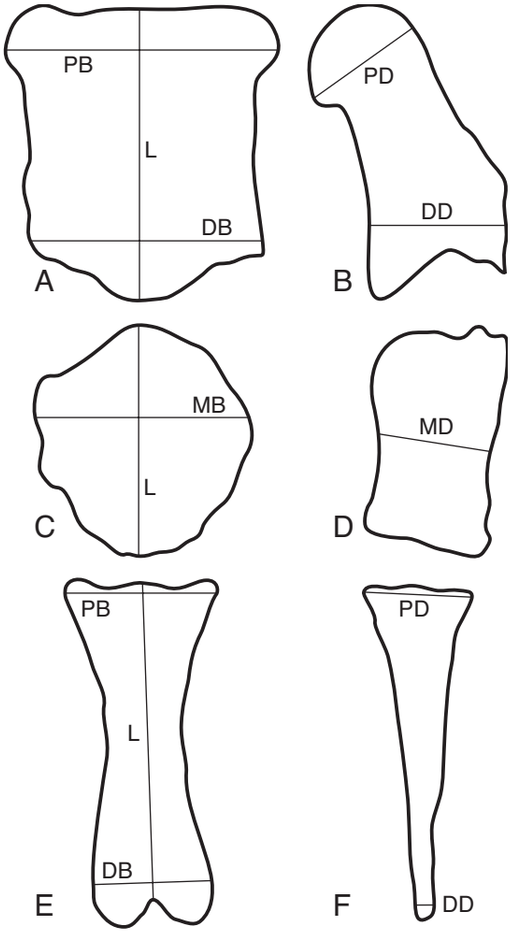

FIGURE 70 — Measurements of sternal elements of *Dorudon atrox*. A-B, manubrium in ventral and lateral view. C-D, representative mesosternal element in ventral and lateral view. E-F, xiphisternum in ventral and lateral view. Measurement values for the sternal elements of *D. atrox* are listed in Appendix VI-B.

Sternum

The sternum of *Dorudon atrox* generally has five bony elements (although a variant is discussed below). The sternebrae [**St1-5**] are numbered from one to five, anterior to posterior. Measurements of sternal elements of *D. atrox* are shown in Figure 70, and summary statistics are shown in Table 13. The posterior edge of the manubrium, the anterior, posterior, and lateral edges of the mesosternal elements, and the anterior edge of the xiphisternum are very roughened. This rough surface articulated with cartilages that were present between the adjacent sternebrae and between the sternebrae and the ribs. These cartilages are the intersternebral and costal cartilages, respectively. One specimen of *D. atrox* (UM 101222, Figs. 71-72) preserves the intersternebral cartilages [**isc**].

TABLE 13 — Summary statistics of measurements of sternal elements of adult *Dorudon atrox*. Measurements are shown in Figure 70 and listed in Appendix VIB. PB is proximal breadth. DB is distal breadth. MB is maximum breadth. L is craniocaudal length. PD is proximal depth. DD is distal depth. The maximum breadths of the manubrium and xiphisternum are on the proximal (cranial) ends. N, sample size; SD, standard deviation; CV, ratio of the standard deviation to the mean (in percent). Measurements are in millimeters.

Bone	Dimension	N	Minimum	Maximum	Mean	SD	CV
Manubrium	PB	3	81.1	98.8	92.5	9.9	10.7
	DB	3	70.8	83.8	79.2	7.3	9.2
	L	3	108.9	118.8	113.5	5.0	4.4
	PD	3	31.9	44.7	36.2	7.3	20.2
	DD	3	42.4	49.0	46.4	3.5	7.6
Sternebra 2	MB	3	68.0	80.1	75.8	6.8	8.9
	L	4	76.9	81.6	79.2	2.1	2.7
	MD	4	33.0	45.0	39.3	4.9	12.5
Sternebra 3	MB	3	67.0	82.5	76.7	8.5	11.0
	L	3	74.6	84.7	79.6	5.1	6.3
	MD	3	34.4	39.2	37.0	2.4	6.5
Sternebra 4	MB	4	72.8	78.0	75.6	2.1	2.8
	L	4	67.8	78.1	72.2	4.8	6.6
	MD	4	28.5	35.1	33.0	3.0	9.1
Xiphisternum	PB	3	50.8	61.4	54.5	6.0	11.0
	DB	2	47.0	53.9	50.5	4.9	9.7
	L	3	96.5	157.0	122.2	31.3	25.6
	PD	3	25.0	36.7	29.0	6.7	23.1
	DD	3	2.5	7.8	4.8	2.7	57.3

Manubrium.— The most anterior sternal element [St1] is also known as the manubrium sterni [**MS**, Fig. 71]. The manubrium is the largest of the sternal elements. It is roughly rectangular and longer than wide. The anterior portion has two large knobs projecting laterally and anteriorly from the main body. The posterior end is rounded to triangular rather than square in outline. The lateral surfaces meet the anterior surface at an approximately right angle, but rounded off. The lateral surfaces meet the dorsal surface in a flowing arc with no real angle. The caudal third of the manubrium is at an angle of about 40° to the rest of the body, bent in a dorsal direction. The anterior, lateral, dorsal, and ventral surfaces are all smooth.

Mesosternum.— The mesosternal elements [**St2**, **St3** and **St4**, Figs. 71-72] are shaped like hexagons that are slightly craniocaudally elongated. St4 is pentagonal when viewed from the ventral surface. St4 is also wedged from anterior to posterior, with the anterior end being dorsoventrally thicker than the posterior end. The ventral and dorsal sides of the mesosternal elements are somewhat rough when compared to the surface of the manubrium, but not as rough as the cranial, caudal, and lateral surfaces, which are extremely rough and irregular.

Xiphisternum.— The fifth sternebra, the xiphisternum [**X**, Fig. 73] is craniocaudally elongated and dorsoventrally flattened. It is widest and thickest at the cranial end and thins toward the caudal end. It is laterally waisted approximately halfway down its length. The caudal end terminates with two flat tongues of bone, one on each side of a midline notch.

A single specimen, UM 101222, has a very different xiphisternum. It appears to be formed from three fused elements. On its cranial end, there are two paired elements (left and right), fused up the midline, that articulate cranially with the fourth pair of intersternebral cartilages. This fused element is also fused to the third element, a flat elongated bone, rather like the standard xiphisternum described above, but much more narrow laterally. The two fused cranial elements are fused to the caudal element by a bulbous synarthrosis on the left side only. It is not clear whether this is a developmental anomaly, evidence of an injury, a variant, or some or all of the above.

Ribs

Ribs of *Dorudon atrox* are illustrated in Figures 74-78. These were measured as shown in Figure 79.

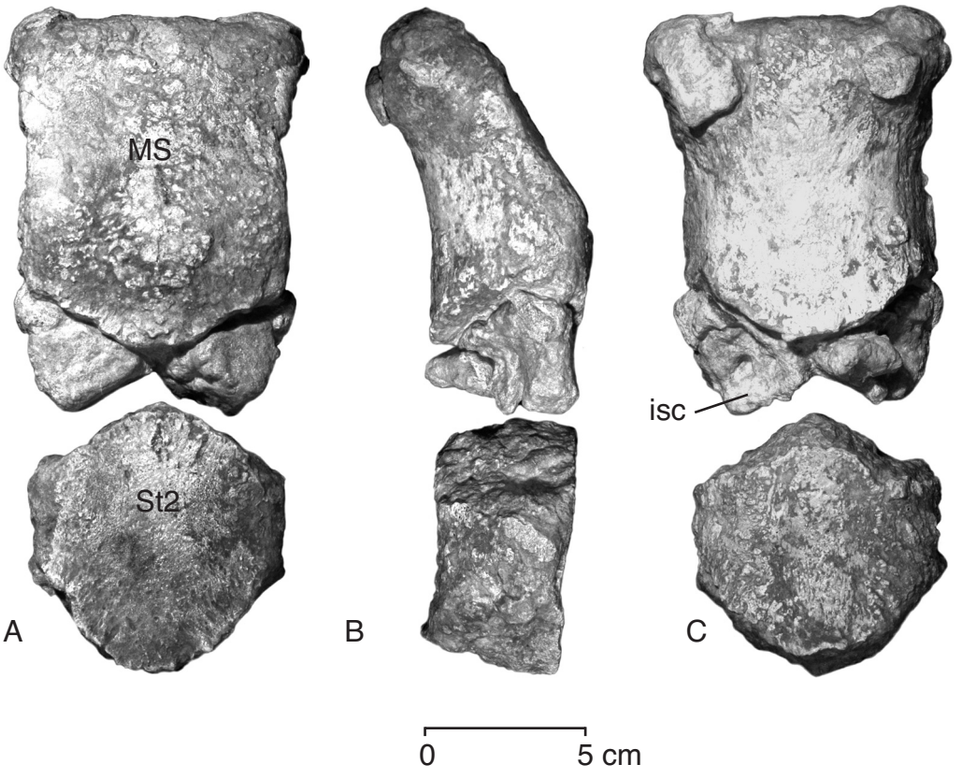

FIGURE 71 — First and second sternal elements (manubrium and St2) of *Dorudon atrox* (UM 101222) in A, ventral, B, lateral, and C, dorsal view. Note the angle in the manubrium in the lateral view. The large triangular ossifications attached to the caudal end of the manubrium are ossified intersternebral cartilages (*isc*). The cranial end of the second sternal element articulates with the caudal surfaces of the cartilages.

The first ten ribs have two separate articular surfaces where they meet the vertebrae, one on the capitulum, the other on the tuberculum. The capitulum articulates with two adjacent vertebrae. Each capitulum articulates with the thoracic vertebra to which it corresponds in number (capitulum of rib R1 with thoracic vertebra T1), and with the vertebra immediately anterior. The capitular articular surfaces on the vertebrae are divided between the two adjacent vertebrae with the more cranial portion of the articular surface on the more cranial vertebra, and the caudal portion of the articular surface on the rib's corresponding vertebra. Ribs eleven and twelve have a single proximal articular surface. The capitulum and the tuberculum are joined and their articular surfaces are confluent. These singular articular surfaces articulate with the thoracic vertebrae at three points. The capitular portion of the articular surface articulates with two adjacent vertebrae as described above. The tubercular portion of the articular surface articulates with the transverse process of the thoracic vertebra corresponding to the rib. Ribs twelve through seventeen have a singular proximal articular surface that articulates with the transverse process of the corresponding thoracic vertebra.

The proximal portions of the bodies of the ribs are composed of thick cortical bone with a small central space filled with trabecular bone. Farther distally, the ribs are composed of mostly trabecular bone. The thick cortex indicates that the ribs are osteosclerotic, but most individuals show no pachyostosis (*sensu* de Buffrénil et al., 1990). A few individuals have moderate inflation of the distal ends of the longest ribs (5-8), and could be described as moderately pachyostotic. These expanded portions of the ribs are composed mainly of trabecular bone, rather than thickened cortex. The ribs do not have a medullary cavity.

No archaeocete whales, including *Dorudon atrox*, are known to have sternal ribs. It is highly unlikely that *D. atrox* could have had sternal ribs that have not been found, since specimen UM 101222 was discovered with most of the thorax in articulation and there were no sternal ribs found. The anterior ribs were discovered articulated with the thoracic vertebrae and the

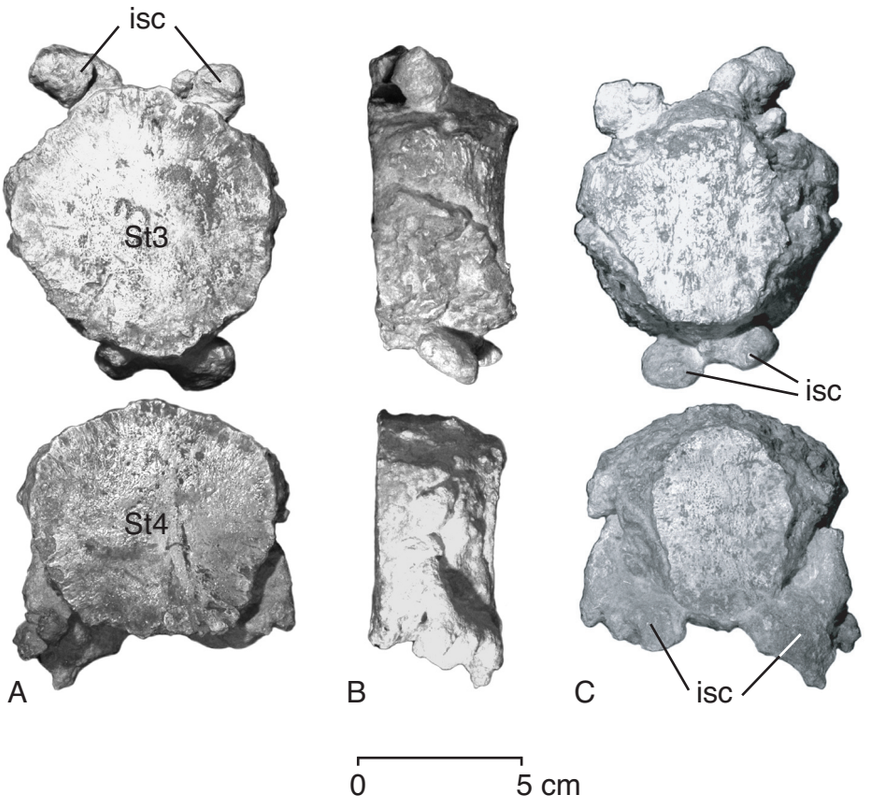

FIGURE 72 — Third and fourth sternal elements (St3 and St4) of *Dorudon atrox* (UM 101222) in A, ventral, B, lateral, and C, dorsal view. Irregular masses attached to the cranial and caudal ends of St3 and the caudal end of St4 are intersternebral cartilages (*isc*). Note the rough texture along the lateral sides of the sternal elements indicating a cartilaginous articulation with the costal cartilages.

sternal elements were found in articulation with each other, with no sternal ribs articulated with either the distal ribs or the sternum. Slijper (1936) illustrates specimens (his Abb. 60, p. 123) and reconstructions of the thorax (his Abb. 61, p. 124) of *Basilosaurus* (*Zeuglodon*) *isis*, showing sternal ribs. The "anterior sternal rib" in his figures is probably a thyrohyal. Its expanded proximal end (his sternal articular end) and long shaft is very similar in morphology to the thyrohyal of *D. atrox*. The "posterior sternal rib" in his figures is very different from the "anterior sternal rib", and it is difficult to judge what it might be from the figure, but it is probably a posterior vertebral rib. It appears to have a capitulum on the proximal end (his sternal articular end) and a long thin shaft that is reminiscent of the posterior vertebral ribs of *D. atrox*. Summary statistics for the measurements of *D. atrox* ribs are shown in Table 14.

Rib articular processes.— The capitula [**cap**] of the ribs are the processes that articulate with the vertebral bodies. The capitula of the ribs of *Dorudon atrox* are large and irregularly hemispherical in shape. Rib R1 is unique in that the capitulum articulates with the caudal end of the seventh cervical vertebra. The tubercula [**tub**] or tubercles of the ribs are the processes that support the surfaces that articulate with the transverse processes of the thoracic vertebrae. The ribs of *D. atrox* have large tubercula with large articular surfaces. The tubercular surfaces are oval in outline and generally flat. The tubercula are well separated from the capitula on ribs R1 to R4. The tubercula are closer to the capitula in R5-7, and this distance of separation decreases further from ribs R8 to R10. The two articular surfaces are almost touching in rib R10.

The capitular articular surfaces of ribs R11 to R13 have merged with the tubercular articular surfaces to form one single articular surface. On rib R11, this merged articular surface articulates with three points on the vertebrae as described above. On ribs R12 and R13, this common articular surface articulates only with the merged articular surface on the transverse process of the corresponding thoracic vertebra.

Rib proximal end.— The neck [**n**] of R1 is short and broad. It is not well differentiated from the shaft. The neck increases

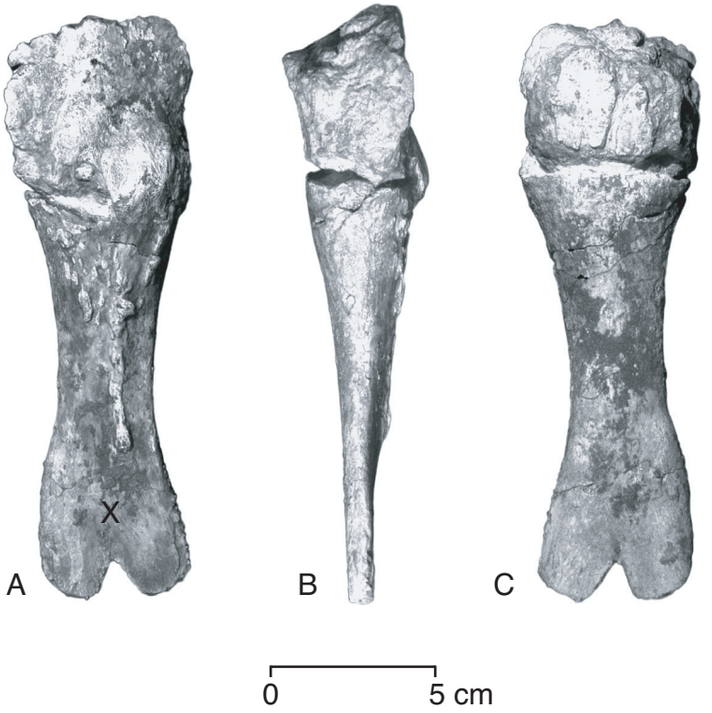

FIGURE 73 — Fifth sternal element (xiphisternum) of *Dorudon atrox* (UM 101222) in A, ventral, B, lateral, and C, dorsal view. This xiphisternum is unique among known specimens of *D. atrox*. It appears to be composed of three fused elements, with two paired elements on the cranial end and a single unpaired element on the caudal end. Note the distinct thinning from the cranial to caudal ends, viewed laterally, which is typical of *D. atrox* xiphisternae.

in length and decreases in robustness from R1 to R7. The necks of R8-10 are shorter than those of R5-7, and they get shorter from R8 to R17.

The curvature at the angle [**an**] of the rib is quite low in rib R1. The amount of curvature at the angle is much higher in ribs R2 to R8. Rib R1 has a low angle since it is much shorter than ribs R2 to R4 and does not need to curve as sharply to direct the distal end near to the manubrium of the sternum along the ventral midline of the chest. This angle significantly decreases between ribs R8 and R9 and decreases less so from rib R9 to rib R10. The amount of curvature at the angle of ribs R11 to R17 is very low. This angle decreases from ribs R14 toR17 and the proximal end develops a different bend just distal to the proximal articular surface.

Rib body.— The body [**b**] of the rib changes dramatically from proximal to distal in the ribs of *Dorudon atrox*. The proximal end of the body and most of the length of the body is craniocaudally flattened. The body is concave on its caudal surface at its most proximal end, between the capitulum and the tuberculum. The body is also concave on its cranial surface at the angle. Most of the length of the body is flat and oval in cross section in the first four ribs, while the bodies of ribs R5 and R6 are much thicker. More posterior ribs become progressively more gracile. The bodies become oval in cross section just distal to the angle. In ribs R5 to R14, the bodies become somewhat triangular in cross section farther distally, with the base of the triangle facing caudally, and the apex cranially. The angles of the triangular cross sections are very rounded. In addition, shallow grooves are present on the caudal surface of the ribs. The bodies of ribs R14 to R17 lack the distinct concavities found on the cranial and caudal surfaces of the more anterior ribs. The bodies of the ribs are generally oval in cross section. Ribs increase in length from R1 to R6, and then gradually decrease in length more posteriorly.

Rib distal end.— The bodies of ribs R1 to R7 are expanded at the distal end to form a large oval surface, covered with rugose, spongy bone. This surface is smaller in ribs R8 and R9, and rib R10 lacks this expansion altogether. The surface texture is indicative of a cartilaginous articulation. These distal ends articulate with the costal cartilages that attach in turn to

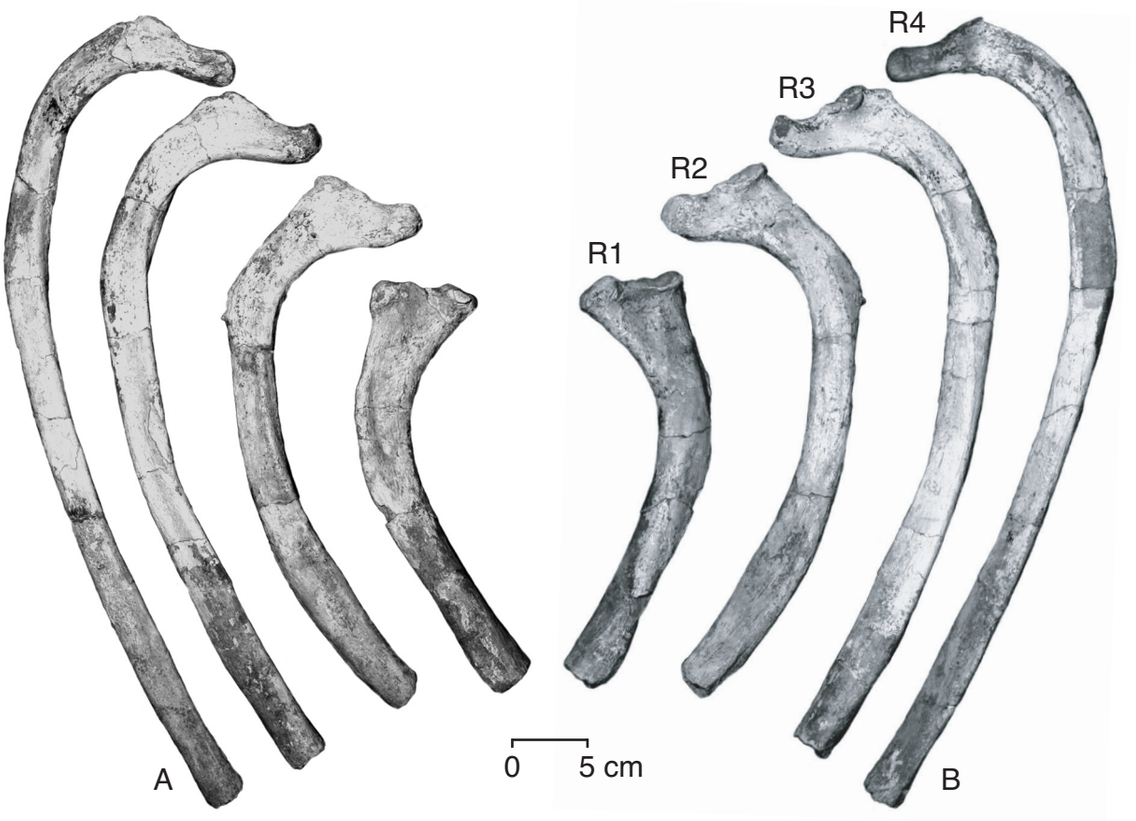

FIGURE 74 — Ribs one to four of *Dorudon atrox* (UM 101222) in A, anterior, and B, posterior view. Note the dramatic increase in length from rib one to rib four.

the sternum. The distal ends of ribs R11 to R13 have a very small flattened expansion. This expansion has a small groove in it running parallel to the long axis of the expanded tip. These ribs do not appear to have been attached to a cartilaginous extension on the distal tip.

Lumbar vertebrae

The number of lumbar vertebrae in *Dorudon atrox* is probably twenty, but this number may be variable or it may simply be slightly higher. No entire lumbar regions have been collected in articulation. Specimen UM 101215 has twenty lumbar vertebrae, but it was found disarticulated. Specimen UM 97512 has twenty lumbar vertebrae, and it was found semi-articulated. The specimen that was found in the best-articulated condition is CGM 42183. It has nineteen lumbar vertebrae, but there is a break in the series, suggesting there is at least one vertebra missing. The lumbar vertebrae are all very similar to one another, so they will all be described together, with trends along the column and any particular differences noted. Summary statistics for the measurements of *D. atrox* lumbar vertebrae are shown in Table 15.

Lumbar vertebrae 1-20

Body.— The bodies [**b**] of the lumbar vertebrae [Figs. 80-87] are roughly oval in cross section and about as long as they are tall. The bodies are not distinctly waisted, but the epiphyses are slightly larger in circumference than the body. The dorsal surface of the body has a ridge running down the midline, on the floor of the neural canal (see Fig. 84). There is a nutrient foramen on both sides of the ridge on each vertebra. These are often asymmetrically developed. The ventral surface of each body is also perforated by nutrient foramina, near the midline, one on either side of the ventral keel. These too are often asymmetrically developed.

The cranial epiphyses [**cre**] are oval in outline, but the oval shape is slightly flattened on the dorsal edge, along the floor of the neural canal (see Fig. 82). The cranial epiphyses are generally flat with a slight indentation in the center, but they are not

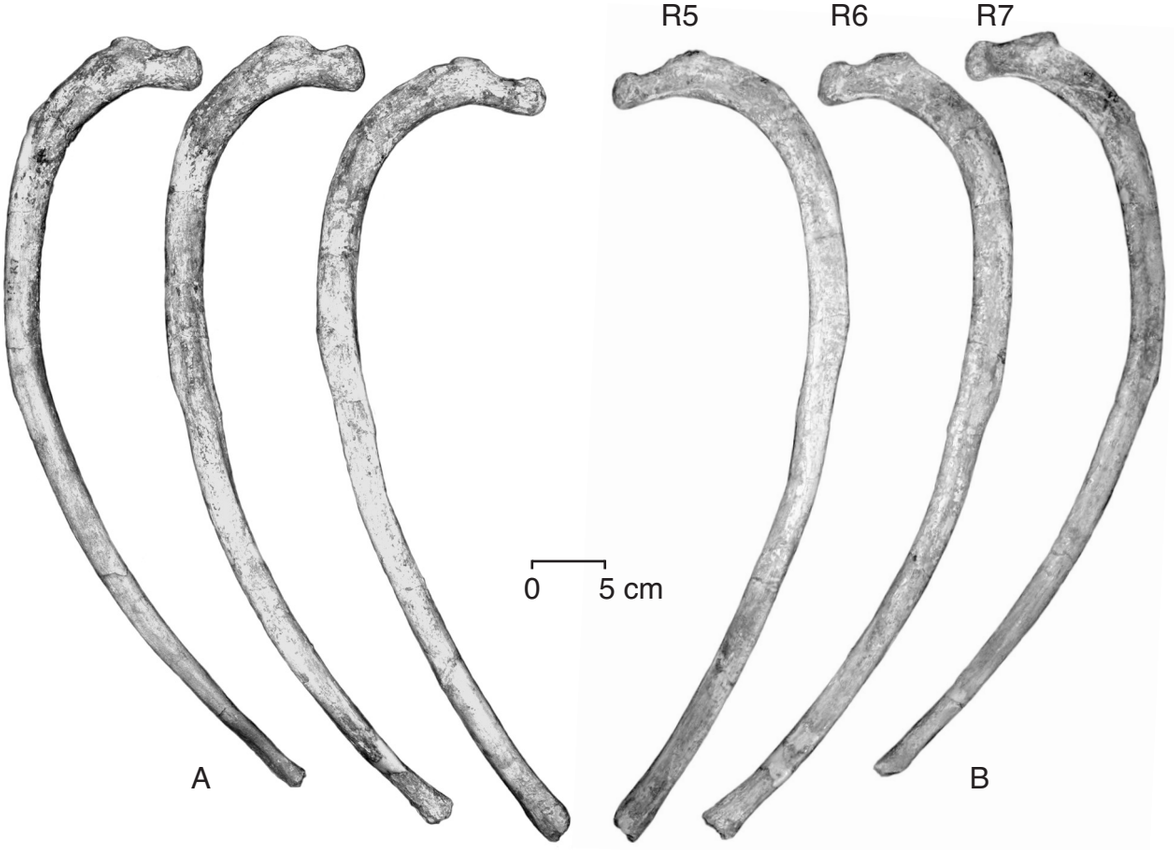

FIGURE 75 — Ribs five to seven of *Dorudon atrox* (UM 101222) in A, anterior, and B, posterior view. Rib six is the longest rib in the entire series.

distinctly procoelous. The caudal epiphyses [**cae**] are also oval in outline, but they lack the distinctly flattened dorsal edge of the cranial epiphyses. The caudal epiphyses are also generally flat, with a slight indentation in the center. The bodies of L1-16 have very small ventral keels [**vk**]. L17 to L20 lack ventral keels altogether. There are variably developed hypapophyses [**hy**] on the caudal end of each ventral body.

Neural arch.— The pedicles [**p**] of L1-2 are very robust at their bases and become thinner at about half their height. These robust bases are very similar to those of the pedicles of the thoracic vertebrae. The pedicles of L3-5 have much more gracile bases and remain thin through their entire height. The pedicles of L6-20 are thin and arise closer to the cranial epiphysis than to the caudal epiphysis. The pedicles arise closer to the midline of the body in L16-20 than in more anterior lumbars.

The pedicles meet with the laminae [**l**] to form the neural arch [**na**]. The laminae are about as thick as the pedicles and are at a high angle to the horizontal in L1. This angle decreases from L1 to L5 such that the roof of the neural canal is almost flat by L5. The laminae decrease in size from L16 to L20. The neural canal [**nc**] is large and in the shape of an inverted heart, with the heart becoming less pointed from L1 to L5 as the roof of the neural canal becomes flat. The neural canal decreases in size from L16 to L20 as the pedicles move closer to the midline of the vertebrae (Figs. 86-87).

The intervertebral foramina [**if**] are formed from the posterior borders of the pedicles and anterior borders of the pedicles of adjacent articulating vertebrae. These are about as long as the pedicles of the vertebrae that they intercalate with. At the ventral edges of the intervertebral foramina, shallow grooves are formed on the bodies between the posterior edge of the pedicles and the posterior epiphyses. In addition, there is a small notch in the posterior border of each transverse process where it meets the body.

Neural spine.— The neural spines [**ns**] of the lumbar vertebrae are broad and tall. The spines arise along the dorsal surface of the neural arch on the midline. The neural spines angle slightly caudally and are roughly rectangular at their dorsal ends. The neural spines increase in height very slightly from the anterior lumbars to somewhere around L12-L16, where they

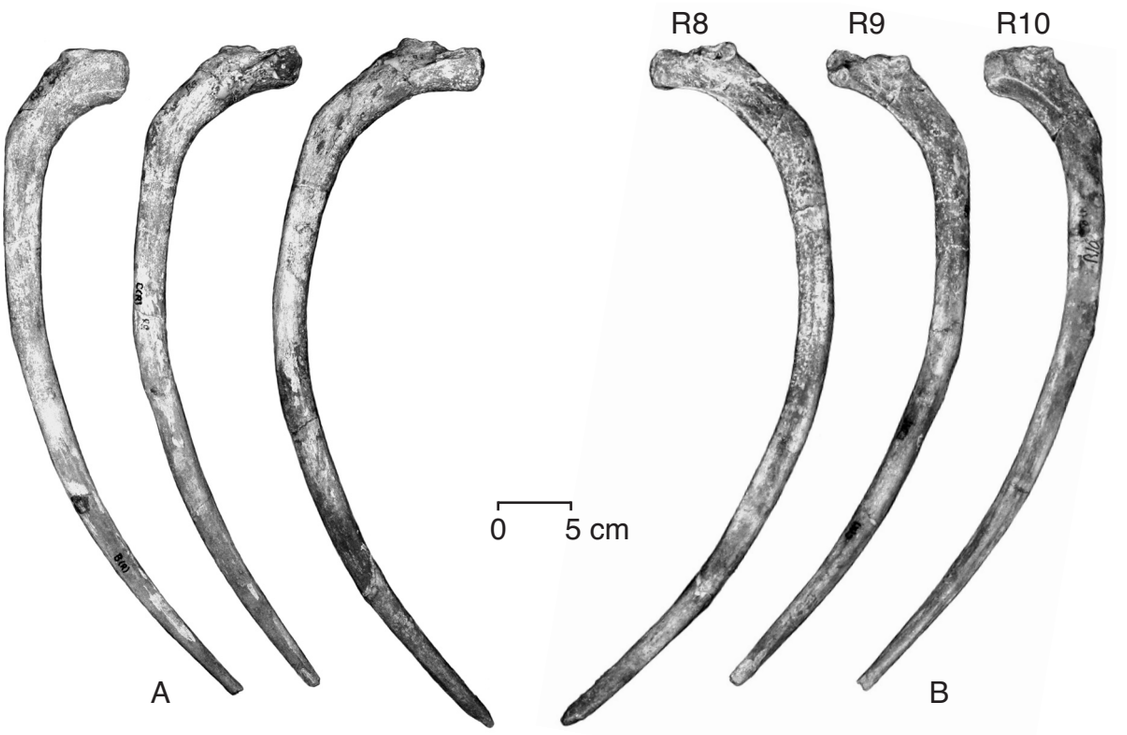

FIGURE 76 — Ribs eight to ten of *Dorudon atrox* (UM 101222) in A, anterior, and B, posterior view. Note the decrease in length from rib eight to rib ten.

begin to decrease in height. Many of the lumbar neural spines are broken in all specimens known, so the exact pattern of height increase and decrease through the lumbar region is difficult to determine.

Zygapophyses.— The prezygapophyses [**prz**] arise from the neural arches where the pedicles and laminae meet. The prezygapophyses project only slightly more cranially than the cranial epiphyses of the bodies. The prezygapophyses of most of the lumbar vertebrae are short, rounded, and non-articulating. The prezygapophyses clearly do not articulate with the postzygapophyses of the next-most-cranial vertebra. The prezygapophyses are much farther apart than the postzygapophyses of the adjacent anterior vertebra, such that they could not articulate. In addition, the neural spines of adjacent vertebrae touch if the zygapophyses are brought into close approximation. As stated earlier, the prezygapophyses and metapophyses arise from the neural arches via a common base. Since the "prezygapophyses" do not articulate with the postzygapophyses of the adjacent vertebrae in the lumbar region, this entire structure will be referred to as a metapophysis [**m**] in this region. Many of the metapophyses of the posterior lumbar vertebrae are missing, but the metapophyses of L20 are present and they are very large, like those of the anterior caudal vertebrae. The lumbar vertebrae still retain small postzygapophyses [**poz**] despite the fact that they do not articulate with the prezygapophyses. The postzygapophyses are small projections that flare out laterally and caudally from the caudal ends of the bases of the neural spines.

Transverse processes.— The transverse processes [**t**] are longer than those of the thoracic vertebrae, but they are much less robust. They increase in length from L1 to L10 and remain about the same length to around L18. The transverse processes decrease in length from L18 to L20. The transverse processes are thick at their bases and thin laterally. The bases of the transverse processes are closer to the posterior ends of the bodies than to the cranial ends. The distal ends of the transverse process are not rectangular but they terminate at an angle away from the midline. The transverse processes are angled ventrally, and slightly cranially. The transverse processes of L18 to L20 are very thick, especially on the caudal border. They increase in thickness from L17 to L20 (Fig. 88). The transverse processes of L19 and L20 are also broad craniocaudally.

Sacrum

Vertebrae that articulate with the innominates are considered to be the sacral vertebrae in terrestrial mammals (Flower, 1876). No vertebrae articulate with the bony remnants of the

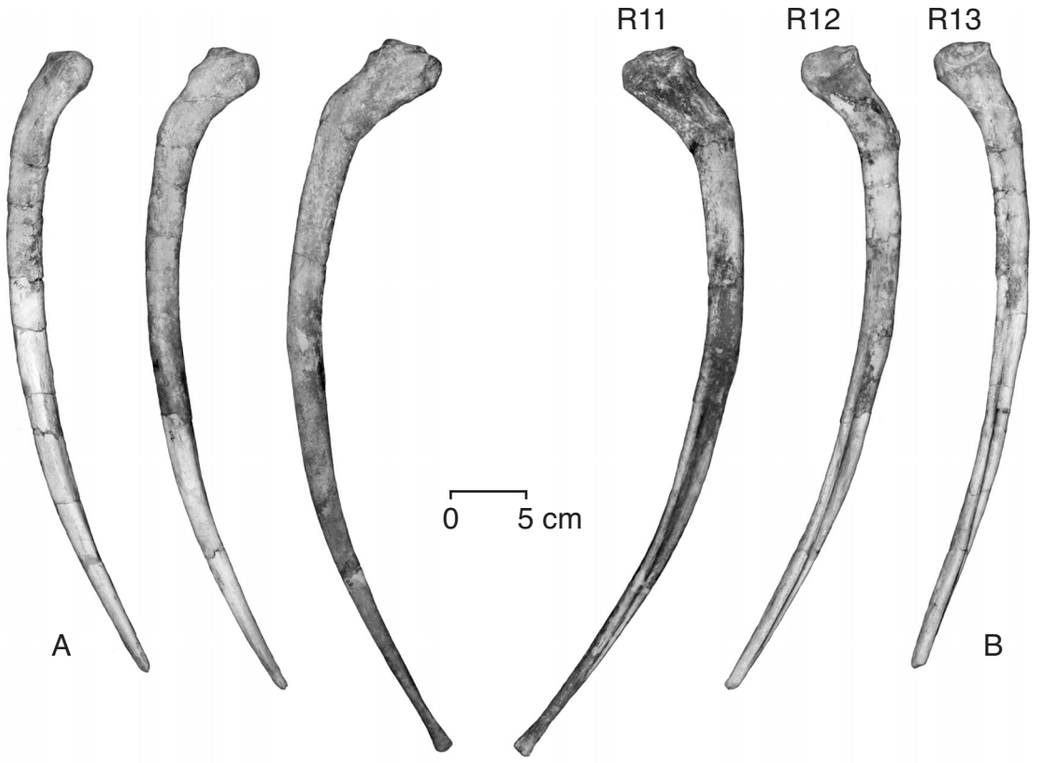

FIGURE 77 — Ribs eleven to thirteen of *Dorudon atrox* (UM 101222) in A, anterior, and B, posterior view. Note the decrease in length and angle from rib eleven to rib thirteen.

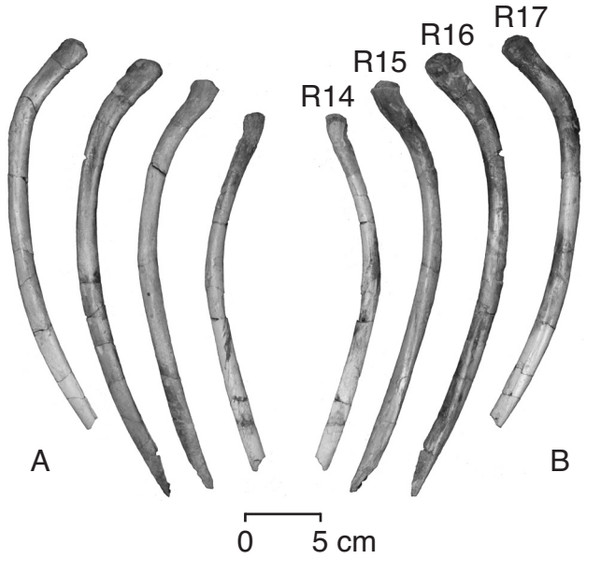

FIGURE 78 — Ribs fourteen to seventeen of *Dorudon atrox* (UM 101222) in A, anterior, and B, posterior view. Note the decrease in length and angle from rib fourteen to rib seventeen.

innominates and the innominates are not connected to any vertebrae with ligaments in modern cetaceans (Slijper, 1962), so this seems to discount the possibility of there being any sacral vertebrae. On the other hand, some fossil cetaceans, such as the protocetids *Protocetus*, *Rodhocetus*, *Gaviacetus*, and others have readily identifiable sacral vertebrae (Fraas, 1904; Gingerich et al., 1994 and 1995).

Slijper (1936) identified sacral vertebrae in modern cetaceans by determining the location of the roots of the pudendal nerve in relation to the vertebral column. These nerve roots arise from the spinal cord and exit through the intervertebral foramina formed by adjacent sacral vertebrae in terrestrial mammals. These vertebrae are anatomically part of the lumbar region. Buchholtz (1998) referred to these vertebrae as sacral lumbars.

No vertebrae articulate with the innominates in *Dorudon atrox*. Thus, by the conventional definition there are no sacral vertebrae. The last lumbar is identified as the caudalmost lumbar vertebra that lacks articular facets for chevron bones. The last few lumbar vertebrae (L17 - L20) have very robust and thickened transverse processes (Fig. 88). The more anterior lumbar vertebrae have transverse processes that are thick at their bases and thin distally. The transverse process of these

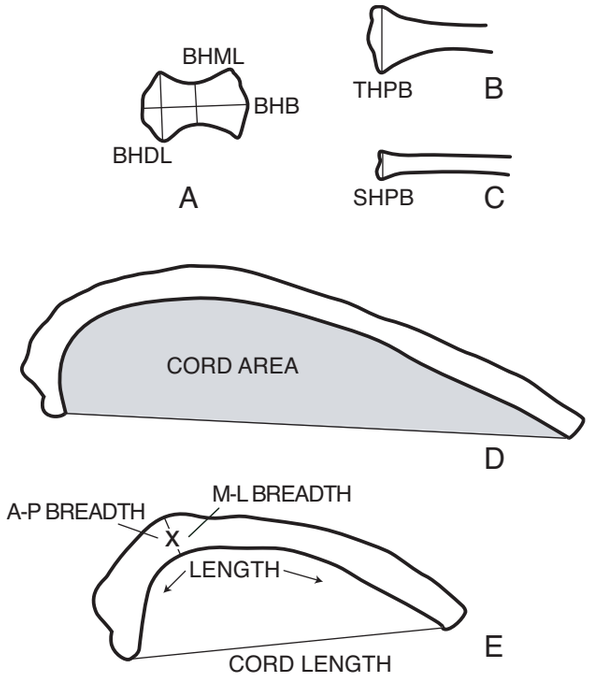

FIGURE 79 — Hyoid and rib measurements for *Dorudon atrox*. A, basihyal; B, thyrohyal; C, stylohyal; D, rib four; E, rib two. Abbreviations: *BHB*, basihyal breadth; *BHML*, basihyal midline length; *BHDL*, basihyal distal length; *SHPB*, stylohyal proximal breadth; *THPB*, thyrohyal proximal breadth. No lengths of stylohyals or thyrohyals are shown since all specimen are broken. The length of the rib in E is the outline length of the edge of the rib. Measurement values for the hyoid elements of *D. atrox* are listed in Appendix IV-C. Measurement values for the ribs of *D. atrox* are listed in Appendix VI-A.

posterior lumbars remain quite thick through much of their length and thin only at their most distal tips. This different morphology suggests that these lumbars could be the former sacral vertebrae, now unfused from each other and disarticulated from the innominates. There are, however, no anatomical features that indicate that any of these vertebrae articulated with the pelvis, and there is no suggestion of an osseous or ligamentous attachment of these vertebrae to the pelvis. The last four lumbar vertebrae (L17-L20) are probably sacral lumbar vertebrae, using the terminology of Buchholtz (1998).

Caudal vertebrae

Classically, cetacean workers have used the presence of the first chevron bone as the start of the caudal region (Flower, 1876). Chevron bones are associated with the preceding vertebra since there is a well-developed synovial joint between the chevron and the preceding vertebra. Thus, the first caudal is the most-anterior vertebra that precedes a chevron bone. The caudal region can be further subdivided into three regions that can be readily identified in modern cetaceans. The first is the anterior caudal region. These are vertebrae that have bodies that are wider than they are tall as viewed from the caudal end. Figure 51 shows the caudal region of a modern spotted dolphin (*Stenella attenuata*) in dorsal and lateral views and illustrates the three divisions of the caudal region. The second caudal division is the peduncular region, which is contained in the caudal peduncle. Peduncular caudals are posterior to the anterior caudals and differ in having bodies that are higher than they are wide when viewed from the caudal end. In addition, the transverse processes, neural arch, and pedicles are very reduced or absent. The third caudal division is the posterior region. Posterior caudals have bodies that are wider than they are high when viewed from the caudal end. The vertebral series goes through a dramatic transition from the peduncular to the posterior caudal vertebrae. As vertebral bodies change from being very high and narrow to being very wide and short. Articular surfaces of the bodies of posterior caudals are almost rectangular in shape: they are broad laterally and short dorsoventrally.

Caudal vertebrae 1-21

There are twenty-one caudal vertebrae in *Dorudon atrox* (see Figs. 89-96). Specimen UM 101222 includes a nearly complete articulated caudal region that is missing only Ca1-4. The caudal region of *D. atrox* cannot be divided into the three regions seen in modern cetaceans. This is because *D. atrox* lacks the peduncular region altogether. This has significant implications for locomotion and reconstruction of the exterior body outline and will be discussed in the next chapter. *D. atrox* caudal vertebrae undergo a series of shape changes down the column from the twelve anterior caudals, which look very much like posterior lumbars but have articulated chevron bones, to the nine posterior caudals, which are very flattened in the plane of the fluke and lack chevron bones. The transition between the anterior and posterior regions is gradual and smooth, but the division is drawn between Ca12 and Ca13, since Ca13 is wider than it is tall. Summary statistics for the measurements of *D. atrox* caudal vertebrae are shown in Table 16.

Body.— The caudal vertebrae decrease in size down the column from cranial to caudal in all vertebral body dimensions. The bodies [**b**] of the anterior caudals (Ca1 to Ca 12) are longer than they are tall or wide, are slightly amphicoelous, and are all moderately waisted, with the deepest constriction at the cranial-caudal midpoint. The posterior caudal vertebrae are wider than they are tall or long, and are not waisted at all. They are flat to convex, with Ca 13 being particularly convex on both its cranial and caudal ends. The last caudal (Ca21) is very small in all dimensions.

The cranial epiphyses [**cre**] of the anterior caudals are generally circular in outline, with slight indentations from circularity in the upper left and upper right quadrants when viewed

TABLE 14 — Measurements of specimens with relatively complete rib cages. Measurements are shown in Figure 79 and are listed in Appendix VIA. Length is the length of the rib measured along the medial edge of the rib from the proximal most point to the distal most point. Cord length is the straight line length from the proximal most point and the distal most point. Cord area is the area enclosed by the length plus cord length lines. A-P breadth is the anterior-posterior thickness of the rib at the angle. M-L breadth is the medial-lateral thickness of the rib at the angle. N, sample size; SD, standard deviation; CV, ratio of the standard deviation to the mean (in percent). All measurements are in millimeters except cord area, which is in square millimeters.

Rib	Measurement	N	Minimum	Maximum	Mean	SD	CV
Rib 1	Length	3	34.6	49.8	40.7	8.1	19.8
	Cord Length	3	14.7	23.3	18.0	4.7	25.9
	Cord Area	3	52.4	81.8	63.4	16.0	25.2
	A-P Breadth	3	10.6	16.7	12.7	3.5	27.3
	M-L Breadth	3	30.6	38.9	34.0	4.3	12.8
Rib 2	Length	4	58.1	69.2	65.0	4.8	7.4
	Cord Length	4	22.7	29.1	26.8	2.9	10.7
	Cord Area	4	121.8	188.7	171.4	33.0	19.3
	A-P Breadth	6	10.4	14.0	12.4	1.6	13.0
	M-L Breadth	6	25.3	37.2	33.2	4.3	13.0
Rib 3	Length	3	66.9	89.2	80.2	11.8	14.7
	Cord Length	3	27.4	38.5	33.3	5.6	16.8
	Cord Area	3	208.7	319.7	276.1	59.2	21.4
	A-P Breadth	5	11.1	16.4	13.1	2.5	18.9
	M-L Breadth	5	19.6	32.0	25.8	5.3	20.7
Rib 4	Length	2	78.8	104.3	91.6	18.0	19.7
	Cord Length	2	31.5	45.3	38.4	9.8	25.4
	Cord Area	2	272.2	387.4	329.8	81.5	24.7
	A-P Breadth	4	10.3	15.7	13.3	2.8	20.8
	M-L Breadth	4	20.9	29.3	26.3	3.9	14.9
Rib 5	Length	3	82.6	109.8	100.0	15.1	15.1
	Cord Length	3	33.5	47.8	41.2	7.2	17.5
	Cord Area	3	310.0	514.2	427.0	105.3	24.7
	A-P Breadth	4	10.3	17.0	13.9	2.8	19.9
	M-L Breadth	4	20.9	30.3	26.7	4.4	16.7
Rib 6	Length	3	81.8	113.9	93.1	18.0	19.3
	Cord Length	3	34.0	49.6	39.8	8.5	21.4
	Cord Area	3	266.8	464.4	346.3	104.3	30.1
	A-P Breadth	5	9.9	17.3	12.9	3.3	25.5
	M-L Breadth	5	21.5	31.7	25.2	4.4	17.3
Rib 7	Length	1	107.6	107.6	107.6	—	—
	Cord Length	1	46.8	46.8	46.8	—	—
	Cord Area	1	451.1	451.1	451.1	—	—
	A-P Breadth	4	10.0	16.7	13.3	3.8	28.5
	M-L Breadth	4	19.4	31.7	25.9	6.2	24.1
Rib 8	Length	2	78.0	97.2	87.6	13.6	15.5
	Cord Length	2	34.5	42.0	38.3	5.3	13.9
	Cord Area	2	230.0	364.6	297.3	95.2	32.0
	A-P Breadth	6	9.1	16.2	12.2	3.0	24.3
	M-L Breadth	6	20.6	33.1	27.8	5.5	19.8
Rib 9	Length	2	76.7	88.5	82.6	8.3	10.1
	Cord Length	2	32.7	40.2	36.5	5.3	14.5
	Cord Area	2	201.0	270.0	235.5	48.8	20.7
	A-P Breadth	5	10.2	15.8	12.4	2.9	23.2
	M-L Breadth	5	21.1	31.6	26.0	4.9	19.0

TABLE 14 (cont.)

Rib	Measurement	N	Minimum	Maximum	Mean	SD	CV
Rib 10	Length	3	74.3	87.3	79.0	7.2	9.2
	Cord Length	3	33.7	40.6	36.4	3.7	10.1
	Cord Area	3	170.5	236.4	196.0	35.4	18.1
	A-P Breadth	5	10.1	13.7	12.0	1.7	14.3
	M-L Breadth	5	19.4	35.3	28.1	7.7	27.2
Rib 11	Length	3	69.5	89.7	81.6	10.7	13.1
	Cord Length	3	32.5	42.1	38.3	5.1	13.3
	Cord Area	3	136.5	236.3	194.6	51.9	26.7
	A-P Breadth	5	9.5	14.6	12.2	2.3	18.5
	M-L Breadth	5	20.7	34.0	27.2	6.0	22.1
Rib 12	Length	1	81.3	81.3	81.3	—	—
	Cord Length	1	38.2	38.2	38.2	—	—
	Cord Area	1	163.9	163.9	163.9	—	—
	A-P Breadth	5	9.4	13.2	12.0	1.5	12.5
	M-L Breadth	5	21.8	29.8	26.9	3.2	12.0
Rib 13	Length	3	62.7	87.6	76.0	12.5	16.5
	Cord Length	3	29.1	38.8	35.2	5.3	15.0
	Cord Area	3	106.4	197.6	142.9	48.3	33.8
	A-P Breadth	4	8.4	14.3	11.2	2.9	26.1
	M-L Breadth	4	17.7	24.5	21.0	3.6	17.3
Rib 14	Length	0	—	—	—	—	—
	Cord Length	0	—	—	—	—	—
	Cord Area	0	—	—	—	—	—
	A-P Breadth	4	8.4	12.4	10.2	2.0	19.4
	M-L Breadth	4	16.1	23.6	19.7	3.6	18.4
Rib 15	Length	1	52.7	52.7	52.7	—	—
	Cord Length	1	25.1	25.1	25.1	—	—
	Cord Area	1	68.7	68.7	68.7	—	—
	A-P Breadth	3	9.5	13.7	10.9	2.4	21.9
	M-L Breadth	3	13.5	22.4	17.0	4.8	28.1
Rib 16	Length	1	68.6	68.6	68.6	—	—
	Cord Length	1	33.1	33.1	33.1	—	—
	Cord Area	1	90.9	90.9	90.9	—	—
	A-P Breadth	3	8.1	10.1	9.1	1.0	11.0
	M-L Breadth	3	13.6	18.0	15.1	2.5	16.9
Rib 17	Length	0	—	—	—	—	—
	Cord Length	0	—	—	—	—	—
	Cord Area	0	—	—	—	—	—
	A-P Breadth	3	8.1	9.4	8.6	0.7	8.4
	M-L Breadth	3	10.0	16.9	12.5	3.8	30.6

from the cranial end. They become more oval in outline down the column, being wider than they are tall. In the posteriormost caudals, the cranial epiphyses are essentially rectangular, being much wider than they are tall. The caudal epiphyses [**cae**] change from very distinctly circular in outline to quite oval in outline from anterior to posterior. The oval forms are wider than they are tall. All are flattened on the ventral border of the epiphysis. In the posteriormost caudals, the caudal epiphyses are rectangular, like the cranial epiphyses.

Deep grooves are present on the lateral sides of the body of Ca13 for the spinal arteries. These grooves are partially enclosed in Ca14, and more so in Ca15, where it is virtually a canal. This structure is a canal in more posterior caudal vertebrae. The canal is approximately midway from cranial to

TABLE 15 — Summary statistics for lumbar vertebra measurements of *Dorudon atrox*. Measurements are shown in Figure 52 and listed in Appendix V. H, cranial centrum height; L, ventral centrum length; W, cranial centrum breadth. N, sample size; SD, standard deviation; CV, ratio of the standard deviation to the mean (in percent). All measurements are in millimeters.

Vertebra	Dimension	N	Minimum	Maximum	Mean	SD	CV
L1	L	3	62.0	70.4	67.1	4.5	6.7
	W	3	74.0	89.5	82.3	7.8	9.5
	H	3	70.0	73.7	71.7	1.9	2.6
L2	L	3	63.0	72.1	68.7	5.0	7.2
	W	2	68.0	93.1	80.6	17.7	22.0
	H	2	69.0	77.9	73.5	6.3	8.6
L3	L	3	64.7	73.0	69.5	4.3	6.2
	W	3	72.0	94.4	83.5	11.2	13.4
	H	3	70.0	81.8	74.6	6.3	8.5
L4	L	3	65.6	74.0	70.6	4.4	6.3
	W	3	75.0	91.1	83.3	8.1	9.7
	H	2	72.3	76.7	74.5	3.1	4.2
L5	L	2	68.8	71.7	70.3	2.1	2.9
	W	2	88.8	92.5	90.7	2.6	2.9
	H	3	71.0	80.1	76.2	4.7	6.2
L6	L	3	72.0	73.0	72.6	0.5	0.7
	W	2	86.9	95.2	91.1	5.9	6.4
	H	3	68.0	81.0	76.5	7.4	9.7
L7	L	3	66.7	74.1	70.6	3.7	5.3
	W	2	70.0	97.6	83.8	19.5	23.3
	H	2	67.0	84.0	75.5	12.0	15.9
L8	L	2	73.0	73.2	73.1	0.1	0.2
	W	2	92.3	92.5	92.4	0.1	0.2
	H	1	88.2	88.2	88.2	—	—
L9	L	3	65.1	78.0	73.3	7.1	9.7
	W	1	98.5	98.5	98.5	—	—
	H	1	83.6	83.6	83.6	—	—
L10	L	2	75.1	77.0	76.1	1.3	1.8
	W	1	96.9	96.9	96.9	—	—
	H	1	86.1	86.1	86.1	—	—
L11	L	3	66.2	80.0	73.4	6.9	9.4
	W	3	77.0	95.8	88.3	9.9	11.3
	H	2	73.0	84.4	78.7	8.1	10.2
L12	L	3	64.0	75.0	70.3	5.7	8.1
	W	1	94.6	94.6	94.6	—	—
	H	1	84.8	84.8	84.8	—	—
L13	L	3	70.0	76.0	72.6	3.1	4.3
	W	1	96.7	96.7	96.7	—	—
	H	2	78.0	81.2	79.6	2.3	2.8
L14	L	2	73.1	76.0	74.6	2.1	2.8
	W	1	95.9	95.9	95.9	—	—
	H	2	77.0	82.8	79.9	4.1	5.1

TABLE 15 (cont.)

Vertebra	Dimension	N	Minimum	Maximum	Mean	SD	CV
L15	L	3	64.5	78.0	73.2	7.6	10.3
	W	2	80.0	94.0	87.0	9.9	11.4
	H	2	75.0	85.7	80.4	7.6	9.4
L16	L	2	74.6	78.0	76.3	2.4	3.2
	W	1	96.3	96.3	96.3	—	—
	H	2	78.0	86.7	82.4	6.2	7.5
L17	L	3	65.0	78.0	73.5	7.3	10.0
	W	1	92.4	92.4	92.4	—	—
	H	2	76.0	82.2	79.1	4.4	5.5
L18	L	3	64.4	78.0	73.2	7.6	10.4
	W	2	78.0	90.0	84.0	8.5	10.1
	H	2	76.0	83.0	79.5	4.9	6.2
L19	L	2	71.0	78.0	74.5	4.9	6.6
	W	1	76.0	76.0	76.0	—	—
	H	1	75.0	75.0	75.0	—	—
L20	L	3	70.0	78.0	75.0	4.4	5.8
	W	2	80.0	92.9	86.5	9.1	10.6
	H	2	79.0	87.6	83.3	6.1	7.3

caudal along the length of the body. The dorsal opening to the spinal arterial canal is farther lateral than the ventral opening in Ca16 to Ca20. Caudal vertebra Ca21 has no canals. The lateral sides of each vertebra are divided into dorsal and ventral processes. Both are somewhat irregular. The dorsal processes project farther laterally than the ventral processes. This inequity is more pronounced in the more caudal vertebrae. The last vertebra, Ca21, is somewhat different. It is not nearly as wide proportionally as Ca17 to Ca20. It is much more square in outline. In addition, it does not have canals for the passage of the spinal arteries.

Paired hemal processes [**hp**] are present on the ventral side of the caudal ends of Ca1 to Ca13. The hemal processes bear articular facets for the chevrons. The hemal processes become less prominent from Ca10 to Ca13. The hemal processes are very reduced in Ca13. These are only a pair of very low tuberosities on the posterior end of the ventral surface of the vertebra. Ca18 to Ca21 have tiny ventral keels that more anterior caudal vertebrae lack.

Neural arch.— The pedicles [**p**] are placed anteriorly on the bodies. They are shorter in this region than in the posterior lumbar region. The pedicles decrease in height from Ca1 to Ca9, especially so from Ca5-9. The pedicles remain the same length in proportion to the length of the body down the column. The pedicles [**p**] of Ca10 to Ca12 are virtually nonexistent. The laminae and metapophyses arise almost directly from the bodies of the vertebrae. The laminae [**l**] become thinned as one moves from Ca1 to Ca12. They also become longer relative to the length of the body. The length of the laminae decreases dramatically from Ca10 to Ca12, to where each is only a very narrow band of bone. Along the midline of the neural arch [**na**] of the caudals, there is a long, stout process that projects posteriorly over the posterior portion of the body. This process projects to the caudal edge of the body. It is broken in all specimens of Ca1 to Ca4, but was almost certainly present. The process becomes more gracile from Ca5 to Ca9, but it remains the same relative length. This process becomes shorter and projects more dorsally as the laminae decrease in length caudal to Ca9. The neural canal [**nc**] decreases in cross sectional area from Ca1 to Ca12. Neural arches and thus neural canals are completely absent from Ca13 to Ca21.

Neural spine.— A single specimen (UM 101215) of *Dorudon atrox* includes the neural spine of one of the first four caudal vertebrae. The spines are broken in all other specimens. This vertebra is a first caudal and has a neural spine that is very short. More posterior caudals starting with Ca5 have low ridges on the midline of the neural arch instead of a neural spine. This suggests that the neural spine dramatically decreases in height from Ca1 to Ca4. The ridge present on Ca5 and Ca6 is absent by Ca7. The sizes of the bases of the neural spines that remain on the neural arches are also consistent with this suggestion. The neural spine is completely absent in more posterior caudals.

Zygapophyses.— The metapophyses [**m**] of Ca1 to Ca9 are very large. These project dorsally and anteriorly beyond the cranial edge of the body. They are very robust and are thickened

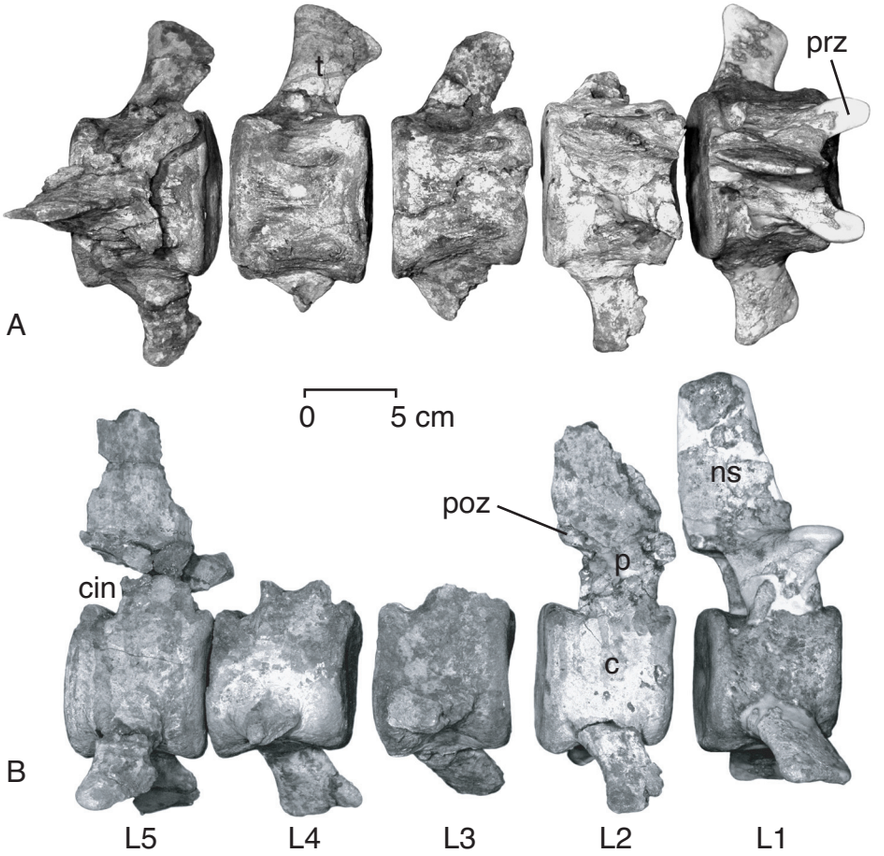

FIGURE 80 — Lumbar vertebrae 1-5 of *Dorudon atrox* (UM 101215) in A, dorsal, and B, right lateral view. The neural arches of L3-4 are missing, as are some transverse processes. The neural spine of L2 is bent laterally to the right. Note the similarity in the size of the vertebral bodies.

at their distal extremities. The metapophyses decrease in size from Ca10 to Ca12 and arise almost directly from the bodies of the vertebrae, since the pedicles are very short to absent. Ca12 is the most posterior caudal vertebra with appreciable metapophyses. No postzygapophyses are present.

Transverse processes.— The transverse processes [**t**] change dramatically from Ca1 to Ca12. Ca1 has a very large, craniocaudally-broad transverse process that is somewhat thickened like those of the posterior lumbar vertebrae. The transverse processes decrease in breadth, thickness, and length from Ca1 to Ca12. More posterior caudals lack transverse processes. The lateral edges of the transverse processes project farther laterally on the cranial ends of the processes, making the lateral edges of the transverse processes angled caudally. The transverse processes of Ca5 to Ca9 change their orientations from ventrally angled to almost horizontal by Ca9. The transverse processes of Ca1-4 are not perforated by foramina for the spinal arteries, with a single exception. The posterior edge of the left transverse process of Ca4 from specimen UM 97512 is perforated by a foramen. Left-right asymmetry of this nature is common in modern odontocetes (personal observation). All of the individuals have the transverse processes of Ca5 to Ca9 perforated by foramina for spinal arteries. The position of the foramen moves from the cranial edge of the transverse process to the caudal edge going from Ca5 to Ca9. It also moves closer to the body as the transverse processes get shorter down the column.

The transverse processes of following vertebrae do not contain foramina for the spinal arteries, rather they are deeply notched for the passage of these blood vessels. This effectively divides each transverse process into two processes, one more anterior, the other more posterior. The more anterior portion projects farther laterally than the more posterior portion. The posterior portion is absent in Ca12, with the last remnant

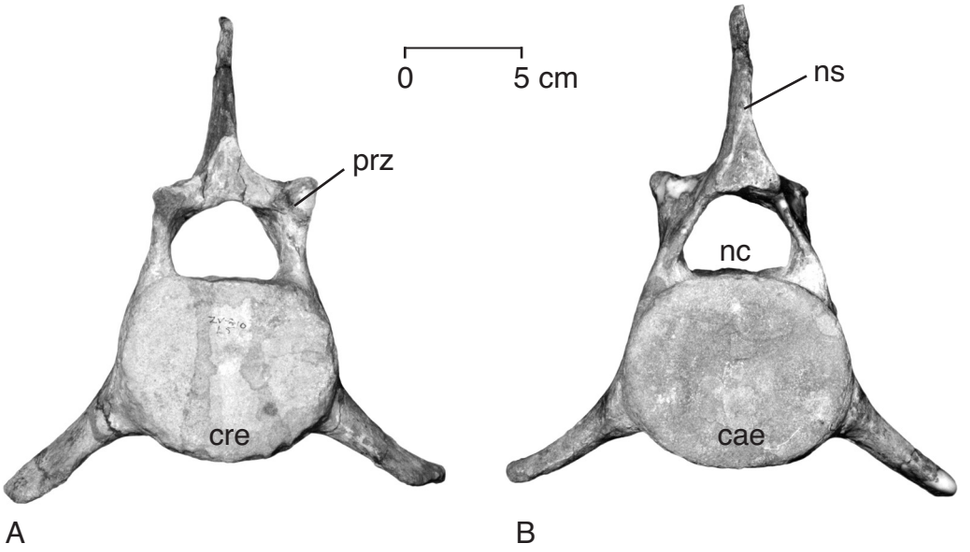

FIGURE 81 — Lumbar vertebra 5 of *Dorudon atrox* (UM 101215) in A, anterior, and B, posterior view. The prezygapophyses and neural spine are damaged.

of the transverse process only represented by the anterior portion. The position of the notch moves from about two thirds of the craniocaudal length of the transverse process to the very caudal end of the process from Ca10 to Ca12.

Chevrons

The chevron bones [**Cv**] articulate with the hemal processes of the anterior caudal vertebrae. Chevrons 1-4 are not known with certainty from any specimen of *Dorudon atrox*, since none have been recovered articulated with these vertebrae. Much of the caudal region of specimen UM 101222 was found in articulation, including many of the chevrons (Fig. 97). Caudal vertebrae seven to twenty one (the ultimate caudal vertebra) were discovered articulated. Additional anterior caudal vertebrae (Ca5 and Ca6) were found disarticulated. The chevron bones of most of the anterior caudal vertebrae represented in this specimen were also recovered, some in articulation with the caudal vertebrae. A chevron bone found disarticulated from the rest of the caudal region may represent one of Cv1 to Cv4. Another specimen CGM 42183 has chevrons Cv7 through Cv9 and Cv11 through Cv12 articulated with the caudal vertebrae. The morphology of these articulated chevrons is consistent with the arrangement of the chevrons described above for UM 101222.

Chevrons seven to nine [**Cv7-9**, Fig. 97] are unpaired **Y**-shaped bones. The anterodorsal ends of the chevrons are the articular surfaces, where they meet the caudal vertebrae they are associated with. The articular surfaces are generally teardrop-shaped, with the apex of the teardrop pointing caudally. The articular surfaces have a slight convexity craniocaudally, and angle toward the midline. The articular processes are joined to the bodies of the chevrons by flat plates of bone reminiscent of the pedicles of the neural arches of the vertebrae. They are flat, with their surfaces parallel to the long axis of the body. They join the bodies of the chevrons on the dorsal side of its cranial end. The bodies of the chevrons are generally flat on their ventral surfaces. The dorsal surfaces of the bodies are concave. There are pronounced bumps on their lateral sides where the articular processes join the bodies. Their cranial edges are **U**-shaped where the articular processes meet the bodies and meet along the midline. The caudal ends of the flat bodies have two small protuberances, one on each side, which are connected by a gently curving edge through the midline.

The chevrons get more robust from Cv7 to Cv9. The bodies are dorsoventrally thicker and the articular processes more stout. In addition, the articular processes are more craniocaudally broad than in the anterior chevron described above. The posterior breadth from one posterior process to the other decreases significantly from Cv7 to Cv9.

Chevrons ten to thirteen are very different from the more anterior chevrons. Rather than a single bone at each position, there is a pair of bones associated with each caudal vertebra, one left, the other right. Each chevron is composed of an articular surface and a plate of bone extending ventrally from the articular surface that are together serially homologous with the articular process of the anterior chevrons. The ventral

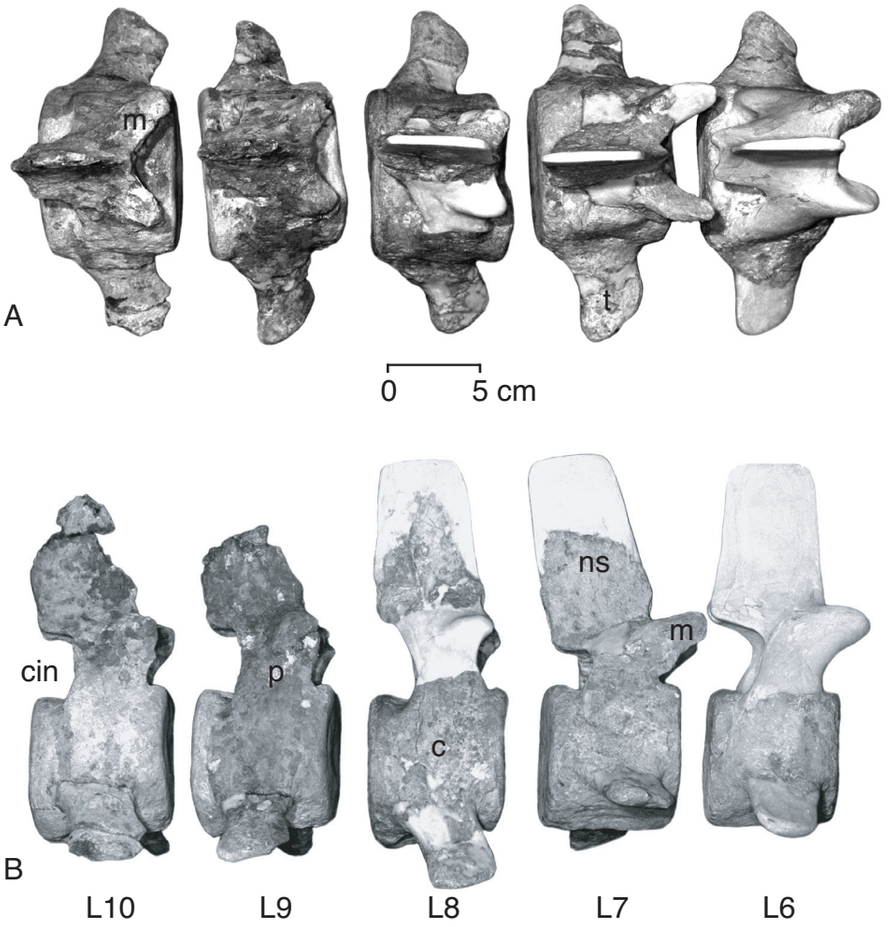

FIGURE 82 — Lumbar vertebrae 6-10 of *Dorudon atrox* (UM 101215) in A, dorsal, and B, right lateral view. Much the anatomy of L6 to L8 has been reconstructed. The neural spines and prezygapophyses of L9 and L10 are broken.

midline body is missing. When viewed laterally, each bone of the pair is in the shape of a rough parallelogram, with the articular (proximal) end cranialmost, and the bony plate angling caudally. This caudal angulation is most pronounced in Cv10 and much less pronounced in Cv11 through Cv13. Chevron 13 is reduced to only a short, teardrop-shaped articular surface, with a small caudoventral projection. The body of each chevron also angles toward the midline.

As in the anterior chevrons, the articular surfaces are teardrop-shaped, with the apex of the teardrop pointing caudally. The shape of the articular surfaces becomes less teardrop-shaped and more oval from Cv10 to Cv12. In addition, they become less craniocaudally elongated. The ventral borders of Cv10 and Cv11 are thickened, with surfaces for the attachment of ligaments and/or tendons. It is unclear whether this thickened border was present in Cv12 due to damage. The chevrons decrease dramatically in size and increase in robustness from Cv10 to Cv13. No chevrons are known posterior to Cv13.

Kellogg (1936) illustrates two different chevron bones for *Zygorhiza kochii* (his Figs. 69 and 70, p. 158). The first (his fig. 69) is very much like the middle chevrons described above. Nothing like the second (his fig. 70) has been seen in *Dorudon atrox*. It may be that the more anterior chevrons are similar to the second type from *Z. kochii* illustrated by Kellogg (1936). In addition, Kellogg (1936) shows the chevrons articulated with the caudal vertebrae of *Zygorhiza kochii* at an odd angle (his plate 1B). He shows the chevrons pointing directly ventrally from the ventral sides of the vertebrae. The chevrons described

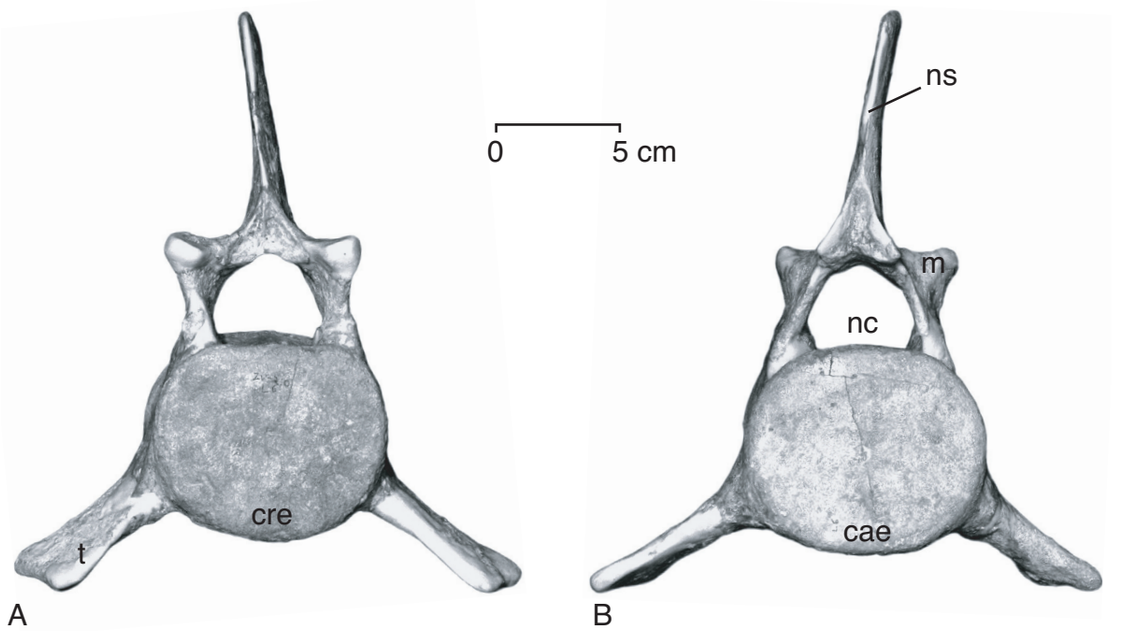

FIGURE 83 — Lumbar vertebra 6 of *Dorudon atrox* (UM 101215) in A, anterior, and B, posterior view. The neural spine is bent laterally to the right. The prezygapophyses have been reconstructed.

here clearly articulated at an angle to the caudal vertebrae based on the preserved positions in articulated specimens, the angle of the plane of their articular surfaces, and the orientation of the plane of the body. When a chevron is articulated at an angle, the body lies flat and the cranial end of the bone forms an opening through which blood vessels can pass and subsequently lie on the dorsal surface of the body of the chevron as they continue in a caudal direction.

FORELIMB

Shoulder girdle

Scapula

The scapula [**Sc**, Fig. 98] of *Dorudon atrox* is very different from that of its terrestrial ancestors and very much like the scapula of modern cetaceans. Most terrestrial mammals, including the relatives of cetaceans, have narrow scapulae that have supraspinous and infraspinous fossae of subequal area. Modern cetaceans and *D. atrox* have broad, fan-shaped scapula with a reduced supraspinous fossa (absent in some modern taxa). *D. atrox* has a large supraspinous fossa relative to most modern cetaceans, but it is relatively small when compared to terrestrial mammals. In addition, *D. atrox* shares large, anteriorly-projecting acromion and coracoid processes with most modern cetaceans. Measurements of the scapula are shown in Figure 99. Summary statistics for the measurements of *D. atrox* scapulae are shown in Table 17.

The surfaces of the scapula are smooth, lacking the vertical striations found in the infraspinous fossae of many modern cetaceans. The spine [**s**] of the scapula arises from the lateral surface. The spine runs from near the vertebral border of the scapula ventrally to the acromion process [**ac**]. The spine is low near the vertebral border and becomes more prominent near the acromion. It is very low when compared to the scapular spines of terrestrial mammals of similar size. In addition, the spine arises nearly perpendicular to the plane of the scapula near the vertebral border, but becomes angled, leaning anteriorly as the spine joins with the acromion process. The spine forms the division between the supraspinous fossa [**spsf**] anterior to the spine and the infraspinous fossa [**isf**] posterior to the spine.

The supraspinous fossa has a moderate to large area in relation to the rest of the scapula for a cetacean. It is delimited by the anterior and vertebral borders of the scapula and by the spine of the scapula. The supraspinous fossa is the site of origin for the supraspinatus muscle.

The infraspinous fossa is delimited by the vertebral border of the scapula, the scapular spine, and a ridge separating the

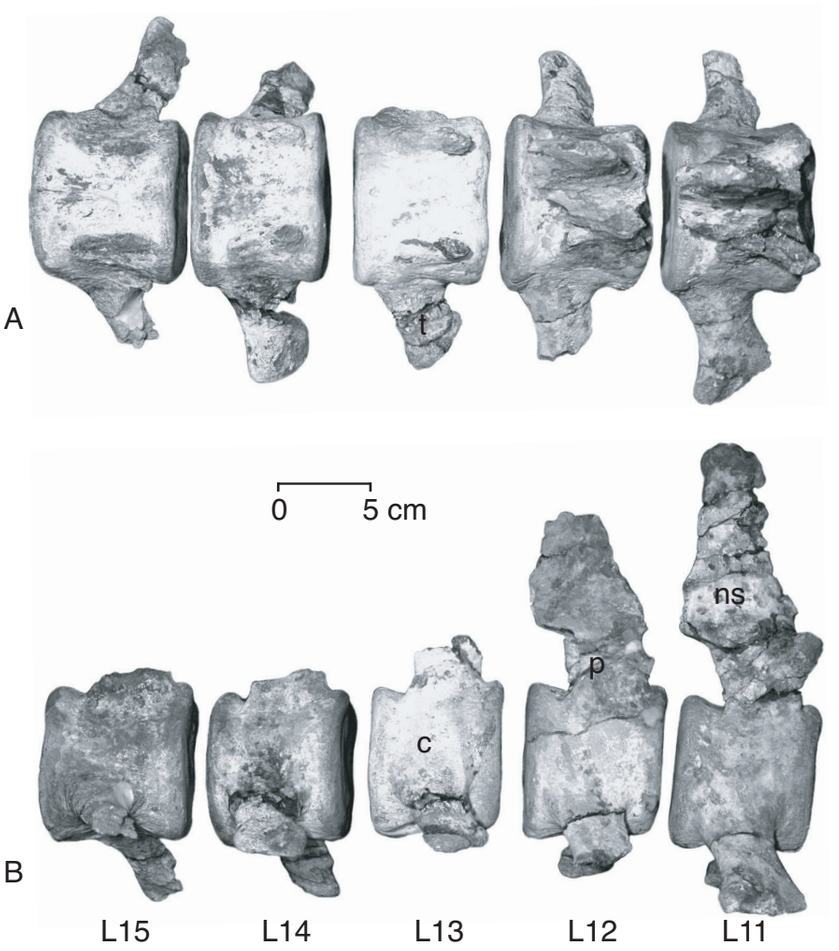

FIGURE 84 — Lumbar vertebrae 11-15 of *Dorudon atrox* (UM 101215) in A, dorsal, and B, right lateral view. The neural arches of L13 to L15 are missing, as are the tips of many transverse processes. Note the presence of nutrient foramina on the dorsal faces of the vertebral bodies missing neural arches.

infraspinous fossa from the teres fossa on its posterior border. The infraspinous fossa is the site of origin for the infraspinatus and deltoideus muscles.

The teres fossa [**tf**] is delimited by a ridge between it and the infraspinous fossa, the vertebral border of the scapula, and the posterior border of the fossa. It is the site of origin of the teres major muscle.

In cetaceans, the acromion process has lost its articulation with the clavicle, since the clavicle is not present in modern cetaceans (but see Klima, 1990). The clavicle appears to be absent in *Dorudon atrox* as well. The lateral face of the acromion is a site of origin for the deltoideus muscle, while the medial side is a site of origin for some fibers of the supraspinatus muscle. The acromion process is very long, flat, and dorsoventrally deep. It projects anteriorly from the base of the scapular spine.

The glenoid cavity [**gc**] is a pear-shaped depression on the ventral border of the scapula that forms the articulation with the humerus. The scapular tuberosity [**sct**] is on the anterior side of the glenoid cavity slightly ventral to the coracoid process. It is the origin of the tendon of the biceps brachii muscle, but is indistinct in *Dorudon atrox*. The edges of the glenoid are rounded rather than sharp. The glenoid cavity is set off from the body of the scapula by a short neck. The caudal border of this neck has an indistinct tubercle for the origin of the long head of the triceps brachii muscle.

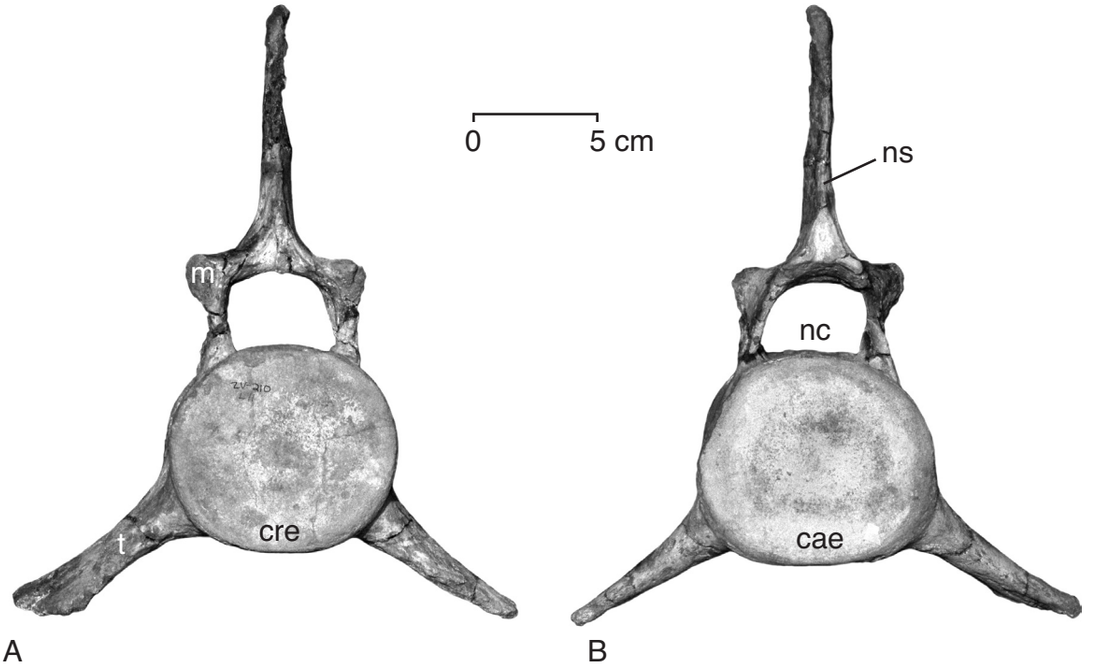

FIGURE 85 — Lumbar vertebra 11 of *Dorudon atrox* (UM 101215) in A, anterior, and B, posterior view. Note the complex triangular area where the neural spine meets the laminae of the neural arch.

The coracoid process [**cp**] of the scapula projects anteriorly and curves ventrally, lying near the medial face of the scapula (Fig. 98b, c). It is much larger than in the terrestrial ancestors of cetaceans. The coracoid process is often large in modern cetaceans. It is usually flat and sometimes lost. In *D. atrox*, the coracoid process is very robust, with a rounded distal end. It forms the origin of the coracobrachialis muscle.

The subscapular fossa [**sbsf**] is on the medial side of the scapula. It is generally flat, with the anterior border turned gently medially. This forms a broad, shallow fossa opposite the supraspinous fossa on the lateral side. There are no spines, ridges, or tuberosities that are distinguishable on the medial side of the scapula. The subscapular fossa is the origin of the subscapularis muscle.

The vertebral border [**vb**] of the scapula is in the shape of a broad arc, with the highest point of the arc on the dorsal-most point of the blade. The vertebral border has a shallow groove in it, and a rough surface. This indicates the presence of the cartilaginous extension of the vertebral border that is present in most modern cetaceans. The cranial border [**crb**] curves cranially (anteriorly) from the neck of the scapula where the blade joins the glenoid cavity. The cranial border then curves back caudally to joint the vertebral border where the spine meets the border on the lateral side. The caudal border [**cab**] is cranially convex, meeting the vertebral border at a rounded angle of about 80°.

Brachium

Humerus

The humerus of *Dorudon atrox* [**H**, Fig. 100] is very much like that of other archaeocetes. It retains some primitive characters of terrestrial quadrupeds including: well-defined greater and lesser tuberosities, long deltopectoral crest, and a synovial-joint surface at the elbow. The humerus of *D. atrox* is like modern cetacean humeri in that it is much less gracile than the humeri of terrestrial mammals. The expanded distal articular surface of the humerus of modern cetaceans, which effectively locks the antebrachial elements in place relative to the humerus, is round in *D. atrox*. Measurements of the humerus are shown in Figure 101. Summary statistics for the measurements of *D. atrox* humeri are shown in Table 18.

The head of the humerus [**h**] articulates with the glenoid cavity of the scapula. The head is hemispherical to somewhat ovoid in shape. The head is slightly elongated craniocaudally. The curvature of the head is much more convex than the glenoid cavity of the scapula is concave (see Scapula, above).

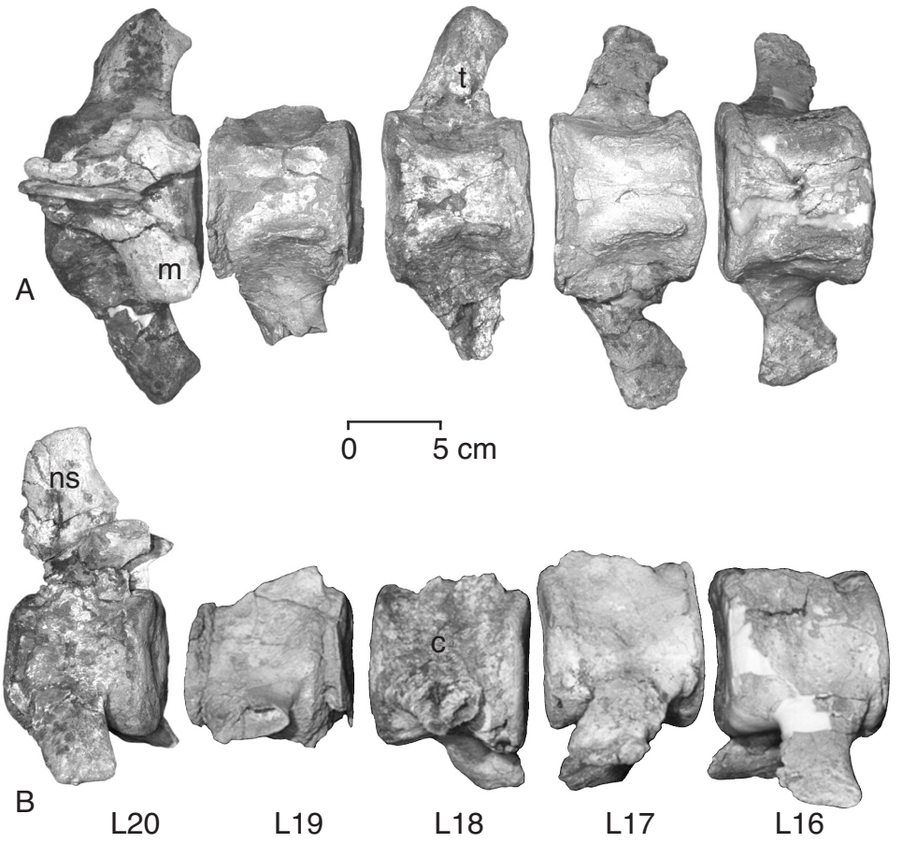

FIGURE 86 — Lumbar vertebrae 16-20 of *Dorudon atrox* (UM 101215) in A, dorsal, and B, right lateral view. The neural arches of L16 to L19 are missing. Note the short neural spine and robust transverse processes of L20.

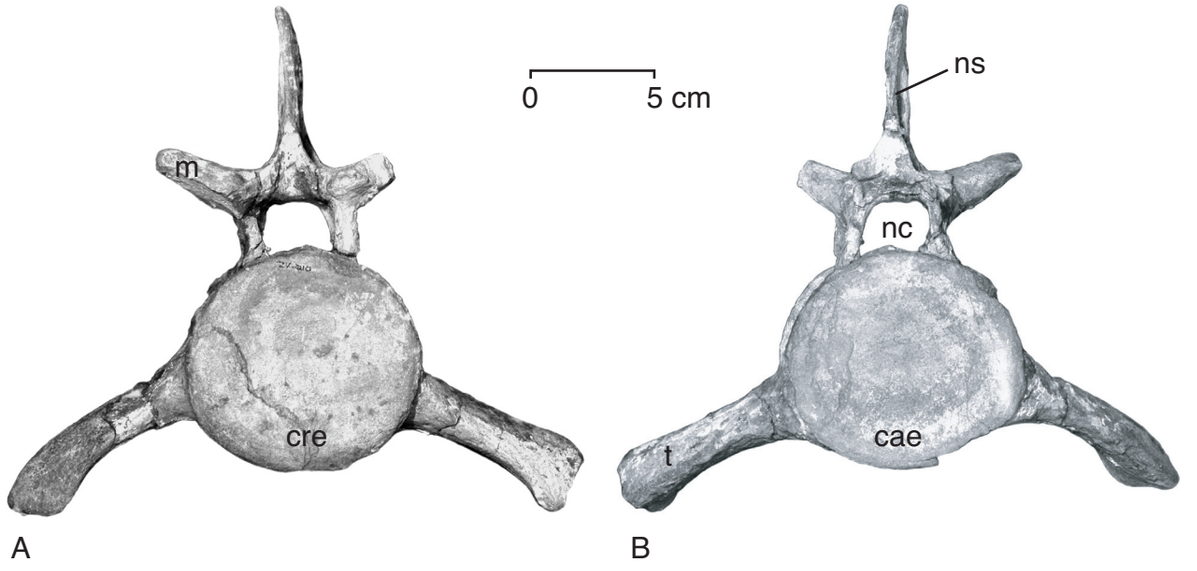

FIGURE 87 — Lumbar vertebra 20 of *Dorudon atrox* (UM 101215) in A, anterior, and B, posterior view. Note the short neural spine, robust transverse processes, and small neural canal.

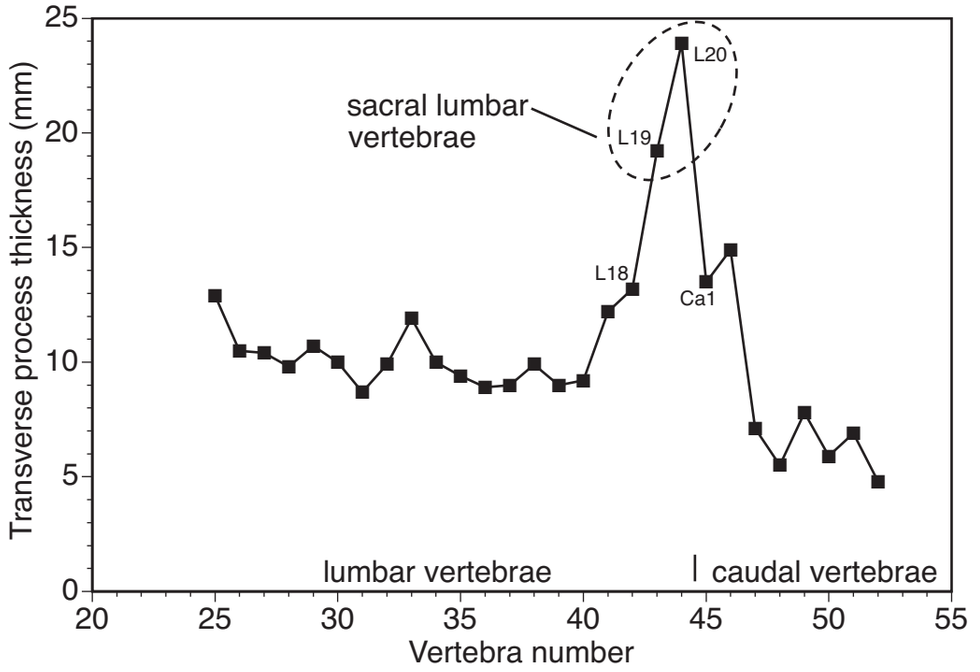

FIGURE 88 — Plot of transverse process thickness of lumbar and anterior caudal vertebrae of *Dorudon atrox*, UM 101215. Note that the thickness is relatively constant in most of the lumbar region, but it goes up dramatically at the end and in the first two caudal vertebrae. The vertebrae with the thickened transverse processes are the ones that Kellogg (1936) identified as sacral vertebrae in *Basilosaurus cetoides.* The last four lumbar vertebrae are here identified as the sacral lumbar vertebrae, using the terminology of Buchholtz (1998).

The medial side of the articular surface of the head grades onto the lesser tubercle via a shallow sulcus. This sulcus continues caudally and changes direction almost 90° and becomes a deep groove that parallels the shaft of the humerus. The groove terminates at the epiphysis-diaphysis suture. The head terminates craniomedially at a continuation of the bicipital groove [**bg**]. The head is separated from the shaft of the humerus by a weakly-developed neck. The neck is most prominent on the caudal edge where the shaft flares out somewhat to meet the distal edge of the caudal border of the head.

The shaft of the humerus [**sh**] is slightly concave medially. In cross section the shaft is teardrop shaped, with the cranial edge much thinner than the caudal edge, due to the presence of a broad deltopectoral crest [**dpc**]. This crest is the point of insertion of the deltoideus and pectoralis major muscles. The caudal edge has a slight caudal expansion at about the same distance proximally from the trochlea as the major expansion of the deltopectoral crest.

The greater tubercle of the humerus [**gt**] is cranial and medial to the head. The greater tubercle is proximal to and confluent with the broad deltopectoral crest on the shaft of the humerus (see below). It projects slightly higher than the head, and is about equal in height to the projection of the lesser tubercle. It is cranial to and separated from the lesser tubercle by the bicipital groove. The greater tubercle is the point of insertion for the supraspinatus muscle.

The lesser tubercle of the humerus [**lt**] is slightly cranial and medial to the head. The lesser tubercle is separated from the head by a shallow sulcus. The lesser tubercle has two broad prominences, one more cranial and the other more caudal. The lesser tubercle is caudal to and separated from the greater tubercle by the bicipital groove. The lesser tubercle is the point of insertion for the subscapularis muscle on the cranial prominence, and the teres major muscle on the caudal prominence.

Articulations with the radius and ulna are different enough from terrestrial mammals to warrant some critical evaluation of the homology of structures. In terrestrial mammals, including cetacean ancestors, the distal ulnar articular surface is divided into the capitulum [**cpt**] (radial articulation) and trochlea [**tr**] (ulnar articulation). The capitulum is usually a shallow sulcus on the lateral border of the articular surface. The trochlea is a deep sulcus on the medial side of the articular surface. There is sometimes a low ridge separating the two surfaces. In modern cetaceans, the radius and ulna rest in a sulcus that covers the

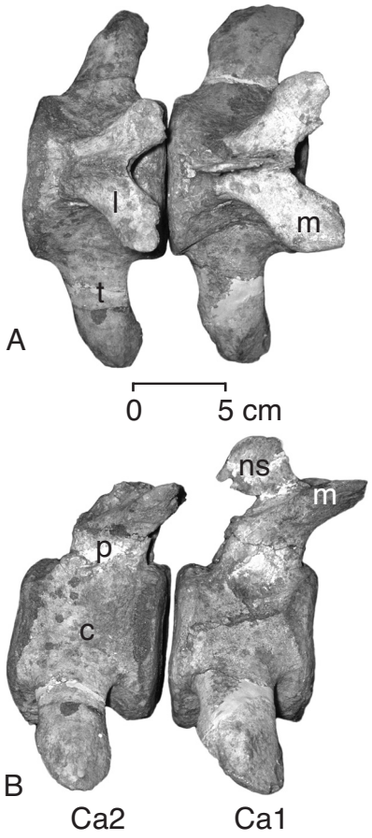

FIGURE 89 — Caudal vertebrae one and two (Ca1 and Ca2) of *Dorudon atrox* (UM 101215) in A, dorsal, and B, right lateral view. Note that the neural spine of Ca2 is broken.

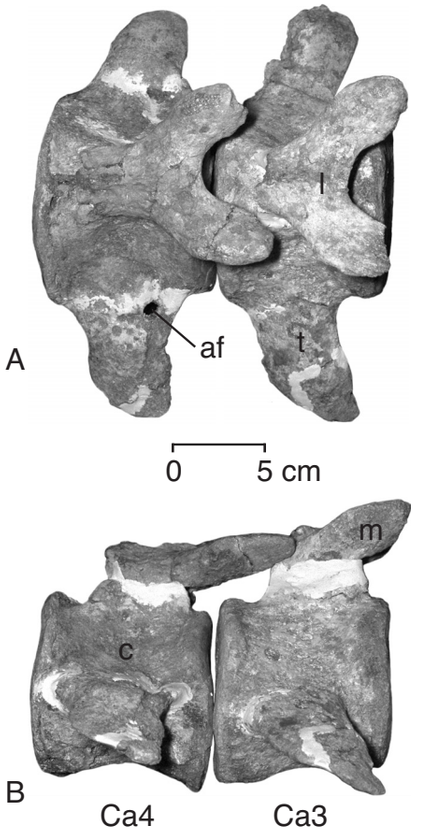

FIGURE 90 — Caudal vertebrae three and four (Ca3 and Ca4) of *Dorudon atrox* (UM 101215) in A, dorsal, and B, right lateral view. Note that the neural spines of both vertebrae are broken. Note also the presence of foramina in the transverse process of caudal vertebra four.

entire distal end of the humerus in two flat surfaces. The distal humerus is expanded craniocaudally with the radius resting on the surface anterior to the ulna. There is little or no movement in modern cetaceans at this joint. There is no division of the distal humerus into capitulum and trochlea. In *Dorudon atrox*, both the radius and ulna articulate with the humerus in a common sulcus, like modern cetaceans, but the articular surface is not broadly expanded like that of modern cetaceans. The joint surface remains synovial and functional in *D. atrox*. In addition, on the lateral side of this articular surface, there is a very low ridge and a very shallow sulcus just on the edge of the articular surface. This structure is positionally equivalent to the capitulum in terrestrial mammals, and is here interpreted as a vestige of this structure. The radius has migrated medially to rest medial to the ulna, on the same articular surface as the ulna, which will subsequently be referred to as the trochlea.

The distal end of the humerus is shaped like an asymmetrical saddle, with the lateral edge extending slightly more distally than the medial edge. The lateral and medial edges of the trochlea are separated by a sulcus that is shallow and broad on the cranial border, becoming deeper and narrower toward the caudal border. The sulcus is in the midline of the saddle formed from the medial border of the trochlea and the low ridge separating the capitulum. The articular surface extends from the cranial border around the distal edge of the humerus up onto the caudal border of the humerus to the olecranon fossa [**of**]. The articular surface is widest at its most distal point and narrows toward the cranial and caudal borders of the humerus. There is no supratrochlear foramen, or entepicondylar foramen.

The medial condyle of the humerus is much larger than the lateral condyle, which is very low. The flexor carpi radialis, flexor carpi ulnaris, and flexor digitiorum communis all originate on the medial condyle.

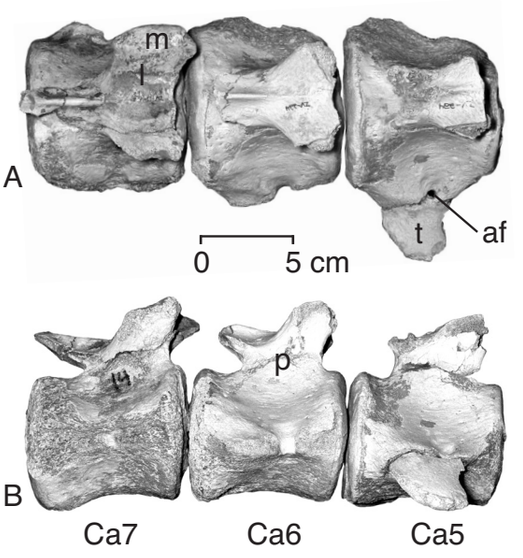

FIGURE 91 — Caudal vertebrae five to seven (Ca5-Ca7) of *Dorudon atrox* (UM 101222) in A, dorsal, and B, right lateral view. Note that the neural spines of the vertebrae are not broken, but they have been reduced such that they are only represented by a midline ridge. Note also the presence of foramina in the transverse process of each of the vertebrae and the very long, caudally-projecting midline processes. The metapophyses are broken on Ca5 and Ca6.

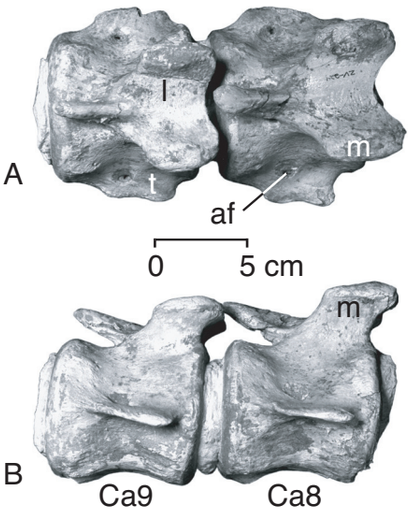

FIGURE 92 — Caudal vertebrae eight and nine (Ca8 and Ca9) of *Dorudon atrox* (UM 101222) in A, dorsal, and B, right lateral view. Note the presence of foramina in the transverse process of each of the vertebrae and the very long, caudally-projecting midline processes. These vertebrae are virtually complete.

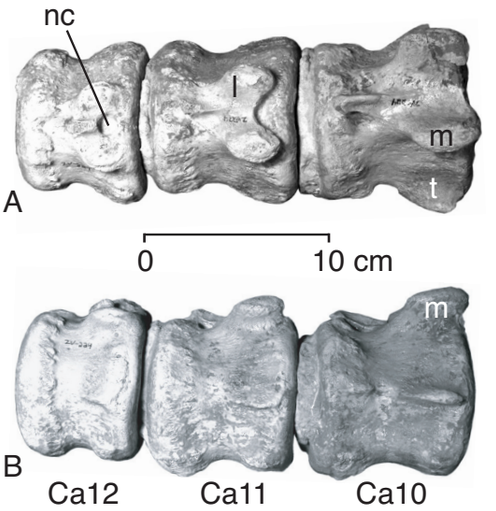

FIGURE 93 — Caudal vertebrae ten to twelve (Ca10-Ca12) of *Dorudon atrox* (UM 101222) in A, dorsal, and B, right lateral view. Note the foramina in the transverse processes are no longer closed, but are represented by a notch in Ca10. The transverse processes are almost completely reduced and the neural arches and neural canals are decreasing in size.

Antebrachium

Ulna

The ulna [**U**, Figs. 102 and 105] articulates proximally with the trochlea of the humerus and the caudal border of the radius. The shaft is flattened in the plane of the flipper. The trochlear notch [**tn**] which contains the surface that articulates with the humerus, is teardrop-shaped in plan view, and saddle-shaped when viewed laterally. There is a notch in the humeral articular surface of the ulna, near the proximal end of the medial border. The trochlear notch articulates with the caudal end of the trochlea of the humerus, behind the radius. The proximal edge of the trochlear notch fits into the olecranon fossa on the caudal border of the humerus. Measurements of the ulna are shown in Figure 103. Summary statistics for the measurements of *D. atrox* ulnae are shown in Table 19.

The olecranon process [**op**] is large and blade-shaped. The length of the olecranon process is about one half of the length of the shaft. The olecranon process thins toward its proximal edge from a maximum thickness where it joins the shaft of the ulna. The olecranon epiphysis is usually unfused to the olecranon process. Only in the oldest individual of *Dorudon atrox* (UM 101215) is the epiphysis fused to the process. The medial side of the proximal edge of the blade is rugose and is the point of insertion of the triceps muscle.

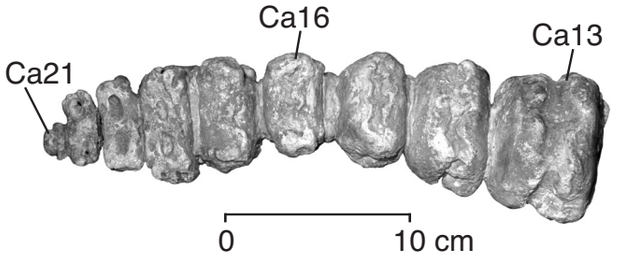

FIGURE 94 — Caudal vertebrae thirteen to twenty-one (Ca13-Ca21) of *Dorudon atrox* (UM 101222) in dorsal view. This series was found articulated in the field and has been left as it was found. There is a slight twist in the series between Ca15 and Ca16. Note the dramatic shape change from anterior to posterior.

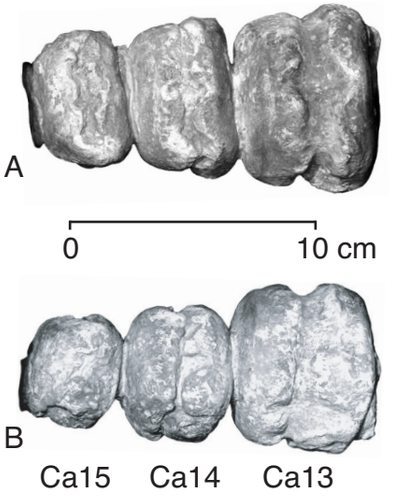

FIGURE 95 — Caudal vertebrae thirteen to fifteen (Ca13-Ca15) of *Dorudon atrox* (UM 101222) in A, dorsal, and B, right lateral view. Note the vertical grooves along the lateral sides of Ca13 and Ca14 that are enclosed in foramina in Ca15. Note also that Ca13 is approximately as wide as it is tall, and that the others are wider than they are tall. This point of shape transition marks the insertion of the fluke on the caudal vertebrae in modern cetaceans.

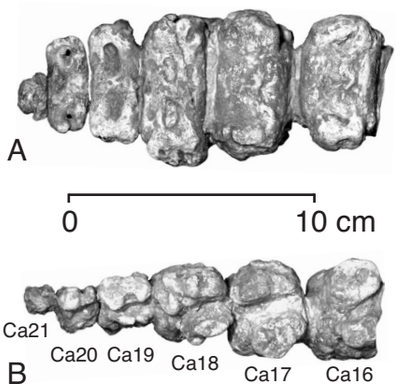

FIGURE 96 — Caudal vertebrae sixteen to twenty-one (Ca16-Ca21) of *Dorudon atrox* (UM 101222) in A, dorsal, and B, right lateral view. Note that the vertebrae are dorsoventrally compressed, and wider than they are tall. These vertebrae were all within the fluke. The last vertebra (Ca21) shown here is almost certainly the last, as no more vertebrae were found this articulated series.

The coronoid process of the ulna [**cnp**] projects cranially from the border of the trochlear notch, on the medial side of the trochlear notch. The coronoid process forms the medialmost contact of the ulna with the radius. The radius articulates with the cranial (radial) edge of the articular surface of the trochlear notch and with the coronoid process. The radial notch [**rn**] which is just distal to the articulation, accepts the projection of the proximal radial articular surface, but does not form part of the articulation itself.

The interosseous crest of the ulna [**uic**] arises from the lateral border of the articular surface of the trochlear notch. It continues distally to join the cranial (radial) border of the ulna. This crest forms the insertion of the interosseous membrane between the radius and ulna.

The distal epiphysis of the ulna articulates with the pisiform, cuneiform, and lunate. The styloid process [**stp**] is somewhat subdued, but present. It forms the articular surface for the pisiform on its caudal border, and for the cuneiform on its more distal/cranial border. The distal ulnar epiphysis has two distinct facets. The more caudal facet articulates with the cuneiform, while the more cranial (radial) facet articulates with the lunate. There is a flattened area on the cranial (radial) border of the shaft and distal epiphysis of the ulna forming the distal articulation with the radius.

Radius

The radius [**Rd**, Fig. 102 and 105] articulates proximally with the trochlea of the humerus and rests anterior to the ulna, which also articulates with the trochlea. The radius is curved cranially in the plane of the flipper, with the apex of the arc of curvature about midshaft. The main portion of the shaft is flattened in the plane of the flipper, but the proximal end is somewhat more cylindrical and the distal end is thicker than the main portion of the shaft. Measurements of the radius are shown in Figure 103. Summary statistics for the measurements of *D. atrox* radii are shown in Table 19.

TABLE 16 — Summary statistics for caudal vertebra measurements of *Dorudon atrox*. Measurements are shown in Figure 52 and listed in Appendix V. H, cranial centrum height; L, ventral centrum length; W, cranial centrum breadth. N, sample size; SD, standard deviation; CV, ratio of the standard deviation to the mean (in percent). All measurements are in millimeters.

Vertebra	Dimension	N	Minimum	Maximum	Mean	SD	CV
Ca1	L	3	70.9	78.0	74.9	3.6	4.9
	W	2	81.0	89.1	85.1	5.7	6.7
	H	2	81.0	87.6	84.3	4.7	5.5
Ca2	L	3	68.6	80.0	74.9	5.8	7.7
	W	3	83.0	94.6	89.2	5.8	6.5
	H	2	81.0	87.3	84.2	4.5	5.3
Ca3	L	3	70.6	78.0	74.8	3.8	5.1
	W	1	85.8	85.8	85.8	—	—
	H	2	77.0	84.6	80.8	5.4	6.7
Ca4	L	3	67.5	78.0	74.0	5.7	7.7
	W	3	85.0	95.9	89.5	5.7	6.4
	H	2	75.0	85.7	80.4	7.6	9.4
Ca5	L	3	72.1	79.0	75.4	3.5	4.6
	W	3	89.0	93.0	90.8	2.0	2.2
	H	2	76.0	82.0	79.0	4.2	5.4
Ca6	L	4	73.5	85.0	78.0	4.9	6.3
	W	3	85.0	95.3	91.4	5.6	6.1
	H	3	75.4	81.5	78.0	3.2	4.1
Ca7	L	5	68.0	85.0	77.8	6.8	8.7
	W	4	81.0	92.9	87.7	6.0	6.9
	H	3	72.0	80.6	76.5	4.3	5.6
Ca8	L	4	70.0	81.0	75.5	4.7	6.2
	W	3	87.9	92.5	90.4	2.3	2.6
	H	2	75.3	82.4	78.9	5.0	6.4
Ca9	L	3	66.5	80.9	74.8	7.4	10.0
	W	2	86.7	88.6	87.7	1.3	1.5
	H	2	74.7	75.0	74.9	0.2	0.3
Ca10	L	3	63.2	79.5	71.2	8.2	11.4
	W	3	83.9	88.4	85.4	2.6	3.0
	H	2	76.7	79.0	77.9	1.6	2.1
Ca11	L	3	61.9	75.0	67.3	6.8	10.2
	W	3	80.0	87.2	83.6	3.6	4.3
	H	2	74.3	79.4	76.9	3.6	4.7
Ca12	L	4	51.0	63.2	57.1	5.0	8.7
	W	3	78.8	85.0	82.1	3.1	3.8
	H	3	74.8	81.0	78.4	3.2	4.1
Ca13	L	4	39.0	54.5	47.8	6.5	13.6
	W	4	68.0	82.4	76.6	6.2	8.1
	H	2	70.1	72.3	71.2	1.6	2.2
Ca14	L	4	34.0	41.1	38.1	3.0	7.8
	W	4	64.6	80.2	69.3	7.4	10.6
	H	3	51.0	67.5	58.7	8.3	14.1

TABLE 16 (cont.)

Vertebra	Dimension	N	Minimum	Maximum	Mean	SD	CV
Ca15	L	5	28.0	31.0	30.1	1.3	4.2
	W	5	51.0	72.8	59.4	8.4	14.2
	H	4	48.3	67.2	56.5	7.9	13.9
Ca16	L	5	27.2	29.5	28.3	0.9	3.1
	W	5	37.0	53.8	46.4	6.1	13.1
	H	4	37.4	59.3	47.5	9.0	18.9
Ca17	L	3	22.7	29.7	26.1	3.5	13.4
	W	2	38.1	46.1	42.1	5.7	13.4
	H	2	31.3	33.2	32.3	1.3	4.2
Ca18	L	2	21.0	26.7	23.9	4.0	16.9
	W	1	34.0	34.0	34.0	—	—
	H	1	28.5	28.5	28.5	—	—
Ca19	L	1	19.8	19.8	19.8	—	—
	W	1	27.4	27.4	27.4	—	—
	H	1	22.3	22.3	22.3	—	—
Ca20	L	2	13.3	15.5	14.4	1.6	10.8
	W	2	24.6	26.7	25.7	1.5	5.8
	H	2	13.0	17.9	15.5	3.5	22.4
Ca21	L	1	11.0	11.0	11.0	—	—
	W	1	14.3	14.3	14.3	—	—
	H	1	9.8	9.8	9.8	—	—

The head of the radius [**rh**] articulates with both the distal humerus and the proximal ulna. The humeral articular surface of the head is a broad saddle-shaped surface, with the upturned edges of the depression on the anterior and posterior edges, and the axis of the depression of the saddle running mediolateral. This surface matches perfectly with the upturned edge of the trochlea on the anterior edge of the distal humerus, with which the radius articulates.

The articular circumference of the radius [**arc**] is a small eminence on the ulnar side of the head. It forms the articular surface with the ulna. Its small size and thus limited range of motion relative to the ulna, in which it can remain articulated with the ulna, indicates that forearm pronation or supination at the elbow was not possible.

The radial neck [**rdn**] is not very prominent. The flattened shaft of the radius flares out gradually in the proximal one-fourth of its length to meet the more cylindrical head. Just distal to the neck are three separate tuberosities. The largest, on the medial side of the radius, is the radial tubercle [**rt**], which is the insertion for the m. biceps brachii. It is in the shape of a ridge that parallels the medial surface of the head but projects from the shaft about 1 cm distal to the head. Another of the tuberosities is on the ulnar (caudal) side of the radius. It is at the most proximal point on the radial interosseous crest [**ric**]. It serves as the most proximal attachment point for the interosseous membrane. The interosseous crest continues distally to merge with the ulnar (caudal) border of the radius. The third tubercle on the proximal end of the radius is a small eminence on the cranial edge, just distal to the neck.

As noted above, the shaft is flattened in the plane of the flipper. The most conspicuous feature of the shaft is the presence of a broad eminence in the plane of the flipper, about one third of the length of the shaft from the proximal end of the radius. Kellogg (1936) interprets this as the insertion of the pronator teres muscles, but since the elbow joint could not allow pronation this seems doubtful.

The distal end of the radius encompasses articulations with the distal ulna, lunate, and scaphoid. The ulnar articulation is in the form of a broad flattened area on the caudal (ulnar) border of the shaft of the radius. This flat area is expanded somewhat by a raised projection from the shaft of the radius. The distal epiphysis of the radius forms the carpal articular surface, which articulates with the lunate and scaphoid. The distal epiphysis has two distinct facets, the larger, more caudal (ulnar) facet for the lunate, and the smaller, more cranial (anterior) facet for the scaphoid.

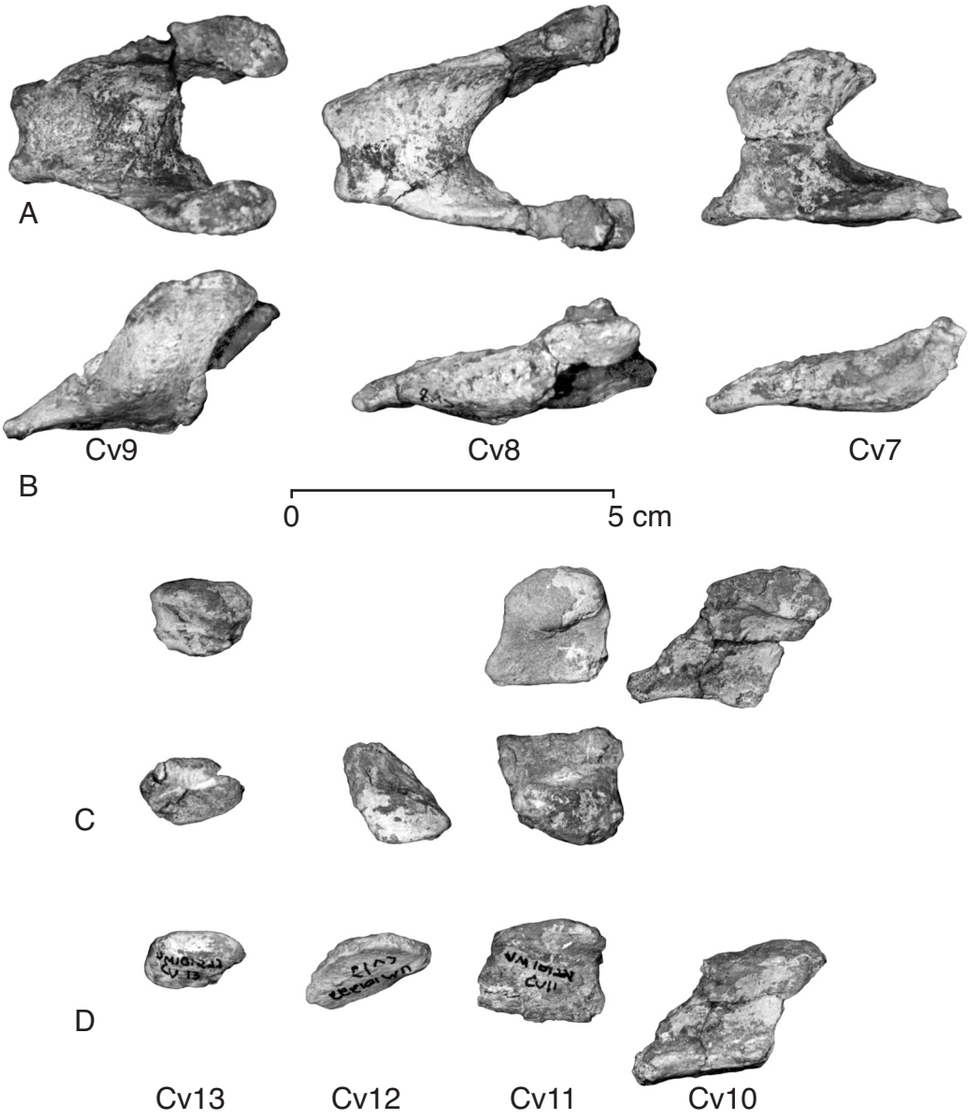

FIGURE 97 — Chevrons *Dorudon atrox* (UM 101222). A-B, Cv7-Cv9 in dorsal and lateral view. C-D, Cv10-Cv13 in dorsal and lateral view. Cv10 is the most anterior chevron that is paired rather than single.

Manus

Carpus

The carpus of *Dorudon atrox* contains six separate elements arranged in two alternating rows, one proximal, articulating with the radius and ulna, the other distal, articulating with the metacarpus (Fig. 104). The carpus contains one accessory element, the pisiform. The pisiform articulates with the ulna and with the cuneiform on the caudal (ulnar) border of the carpus.

The scaphoid [**Sca**, Figs. 104 and 105] is the second smallest bone in the carpus of *Dorudon atrox* (second only to the trapezium). The scaphoid is the first carpal element in the proximal row on the cranial (radial) side of the carpus. It articulates proximally with the distal radial epiphysis, distally with the trapezium and trapezoid, and caudally with the trapezoid and lunate. There is no articulation on the cranial border.

The radial facet [**rf**] is generally flat, with a small projection from the scaphoid on the medial/cranial corner of the facet,

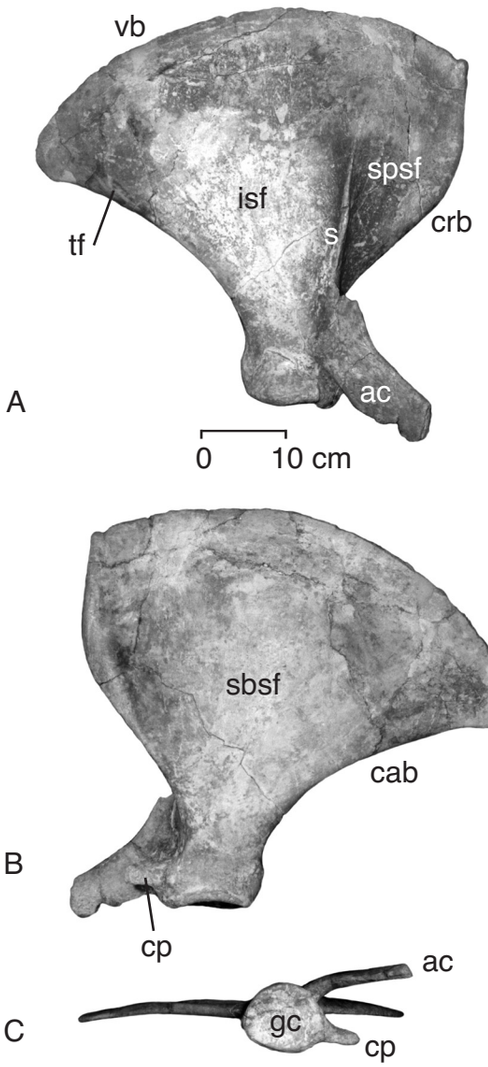

FIGURE 98 — Right scapula of *Dorudon atrox* (UM 101222) in A, lateral, B, medial, and C, glenoid (distal) view. Note the broad fan-shaped scapular blade. The lateral side is divided into the supraspinous and infraspinous portions by the nearly vertical spine. The teres fossa is along the caudal border on the lateral side. Note the orientations of the acromion and coracoid process in each of the views.

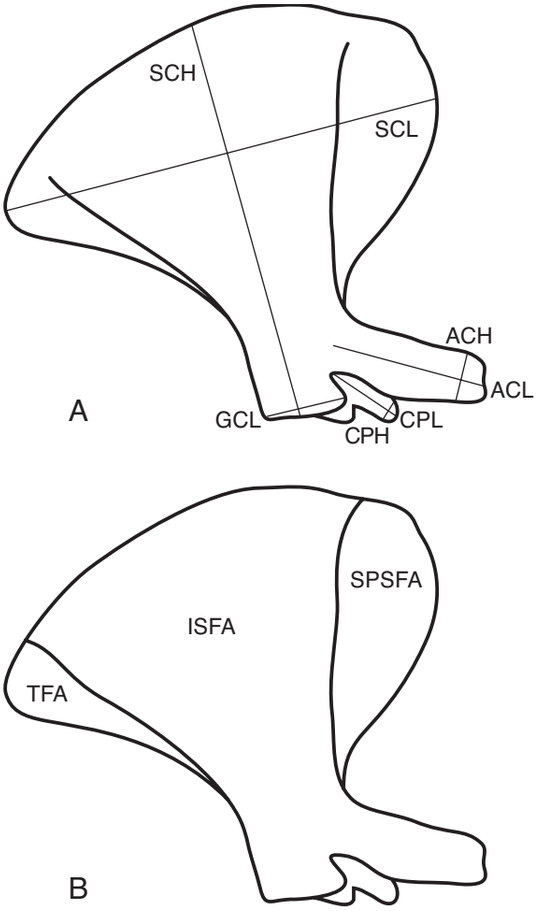

FIGURE 99 — Scapula measurements of *Dorudon atrox*. A, linear measurements. B, area measurements. Abbreviations: *SCH*, scapula height; *SCL*, scapula length; *ACL*, acromion process length; *ACH*, acromion process height; *CPH*, coracoid process height; *CPL*, coracoid process length; *GCL*, glenoid cavity length; *SPSFA*, supraspinous fossa area; *ISFA*, infraspinous fossa area; *TFA*, teres fossa area. Measurement values for the scapulae of *D. atrox* are listed in Appendix VII-A.

and another projection on the caudal (ulnar) edge of the facet. These projections fit into depressions on the scaphoid articular surface of the distal radius. The lunar facet is on the caudal (ulnar) border of the scaphoid. It is a complex surface that is generally saddle-shaped, with the axis of the saddle-shaped fold running perpendicular to the plane of the flipper. The trapezoid facet is on the cranial (radial) side of the distal border of the scaphoid. It is separated from the trapezium facet by a low ridge. It has a small convexity that articulates with a shallow depression on the trapezium. The trapezium facet is on the caudal (ulnar) side of the distal border of the scaphoid. It is curved and convex, with no major projections. The cranial border of the scaphoid is thinner (in the plane of the flipper) than the caudal border. The cranial border thins to a rounded edge.

The lunate [**Lun**, Figs. 104 and 105] is the central element in the proximal row of carpals. It articulates proximally with the radius and ulna, distally with the trapezoid and unciform, cranially with the scaphoid, and caudally with the cuneiform.

TABLE 17 — Summary statistics of scapula measurements for adult *Dorudon atrox*. Measurements are shown in Figure 99 and are listed in Appendix VIIA. SCH, scapula height; SCL, scapula length; ACL, acromion process length.; ACH, acromion process height. CPH, coracoid process height; CPL, coracoid process length.; GCL, glenoid cavity length; SPSFA, supraspinous fossa area; ISFA, infraspinous fossa area; TFA, teres fossa area. N, sample size; SD, standard deviation; CV, ratio of the standard deviation to the mean (in percent). All measurements are in millimeters except SPSFA, ISFA, and TFA which are in square centimeters.

Measurement	N	Minimum	Maximum	Mean	SD	CV
SCH	6	240.0	311.0	271.7	28.6	10.5
SCL	6	230.0	282.0	255.2	16.9	6.6
ACL	3	25.4	31.6	29.2	3.3	11.3
ACH	3	87.7	105.8	96.8	9.1	9.4
CPH	6	16.1	20.0	18.8	1.4	7.6
CPL	6	48.0	61.3	55.2	5.2	9.4
GCL	6	52.7	55.5	53.8	1.1	2.0
SPSFA	6	59.5	101.0	84.2	17.3	20.6
ISFA	6	247.2	344.0	310.3	35.7	11.5
TFA	7	5.2	28.0	14.2	8.1	57.4

The radial facet [**rf**] is broadly dish-shaped. It is separated from the scaphoid facet by a ridge, and from the ulnar facet by a ridge which has an expansion on the medial side. The ulnar facet is roughly triangular in outline and broadly convex. It is separated from the cuneiform facet only by a change in orientation of the plane of articulation via a broad gentle curve. The cuneiform facet is very small. The proximal ulnar corner of the lunate forms the articulation with the cuneiform. The scaphoid facet is on the radial side of the lunate. It, together with the scaphoid facet of the trapezoid, forms a shallow concavity with which the ulnar side of the scaphoid articulates. The magnum facet is on the distal side of the lunate. The magnum facet is large, roughly rectangular to square in shape, and deeply concave. The magnum facet accommodates the articulation with the magnum portion of the fused trapezoid + magnum. The unciform facet is also rectangular to square in shape. It is deeply concave and accommodates the articular surface of the unciform.

The cuneiform [**Cun**, Figs. 104 and 105] is the ulnarmost carpal in the first row. The cuneiform articulates proximally with the ulna. The ulnar facet is laterally elongated, and flat to uneven in its texture. The lunar facet is very small and generally flat. The pisiform facet is on the ulnar side of the cuneiform. It is long, thin, and flat, articulating with the more distal of the two articular surfaces on the pisiform. The unciform facet is the largest articular surface on the cuneiform. It is gently curved from medial to lateral, and slightly convex.

The pisiform [**Pis**, Figs. 104 and 105] is very large. It is broad proximodistally and flattened in the plane of the flipper. It is thickest near the articular surfaces and thins toward the edge. The pisiform is slightly curved in the palmar direction. The pisiform articulates with the ulna and the cuneiform. The ulnar facet is more proximal and slightly shorter than the cuneiform facet. The cuneiform facet is longer and thins from proximal to distal. The caudal margin of the pisiform is gently rounded.

The unciform [**Unc**, Figs. 104 and 105] is one of the largest carpals, approximately the same size as the lunate. It is also the ulnarmost carpal in the distal row. The unciform articulates proximally on the ulnar side with the cuneiform. The cuneiform facet is the longest articular facet on the unciform. It is gently curving from medial to distal and is slightly concave. The unciform articulates proximally on the radial side with the lunate. The lunar facet is rectangular in outline and slightly convex. The magnum facet is on the radial side of the unciform. It is roughly rectangular in outline, but its surface is complex. The dorsal border of the articular surface is flat, but the palmar surface is deeply concave. On some specimens, the concavity reaches the dorsal border of the magnum facet, effectively dividing it into two portions, one proximal and one distal. The distal border of the unciform contains three articular facets for metacarpals. The two more ulnar facets are laterally elongate and concave. The ulnarmost facet is for metacarpal V, with the more ulnar facet for metacarpal IV. The

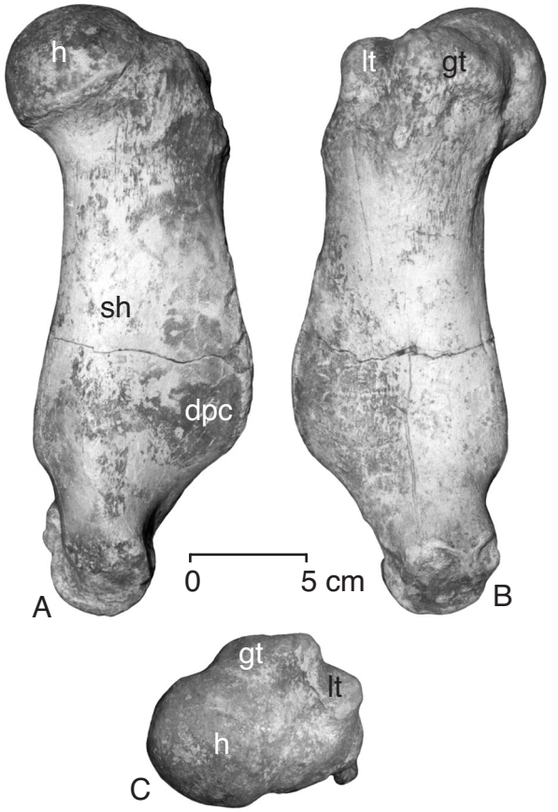

FIGURE 100 — Right humerus of *Dorudon atrox* (UM 101222) in A, lateral, B, medial, and C, proximal view. Note the large, hemispherical head and long robust shaft. The deltopectoral crest along the cranial margin of the humerus is greatly developed, especially at its distal end. Scale is in centimeters.

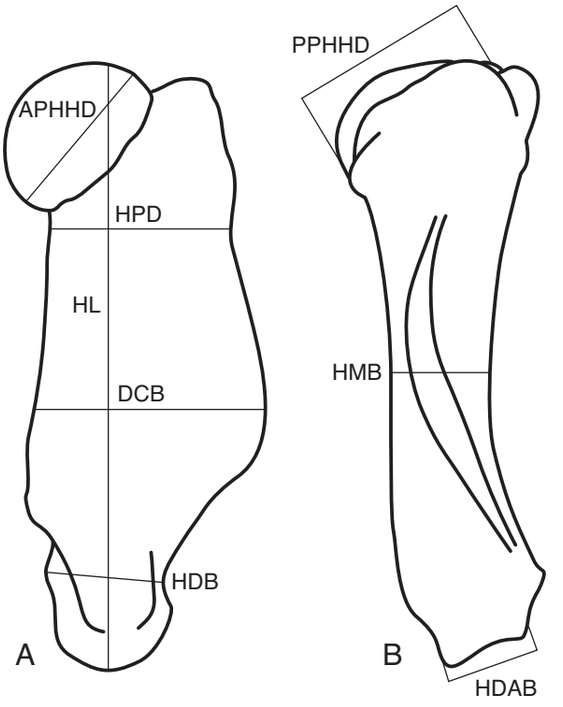

FIGURE 101 — Humerus measurements of *Dorudon atrox*. Abbreviations: *HL*, humerus length; *HMSD*, humeral mid-shaft diameter; *HMB*, humeral shaft mid breadth; *DCB*, deltopectoral crest breadth; *HDB*, humeral distal breadth; *PDHHD*, proximal-distal humeral head diameter; *APHHD*, anterior-posterior humeral head diameter; *HDAB*, humeral distal articular breadth. Measurement values for the humeri of *D. atrox* are in Appendix VII-B.

radialmost facet is much shorter, and it is for the ulnar edge of the proximal articular surface of metacarpal III.

The magnum of *Dorudon atrox* is fused with the trapezoid. All specimens show this fusion, but with varying degrees of completeness. This pair can either be referred to as magnum + trapezoid or alternatively just trapezoid [**Trd**, Figs. 104 and 105]. The former term is used here when it is convenient to distinguish between the two parts of the bone, and the latter is used when the bone simply needs identification. Trapezoid was chosen over magnum for the pair since other authors have identified the bone in this position in modern cetaceans as the trapezoid (see Rommel, 1990, *e.g.*).

The magnum portion is larger than, and ulnar to, the trapezoid portion of the bone. The magnum portion articulates proximally with the lunate. The lunar facet is roughly rectangular in outline and slightly convex. The unciform facet is also roughly rectangular. There is a concavity on the unciform facet that is variably developed. Its degree of development is correlated with that of the concavity on the magnum facet of the unciform. The magnum+trapezoid articulates distally with two metacarpals. The articular facet on the trapezoid portion is for metacarpal II. The articular facet on the magnum portion is for metacarpal III. The articular facet for metacarpal II extends over the entire distal surface of the trapezoid portion and onto the magnum portion of the bone. The radial side of the trapezoid portion articulates with the trapezium. The trapezium facet is rather small and flat.

There does not appear to have been and os centrale *Dorudon atrox*.

The trapezium [**Tzm**, Fig. 104 and 105] is the smallest of the carpals, and is the radialmost carpal of the distal row. The trapezium articulates proximally with the scaphoid. The scaphoid facet is in the shape of a rounded square, and it is generally flat. The ulnar side of the trapezium articulates with the trapezoid portion of the trapezoid+magnum. The trapezoid facet is in the shape of half of an oval, the cut edge being proximal and the rounded edge being distal. The trapezium articulates distally with metacarpal I. The articular surfaces are ill-defined and poorly developed.

TABLE 18 — Summary statistics of humeral measurements for adult *Dorudon atrox*. Measurements are shown in Figure 101 and are listed in Appendix VIIB. HL is humerus length. HMSD is humeral mid-shaft diameter. HMB is humeral shaft mid breadth. DCB is deltopectoral crest breadth. HDB is humeral distal breadth. PDHHD is proximal-distal humeral head diameter. APHHD is anterior-posterior humeral head diameter. HDAB is humeral distal articular breadth. N, sample size; SD, standard deviation; CV, ratio of the standard deviation to the mean (in percent). All measurements are in millimeters.

Measurement	N	Minimum	Maximum	Mean	SD	CV
HL	5	224.0	253.0	237.4	13.1	5.5
HMSD	5	29.9	35.4	33.3	2.8	8.5
HMB	4	66.3	69.0	67.4	1.1	1.7
DCB	5	86.6	91.0	88.5	1.9	2.1
HDB	6	42.7	47.8	44.9	2.1	4.6
PDHHD	4	52.4	60.0	54.7	3.5	6.5
APHHD	4	60.3	67.0	63.7	2.9	4.6
HDAB	6	31.8	35.0	33.7	1.3	3.8

Metacarpus

Dorudon atrox retains five digits on the forelimb, and thus there are five metacarpals, numbered with Roman numerals from medial to lateral. Measurements taken on the metacarpals are shown in Figure 103. Summary statistics for the measurements of *D. atrox* metacarpals are shown in Table 20. Each of the metacarpals is composed of a long shaft that is oval in cross section, flattened in the plane of the flipper, with articular surfaces on the proximal and distal ends.

There are four projections on the proximal end of each metacarpal, two on the dorsal margin of the proximal articulation, and two on the palmar margin of the proximal articulation. These processes project laterally from the shaft. The pair of processes on each side forms a shallow notch on each side of the proximal end of the shaft. These notches are for insertion of the interosseous metacarpal ligaments that link adjacent metacarpals. The dorsal process on the ulnar side of the shaft of each metacarpal has an articular surface for articulation with the laterally adjacent metacarpal (except on Mc V). There is a well-developed articular surface on the radial side of the proximal shaft of each metacarpal for articulation with the medially adjacent metacarpal (except on Mc I).

The first metacarpal [**Mc I**, Fig. 104 and 105] is the smallest of all the metacarpals. It is very short and has a small cross-sectional area. The cross-sectional area is largest at its proximal end and decreases to the distal end. Metacarpal I is much more rounded in cross section than metacarpals II-V. The proximal end of metacarpal I articulates with the trapezium. The distal end of metacarpal I is fused to the proximal end of the proximal phalanx, which is also the terminal phalanx. There is a slight swelling where the two bones are fused together, but otherwise the fusion is complete. This phalanx is discussed further below.

The second metacarpal [**Mc II**, Fig. 104 and 105] is much more substantial than metacarpal I. The shaft is not very flattened in the plane of the flipper. The shaft is about twice as long as metacarpal I and it is the third longest of all the metacarpals. The shaft is slightly curved in the palmar direction. Metacarpal II articulates proximally with the trapezoid via a convex articular surface. The distal articulation is oval to round in shape and also gently convex.

The third metacarpal [**Mc III**, Fig. 104 and 105] is the largest of all the metacarpals. It is the greatest in length, breadth, and cross-sectional area. The shaft is very flattened in the plane of the flipper. The proximal articular surface is divided into two portions. The larger portion is generally perpendicular to the shaft and saddle-shaped. This surface is laterally elongate and is the articulation of metacarpal III with the magnum portion of the fused trapezoid + magnum. The smaller surface is the articulation of metacarpal III with the unciform. It is confluent with the larger one, is at a slight angle, and is on the ulnar side of the metacarpal. The distal articular surface is oval in shape and gently convex. There is a small palmar projection on the radial side of the distal shaft.

The fourth metacarpal [**Mc IV**, Fig. 104 and 105] is the second longest of the metacarpals. The proximal articular surface is in the shape of a laterally elongated, rounded rectangle, and it is flat to slightly convex. Metacarpal IV articulates proximally with the unciform. The distal articular surface is oval in

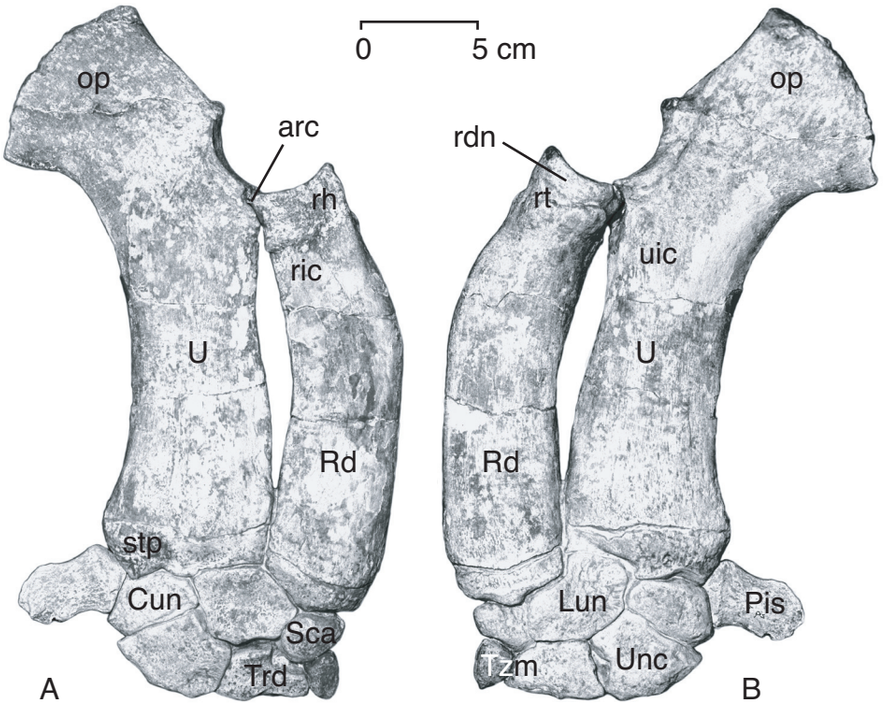

FIGURE 102 — Right radius, ulna, and carpus of *Dorudon atrox* (UM 101222) in A, lateral, and B, medial view. Note that both the radius and ulna are flattened in the plane of the flipper, especially at their distal ends. The articulated radius and ulna form a semicircular articular surface on their proximal ends for articulation with the distal humerus. This surface is shown in Figure 105. Note also the very large olecranon process on the ulna.

shape and slightly convex. There is a small process on the radial side of the distal shaft. The flattened shaft forms a rather sharp edge on the ulnar side of the distal shaft.

The fifth metacarpal [**Mc V**, Fig. 104 and 105] is the second shortest metacarpal, second only to metacarpal I. It is short and stout, less flattened than metacarpal IV. The shaft is slightly curved in a palmar direction. The proximal articular surface is at an angle perpendicular to the shaft. It is oval to rectangular in outline and is slightly convex. There is a large process on the ulnar side of the shaft that projects out over the pisiform. This surface does not appear to be an articulation with the pisiform. The distal articular surface is oval in shape and very flat. The ulnar side of the distal shaft is quite sharp, as in metacarpal IV.

Phalanges

Dorudon atrox retains five digits on the forelimb, and thus there are five sets of phalanges, numbered with Roman numerals from medial to lateral in Figure 104. Phalanges are also numbered from proximal to distal with Arabic numbers, with 1 being the most proximal and higher numbers being successively more distal. Measurements taken on the phalanges are shown in Figure 103. Summary statistics for the measurements of *D. atrox* phalanges are shown in Table 21.

The phalangeal formula of *Dorudon atrox* is unclear. The only phalanges found in articulation with the rest of the manus are the proximal phalanges. No middle or distal phalanges have been found in articulation with the proximal phalanges. However, additional proximal ends, distal ends, and complete phalanges have been recovered from two specimens of *Dorudon atrox* (UM 97506 and UM 101222), and it is clear that *Dorudon atrox* had middle phalanges on some or all carpal digits.

Proximal phalanges.— The proximal phalanges are long shafts that are generally oval in cross section and broadest at their proximal ends and narrowest from the midpoint to near the distal ends. The shafts are generally slightly curved dorsally and slightly curved toward the midline of the flipper. There are articular surfaces on the proximal ends for articulation with the metacarpal that are generally oval in outline and slightly concave. The distal articular surface on each proximal phalanx is teardrop-shaped, with the rounded side toward the ulnar border of the flipper. The thin, pointed end of the distal articular

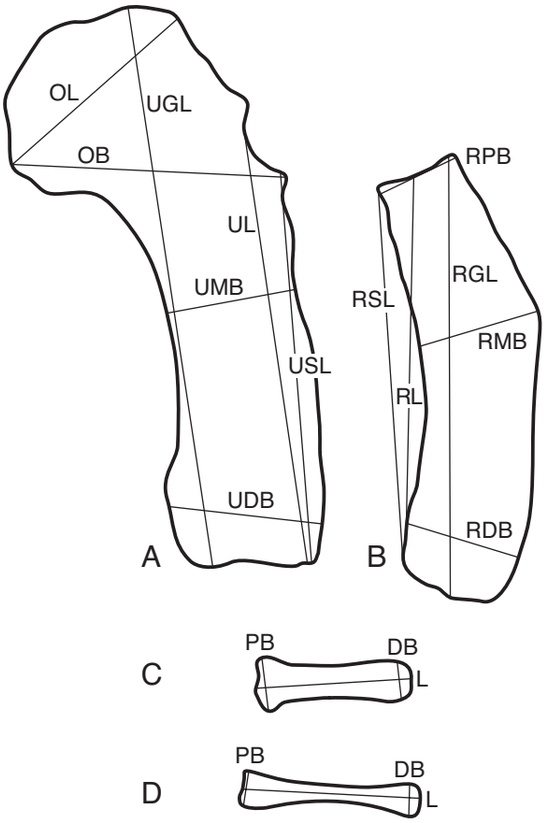

FIGURE 103 — Radius, ulna, metacarpal, and phalanx measurements of *Dorudon atrox*. Abbreviations: *UGL*, ulna greatest length; *USL*, ulna shaft length; *UL*, ulna length; *OL*, olecranon length; *OB*, olecranon breadth; *UMB*, ulna mid-shaft breadth; *UDB*, ulna distal breadth; *RGL*, radius greatest breadth; *RSL*, radius shaft length; *RL*, radius length; *RPB*, radius proximal breadth; *RMB*, radius mid-shaft breadth; *RDB*, radius distal breadth; *PB*, proximal breadth; *DB*, distal breadth; *L*, length. Measurement values for the ulnae, radii, metacarpals, and phalanges of *D. atrox* are listed in Appendices VII-C, VII-D, and VII-E.

surface is formed by a thin flange of bone that projects from the shaft of the phalanx. The first digit lacks a distal articular surface.

The proximal phalanx of digit I [**Ph I-1**, Fig. 104 and 105] is fused to the distal end of metacarpal I. It is very short, has a very small cross-sectional area, and decreases in girth from proximal to distal. This proximal phalanx is also the terminal phalanx for digit I. It is slightly expanded near the distal tip, and then tapers to a rounded point with no distal articular surface.

The proximal phalanx of digit II [**Ph II-1**, Fig. 104 and 105] is longer than Ph I-1, shorter than Ph III-1 and Ph IV-1, and approximately equal in length to Ph V-1. Ph II-1 is considerably longer than Mc II.. There is variation in the shape of the shaft cross section. The left Ph II-1 in specimen UM 101222 is distinctly oval, with the shaft being flattened in the plane of the flipper. The right Ph II-2 in the same specimen is much more round.

The proximal phalanx of digit III [**Ph III-1**, Fig. 104 and 105] is the longest of all the proximal phalanges. It is also longer than Mc III. The proximal articular surface is generally oval in outline and quite concave. The proximal end of the shaft is very thick. It is flat on the palmar surface and domed on the dorsal surface. The shaft is oval in cross section, thinning from the proximal end to about two thirds of its length, where the shaft begins to flare out.

The proximal phalanx of the fourth digit [**Ph IV-1**, Fig. 104 and 105] is a bit shorter than Ph III-1, but longer than all of the other proximal phalanges and Mc IV. The proximal end of the shaft is very thick, flat on the palmar surface, and domed on the dorsal surface.

The proximal phalanx of the fifth digit [**Ph V-1**, Fig. 104 and 105] is shorter than those of digits III and IV, but approximately equal to that of digit II. It, like the proximal phalanx of digit II, is variable in shape. In specimen UM 101222, the proximal articular surface and shaft are oval, while in another specimen, UM 97512, the proximal articular surface is deeply concave to accommodate a much more convex distal articular surface on Mc V than is seen in other individuals.

Middle phalanges.— The proximal ends of these phalanges appear to be the appropriate size to articulate with the distal ends of the proximal phalanges. Their distal ends however are thin, broad planes that do not appear to articulate with additional phalanges. This would suggest that *Dorudon atrox* had only two phalanges per digit rather than the primitive three. In addition, the proximal phalanx of digit I that is fused to metacarpal I does not appear to articulate with another phalanx distally, which would suggest there was a single phalanx in digit I. These additional phalanges are described below as middle phalanges and are not assigned to any particular digits. Their identification as middle phalanges is only tentative, until a completely-articulated flipper is found. Note that the term middle phalanges is used for these bones to identify them as positional homologues of the middle phalanges of terrestrial mammals, despite their functional role in the distal position on each digit.

The middle phalanges are shorter than all of the proximal phalanges. They are greatly expanded on their proximal ends. The proximal articular surfaces are oval-shaped in outline and are slightly concave. Some proximal articular surfaces are more round than oval. The expanded proximal shaft of each phalanx narrows to just proximal to the distal end where it flares out. There is a small flange of bone on one side of the shaft at the distal end of each phalanx. The distal ends are very flat.

TABLE 19 — Summary statistics of antebrachial measurements for adult *Dorudon atrox*. Measurements are shown in Figure 103 and are listed in Appendix VIIC and Appendix VIID. UGL is ulna greatest length. USL is ulna shaft length. UL is ulna length. OL is olecranon length. OB is olecranon breadth. UMB is ulna mid-shaft breadth. UDB is ulna distal breadth. RGL is radius greatest breadth. RSL is radius shaft length. RL is radius length. RPB is radius proximal breadth. RMB is radius mid-shaft breadth. RDB is radius distal breadth. N, sample size; SD, standard deviation; CV, ratio of the standard deviation to the mean (in percent). All measurements are in millimeters.

Measurement	N	Minimum	Maximum	Mean	SD	CV
UGL	5	214.0	218.0	215.2	1.8	0.8
USL	5	139.0	153.0	143.4	5.6	3.9
UL	5	152.0	169.0	159.2	6.3	4.0
OL	6	66.7	80.6	75.4	5.3	7.1
OB	5	93.4	100.4	97.7	3.6	3.6
UMB	6	43.2	49.3	47.4	2.2	4.6
UDB	7	52.7	66.3	58.4	4.4	7.5
RGL	4	164.0	167.0	165.5	1.3	0.8
RSL	4	140.0	145.0	142.8	2.3	1.6
RL	4	156.0	161.0	157.5	2.4	1.5
RPB	4	30.1	35.5	33.6	2.4	7.1
RMB	6	40.6	50.0	44.6	3.5	7.9
RDB	5	41.9	46.4	43.9	2.0	4.6

HIND LIMB

The hind limb of *Dorudon atrox* is still poorly known. One individual, UM 97506, preserves three hind limb elements. These are a proximal femur, lateral portion of an astragalus, and a complete patella. All are smaller but otherwise similar to comparable parts of *Basilosaurus isis* (Gingerich et al., 1990).

Innominate

The innominate of *Dorudon atrox* is unknown, but it was probably similar to that of *Basilosaurus isis* (Gingerich et al., 1990) and *Chrysocetus healyorum* (Uhen and Gingerich, 2001), based on the similarity of other hind limb elements to those of *Basilosaurus*, and the similarity of the innominates of *Basilosaurus* and *Chrysocetus*.

Crus

Femur

The femur [**Fe**, Fig. 106A-B] of *Dorudon atrox* is known from a proximal shaft of the right femur of specimen UM 97506. The proximal epiphysis is missing, and with it, the head of the femur. The femur was identified based on comparison with the femur of *Basilosaurus*.

The proximal end of the shaft is flattened mediolaterally. The anterior and posterior edges of the shaft flare anteriorly and posteriorly, respectively. Since the head is missing, it is impossible to assess length of the neck. The anterior and posterior edges of this flattened portion of the shaft are gently curved medially, creating a shallow sulcus running parallel to the shaft on the medial side of the flattened anterior end.

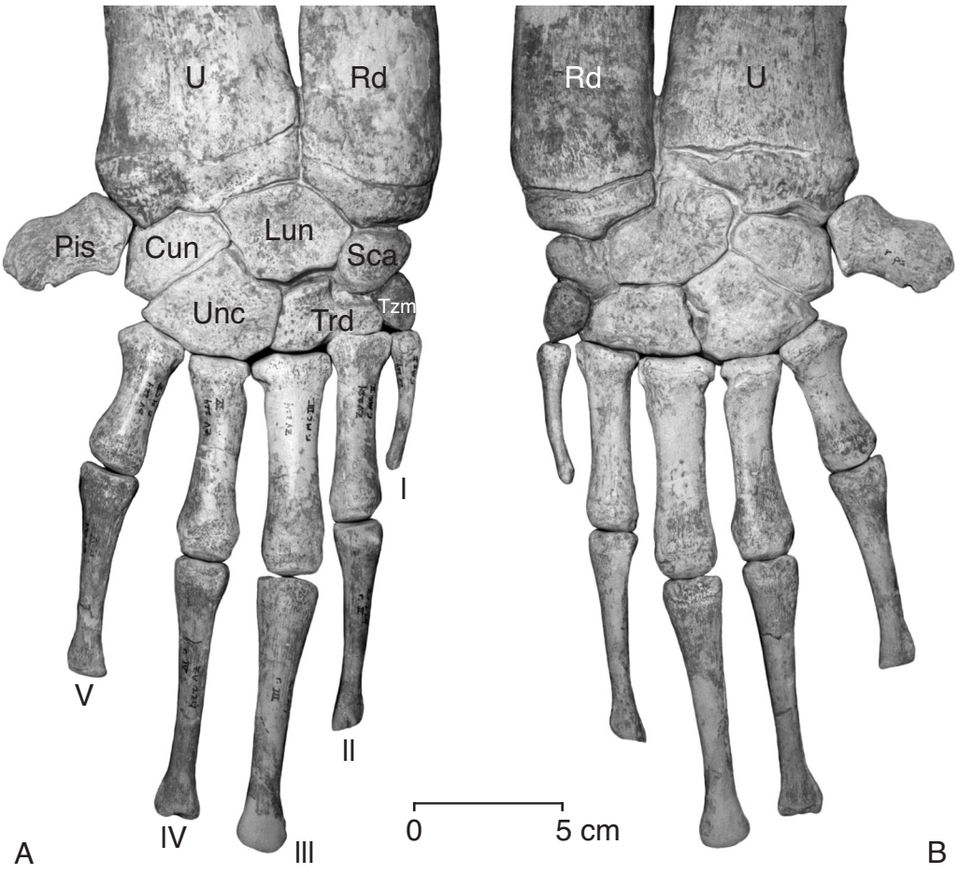

FIGURE 104 — Right manus of *Dorudon atrox* (UM 101222) in A, lateral, and B, medial view. Note the alternating rows of carpals, the extremely large pisiform, and the fusion of the trapezoid and magnum. Digit I appears to be formed from the fusion of metacarpal I and proximal phalanx I. All of these bones were found in articulation. It is unclear whether *Dorudon atrox* had two or three phalanges per digit, since no middle phalanges have been found in articulation with proximal phalanges.

The greater trochanter is present on the specimen, but much of the proximal extent is missing. The greater trochanter extends down onto the shaft of the femur, where it terminates in a strong ridge, running at an angle to the length of the shaft. It extends down the shaft farthest on the caudal border of the shaft. The lesser trochanter is difficult to differentiate from the shaft of the femur. The cranial border of the femur is thickened relative to the central portion of the proximal shaft. This is the only hint of the presence of the lesser trochanter. There is no readily identifiable trochanteric fossa.

The shaft of the femur narrows distal to the anterior end and becomes oval in cross section. The long axis of the oval is oriented craniocaudally. The shaft also appears to be slightly curved in a lateral direction, although most of the shaft is missing. The distal end of the femur is unknown.

Patella

A relatively well-preserved right patella [**P**, Fig. 106C-D] is known from specimen UM 97506. It is very similar to the patella of *Basilosaurus isis* (Gingerich et al., 1990). The base of the patella is more pointed than in most mammalian patellae. It is rather difficult to distinguish between the base and the apex because of their similarity in shape. The body of the patella is very thick and shaped like a pointed oval in outline view. There is a weak midline ridge running from the base to the apex on the cranial (anterior) surface. The articular surface is saddle-shaped, with the axis of the sulcus running mediolaterally. The edges of the articular surface are abraded, so its outline shape is unclear, but it was probably oval. This surface articulated with the patellar groove of the distal femur. This large well-formed patella indicates that the distal femur had a functional knee joint, despite the lack of a specimen of the distal femur.

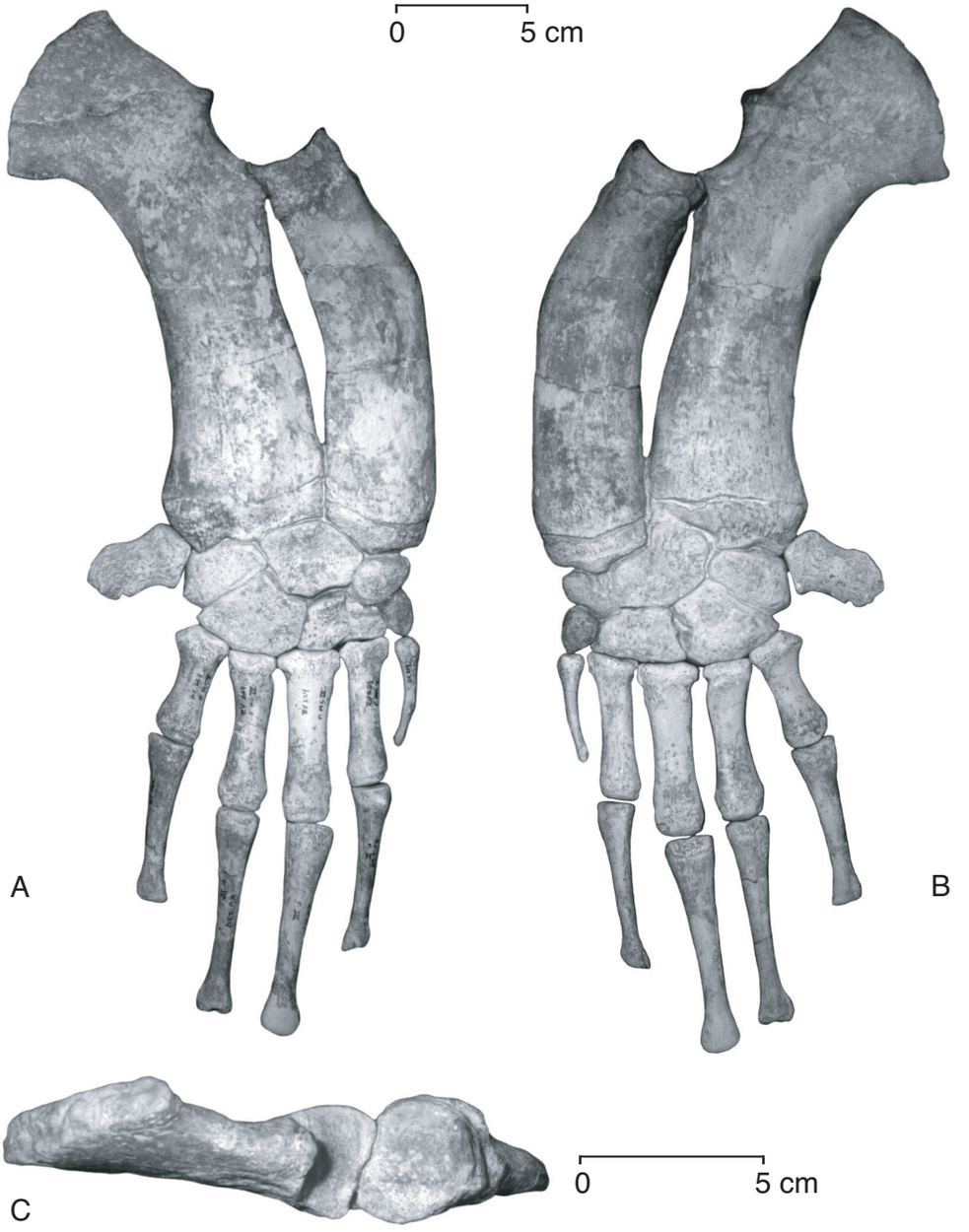

FIGURE 105 — Right articulated antebrachium and manus of *Dorudon atrox* (UM 101222) in A, lateral, B, medial, and C, proximal view. Note that the longest digit is the central digit (III). The anterior view of the radius and ulna shows the articular surface for the humerus. Note the shape of the articulation of the radius with the ulna. This articulation would not allow pronation or supination at the elbow.

Tibia

No tibia is known from any specimen of *Dorudon atrox*. The tibia is hypothesized to have been present due to the presence of a well-formed patella, and thus a functioning knee joint, which would indicate the presence of hind limb elements just distal to the knee, either the tibia, fibula, or both. In addition,

TABLE 20 — Summary statistics of metacarpal measurements for adult *Dorudon atrox*. Measurements are shown in Figure 103 and are listed in Appendix VIID. The measurements for metacarpal I include the fused phalanx I. L is length. PB is proximal breadth. DB is distal breadth. N, sample size; SD, standard deviation; CV, ratio of the standard deviation to the mean (in percent). All measurements are in millimeters.

Bone	Dimension	N	Minimum	Maximum	Mean	SD	CV
Mc I	L	1	44.3	44.3	44.3	—	—
	PB	2	11.0	11.3	11.2	0.2	1.9
	DB	1	5.2	5.2	5.2	—	—
Mc II	L	3	56.1	59.6	57.9	1.8	3.0
	PB	4	18.2	22.0	20.6	1.7	8.1
	DB	4	15.8	16.9	16.4	0.5	2.8
Mc III	L	3	68.7	71.6	69.9	1.5	2.2
	PB	3	24.3	24.6	24.5	0.2	0.6
	DB	3	18.6	20.2	19.6	0.9	4.4
Mc IV	L	5	61.8	65.8	63.1	1.6	2.6
	PB	5	18.2	19.7	19.1	0.6	3.2
	DB	4	15.1	19.5	18.0	2.0	10.9
Mc V	L	5	45.1	48.2	46.8	1.1	2.4
	PB	6	21.1	24.3	22.9	1.2	5.4
	DB	5	18.2	19.3	18.7	0.4	2.2

TABLE 21 — Summary statistics of proximal phalanx measurements for adult *Dorudon atrox*. Measurements are shown in Figure 103 and are listed in Appendix VIIE. Proximal phalanx I is not listed since it is fused to metacarpal I. L is length. PB is proximal breadth. DB is distal breadth. N, sample size; SD, standard deviation; CV, ratio of the standard deviation to the mean (in percent). All measurements are in millimeters.

Bone	Dimension	N	Minimum	Maximum	Mean	SD	CV
Ph II-1	L	1	64.4	64.4	64.4	—	—
	PB	3	14.1	16.0	15.2	1.0	6.4
	DB	1	12.2	12.2	12.2	—	—
Ph III-1	L	4	84.3	93.2	89.7	3.8	4.2
	PB	4	18.3	19.3	19.0	0.5	2.5
	DB	4	12.6	16.2	14.6	1.5	10.3
Ph IV-1	L	3	79.1	90.4	83.0	6.4	7.7
	PB	3	17.2	18.5	17.8	0.7	3.7
	DB	3	14.2	15.9	14.8	1.0	6.4
Ph V-1	L	3	63.3	71.9	67.5	4.3	6.4
	PB	3	18.8	19.2	19.0	0.2	1.1
	DB	3	12.9	15.0	14.0	1.1	7.6

the astragalus (described below) has an articular facet for the distal tibia, again indicating its presence, despite the lack of a specimen.

Fibula

No fibula is known for any specimen of *Dorudon atrox*. It is likely to have been present for the reasons given above.

Pes

Only a single bone is known with certainty from the pes of *Dorudon atrox*. It is the lateral portion and much of the body of a right astragalus. No other tarsal elements are known with certainty, although some fragments from specimen UM 97506 may represent other tarsals, metatarsals, or pedal phalanges.

Astragalus

Specimen UM 97506 preserves the lateral (calcaneal) aspect of the astragalus [**A**, Fig. 106E-F], including most of the proximal articular surfaces. The tarsal elements of *Dorudon atrox* were compared with the tarsal elements of *Basilosaurus isis*, as identified by Gingerich et al. (1990). The astragalus appears to have been free of fusion with other tarsal elements, but it may have been fused with the calcaneum, the navicular or both. This is difficult to determine since the medial side of the bone is missing. In addition, the tarsal bones of *Basilosaurus*, which are very similar to those of *Dorudon atrox*, exhibit a variable pattern of fusion (Gingerich et al., 1990), so even if one specimen of *D. atrox* could be shown to have free tarsals, it is doubtful that this would necessarily be the case for all individuals.

The astragalus of *Dorudon atrox* lacks a trochlea. It has a flat tibial facet [**tfa**] that articulated with the tibia. The head of the astragalus is merged with the body, and there is no discernible neck. The fibular facet is separated from the tibial facet by a high ridge along the midline of the proximal end of the astragalus. The fibular facet is the lateral side of the ridge. The fibular facet is confluent with the ectal facet. The fibular facet and ectal facet combined are subequal in size to the tibial facet. These two surfaces slope away from the midline ridge at about the same angle, making the proximal end of the astragalus sharply pointed.

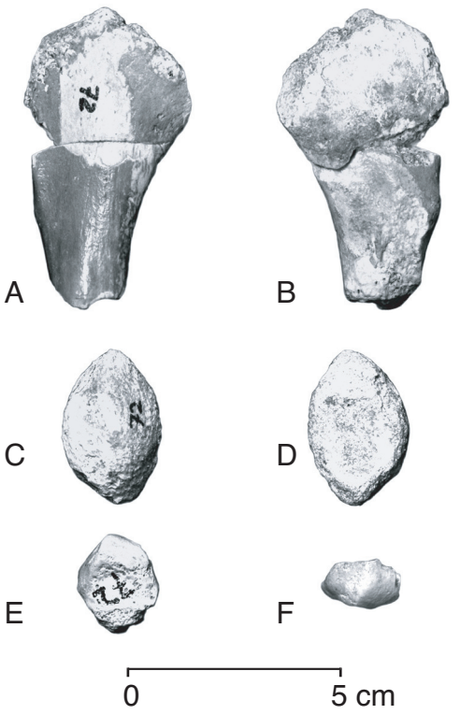

FIGURE 106 — Hind limb elements of a juvenile *Dorudon atrox* (UM 97506). A, lateral view of proximal right femur; B, medial view of proximal right femur; C, anterior view of right patella; D, posterior view of right patella; E, anterior view of right astragalus; F, proximal view of right astragalus. The head is missing from the proximal femur. The patella is complete. The distal astragalus has been damaged by weathering.

IV

ANATOMICAL RECONSTRUCTION

Osteological remains of mammals can be used to reconstruct some of their soft anatomy. One goal of anatomical reconstruction is to emphasize that fossil mammals were once living, breathing, eating, reproducing animals. The simple fact that there were enough carcasses around to be incorporated into the fossil record and discovered today is testament to success in their own time. Reconstruction of soft anatomy of extinct organisms from their osteology alone requires accurate identification of the osteological correlates of soft anatomy. Many cranial foramina, for instance, are identified only by what soft structure passes through them. The hypoglossal foramen is only the hypoglossal foramen if the hypoglossal nerve passed through it. Other soft structures (many muscles for instance) do not have such an intimate relationship with named hard parts. Epaxial muscles of extant cetaceans are certainly homologous with the back muscles of other mammals at some level, and yet their novel origins, insertions, and relationships have baffled comparative morphologists to the point where some of the muscles have been given new names to indicate the lack of identifiable homologies (Pabst, 1990).

Soft anatomy of *Dorudon atrox* was reconstructed by comparing the skeletal anatomy of *D. atrox* to modern cetaceans and modern artiodactyls. Modern cetaceans probably descended from the subfamily Dorudontinae, to which *D. atrox* belongs (see the phylogenetic analysis), and artiodactyls are thought to be the next closest living outgroup to Cetacea (Gatesy, 1998; Gingerich et al., 2001; Thewissen et al., 2001). If both of the extant groups have the same soft tissue structure associated with the same osteological correlate, and the osteological correlate is present in the extinct fossil taxon, then the osteological correlate passes Patterson's (1982) test of congruence for homology, and the soft tissue structure can be strongly inferred to have been present in the entire holophyletic group including the extinct fossil taxon, in this case *Dorudon atrox*. This essentially follows the suggestions for reconstruction of soft anatomy in fossil taxa listed by Witmer (1995).

An added difficulty in reconstructing the soft anatomy of *Dorudon atrox* is that the two extant bracketing taxa (Artiodactyla and Neoceti) are both highly derived from their most recent common ancestor. Artiodactyls are highly specialized terrestrial cursors, while modern cetaceans are highly specialized aquatic swimmers. Thus it is difficult to identify homologies in both extant outgroups and *Dorudon atrox*. Modern cetaceans have numerous autapomorphies relative to other modern mammals. Since dorudontines are thought to be ancestral to modern cetaceans, any autapomorphies of the skeleton that they share with modern cetaceans (thus more correctly termed synapomorphies) will be taken as indicative of possession of the soft anatomical correlates associated with the skeletal features in modern cetaceans.

Some soft tissue structures of *Dorudon atrox* could be reconstructed with more confidence than others based on the mode of preservation of some specimens. Often the endocranial cavity and many of the cranial nerve tracts were filled with very hard sediment, that is much more resistant to weathering than the bone of the skull. When the bone is removed, a natural endocast of these structures remains. In addition, some soft tissue spaces of the skull were imaged using computed tomography (CT) scans.

BODY MASS AND FORM

Body mass estimation

Body mass in fossil mammals has been estimated using three basic methods. The first method uses some measure of tooth size to predict body mass. Legendre (1986) correlated the natural log of M_1 area with body mass for a number of groups of modern mammals. The problem with using this method to determine the body size of *Dorudon atrox* is that modern mysticetes and even some odontocetes have no cheek teeth, and those odontocetes with teeth do not use them in the same manner as archaeocetes and other mammals. Gingerich (1990) used limb bone lengths and cross sectional areas to estimate body size. This is also not applicable to *Dorudon atrox* since it assumes that limb bone measurements are good predictors of body mass because they support the body on land. The limbs of *D. atrox* no longer support the body mass, and they are the size that they are due to other forces placed on them.

Jerison (1973), used body length of modern carnivores and ungulates to estimate body mass. Jerison's body mass equations are inappropriate for *Dorudon atrox*, since cetaceans have undergone a multiplication of the number of lumbar and caudal vertebrae, increasing their body length. They have almost certainly changed the relationship between body length and body mass relative to terrestrial mammals as part of an integrated evolutionary response to living in water.

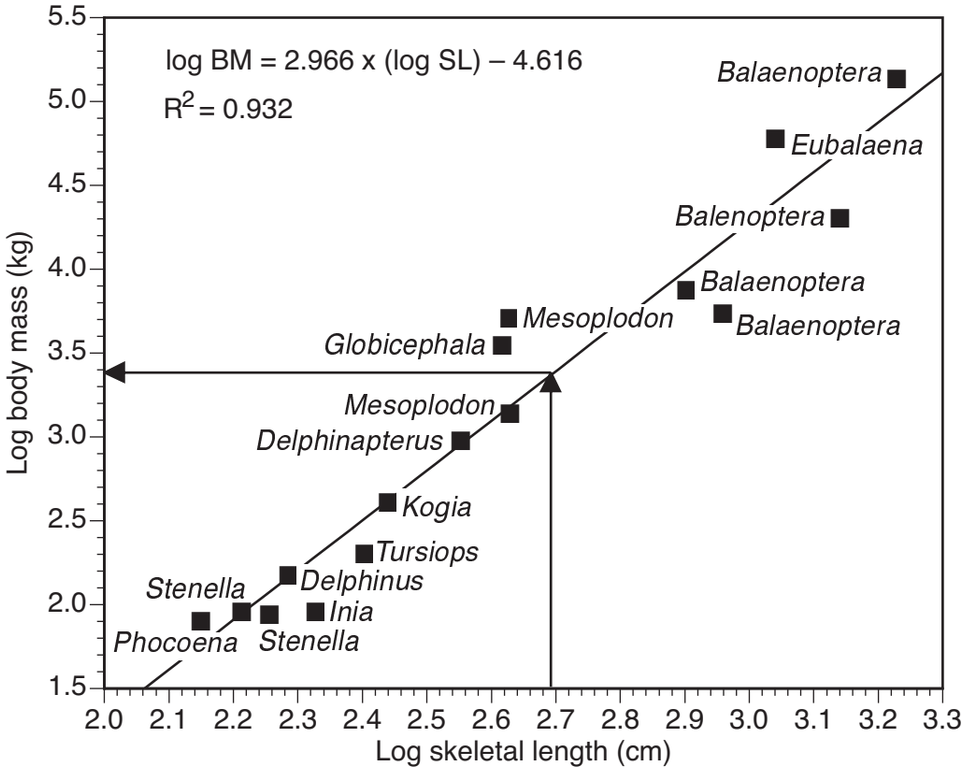

FIGURE 107 — Relationship of body mass and skeletal length in modern cetaceans. Note the generally good relationship between skeletal length and body mass. There are fewer data points at large body size due to the high proportion of small cetaceans (mainly delphinids) relative to large cetaceans (mainly mysticetes). Arrows indicate the skeletal length and predicted mass of *Dorudon atrox*.

Body mass of Dorudon atrox

Following Jerison's lead, a regression equation was constructed based on modern cetaceans to predict body mass from skeletal length, since skeletal length is a variable that is known in *Dorudon atrox*. This assumes that *D. atrox* had a similar body length-body mass relationship as modern cetaceans. Skeletal lengths of modern cetacean were collected from literature sources (Nishiwaki and Kamiya, 1958; Omura, 1958 and 1975; Nishiwaki and Kasuya, 1970; Omura et al., 1981) and personal observations. These were correlated with body masses tabulated from Silva and Downing (1995) to construct a regression equation predicting log body mass from log skeletal length. The regression is shown graphically in Figure 107. The equation for the regression line is

$$\log_{10} \mathrm{BM} = 2.966 \cdot \log_{10} \mathrm{SL} - 4.616 \qquad (1)$$

where *BM* is body mass in kilograms and *SL* is skeletal length in centimeters. The coefficient of determination of the equation is 0.93. The skeletal length of *Dorudon atrox*, based on measurements of vertebrae and skulls of two relatively complete adult specimens (UM 101215 and UM 101222), is around 485 cm. Using this calculation in Equation 1, the estimated body mass of *D. atrox* is about 2,240 kg. This is about the size of a beluga whale (*Delphinapterus leucas*).

Body form

The external body form of *Dorudon atrox* was probably fusiform, like modern cetaceans. There are some indications of this shape in the skeleton. In essence, a fusiform shape is a cylinder that tapers to a point at both ends. The maximum diameter of the body of *D. atrox* is in the thorax at about the level of the sixth thoracic vertebra. The body narrows anteriorly, with each of the preceding ribs being shorter than the caudally adjacent ribs. In addition, the skull is greatly elongated in the face, narrowing to a blunt point from the frontal shield forward. The body has become greatly elongated relative to terrestrial mammals due to the addition of more lumbar vertebrae. The diameter of the body tapers posteriorly, as indicated by the neural spines and transverse processes of the vertebrae, which get shorter from the posterior lumbar region

TABLE 22 — Endocranial volumes of *Dorudon atrox* and *Zygorhiza kochii* individuals. Age classes are delimited by epiphyseal fusion state and dental wear class. CT and *Z. kochii* values from Marino et al. (2000).

Specimen	Age class	Endocranial volume (cm^3)	Rete mirabile volume (cm^3)	CT scan (cm^3)	Est. brain weight	Retial % of total
D. atrox						
BMNH M9265	4	800.0	135.8		664.2	17.0
BMNH M10173	4	785.0	153.1		631.9	
UM 93235	3	1046.0	245.2		800.8	23.4
UM 93234	1	780.0	126.3		653.7	16.2
UM 94795	5	1170.0	245.1		924.9	20.9
UM 94796	4	1225.0	246.7		978.3	20.1
UM 97506	4		189.2	970.0	780.8	
UM 100139	1		97.5	500.0	402.5	
UM 101222	10		228.7	1173.0	944.3	
Z. kochii						
USNM 16638	10		178.8	917.0	738.2	
USNM 16639	7		146.4	751.0	604.6	

into the caudal region where they completely disappear. The body narrows to the point where the posterior caudal vertebrae enter the tail stock of the fluke. Changes in the caudal vertebrae associated with the fluke are discussed in detail in the next chapter.

The forelimbs of *Dorudon atrox* are modified into flippers. The antebrachial elements are flattened, and movements of joints have become restricted. The elbow can only flex and extend, and the carpals are restricted to very slight flexion and extension. Possible movements of the forelimb are discussed in detail in the next chapter. The only other element of external body form found in modern cetaceans is the dorsal fin. The dorsal fin is a completely cutaneous structure with no osteological correlates. Without such correlates, its presence or absence is difficult to determine. Since the dorsal fin is thought to be primitive for all modern cetaceans, the proximal common ancestor of modern cetaceans should have a dorsal fin as well. It is not clear that *D. atrox* fills the role of proximal common ancestor since it is not the ancestor or even the sister taxon to modern cetaceans in the phylogenetic analysis. Thus, the question of whether *D. atrox* had a dorsal fin must remain unanswered.

NERVOUS SYSTEM

Central nervous system

The endocranial space is well-preserved in numerous natural casts of the skull of *Dorudon atrox*. Jerison (1973) warned against the use of the entire endocranial volume as the volume of the brain, because the endocranial space also includes the proximal ends of cranial nerves and vascular structures, particularly venous sinuses. These do not contribute a great deal to overall endocranial volume in some mammals, but in others, these venous sinuses are large and elaborate. A case in point is the archaeocete whales. Dart (1923) correctly identified the dorsal sagittal sinus [**dss**] and the "jugular leash" (jugular vein) in endocranial casts of what are now called *Saghacetus osiris* and *Dorudon atrox*, but he incorrectly identified other venous structures. As others have pointed out, (Marples, 1949; Breathnach, 1955; Pilleri, 1991) what Dart (1923) identified as the "lobus medius cerebelli" is a *rete mirabile* (a complex venous network) rather than part of the brain. This structure will be discussed in more detail along with the circulatory system. It is difficult to separate the *rete mirabile* from the brain to measure the brain volume accurately.

Endocranial volume

Previous measurements of endocranial volume *Dorudon atrox* measured by Dart include the following: BMNH M10173, *Dorudon atrox* (= Zeuglodon *intermedius*) 785 cc as measured, no corrections indicated (Dart, 1923, p. 634); BMNH M9265, *Dorudon atrox* (= "*Prozeuglodon atrox*:") 790 cc as measured, estimated to be 800 cc since the anterior portion is missing (Dart, 1923, p. 634). Additional specimens of both natural cranial endocasts, as well as intact skulls that have been subjected to serial computed tomography (CT) scans of have recently been measured for endocranial volume. Volumes of specimens of natural endocasts were measured using water displacement. Endocranial volumes of specimens that were CT scanned were measured by measuring the areas of endocranial space on each serial scan and then multiplying by the space between the scans. All specimens of *D. atrox* that have endocranial volumes are listed in Table 22.

The volume of the endocranial space in an overestimate of actual brain size, since it includes the volume of the cranial *rete mirabile*. The size of the *rete mirabile* was measured in cranial endocast specimens by shaping a model of the *rete mirabile* in clay and measuring the volume of the model. This volume was

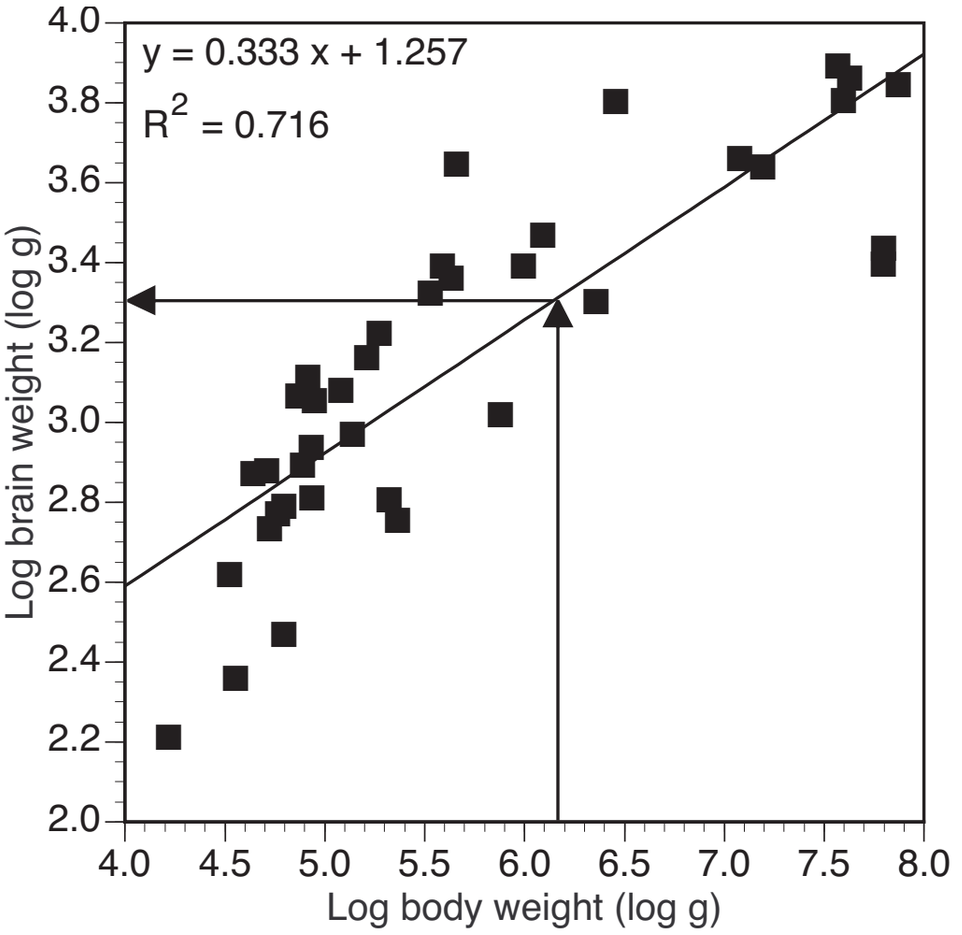

FIGURE 108 — Relationship of log brain weight to log body mass in modern cetaceans. Note that the slope of the least-squares linear regression is around 0.35. The body mass of *Dorudon atrox* is indicated by the vertical arrow drawn to the regression line. The horizontal arrow indicates the expected brain size of a modern cetacean of the body weight of *D. atrox*. Data are from a compilation of mammalian brain and body sizes by Gingerich (1998).

then subtracted from the endocranial volume to calculate and estimated brain volume for *Dorudon atrox*. These values are listed in Table 22 The average size of the *rete mirabile* was about 18.8% of the endocranial volume. This figure was used to calculate the size of the brain in those specimens for which endocasts were inaccessible or unavailable.

Together, the adult endocranial volume and estimated body mass can be used to calculate an encephalization quotient (EQ) for *Dorudon atrox*. An encephalization quotient is the ratio of the actual brain volume divided by the brain volume expected for an animal of the same body size (Jerison, 1973). Thewissen and Gingerich (1989) noted that there are several ways to calculate the expected brain weight for a given body size. Jerison (1973) suggested that brain weight in mammals scales as a function of body surface area, yielding a slope of the linear correlation between brain weight and body weight in log-log space around 0.67. Martin (1981) suggested that mammalian brain weight scales in relation to metabolic rate, yielding a slope of the linear correlation between brain weight and body weight in log-log space around 0.76. Gingerich (2001) calculated an expected slope of the linear correlation between brain weight and body weight in log-log space of 0.704 based on a large sample of terrestrial mammals.

Neither of the these appear to be the case for cetaceans. The linear correlation between brain weight and body weight in log-log space for modern cetaceans is shown in Figure 108. The slope of this line is around 0.35, which is not very close to either expectation. It may be that the cetacean brain size/body size relationship is very different from that of terrestrial mammals due to their large increase in body mass due to the addition of a large amount of blubber. Since this tissue is not under nervous control like the skin, muscles, and viscera, it may alter

the brain weight/body weight relationship in cetaceans. This would only be the case if larger cetaceans had relatively more blubber than smaller cetaceans. This possibility will be investigated in the future. If this is the case, it suggests that encephalization quotients for marine mammals should be calculated using an estimate of lean body weight, rather than total body weight.

No matter what the cause of the relationship of brain weight and body weight, adopting a standardized formulation for EQ allows the comparison of the relative brain sizes of the animals under study, in this case *Dorudon*, to the group the equation was based on. Here, Jerison's equation for mammals will be used because it has been widely used before, an allows the comparison of *Dorudon* brain size to other mammals.

$$EQ = \text{brain weight} / 0.12\ (\text{body weight})^{0.67}$$

The estimated body weight listed above is 2,240 kg. Using Jerison's equation shown above, and the actual brain size of adult *D. atrox* (UM 1001222, 944 g), yields an EQ of 0.438. Since the expectation of an average mammal is an EQ of 1.0, this indicates that *D. atrox* has a relatively small brain.

Marino et al., (2000) report the result of a CT study of the endocranial volume of *Zygorhiza kochii*, and include calculations of *Dorudon atrox* encephalization quotients as well. Their results also indicate that *D. atrox* and *Z. kochii* were not highly encephalized like modern cetaceans. Based on equation calculated from modern odontocetes (Marino, 1995), the mean EQ values of 0.39 for *D. atrox* and 0.26 for *Z. kochii* are much lower than those for modern odontocetes which range between 0.5 to 2.7 (Marino, 1998). It is important to note that these observations are not dependent upon the estimates of endocranial rete volume. When no endocranial rete volume is subtracted and total endocranial volume is used in calculating EQ, the results lead to the same conclusion. In this case, the EQ, based on Jerison's EQ equation, based on a large sample of modern mammals, for *D. atrox* is 0.48 and for *Z. kochii* 0.32 (Marino et al., 2000).

Table 22 also includes brain size data on several sub-adult specimens of *Dorudon atrox*. These values indicate that, as expected, brain size increases with ontogenetic age in *Dorudon*. Beyond that, it is difficult to say much more about the change in relative brain size, because while endocranial volume is relatively easy to measure, body mass is not. Since there is no reliable way to calculated body size in these subadult individuals, there is no reliable way to calculate their encephalization quotients as well.

Brain

Cerebrum

The dorsal surface of the cerebrum [**cbr**] of *Dorudon atrox* is visible lateral to the midline in cranial endocasts, anterior to the *rete mirabile* that covers the dorsal surface of the cerebellum (Figures 109A and 110A). Dart (1923) described the dorsal surface of the cerebrum as "flattened", but it is unclear what he meant by this term. The surface of the cerebrum visible between the dorsal sagittal sinus and the dorsal surface of the ophthalmic division of the trigeminal nerve (V_1) is quite convex and at a high angle to the ventral and dorsal surfaces of the brain, not flat. The cerebrum is obscured along the midline by the dorsal sagittal sinus. No bony falx cerebri or tentorium cerebelli is present in *Dorudon atrox*. In addition, many features of the surface of the cerebellum, such as the longitudinal fissure or the larger sulci often preserved in cranial endocasts are not visible since they are obscured by vascular structures.

The olfactory bulb [**ob**] in most mammals rests on the cribriform plate of the ethmoid and sends nerve fibers through perforations in the cribriform plate into the nasal cavity. These fibers constitute the olfactory nerve (Cr. I, discussed below). In archaeocetes, the intertemporal region of the skull has become greatly elongated, separating the cribriform plate from the bulk of the brain by a great distance, bridged by the elongated olfactory nerve of *Dorudon atrox*. The olfactory nerve is the dorsalmost nerve of all the cranial nerves extending anteriorly from the brain.

Cerebellum

Little of the cerebellum [**cbl**] is visible on cranial endocasts of *Dorudon atrox* (Figures 109A and 110A). The dorsal surface of the cerebellum is covered with a large *rete mirabile* as noted above. The *rete* also covers much of the lateral side of the cerebellum as well. The ventral aspect of the cerebellum is a bit troublesome to identify, as many landmarks on the ventral aspect of endocranial casts are obscured. The cerebellum is most easily seen from the posterior end. The dorsal *rete mirabile* clearly ends somewhat dorsal to the foramen magnum, exposing the cerebellum. It is difficult to pinpoint the junction between the cerebellum and the brain stem, as this feature is not always readily apparent in cranial endocasts.

Brain stem

The difficulty in distinguishing the brain stem from the ventral aspects of the cerebrum and cerebellum has led to some confusion as to the identity of particular structures. Pilleri (1991, plate II) illustrated the ventral aspect of a dorudontine (*Dorudon* sp., possibly *D. atrox*) and identified parts of the brain and cranial nerves. The identifications differ somewhat from those of Dart (1923, text-figure 3). Both agree on the identity of the trigeminal nerve. Dart (1923) identified the "tuberculum olfactorium" lateral to the midline "intertubercular sulcus". The bulges of the tubercula olfactorium do not appear to connect to the olfactory nerve, which is not even visible on the ventral view of the cranial endocast. It is possible that Dart's "tubercula olfactorium" are the roots of the optic nerve. This interpretation would suggest that the area just anterior these structures is the optic chiasma. There is no obvious representation of the optic chiasma on any of the cranial endocasts.

The hypophysis [**hyp**] is apparent along the midline of the ventral surface of cranial endocasts of *Dorudon atrox* (Figures 109B and 110B). The hypophysis projects ventrally into a small

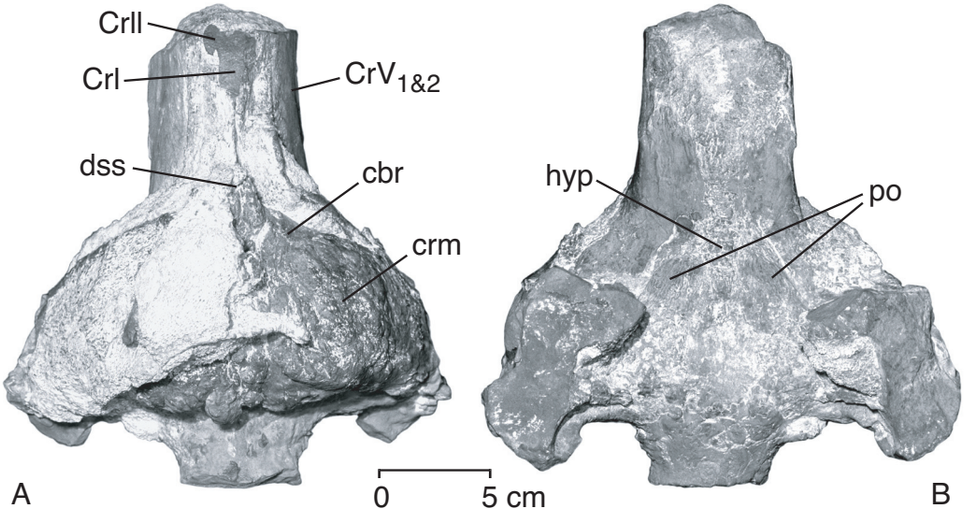

FIGURE 109 — Cranial endocast of *Dorudon atrox* (UM 100144) in A, dorsal, and B, ventral view. Note the large-meshwork texture on the dorsal surface of the endocast. This is almost certainly a cranial rete mirabile [*crm*]. Note also the presence of well-preserved casts of cranial nerves on the anterior end of the endocast. The large structures on the lateral edges of the endocast seen in ventral view are casts of the tympanic cavity that are confluent with the endocranial space via the cranial hiatus.

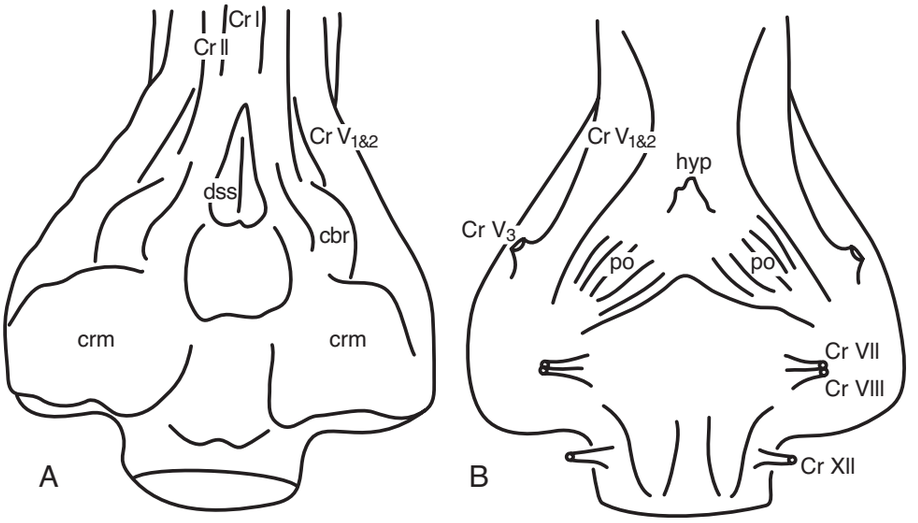

FIGURE 110 — Brain anatomy of *Dorudon atrox* in A, dorsal, and B, ventral view. These drawings are based on numerous cranial endocasts of *D. atrox* individuals, CT scans of skulls, and additional skulls. The origins of some of the cranial nerves, such as the olfactory and optic nerves, are obscured by other structures.

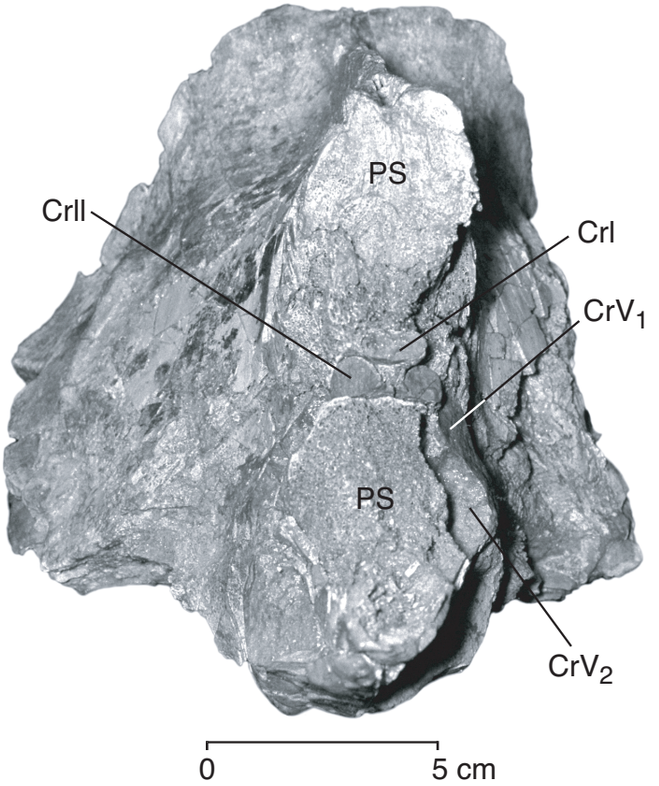

FIGURE 111 — Cranial nerves of *Dorudon atrox* (UM 94797), anterior view. Note the well-preserved and well-differentiated casts of the olfactory nerve [*Cr I*], optic nerves [*Cr II*], ophthalmic nerves [*Cr* V_1], and maxillary nerves [*Cr* V_2].

depression along the midline of the endocranial surface of the basisphenoid. It is just posterior to the point where the ophthalmic and maxillary divisions of the trigeminal are closest to the midline (this is the constriction in the hourglass shape visible on the endocranial surface of the basisphenoid).

Lateral to and posterior to the hypophysis are a pair of bulges that are separated along the midline by a groove. The bulges trend anteroposteriorly on their anterior ends and turn to run lateroposteriorly on their posterior ends. These bulges are covered with fine striations that parallel the trend of the structures themselves. Pilleri (1991) identified the bulges as the hypophysis. This is almost certainly not the case, simply based on size, and since there is another structure of the appropriate size and in the correct position to be the hypophysis. Dart (1923) does not identify the bulges in any of his figures, but he does identify the area posterior to them as the medulla oblongata. The bulges are much more likely to be the pons [**po**] than the hypophysis. Pilleri (1991) suggested that this area is the pons and the medulla oblongata is more posterior yet.

The pair of bulges is likely to be the pons for three reasons. First, its position and size relative to the hypophysis is consistent with this structure being the pons. It is mainly posterior and lateral to the hypophysis. Second, the surface is prominently striated with the striations running parallel to the structure. This surface texture is typical of the pons. Lastly, the flat area behind the bulges is just anterior to the spinal cord and at least part of this flat area must be medulla oblongata [**mo**].

Cranial nerves

Olfactory nerve

The olfactory peduncles are elongated in archaeocetes into the olfactory nerve [**Cr. I**, Figure 111]. The large olfactory nerve is extremely different than that seen in modern cetaceans, which lack olfactory nerve fibers altogether as adults, but retain a few nerve fibers in fetal development (most odontocetes) or have only a few fibers as adults (most mysticetes [Morgane and Jacobs, 1972]). The olfactory nerve can be seen in Figures 28 and 111. The olfactory nerve arises from the cerebrum somewhere dorsal to (and possibly anterior to) the optic nerve and follows along the midline of the skull with the parietal posteriorly, the frontal anteriorly dorsal, and the presphenoid ventrally. The olfactory nerve meets the cribriform plate just anterior to the

orbit and fibers pass through the cribriform plate into the posterodorsal narial cavity (Figure 28).

Optic nerve

The optic nerve [**Cr. II**, Figure 111] arises from the brain stem and proceeds anteriorly towards the optic foramen in the orbit. The optic nerve is visible in Figures 28 and 111. The precise point where the optic nerve arises from the cerebrum is not evident in any cranial endocasts of *Dorudon atrox*. In addition, no optic chiasma is visible in endocasts of the brain of *D. atrox*, although one was almost certainly present since the optic chiasma is present in artiodactyls and in modern cetaceans. There are no grooves on the endocranial surface of well-preserved basisphenoids where the optic chiasma would be. The optic nerve follows a path that is parallel to that of the olfactory nerve, with the presphenoid ventral and the parietal and frontal dorsal to the nerve tract. The optic nerve lies slightly ventral and lateral to the midline olfactory nerve. At the optic foramen of the frontal, the optic nerve turns laterally and enters the orbit. The nerve follows the dorsal border of the orbit along the underside of the frontal shield lateral to the eye.

Oculomotor nerve and trochlear nerve

The oculomotor nerve [**Cr. III**] and the trochlear nerve [**Cr. IV**] cannot be identified in any specimen of *Dorudon atrox*. They, along with the abducens nerve, probably followed the path of the trigeminal nerve (ophthalmic division, V_1) from the endocranial space to the orbital fissure. Here they enter the orbit and distribute to the appropriate eye muscles. They probably cannot be distinguished since they are not in separate tracts from the trigeminal nerve and because they are so small in relation to the trigeminal nerve. Hosokawa (1951) indicated that the oculomotor, trochlear, and abducens nerves follow the course of the trigeminal from the endocranial space to the orbit in modern cetaceans, as is the case in artiodactyls (Getty, 1975).

Trigeminal nerve

The trigeminal nerve [**Cr. V**, Figure 111] is the largest of all the cranial nerves in *Dorudon atrox*. It originates from the pons and almost immediately divides into its main trunks (Figure 109B, 110B). The base of the trigeminal nerve appears to emerge from the anterolateral surface of the pons. Breathnach (1955) states that casts of the trigeminal nerve tract in modern cetaceans bear little resemblance to the nerve itself due to the presence of a *rete mirabile* surrounding the trigeminal nerve. The apparent large size of the cast of the trigeminal nerve may be due to the inclusion of retial tissue in the cast (Breathnach, 1955). Casts of the trigeminal nerve in *D. atrox* have a surface that appears to be covered with a fine mesh of threadlike fibers indicating an ophthalmic *rete mirabile*. In addition, the first two divisions of the trigeminal, (ophthalmic and maxillary) seem to be much more distinct from one another in younger individuals. This may indicate that the retial tissue becomes thicker in older individuals, obscuring the division between the two portions of the nerve.

The trigeminal is divided into the ophthalmic nerve (**Cr. V_1**), maxillary nerve (**Cr. V_2**), and mandibular nerve (**Cr. V_3**). The first branch to diverge is the mandibular nerve, which splits off from the ophthalmic and maxillary trunks just anterior to the otic region. The mandibular nerve proceeds laterally to leave the cranial cavity via the foramen pseudo-ovale of the squamosal. A portion of the mandibular nerve entered the large mandibular foramen of the dentary and proceeded anteriorly along the mandibular canal to innervate the lower teeth. Presumably, a branch of the mandibular nerve entered the oral cavity to innervate part of the tongue, but there are no osteological indicators of this branch. The ophthalmic and maxillary divisions proceed anteriorly dorsolateral to the presphenoid and ventromedial to the parietals and then frontals (Figure 111). Upon entering the orbit via the orbital fissure, the ophthalmic nerve (Cr. V_1) continues into the orbit to the eye. It is unclear whether there are any ethmoidal branches of the ophthalmic nerve. There is no supraorbital foramen nor notch for a frontal branch of the ophthalmic nerve. The maxillary nerve (Cr. V_2) continues through the orbit and runs anteriorly into a long extension of the orbital space. The maxillary nerve enters the antorbital canal of the maxilla at the anterior end of this space via the internal maxillary foramen and proceeds onto the face via the antorbital foramen. This foramen is sometimes singular, but often it is divided into multiple foramina. A branch of the maxillary nerve also continues anteriorly in the maxilla to innervate the maxillary and premaxillary alveoli.

Abducens nerve

The abducens nerve [**Cr. VI**] cannot be identified in any specimen of *Dorudon atrox*. Its probable path is discussed above along with the oculomotor and trochlear nerves.

Facial nerve

The facial nerve [**Cr. VII**] leaves the endocranial cavity by entering the internal acoustic meatus of the periotic. This structure has multiple foramina that are described along with the rest of the periotic. The opening for the facial nerve is referred to here as the facial canal. The origin of the facial nerve is obscured in cranial endocasts of *Dorudon atrox*, since the entire tympanic cavity is cast along with the brain. Some cranial endocasts do preserve a cast of the internal acoustic meatus of the periotic, and thus show the entrance of the facial nerve into the body of the periotic. The facial nerve passes through the periotic, exiting via the lateral opening of the facial canal. Kellogg (1936) calls this opening the "epitympanic orifice of the aqueductus Falopii." It is a small foramen that is situated between the main portion of the body and the fossa for the head of the malleus. It opens posteriorly into a well-defined groove that runs posteriorly, dorsal to the fenestra ovalis. The facial nerve leaves the tympanic cavity via the elliptical foramen of

the auditory bulla. It presumably then turned anteriorly to distribute to many structures of the face, for which there are no osteological indicators.

Vestibulocochlear nerve

The vestibulocochlear nerve [**Cr. VIII**] has a very short path from the brain to the internal acoustic meatus of the periotic. Numerous foramina in this structure are described above (with the periotic). The origin of the vestibulocochlear nerve in the brain is obscured, as described above for the facial nerve. Casts of the internal acoustic meatus also preserve casts of the vestibulocochlear nerve entering the periotic. The vestibulocochlear nerve divides into its vestibular and cochlear components even before it enters the periotic. The largest and most posterior of these foramina is for the cochlear portion of the vestibulocochlear nerve (cochlear nerve). The cochlear nerve innervates the cochlea inside the periotic. The next most anterior foramen is for the vestibular portion of the vestibulocochlear nerve (vestibular nerve). The vestibular nerve innervates the semicircular canals, the utricle, and saccule inside the periotic.

Glossopharyngeal, vagus, and accessory nerves

The glossopharyngeal [**Cr. IX**], vagus [**Cr. X**], and accessory nerves [**Cr. XI**] do not leave the skull via their own foramina in *Dorudon atrox*. Presumably, their exit was via the posterior lacerate foramen.

Hypoglossal nerve

The hypoglossal nerve [**Cr. XII**] leaves the skull via the hypoglossal foramen in the jugular notch. The position of the hypoglossal foramen in or near the jugular notch is a characteristic of all cetaceans.

Spinal cord and spinal nerve*s*

The spinal cord of *Dorudon atrox* extended from the brain stem, through the foramen magnum of the skull, into the neural canal of the vertebral column. The last vertebra that has a neural canal is around caudal vertebra 12. This indicates that the spinal cord itself terminated at some point cranial to Ca12, since the spinal cord terminates anterior to the end of the bony neural canal in mammals. The spinal cord of *Lagenorhynchus albirostris* (*Delphinus albirostris*) terminates between L6 and L7 (Cunningham, 1877), while the spinal cord of the bottlenose dolphin (*Tursiops truncatus*) ends at about L3 (Ridgway, 1990). In the pig it ends at the third sacral vertebra (Getty, 1975). It is likely that the spinal cord terminated somewhere in the lumbar region of *Dorudon atrox*. Posterior to the termination of the spinal cord, the neural canal houses only the filum terminale and the more posterior spinal nerves, rather than the spinal cord itself.

The size of the neural canal has been used to determine the amount of neural control over the fore and hind limbs. The spinal cord is expanded in the regions of the brachial plexus (for forelimb control) and the lumbar plexus and sacral plexus (for hindlimb control) in mammals. The size of the neural canal reflects the size of the spinal cord and can be used to gauge the contributions from the fore- and hind limbs in locomotion in pinnipeds (Giffin, 1992). Unfortunately, this method cannot be used in cetaceans since the size of the neural canal does not reflect the size of the spinal cord. The neural canal of modern cetaceans contains both the spinal cord and a voluminous *rete mirabile* (Turner, 1872; McFarland et al., 1979). This extra vascularization precludes interpretation of the size of the spinal cord from the size of the bony neural canal.

Spinal nerves leave the neural canal through the intervertebral foramina formed by adjacent articulating vertebrae. Little more can be said about the spinal nerves since the sizes of the foramina only limit the sizes of the nerves, and the foramina are larger than the neural canal itself.

CIRCULATORY SYSTEM

Blood supply to the brain

The blood supply to the brain of *Dorudon atrox* is difficult to reconstruct because both artiodactyls and modern cetaceans are highly autapomorphic in their cranial blood supply. Blood flows from the heart to the brain via the aorta, common carotid, and external carotid artery in extant artiodactyls (McFarland et al., 1979). This pattern is unusual for mammals, which primitively supply the brain with blood from the internal carotid artery. Modern cetaceans receive blood flowing to the brain from the aorta via the intercostal arteries that feed into a thoracic *rete mirabile* (McFarland et al. 1979). This gives rise to smaller retial structures that enter the vertebral canal via the intervertebral foramina. Here they form the spinal *rete mirabile* through which blood flows into the cranial cavity via the spinal meningeal artery to supply the brain. The second problem in determining the blood supply to the brain of archaeocetes is that there are no separate foramina for the blood vessels that supply the brain with blood and those that drain deoxygenated blood. Both the internal carotid artery and the jugular vein enter and leave the skull, respectively, via the posterior lacerate foramen, thus leaving no indication of their size.

However blood got to the brain of *Dorudon atrox*, cranial endocasts show the presence of a cranial *rete mirabile* [**crm**] on the dorsal surface of the cerebrum, visible in Figure 109A, 110A. This network appears to be linked to the dorsal sagittal sinus [**dss**], which projects anteriorly from the dorsal cerebellar surface. Thus the network is probably a venous *rete mirabile*. Modern cetaceans have endocranial *retia* (Breathnach, 1955), but they are not found on the dorsal surface of the cerebrum.

Cranial endocasts also show blood vessels that are found in the bones of the skull, either on the surface of the brain, or just off the surface of the brain within the bones (Figure 112A). A large blood vessel leaves the otic region just anterior to the periotic and travels dorsally and slightly anteriorly within the

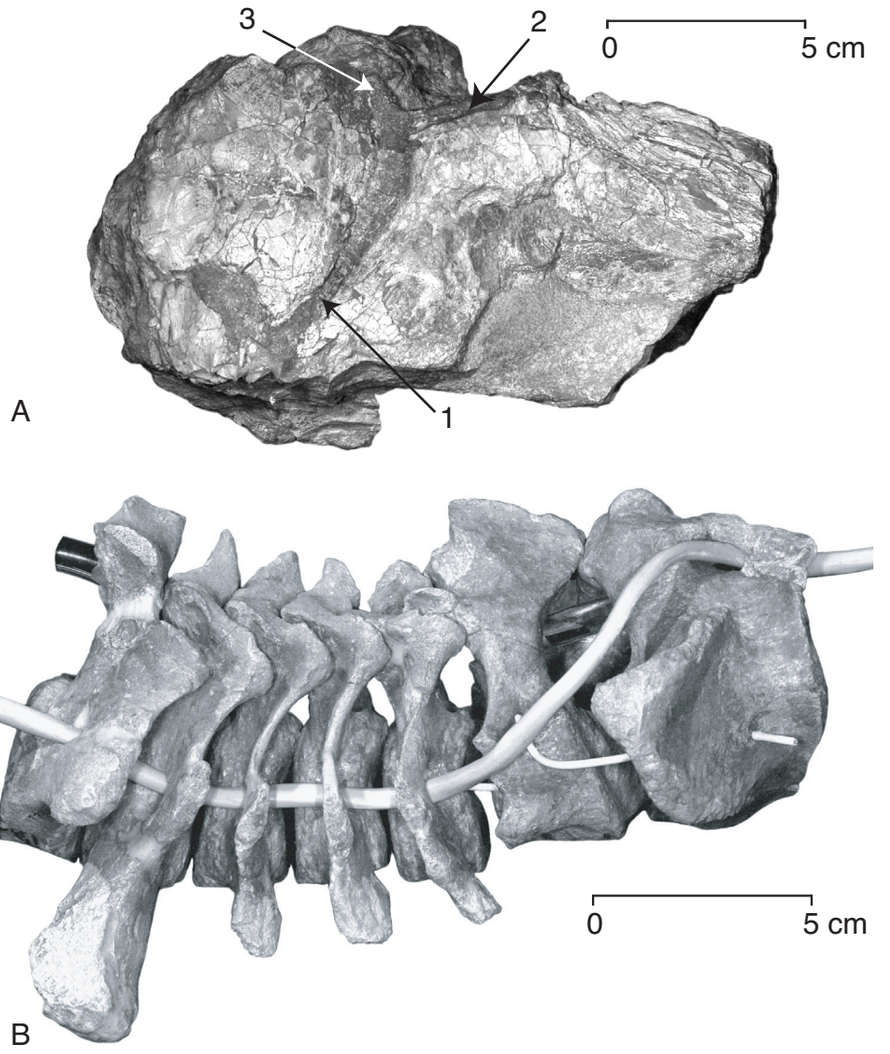

FIGURE 112 — Paths of blood vessels of *Dorudon atrox*. A, cranial vessels in UM 97519. Vessel 1 leads away from the tympanic cavity and trends anteriorly and dorsally through the squamosal bone. Vessel 2 is a branch heading anteriorly and medially. Part of it becomes lost in the bone of the intertemporal region, while another branch appears to continue anteriorly, possibly representing the ophthalmic artery. Vessel 3 is a second branch of vessel 1 that exits the skull via the post-parietal foramen. B, path of the vertebral artery of UM 94814. This passes through the arterial foramina in C7 to C3. The foramen in C2 is much smaller, suggesting that only a small branch of the vertebral artery passes through it, exiting on the lateral side of the body and entering the posterior side of C1. The main portion of the vertebral artery probably passes around C2, enters the neural canal via the lateral foramen of C1, and enters the skull through the foramen magnum.

squamosal. A small branch of this vessel continues anteriorly in the squamosal just dorsal to the ophthalmic division of the trigeminal nerve. This is probably the ophthalmic artery. The main trunk of the vessel leaving the otic region continues dorsally. Near the level of the dorsal sagittal sinus, the vessel divides into two branches of approximately equal size. One leads anteriorly and appears to become lost in the spongy bone of the squamosal, anterior and dorsal to the dorsal sagittal sinus. This vessel is possibly a nutrient artery, supplying this thick bony area with blood. The other branch leads to the postparietal foramen and leaves the parietal bone. The positions of the branches of these vessels vary from specimen to specimen, but the general pattern is the same.

Another artery that can be traced with some certainty in *Dorudon atrox* is the vertebral artery. The vertebral artery branches off from the brachiocephalic artery and travels up the

cervical region of the spinal column to the brain (Figure 112B). The vertebral artery travels through the foramina in the transverse processes, passing from the posterior to the anterior side of the cervical vertebrae from C7 to C3. At C2 the artery probably passed laterally around the transverse process, possibly through a notch in the transverse process. A small branch enters the posterior side of the transverse process. The reason for thinking that the main vertebral artery passed around C2 rather than through C2 is that the transverse foramen of C2 is less than half the size of the transverse foramina of C3 to C7. Inside the transverse process, the canal takes a 90° turn laterally, such that the "anterior" opening of the canal is on the lateral side of the transverse process.

On C1, the transverse foramen is located directly anterior to the transverse foramen of C2. This foramen is variably present. Of six C1 specimens examined closely, two have transverse foramina on both sides and four have a foramen on only one side. The anterior opening is lateral to the cranial articular surface. These foramina are even smaller than those in C2 and probably only transmit a small branch of the vertebral artery. The main portion of the vertebral artery probably passed dorsal to the transverse process of the atlas and passed through the lateral vertebral foramen from the posterolateral side into the neural canal. The lateral vertebral foramina of C1 are much larger than the transverse foramina of C2. If the same artery that exited the transverse foramen of C2 passed through the lateral vertebral foramen of C1, it is odd that they are so disparate in size. Some mammals receive an anastomosis (the occipital artery) from the external carotid artery before the vertebral artery enters the lateral vertebral foramen. If the disparity in size of foramina of C2 and C1 is any guide, this may also have been the case in *Dorudon atrox*. The vertebral artery then passed into the skull via the foramen magnum. In addition, the large size of the lateral vertebral foramen of C1 suggests that it transmitted a substantial artery that would have significantly contributed to the cranial blood supply.

The last set of arteries that can be described in *Dorudon atrox* are the caudal intervertebral arteries. In modern cetaceans, the caudal extension of the abdominal aorta gives rise to a number of arteries the pass dorsally to feed into the tail stock and fluke (Slijper, 1936). In *D. atrox*, these arteries pass between the transverse processes of the vertebrae in the posterior lumbar and anteriormost caudal regions. The transverse processes from approximately caudal vertebrae Ca4 to Ca10 in *D. atrox* are perforated by foramina that transmitted these arteries. Posterior to Ca10, the transverse processes are very reduced, but still contain a notch in which the artery rested. These features of the caudal vertebrae are similar to those found in modern cetaceans, suggesting similar paths for the caudal intervertebral arteries.

MUSCLES

One can be relatively confident that a given soft tissue structure, such as a muscle, was present in *Dorudon atrox* based on its presence in modern cetaceans and modern artiodactyls, but the precise position of the origin or insertion may not be clear in *D. atrox*. The origins and insertions of muscles of *D. atrox* described below are considered to be the best hypotheses of positional relationships based on the following criteria, applied in order from first to last.

First, muscles that are present in artiodactyls and extant cetaceans are present in *Dorudon atrox*. Second, muscles present in both artiodactyls and extant cetaceans that have distinctive osteological correlates have the same relationship between muscles and correlates as in modern artiodactyls and cetaceans. Third, for those muscles that lack distinctive osteological correlates in extant bracket taxa, their origins and insertions are determined by finding sites of origin and insertion in *Dorudon atrox* that are in similar positions relative to the origins and insertions that are known with more certainty. Fourth, for all of the origins and insertions, it was determined whether the muscle in question can function in its hypothesized position.

Muscles are listed here by the joints that they cross and the bones that they move. More detailed descriptions of particular movements and the muscles that contribute to them are discussed in a subsequent chapter on functional morphology. In addition, muscles are usually assigned an origin and an insertion based on the point that is considered to be more stationary during a given movement. Many of these relationships are reversed in cetaceans from their typical usage, particularly in the musculature of the back and trunk. Since *Dorudon atrox* is a cetacean and has many of the same anatomical features of modern cetaceans, the cetacean usages of origin and insertion for particular muscles are followed here, usually derived from Strickler (1980) or Pabst (1990). Also, when describing the same muscles in modern artiodactyls, the cetacean usages of origin and insertion are used to avoid confusion, even though they are often reversed from the normal application to artiodactyls.

Muscles of mastication

The muscles of mastication of *Dorudon atrox* have never before been reconstructed, although they have been for *Zygorhiza kochii*. Carpenter and White (1986) reconstructed the muscles of mastication based on Kellogg's (1936) reconstruction of the skull of *Zygorhiza*. Some of the origins and insertions of the muscles shown are likely to be generally correct, but others are almost certainly wrong. Each will be discussed below along with the reconstruction for *Dorudon atrox*. The muscles of mastication are shown in Figure 113.

One muscle that Carpenter and White reconstruct that is almost certainly not present is the zygomaticomandibularis. The zygomaticomandibularis muscle is not found in extant Artiodactyla, nor in modern Cetacea. There is no anatomical evidence of it on the skull of *D. atrox* in the form of ridges or roughened areas of muscular attachment that would indicate that three separate muscles originated on the zygomatic arch (superficial masseter, deep masseter, and zygomaticomandibularis), nor is there evidence for insertions on the lateral side of the

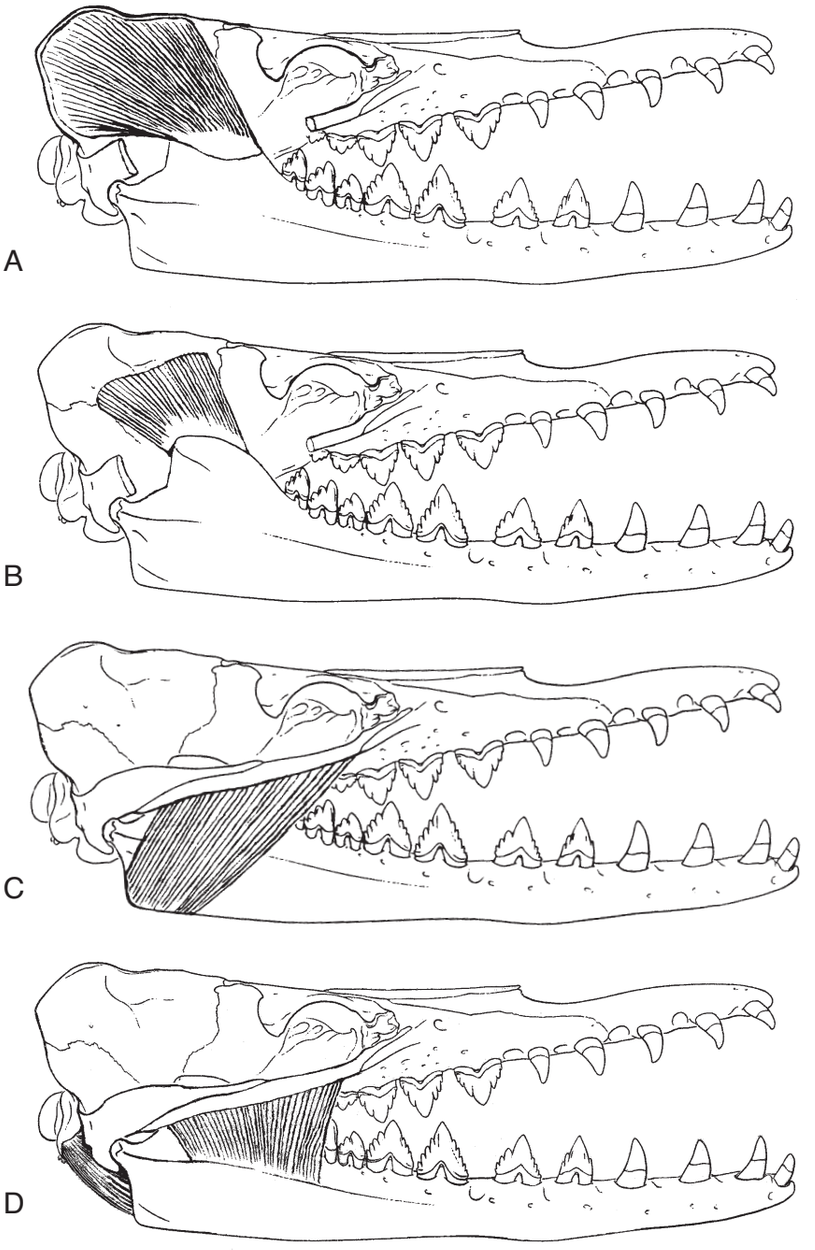

FIGURE 113 — Muscles of mastication of *Dorudon atrox*, in lateral view. A, superficial temporal; B, deep temporal; C, superficial masseter; D, deep masseter and digastric. Note the large temporalis muscles and masseter muscles. This reconstruction differs significantly from that of Carpenter and White (1986) for *Zygorhiza kochii* in lacking the zygomaticomandibularis muscle and in placement of the pterygoid muscles.

mandible (deep masseter and zygomaticomandibularis). For these reasons, the zygomaticomandibularis is not reconstructed here.

Muscles that close the jaw

Temporalis pars superficialis.— The temporalis muscles originate on the lateral wall of the skull, on the parietal bone.

Carpenter and White (1986) show a very large origin for the superficial temporalis of *Zygorhiza*, with the anterior fibers originating on the frontal just behind the frontal shield, and the posterior fibers originating on the squamosal. In *Dorudon atrox* there is a prominent ridge that forms a discontinuity in the surface of the parietal. This ridge is anterior to the postparietal foramen. It probably forms the division between the origin of the superficial temporal and deep temporal muscles. Also, it seems unlikely that the anterior fibers of the superficial temporal muscle would have originated on the frontal, since their orientation would be such that they would pull the jaw up and forward, rather than up and back. There is also another low vertical ridge on the anterior face of the squamosal. This ridge probably marks the medial side of the origin of the temporalis on the squamosal. Temporalis pars superficialis inserted on the lateral side of the coronoid process of the dentary. There is a well-developed muscular fossa on the coronoid for the insertion. The fossa is delimited by a low ridge on the ventral border. The main action of the superficial temporal is to pull the mandible up and back.

Temporalis pars profundus.— The deep temporal muscle originates on the lateral wall of the skull, just ventral to the origin of temporalis pars superficialis. Carpenter and White (1986) showed a very large origin for the deep temporal for *Zygorhiza* that parallels that of the superficial temporal. Anterior fibers originate on the frontal, while posterior fibers originate on the squamosal. It is unlikely that the anterior fibers originated so far forward. The origin of the deep temporal muscle shown for *Dorudon atrox* is much more restricted. It is bordered dorsally and laterally by the origin of the superficial temporal muscle. Its anterior and ventral margins are probably near the frontoparietal suture. The temporalis pars profundus inserts on the medial side of the coronoid process of the dentary. There is a well-developed fossa for the insertion that is the mirror image of the insertion for the superficial temporal on the lateral side of the coronoid process. The main action of the deep temporal muscle is to pull the mandible up and back.

Masseter pars superficialis.— The superficial masseter originates on the maxillary portion of the zygomatic arch and from the ventral jugal. The fibers of the superficial masseter angle ventrally and posteriorly to the insertion on the angle of the dentary. This region is very poorly preserved in most specimens of *Dorudon atrox*, so other archaeocetes were also used to reconstruct the insertion. This reconstruction is very similar to that of Carpenter and White (1986) for *Zygorhiza kochii*. The main action of the superficial masseter is to pull the mandible up and forward.

Masseter pars profundus.— The deep masseter originates on the ventral and lateral margins of the zygomatic arch, on the jugal and zygomatic process of the squamosal. The fibers of the deep masseter run almost directly ventrally to insert on the condyloid crest of the mandible. The main action of the deep masseter is to pull the mandible up.

Muscles that open the jaw

Digastricus.— The digastric muscle in mammals is usually divided into two bellies connected by a dividing tendon (Turnbull, 1970). The posterior belly originates on the lateral side of the paroccipital process of the exoccipital and inserts on the dividing tendon. The anterior belly originates on the dividing tendon and inserts on the ventral border of the dentary. Carpenter and White (1986) show this arrangement for *Zygorhiza kochii* and state that the digastric "crosses over the lateral surface of the auditory bulla". If the digastric originates on the paroccipital process, the muscle certainly must pass over either the lateral surface of the bulla or the posterior process of the bulla, as the bulla is directly in the path that the muscle would take from the paroccipital process to any point on the dentary.

Unfortunately, there is no clear muscle scar for either the origin of the digastric on the paroccipital process, or for the insertion on the ventral border of the dentary. In addition, the condition of the digastric in modern cetaceans is very different from that of primitive mammals. In odontocetes the digastric muscle has only a single belly, and it originates on the "mastoid notch of the temporal bone" and/or on the basihyoid and stylohyoid (Werth, 1992). The relatively small paroccipital process is the articulation for the stylohyoid in *Dorudon atrox*, making it difficult to give origin to the digastric muscle since there does not appear to be enough area for both. Given the problems associated with the placement of the origin of the digastric in relation to the auditory bulla and stylohyoid, and its shifted origin in modern odontocetes, a different origin of the digastric is likely. The digastric may take origin from the squamosal, posterior to the external auditory meatus and anterior to the posterior process of the periotic. This complicated area is rugose, suggesting a possible muscle origin, and it would place the belly of the digastric lateral to the bulla and stylohyoid, keeping it from interfering with the auditory apparatus. The main action of the digastric is to depress the mandible.

Muscles that stabilize the jaw

The origins of the pterygoideus muscles in modern cetaceans have been greatly altered from their condition in primitive mammals by development of the pterygoid sinuses. The medial and lateral laminae of the pterygoid bone form a space between them that is the foam-filled sinus. The pterygoid sinus is present in *Dorudon atrox* and other basilosaurid archaeocetes, but it is quite different in form from modern cetaceans. In addition, since the laminae of the pterygoid are very thin and fragile, they are not often preserved, and when they are, they are often in poor condition, making any muscle scars difficult to observe. For these reasons, any hypothesis concerning the origins of the pterygoid muscles must be considered speculative.

The reconstruction of the pterygoid muscles in *Zygorhiza kochii* by Carpenter and White (1986) is problematic. The skull of *Zygorhiza* in their reconstruction completely lacks the pterygoid sinuses, and only one lamina of the pterygoid is shown. This is clearly not the case, as *Zygorhiza* has pterygoid sinuses similar to those of *Dorudon atrox* (Kellogg, 1936; personal observation). In addition, the lateral pterygoid (pterygoideus externus) is shown running dorsal to the bulla and ventral to the skull. This reconstruction is certainly wrong

since the pterygoid and squamosal bones are there, which would prevent any muscles from traversing the space.

Pterygoideus medialis.— The medial pterygoid probably originated on the lateral side of the lateral lamina of the pterygoid and anteriorly on the lateral side of the posterior palatine. There is a large depressed area with some rugosity in this position, which indicates a site of muscle origin. There is no obvious muscle scar for the insertion of the medial pterygoid on the dentary, but the fibers probably ran ventrolaterally to insert ventral to the mandibular foramen.

Pterygoideus lateralis.— The lateral pterygoid probably inserted on the lateral side of the lateral lamina of the pterygoid posterior to the origin of the medial pterygoid. The fibers ran ventrolaterally to insert on the dentary dorsal to the mandibular foramen. There is a small fossa in this position, which could indicate the insertion of the lateral pterygoid. The main action of the pterygoids is to pull the mandible medially during chewing. As stated earlier, the reconstructions of these muscles is speculative, but it is consistent with known skeletal anatomy and has the muscles in functional positions.

Hyoid musculature

Many of the muscles of the throat region are small or only originate or insert on soft tissues structures. Small muscles rarely leave muscle scars on bone, and those that attach only to soft tissue structures would not be expected to leave any trace. Since any reconstruction of these muscles would be based on speculation, only those muscles that have large origins and insertions on bony structures are discussed here. No obvious muscle scars can be found on the medial or ventral borders of the dentary, so those muscles of the sublingual region that originated on the dentary and inserted on the tongue are also not reconstructed.

Geniohyoideus.— The geniohyoideus originates at the mandibular symphysis and inserts on the cranial border of the basihyal. The cranial border of the basihyal is narrow but flat when compared to the caudal border. Laterally, its quite rugose in some specimens. It is likely that the geniohyoideus inserts on this flat area and the rugose area. The main action of the geniohyoideus is to raise the hyoid apparatus.

Hyoglossus.— There is a large, roughly triangularly shaped area on the craniomedial aspect of the medial end of the thyrohyal. This is probably the origin of the hyoglossus muscle. This muscle may also take its origin from the dorsal side of the basihyal, as it does in modern cetaceans (Reidenberg and Laitman, 1994). The hyoglossus inserts into the base of the tongue, so this insertion cannot be observed in *Dorudon atrox*. The main action of the hyoglossus is to depress the tongue.

Styloglossus.— The shaft of the stylohyal is somewhat flattened dorsoventrally, especially away from the articulation with the basihyal. The flattened ventral side presents a shallow fossa that is the site of origin of the styloglossus muscle. The styloglossus inserts into the base of the tongue, so this insertion cannot be observed in *Dorudon atrox*. The main action of the styloglossus is to depress the tongue.

Sternohyoideus and thyrohyoideus.— The shaft of the thyrohyal is somewhat triangular in cross section. One of the flat sides of the triangle faces caudally, and is probably the site of insertion of the sternohyoideus and thyrohyoideus muscles. The sternohyoideus originates on the manubrium of the sternum, anterior to the angle. The thyrohyoideus inserts on the thyroid cartilage in artiodactyls and modern cetaceans, but since this is not preserved it cannot be assessed in *Dorudon atrox*. The main action of the sternohyoideus is to move the hyoid apparatus caudally. The main action of the thyrohyoideus is to move the thyroid cartilage cranially.

Interhyoideus.— The interhyoideus connects the thyrohyal and the stylohyal. One of the sides of the triangular shaft of the thyrohyal faces the caudal border of the stylohyal. The caudal border of the stylohyal is flattened just distal to its articulation with the basihyal. It is likely that these two flat surfaces were connected by the interhyoideus in *Dorudon atrox*.

Other head and neck muscles

Muscles that extend the head and neck

Rectus capitis posterior.— The rectus capitis posterior is usually described as two separate muscles, the rectus capitis posterior major, which originates on the neural spine of C2, and the rectus capitis posterior minor, which originates on the dorsal side of the neural arch of the atlas of the skull in *Pontoporia blainvillei* (Strickler, 1980). The fibers of both portions merge cranially and insert along the crests between the supraoccipital and parietal bones (nuchal crest). The neural spine of C2 in *Dorudon atrox* is very robust, and the nuchal crest is very well developed. In addition, the dorsal side of the neural arch of the atlas of *Dorudon atrox*, lateral to the small neural spine, is a large flat area that is likely to be the origin of the rectus capitis posterior minor. These features suggest a very powerful rectus capitis posterior that originated on the first two cervical vertebrae. The main action of this muscle is to extend the head.

Obliquus capitis.— The obliquus capitis is also often described in two portions, the obliquus capitis superior, which originates on the transverse process of the atlas and inserts on the lateral portion of the exoccipital, and the obliquus capitis inferior, which originates on the lateral side of the neural spine of the axis and inserts on the transverse process of the atlas (Strickler, 1980). The large transverse processes of the atlas of *Dorudon atrox* were probably the origin of the obliquus capitis superior, as well as the insertion of the obliquus capitis inferior. In addition, the large neural spine of the axis is also likely to be the origin of the obliquus capitis inferior. The main action of this muscle is to extend the head. In unilateral action these muscles would also assist in rotation of the head (Getty, 1975).

Longissimus capitis.— There is no clear origin for the longissimus on the cranium and no clear insertion on the transverse processes of the cervical or thoracic vertebrae in *Dorudon atrox*. Despite this, since both modern artiodactyls and modern cetaceans (Pabst, 1990) have longissimus muscles, these were al-

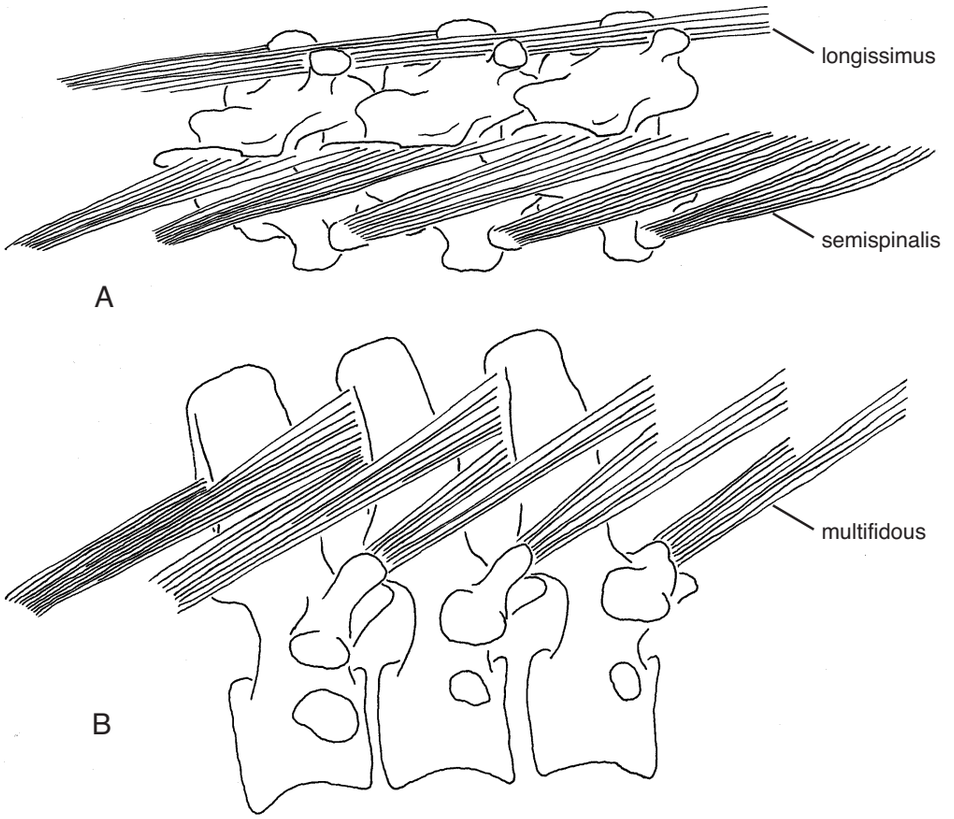

FIGURE 114 — Epaxial muscles of the thorax of *Dorudon atrox*, in A, dorsal, and B, lateral view. Note that individual muscles are shown in only one view and on one side for purposes of illustration. The fibers of the longissimus muscle originate on the posterior borders of the transverse processes of the thoracic vertebrae and insert on the transverses process of the lumbar vertebrae (see Figure 115). The fibers of the semispinalis originate on the supraspinous ligament as well as the tips of the neural spines. Fibers of the multifidus were probably not so regularly arranged as shown. Some fibers probably originated multiple vertebrae anterior to their insertions rather than one or two as shown.

most certainly present in *Dorudon atrox*. It is not surprising that clear muscle insertions are not found on the transverse processes in *D. atrox*, since they are often not present on the transverse processes in modern cetaceans.

Intertransversarii dorsales cervicis.— The cervical dorsal intertransversarii originate just anterior and ventral to the prezygapophyses of the third cervical to first thoracic vertebrae. Each muscle belly trends anteroventrally to insert on the posterior side of the transverse process of the anteriorly adjacent vertebra. Both the origins and insertions of this muscle are indistinct, and the muscles are lacking in modern cetaceans, since many have fused cervical vertebrae. These muscles may not have been present, but the space for the muscles is present, as are well-developed transverse processes and other muscle origins and insertions. All of these additional factors suggest that *Dorudon atrox* had a rather flexible neck, and the cervical dorsal intertransversarii would have added mobility to this.

Muscles that flex the head and neck

Longus coli.— The longus coli muscle is divided into two portions, the cervical and thoracic. The cervical portion originates on the transverse process of the sixth cervical vertebra, with additional bellies arising from the transverse processes of C3 to C5 as well. These bellies insert on the ventral side of the bodies of C2 to C5. The most cranial fibers of the muscle insert on the ventral process of the atlas. The thoracic portion of the longus coli originates from the ventral sides of the bodies of T1 to T6, each giving rise to a muscle belly. These muscle bellies all insert on the transverse process of the sixth cervical

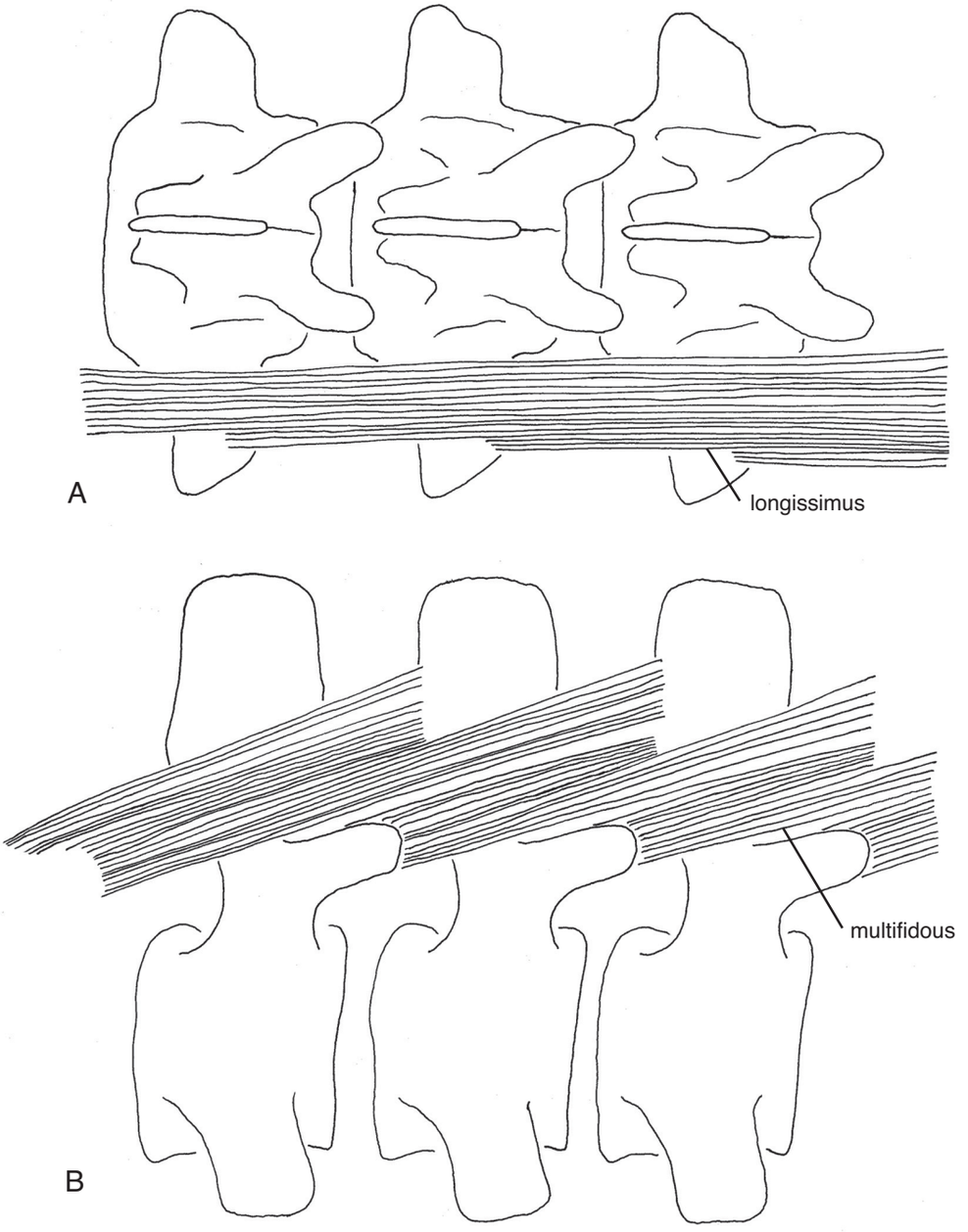

FIGURE 115 — Epaxial muscles of the lumbus of *Dorudon atrox*, in A, dorsal, and B, lateral view. The insertions of the longissimus fibers are not clearly defined on the transverse processes of the lumbar vertebrae. The large metapophyses on the lumbar vertebrae suggest an arrangement of multifidus fibers like that of the thoracic vertebrae, but the neural spines lack the well-defined sites of origin on their posterior borders.

vertebra, with some fibers inserting on the transverse process of the seventh cervical vertebra. The main action of the longus coli is to flex the neck.

Longus capitis.— While *Dorudon atrox* probably possessed the longus capitis, neither the origins nor the insertions are clear. The main action of the longus capitis is to flex the neck ventrolaterally.

Intertransversarii ventrales cervicis.— The cervical ventral intertransversarii originate on the very large ventrolaterally projecting transverse process of the sixth cervical verte-

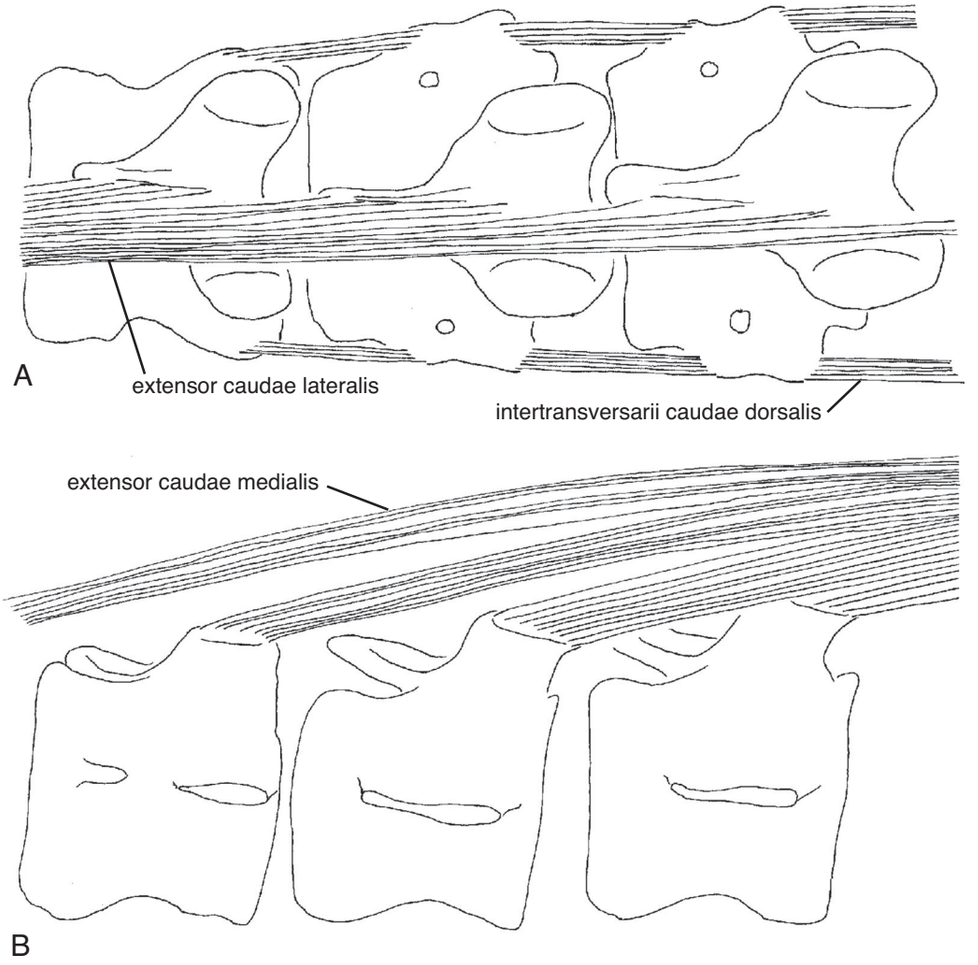

FIGURE 116 — Epaxial muscles of the anterior caudal region of *Dorudon atrox*, in A, dorsal, and B, lateral views. The extensor caudae lateralis fibers insert on the dorsal surfaces of the posterior caudal vertebrae. The extensor caudae medialis is the caudal extension of the multifidus, inserting on the large metapophyses of the anterior caudal vertebrae.

bra. This muscle has multiple insertions on the caudal sides of the transverse processes of atlas, axis, C3, and C4. The main action of the intertransversarii ventrales cervicis is to flex the neck laterally.

Epaxial muscles

The epaxial muscles are those that are dorsal to the transverse processes of the vertebrae. Reconstructions of the epaxial and hypaxial muscles of *Dorudon atrox* are shown in Figures 114-116.

Semispinalis.— In artiodactyls, the semispinalis originates on the occiput and inserts on the posterior cervical vertebrae, the nuchal ligament, and the transverse processes of the anterior thoracic vertebrae (Getty, 1975). In cetaceans, the semispinalis originates on the posterior skull along the nuchal crest and becomes intermingled with the fibers of the longissimus in the thoracic region (Strickler, 1980; Pabst, 1990). The insertion of the semispinalis + longissimus in modern cetaceans is discussed below with the longissimus. The semispinalis originates along the nuchal crest, the tips of the neural spines and the supraspinous ligament in *Dorudon atrox*. The semispinalis apparently retains its separate identity posteriorly in *D. atrox* (Figure 114). The large metapophyses on the thoracic vertebrae are probably the points of insertion for the semispinalis, as they are in the same positions as similar processes found on artiodactyl vertebrae where the semispinalis inserts. The main action of the semispinalis in both modern artiodactyls and modern cetaceans is to extend the head and in unilateral action to turn the head (Getty, 1975; Pabst, 1990).

Multifidus.— The multifidus originates on the posterior edge and lateral sides of the neural spines of the posterior cervical,

thoracic, and anterior lumbar vertebrae in modern artiodactyls. Individual slips of multifidus insert on the metapophyses of vertebrae that are one to several vertebrae caudal to their origin (Getty, 1975). In modern cetaceans the multifidus originates on the lateral sides of the neural spines of the posterior cervical, thoracic, lumbar and some anterior caudal vertebrae and inserts on the deep tendon (Strickler, 1980; Pabst, 1990). The deep tendon originates from the ventral surface of the multifidus and inserts on the metapophyses of the vertebrae from the first thoracic to the fluke insertion (Strickler, 1980; Pabst, 1990).

The multifidus in *Dorudon atrox* probably retained a condition more similar to that in artiodactyls rather than having the more derived cetacean condition (Figures 114 and 115), as indicated by features of the vertebrae. First, the posterior margins of the neural spines of the anterior thoracic vertebrae have well-defined fossae for the origin of multifidus like those of artiodactyls, and unlike modern cetaceans. These fossae decrease in their distinctiveness caudally until about T13-T14, where they disappear completely. Presumably, the multifidus originated on the lateral sides of the neural spines from this point and more posteriorly. Second, *Dorudon atrox* retains large, robust metapophyses on all of the thoracic, lumbar, and anterior caudal vertebrae. In modern cetaceans, the metapophyses are prominent on the anterior thoracic vertebrae and become reduced in the posterior thorax and lumbar regions. In some taxa they become larger again in the posterior lumbar and anterior caudal regions. The metapophyses are also positioned near the apex of the neural arch, very close to the midline. These metapophyses can be reduced in modern cetaceans since they are the site of insertion for the deep tendon rather than the entire multifidus complex. The metapophyses remain large and robust in *D. atrox* because they are the site of insertion for the multifidus muscles themselves. In addition, the metapophyses remain far removed from the midline, giving the multifidus muscle some distance over which to exert force, as it does in modern cetaceans where it inserts on the deep tendon. The action of the multifidus is to extend the anterior caudal region.

Extensor caudae medialis.— The sacrocaudalis dorsalis medialis is the caudal extension of the multifidus in both modern artiodactyls and modern cetaceans (Getty, 1975; Pabst, 1990). Slips of this muscle have a similar origin and insertion as the slips of the multifidus. They originate from the lateral surfaces of the neural spines of the sacral vertebrae and insert on the dorsal surfaces of the caudal vertebrae. The main action of this muscle is to extend the tail. The extensor caudae medialis in *Dorudon atrox* presumably has a similar origin and insertion to the multifidus, originating on the lateral sides of the neural spines of the posterior lumbar and anteriormost caudal vertebrae, and inserting on the large metapophyses of the anterior caudal vertebrae (Figure 116). The last caudal vertebra with significant metapophyses, and presumably the last with an insertion of the extensor caudae medialis, is around Ca 12. The main action of the extensor caudae medialis is to extend the tail.

Longissimus.— The longissimus originates from the mastoid process of the exoccipital, the lateral border of the atlas, the transverse processes of the cervical vertebrae, and the transverse processes of the thoracic and lumbar vertebrae, and inserts on the cranioventral surface of the ilium, spines of the sacral vertebrae, and neural spines of the thoracic and lumbar vertebrae in modern artiodactyls (Getty, 1975). In modern cetaceans, the longissimus originates from the zygomatic process of the squamosal, the lateral margin of the exoccipital, the lateral sides of the cervical vertebrae, the transverse processes and neural arches of the thoracic and anterior lumbar vertebrae, the dorsal surfaces of the ribs, and the ventral surface of the deep tendon. The longissimus inserts on the transverse processes of anterior thoracic vertebrae and the superficial tendon. The superficial tendon inserts on the neural spines of the posterior thoracic, lumbar, and anterior caudal vertebrae (Pabst, 1990). Its main action is to extend the back and neck in modern artiodactyls and cetaceans.

The relationships of the longissimus muscle in *Dorudon atrox* (Figures 114 and 115) must be very different from those in modern artiodactyls since the innominate, and thus the ilium, which provides the insertion of the longissimus, is greatly reduced. In addition, the entire hind limb is no longer connected to the vertebral column and is thought to be positioned far from the vertebral column against the ventral body wall. The longissimus originates on the posterior surfaces of the transverse processes of the thoracic vertebrae. There are no clear sites of muscle attachment on the transverse process of the lumbar vertebrae, but the posteriormost lumbars and anterior caudals have very robust transverse processes. It is unclear whether the longissimus muscle inserted directly onto the transverse processes or onto a superficial tendon like in modern cetaceans. In either case, the main action of the longissimus is extension of the anterior caudal region or to extend the head, depending on which portions are active (Pabst, 1990).

Extensor caudae lateralis.— Getty (1975) described the sacrocaudalis dorsalis lateralis as the caudal continuation of the longissimus in artiodactyls. It has a common origin with the longissimus and it inserts on the transverse processes, spines, and lateral surfaces of the caudal vertebrae. Its main action is to extend the tail, and in unilateral action to flex the tail laterally. Pabst (1990) described the extensor caudae lateralis as the caudal extension of the longissimus. It originates on the transverse processes and neural arches of the posterior lumbar vertebrae and anterior caudal vertebrae, and inserts on the tendons of the extensor caudae lateralis. These tendons (with contributions from the longissimus) coalesce into a group of distinct cylindrical tendons that insert onto the dorsal surfaces of the posterior caudal vertebrae.

The origin of the extensor caudae lateralis is similar in modern artiodactyls and modern cetaceans, and was probably similar in *Dorudon atrox* as well. The insertion of the muscle was probably more similar to that of modern artiodactyls, rather than like that of modern cetaceans, since other evidence suggests that the elaborate tendinous origins and insertions of modern cetaceans were not yet developed in *D. atrox* (Figure 116). The position where the caudal vertebrae become dorsoventrally compressed in *D. atrox* is around Ca13, suggesting that the insertion of the extensor caudae lateralis on the dorsal surfaces of the caudal vertebrae started around there, and continued posteriorly.

Iliocostalis.— In artiodactyls the iliocostalis originates on the caudal border of the ribs and transverse process of C7, while it inserts on the cranial border and lateral surface of the ribs and the tips of the lumbar transverse processes, as well as some on the thoracolumbar fascia (Getty, 1975). In modern cetaceans, the iliocostalis originates from the lateral side of the longissimus muscle, the lateral edge of the transverse processes of the atlas and axis, and the dorsolateral aspect of each of the ribs. It inserts on the subdermal sheath (Pabst, 1990).

The iliocostalis probably took origin from the caudal border of the ribs and transverse process of C7 in *Dorudon atrox*. Unfortunately, there are no known osteological correlates of the subdermal sheath, so its presence in *D. atrox* must remain equivocal. The iliocostalis certainly could have inserted on the cranial borders of the posterior ribs and tips of the lumbar vertebral transverse processes as in artiodactyls. This arrangement seems more likely since, as stated earlier, the insertions of other muscle groups suggest that the complex system of tendinous insertions seen in modern cetaceans was not developed in *D. atrox*.

Intertransversarius caudae dorsalis.— The intertransversarius caudae dorsalis originates from the dorsal surfaces of the transverse processes of the posterior lumbar and anterior caudal vertebrae in modern cetaceans. The individual muscle slips insert on the anterior edges of transverse processes and vertebral bodies of adjacent or nearly adjacent vertebrae, or insert onto the subdermal sheath (Pabst, 1990). The action of the intertransversarius caudae dorsalis is to aid in extension of the anterior tail and in unilateral action to move the tail laterally. In modern artiodactyls, the intertransversarii are present in the lumbar region and connect the transverse processes of adjacent vertebrae. The unilateral action of these muscles is to move the tail laterally. Since the origin of the intertransversarius caudae dorsalis is similar in artiodactyls and modern cetaceans, it is likely to be similar in *Dorudon atrox* as well, arising from the dorsal surfaces of the transverse processes of the posterior lumbar and anterior caudal vertebrae (Figure 116). The insertion was probably on the anterior edge of the transverse processes of more posterior vertebrae, since the subdermal sheath was probably absent as stated above.

Hypaxial muscles

The hypaxial muscles are those that are dorsal to the transverse processes of the vertebrae. Reconstructions of the hypaxial and epaxial muscles of *Dorudon atrox* are shown in Figures 114-116.

Hypaxialis lumborum.— The hypaxialis lumborum is difficult to homologize with muscles in primitive mammals or artiodactyls. In modern cetaceans it originates from the ventral surfaces of the posterior thoracic through anterior caudal vertebrae, including the chevron bones. It inserts on the ventral and medial tendons. The ventral tendon inserts on the ventral sides of the posterior lumbar and anterior caudal vertebrae, while the medial tendon inserts on the ventral sides of the posterior caudal vertebrae (Pabst, 1990). Howell (1927) suggested that the hypaxialis lumborum is composed of parts of the psoas, iliacus, and quadratus lumborum muscles, but he did not provide any evidence for this idea. It is unclear what arrangement of hypaxial muscles was present in *Dorudon atrox*, since the origins of these muscles are not clearly present. This is not surprising, since the origins of the hypaxialis lumborum in modern cetaceans does not leave obvious muscle scars on the ventral sides of the vertebrae. No doubt some kind of hypaxial muscles inserted on the chevrons and the ventral sides of both the anterior and posterior caudal vertebrae. The main action of these muscles is to flex the tail.

Intertransversarius caudae ventralis.— The intertransversarii of modern artiodactyls are not usually differentiated into dorsal and ventral portions. In modern cetaceans those that originate from the dorsal aspect are termed intertransversarii caudae dorsalis (see above), while those that originate from the ventral aspect are termed intertransversarii caudae ventralis (Pabst, 1990). The ventral intertransversarius caudae muscles have a similar insertion and action to the dorsal muscles described above.

Forelimb muscles

Many of the major muscles of the forelimb have left readily interpretable indications of their presence, but many of the minor muscles have not. In addition, many of the minor muscles of the forelimb attach to fasciae, rather than inserting on bones in modern cetaceans (Klima et al., 1980; Benke, 1993). Reconstructions of the forelimb muscles of *Dorudon atrox* are shown in Figures 117 and 118.

Muscles that move the scapula

Most of the muscles that move the scapula do not have well-developed osteological markers of insertion on the scapula. The omohyoideus and levator scapulae insert on the deltoideus fascia in some odontocetes (Klima et al., 1980) and have only a small insertion on the scapula in others (Benke, 1993); thus, they are unlikely to have left any trace on the scapula. The rhomboideus and serratus muscles insert, respectively, along the lateral and medial sides of the vertebral border of the scapula. These muscles usually do not leave any obvious muscle scars in modern cetaceans, and they did not leave muscle scars on the scapula of *Dorudon atrox* .

Muscles of the glenohumeral joint

Supraspinatus.— The supraspinatus muscle originates in the supraspinous fossa of the scapula. The supraspinous fossa of *Dorudon atrox* is larger than that of most modern cetaceans, but it is similarly oriented relative to the glenoid fossa. The supraspinous fossa narrows towards the medial side of the acromion of the scapula. In most modern cetaceans, some fibers of the supraspinous muscle originate from the medial side of the acromion as well as the supraspinous fossa. This was probably the case in *Dorudon atrox* as well. The supraspinatus muscle inserts on the greater tuberosity of the humerus. Its main action is to abduct the humerus.

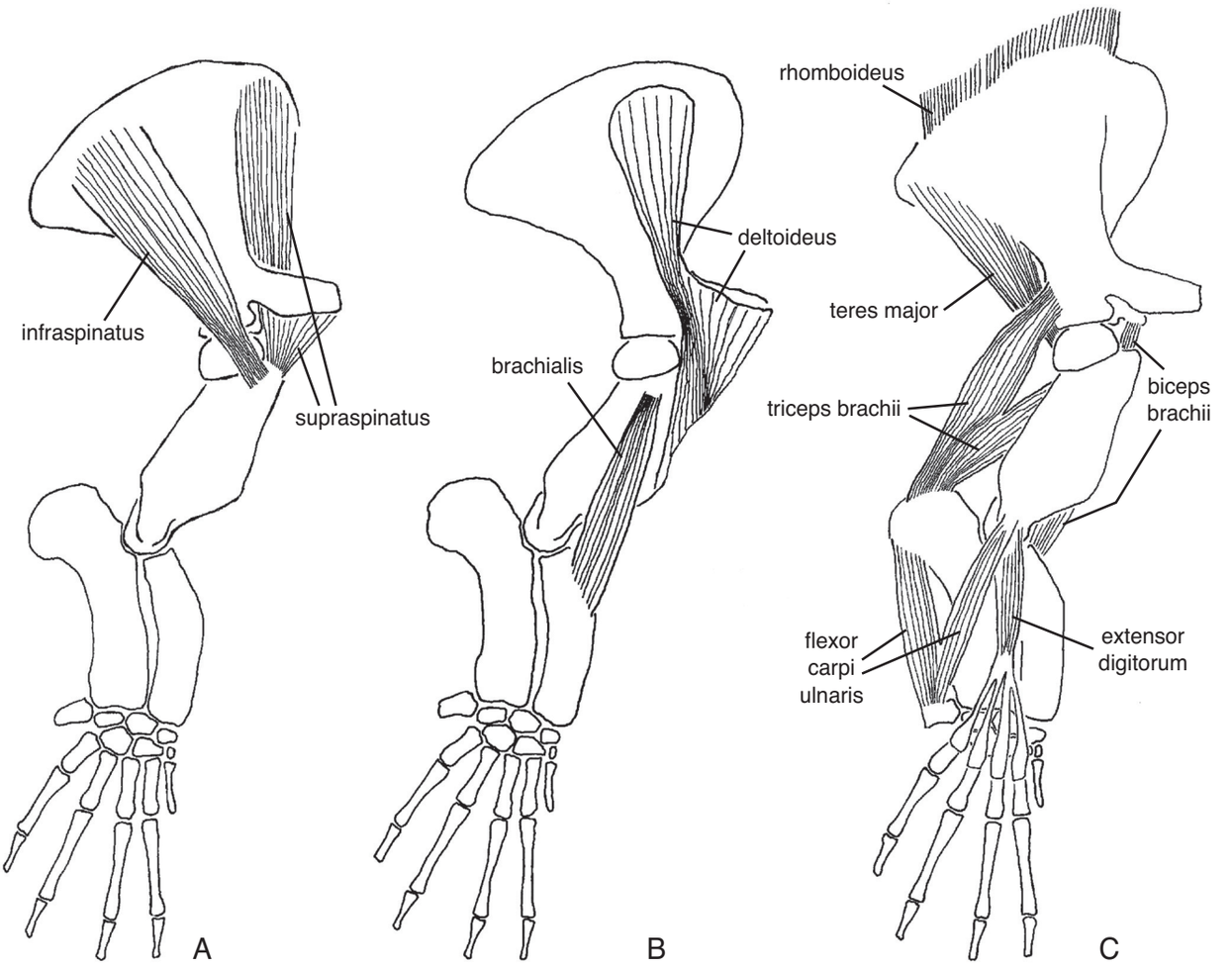

FIGURE 117 — Muscles of the lateral forelimb of *Dorudon atrox*. A-C, different muscles, generally from shallow in A to deep in C. The large olecranon process of the ulna and a large pisiform indicate powerful extension of the elbow and wrist in *D. atrox*. This action would keep forelimb elements in a position similar to that fixed by the immobile joints found in modern cetaceans.

Deltoideous.— The deltoideous originates from the infraspinous fossa, spine, and lateral surface of the acromial process of the scapula. The division of the infraspinous fossa into deltoideus and infraspinous portions is not clear in *Dorudon atrox*. The deltoideus inserts on the lateral side of the anterior edge of the deltopectoral crest of the humerus. The main action of the infraspinous fibers of the deltoideus is to extend the humerus. The acromial fibers of the deltoideus also contribute to abduction of the humerus.

Infraspinatus.— The infraspinatus originates from the infraspinous fossa. It is found just caudal to the insertion of the deltoideous muscle. Its origin is fan-shaped, narrowing toward the glenoid fossa, and expanding toward the vertebral border of the scapula. The infraspinatus inserts on a small tubercle on the lateral side of the proximal humerus. This tubercle is lateral to the greater tuberosity, and is thus lateral to the insertion of the supraspinatus muscle. The main action of this muscle is to extend the humerus.

Teres major.— The teres major originates from the caudal margin of the lateral side of the scapula. There is a distinctive fossa for the teres major in most modern cetaceans. It is roughly triangular in shape, coming to a point toward the glenoid, and expanding toward the vertebral border of the scapula. *Dorudon atrox* has a similar fossa on the caudal border of the scapula for the origin of the teres major. The insertion of the teres major is on a tuberosity on the medial side of the proximal humerus. This tuberosity is directly caudal to the lesser tuberosity of the humerus, separated from it by a shallow sulcus. The main action of the teres major is to adduct the humerus.

Subscapularis.— The subscapularis muscle originates over most of the medial surface of the scapula. The origin is fan-shaped, like the medial scapular surface. The subscapularis

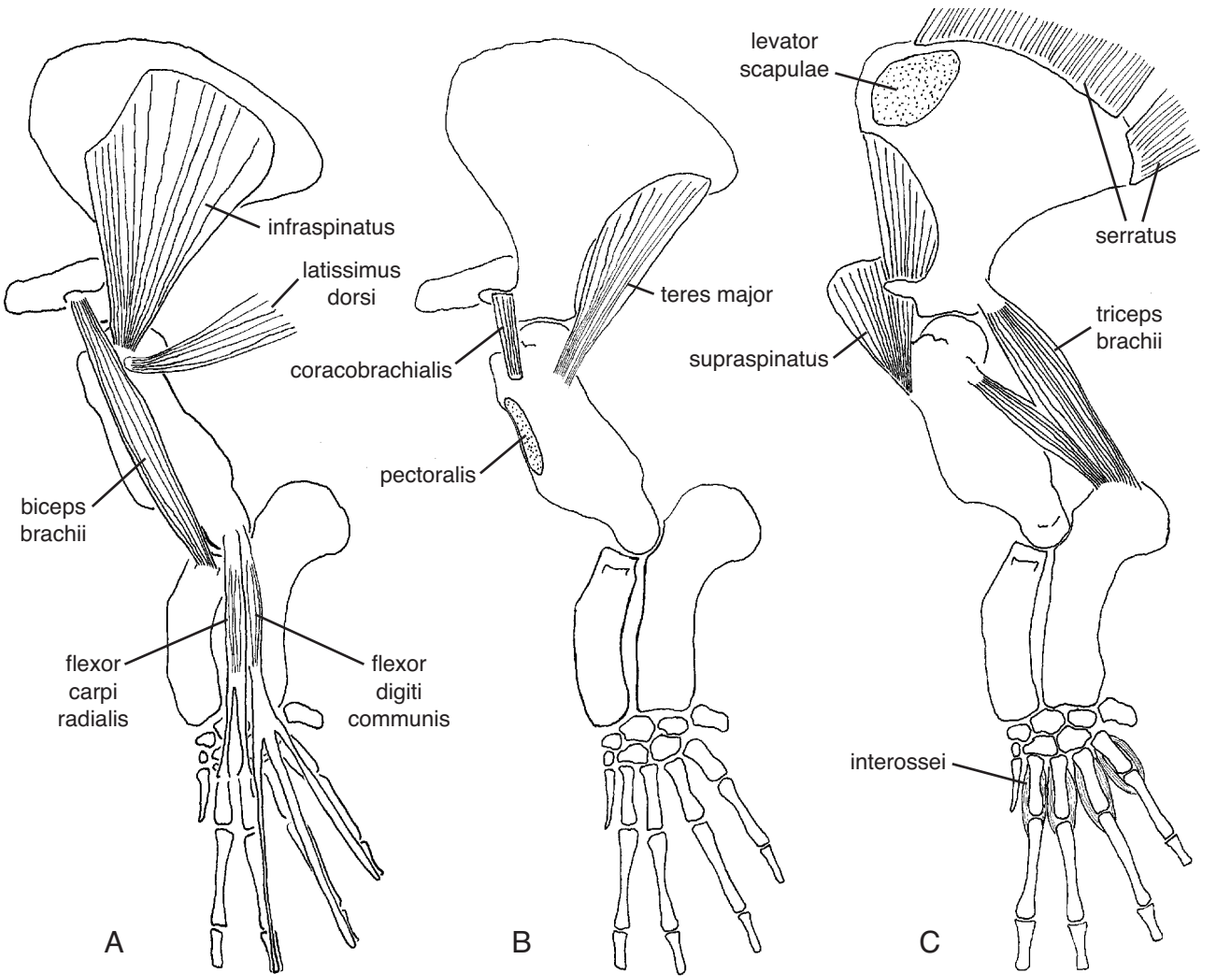

FIGURE 118 — Muscles of the medial forelimb of *Dorudon atrox*. A-C, different muscles generally from shallow in A to deep in C. There is no clear insertion for the serratus (or rhomboideus from the lateral view) along the vertebral border of the scapula. Most modern cetaceans have a cartilaginous extension of the scapula along this border for insertion of these muscles that may have been present in *D. atrox* as well.

inserts on the greater tuberosity on the medial side of the humerus. The main action of the subscapularis is to flex the humerus.

Latissimus dorsi.— The latissimus dorsi muscle originates from a broad aponeurosis connected to the posterior thoracic and anterior lumbar vertebrae in both modern artiodactyls and modern cetaceans. This site of origin is not easily located in *Dorudon atrox*. The latissimus dorsi probably inserted on the medial side of the humerus, just distal to the insertion of the subscapularis on the lateral side of the greater tuberosity. The action of the latissimus dorsi is to adduct the humerus.

Coracobrachialis.— The coracobrachialis muscle originates from the medial side of the coracoid process of the scapula in modern artiodactyls, cetaceans, and most likely *Dorudon atrox* as well. It inserts on the medial side of the humerus, just distal to the insertion of the latissimus dorsi. The action of the coracobrachialis is to assist in flexion of the humerus, adduction of the humerus, and stabilization of the glenohumeral joint during other movements.

Muscles of the elbow joint

Triceps brachii.— The triceps brachii has multiple origins in most mammals. In *Dorudon atrox* the long head of the triceps originates from a small tubercle on the caudal side of the scapular neck. The medial head of the triceps originates from a small tubercle on the medial side of the proximal humerus. This tubercle is just distal to the point of insertion of the teres major. The insertion of the triceps brachii is the olecranon process of the ulna. The main action of the triceps brachii is extension of the elbow.

Biceps brachii.— The biceps brachii is present in primitive terrestrial mammals and artiodactyls, but not present in modern cetaceans; thus its presence or absence in *Dorudon atrox* based on these taxa is unclear. The bones of the forelimb of *D. atrox*, however, appear to have osteological traces of both the origin and insertion of the biceps brachii. The origin of the biceps brachii is on the scapular tuberosity. This tuberosity is on the anterior side of the glenoid fossa next to the coracoid process. The insertion of the biceps brachii is on the radial tuberosity. The radial tuberosity is a strongly developed ridge near the head of the radius on the medial side. The main action of the biceps brachii is flexion of the elbow joint.

Brachialis.— The brachialis muscle is present in primitive mammals and artiodactyls, but it is not present in modern cetaceans. Osteological features suggest that it was present in *Dorudon atrox*. The brachialis muscle originates on the lateral side of the proximal humerus, distal to the insertion of the infraspinatus. The brachialis inserts on the radius just distal to the head, on the cranial border. The action of the brachialis is to flex the elbow joint.

Muscles of the carpal joints

Flexor carpi ulnaris.— The flexor carpi ulnaris is found in modern artiodactyls, modern cetaceans, and *Dorudon atrox*. In modern artiodactyls the flexor carpi ulnaris has two heads of origin. The humeral head originates from the medial epicondyle of the humerus, near to the caudal end. *D. atrox* has a well-defined muscular attachment pit in this position that appears to be for the humeral head of the flexor carpi ulnaris. The other head originates from the medial side of the distal portion of the olecranon process. This head is present in modern artiodactyls, modern cetaceans, and *D. atrox* as well. The insertion of the flexor carpi ulnaris is on the proximal or lateral side of the pisiform in both modern artiodactyls and modern cetaceans. *D. atrox* has a very large pisiform, which indicates a very large and powerful flexor carpi ulnaris. The action of the flexor carpi ulnaris is to flex the carpus and extend the elbow.

Flexor carpi radialis.— The flexor carpi radialis muscle is present in primitive mammals and artiodactyls, but not in modern cetaceans. *Dorudon atrox* has a site of muscular attachment in the position where the origin of the flexor carpi radialis should be. The origin is on the medial epicondyle of the humerus, anterior to the site of origin for the flexor carpi ulnaris. The flexor carpi radialis inserts on the proximal ends of the palmar sides of metacarpals II and III. There are muscle attachment sites in this position on metacarpals II and III of *D. atrox*, but there are similar muscle attachment sites in the same position on all of the metacarpals, so there is not an obvious separate insertion point for the flexor carpi radialis. The main action of this muscle is to flex the carpal joint.

Extensor carpi radialis and extensor carpi ulnaris.— Both of these muscles are present in primitive mammals and artiodactyls, but they are lacking in modern cetaceans. It is unclear whether they were present in *Dorudon atrox*. The lateral epicondyle of the humerus, where these muscles originate, has a poorly developed site for muscle attachment compared to the lateral epicondyle. In addition to the carpal extensors, the digital extensors also have a site of origin on the lateral epicondyle, so it is unclear which of these muscles originated on the lateral epicondyle. The sites of insertion are on the proximal ends of the dorsal surfaces of the metacarpals. These have weakly developed muscular attachment surfaces, indicating the likely presence of the extensor carpi radialis and extensor carpi ulnaris. The action of both of these muscles is extension of the carpus. A single digital extensor with a common tendon is shown in Figure 117.

Muscles of the metacarpal-phalangeal and interphalangeal joints

Digital flexors.— Benke (1993) termed a digital flexor that originates on the medial epicondyle of the humerus the "flexor digiti communis." Most primitive terrestrial mammals and artiodactyls have two sets of digital flexors, the flexor digitorum profundus and the flexor digitorum superficialis. Both originate from the medial epicondyle of the humerus and insert on the phalanges. The flexor digitorum profundus inserts on the distal phalanges, while the flexor digitorum superficialis inserts on the middle phalanges. It is unclear which phalanges of modern cetaceans are homologous with the proximal, middle, and distal phalanges of terrestrial mammals, since modern cetaceans exhibit hyperphalangy. Thus, it is difficult to know with which digital flexor the flexor digiti communis is homologous, since its identity is dependent on its point of insertion on the phalanges. Despite this, the flexor digiti communis appears to insert on the distalmost phalanges as shown by Benke (1993; figure 64). Since the middle and distal phalanges are not known with certainty in *Dorudon atrox*, it is unclear whether one or both of the digital flexors is present. The medial epicondyle of the humerus has a large area of muscular attachment that could easily include the origin of one or both digital flexors. The action of the digital flexors is to bend the digits in a palmar (medial) direction.

Interossei.— The interosseous muscles originate from the palmar (medial) sides of the proximal ends of the metacarpals and insert on the palmar (medial) sides of the proximal ends of the proximal phalanges in primitive mammals and artiodactyls. There are no intrinsic muscles of the manus in modern cetaceans. The medial sides of the proximal ends of the metacarpals of *Dorudon atrox* appear to be sites for muscle attachment, as well as the medial sides of the proximal ends of the proximal metacarpals. These are probably the origins and insertions of the interossei, respectively. The action of the interossei is to flex the metacarpophalangeal joints and draw the digits toward the midline.

An additional note should be made here of the prominent pits that are present on the sides of proximal metacarpals II to V. These pits are the sites of attachment of the interosseous metacarpal ligaments. These ligaments prevent extreme extension of the metacarpal-phalangeal joints, and prevent the digits from spreading too far from the midline. These pits are very well developed in *Dorudon atrox*.

Costal muscles

Internal and external intercostal muscles

Modern artiodactyls and cetaceans both have intercostal muscles in similar positions (Getty, 1975; Howell, 1930), so *Dorudon atrox* is likely to have them in the same positions as well. Both the cranial and caudal surfaces of the ribs of *D. atrox* are thickened along their medial and lateral margins, especially toward the proximal ends. These thickened margins are the sites of attachment for the internal and external intercostal muscles. The internal intercostals attach along the medial borders of the ribs, while the external intercostals attach along the lateral borders of the ribs. The main action of the intercostal muscles is to bring the ribs closer together to aid in expiration.

Other muscles

Other muscles certainly attached to the ribs, but their origins and insertions are unclear. Some of the muscles described with the epaxial musculature (like the iliocostalis) almost certainly originated from the ribs, but there are no other obvious muscle scars. In addition, a number of other muscles like the serratus muscles and some abdominal muscles attach to the ribs or costal cartilages in both modern artiodactyls, modern cetaceans, and probably *Dorudon atrox*, but their attachments are not apparent, so they are not discussed here.

FLUKES

Both modern cetaceans and basilosaurids (including *Dorudon atrox*) share distinctive features of the caudal region of the vertebral column that are very different from terrestrial mammals. Most terrestrial mammals have posterior caudal vertebrae that are very long and thin. These long caudals are generally about as wide as they are high. Modern cetaceans display a series of shape changes in the caudal region that are briefly outlined here and discussed more fully in the chapter on functional morphology.

All modern cetacean caudal vertebrae are relatively much wider and higher than their terrestrial counterparts. The anterior caudals are about as wide as they are high and long. More posteriorly, in the peduncular region, the caudals become very high relative to their width and length. At the posterior end of the caudal series, the vertebrae are dorsoventrally compressed. The anteriormost caudal vertebra that is wider than it is high is where the fluke inserts relative to the vertebral column in modern cetaceans. *Dorudon atrox* also exhibits this distinctive shape change, suggesting that it too had a fluke that inserted onto the caudal vertebral column.

V

FUNCTIONAL MORPHOLOGY AND LIFE HISTORY

Paleontologists can only suggest possible functions for anatomical structures, since the opportunity to observe the use of these structures in living animals has long passed. The goal of this chapter is to propose likely uses for of some of the anatomical structures described in the previous chapter. These suggested functions are developed in three ways. The first method of determination of function is from basic physical constraints such as range of movement between articulating bones. The second is from indications of use retained in the specimens themselves, such as the presence wear facets on teeth. The third is by analogy with living mammals in which function can be observed. Animals that have osteological structures that are similar but not necessarily homologous to those in *Dorudon atrox* were studied to determine if the osteological similarities seem to be functionally constrained. If so, *D. atrox* is suggested to be similarly constrained. This chapter is arranged by activity, with each activity being explored by drawing on different anatomical structures described in the previous chapter that have some bearing on the activity.

LOCOMOTION

Mode of locomotion

Mammalian locomotion can be classified in many different ways. One of the simplest categorizations of locomotor patterns was presented by Gambaryan (1974), who organized mammals into locomotor groups by the contribution of the forelimbs, hindlimbs, and the vertebral column to the production of forward movement. Those mammals that use flexion and extension of the vertebral column to help extend the stride are called *dorsomobile*, emphasizing the mobility of the vertebral column during locomotion. Those mammals that keep their vertebral columns relatively immobile during locomotion are termed *dorsostable*. In addition, mammals that use both the fore and hind limbs in the production of forward movement are termed *dilocomotory*. Those that use only the hind limbs in the production of forward movement are termed *metalocomotory*. Combinations of these terms for mammals that use both the vertebral column and limbs for locomotion can categorize most mammalian locomotion. Unfortunately, his categorization did not extend to mammals like the cetaceans and sirenians that have virtually no contribution from the limbs to forward motion. Gambaryan did not discuss fully aquatic mammals, but they fit well into an extended classification as simply dorsomobile mammals (Uhen, 1991). Figure 119 shows the locomotor categories and some representative taxa that utilize each particular mode of locomotion.

Fortunately, there is a general correspondence of locomotor category with patterns of vertebral body measurements. Figure 120 shows a profile of log length of vertebral bodies down the vertebral column for a selection of terrestrial taxa in the different locomotor groups listed in Figure 119. Figure 121 shows the same plot for a selection of cetaceans, including *Dorudon atrox*, and Figure 122 includes a sirenian (*Trichechus manatus*). One can immediately see that one of the most distinct patterns is that for purely dorsomobile mammals. The trunk vertebrae (posterior thoracic, lumbar, and anterior caudal vertebrae) of dorsomobile mammals have relatively uniform lengths. In addition, cetaceans exhibit a multiplication of the number of lumbar vertebrae, effectively increasing trunk length.

The pattern seen in the cetaceans and sirenians is very different from other mammals for two reasons. The first is that the vertebral column of terrestrial mammals is used for locomotion (in some groups,) for support of the body in resistance to the force of gravity, and as support for some type of limb based locomotion. Cetaceans and sirenians do not need to contend with gravity due to their nearly neutral buoyancy in an aquatic medium (Slijper, 1946). Second, cetaceans and sirenians use dorsoventral flexion and extension of the vertebral column exclusively to propel themselves through water. The forelimbs are used very little for propulsion, and there are no external hind limbs at all (although internal skeletal vestiges remain).

It is interesting to observe the third group of mammals that are usually classified as aquatic mammals, the Pinnipedia. Pinnipeds are considered to be arctoid carnivores, although their particular placement within this group is debated (Wyss, 1989). Pinnipeds differ from cetaceans and sirenians in two important ways. First, pinnipeds retain vertebral columns that can support them on land, since they still return to land to breed. The fully aquatic cetaceans and sirenians do not have this functional constraint on their vertebral columns. Second, all pinnipeds use some form of limb-based locomotion (Gordon, 1981). With this in mind, it is not surprising to see in Figure 120 that pinnipeds retain a pattern of vertebral body lengths very much like their terrestrial arctoid carnivore relatives.

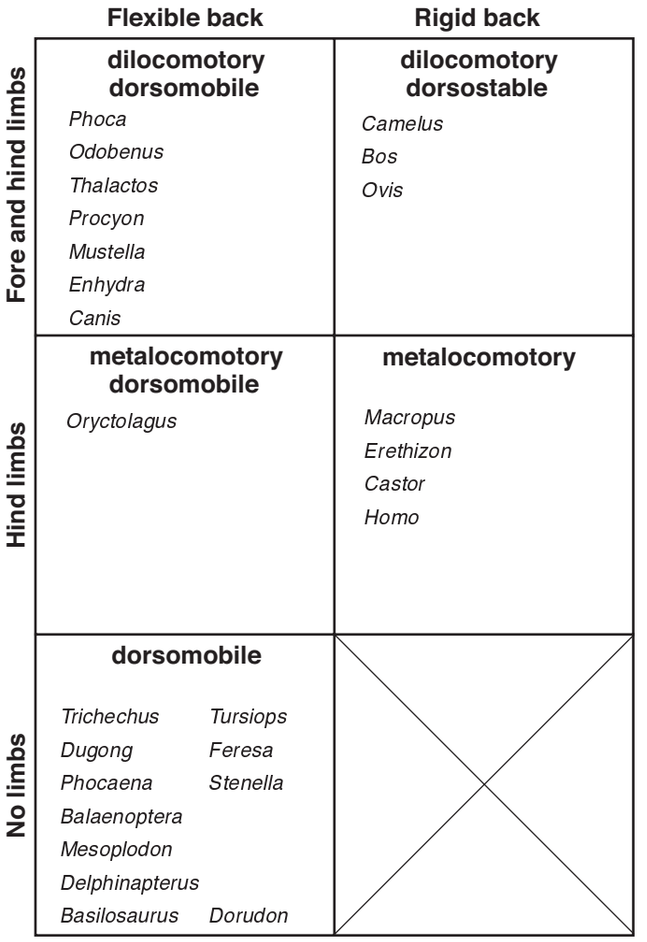

FIGURE 119 — Classification of mammalian locomotor categories (extended from Gambaryan, 1974). The two axes in this classification are contributions to locomotion from the back and from the limbs, respectively. The back can either be flexed and extended to contribute to locomotion, or held rigid. Both sets of limbs, hind limbs alone, or no limbs can contribute to locomotion. The box in the bottom right hand corner (no contribution from the limbs or the back to locomotion) is not occupied by any mammals. Cetaceans and sirenians use only their backs to produce significant locomotion.

The features that make the pattern of vertebral body lengths in Cetacea and Sirenia unique are: very short cervical vertebrae, increasing thoracic length, relatively uniform lumbar lengths, and a distinctive shortening in the posterior caudal region. No other mammals have this combination of features in plots of vertebral body length. However, there are two patterns within the basic fully aquatic pattern. The functional interpretation of these patterns are discussed below under Swimming Speed.

A gradually increasing thoracic length indicates a smooth transition from a short cervical vertebrae to a relatively uniform lumbar vertebral length. Uniform vertebral length is associated with the lack of loading due to gravity concentrated at two points, the forelimb and hindlimb. Other fully aquatic vertebrates (fish, ichthyosaurs) , as well as non-aquatic legless vertebrates (snakes), have similarly uniform vertebral body lengths. The different lengths of vertebrae in the posterior thoracic and lumbar regions in terrestrial mammals are due to different stresses on the vertebral column resulting from gravity and from forces generated by their particular style of locomotion. Since the lumbar region of aquatic animals is not affected by gravity, and motion of the vertebrae during locomotion is concentrated in the caudal region, the lumbar vertebrae are relatively uniform in length.

The caudal vertebrae just anterior to the insertion of the fluke are tall and narrow in modern cetaceans and they lack transverse processes. Sirenians have broad bodies with transverse processes anterior to the fluke insertion. Both of these

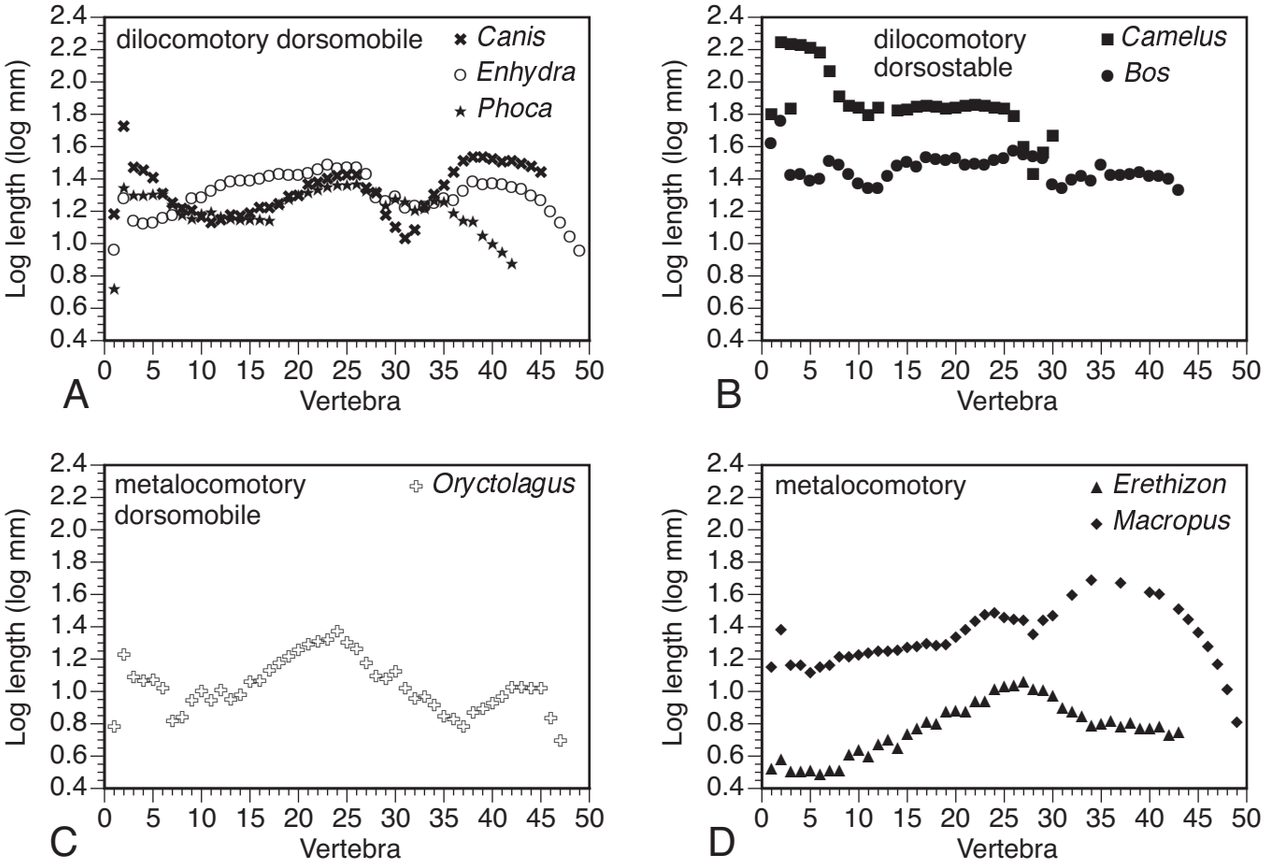

FIGURE 120 — Vertebral column plots of mammals by locomotor category. Note that pinnipeds (here represented by *Phoca*) retain the pattern of vertebral body lengths of other carnivores. Compare these with the patterns for cetaceans in Figure 121. Note also that there is great variation in body length down the vertebral column in each locomotor category that is not seen in cetaceans.

differences are related to the fact that modern cetaceans all have a caudal peduncle that sirenians lack. The peduncle is the narrow region on the cetacean body just anterior to the insertion of the fluke. Figure 123 shows an outline of a typical cetacean and a manatee. Note that the manatee does not display the extreme narrowing anterior to the fluke insertion. Figure 124 shows a plot of vertebral body height relative to breadth for a modern cetacean and for *Dorudon atrox*. The vertebrae of the peduncle in *Delphinapterus* show a rapid rise in the height/width ratio. More caudally, the height/width ratio falls rapidly as the vertebrae change shape to become very short and wide as they enter the tail stock. *D. atrox* does not display the rapid rise in the height/width ratio seen in the peduncle of *Delphinapterus*. This indicates that *D. atrox* lacks the narrow peduncle of modern cetaceans.

All fully aquatic mammals (cetaceans and sirenians) have anteroposteriorly short, laterally wide, and dorsoventrally flattened caudal vertebrae. These vertebrae are within the thickened central portion of the fluke (the tail stock). Most typical mammals have long rod-like caudal vertebrae that are similar to each other and diminish in size down the vertebral column.

Dorudon atrox shares all of the characteristics listed above with modern caudally propelled swimmers. Figure 121 shows a plot of log vertebral body length vs. vertebral number for *D. atrox* and some representative modern cetaceans. *D. atrox* has compressed cervical vertebrae, increasing thoracic length, relatively uniform posterior thoracic and lumbar lengths, and short posterior caudal vertebrae. In addition, the posterior caudal vertebrae lack transverse processes, like modern cetaceans, and display a dramatic shape change as the vertebral column enters the fluke. Log vertebral body length and width are plotted vs. vertebral number for a representative modern cetacean, *D. atrox*, and a manatee in Figure 122. The shape change can be clearly seen in the cetaceans where the length and width plots converge. This is the point where the vertebrae become wider than they are tall. Note that the plots do not converge in the anterior caudal region of the manatee since all of the caudal vertebrae are wider than they are tall. The relationship of this

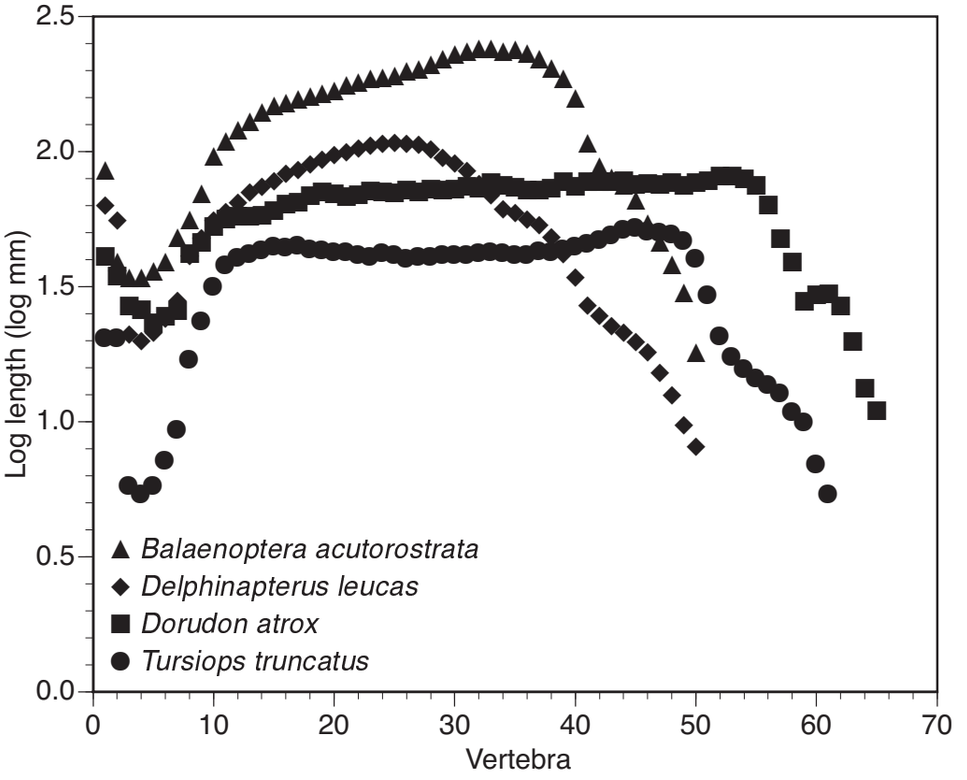

FIGURE 121 — Vertebral column plots of cetaceans. Note that all modern cetaceans have a sigmoid curve in the caudal region. The fluke inserts on the vertebral column at the anterior end of this sigmoid curve. Note also that *Dorudon atrox* follows a similar pattern, suggesting that it too had a tail fluke that inserted in the same position.

crossover point to the insertion of the tail fluke can be seen in Figure 125. Here two x-rays of the caudal region of a modern cetacean are shown, one in lateral and the other in dorsal view. The flattening (dorsal-ventral) of the vertebrae can be seen in the lateral view, while the widening of the vertebrae can be seen in the dorsal view. Note that this shape change takes place where the fluke inserts on the vertebral column.

In addition to articulations on the anterior and posterior ends of the bodies, vertebrae can articulate with each other via zygapophyses. The pre- and postzygapophyses are very well-developed in the vertebrae of modern ungulates. Modern ungulates have articulating zygapophyses through the thoracic, lumbar, sacral (sacral vertebrae are fused to one another), and anterior caudal regions. In many modern ungulates these zygapophyses are revolute, that is, the postzygapophyses are curved such that they embrace the prezygapophyses of the vertebrae with which they articulate (Slijper, 1946). The zygapophyses of ungulates and mesonychids are thought to severely limit both flexion and extension of the vertebral column, as well as bending in the lateral direction (Slijper, 1946).

Modern cetaceans exhibit an extreme reduction of the number of vertebrae that have articular zygapophyses: only the anterior thoracic vertebrae have articular zygapophyses. Posterior thoracic and a few anterior lumbar vertebrae have metapophyses (which are serially homologous with the articular prezygapophyses, as outlined in chapter 2) that are laterally

FIGURE 122 — Graph showing log length and log width of each vertebral body down the vertebral column in A, *Delphinus delphis*; B, *Dorudon atrox*; and C, *Trichechus manatus*. The tail fluke of modern cetaceans inserts at the point where caudal vertebrae become wider than they are tall (where the plots converge). This point is visible in *Dorudon atrox* as well. Note that this is not the case for *Trichechus*.

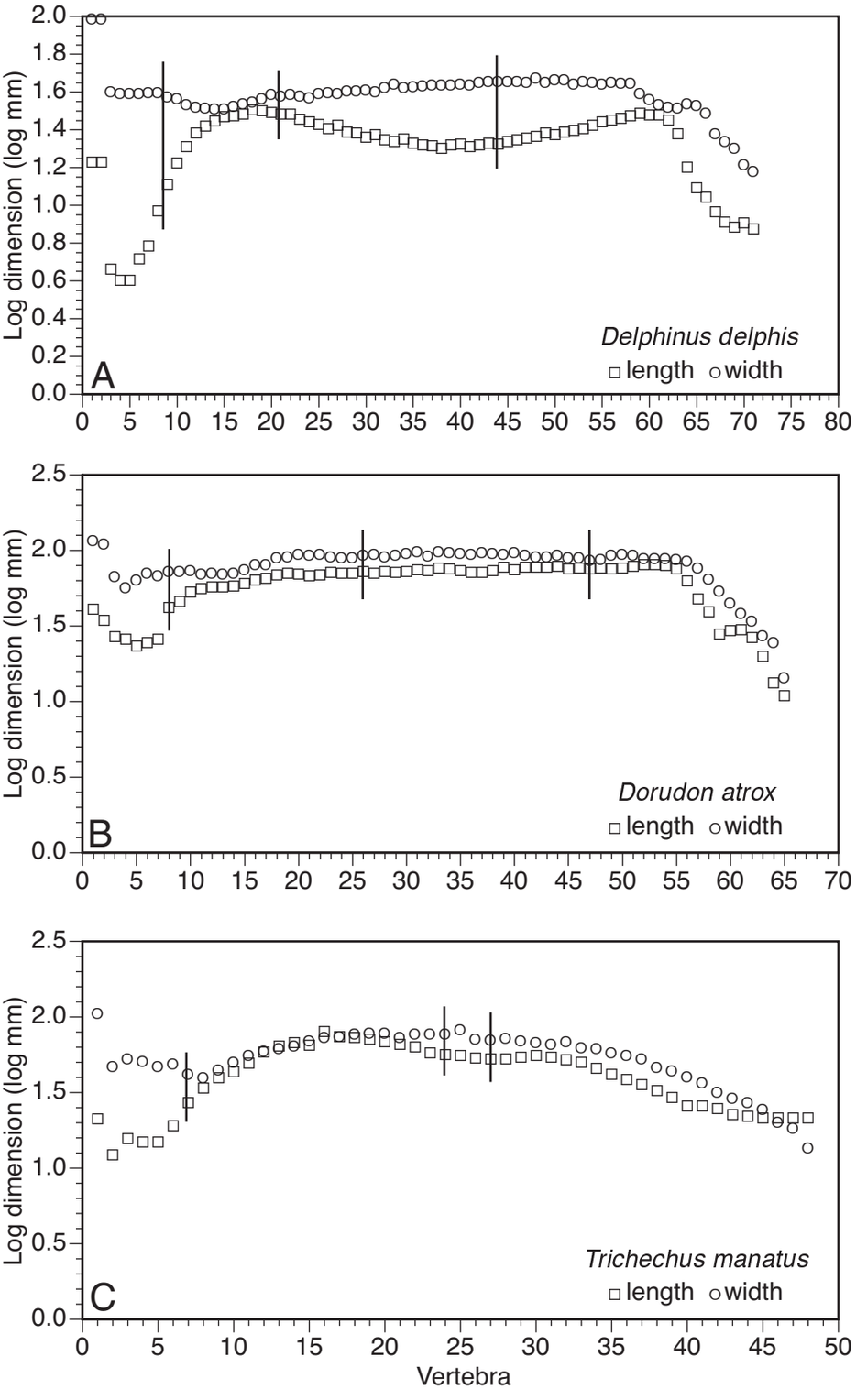
Log dimension (log mm)
Delphinus delphis
length
width
A
Log dimension (log mm)
Dorudon atrox
length
width
B
Log dimension (log mm)
Trichechus manatus
length
width
C
Vertebra

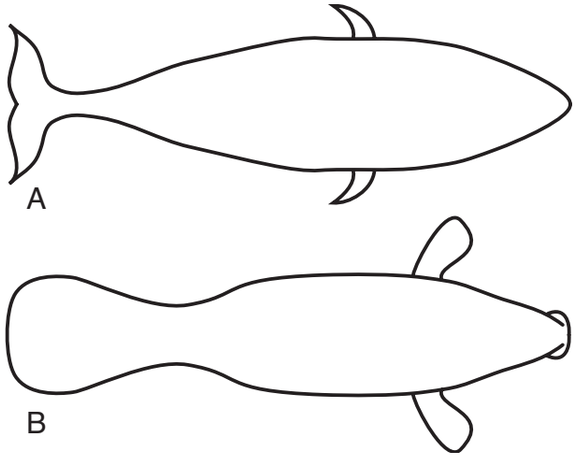

FIGURE 123 — Body outlines of A, a cetacean; B, a manatee. Note the presence of a peduncle in the cetacean. This is the narrow region just anterior to the fluke. The manatee lacks the peduncle, as did *Dorudon atrox* (see Fig. 124).

flattened and project anteriorly from the neural arches. The paired metapophyses form a "slot" between them that accepts the posterior margin of the neural spine of the cranially adjacent vertebra. These metapophyses lack articular surfaces, but certainly restrict lateral motion between adjacent vertebrae. The posterior lumbar and caudal vertebrae also lack articular zygapophyses.

Dorudon atrox has well-developed, articular zygapophyses in the anterior thoracic region. These articular surfaces are flat, rather than revolute as in ungulates. This conformation would have restricted flexion and extension of the vertebral column in the anterior thoracic region. The pre- and postzygapophyses become smaller in the last few thoracic vertebrae. By the first lumbar, the postzygapophyses are so small that they could not have articulated with the prezygapophyses of the caudally adjacent vertebrae. *Dorudon atrox* retains metapophyses on the vertebrae from this point well into the caudal region for the attachment of muscles.

Despite differences between *Dorudon atrox* and modern cetaceans, the epaxial muscles of *D. atrox* are arranged to effectively move the vertebral column through the motions necessary for a similar style of locomotion as modern cetaceans. The addition of many lumbar vertebrae also suggests a modern cetacean style of locomotion. Contraction of the epaxial muscles in modern cetaceans produces only a small amount of displacement between adjacent vertebrae (Bennett et al., 1987). Having more vertebrae in the lumbar region allows a greater range of motion for the entire fluke stroke since each of the small displacements between adjacent vertebrae can be added to produce a large overall motion. The multifidus and longissimus functioned together to lift the posterior trunk and tail during the upstroke, while the extensor caudae medialis and lateralis functioned together to further lift the tail (Arkowitz and Rommel, 1985). The tail could be kept horizontal relative to the trunk of the body by contracting both left and right sides of the muscles together at the same time. The angle of the tail could be changed to produce motion in a different direction by unilateral or unequal contraction of the epaxial musculature.

From these observations on the vertebral column of *Dorudon atrox* the following conclusions can be drawn: (1) *D. atrox* used dorsal-ventral flexion and extension of the vertebral column for propulsion; (2) *D. atrox* had a tail fluke like that of modern cetaceans; and (3) *D. atrox* lacked a caudal peduncle like that of more derived cetaceans.

Swimming speed

The single most difficult problem for determining the swimming speed of an extinct cetacean is the lack of data on swimming speed in living cetaceans. Many modern cetacean species have little or no ecological or behavioral data known for them. In addition, recording and reporting of swimming speed is not standardized, and the reliability of many reports of swimming speed is questionable (Fish and Hui, 1991). For this study, only speeds that are reported as maximum, burst, or sprint speeds are included. This was done in an attempt to remove records of individuals swimming at less than maximum speed. In addition, individuals reported to be bow wave riding or performing unusual locomotor patterns were excluded.

It is difficult to compare absolute swimming speeds in creatures ranging from the size of a harbor porpoise (around 1.5 m) to a blue whale (33.5 m). Swimming speeds were converted to a relative metric of speed: body lengths per second. Thus, the speeds compared are all relative to the scale of the animals themselves.

One possible indicator of swimming speed is the cross sectional area of the locomotory muscles. While the muscles themselves are missing from osteological specimens, a rough approximation of the cross sectional area of the epaxial muscles can be made from just the vertebrae of the lumbar and caudal regions. Pabst (1990) illustrates whole-body cross sections of *Tursiops truncatus* that show that the epaxial musculature is enclosed in a space roughly bounded by the neural spines, transverse processes and the external body wall in the lumbar and caudal regions. The muscles actually extend slightly beyond the neural spines and transverse processes along intermuscular septa that also attach to the tips of the processes. Video images of the anterior aspect of the first lumbar vertebra, a mid-lumbar vertebra, and the first caudal vertebra were captured from osteological specimens representing a selection of modern cetacean species. The epaxial muscle cross-sectional area was estimated on each vertebra by joining the tips of the neural spine and transverse process with an arc from an ellipse centered on the vertebral body. Unfortunately, the correlation of cross-sectional area of the epaxial musculature with maximum relative swimming speed is very weak.

Many different osteological characters have been suggested by cetacean workers to be correlated with swimming speed or some other poorly defined term like "efficiency" or "mobility." Slijper (1961) suggested that the length of the lumbar region

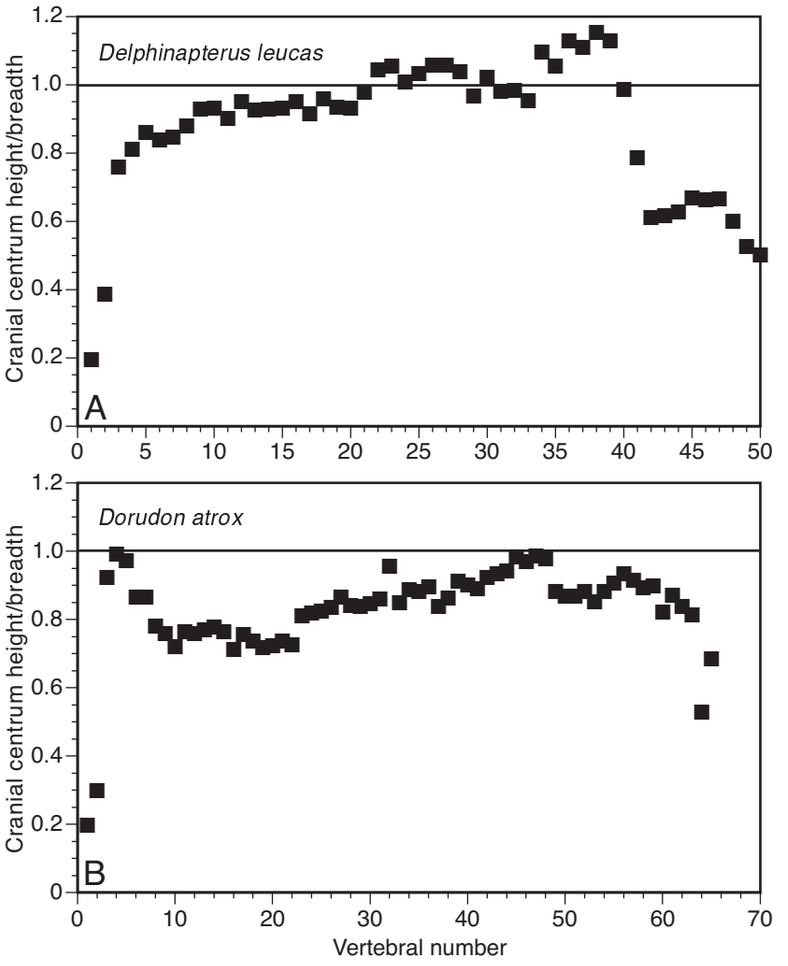

FIGURE 124 — Plot of height divided by breadth for vertebral bodies of A, *Delphinapterus lecuas* (beluga), and B, *Dorudon atrox*. Note that the ratio is above one (vertebral bodies are taller than they are wide) in the peduncular region just anterior to the fluke in *Delphinapterus*, while this is not the case in *Dorudon atrox*, suggesting that *Dorudon* lacked a peduncle.

has increased in cetaceans from their terrestrial ancestors to increase the mobility and elasticity of the lumbar region of the vertebral column. The column is made more mobile by increasing the number of vertebrae, since more intervertebral disks and more points for movement are also included along with the vertebrae. While the association of more intervertebral spaces with increased mobility seems self-evident, Slijper (1946) himself states that "the thoracic and lumbar region of the porpoises and dolphins (Phocoenidae and Delphinidae) is comparatively stiff and that the swimming movements almost completely are exercised by the tail." It might be the case, since most the propulsive musculature of the fluke is formed from many slips of muscle originating on the vertebral processes (Slijper, 1946: Pabst, 1990), that an increase in the number of vertebrae increases the functional amount of muscle mass by increasing the number of points of origination.

The number of vertebrae in the entire vertebral column, in the post-thoracic region, the lumbar region, and the caudal region were all investigated as possible correlates of swimming speed. Generally, *the total number of vertebrae is a good indicator of swimming speed* (Figure 126). One might suspect that this number is just an indicator of body size since, as stated above, smaller cetaceans generally swim faster than large cetaceans (Webb, 1975). This is not the case. Smaller cetaceans generally have many more vertebrae than larger cetaceans. The number of lumbar vertebrae does not seem to be a very good indicator of swimming speed, as the coefficient of determination of this relationship is rather low. The number of caudal vertebrae and the number of post-thoracic vertebrae both perform much better. Also, it is clear that *Dorudon atrox*, with 20 lumbar vertebrae, has many more lumbars than most modern cetaceans. *Dorudon atrox* also appears to have a relatively

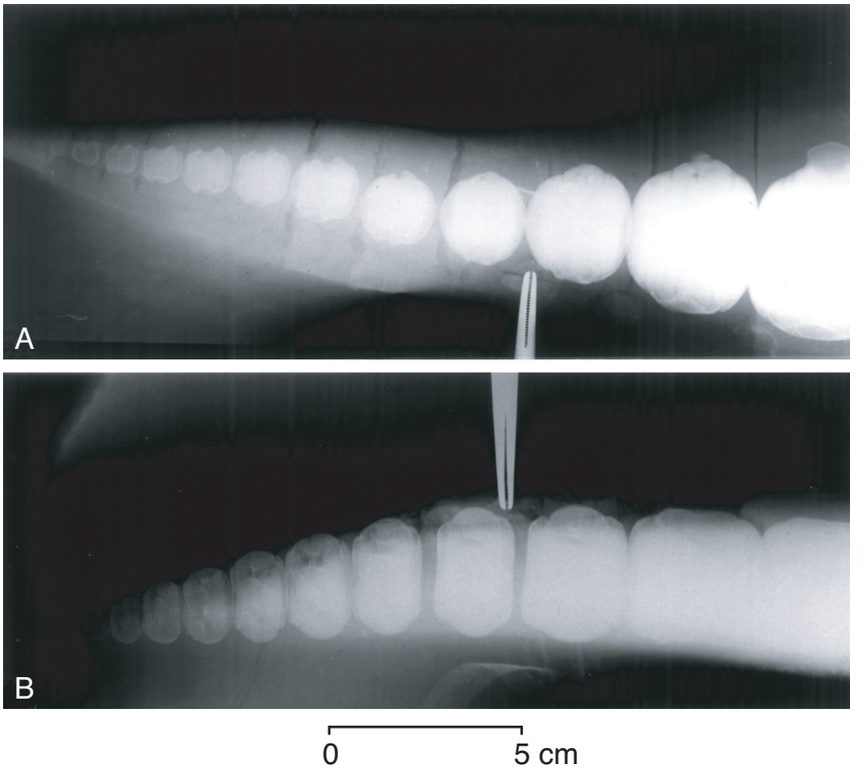

FIGURE 125 — X-rays of the tail of *Lagenorhynchus acutus* in A, lateral, and B, dorsal views. The tip of the hemostat marks the anterior margin of the fluke. Note that this is the point where the vertebrae become wider than they are tall.

low number of caudals at 21. It appears that modern cetaceans have "caudalized" a number of lumbar vertebrae over the course of their evolution. For this reason, the number of post-thoracic vertebrae (lumbars + caudals) was used to infer swimming speed in *Dorudon atrox*, to avoid any confounding effects of this caudalization of lumbars. *D. atrox* has 41 post-thoracic vertebrae, which yields a predicted sprint swimming speed of around 2.4 body lengths per second. This translates into an absolute speed of about 12 meters per second.

FORELIMB USE

There are two basic problems in attempting to relate the morphology of archaeocete forelimbs to their functional ability. The first is that both modern cetaceans and modern artiodactyls have very differently derived forelimbs and both share few features with archaeocetes. Many of the forelimb elements of archaeocetes are unlike their terrestrial artiodactyl relatives or their modern cetacean descendants. Some features, however, especially of the scapula, are shared with modern cetaceans, which at least allows the possibility of using modern cetaceans to help determine the function of these features in archaeocetes.

The second problem is that little information is available on how modern cetaceans use their forelimbs, and virtually nothing is known of how forelimb form relates to forelimb function. Modern cetaceans use their forelimbs for three different classes of activities: steering, starting and stopping, and social touching (Benke, 1993). A few generalizations about the shapes of cetacean flippers in relation to their uses have been made. Species that have broad flippers tend to use their flippers more for steering than others, and they also seem to be more agile, particularly at slow speeds (Benke, 1993; Klima, 1980). An additional observation is that *Megaptera novaeangliae*, the humpback whale, is the most acrobatic of mysticetes, yet it has very long narrow flippers (Benke, 1993). It appears that species with relatively narrow, falcate flippers, like those typical of delphinids, use their flippers very subtly during steering, but most steering is done with their bodies and flukes (Benke, 1993). Since the form of the flippers of archaeocetes is different from those in modern cetaceans, it is difficult to say how these observations should be applied to *Dorudon atrox*.

One recent study attempted to describe the forms of cetacean humeri using eigenshape analysis and to relate this description of form to function (Dawson, 1993). This study showed that archaeocete humeri are very different from those

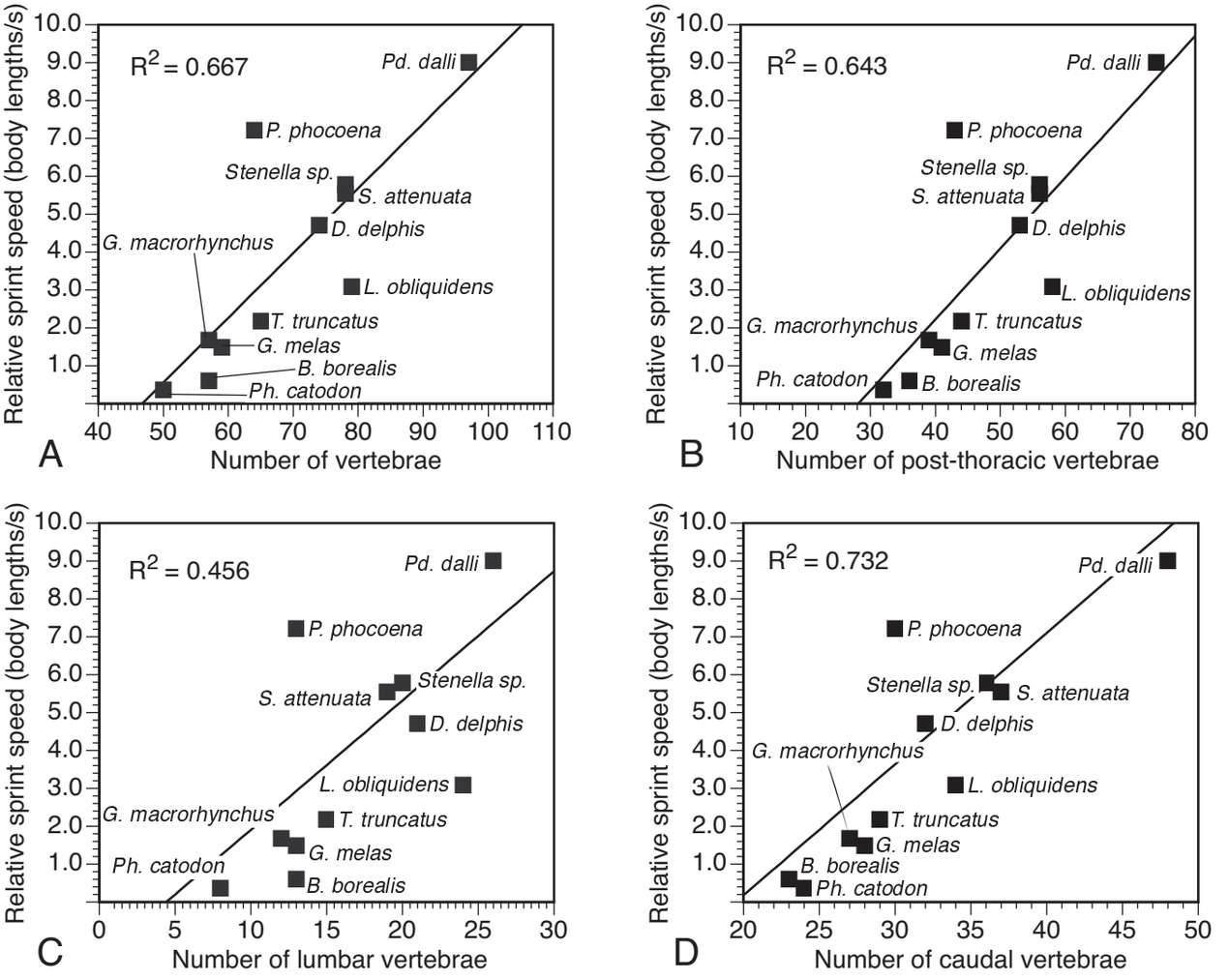

FIGURE 126 — Correlations of different vertebral counts with relative swimming speed in modern cetaceans. The number of caudal vertebrae has the best coefficient of determination. Note that none of these vertebral counts correlates with body size, since smaller cetaceans generally have more vertebrae than larger ones. These correlations suggest that *Dorudon atrox* was a relatively slow swimmer since it has a relatively low number of caudal vertebrae (21). *Phocoena phocoena* (harbor porpoise) is an anomaly in every plot. It has a low number of vertebrae in each region despite its high relative swimming speed. Data on modern cetacean swimming speeds are taken from Au and Perryman (1982), Gawn (1948), Hui (1987), Johannessen and Harder (1960), Lang and Norris (1966), Lang and Pryor (1966), Law and Blake (1994), and Watkins *et al*. (1993).

of modern cetaceans. The characters that distinguished them from modern cetaceans were the narrow distal end (broad in modern cetaceans), and the broad deltopectoral crest (reduced or absent in modern cetaceans). The relation of form to function in this study was again hampered by the lack of good data on forelimb use in modern cetaceans.

The forelimb of *Dorudon atrox* shows a mix of derived characters that it shares with the forelimb of modern cetaceans, and primitive characters that it shares with the forelimb of terrestrial mammals. In particular, the scapula is quite derived, being broadly expanded into a fan-shape like the scapulae of modern cetaceans. The humerus of *D. atrox* is rather unlike both the gracile and long humeri of artiodactyls, and the short and stout humeri of modern cetaceans. The radius and ulna of *D. atrox* have the same relative positions as modern cetaceans, with the radius cranial to the ulna. The radius and ulna are restricted to flexion and extension at the elbow, with no pronation or supination. Artiodactyls are capable of all of these movements of the elbow, while modern cetaceans are capable of none. The carpals of *D. atrox* lack saddle-shaped articular

surfaces, so they are incapable of much movement out of the horizontal plane defined by the flat radius and ulna. The rounded articular surfaces of the metacarpals and phalanges indicate that they were capable of limited flexion and extension.

Discrete forelimb motions

Most of the motion of the forelimb of modern cetaceans is centered on the glenohumeral joint, since it is the only functional synovial joint in the forelimb (Benke, 1993). *Dorudon atrox* has a similar glenohumeral joint with a similar range of motion. The range of motion of the humerus relative to the scapula of *D. atrox* was explored using three dimensional digitization. First, the outline of the scapula and the outline of the glenoid fossa were digitized. Then the humeral head and the glenoid fossa were brought into articulation. Next the humerus was moved through its maximum range of motion by moving the humerus while keeping the edge of the articular surface of the humerus in contact with the edge of the articular surface of the glenoid fossa. The position of the distal humerus was digitized at many points along this maximum range. Lastly, intermediate points representing the position of the distal humerus at less extreme positions of articulation were also digitized, to form a surface that represents all the possible positions of the distal humerus relative to the glenoid. This surface is roughly saddle-shaped. It shows that the humerus can be moved freely in most directions relative to the scapula, except cranially. Motion is restricted in the cranial direction by the tuberosities of the humerus.

Six discrete motions are described for the shoulder of *Dorudon atrox*. All combine to yield the complete range of motion at the shoulder, and their use is not meant to imply that *D. atrox* moved its forelimb in such a discrete fashion. They are helpful in describing the separate and combined actions of muscles and muscle groups.

Motions of the shoulder

Flexion of the glenohumeral joint moves the forelimb toward the ventral surface of the body. The humerus could be moved such that it was parallel with the midsagittal plane, or even beyond, such that the two forelimbs could touch each other across the midsaggital plane on the ventral side of the body. The main muscles involved in flexion of the shoulder are the subscapularis and the pectoralis.

Extension of the glenohumeral joint moves the forelimb away from the ventral surface of the body. The humerus could not be any more dorsal than 90° to the midsaggital plane. Thus, at full extension the forelimb is straight out laterally from the body. The main muscles involved in extension of the shoulder are the deltoid and infraspinatus muscles.

Abduction of the glenohumeral joint moves the distal tip of the forelimb cranially. The humerus could not be moved very far in the cranial direction. This is in contrast to most modern cetaceans that can move the flipper approximately parallel to the long axis of the body while pointing cranially. The main muscles involved in abduction are the supraspinatus and the acromial fibers of the deltoid.

Adduction of the glenohumeral joint moves the distal tip of the forelimb caudally. The humerus could be moved approximately parallel to the long axis of the body during adduction. The main muscle involved in adduction is the teres major.

Inward rotation of the glenohumeral joint moves the cranial margin of the forelimb ventrally. The limit on inward rotation is imposed by the short action of the muscles that are involved in rotation of the shoulder. The main muscle involved in inward rotation is the teres major.

Outward rotation of the glenohumeral joint moves the cranial margin of the forelimb dorsally. The limit on outward rotation is imposed by the short action of the muscles that are involved in rotation of the shoulder. The main muscle involved in outward rotation is the supraspinatus.

Motions of the elbow

The elbow of *Dorudon atrox* and other archaeocetes retains a functional synovial joint, based on the presence of a well-formed articular surface. The motion of this joint is greatly restricted relative to terrestrial mammals. The antebrachium can only be flexed and extended relative to the humerus. There was no pronation or supination possible at the elbow. Well-preserved forelimbs were studied to determine the range of motion available at the elbow. The humerus was articulated with the radius and ulna in both the fully flexed and fully extended positions, keeping the radius and ulna properly articulated with each other and with the distal humerus. The angle between the shaft of the humerus and the shaft of the ulna was measured, and the angular range of motion between the two positions was calculated. Angular motion at the elbow ranges from 30° to 40° in five different forelimbs (from three individuals) of *Dorudon atrox*.

Flexion of the elbow closes the angle between the cranial edge of the humerus and the cranial edge of the antebrachium. The limit on the range of flexion is due to the size of the articular surface of the radial head and the size of the distal humeral (trochlear) articulation. The main muscles involved in flexion of the elbow are the biceps brachii and the brachialis muscles.

Extension of the elbow opens the angle between the cranial edge of the humerus and the cranial edge of the antebrachium. The limit on the range of extension is due to the size of the articular surface of the trochlear notch and the size of the distal humeral (trochlear) articulation. The main muscle involved in extension of the elbow is the triceps brachii.

Motions of the manus

Joint surfaces between the distal antebrachial elements (radius and ulna) and the proximal carpals (scaphoid, lunate, and cuneiform), and between the proximal carpals and distal carpals (trapezium, trapezoid, and unciform) indicate limited movement at these joints. The joint surfaces are restricted to the proximal and distal surfaces of the bones. They do not extend onto the medial and lateral sides of the carpals (primitively the dorsal and palmar surfaces, respectively), which would allow more movement at these joints. Without these extended articular surfaces, flexion and extension are very limited and are es-

TABLE 23 — Flexibility and extensibility at the metacarpal-phalangeal joints of *Dorudon atrox*. The figures show the angle to which each phalanx can be flexed or extended relative to the fixed metacarpal.

Digit	n	Flexibility			Extensibility		
		min	mean	max	min	mean	max
I	1	0°	0°	0°	0°	0°	0°
II	2	13°	13°	13°	24°	25°	25°
III	2	24°	26°	27°	8°	9°	10°
IV	3	7°	11°	18°	15°	18°	21°
V	3	0°	2°	6°	20°	24°	29°

sentially limited by the amount of space between adjacent carpal elements and the amount of compressibility of the intervening soft tissues. Abduction and adduction of the manus at the wrist is also limited by similar factors.

The metacarpal-phalangeal joints all have different degrees of flexibility. The proximal phalanx of digit I is fused to the metacarpal, so it can neither flex nor extend. The flexibility of the other metacarpal-phalangeal joints was investigated by moving each joint through its full range of motion while keeping the articular surfaces in contact. The results of these experiments are shown in Table 23.

Combined forelimb motions

Despite the differences between *Dorudon atrox* forelimbs and the forelimbs of modern cetaceans, *D. atrox* had a similar total range of motion of the forelimb to modern cetaceans. Virtually all of the motion of the forelimb is at the glenohumeral joint in modern cetaceans, and most of the motion of the forelimb is at the glenohumeral joint in *D. atrox*. *D. atrox* has some additional movement at the elbow joint, at the carpal-metacarpal joints, and the interphalangeal joints, but these additional motions do not extend the range of motion much beyond that achieved by movement at the glenohumeral joint alone. The additional motions possible in *Dorudon atrox* are in two perpendicular planes. Flexion and extension of the elbow of *D. atrox* is within the plane of the flipper. Flexion and extension of the carpal-metacarpal joints and interphalangeal joints bend the distal end of the flipper out of the plane of the flipper.

The total combined motions of the forelimb of *Dorudon atrox* suggest that the forelimb could have been used for the same functions as the forelimbs of modern cetaceans. The flattened shape of the forelimb suggests that it would function as an effective hydrofoil, and thus could have been used for steering. The similar freedom of motion at the glenohumeral joint between *D. atrox* and modern cetaceans indicates that the forelimb of *D. atrox* could have been used for stopping and starting locomotion as in some modern cetaceans. The extra flexibility of the forelimb of *D. atrox* might have been useful during social touching, which has been seen in modern cetaceans as well.

BUOYANCY CONTROL

Secondarily aquatic mammals and birds utilize many adaptive strategies to alter the density of their bodies relative to that of water. These strategies include the following: pachyostosis (thickening of bone, Domning and de Buffrénil, 1991), osteosclerosis (replacement of cancellous bone with compact bone, Domning and de Buffrénil, 1991), swallowing of stones (gastroliths, Taylor, 1993), augmentation of fatty tissue, lightening of the skeleton (Wall, 1983), and collapse of the lungs during diving (Ridgway and Howard, 1979).

Modern aquatic mammals use different combinations of these adaptive strategies. Modern sirenians use pachyosteosclerosis (a combination of pachyostosis and osteosclerosis) to maintain neutral buoyancy and horizontal trim (Domning and de Buffrénil, 1991). Many pinnipeds are known to swallow stones (Taylor, 1993), and some pinnipeds have somewhat pachyostotic limbs, while others have less dense limbs (Wall, 1983). Modern cetaceans all have lightened skeletons (de Buffrénil et al., 1985). In addition, modern cetaceans have lungs that collapse when they dive deeply (Ridgway and Howard, 1979). All modern marine mammals also have some subcutaneous fat or blubber (Ling, 1974). This fat layer insulates the body from cold, but since the lipids in blubber are significantly lighter than water, blubber significantly affects hydrostatic adaptation.

Evidence for some of these adaptive strategies can be found in the fossil record. For instance, pachyostosis and osteosclerosis can be (and have been) identified in fossil sirenians and cetaceans. Stomach stones could potentially be preserved as

stomach contents. The ability to collapse the lungs in cetaceans does not have any osteological correlates, so this ability cannot be assessed in fossil marine mammals. In addition, the development of blubber cannot be assessed in fossil cetaceans for the same reason. It is worthwhile to note that all modern marine mammals have blubber layers, and the fully aquatic mammals (Sirenia and Cetacea) have extensive blubber deposits. These blubber layers are insulative as mentioned above, and they also contribute significantly to external body shape, in this case to streamline it (Ling, 1974). Since *Dorudon* was fully aquatic, based on other evidence, it likely that it too had an extensive blubber layer and a streamlined shape. This would decrease the density of the body overall.

Dorudon has some of the hydrostatic adaptations seen in recent and fossil sirenians, but these are developed to a lesser degree. The long bones and ribs of *Dorudon atrox* lack medullary cavities altogether with the space being filled with bone. In addition, the ribs are somewhat osteosclerotic, having a high proportion of dense cortical bone relative to the amount of trabecular bone. In all ribs, the articular processes are composed of trabecular bone, with relatively thin cortical surfaces. The part of the shaft near and just distal to the angle is composed mostly of dense cortical bone with a small cancellous medulla of trabecular bone. The more anterior ribs expand this area of trabecular bone to encompass most of the shaft, with only a thin cortical surface. More distal ribs have a smaller trabecular center and are composed mostly of dense cortical bone, except on the very distal tip, which is again trabecular. The cancellous medulla is not centrally located in these ribs. The medial side has a much greater thickness of compact cortical bone than the lateral side, placing the trabecular interior area nearer to the lateral margin.

These observations on the ribs match those made on another dorudontine archaeocete, *Zygorhiza kochii*, described by de Buffrénil et al. (1990). Despite these similarities in fine anatomical structure, other characterizations of the ribs of dorudontine archaeocetes by de Buffrénil et al. (1990), are somewhat misleading. These authors describe the morphology of the ribs as "pestle-like," emphasizing the distal expansion of the ribs. This distal expansion is expressed most profoundly in rib one and persists, while declining in its expression, to rib six. Rib seven is somewhat transitional, and more caudal ribs become pointed at their distal ends. In addition, the cortical thickening described in the ribs of *Zygorhiza* and *Dorudon* is most prominent in the very flat shafts of these more anterior ribs, while the expanded distal ends are composed mostly of cancellous bone. The ribs of *Dorudon* are best described, in the terms of Domning and de Buffrénil, as lacking a medullary cavity, and somewhat osteosclerotic, but only slightly pachyostotic (anterior ribs only).

The relative densities of fossilized bones can be determined by direct measurement if they are not permineralized. The densities of bones of *Dorudon* were measured by weighing the bones in air and then weighing the bones in water. The difference in these two figures is the weight of the water displaced by the bones when they are submerged. Since the weight of water in grams is equal to the volume of water in cubic centimeters, the volume of the bones is also known, and the density of the bones can be calculated. This was done for the ribs, sternebrae, periotic, auditory bullae, and auditory ossicles. The ribs are discussed below and the bones of the auditory region are discussed in the section on hearing.

The ribs of *Dorudon* are also compared with those of a fossil sirenian, *Eosiren abeli*, in Figure 127. The density of each rib is the average of left and right sides. One can see that the ribs of *Eosiren* are much more dense than those of *Dorudon*. The density of the ribs of *Eosiren* are around 2.3 g/cm^3, while those of *Dorudon* are around 1.8 g/cm^3. This is not surprising, since the ribs of *Eosiren* are composed entirely of dense cortical bone, with no cancellous trabecular bone at all. The exception that proves this observation, is the last two ribs of *Eosiren*, which are very small and contain trabeculae, and are consequently much less dense. *Dorudon* shows an overall somewhat increased skeletal density, rather than the extreme pachyosteosclerosis. This further emphasizes the difference between the ribs of dorudontine archaeocetes and those of truly pachyosteosclerotic sirenians.

The densities of the sternebrae are higher than those of the ribs. The average density of the manubrium is about 2.12 g/cm^3. The density of sternal elements two and three averages about 2.15 g/cm^3, while sternal element four is about 2.00 g/cm^3 and the xiphisternum is about 1.76 g/cm^3. The xiphisternum is about the same density as the ribs, while the more anterior sternal elements are somewhat more dense. These sternal elements are also very large when compared to either the terrestrial ancestors of archaeocetes or their descendants, the modern cetaceans. Modern mysticetes have extremely reduced sternebrae, and odontocetes, while retaining a relatively large sternum, have very flat and light sternal elements. Having a large volume of relatively dense bone ventral to the thorax would form an effective counterbalance to the highly buoyant lungs. The large dense sternum would also help keep *Dorudon atrox* trim since the extra weight is carried along the midline of the body, which would help prevent roll while swimming or at rest.

FEEDING

Feeding in *Dorudon atrox* can be studied by assessing the masticatory abilities of *Dorudon atrox* from the morphology of the teeth and skull, observing dental wear patterns, and by identifying the organisms present in preserved stomach contents. Each of these approaches is used to study feeding in modern odontocetes since direct observation of feeding is difficult (if not impossible) in animals that feed at depth (see Caldwell and Brown, 1964; Fitch and Brownell, 1968; Werth, 1992). Each of these approaches is outlined below, although more information, especially on stomach contents, could greatly expand our knowledge of archaeocete feeding and behavior.

Head and neck movements

The nuchal crest of *Dorudon atrox* is very different from the nuchal crests of most mammals. In most mammals that

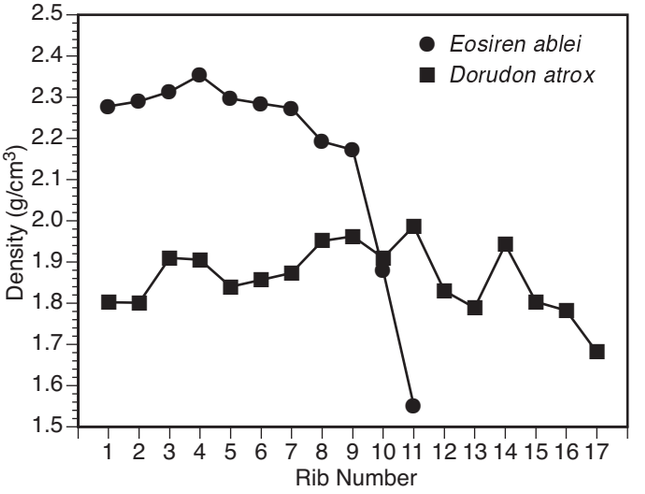

FIGURE 127 — Rib density in *Dorudon atrox* (UM 93220) and *Eosiren abeli*. The ribs of *Eosiren abeli* (UM 97514) are distinctly pachyosteosclerotic and very dense, almost entirely lacking cancellous bone. The last two ribs of *Eosiren* are much smaller and less dense than the other ribs. Those of *Dorudon atrox* have a high proportion of cancellous bone, and are not nearly as dense as those of *Eosiren*. There is no discernible pattern of density change down the series of ribs in *D. atrox*.

have nuchal crests, the lateral edges are slightly curved anteriorly, forming a concavity where the temporalis muscles originate on the anterior side. This slight curvature can be found across many modern mammalian orders. The edges of the nuchal crest of *Dorudon atrox* project almost directly posteriorly, even curving back slightly toward the midline (Figure 39A). The edge of the nuchal crest also projects vertically, far above the occipital condyles (Figure 39B).

Modern cetaceans have no nuchal crest, so they are not of much help in determining the function of the crest in *D. atrox*. The shape of the nuchal crest appears to be closely related to the origin of the temporalis muscles in most modern mammals. Since this does not appear to be the case in *D. atrox*, it may be that the high, posteriorly-projecting nuchal crest gives a longer lever arm for muscles that are attached to the nuchal crest and to the cervical vertebrae. This would be advantageous for an animal that needed to move a large, heavy head during prey capture such as *D. atrox*.

Shortened cervical vertebrae decrease the flexibility of the neck. Modern cetaceans and sirenians all have shortened cervical vertebrae, but some have carried the trend even farther to fusion of the cervical vertebrae. The shortening of the cervical vertebrae is associated with stabilization of the head on the trunk of the body (Slijper, 1962). There is a wide range of cervical fusion among modern cetaceans. Some, such as the beluga (*Delphinapterus leucas*), have all of the vertebrae free. Correspondingly, belugas have been observed to have one of the most flexible necks among the Cetacea (Kleinenberg et al., 1964). *Dorudon atrox* has shortened cervicals like those in other cetaceans, but they are completely unfused. They are similar to the cervicals of some ziphiids and the beluga. The sixth cervical has very enlarged ventral laminae of the transverse processes for attachment of powerful ventral neck flexors. Based on the size and shape of the cervical vertebrae, the neck of *Dorudon atrox* was at least as flexible that of the beluga.

Masticatory apparatus and dental morphology

The jaws of *Dorudon atrox* differ significantly from those of primitive mammals in the elongation of the anterior portion of the lower jaw and premaxillary region of the skull. This elongation gives *D. atrox* a skull form similar to that of gavials, some raptorial birds, and many odontocete cetaceans, such as the river dolphins and many delphinids (Werth, 1992). Werth (1992) indicated that the cranial shape and hyoid musculature of dorudontine archaeocetes is unsuited for suction feeding, which is a method of prey capture utilized by some modern odontocetes. Instead, the anterior teeth placed in the long, relatively slender snout are used to catch, debilitate, and retain prey items than can then be moved to the cheek teeth to be chewed into smaller pieces and swallowed. This is discussed in more detail below.

The mandibular condyle of archaeocetes, including *Dorudon atrox*, is robust, with an articular surface that is oriented almost vertically on its posterior surface and that curves anteriorly such that is almost horizontal on its dorsal surface. The curved condyle articulates with the vertical postglenoid process and the horizontal glenoid fossa. There is no preglenoid process in *D. atrox*, which allowed the mandible to slide forward along the glenoid fossa unimpeded. It is possible that this action was used during prey capture with the anterior dentition, while the mandible rested snugly against the postglenoid process during food processing.

Two groups of masticatory muscles were reconstructed for *Dorudon atrox* in the previous chapter, the temporalis group and the masseter group. The temporalis group, consisting of the superficial and deep temporalis muscles, functions to pull the lower jaw up and back. The temporal fossa of *D. atrox* is large, indicating that the temporalis muscles that filled the temporal fossa had large cross-sectional areas, and thus were powerful muscles. The skull of *D. atrox* is also very long between the posterior end of the frontal shield and the anterior end of the nuchal crest (intertemporal region). The fibers of the temporalis group muscles traversed much of this long distance between their origin and insertion, and thus acted slowly. The temporalis muscles were probably used for oral processing of food, powerfully bringing the lower cheek teeth into occlusion with the upper cheek teeth to shear food into smaller pieces to be swallowed.

The second group of masticatory muscles reconstructed for *Dorudon atrox* is the masseter group, consisting of the superficial and deep masseter muscles. The masseter muscle group functions to draw the mandible up and forward. Since the masseter muscles attached to the thin zygomatic arch, they probably had a much smaller cross-sectional area than the temporalis muscles. In addition, the fibers of the masseter muscles traversed a relatively short distance from the zygomatic arch to the angle of the dentary (superficial masseter) and condyloid crest (deep masseter). Thus they could act more quickly than the long fibers of the temporalis group muscle. The action and length of the masseter muscle fibers suggest that the masseter muscle group was used to close the jaw quickly. This action is likely to have been used during prey capture with the anterior teeth.

Dental occlusion

Dental wear patterns are extremely important in reconstruction of the diet of extinct mammals for two reasons. The first is that wear patterns can indicate something about the resistance of food to oral mechanical processing. The second is that dental wear can indicate how the upper and lower teeth contacted one another in the chewing cycle. Thus dental wear can help characterize the mode of chewing along with the skeletal anatomy and musculature as described above.

The premolars of *Pakicetus* are simple triangles, with a single large central cusp. Both uppers and lowers show this morphology and are laterally compressed. P^3_3 and P^4_4 are the tallest cheek teeth in *Pakicetus*. These triangular premolars form an effective shearing mechanism when the uppers and lowers are brought into occlusion. The posterior edge of the lower premolar shears past the anterior edge of the corresponding upper premolar.

The emphasis of shearing between the elongated and laterally compressed lower molars, and the buccal cusps of the upper molars is pronounced in early archaeocetes. *Pakicetus* reduces the protocone on the upper molars and effectively widens the **V**-shaped groove between the protocone and the buccal cusps (Gingerich and Russell, 1990). Later protocetids lost the protocone but retained a lingual expansion on the three-rooted upper molars.

Rather than being in a row across the anterior of the skull and jaw, the incisors of *Dorudon atrox* are in an anteroposterior row in line with the cheek teeth. This arrangement of conical anterior teeth is found in modern aquatic predators, such as gavials and long-snouted odontocetes that snap up individual prey items (Werth, 1992). In addition, the canines are much reduced when compared to generalized mammals and are only slightly larger than the posterior incisors. The premolars grade from P^1_1 to P^4_4, with P^1_1 being rather like the incisors and canines but with more pronounced lateral compression and small accessory denticles. P^2_2-P^4_4 are much larger triangular teeth with well-developed and numerous accessory denticles. These cheek teeth also functioned as shear blades, like those of *Pakicetus*.

Lower molars of *Dorudon atrox* and other basilosaurids are also laterally compressed, but they have elaborated the primitive "cristid obliqua" into a series of accessory denticles. The anterior edge of the lower molars is marked by a reentrant groove. This groove accepts the posterior edge of the preceding tooth. This groove is reminiscent of the groove present in lower molars of Hapalodectinae (Szalay, 1969). The upper molars of basilosaurids are also dramatically different from the ancestral condition. The entire lingual expansion is gone, including the protocone and the lingual third root. The upper third molar is lost, and $M^{1\text{-}2}$ are reduced in size. As in the earlier groups, the lower molars shear past the buccal cusps of the upper molars that now form the lingual side of the tooth.

Dental wear patterns

There are three general types of cheek tooth wear in *Dorudon atrox*. The first is apical cusp wear. This type of wear is found on the apices of the central cusps and on the apices of accessory denticles of the cheek teeth. The second type of wear is surficial wear. This type of wear is found on the relatively flat sides of the crowns of the cheek teeth. The particular location of wear facets of these first two types is discussed below, along with an interpretation of chewing mechanics. The third type of wear is here termed cingular erosion. It is found around the base of the crown of the teeth, particularly the anterior teeth, in old individuals. The enamel is often completely worn away on the wear facets of *D. atrox* teeth.

Apical wear is prevalent on the anterior teeth of *Dorudon atrox* (Figure 128B-C). Each of the anterior teeth wears down from the apex toward the root. The wear facet is almost flat in a plane parallel to the palate. In the oldest individual, UM 101215, the anterior teeth, upper and lower, are also heavily worn on their medial sides.

Apical wear in *Dorudon atrox* lower premolars is concentrated on the central cusp and the anterior accessory denticles. The apical cusp wears relatively flat, while the wear facets on the accessory denticles angle anteriorly . Wear is rarely found on the posterior accessory denticles, and, when present, it is

very light but heaviest nearest to the apical cusp. Those few posterior accessory denticles that show wear have wear facets that angle posteriorly. Apical wear is heaviest on the central cusp of the lower premolars and decreases in intensity towards the anteriormost accessory denticle (Figure 128D). On the lower premolars, apical wear is usually heaviest on P_2, and decreases from P_2 to P_4. P_1 usually shows little apical wear.

Apical wear on the molars is heaviest on M_1 and decreases from M_1 to M_3 within individuals (Figure 128D-E). On a given molar, the amount of wear is heaviest on the anteriormost cusp (the protoconid) and decreases on successively more posterior cusps. In heavily worn individuals, the anteriormost cusp of M_1 is completely worn away and the apical wear facet is confluent with the lateral wear facet on the anterolateral side of the tooth. There is no apical wear present on any of the cusps of any M_3.

Apical wear in *Dorudon atrox* upper premolars is also concentrated on the central cusp and the anterior accessory denticles. Wear on the accessory denticles is heaviest nearest to the central cusp and decreases toward more distal cusps. The posterior accessory denticles of the upper premolars show slightly more wear than the posterior accessory denticles of the lower premolars. The upper molars show little or no apical wear. Wear on the upper molars is mostly surficial, and is restricted to the lingual sides of the teeth, where they occlude with the buccal surfaces of the lower molars (Figure 128A).

Apical wear in archaeocete teeth is certainly due to abrasion against food objects, since the upper and lower teeth do not occlude cusp to cusp, even when the mouth is completely closed. The anterior teeth (incisors plus canines) alternately interlock along the jawline, with the apices of the teeth inserting into corresponding embrasure pits. The lower anterior teeth insert into embrasure pits that are anterior to the adjacent upper teeth on the outer margin of the upper jaw. The lower canine has a rather small embrasure pit, since it is a rather small tooth. This embrasure pit is directly in line with the upper tooth row, rather than on the outer margin of the jaw. The embrasure pit for P_1 is just lingual to the cheek tooth row, and the pits for P_2 to M_3 are all in line with each other and lingual to the cheek tooth row.

The positions of the embrasure pits and the positions of the teeth when the lower jaws are in occlusion with the palate indicate that the upper and lower teeth form alternating, interlocking rows from the tip of the snout back to $P^1{}_1$. At this point the lower teeth cross over the upper tooth row, and distal (posterior) to this point the lower cheek teeth occlude lingual to the upper cheek teeth. The embrasure pits for the upper teeth remain on the buccal side of the mandible.

There are no embrasure pits for $M^{1\text{-}2}$ on the mandible, and the low crowns of these teeth do not reach the lower jaw. This suggests that the embrasure pits form in response to occlusion of the high-crowned cheek teeth with the palate and the buccal side of the lower jaw. This idea is supported by specimen UM 101222, which has a broken right P_1. The crown of this tooth was completely broken off and subsequently worn smooth, indicating that this tooth was broken during life and that the individual lived for a significant period of time after the tooth was broken. The embrasure pit that corresponds to the tooth is significantly shallower than the same embrasure pit on the other side of the jaw. This further suggests that the bone is actively remodeled in response to occlusion.

In addition to crossing over, the cheek teeth become closely spaced distally (posteriorly). There are diastemata between all adjacent anterior teeth back to $P^2{}_2$ and $P^3{}_3$, but there are no diastemata between $P^3{}_3$ and $P^4{}_4$ or between all subsequent adjacent pairs of cheek teeth. When in occlusion, the upper and lower teeth still alternate, with the corresponding lower teeth occluding anterior to the corresponding upper teeth. As the cheek teeth are brought together as the jaw closes, the posterior edge of the lower cheek teeth shears past the anterior edge of the upper cheek teeth. As the central cusp of the uppers moves past the posterior edge of the anterior lower tooth and the posterior lower tooth, the lingual side of the upper is brought into contact with the buccal side of the lower. This action produces surficial wear discussed below. At no time during this chewing stroke do the cusps of cheek teeth come into contact. Thus apical wear must be produced by something other than tooth-to-tooth contact.

The only source of apical wear is food-to-tooth contact. Food items processed by the cheek teeth are held by the posterior edge of a lower cheek tooth and the anterior edge of an upper cheek tooth and sheared by the blades as they pass one another. The resistant food items cause apical wear on the central cusps and accessory denticles of the cheek teeth. This idea is supported by the lack of apical wear on M_3. Since the palate terminates posterior to M^2, there is no corresponding embrasure pit for M_3. Since the apical cusp of M_3 cannot push food items into an embrasure pit, there is no opportunity for tooth-food wear on the apical cups of M_3. The palate and mandible are covered with soft oral epithelium that could not cause abrasive wear on enamel covered cusps.

Surficial wear is found on the lateral sides of lower cheek teeth and medial sides of upper cheek teeth (O'Leary and Uhen, 1999). Surficial wear facets are elongated vertically, parallel to the direction that the jaw moved during oral processing of food. Most of the surficial wear facets are completely worn through the enamel, exposing dentin from below. There are striations on the enamel of those wear facets that are not worn through that have striations parallel to the vertical elongation of the facets. Multiple specimens show almost the entire height of the crown of M_1 on the anterior edge of the buccal side of the tooth worn away. Surficial wear decreases from M_1 to M_3 within individuals. Wear on M_3 is quite variable, and this variation does not correlate well with age as assessed from other teeth. Specimen UM 100215, the oldest *Dorudon atrox* individual known, has only light on M_3, while other younger individuals have light to heavy wear on M_3. In addition, many upper molars have their entire lingual surfaces worn off (Figure 128A).

These observations stand in direct contrast to those of Carpenter and White (1986), who report no wear of this nature on

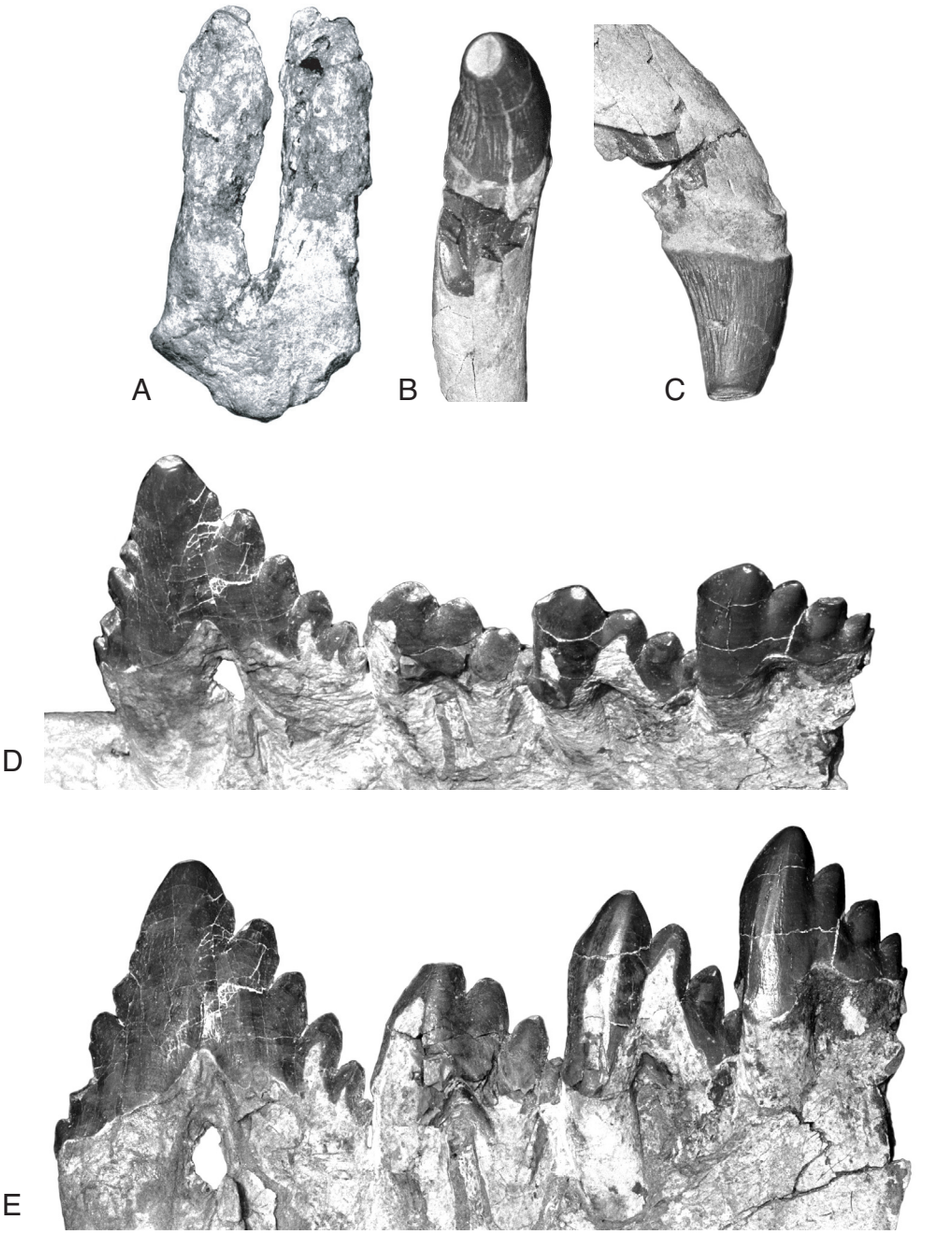

FIGURE 128 — Tooth wear in *Dorudon atrox*. A, medial side of an upper molar with the enamel completely worn away. B, apical view of an incisor with moderate apical wear. C, same incisor as B, in a lateral view. D, P_4-M_3 in lateral oblique view. Note the presence of both apical and lateral wear facets. E, same teeth as D, to highlight the lateral wear facets. Note that in both D and E, wear is heaviest on M_1, decreases on M_2, and there is only a facet on the surface of the enamel on M_3.

a single specimen of *Zygorhiza kochii*. They concluded from this observation that there was no shear between the upper and lower cheek teeth. Some specimens of *D. atrox* also show little or no surficial wear, but this can be directly linked to the age of the individuals. Those individuals with heavy wear are also skeletally mature, while those with little or no wear are skeletally immature. Lack of surficial wear on the cheek teeth thus indicates a young age, rather than a lack of shearing.

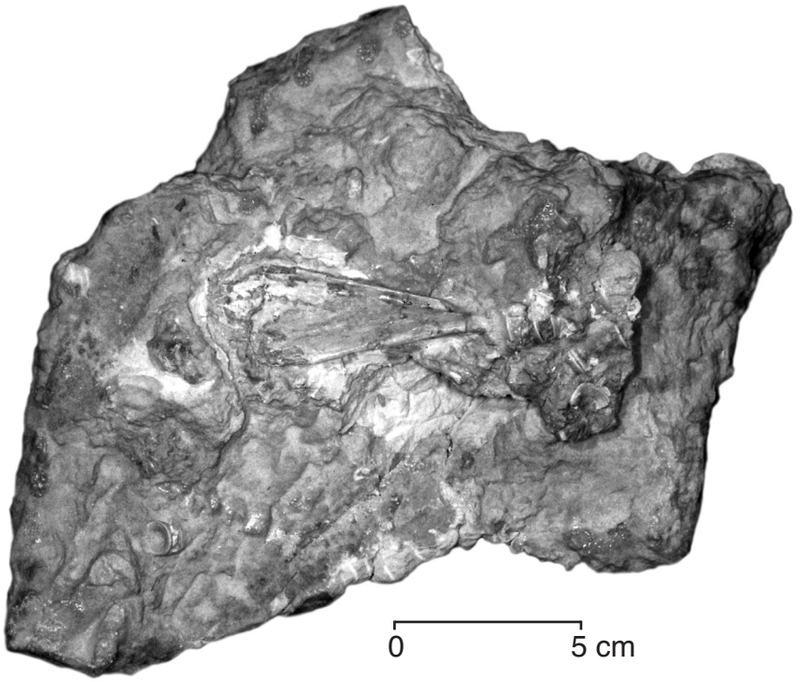

FIGURE 129 — Stomach contents of *Dorudon atrox*. This concentration of fish bones was found near rib 10 in UM 101222. The concentration includes at least two different fish, based on the presence of two sizes of vertebrae.

Cingular erosion can be seen around the bases of the crowns of the teeth in the oldest individual of *Dorudon atrox* known, UM 101215. The enamel at the bases of the crowns of the anterior teeth is entirely missing and the dentin in the same area is eroded away, leaving a broad shallow groove. This is similar to a condition found in many modern odontocete teeth, particularly *Orcinus orca* (Caldwell et al., 1956). These authors do not offer a hypothesis for the cause of this type of feature. It may be due to some kind of gum infection that leads to an acidic environment around the cingulum, thus eroding the enamel and dentin.

Apical and surficial wear on both the anterior teeth and on cheek teeth support the hypothesis that *Dorudon atrox* uses its anterior teeth to capture prey and the cheek teeth to process prey items. Further studies of dental wear in early mysticetes and odontocetes should be able to illuminate the adoption of modern modes of feeding (filter feeding and swallowing prey whole, respectively) in these groups.

Stomach contents

A skeleton of *Dorudon atrox* (UM 101222) that was found largely articulated included a small association of fish bones in the posterior thoracic region. The association includes vertebrae and skull bones of at least two different fish, one small and one large, and is shown in Figure 129. The bones are mostly disarticulated, but some of the vertebrae of the smaller individual are semi-articulated. The association of bones was found near right rib ten. It is possible that this association of fish bones is the remains of the stomach contents of this individual of *D. atrox*. There is no obvious evidence of corrosion of the bones from stomach acid, nor are there any clear bite marks on the fish bones.

If this association of fish bones really is stomach contents, it reveals that *Dorudon atrox* preyed on fish. Most modern odontocetes generally prey on fish or squid or some combination thereof, although there are some exceptions. It is unlikely that any remains of squid would be preserved as fossils, since they almost completely lack hard parts. A larger association of fish bones has been identified in *Basilosaurus cetoides* (Swift and Barnes, 1996) indicating that *Basilosaurus* also consumed a variety of fish.

It is possible that future finds of *Dorudon atrox* specimens will yield a clearer association of skeleton and stomach contents. Identification of the fish from the stomach contents could also give some clues as to the depths at which *D. atrox* fed, since many fish have specific depths at which they live. Recovery in the stomach contents of *D. atrox* would indicate that *D. atrox* had to have been at that depth to capture the fish.

HEARING

Much recent work has shown that hearing in cetaceans is highly specialized, and many features associated with

specialized hearing are reflected in the bones of the skull and jaw including the periotic, auditory bulla, ossicles (malleus, incus, stapes), and dentary (Fleischer, 1976). The discussion of hearing in *Dorudon atrox* will include three somewhat separate topics. The first is the general problem associated with sound perception underwater. The second is the range of frequencies that could have been perceived by *D. atrox*. Third is the protection of the auditory region of the skull from regions of sound production in the skull.

Underwater sound perception

Sound perception underwater presents a set of physical conditions that are very different from those for sound perception in air. Sound travels about four times faster in water than in air (Reysenbach de Haan, 1960). In addition, water, being a much denser medium than air, is much closer to the density of mammalian tissues. The densest bone of a terrestrial animal is around 10^4 times the density of air, while the densest bone of the same animal submerged is only around 8 times the density of water (Norris, 1968). Investigations on modern cetaceans show that a number of features of cetacean cranial and mandibular anatomy aid in sound perception in water. These features can be preserved in fossils since many of them are osteological.

Sound channels

Mammals that live subaerially have a sound channel that conducts sound waves from the external environment to the middle ear from the pinna, through the auditory tube, and the external auditory meatus (EAM). This anatomical system collects and directs sound towards the tympanic membrane where sound waves are converted to mechanical motion of the ossicular chain. This system does not function in the same manner when placed under water. As stated above, the soft and hard tissues are much closer to the density of water than they are to the density of air. Sound waves can propagate from the water to the tympanic membrane from almost any point on the head since both the soft and hard tissues of the skull have acoustic impedances that are very close to the acoustic impedance of water (Reysenbach de Haan, 1960; Norris, 1968).

This would not be a particularly significant problem if simple perception of sound is the only sensory modality of the ears. While sound itself carries information that is sensed by the ears, one of the most important aspects of sound is the direction in which the sound waves are moving. Directionality of sound is perceived by the slight separation between the time when sound waves reach the left and right ears (Reysenbach de Haan, 1957). When sound waves are propagated through the skull in a diffuse manner, this time difference is obscured as vibrations move through the head and strike each tympanic membrane at approximately the same time (Reysenbach de Haan, 1960).

Modern cetaceans have anatomical peculiarities indicating that they have a different sound channel from that used by terrestrial mammals. Modern cetaceans lack pinnae, but retain an external auditory meatus. The external opening of the EAM is always very small and the outer edges are appressed despite the presence of a patent lumen. Mysticetes also have a large wax plug that fills the lumen of the EAM (Fraser and Purves, 1960).

Modern cetaceans appear to have abandoned the primitive sound channel (Reysenbach de Haan, 1957), although this is by no means universally accepted (see Fraser and Purves, 1960). Instead, modern cetaceans channel sound through the lower jaw to the ear region. The mandibular foramen of modern cetaceans is very large, occupying most of the area of the medial side of the posterior dentary. In addition, the lateral wall of the dentary is covered by very thin bone lateral to the mandibular foramen. This large foramen houses a large fat pad that extends posteriorly and attaches to the auditory bulla. Sound waves preferentially propagate from water, through the lateral wall of the dentary, and through the fat pad to the auditory bulla (Norris, 1968). In addition, the fat of the fat pad has chemical and acoustic properties that are different from those of normal body fat, further supporting the hypothesis that it plays a special role in sound conduction (Norris, 1980). This new sound channel allows cetaceans to hear directionally underwater, since there is a separate sound channel for each ear (Norris, 1968).

While the soft tissues associated with the sound channel found in modern cetaceans have not been preserved as fossils, the osteological anatomy has been preserved. The bony external auditory meatus is present in *Dorudon atrox*, as it is in modern cetaceans. In addition, *D. atrox* has a very large mandibular foramen with a thin covering of bone on the lateral side of the dentary. It is impossible to know whether *D. atrox* retained pinnae, since the pinnae were composed entirely of soft tissues. Thus it is unclear whether the primitive terrestrial sound channel was still present in *D. atrox*. It is clear, however, that the mandibular sound channel was likely to be present, since the osteological correlates associated with the soft tissue structures are present. Since *D. atrox* has a sound channel like that of modern cetaceans, *D. atrox* was capable of directional hearing underwater.

Mechanical sound reception

The tympanic membrane in modern cetaceans is stretched into a conical shape, often described in two portions, the tympanic membrane itself and the tympanic ligament, which is the long apical portion of the cone (Fraser and Purves, 1960). The entire structure is called the tympanic conus. The circumference of the tympanic membrane is attached to the sigmoid process and to the body of the auditory bulla in modern cetaceans. The apex of the tympanic conus is attached to the malleus. In addition, when the ossicular chain is articulated, the malleus is out of the plane of the tympanic membrane, thus "pulling" the apex of the tympanic conus away from the plane. If one could demonstrate that the ossicular chain of a fossil cetacean placed the malleus out of the plane of the tympanic membrane, this would suggest that a tympanic conus was present. As stated earlier, the one ossicular chain found in place in *Dorudon atrox*

is at best semi-articulated, which makes the position of the malleus difficult to determine. Lancaster (1990) described the rotation of the ossicular chain of *Zygorhiza kochii*, a close relative of *D. atrox*, and suggested that *Zygorhiza* had a tympanic conus similar to that of modern cetaceans. Since the periotic, bulla, and ossicular chain of *D. atrox* is very similar to that of *Zygorhiza* when disarticulated, it is reasonable to assume that they articulated in the same way and that the ossicular chain of *D. atrox* was similarly rotated. Therefore, *D. atrox* probably had a tympanic conus.

The auditory bulla of cetaceans is also very different from those of terrestrial mammals. All cetaceans have a large bulla with a heavy involucrum on the medial wall of the bulla. The lateral wall of the bulla is very thin and supports the sigmoid process. The sigmoid process in turn supports the tympanic conus. In addition, Lancaster (1990) states that the malleus is fused to the lateral wall of the bulla in *Zygorhiza*, as it is in modern cetaceans, although this is difficult to assess for *Dorudon atrox*. Both the large involucrum and fusion of the malleus are thought to make the mechanical system more rigid (Fleischer, 1973). The acoustic fat pad described above is attached to the thin lateral wall of the bulla in modern cetaceans. It is thought that acoustic waves that have been transmitted through the fat pad cause the lateral wall of the bulla to vibrate (Norris, 1968) and thus to move the malleus that is fused to the lateral wall. This initiates the transfer of mechanical motion down the ossicular chain to the stapes.

The bones of the ossicular chain are much more dense in cetaceans than the ossicles of terrestrial mammals (Girard-Sauveur, 1969). Archaeocetes also have ossicles that are as dense or even slightly more dense than those of modern cetaceans (Lancaster, 1990). The specific gravity of *Basilosaurus cetoides* and *Zygorhiza kochii* ossicles are around 2.9 (Lancaster, 1990), while the specific gravity of modern cetacean ossicles range from around 2.3 to 2.8, and the specific gravity of terrestrial and semi-aquatic mammals (pinnipeds and others) range from around 2.0 to 2.3 (Girard-Sauveur, 1969). The auditory ossicles of *Dorudon atrox* have a specific gravity of 2.64 for the malleus, 2.56 for the incus, and 2.39 for the stapes. These values are comparable to those of modern cetaceans, and not very different from those of other archaeocetes.

The range of frequencies of sound that causes the cetacean middle ear to vibrate is directly linked to the rigidity and density of the bulla and ossicular chain. Increasing the stiffness of the mechanical transmission system increases the sensitivity to high frequency vibrations. Increasing the density of the system increases the sensitivity to low frequency vibrations (Reysenbach de Haan, 1957). Modern cetaceans achieve a balance between these two effects to allow the ossicular chain to transmit vibrations of a wide range of frequencies. This is discussed in more detail below.

Frequency range

The cetacean cochlea has features that are thought to be related to the range of frequencies that can be perceived. The ratio of the height of the cochlea to the diameter indicates the position of the frequency range. A short height relative to the diameter indicates that the frequency range includes high frequencies (Fleischer, 1976). Modern odontocetes have a very low-spired cochlea, and they have been demonstrated to hear very high frequencies (Reysenbach de Haan, 1957). Mysticetes, on the other hand have a higher-spired cochlea and have a frequency range that includes lower frequencies (Reysenbach de Haan, 1957). Archaeocetes have a cochlea that is even more high-spired than that of mysticetes (Fleischer, 1976; this study). The basal turn of the cochlea of *Zygorhiza kochii* has a diameter of 8 mm, and the entire cochlea has a height of 11.5 mm according to Kellogg (1936). This is similar to the values measured in *Dorudon atrox*. The basal turn of the cochlea of *D. atrox* has a diameter of 11 mm, and the entire cochlea has a height of around 10 mm. Both of these figures are estimates from a cochlea (described below) that was not fractured directly through the axis of coiling.

Another feature of the cochlea that is correlated with the range of perceived frequencies in modern cetaceans is the width of the basilar membrane. The basilar membrane spans the gap between the primary and secondary bony laminae. Together, these three structures (primary bony lamina, basilar membrane, secondary bony lamina) divide the coiled tube of the cochlea into two sections, the scala vestibuli dorsad to the division and the scala tympani ventrad to the division. The width of the basilar membrane is thought to be directly related to frequencies that can be perceived. The basilar membrane is in the shape of an elongated wedge that is narrowest at the bottom and widest at the apex of the cochlea. Lower frequency sounds are perceived where the membrane is broadest, and higher frequencies are perceived where the membrane is narrow. Since the membrane is narrowest in the basal turn, the width of the membrane in the basal turn is correlated with the upper frequency limit (Fleischer, 1976).

These same observations can be made of the cochlea of *Dorudon atrox*. The right periotic of specimen UM 101223 is fractured in three planes through the cochlea. It fractured such that the interior of the cochlea can be seen in a parasagittal section (relative to the axis of coiling). In addition, the base of the basal turn of the cochlea was broken such that the primary and secondary bony laminae of the basal turn can be observed from below. The primary bony lamina is large and divides the basal turn into unequal partitions. The scala vestibuli is much smaller than the scala tympani in the basal turn. Both chambers are of similar size in the second turn, and the scala vestibuli is reduced to nothing by the end of the last turn. This structure is very similar to that of *Zygorhiza kochii* (Fleischer, 1976).

Since the primary and secondary bony laminae are both visible in the basal turn of the cochlea, the gap between them that was covered by the basilar membrane in life is also visible. The gap measures about 0.35 mm across at around one quarter turn. This value is in the range of modern mysticetes and is much higher than that of modern odontocetes (Fleischer, 1976). Taken together these numbers suggest that *Dorudon atrox* lacks

the high frequency specializations found in modern odontocetes (low spired cochlea, narrow basilar width, slow increase in basilar width). Thus *D. atrox* and other archaeocetes almost certainly lacked any echolocation capabilities and perceived only low and mid range frequency sounds, like modern mysticetes.

Isolation of the auditory region

The auditory region of modern cetaceans is isolated from the nasal passages and pharynx by a number of sinuses that are filled with a foamy substance that is mostly air, and they are lined with a richly-vascularized mucous membrane (Purves, 1966). These sinuses are thought to maintain a constant pressure balance in the tympanic cavity, with which they are confluent (Reysenbach de Haan, 1957), through blood engorgement during dives (Norris, 1968).

In addition, these foam-filled cavities isolate the middle and inner ear acoustically from the surrounding area (Reysenbach de Haan, 1957; Norris, 1968). This isolation would help delimit the sound channel or sound channels that conduct incoming sound waves to the tympanic membrane. This is clearly important and related to the acuteness of directionality of hearing underwater. Norris (1968) also suggests that the air sinuses help to isolate the auditory region from extraneous outgoing sound. At least some odontocetes are thought to generate very intense bursts of sound, which may even be used to stun potential prey (Norris and Møhl, 1983). It is important to shield the auditory region from these outgoing sounds to protect the ear and to keep it free to hear incoming sounds rather than being overwhelmed by outgoing sounds that do not necessarily need to be perceived.

Dorudon atrox has a large peribullary sinus anterior to the bulla. The walls and floor of the sinus are formed by the pterygoid bone. The posterior end of the sinus is confluent with the tympanic cavity, and it is open ventrally. Basilosaurid archaeocetes such as *D. atrox* are the earliest cetaceans to have any hint of accessory air sinuses, as non-basilosaurid archaeocetes lack them altogether (but see Thewissen et al., 1996 for an alternative view of *Ambulocetus natans)*. Presence of the pterygoid air sinuses indicates that the middle ear of *D. atrox* was well insulated and that incoming sound waves were being channeled through the lower jaw, as discussed earlier. The presence of pterygoid air sinuses may also indicate that *D. atrox* was capable of deeper diving than earlier cetaceans. If the sinuses were lined with vascularized mucosa, as in modern cetaceans, this would provide protection against pressure differences associated with diving.

VISION

Two osteological features, the size of the orbit and the size of the optic nerve, may indicate something about the vision of *Dorudon atrox*. *D. atrox* has relatively large orbits when compared to some early protocetids and modern cetaceans. Slijper (1962) implies that the size of the eye is directly related to visual acuity. As an example he illustrates the Ganges river dolphin (*Platanista gangetica*) and points out that it has a very small eye and feeds in turbid bottom water where vision would not help in prey capture. In addition, he also points out that the sperm whale (*Physeter catodon*) has an eye that weighs about one third of what a humpback (*Megaptera novaeangliae*) eye weighs, although both animals have a similar body mass. He suggests that sperm whales do not need good vision to capture prey at great depths where they feed. While these are clearly salient examples of small eyes in cetaceans that do not need good vision, it is not clear that the size of the eye is directly related to visual acuity.

It is also difficult to interpret the meaning of the size of the optic nerve. Jansen and Jansen (1969) state that modern cetaceans have optic nerves of "moderate size". It is unclear what they are comparing the size of the nerve to. In addition, the optic nerve is covered with a thick *rete mirabile* in modern cetaceans (Jansen and Jansen, 1969). If the same is true of the optic nerve of *Dorudon atrox*, it would be impossible to determine the size of the nerve itself, since only the size of the canal housing the nerve and associated tissues is known. If there were a thick *rete* also in the canal, this would make the canal much larger than the size of the nerve itself. It is only safe to conclude that *D. atrox* had adequate visual perception and did not have extremely reduced eyes like *Platanista*.

LIFE HISTORY

It is difficult to study the life history of cetaceans for numerous reasons. One obvious problem is access to the organisms. As aquatic mammals, cetaceans inhabit a medium that is difficult for humans to work in since our senses and physiology are not adapted to function well under water. Long term studies of marine mammals must be limited to intermittent surface observations for varying periods of time, or some type of short term study under the surface such as sound recording or radio tracking. For these and other reasons, cetologists studying modern cetaceans have developed some techniques to acquire life history data from dead cetaceans that can be applied to fossil cetaceans as well. These are discussed below along with other techniques that are used to study non-cetacean mammals.

AGE OF *DORUDON ATROX* INDIVIDUALS

Relative age

Dental eruption sequence

Dental eruption in mammals provides a sequence of events in individual development that can be linked to other life history parameters. Dental eruption is a very stable indicator of maturation (Smith, 1989) that can be compared to other measures of growth such as epiphyseal fusion and size increase. Dental eruption sequence has been correlated with the rate of development in recent mammals. Mammals that have molars that erupt early in the dental eruption sequence tend to mature

TABLE 24 — Dental eruption and wear status of dorudontine individuals. Specimens are listed in the first column in order of age at death from youngest to oldest as determined from their dental eruption sequence. Specimens USNM 4748 and 16639 are *Zygorhiza kochii*, while all others are *Dorudon atrox*. Teeth are listed across the first row in order that they erupt as determined from these individuals. Each cell indicates the status of each tooth in each individual using the following code: 0, not present; 1, forming in the crypt; 2, less than half of the crown erupted; 3, greater than half the crown erupted; 4, erupted with no wear; 5, erupted with wear that has not broken the enamel surface; 6, moderate wear with patches of dentin expose; 7, heavy wear with dentine swaths exposed; 8, very heavy wear with greater than fifty percent of the enamel worn away. A dash indicates that the tooth is not preserved in the specimen. The form of the table is after Fisher (pers. com., 1996).

Specimen	M_1	M^1	dP_1	dP^1	M_2	M^2	M_3	P^4	P_4	P^3	I^1	P_3	I_1	P^2	I^2	P_2	I_2	P^1	I^3	P_1	I_3	C^1	C_1
UM 100139	—	1	—	2	—	0	—	0	—	0	0	—	—	0	0	—	—	0	0	—	—	0	—
UM 94811	—	4	—	4	—	0	—	0	—	0	0	—	—	0	0	—	—	0	0	—	—	0	—
UM 83902	4	—	4	—	2	—	0	—	0	—	—	0	—	—	—	0	—	—	—	0	—	—	0
UM 94814	4	4	4	4	3	0	0	0	0	0	0	0	0	0	0	0	0	0	0	0	0	0	0
UM 93220	4	4	4	4	4	4	2	0	1	0	1	0	—	0	0	0	0	0	0	0	0	0	0
UM 94796	4	—	—	—	4	—	4	—	3	—	—	0	—	—	—	—	—	—	—	—	—	—	—
USNM 4748	—	—	—	—	—	—	—	—	—	—	—	2	—	—	—	2	—	—	—	—	1	—	1
USNM 16639	4	4	4	4	4	4	4	4	4	3	—	3	—	2	—	2	—	—	—	1	—	1	—
UM 100146	6	—	—	—	6	—	5	—	6	—	—	—	—	—	—	—	—	—	—	5	—	—	—
UM 101222	7	7	—	—	7	7	5	6	7	6	—	6	—	6	—	7	—	—	—	—	—	—	—
UM 97506	7	—	—	—	7	—	7	—	5	—	—	—	—	—	—	—	—	—	—	—	—	—	—
UM 101215	7	6	—	—	6	8	5	6	6	6	8	6	—	—	8	6	—	—	7	6	—	—	7

rapidly (Smith, 1992). Mammals that mature rapidly also live their entire lives rapidly, and consequently, die young (Promislow and Harvey, 1990).

Modern cetaceans have abandoned primitive mammalian tooth replacement altogether, with mysticetes developing tooth buds and sometimes teeth *in utero* that are subsequently resorbed, and odontocetes developing only a single set of unreplaced teeth. In addition, odontocetes lack differentiated dentitions characteristic of most mammals, and thus no dental eruption sequence can be developed for modern cetaceans. Archaeocete cetaceans, however, are diphyodont and retain differentiated dentitions. Thus, a dental eruption sequence can be determined from multiple individuals that died in various stages of dental development.

Kellogg (1936) published the dental eruption sequence for *Zygorhiza kochii* constructed from a single specimen, USNM 16639, that was originally housed at Millsaps College Museum. He list the eruption sequence as follows: $M^1{}_1$, $M^2{}_2$, M_3, $P^4{}_4$, $I^3{}_3$, $P^3{}_3$, $I^2{}_2$, $I^1{}_1$, $P^2{}_2$, $P^1{}_1$, $C^1{}_1$. Kellogg (1936) appropriately described this dental eruption sequence as tentative, since some of the relative eruption times could not be determined with the single specimen he was studying. Uhen (2000) confirmed the dental eruption sequence for *Zygorhiza* and added that for *Dorudon atrox*. Uhen (2000) also confirmed the suggestion by Kellogg (1936) that the first premolars of *Zygorhiza* are replaced (as well as those of *Dorudon*), which is an unusual condition for mammals. The sequence for *D. atrox* is based on the many individuals that preserve a mixture of deciduous and permanent teeth. Table 24 shows the dental eruption and wear status of dorudontine individuals studied here. The dental eruption sequence of *D. atrox* is reproduced below.

									I^1	I^2	I^3	C^1
Upper teeth—	DD			M^1	dP^1	M^2	P^4	P^3	P^2	P^1
Lower teeth—	DD	M_1	dP_1	M_2	M_3	P_4	P_3	P_2	P_1
						I_1	I_2	I_3	C_1

Since sexual maturity cannot be directly determined from fossils, another criterion that can be preserved in the fossil record can be used to separate juveniles from adults. Many mammalian paleontologists use the completion of the eruption of the adult dentition to indicate maturity. This criterion is adopted here. Specimens that are in the process of erupting their adult teeth are considered juveniles while those with all of their teeth erupted are considered adults. A single specimen of *Dorudon atrox* (UM 100139) has been collected that died while erupting its deciduous dentition. This individual died in the process of erupting its deciduous first upper premolars and upper first molars. This individual does not have the lower jaws, so the state of its lower dentition is not known. An individual that does not have any teeth preserved appears to be younger than UM 100139 based on the stage of fusion of cranial bones. This individual (UM 100141) is discussed below.

Fusion of bones

Mammalian bones generally develop in a number of ways. Bones of the skull may develop by ossification of cartilage or in membranes (Evans, 1993). In either case, skull bones develop from centers of ossification and then ossify out from the center and fuse with adjacent skull bones along their edges. Mammalian limb bones develop by ossifying from the center (diaphysis) and from the ends (epiphyses) with cartilaginous growth plates separating the diaphyses from the epiphyses. When growth is

TABLE 25 — Fusion status of *Dorudon atrox* individuals. Specimens are listed in the first column in order of age at death from youngest to oldest as determined from fusion status. Sutures are listed across the first row in order that they fuse as determined from these individuals. Each cell indicates the status of each suture in each individual using the following code: 0, unfused; 1 partly fused; 2, fused. A dash indicates that the tooth is not preserved in the specimen. The form of the table is after Fisher (pers. com., 1996).

Specimen	SQ/PA	Occipt.	dors. C1	F/Pa	cerv. ep.	caud. ep.	thor. ep.	lum. ep.	BO/BS	PM/MX	N/F	R/U
UM 100142	0	0	0	0	—	—	—	—	0	—	0	—
UM 100139	—	1	—	2	—	—	—	—	2	—	0	—
UM 94811	—	—	—	2	—	—	—	—	—	0	0	—
UM 94814	2	2	2	2	2	—	0	—	2	0	0	—
UM 93220	2	2	2	2	2	—	0	0	2	0	2	—
UM 101222	2	2	2	2	2	2	2	—	2	2	2	1
UM 101215	2	2	2	2	2	2	2	2	2	—	—	2

complete, the growth plates disappear and the epiphyses fuse to the diaphyses. Relative ages of individuals can be determined by comparing the stage of fusion of skull bones and limb bones and dental eruption stages to fusion stages and dental eruption stages of other individuals .

Several *Dorudon atrox* individuals in different stages of fusion are shown in Table 25. The individual with the least fusion is UM 100142. This individual has all of the occipitals (basioccipital, exoccipital, and supraoccipital) free from each other and free from any other cranial bones. The frontals are free from the parietals, maxillae, and nasals. The squamosals, parietals, and jugals are all unfused. The only postcranial element in association with this partial skull is an atlas (C1). The left and right halves of the neural arch of the atlas are closely approximated, but unfused. The maxillae and premaxillae are not present in this individual, so its stage of dental eruption is not known.

The next oldest individual is UM 100139. In this individual, the occipitals are fused together and the supraoccipital appears to be fused to the parietals. The squamosals are fused to the parietals, with the frontals and parietals partly fused to each other. The basioccipital is directly approximated to the posterior basisphenoid, but they do not appear to be fused. The frontal is free from the nasals and maxilla, and the maxilla is free from the premaxilla.

The next oldest individuals are UM 94814 and UM 94811, which are approximately the same age. They are both very similar to UM 100139, but are slightly older based on dental eruption . Their frontals and parietals are fused. Some postcranial elements are associated with UM 94814. An atlas vertebra (C1) has the sides of the neural arch fused together. The neural arches of the cervical vertebrae are fused to the centra, as are the cranial and caudal epiphyses. The neural arch of an anterior thoracic vertebrae is free from the centrum, but the centrum is not preserved so the state of its cranial and caudal epiphyses are unknown.

The next oldest individuals are UM 93220 and UM 101223. These two are approximately the same age. Both are in the process of erupting M_3 and have P_4 in the crypt. All observable cranial sutures fused in both of these individuals, with the exception of the maxilla/premaxilla suture. The cervical vertebrae are preserved in UM 93220. These all have their cranial and caudal epiphyses fused to the centra. The thoracic vertebrae are present in both individuals. All of the neural arches are fused to the centra, but none of the cranial or caudal epiphyses are fused to the centra. Individual UM 93220 has a few poorly preserved anterior lumbar vertebrae that appear to have been in the process of fusing their cranial and caudal epiphyses to the centra at the time of death.

The oldest juvenile individual known is UM 94795. This specimen includes a cranial endocast and the posterior portion of the right mandible. This mandible has $M_{1\text{-}3}$ in place, P_4 partially erupted, and dP_3 in place. This sequence of individuals shows that the bones of the cranium tend to fuse from posterior to anterior. The first sutures to close are those between the various occipital bones and the supra- and exoccipitals to the parietals. Fusion proceeds anteriorly, such that the next suture to close is the frontal/parietal suture. It is unclear when sutures on the basicranium and lateral side of the cranium, such as the squamosal/alisphenoid suture closed due to the difficulty of finding these sutures in the first place. The last set of sutures to close on the cranium are those between the nasals, premaxillae, and frontals. A recent study showed that many of the same cranial sutures listed here for *Dorudon atrox* all closed in about the same order in the modern phocoenid *Phocoenoides dalli* (Yoshida et al., 1994).

Complete vertebral columns are not known from juvenile individuals. The youngest individual known, UM 100142, includes an atlas vertebra with the dorsal arch unfused. No other vertebrae are known from this individual. A slightly older individual, UM 94814 includes all of the cervical vertebrae and a single neural arch from an anterior thoracic vertebra. The dorsal arch of the atlas is fused, and all of the arches and epiphyses are fused to the centra of C1-C7. The bases of the pedicles of the thoracic neural arch have a spongy surface indicative of a

cartilaginous articulation. Thus at least some of the thoracic neural arches fused to the centra after the cervical epiphyses fused.

The most complete juvenile column is from UM 93220. This individual includes all of the cervical and thoracic vertebrae, and two lumbar vertebrae. The cervical vertebrae have their epiphyses fused to the centra, but the line of fusion is prominent. None of the thoracic and lumbar vertebrae have their epiphyses fused to the centra. Another individual, UM 101223, which is in the same dental eruption stage as UM 93220, has vertebrae in a similar state of fusion. No caudal vertebrae are known from juvenile individuals. What is known about the fusion of vertebral epiphyses is consistent with what is known from modern cetaceans. Yoshida et al. (1994) found that *Phocoenoides dalli* vertebral epiphyses fused from the anterior and posterior ends of the column, with fusion proceeding from both ends towards the middle of the column. This pattern of fusion of the vertebral epiphyses from both ends of the column is also found in *Balaenoptera acutorostrata* (Kato, 1988).

Fusion stages of the forelimb are virtually unknown. A presumably young individual, UM 94807, includes a distal ulna with an unfused epiphysis and a proximal humerus. The proximal epiphysis of the humerus appears to be partly fused to the diaphysis. All other forelimb bones known are from adults. All of the adults have the humeral head fused to the shaft of the humerus, as are the distal ulnar and distal radial epiphyses. All of the adult specimens except UM 100215 have a visible fusion line on the distal ulna and radius. In addition, all of the adults except UM 100215 do not have the proximal ulnar (olecranon) epiphysis fused to the shaft. A single individual, UM 100222, has the epiphysis present but unfused. Specimen UM 100215 clearly has this epiphysis fused to the olecranon process and the distal ulnar and radial fusion lines are obliterated.

Growth layers in teeth

A technique that has great potential for application to fossil marine mammals is the study of growth laminae in teeth. Laminae in dental tissues (enamel, dentin, and cementum) have been observed in both modern and fossil mammals. Growth layers in dentin have been used extensively to assess the age of modern odontocetes. The pulp cavities of odontocete teeth are open for most of their lives, so dentin continues to be deposited. Two problems plague estimation of age in odontocetes. The first is that dentine is deposited in subannual periods as well as annual periods. It is sometimes difficult to distinguish subannual from annual bands (Hohn et al., 1989). The second problem is that long-lived individuals begin to fill up the pulp cavity, and it becomes difficult to distinguish bands at all in this thin, late-deposited dentin (Hohn et al., 1989).

An overwhelming problem is found in archaeocetes. Archaeocetes follow the more typical mammalian pattern of depositing dentin in the pulp cavity for a limited amount of time, and then ceasing dentin deposition long before the end of life. Thus, any incremental lines in the dentin will only have been deposited over a short portion of the life span, thus they cannot be used to assess the age of *D. atrox* individuals. Nonetheless, teeth of *Dorudon atrox* were sectioned to determine if any life history variables can be assessed from incremental growth structures in the teeth. Incremental growth layers in dental tissues have the potential to help determine the length of time over which individual teeth develop, and the age of individuals at birth.

The method of sectioning *Dorudon atrox* teeth generally followed the methods outlined in Fisher (1988) with the following exceptions. Dentin was observed using a petrographic microscope with uncrossed polars in transmitted light. Black and white photographs were taken of the enamel sections and high-contrast prints were made for data collection. This process was used for observation of laminations in enamel because the laminations are difficult to observe directly. Data were collected using the BioScan Optimas image analysis program (BioScan, 1992). Optimas allows the user to enhance video images of the thin sections or photographs to accentuate the features of interest and to collect data directly from the images. For *Dorudon* teeth, luminance transects were taken along transects perpendicular to the laminations.

Incremental growth structures were found in all dental tissues. Each of these features is introduced here and discussed in more detail below. Faint striations are visible in some sections of enamel. There is no apparent hierarchical arrangement of these striations. Much larger contour lines of Owen are visible in the dentin, but the contour lines of Owen are not always preserved. Diagenesis has eradicated the lines in some portions of each of the teeth sectioned, although each of the teeth sectioned had some lines preserved. Permineralization often darkens the color of dentin in transmitted light, making the darker lines difficult to distinguish from the lighter background. Lastly, incremental growth lines were also found in the cementum, where it was preserved. The cementum often spalls off the roots of the teeth and is missing.

Enamel.— The enamel on the crowns of the teeth of *Dorudon atrox* sectioned ranges in thickness from ~0.35 mm to ~0.78 mm. The enamel is thicker at the tips of denticles and thinner on the slopes of cusps and valleys in between cusps. Striations were observed in one section of an upper premolar near the base of the crown. The striations do not form perikymata where they crop out on the surface of the enamel. The striations are not obviously grouped into any hierarchical structure.

Two types of striations have been observed in the enamel of other mammals. The smallest scale striations are called cross striations and are thought to represent a single day of enamel growth (Bromage and Dean, 1985). The larger scale striations are called striae of Retzius and represent groups of seven to eight cross striations, and thus represent one week of enamel deposition (Bromage and Dean, 1985). Striae of Retzius often form perikymata where they crop out on the enamel surface.

The striations in the teeth of *Dorudon atrox* appear as dark, slightly wavy lines against a light background and are shown in Figure 130. The striations seem to disappear when viewed at high magnification. In the small section of enamel where the

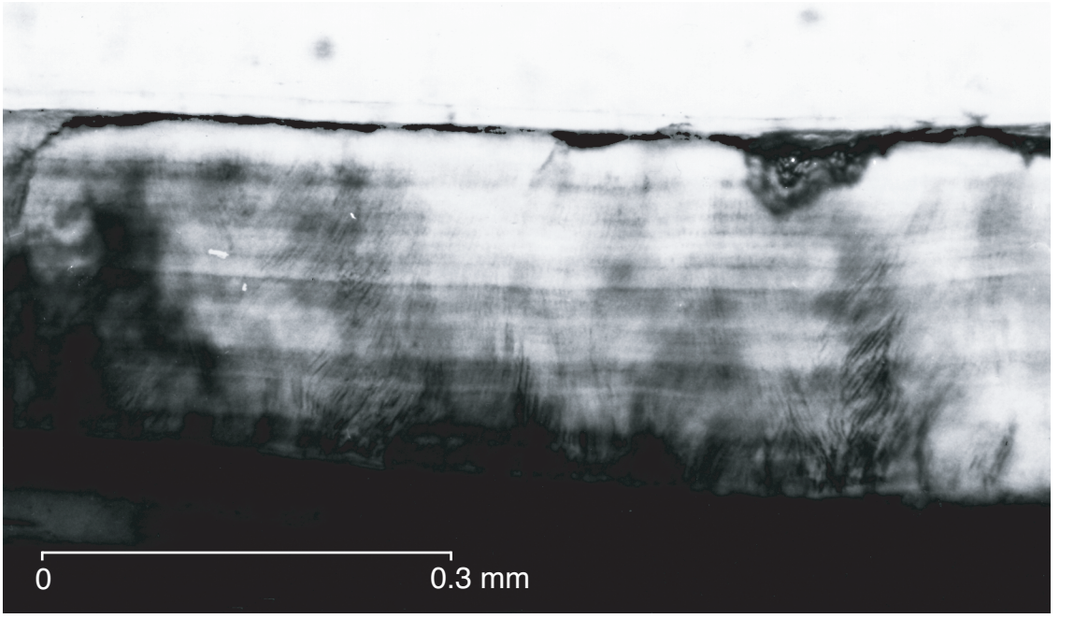

FIGURE 130 — Cross striations in the enamel of *Dorudon atrox*. The section shows the enamel of an upper third premolar near the base of the crown. The enamel dentin junction (EDJ) is towards the top. The external surface of the enamel is towards the bottom. Scale bar is 0.3 mm long. The apex of the crown is towards the left, and the root is towards the right. The enamel is about 0.27 mm thick in this section. The cross striations are difficult to see using a microscope, but show up well in high contrast photographs such as the one shown. Each couplet (one dark plus one light band) is interpreted to be a single days worth of enamel deposition. Note the striations angle slightly towards the EDJ towards the root.

cross striations are visible, there are about 30 bands, with an average band width of around 9 mm. The striations in the enamel of *D. atrox* are similar in width to the cross striations in other mammals (4-8 mm). Cross striations have been interpreted as representing daily increments of enamel deposition (Bromage, 1991; Mimura, 1939; Okada, 1943).

Each striation meets the outer surface of the enamel towards the tooth apex and meets the EDJ towards the tooth root. This geometry is consistent with the expected pattern of enamel mineralization for mammals, that usually begins at the top of each cups and proceeds towards the roots. As enamel deposition proceeds down the tooth, it ceases at the apices of cusps and continues in the shape of a "ring" around the cusp or tooth (Carlson, 1990). This results in successive layers that intersect the outer enamel surface towards the apex (where they have been deposited on previous layers) and that intersect the EDJ towards the root (where they have been newly deposited on the dentin).

If the laminations seen in the enamel of *Dorudon atrox* also represent daily increments of growth, at least 30 days of crown formation are represented in the small section of enamel measured. Since the small portion of the crown studied only includes a few of the last deposited layers of enamel, there must be a large number missing cross striations that were not counted. If this is so, the total number of striae would indicate that crown formation must have taken some number of months if the cross striations represent daily increments of growth, as seen in other mammals.

Dentin.— Contour lines of Owen are visible in the dentin of all teeth sectioned and can be seen in Figure 131. These

FIGURE 131 — Contour lines of Owen in the dentin of *Dorudon atrox*. White arrows point to individual contour lines of Owen in the dentin. These sections show the dentin of upper premolars in the root. A is from UM 101230 while B is from UM 101215. In both photos the dentin cementum junction is towards the top and the pulp cavity is towards the bottom. The lineations up and towards the right in A and almost vertical in B are dentinal tubules. A large crack is present in A angling down from left to right. The contour lines of Owen are horizontal in both photographs. Note that the laminations are obliterated around the crack. Some of the contour lines of Owen are difficult to see in figure A, and seem to fade in certain portions across the field of view. The regularity of the laminations is easier to observe in B because the quality of preservation is more even across the field of view. Scale bar is 0.3 mm long.

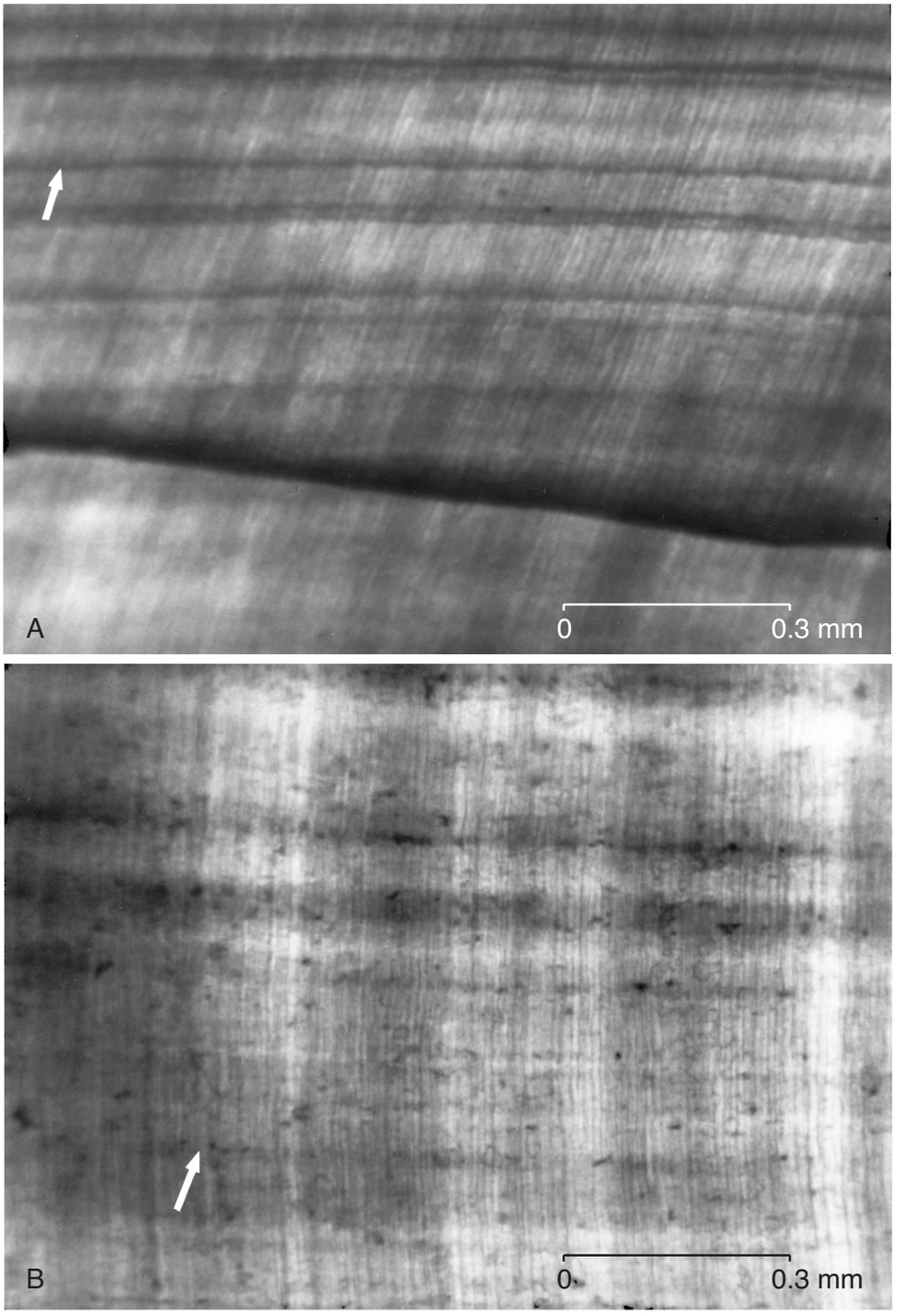
A
0
0.3 mm
B
0
0.3 mm

FIGURE 132 — Cementum of *Dorudon atrox*. Scale bar is 0.3 mm long. The outer surface of the cementum is towards the top of the photograph, while the dentin cementum junction is towards the bottom. There are striking laminations in the cementum that seem to be best developed in the center of the thickness of cementum. It is unclear whether these represent periodic growth structures or episodic growth structures.

structures are laminations that are oblique to the EDJ and dentin-cementum junction, and perpendicular to the dentinal tubules (Carlson, 1990). While the contour lines of Owen were found in all teeth sectioned, they are not easily seen throughout the entire tooth. Diagenesis has obliterated the lines in some sections of the teeth, and made them indistinct in other sections.

A composite transect from the pulp cavity to the EDJ (or to the dentin-cementum junction where applicable) was made for each tooth sectioned. Position of each observable lamination was marked using the Optimas image analysis system as described above and the data on lamination spacing was investigated to determine if any patterns were present.

The distance between adjacent laminations (band width) displayed a range of values that were then plotted in a histogram. Some of the very high values are definitely attributable to the transect crossing an area obliterated by diagenesis and/or cracks. Most of the remaining band widths clustered around two small ranges of values. The higher range of values was

always twice the lower range, suggesting that these represent instances in which a lamination was missed and not counted, effectively making the measured band width twice the actual width. The lower cluster of values was taken to represent a signal of a single period of dentin deposition. The average band width for these single periods of dentin deposition was ~0.035 mm for one of the teeth measured and ~0.059 for another. Using the thickness of dentin in the teeth and the average band width, one can calculate the number of periods over which the tooth formed. This calculation indicates that posterior upper premolars of *Dorudon atrox* take from around 105 to 180 periods to form.

Based on life history, developmental, and dentinal growth band data from other species, one can estimate the period of dentin deposition in *Dorudon atrox*. The life span of *D. atrox* (discussed below) is estimated to be 40-50 years. With a minimum of around 100 periods of deposition, an annual period is clearly too long.

The length of time over which mammalian teeth develop varies among species. Emily and Penman (1994) state that dentin deposition continues in canines of the dog for up to four years. Hillson (1986) reports data that shown domestic pigs take from around 8 months to over a year to form cheek teeth, and that cattle take from two to three years to form their cheek teeth. Fisher (1988) shows that dentin in proboscidean tusks is deposited in daily, weekly or fortnightly, and annual increments and deposition continues throughout the entire life span since their tusks are ever growing. Klevezal' and Kleinenberg (1967) show annual dentin deposition increments in many mammalian taxa. Hohn et al. (1989) have shown that in addition to displaying annual incremental growth of dentin, odontocetes often also shown monthly incremental features.

If each lamination in the dentin of *Dorudon atrox* is taken to represent a week of ontogenetic time, it would have taken from 2 to 3.5 years to form one of the posterior premolars based on the number of laminations present. If each lamination in the dentin represents a fortnight (two weeks) of ontogenetic time, dentin deposition would have lasted 4 to 7 years. If each lamination in the dentin represents a month of ontogenetic time, dentin deposition would have lasted 8 to 14 years.

Cementum.— Layered structures are found in the cementum of *Dorudon atrox* (Figure 132). It is unclear whether these structures represent periodic deposition of cementum, or episodic deposition of cementum. They could also represent periodic or episodic resorption and initiation of redeposition of cementum, since cementum can be remodeled after being initially deposited. The layered structures in the cementum are generally parallel to the dentine-cementum junction. In one deciduous tooth, the cementum layer formed large crenulations on the surface of the root, and the layering in the cementum followed the crenulations, rather than the crenulations representing some surficial reflection of the banded structure of the cementum. Some of the lamination in the cementum are continuous, while others are somewhat discontinuous and difficult to trace. This may be due to varying quality of preservation, or it may represent the original nature of the structures.

Duration of tooth formation

While laminations in the dental tissues of *Dorudon atrox* cannot help determine the absolute age of individuals as they can in modern cetaceans, laminations can help bracket the amount of time it took to form both the crowns and roots of *D. atrox* teeth. Based on the number of cross striations in the small section of enamel where they are visible in one of the crowns sectioned, crown formation took some number of months to over a year. Based on the amount of time it takes to complete dentin deposition in the molars of modern artiodactyls and other mammals, either weekly or fortnightly depositional periods is reasonable. A monthly period of dentinal deposition, like that seen in modern odontocetes, yields root formation times that greatly exceed those of modern mammals.

Life span estimation

Both body weight and brain weight can be used to estimate life span. Body weight is more difficult to use, only because it is harder to estimate body weight in fossil mammals than it is to estimate brain weight. Brain weight, on the other hand, is measured directly from cranial endocasts, with a smaller relative error in the estimate than body weight. The relationship of maximum life span for species of mammals with body weight is shown in Equation 1 (after Sacher, 1959):

$$\text{Ln } y = 1.085 + (\text{Ln } x) \quad (1)$$

In Equation 1, y = life span in years and x = body weight in grams. The relationship of maximum life span for species of mammals with brain weight is shown in Equation 2 (after Sacher, 1959):

$$\text{Ln } y = 1.575 + 0.325\ (\text{Ln } x) \quad (2)$$

In Equation 2, y = life span in years and x = brain weight in grams. The relationship of maximum life span for species of cetaceans with body length is shown in Equation 3:

$$\text{Ln } y = 0.354 + 0.432\ (\text{Ln } x) \quad (3)$$

In Equation 3, y = life span in years an x = total body length in centimeters. The relationship of maximum life span for species of cetaceans with brain weight is shown in Equation 4:

$$\text{Ln } y = 0.354 + 0.432\ (\text{Ln } x) \quad (4)$$

In Equation 4, y = life span in years an x = brain weight in grams.

The body mass of adult *Dorudon atrox* was estimated at 2,700 kg. When this body mass is used in Equation 1, the estimated life span of *D. atrox* is ~56 years. The adult brain mass of *D. atrox* was previously estimated to be around 976 g in the section on reconstructed anatomy. When this brain mass is used in Equation 2, the estimated life span of *D. atrox* is ~45 years. The total body length of *D. atrox* was previously

TABLE 26 — Age classes of *Dorudon atrox* based on dental eruption sequence and tooth wear. Age classes 1-10 are based on position in the dental eruption sequence. Classes 10-13 represents individuals with all of their adult teeth in place and they are based on dental wear. Age class 10 includes individuals with low wear. Age class 11 includes individuals with moderate wear. Age class 12 includes individuals with heavy wear. Age class 13 includes individuals with very heavy wear.

1	2	3	4	5	6	7	8	9	10	11	12	13
						I^1	I^2	I^3	C^1			
DD		M^1	dP^1	M^2	P^4	P^3	P^2	P^1				
DD	M1	dP_1	M_2	M_3	P_4	P_3	P_2	P_1				
						I_1	I_2	I_3	C_1			
UM 100139	UM 94794	NHML M21896	NHML M9266a	UM 93220	UM 94795				CGM 42183	NSFM 4451	UM 101222	UM 101215
		SMNS US I	NHML M10173	UM 94796					UM 97506	SMNS 11417a	UM 100146	
		SMNS 11951a	UM 83902	UM 101223						UM 97512		
		UM 94811	UM 94814							UM 100144		
			UM 94834									

estimated at 535 cm. Using this figure in Equation 3, yields a life span estimate of ~40 years. When the brain mass of 976 g is used in Equation 4, the estimated life span of *D. atrox* is around 28 years.

Given these different life span estimate for *Dorudon atrox*, additional criteria must be applied to choose among them. Two of the equations (1 and 2) are for mammals in general, while two (3 and 4) are specifically for cetaceans. Since cetaceans are very different from other mammals in many aspects of their biology, the cetacean-specific life span equations are a better choice. In addition, many authors have suggested that brain weight has a special relationship with growth and life span, apart from its correlation with body size (Sacher, 1959; Hoffman, 1983; Smith, 1989; Smith et al., 1994). These two factors combined suggest that the correlation of cetacean brain size and maximum life span is the best equation to use to estimate life span of fossil cetaceans, giving *D. atrox* an estimated maximum life span of around 28 years.

AGE STRUCTURE OF DEATH ASSEMBLAGE

Ontogenetic age structure of the sample of *Dorudon atrox* individuals was assessed using dental eruption sequence and tooth wear. A series of thirteen age classes was constructed using the dental eruption sequence discussed above. Classes one to nine are based on dental eruption, while ten to thirteen are based on tooth wear. Age classes are shown in Table 26. Individuals in age class 10 and above had completely erupted their adult dentition. A single individual (UM 100139) is erupting a deciduous tooth (dP^1, the last deciduous tooth to erupt). Another individual (UM 100142), is probably younger based on its stage of cranial fusion, but this specimen does not include any teeth. Age class ten is further subdivided into three age classes based on wear of the cheek teeth, ranging from low to moderate to high.

Table 26 shows the individuals assigned to age classes based on dental eruption sequence. Those specimens that have completed the eruption of their adult dentition are considered to be adults, while those that are still erupting their permanent dentition and retain deciduous teeth are considered juveniles. The age of completion of the permanent dentition is highly correlated with the age of sexual maturity in most mammals (see Smith, 1989 for an example from primates). This cannot be assessed for modern cetaceans since they have abandoned the primitive mammalian dental eruption pattern, and erupt only a single set of teeth.

Note that there is high mortality of young juveniles. No individuals have been recovered that are in the process of erupting their anterior premolars, incisors, or canines. Around 63% of the specimens listed in Table 26 are sub-adult based on their

dental eruption. This type of mortality pattern is similar to that expected for a population of mammals in which females give birth once per year (Klein and Cruz-Uribe, 1984; Barlow and Boveng, 1991). This expectation does assume that the death assemblage is an attritional accumulation of individuals dying from a stable population. One discrepancy from the expectation is that the number of deaths should be higher in older adults.

An alternative hypothesis is that the death assemblage represents a behaviorally differentiated subgroup of the original *Dorudon atrox* population. This hypothesis would necessitate separating young juveniles and young adults from the older juveniles and older adults. A simple explanation for this separation is that the adults in the sample represent reproductive adults, and the juveniles represent their newborn and young offspring. Modern cetaceans are commonly found in this type of association (Urbán and Aguayo, 1987; Shane et al., 1986). Reproductive age adults migrate and associate in breeding grounds (often warm, shallow, tropical waters). The depositional environment of the rocks in which *D. atrox* fossils have been found represent ideal calving grounds for cetaceans. No juveniles of *B. isis* have ever been recovered from these deposits (Gingerich et al., 1990). It is possible that the lack of *B. isis* juveniles is because *B. isis* used some other locality for calving, but the adults are in the Egyptian waters to take advantage of a relatively abundant and vulnerable food source: the calving *D. atrox*. This is of course highly speculative, and in need of further study. Larger sample sizes and samples from other depositional environments (like the southeastern United States) could help choose between these hypotheses, or suggest additional alternatives.

SKELETAL GROWTH

Growth in *Dorudon atrox* is difficult to assess for two reasons. First, the same skeletal elements are not preserved in individuals representing different ages. Second, not all age classes are represented in the sample. No older juveniles are present in the sample, and this is potentially a period during which significant growth could occur.

Four plots of size vs. age class are shown in Figure 133. Four skeletal measurements, mandible depth at C_1, mandible depth at P_4, frontal shield breadth, and auditory bulla length, in addition to endocranial volume are shown. All indicate some increase in size with increasing age. While each of the plots have different scales on the vertical axis that are appropriate to each measurement, the correlation of auditory bulla length with age (Figure 133D) has the lowest slope. This is not due to a different magnitude of measurement, since the mandibular depth measurements are similar in magnitude, yet have a much higher range of values over ontogenetic age. This suggests that auditory bullae reach almost adult size early in life.

The other measurements of the mandible, frontal shield, and endocranial volume all show a marked increase in size over ontogenetic time. Presumably, older juveniles fill the gap between the younger juveniles and adults that is evident in the plots. It is difficult to comment on the allometric relationships among these growing body parts in *Dorudon atrox* because the horizontal axis in each of the plots in Figure 133 is not age, but rank age class. It is safe to conclude only that most skeletal elements of *D. atrox* show an increase in size to adulthood, while others (like the auditory bulla) achieve their adult size early on in ontogeny.

SEXUAL DIMORPHISM

There is no obvious evidence of sexual dimorphism in *Dorudon atrox*. Sexual dimorphism is manifested in modern cetaceans in a number of ways. Often, females are much larger than males (*e.g.* Ohsumi, 1960). Some odontocetes show sexual dimorphism in the dentition, usually with males having display or battle teeth that females lack (*e.g. Monodon*, Ziphiidae [Mead, 1989]). In addition, some cetaceans are sexually dimorphic in other osteological characters, like the development of maxillary crests in *Hyperoodon* (Mead, 1989) length of some ribs, length of the sternum, length of the scapula, and all dimensions of the pelvic bone in *Neophocaena* (Yoshida et al., 1994). Male *Hyperoodon* have very large maxillary crests that increase in size with age (Mead, 1989). All of the dimorphic postcranial measurements in *Neophocaena* are larger in females, except for those of the innominate, which are larger in males. Males also have a differently shaped innominate from females (Yoshida et al., 1994).

Most of these types of sexually dimorphic differences are impossible to demonstrate in *Dorudon atrox* due to the small sample size. As noted above, most of the known individuals of *D. atrox* are juveniles, so any size measurements would be overwhelmingly affected by the age of the individual, obscuring potential sexual differences. In addition, no innominata have been recovered from *Dorudon atrox*.

One skeletal element that is present in many specimens is M_1. M_1 erupts early on in ontogeny, so it is present in many of the juvenile specimens as well as the adults. M_1 length, width and height were investigated for any indication of sexual dimorphism. While there is a range of variation in the size of M_1, there is no obvious separation into two populations that could be males and females. There is no consistent relationship between length, width, and height of M_1, that is, the teeth with the lowest lengths are not necessarily the teeth with the lowest widths and heights.

One other possible skeletal indicator of sexual dimorphism is the shape of the cranial crests. All individuals assigned to *Dorudon atrox* have similarly shaped nuchal crests that lack the pinching seen in *Saghacetus osiris*. Of the four adult specimens that have well-preserved sagittal crests, a single individual, UM 101215 has a distinct concavity in the crest just anterior the point where the sagittal crest meets the nuchal crest. It is unclear whether this is simply individual variation, an effect of its age (since it is the ontogenetically oldest individual known), or sexual dimorphism. More adult

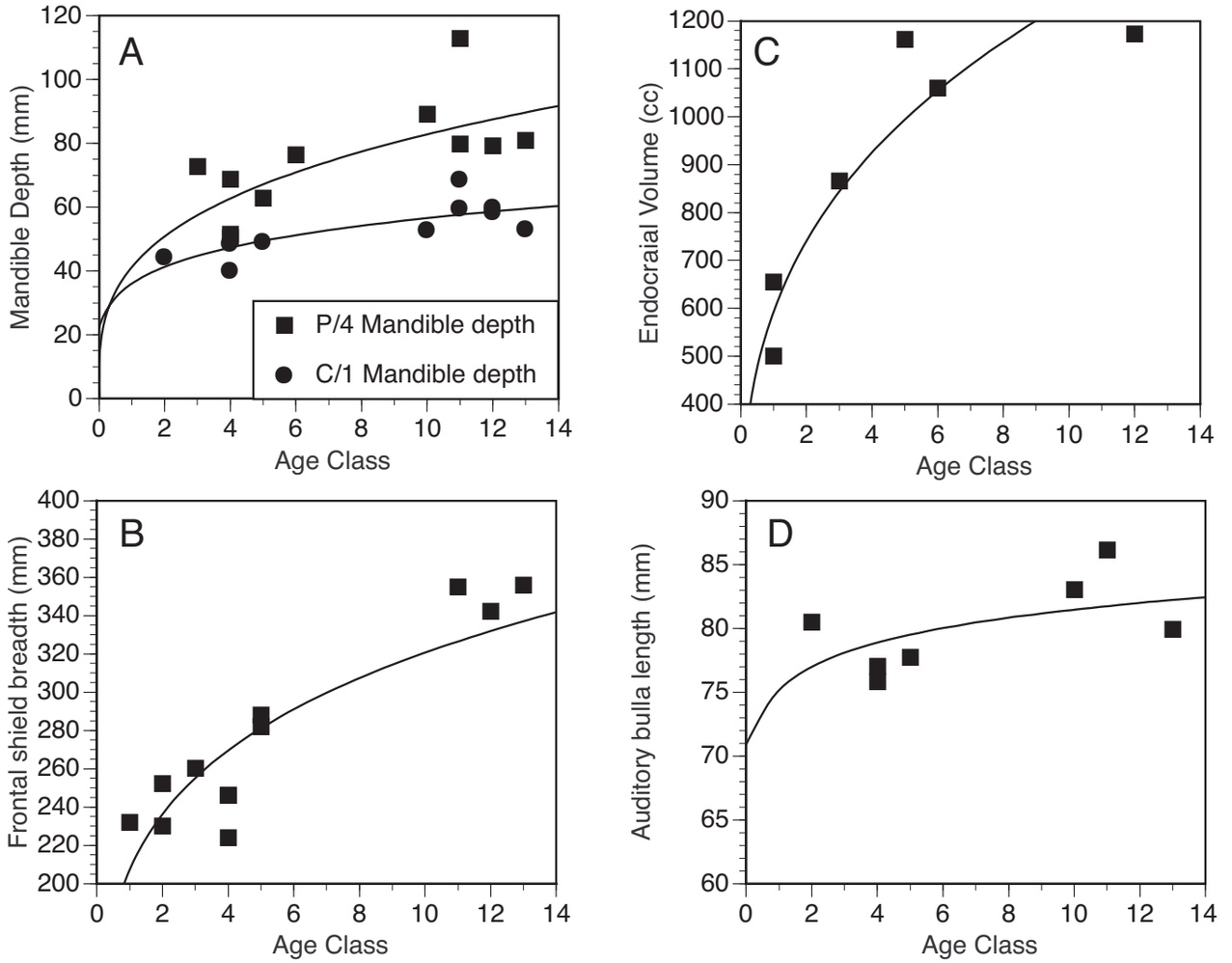

FIGURE 133 — Ontogenetic growth curves for anatomical features of *Dorudon atrox*. A is illustrates the changes in the depth of the mandible at C_1 and P_4. B shows growth in the breadth of the frontal shield. C shows increase in the endocranial volume. D shows change in the size of the auditory bulla. Note that the auditory bulla does not grow much from a very early age to adulthood.

specimens of different ages need to be studied before this question can be answered.

PREDATION AND PATHOLOGY

Evidence of lethal predation or scavenging

Three individuals of *Dorudon atrox* show evidence of lethal predation or scavenging. All individuals have unhealed bite marks on their frontal shields, although the bite marks are very different. All are very young individuals. The youngest, UM 100139, is erupting M_1. The others are approximately the same age, at M_2 eruption.

The first individual, UM 100139, has a single deep bite mark on the right side of the frontal shield (Figure 134). The bite is rather deep (H" 10 mm) and oval in shape. The long axis of the oval is approximately 16 mm long and the short axis is about 10 mm long. The depression itself is conical.

The second bitten individual, UM 94814, has three bite marks in a row across the frontal shield (Figure 135). The bite marks are numbered from left to right across the frontal shield. Bite marks numbers one and two are to the left of the midline, while bite mark number three is to the right of the midline. Bite mark one is separated from bite mark two by approximately 15 mm, measuring from center to center of the bite marks. Bite mark two is separated from bite mark three by approximately 49 mm, more than three times the distance between one and two.

FIGURE 134 — Skull of a juvenile *Dorudon atrox*, UM 100139. The small oval depression in the frontal shield to the right of the midline is interpreted as a possible bite mark. It is the deepest of the bite marks found, and different in form from the other marks.

All of the bite marks on the second individual are similar in morphology. They are small, circular to oval depressions. The maximum length of the long axis of one of the marks is about 7 mm and the minimum length of the short axis of one of the marks is about 5 mm. It is difficult to closely observe the bone in the depressions, since the bite marks are coated with iron oxide that is difficult to remove without damaging the bone. Despite this, the coating appears thin and the depressions seem smooth and rounded.

All three bite marks on the second individual are in a straight line and they all appear to be a uniform depth. This suggest that the bite marks are from to a single bite by a predator or scavenger. Although the ventral portion of the skull is missing due to weathering, It is likely that the predator or scavenger bit this individual across the top of the skull over the orbit with its upper teeth, while the lower teeth bit into the dentaries. There are no obvious bite marks on the dentaries where the lower teeth would have struck the bone had the dentaries been in articulation with the skull when the bite was made.

The third individual, UM 94811, has a single, large bite mark on the left side of its frontal shield (Figure 136). This bite mark is very different from the others. It is very shallow for its size, around 6 mm at the deepest point. It is shaped like the outline of a figure 8, an elongate oval that is constricted in the middle. The long axis of the bite is about 33 mm long. The short axis cannot be measured because one side of it has been weathered away. The deepest part of the bite mark is at one end The bottom of the bite is lined with the crushed surface of the frontal in many small fragments. It is not clear whether more bites were present on this specimen, since much of the frontal shield and the rest of the skull have been weathered away.

Three types of possible predators or scavengers have been found in the same deposits as specimens of *Dorudon atrox*. They are sharks, marine crocodiles, and other archaeocetes. The marks on the bitten skulls were compared to shark-bitten cetacean bones from the Miocene Eastover Formation of North Carolina. These bite marks are known to be make by sharks because shark teeth have been found embedded in some of the marks. Shark bites are

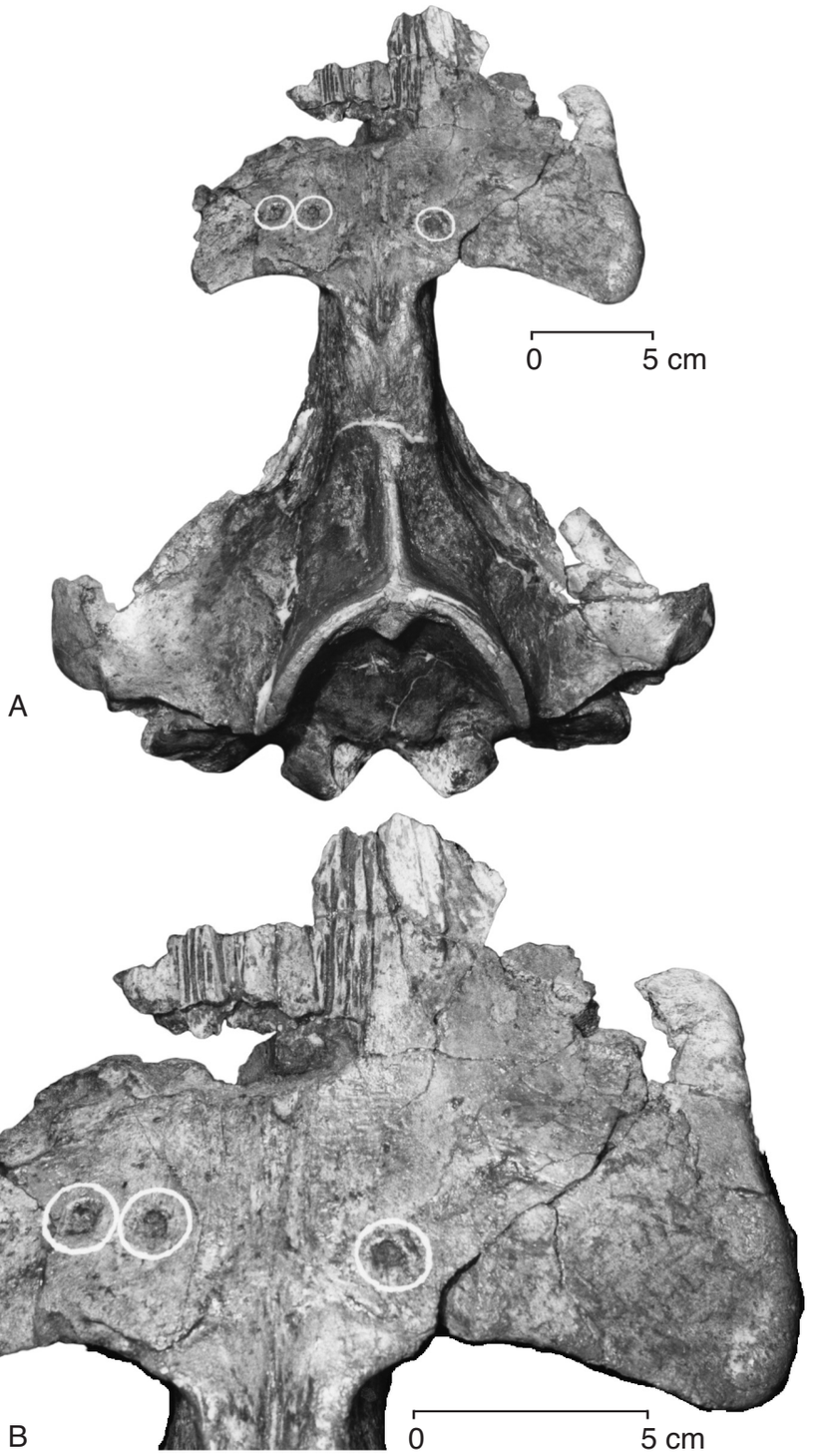

FIGURE 135 — Skull of a juvenile *Dorudon atrox*, UM 94814. The small depressions circled on the frontal shield are interpreted as a series of bite marks. Figure A shows the skull in a distant view, while B shows the bite marks close up. The marks are very shallow, and the two on the left side of the skull are very closely spaced and far from the third mark.

FIGURE 136 — Skull of a juvenile *Dorudon atrox*, UM 94811. The large depression on the left side of the frontal shield is some kind of crushing injury. No other marks are apparent on this skull.

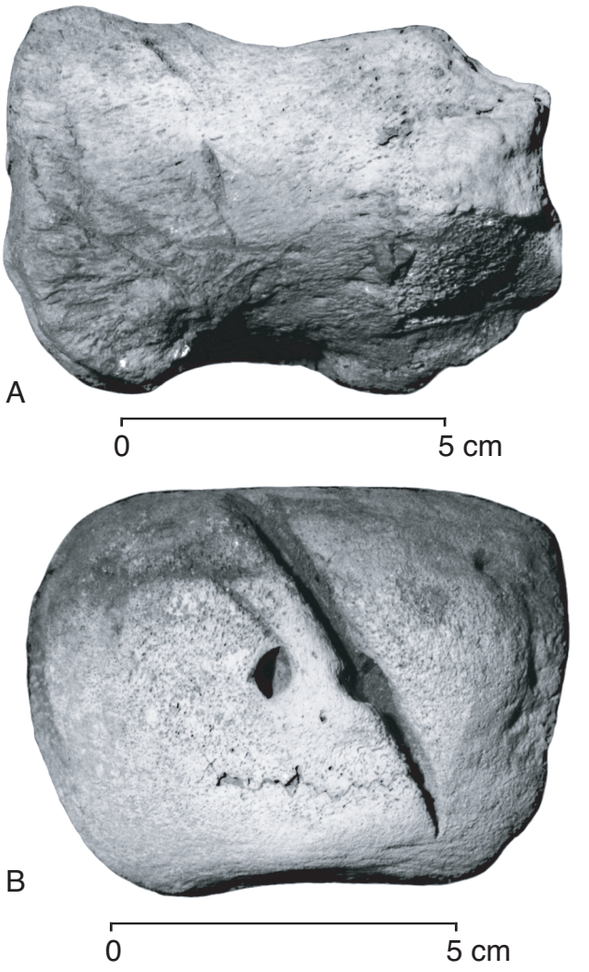

FIGURE 137 — Shark bites on Miocene cetacean bones from the Eastover Formation, North Carolina. A shows a humerus and B shows a caudal vertebra with typical shark bite marks. Note the characteristic long slashing grove that is typical of sharks. These marks are very different from those found on the skulls of *Dorudon atrox*.

TABLE 27 — Distribution of locations of shark bites on 39 cetacean bones from the Eastover Formation, Lee Creek Mine, Aurora, North Carolina. Note that most bites are concentrated on the extremities (distal forelimb, tail) and the ribs.

Mandible	Tooth	Humerus	Radius/Ulna	Rib	Lumbar Vertebrae	Caudal Vertebrae
5	1	2	14	8	2	7

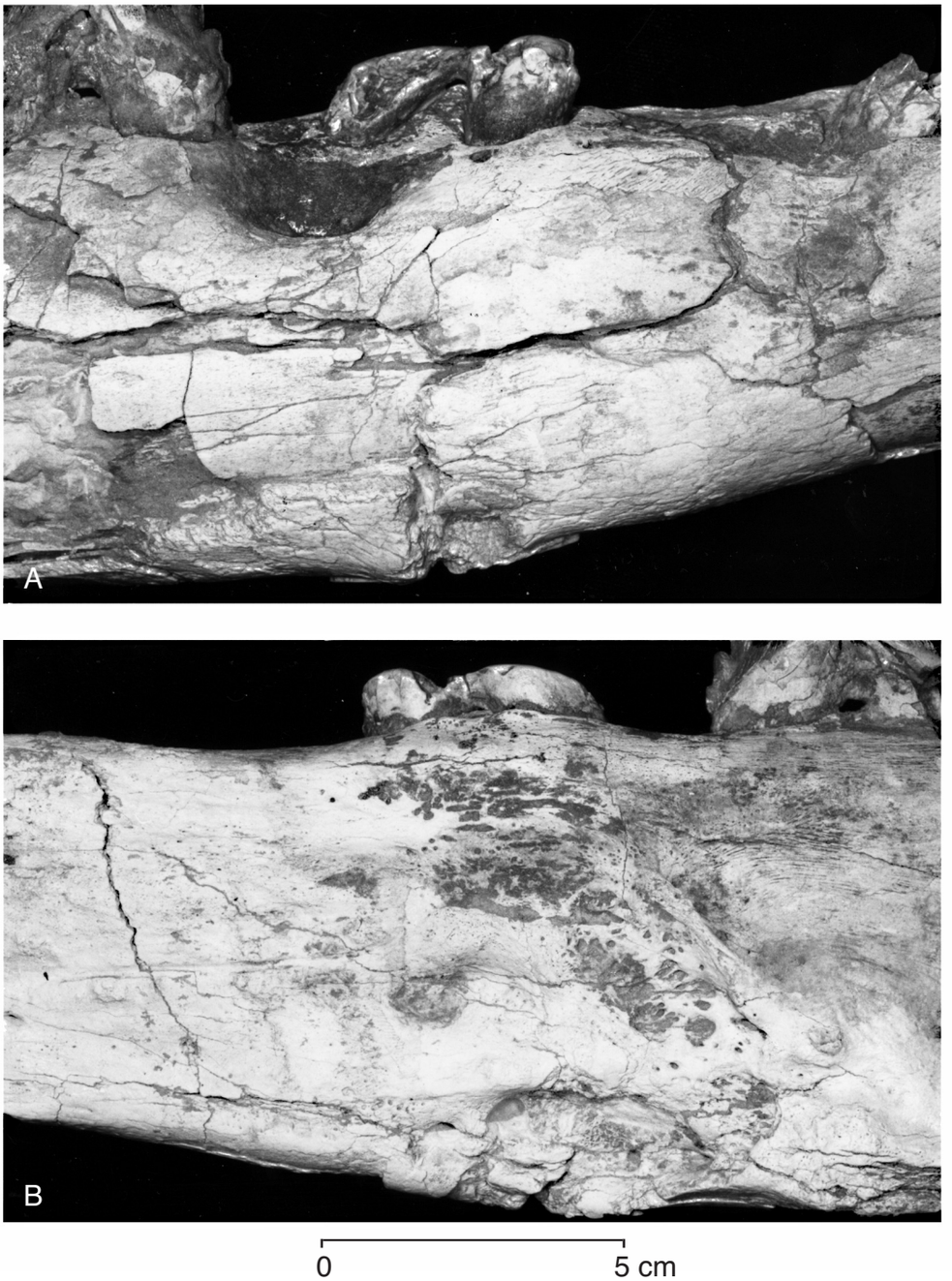

FIGURE 138 — Damaged right dentary of *Dorudon atrox* in A, lateral view, B, medial view. Note the remodeled bone at the ventral margin of the jaw. Also note the broken and subsequently worn P_1 above the damaged bone.

always long, narrow cuts formed by the teeth slicing across the bone (Figure 137). Often there are multiple parallel slice marks on the same bone from adjacent teeth that were dragged across the bone (Figure 137A). In addition, most of the shark-bitten bones from the Eastover Formation are from extremities rather than the skull. Table 27 shows the number of bones with shark bites at different locations for 39 different bitten bones. None of the bites recorded are from skulls, although three are from

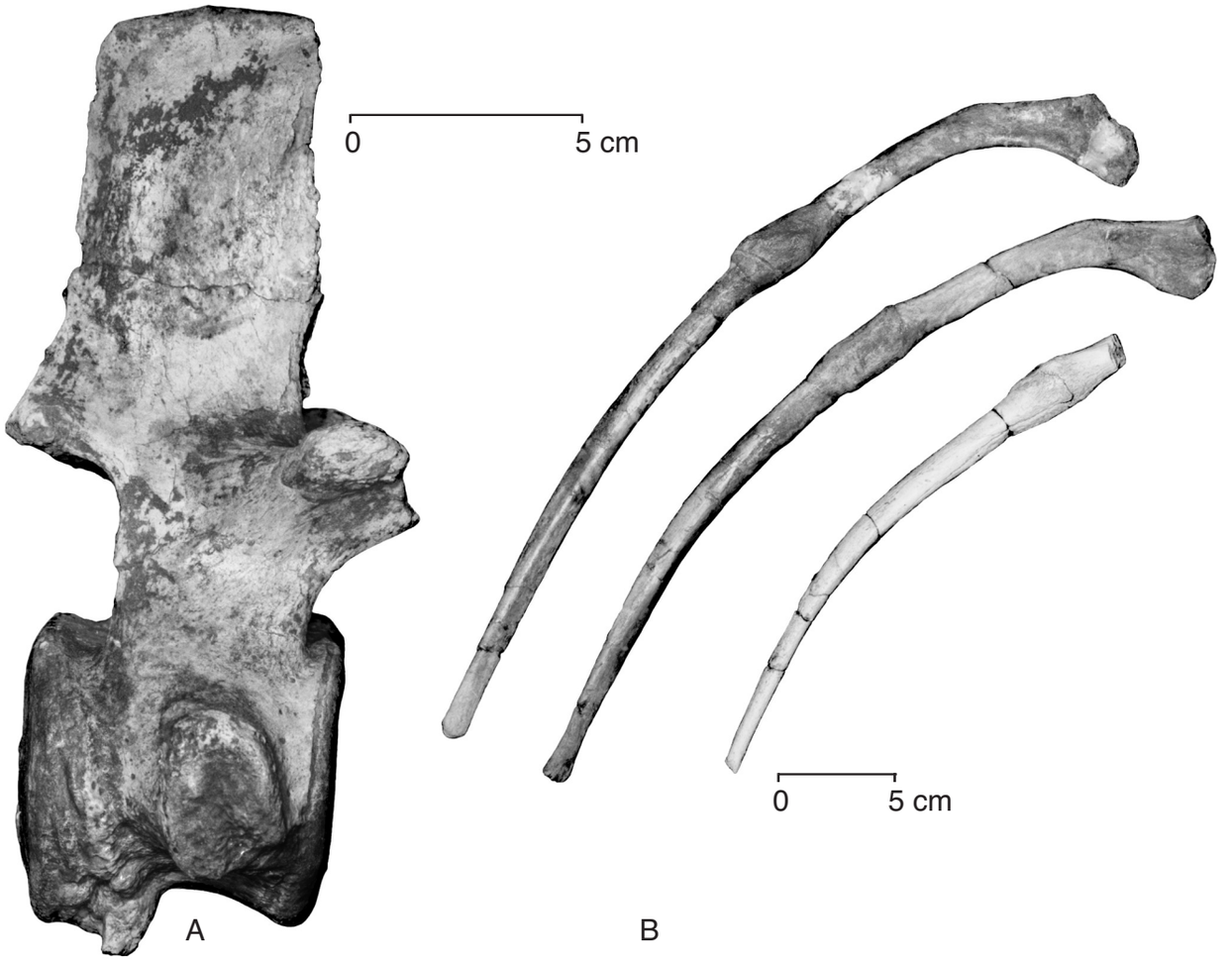

FIGURE 139 — Additional pathological bones of *Dorudon atrox*. A is a right lateral view of T13 from UM 101222. Note the exostosis on the ventral side of the vertebra near the posterior epiphysis. B are ribs 10, 11, and 12 in anterior view. Each of the ribs shows a healed break, probably from a single impact injury to the rib cage.

mandibles. This sample is very likely to be biased against recovery of bitten skulls since the collection of bitten bones was made from spoil piles of a mine in which skulls are likely to have been destroyed. Despite this, all of the shark bites have a similar morphology and it appears that bites are much more common on extremities than on the trunk. The morphology and the location of the bites on the specimens of *Dorudon atrox* suggest that they were not made by sharks.

Crocodilians are also found as fossils from the marine beds of the Fayum. It is possible that the bite marks on UM 94814 were made by a marine crocodile. Bite marks one and two are about the same distance apart as the anterior teeth of *Crocodilus articeps* (Andrews, 1906, plate XXII). The larger space between bite marks two and three may be due to missing or broken teeth. In addition, the size and shape of the bite marks is consistent with small conical teeth like those of a crocodile. The marine crocodiles were probably too small to have preyed on archaeocetes, even very young ones such as UM 94184, but it is possible this is evidence of scavenging. As mentioned earlier, the dentaries of this individual did not show evidence of injury. If the skull had been bitten while the individual was alive, the lower jaws of the predator would have had to have close on the dentaries of the *Dorudon atrox* individual. If the skull was bitten after the individual had died, it is likely that the dentaries would have been disarticulated from the skull, since they are lost early on in the decay sequence for cetaceans (Schäfer, 1972). In this scenario, a marine crocodile could have bitten down on the skull during scavenging and not bitten the dentaries.

Lastly, other archaeocetes are possible predators or scavengers on *Dorudon atrox*. The single crushing bite mark on

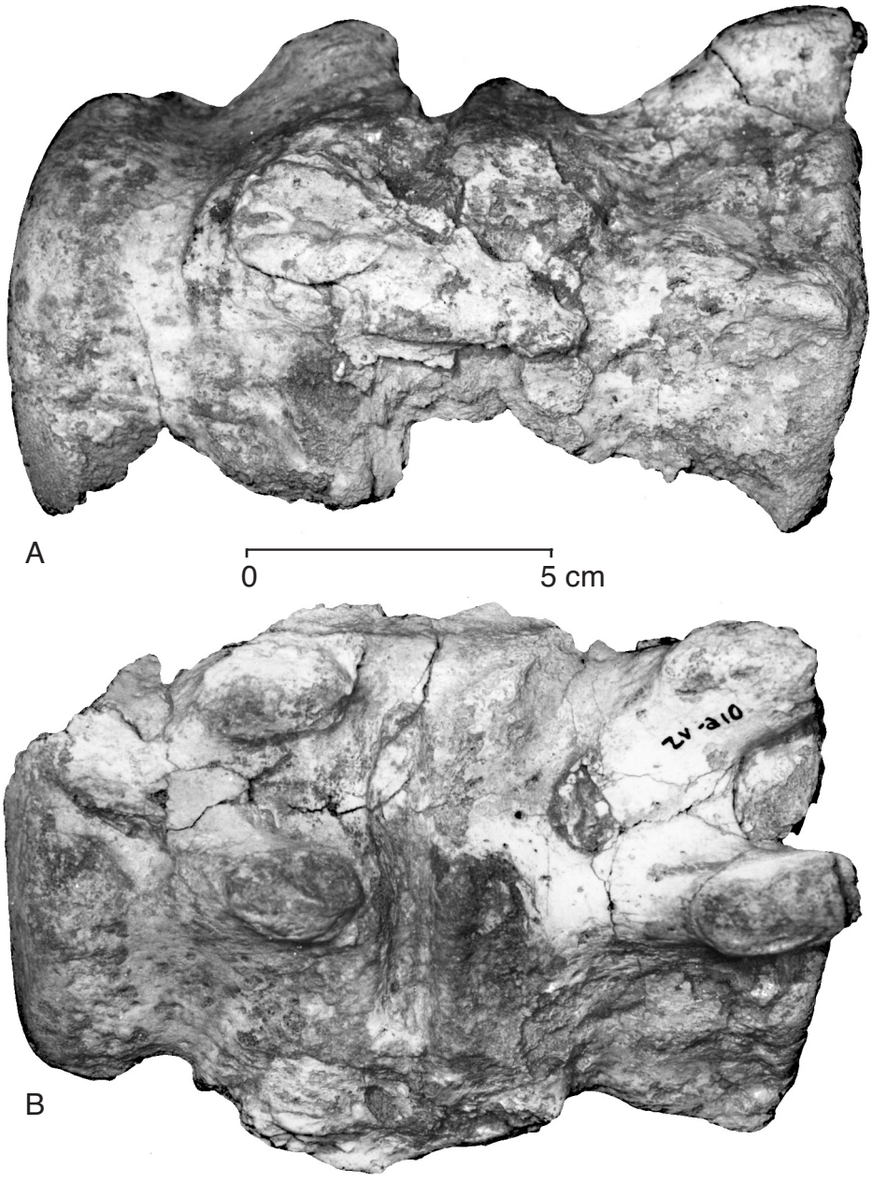

FIGURE 140 — Pathological caudal vertebrae of *Dorudon atrox*, UM 101215: A right lateral view, B left lateral view. These two vertebrae are fused and have a large volume of exostoseal bone around the fusion. Much of the volume of these vertebrae were weathered away, and the original injury has been obscured both by weathering and new bone growth.

UM 94811 could have been made by an archaeocete tooth. The mark appears to have been made by a blunt tooth since the depression is shallow and broadly convex rather than conical. The size of the bite mark is consistent with it being made by a worn tooth of *Basilosaurus isis*, such as the upper incisors, C^1, or P^1. More posterior teeth do not usually wear down enough to have been blunt enough to make the bite mark. The bite mark on UM 100139 is very different from that on UM 94811, but it too could have been made by an archaeocete. It appears to have been made by a conical upper tooth, rather than a blunt tooth. Any of the upper incisors or canine of *Basilosaurus isis* or an adult *Dorudon atrox* could have made this bite mark. It is

unclear whether these marks were made during life by a predator or after death by a scavenger.

Evidence of non-lethal predation or injury

A few other pathological specimens of *Dorudon atrox* have been recovered. Two of these specimens (UM 101222 and UM 101215) are full adults and the other is a juvenile (UM 93220) erupting M^2 and M_3.

One of the adults, UM 101222, exhibits three pathological conditions, two of which may be related, while the third is certainly not. The right dentary of this individual (Figure 138) has a broken and subsequently worn P_1. In addition, the ventral margin of the dentary appears to have been crushed over a small area directly below P_1. It is difficult to determine the true extent of the damage to the dentary because the injury is near the posterior margin of the mandibular symphysis, which gives the bone an odd texture to begin with, and the dentary has undergone postdepositional breakage. It may be that a single injury during prey capture or food processing both caused the tooth to break and the dentary to be compromised.

The third condition seen in UM 101222 is an exostosis on the centrum of thoracic vertebra 13 (Figure 139A). The exostosis is located on the caudal end of the ventral side of the centrum. It projects caudally and laterally. It is somewhat irregular in shape and is surrounded by remodeled bone that is pitted. The bone is nearly normal in appearance anterior to the exostosis and much more remodeled caudal and lateral to the exostosis. A groove nearly parallel to the caudal epiphysis runs up the right side of the centrum and becomes so shallow that it disappears as it angles towards the caudal epiphysis near the dorsum of the centrum. It is unclear whether this pathology is due to an injury, developmental anomaly, or ossification of connective tissue. Unfortunately, the vertebra caudally adjacent to T13 is not preserved in this specimen. T12 and the other thoracic vertebrae completely lack any similar pathology.

A juvenile individual, UM 93220, exhibits a non-lethal pathology in which ribs 10, 11, and 12 were broken and healed during life (Figure 139B). Each rib has a large swelling of the shaft approximately one third of the length of the shaft from the proximal end. All of the swellings line up when the ribs are articulated with the thoracic vertebrae, so it appears that they are all due to a single injury.

Lastly, the other adult, UM 101215, has two fused caudal vertebrae, caudals 10 and 11. These vertebrae are shown in Figure 140. Much of the left sides and ventral sides of these vertebrae have been destroyed by weathering. What remains shows that these vertebrae were completely fused during life. Exostoseal bone is present over the right side of the gap between the edges of the caudal epiphysis of Ca10 and the anterior epiphysis of Ca11. There is no room between the epiphysis for an intervertebral disk. There is also extra bone growth on the left side of the dorsal surface of the vertebrae. Ca10 has an open neural arch and Ca 11 is closed on its posterior end on the left side. There is no obvious evidence of injury, but it is possible that evidence of injury was on the weathered portions of these vertebrae or the evidence has been obscured by subsequent bone growth.

VI

PHYLOGENY

INTRODUCTION

The primary goal of phylogenetic analysis is to discover the pattern of relationships among the organisms under study. Previous phylogenetic analyses of archaeocete whales are reviewed here and a new analysis is presented to accomplish two goals. The first is to provide a phylogenetic framework upon which the taxonomy of archaeocetes discussed earlier is based. The taxonomic philosophy followed here is that all members of a taxonomic group should be derived from a common ancestor, that is taxonomic groups should be non-polyphyletic. A phylogenetic analysis is necessary to determine if taxonomic groups meet this criterion. The second goal is to provide a method of testing evolutionary hypotheses. Particularly, hypotheses regarding the origins of Odontoceti and Mysticeti from Archaeoceti are dependant on a well-supported phylogeny of archaeocetes, and in particular, dorudontines.

NON-CLADISTIC PHYLOGENETIC HYPOTHESES

Many authors have speculated about the broad evolutionary relationships of Archaeoceti to other mammals, and to Mysticeti and Odontoceti, but few have performed detailed phylogenetic analyses to determine the relationships among archaeocetes. Stromer (1908, p. 152) illustrated his conception of the phylogenetic relationships among the species of archaeocetes that had been described at that time. He presented the information in a chart showing stratigraphy (and thus relative time) in the vertical dimension, and geography separated into three areas (Egypt, North America, and England) in the horizontal dimension. This diagram is problematic because many of the taxa in this figure have now been synonomized ("*Zeuglodon*" *zitteli* = "*Zeuglodon*" *osiris* = *Saghacetus osiris* [Gingerich, 1992]). Others have been separated into different genera (*Basilosaurus*, *Saghacetus*, *Pontogeneus*, *Dorudon*). In addition, it is unclear how Stromer arrived at his conclusions about the relationships among the taxa.

Kellogg (1936) reviewed the possible relationships of Archaeoceti to different groups from marsupials and edentates to carnivores and ungulates. He also reviewed the possible relationship of archaeocetes to Mysticeti and Odontoceti, but he made no firm conclusions on any of these possible relationships. Kellogg also failed to elucidate any relationships among archaeocetes beyond his placement of individual species into one of three families: Protocetidae, the ancestral archaeocete group; Dorudontidae, the derived group with normally-proportioned vertebrae; and Basilosauridae, the derived group with elongate vertebrae. He hinted that basilosaurids are derived from dorudontines in one discussion, while describing this relationship as "distant" in another.

More recent phylogenetic reconstructions include those of Barnes and Mitchell (1978), Barnes et al., (1985), and Marino et al. (2003). The phylogeny of Barnes and Mitchell (1978) includes many archaeocetes identified at the species level, but they did not critically evaluate the validity of these species. Since then, many of the species listed by Barnes and Mitchell have been synonomized with other taxa (Gingerich, 1992; Uhen, 1998). In addition, the method of phylogenetic reconstruction utilized by Barnes and Mitchell is ill-defined at best. Barnes et al. (1985) showed a phylogeny of Cetacea at the family level, with a dashed line leading toward modern cetaceans that curves from Protocetidae, hinting that modern cetaceans were derived from Protocetidae. Yet, they stated in the text that the modern suborders are likely to be derived from the Dorudontinae (p. 19). Marino et al. (2003) recently published a phylogenetic tree of all currently recognized fossil and recent cetacean families (essentially an update to Barnes et al., [1985]), but this tree too suffers from the fact that it is a compilation of a multitude of previous phylogenetic analyses rather than a new analysis of all available data.

Finally, there have been several good reviews of fossil cetaceans including Fordyce and Barnes (1994) and Fordyce and de Muizon (2001) that include helpful discussions of the paleobiology of extinct cetaceans, their stratigraphic ranges, and even their interrelationships, but they also lack a phylogenetic analysis.

CLADISTIC PHYLOGENETIC HYPOTHESIS

Since older phylogenetic analyses of archaeocetes have some shortcomings, and many new taxa have recently been described, more recent phylogenetic analysis of archaeocetes better meet the goals outlined above. Recent phylogenetic analyses of archaeocetes have been presented by Hulbert (1994); Luo and

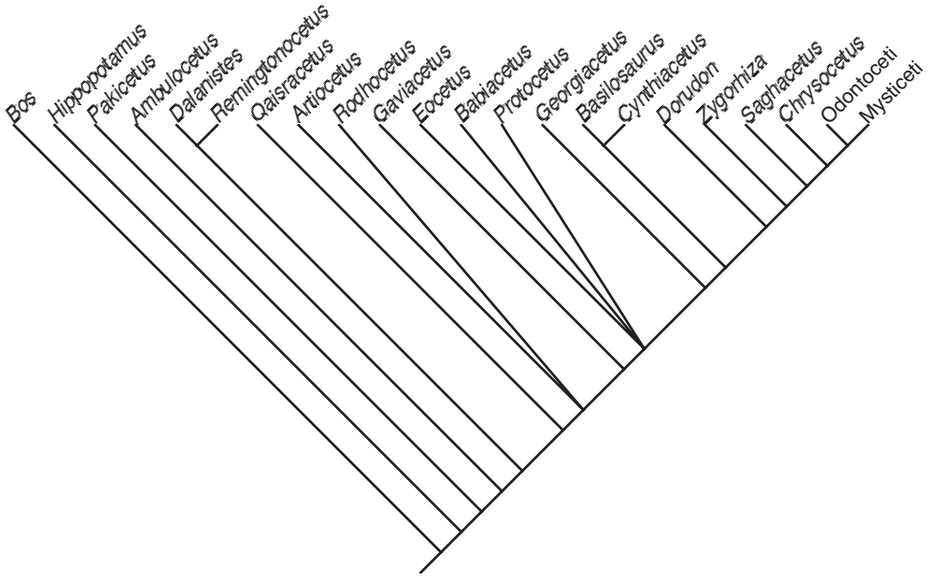

FIGURE 141 — Strict consensus cladogram of six equally overall most parsimonious cladograms resulting from the procedure outlined in the text. The stratigraphic character was not included in the morphological cladistic analysis. Basilosaurinae is represented by *Basilosaurus*. Basilosaurines have elongate posterior thoracic, lumbar and anterior caudal vertebrae. Dorudontinae are a paraphyletic assemblage including *Dorudon* that give rise to Neoceti and Basilosaurinae. Note that *Dorudon* is the sister taxon to the rest of the Dorudontinae, with the exception of *Pontogeneus*, which groups with *Basilosaurus*. Neoceti (Odontoceti + Mysticeti) arise from within the Dorudontinae. Early Neoceti share a number of derived features with basilosaurids and lack the autapomorphic features of basilosaurines.

Gingerich (1999); O'Leary and Geisler (1999; reviewed by Gatsey and O'Leary, 2001); Uhen and Gingerich (2001) in their work on *Chrysocetus healyorum*; Geisler (2001) in an analysis of the origins of Cetacea; and by Thewissen et al. (2001) in their work on *Pakicetus* and *Ichthyolestes*. Hulbert (1994) used cladistic analysis to form a hypothesis of sister group relationships among many of the archaeocete taxa known at that time. Hulbert's analysis supported the paraphyly of the primitive Protocetidae, and the monophyly of Basilosauridae. Unfortunately, this work has only been published as an abstract, so a critical evaluation of the characters used is not possible. Luo and Gingerich (1999) present a thorough description of characters and a cladistic analysis, but their study only includes cranial characters, and does not include all of the relevant basilosaurid taxa. The studies by O'Leary and Geisler (1999), Uhen and Gingerich (2001), and Geisler (2001) all suffer because they were published prior to the publication of work by Gingerich et al., (2001) and Thewissen et al. (2001) that clearly identify artiodactyls (or some subset thereof) as the sister taxa to Cetacea. Gingerich et al. (2001) do not include an explicit phylogenetic analysis and Thewissen et al. (2001) do not include all of the taxa relevant to this study of *Dorudon atrox*. The most recent phylogenetic analysis of Cetacea is that of Geisler and Sanders (2003). This study includes only two archaeocetes (*Georgiacetus* and *Zygorhiza*), and concentrates mainly on the Neoceti.

Since all previous phylogenetic analyses of Cetacea (particularly archaeocetes) are lacking in some way, a new analysis was performed here. This analysis is based on the study of Uhen and Gingerich (2001), with the mesonychian outgroup used there replaced with an artiodactyl outgroup, and with new information on *Rodhocetus* from Gingerich et al. (2001), and *Pakicetus* from Thewissen et al. (2001), and the new taxon *Artiocetus* from Gingerich et al. (2001). The new taxa and character codings are listed in Appendix VIII. All character descriptions and character codings follow Uhen and Gingerich (2001). Hypothetical ancestral odontocetes and mysticetes were included to generally assess the relationship of archaeocetes to the modern suborders.

Stratocladistic analyses must be performed in multiple steps since no phylogenetic analysis program includes both optimal tree finding algorithms and the stratigraphic character type. First, a preliminary phylogenetic analysis was performed on 22 taxa using the morphologic characters from Uhen & Gingerich (2001) using PAUP 4.0b3 (Swofford, 2000). Character states for additional taxa are listed in Appendix VIII. Two artiodactyl genera (*Bos* and *Hippopotamus*) were considered outgroup taxa, while the rest (20) were ingroup taxa. Characters were equally weighted, and multistate characters were ordered. Characters were chosen that vary in state among taxa in the analysis. A branch and bound search was performed, which guarantees to find the optimal tree. 229 morphologically most

parsimonious trees of length 176 were found. The matrix and these trees were then taken into MacClade 4.0 (Maddison and Maddison, 2000), where the stratigraphic character (character 69) was added. The trees with the stratigraphic character added ranged in length from 217 to 222. These trees were further explored by in MacClade and by swapping branches by hand. Six overall most parsimonious topologies of length 217 were found, although others may exist. These six trees were taken back into PAUP, where a strict consensus was computed, which is shown in Figure 141. The trees differ in the relative positions of *Eocetus*, *Protocetus*, and *Babiacetus*, as well as *Artiocetus* and *Rhodocetus*.

Relationships among the Dorudontinae are not well-defined, either by morphology or stratigraphy. Different rearrangements among the Dorudontinae result in phylogenetic trees that are only one or two steps longer than the tree shown. In addition, the relationships among the Dorudontinae cannot be determined until the taxa within the Dorudontinae are clearly delimited. Currently, *Dorudon serratus* is not included in the analysis because it is only known from a handful of deciduous teeth and cranial fragments. The last time *Dorudon serratus* was compared to *Zygorhiza kochii*, they were thought to be very different (True, 1908), but the teeth of *D. serratus* were not recognized as deciduous teeth. Most of the characters listed to distinguish the two species distinguish between juvenile and adult dorudontines, so it is possible that this species is a senior synonym of *Zygorhiza kochii*. *Pontogeneus brachyspondylus*, known from both North America and Egypt is a large dorudontine with trunk vertebrae that lack the elongation seen in the trunk vertebrae of *Basilosaurus*.

Many characters indicate that the Odontoceti and Mysticeti form a monophyletic group that is derived from Dorudontinae. These characters include: loss of the sacrum, rotation of the pelvis, reduction of the pelvic girdle and hind limb, presence of multiple accessory denticles on the cheek teeth (later lost in odontocetes and mysticetes), radius and ulna articulating with the humerus in a common trochlea, and lack of saddle-shaped articular surfaces on the carpals. Uhen and Gingerich (2001), linked *Chrysocetus* to Neoceti based on the shared derived character of monophyodonty, a condition not found in any other dorudontine.

Dorudon occupies an important position in these phylogenetic trees. In the more conservative hypothesis (Figure 141A) is the sister taxon and in the more liberal hypothesis (Figure 141B) is the ancestor to the other dorudontines plus neocetes. It is also important to note that the position of *Basilosaurus* (not to mention *Pontogeneus*, which is not included in this analysis) is not well fixed either. Trees of only a single step longer than those shown here place *Dorudon* as the ancestor to all other basilosaurids plus neocetes. Further study of *Basilosaurus* (which was last extensively reviewed by Kellogg in 1936) and more information on *Saghacetus* (which has never been adequately redescribed since the genus was named by Gingerich in 1992) and *Pontogeneus* (noted as a problem previously by Uhen, 1998) will hopefully clarify the positions of all dorudontines. When combined with information from studies like that of Geisler and Sanders (2003) on early Neoceti, the relationships of dorudontines to the origin of modern cetacean groups should become clear.

VII

SUMMARY

Dorudon atrox occupies a transitional position in the evolution of cetaceans. It is one of the earliest fully-aquatic cetaceans and it is much more primitive than modern cetaceans. Despite this conclusion about its position in cetacean history, one should not view *Dorudon atrox* as a poorly-adapted version of a modern cetacean. *Dorudon atrox* has aquatic adaptations shared with modern cetaceans, and other characteristics that are not. These others are not inferior to those adaptations seen in modern cetaceans, just different. *Dorudon atrox* individuals were adequately adapted to living in the warm shallow seas of the Eocene of Egypt.

Dorudon atrox has anatomical features that suggest it was completely aquatic. The hind limbs of *D. atrox* are very reduced and not connected to the vertebral column, and thus could not have supported the weight of the body on land. In addition, the forelimbs of *D. atrox* are modified into flippers that would be ineffective in supporting the body on land. Movement at the elbow is restricted such that pronation and supination were not possible. Also, the carpals lack saddle-shaped articular surfaces that would allow the manus to be oriented at an angle to the forearm to be used in supporting the body on land.

In addition to lacking these anatomical features that would allow *Dorudon atrox* to come out onto land, *D. atrox* also has features that facilitate life in the water. The external nares are positioned far posterior on the snout to facilitate breathing. The sternum is large and dense, which weighs down the ventral midline to keep the body trim in the water. The forelimbs are modified into flippers that are effective hydrofoils for steering while swimming. The system that is one of the most different from primitive terrestrial mammals is the hearing system. All of the differences in the auditory region between *D. atrox* and terrestrial mammals are shared with modern cetaceans. *D. atrox* has a large, dense auditory bulla that is loosely attached to the basicranium. In addition, the auditory ossicular chain is rotated such that it would have pulled the tympanic membrane into a cone in life. These features are thought to adjust the auditory apparatus for effective sound perception under water.

Dorudon atrox shares many of the osteological features of this system with modern cetaceans. The mandible has a large mandibular foramen and mandibular canal, as well as thin bone on the lateral wall of the mandible over the foramen. As noted earlier, *D. atrox* has a large, dense auditory bulla. These features indicate that *D. atrox* used a mandibular sound channel like modern cetaceans, and was fully capable of directional sound perception under water.

The cochlea of *Dorudon atrox* is very tall relative to the breadth of the basal turn, and the width of the basilar membrane is very wide in the basal turn of the cochlea. These osteological features indicate that *D. atrox* could perceive a range of sound frequencies that are comparable to those of modern mysticetes and that *D. atrox* could not hear the very high frequencies that are perceived by modern odontocetes.

Feeding in *Dorudon atrox* is different from both primitive mammals and modern cetaceans. The skull and jaws of *D. atrox* are elongated, with the anterior teeth in line with the cheek teeth. This is a feature seen in many piscivores, including modern odontocetes, suggesting that *D. atrox* was also piscivorous. This is confirmed by the presence of fish bones in the remains identified as stomach contents in *D. atrox*. The upper and lower anterior teeth interlock when the jaws are closed and moved slightly forward. *D. atrox* used these anterior teeth for prey acquisition and subsequently moved prey items to the back of the oral cavity for processing. The cheek teeth of *Dorudon atrox* are buccolingually-compressed, serrated blades that sheared large food items into smaller pieces when the lower jaws were brought into occlusion with the uppers. This is very different from feeding in odontocetes. Most odontocetes use their teeth only during prey acquisition, and then swallow prey whole.

Locomotion in *Dorudon atrox* was basically like that of modern cetaceans. The vertebral column of *D. atrox* shows many characters typical of modern cetaceans including a great increase in the number of lumbar vertebrae; relatively uniform vertebral body size in the posterior thoracic, lumbar, and anterior caudal vertebrae; and dorsoventrally compressed posterior caudal vertebrae. More lumbar vertebrae also indicates the presence of greater epaxial and hypaxial muscle mass to move the tail. This is significant since modern cetaceans have abandoned primitive mammalian limb-based locomotion in favor of a new tail-based locomotion. The compressed posterior caudal vertebrae of *D. atrox* further indicate that *D. atrox* used its tail for locomotion, since in modern mammals, compressed posterior caudal vertebrae are found only within the tail flukes of mammals with tail-based propulsion. The processes for muscle attachment on the vertebrae of *Dorudon atrox* indicate that the epaxial muscles were arranged in a more primitive manner

in *D. atrox* than in modern cetaceans. Modern cetaceans have a complex system of tendons and connective tissue sheaths that many muscles attach to. Well-developed processes on the vertebrae of *D. atrox* indicate that muscles attached directly to the vertebrae, and thus that *D. atrox* lacked this complex tendon system.

Phylogenetic analysis indicates that *Dorudon atrox* is an early occurring member of the family Basilosauridae. This family includes the subfamily Dorudontinae, and *Dorudon atrox* is the sister taxon to other known dorudontines. Basilosaurids are the earliest occurring cetaceans that had adopted a fully aquatic lifestyle. The reduced hind limbs and modifications of the forelimb mentioned above in relation to *D. atrox* are characteristic of the whole family Basilosauridae. Phylogenetic analysis also indicates that Dorudontinae was ancestral to modern cetaceans.

There are three key points in the evolutionary history of Cetacea that involve dramatic shifts in behavior, ecology, and anatomy. The first is the initial invasion of aquatic habitats by the terrestrial ancestors of Archaeoceti. This transition has recently become much better known from studies of early cetaceans from Indo-Pakistan. This transition is proving to be rather complex, with numerous lineages of cetaceans evolving in different directions. The second key point is the adoption of a fully aquatic existence. Studies such as this one of *Dorudon atrox* are pivotal for an understanding this period of cetacean evolution. Studies of other basilosaurids may show that this transition is similar to the origin of Cetacea in complexity. The last key point in cetacean evolution is the origin of the modern suborders of Cetacea. The fossil record of early mysticetes and odontocetes is currently improving. The fossils now known suggest a very complex early history for these groups. More studies of dorudontine archaeocetes are essential to the study of early mysticetes and early odontocetes, since both groups are thought to have originated from dorudontines.

VIII

LITERATURE CITED

ABEL, O. 1914. Die vorfahren der bartenwale. Denkschriften der Kaiserlichen Akademie der Wissenschaften Mathematisch-Naturwissenschaftliche Klasse, 90: 155-224.

ALLISON, P. A., C. R. SMITH, H. KUKERT, J. W. DEMING, and B. BENNETT. 1991. Deep-water taphonomy of vertebrate carcasses: a whale skeleton in the bathyal Santa Catalina Basin. Paleobiology, 17(1): 78-89.

ANDREWS, C. W. 1904. Further notes on the mammals of the Eocene of Egypt. Geological Magazine, London, Series 5, 1: 211-215.

———. 1906. A Descriptive Catalogue of the Tertiary Vertebrata of Fayum, Egypt. British Museum of Natural History, London, 324 pp.

ARKOWITZ, R. and S. ROMMEL. 1985. Force and bending moment of the caudal muscles in the shortfin pilot whale. Marine Mammal Science, 1(3): 203-209.

ARVY, L. 1979. The abdominal bones of Cetaceans. Investigations on Cetacea, 10: 215-227.

AU, D. and W. PERRYMAN. 1982. Movement and speed of dolphin schools responding to an approaching ship. Fishery Bulletin, 80(2): 371-379.

BARLOW, J. and P. BOVENG. 1991. Modeling age-specific mortality for marine mammal populations. Marine Mammal Science, 7(1): 50-65.

BARNES, L. G., D. P. DOMNING, and C. E. RAY. 1985. Status of studies on fossil marine mammals. Marine Mammal Science, 1(1): 15-53.

BARNES, L. G. and E. D. MITCHELL. 1978. Cetacea. *In*: V. J. Maglio and H. B. S. Cooke (eds.), Evolution of African Mammals, Harvard University Press, Cambridge, pp. 582-602.

BEADNELL, H. J. L. 1905. The Topography and Geology of the Fayum Province of Egypt. Survey Department Egypt, Cairo, 101 pp.

BENKE, H. 1993. Investigations on the osteology and the functional morphology of the flipper of whales and dolphins (Cetacea). Investigations on Cetacea, 24: 9-252.

BENNETT, M. B., R. F. KER, and R. M. ALEXANDER. 1987. Elastic properties of structures in the tails of cetaceans (*Phocaena* and *Lagenorhynchus*) and their effect on the energy cost of swimming. Journal of Zoology, London, 211: 177-192.

BERGGREN, W. A., D. V. KENT, C. C. SWISHER III, and M.-P. AUBRY. 1995. A revised Cenozoic geochronology and chronostratigraphy. *In*: W. A. Berggren, D. V. Kent, M.-P. Aubry, and J. Hardenbol (eds.), Geochronology, Time Scales and Global Stratigraphic Correlation, Society for Sedimentary Geology, Tulsa, pp. 129-212.

BIOSCAN. 1992. Optimas User's Guide. BioScan Incorporated, Edmonds, Washington, 338 pp.

BONAPARTE, C. L. 1849. [Classification af Havapatedyrene i Pinnipedia, Cete og Sirenia]. Forhandlinger ved de skandinaviske Naturforskeres femte Møde Kjøbenhaven, 1847: 618 pp.

———. 1850. Conspectus Systematis. E. J. Brill, Leiden, 1 p.

BRANDT, J. F. 1873. Untersuchungen über die fossilen und subfossilen cetaceen Europa's. Mémoires de L'Académie Impériale des Sciences de Saint-Petersbourg, Series 7, 20(1): 1-372.

BREATHNACH, A. S. 1955. Observations on endocranial casts of recent and fossil cetaceans. Journal of Anatomy, 89(4): 532-546.

BROMAGE, T. G. 1991. Enamel incremental periodicity in the pig-tailed macaque: a polychrome fluorescent labeling study of dental hard tissues. American Journal of Physical Anthropology, 86: 205-214.

——— and M. C. DEAN. 1985. Re-evaluation of the age at death of immature fossil hominids. Nature, 317: 525-527 pp.

BUCHHOLTZ, E. A. 1998. Implications of vertebral morphology for locomotor evolution in early Cetacea. *In*: J. G. M. Thewissen (ed.), The Emergence of Whales: Evolutionary Patterns in the Origin of Cetacea, Plenum Press, New York, pp. 325-352.

BUFFRÉNIL, V. D., A. COLLET, and M. PASCAL. 1985. Ontogenetic development of skeletal weight in a small delphinid, *Delphinus delphis* (Cetacea, Odontoceti). Zoomorphology, 105: 336-344.

BUFFRÉNIL, V. D., A. D. RICQLES, C. E. RAY, and D. P. DOMNING. 1990. Bone histology of the ribs of the archaeocetes (Mammalia: Cetacea). Journal of Vertebrate Paleontology, 10(4): 455-466.

CALDWELL, D. K. and D. H. BROWN. 1964. Tooth wear as a correlate of described feeding behavior by the killer whale, with notes on a captive specimen. Southern California Academy of Sciences, 63(3): 128-140.

———, J. N. LAYNE, and J. B. SIEBENALER. 1956. Notes on a killer whale (*Orcinus orca*) from the northeastern Gulf of Mexico. The Quarterly Journal of the Florida Academy of Sciences, 19(4): 189-196.

CARLSON, S. J. 1990. Skeletal Biomineralization: Patterns, Processes and Evolutionary Trends, Volume I. *In*: Carter, J. G., (ed.), Vertebrate Dental Structures. Van Nostrand Reinhold, New York, 531-556 pp.

CARPENTER, K. and D. WHITE. 1986. Feeding in the archaeocete whale *Zygorhiza kochii* (Cetacea: Archaeoceti). Mississippi Geology, 7(2): 1-15.

COPE, E. D. 1867(1868). An addition to the vertebrate fauna of the Miocene period, with a synopsis of the extinct Cetacea of the United States. Proceedings of the Academy of Natural Sciences of Philadelphia, 19: 138-156.

———. 1868. Second contribution to the history of the Vertebrata of the Miocene period of the United States. Proceedings of the Academy of Natural Science of Philadelphia, 20: 184-194.

CUNNINGHAM, D. J. 1877. The spinal nervous system of the porpoise and dolphin. Journal of Anatomy and Physiology, 11: 207-228.

DAMES, W. B. 1894. Über Zeuglodonten aus Aegypten und die Beziehungen der Archaeoceten zu den übrigen Cetaceen. Palæontologische Abhandlungen Jena n. F., 1(5): 189-222.

DART, R. A. 1923. The brain of the Zeuglodontidae (Cetacea). Proceedings of the Zoological Society of London, 42(33): 615-654.

DAWSON, S. D. 1993. Functional Morphology and Evolution of Marine Mammal Limb Bones: Adaptations to Aquatic Locomotion in Recent and Fossil Cetaceans. Ph.D. dissertation, University of Pennsylvania, Philadelphia.

DOMNING, D. P. 1982. Evolution of manatees: a speculative history. Journal of Paleontology, 56(3): 599-619.

——— and V. D. BUFFRÉNIL. 1991. Hydrostasis in the Sirenia: Quantitative data and functional interpretations. Marine Mammal Science, 7(4): 331-368.

———, G. S. MORGAN, and C. E. RAY. 1982. North American Eocene sea cows (Mammalia, Sirenia). Smithsonian Contributions to Paleobiology, 52: 1-69.

EALES, N. B. 1950. The skull of the foetal narwhal *Monodon monoceros* L. Philosophical Transactions of the Royal Society of London, 235(621): 1-33.

EMILY, P. and S. PENMAN. 1994. Handbook of Small Animal Dentistry. Pergamon Press, Oxford, 117 pp.

EVANS, H. E. 1993. Miller's Anatomy of the Dog. W. B. Saunders Company, Philadelphia, 1113 pp.

FISH, F. E. and C. A. HUI. 1991. Dolphin swimming--a review. Mammal Review, 21(4): 181-195.

FISHER, D. C. 1988. Season of death of the Hiscock mastodonts. Late Pleistocene and Early Holocene Paleoecology and Archeology of the Eastern Great Lakes Region. Bulletin of the Buffalo Society of Natural Sciences, 33: 115-125.

———. 1992. Stratigraphic Parsimony. *In*: Maddison, W. P. and D. R. Maddison, (MacClade 3.0 Manual. Sinauer Associates, Sunderland, MA, pp. 124-129.

FITCH, J. E. and R. L. BROWNELL. 1968. Fish otoliths in cetacean stomachs and their importance in interpreting feeding habits. Journal of the Fisheries Research Board, Canada, 25(12): 2561-2574.

FLEISCHER, G. 1973. Structural analysis of the tympanicum complex in the bottle-nosed dolphin (*Tursiops truncatus*). Journal of Auditory Research, 13: 178-190.

———. 1976. Hearing in extinct cetaceans as determined by cochlear structure. Journal of Paleontology, 50(1): 133-152.

FLOWER, W. H. 1876. An Introduction to the Osteology of the Mammalia. MacMillan and Co., London, 344 pp.

———. 1883. On the arrangement of the orders and families of existing Mammalia. Proceedings of the Zoological Society of London, 1883: 178-186.

FORDYCE, R. E. 1994. *Waipatia maerewhenua*, new genus and new species (Waipatiidae, new family), an archaic late Oligocene dolphin (Cetacea: Odontoceti: Platanistoidea) from New Zealand. Proceedings of the San Diego Society of Natural History, 29: 147-176.

——— and L. G. BARNES. 1994. The evolutionary history of whales and dolphins. Annual Review of Earth and Planetary Sciences, 22: 419-455.

——— and C. MUIZON DE. 2001. Evolutionary history of cetaceans: a review. *In*: Mazin, J.-M. and V. Buffrénile, (eds.), Secondary Adaptation of Tetrapods to Life in Water. Verlag Dr. Friedrich Pfeil, München, Germany, pp 169-223.

FRAAS, E. 1904. Neue Zeuglodonten aus dem unteren Mittelecocän vom Mokattam bei Cairo. Geologische und Palæontologische Abhandlungen, Jena, Neue Folge, 6(3): 199-220.

FRASER, F. C. and P. E. PURVES. 1960. Anatomy and function of the cetacean ear. Proceedings of the Royal Society of London, 152b: 62-77.

GAMBARYAN, P. P. 1974. How Mammals Run: Anatomical Adaptations. John Wiley & Sons, New York, 367 pp.

GATESY, J. 1998. Molecular evidence for the phylogenetic affinities of Cetacea. *In*: J. G. M. Thewissen (ed.), The Emergence of Whales: Evolutionary Patterns in the Origin of Cetacea, Plenum Press, New York, pp. 63-112.

——— and M. A. O'LEARY. 2001. Deciphering whale origins with molecules and fossils. Trends in Ecology & Evolution, 16(10): 562-570.

GAWN, R. W. L. 1948. Aspects of the locomotion of whales. Nature, 161(4080): 44-46.

GEISLER, J. H. 2001. New morphological evidence for the phylogeny of Artiodactyla, Cetacea, and Mesonychidae. American Museum Novitates, 3344: 1-53.

——— and A. E. SANDERS. 2003. Morphological evidence for the phylogeny of Cetacea. Journal of Mammalian Evolution, 10(1): 23-129.

GETTY, R. 1975. The Anatomy of the Domestic Animals. W. B. Saunders, Philadelphia, 2095 pp.

GIBBES, R. W. 1845. Description of the teeth of a new fossil animal found in the Green Sand of South Carolina. Proceedings of the Academy of Natural Sciences, Philadelphia, 2: 254-256.

———. 1847. On the fossil genus *Basilosaurus*, Harlan, (*Zeuglodon*, Owen) with a notice of specimens from the Eocene Green Sand of South Carolina. Journal of the Academy of Natural Sciences of Philadelphia, 1 (new series): 2-15.

GIFFIN, E. B. 1992. Functional implications of neural canal anatomy in recent and fossil marine carnivores. Journal of Morphology, 214: 357-374.

——— and M. GILLETT. 1995. Exceptions to the rule of seven: defining "cervical" in mammals with non-traditional vertebral counts (abstract). Journal of Vertebrate Paleontology, 15(3): 31A-32A.

GILL, T. 1872. Arrangement of the families of mammals. Smithsonian Miscellaneous Collections, 11: 1-97.

GINGERICH, P. D. 1990. Prediction of body mass in mammalian species from long bone lengths and diameters. Contributions from the Museum of Paleontology, University of Michigan, 28(4): 79-92.

———. 1991. Provenance of Fourtau's Egyptian archaeocete. Investigations on Cetacea, 23: 213-214.

———. 1992. Marine mammals (Cetacea and Sirenia) from the Eocene of Gebel Mokattam and Fayum, Egypt: stratigraphy, age and paleoenvironments. University of Michigan Museum of Paleontology Papers on Paleontology, 30: 1-84.

———. 1998. Paleobiological perspectives on Mesonychia, Archaeoceti, and the origin of whales. *In* J. G. M. Thewissen (ed.), The Emergence of Whales: Evolutionary Patterns in the Origin of Cetacea, Plenum Publishing Corporation, New York, pp. 423-449.

———, M. ARIF, M. A. BHATTI, M. ANWAR, and W. J. SANDERS. 1997. *Basilosaurus drazindai* and *Basiloterus hussaini*, new Archaeoceti (Mammalia, Cetacea) from the middle Eocene Drazinda Formation, with a revised interpretation of ages of whale-bearing strata in the Kirthar Group of the Sulaiman Range, Punjab (Pakistan). Contributions from the Museum of Paleontology, University of Michigan, 30(2): 55-81.

———, M. ARIF, and W. C. CLYDE. 1995. New archaeocetes (Mammalia, Cetacea) from the middle Eocene Domanda Formation of the Sulaiman Range, Punjab (Pakistan). Contributions from the Museum of Paleontology, University of Michigan, 29(11): 291-330.

———, M. ul-HAQ, I. S. ZALMOUT, I. H. KHAN, and M. S. MALAKANI. 2001. Origin of whales from early artiodactyls: Hands and feet of Eocene Protocetidae from Pakistan. Science, 293: 2239-2242.

———, S. M. RAZA, M. ARIF, M. ANWAR, and X. ZHOU. 1994. New whale from the Eocene of Pakistan and the origin of cetacean swimming. Nature, 368: 844-847.

——— and D. E. RUSSELL. 1990. Dentition of early Eocene *Pakicetus* (Mammalia, Cetacea). Contributions from the Museum of Paleontology, University of Michigan, 28(1): 1-20.

———, B. H. SMITH, and E. L. SIMONS. 1990. Hind limbs of Eocene *Basilosaurus*: evidence of feet in whales. Science, 229: 154-157.

——— and M. D. UHEN. 1996. *Ancalecetus simonsi*, a new dorudontine archaeocete (Mammalia, Cetacea) from the early late Eocene of Wadi Hitan, Egypt. Contributions from the Museum of Paleontology, University of Michigan, 29(13): 359-401.

GIRAUD-SAUVEUR, D. 1969. Recherches biophysiques sur les osselets des cetaces. Mammalia, 33(2): 285-340.

GORDON, K. R. 1981. Locomotor behavior of the walrus (*Odobenus*). Journal of Zoology, London, 195: 349-367.

HARLAN, R. 1834. Notice of fossil bones found in the Tertiary formation of the state of Louisiana. Transactions of the American Philosophical Society Philadelphia, 4(12): 397-403.

HAZEL, J. E., L. M. BYBELL, R. A. CHRISTOPHER, N. O. FREDERICKSEN, F. E. MAY, D. M. MCLEAN, R. Z. POORE, C. C. SMITH, N. F. SOHL, P. C. VALENTINE, and R. J. WITMER. 1977. Biostratigraphy of the deep corehole (Clubhouse Crossroads corehole 1) near Charleston, South Carolina. United States Geological Survey Professional Paper, 1028(E): 71-89.

HILLSON, S. 1986. Teeth. Cambridge University Press, Cambridge, 376 pp.

HOFFMAN, M. A. 1983. Energy metabolism, brain size and longevity in mammals. The Quarterly Review of Biology, 58(4): 495-512.

HOHN, A. A., M. D. SCOTT, R. S. WELLS, J. C. SWEENEY, and IRVINE A. BLAIR. 1989. Growth layers in teeth from known-age, free-ranging bottlenose dolphins. Marine Mammal Science, 5(4): 315-342.

HOSOKAWA, H. 1951. On the extrinsic eye muscles of the whale, with special remarks on the innervation and function of the musculus retractor bulbi. Scientific Reports of the Whales Research Institute, 6: 1-33.

HOWELL, A. B. 1927. Contribution to the anatomy of the Chinese finless porpoise, *Neomeris phocaenoides*. Proceedings of the United States National Museum, 70(13): 1-43.

———. 1930. Myology of the narwhal (*Monodon monoceros*). The American Journal of Anatomy, 46(2): 187-215.

HUI, C. A. 1987. Power and speed of swimming dolphins. Journal of Mammalogy, 68(1): 126-132.

HULBERT, R. C. 1994. Phylogenetic analysis of Eocene whales ("Archaeoceti") with a diagnosis of a new North American protocetid genus. Journal of Vertebrate Paleontology, 14(3): 30A.

JANSEN, J. and JANSEN J. K. S. 1969. The nervous system of Cetacea. *In*: H. T. Anderson (ed.), The Biology of Marine Mammals, Academic Press, New York, pp. 175-252.

JERISON, H. J. 1973. Evolution of the Brain and Intelligence. Academic Press, New York, 428 pp.

JOHANNESSEN, C. L. and J. A. HARDER. 1960. Sustained swimming speeds in dolphins. Science, 132: 1550-1551.

KASUYA, T. 1973. Systematic consideration of recent toothed whales based on the morphology of tympano-periotic bone. Scientific Reports of the Whales Research Institute, 25: 1-103.

KATO, H. 1988. Ossification pattern of the vertebral epiphyses in the southern minke whale. Scientific Reports of the Whales Research Institute, 39: 11-19.

KELLOGG, R. 1928. The history of whales- Their adaptation to life in the water. The Quarterly Review of Biology, 3(1): 29-76.

———. 1936. A Review of the Archaeoceti. Carnegie Institute of Washington Special Publication, 482: 1-366.

KELLUM, L. B. 1926. Paleontology and stratigraphy of the Castle Hayne and Trent Marls in North Carolina. Unites States Geological Survey Professional Paper, 143: 1-56.

KLEIN, R. G. and CRUZ-URIBE KATHRYN. 1984. The Analysis of Animal Bones from Archeological Sites. The University of Chicago Press, Chicago, 266 pp.

KLEINENBERG, S. E., A. V. YABLOKOV, B. M. BEL'KOVICH, and M. N. TARASEVICH. 1964. Beluga (*Delphinapterus leucas*): Investigation of the Species. Academy of Sciences of the USSR, The A. N. Severtsov Institute of Animal Morphology, Moscow, 455 pp.

KLEVEZAL', G. A. and S. E. KLEINENBERG. 1967. Age determination of mammals from annual layers in teeth and bones. Academy of Science of the USSR. Severtsov Institute of Animal Morphology, Moscow, 128 pp.

KLIMA, M. 1990. Rudiments of the clavicle in the embryos of whales (Cetacea). Zeitschrift für Saügetierkunde, 55: 202-212.

———, H. A. OELSCHLÄGER, and D. WÜNSCH. 1980. Morphology of the pectoral girdle in the Amazon dolphin *Inia geoffrensis* with special reference to the shoulder joint and the movements of the flippers. Zeitschrift für Saügetierkunde, 45: 288-309.

KÖHLER, R. and R. E. FORDYCE. 1997. An archaeocete whale (Cetacea: Archaeoceti) from the Eocene Waihao Greensand, New Zealand. Journal of Vertebrate Paleontology, 17(3): 574-583.

LANCASTER, W. C. 1986. The taphonomy of an archaeocete skeleton and its associated fauna. *In*: J. A. Schiebout and W. van den Bold (eds.), Montgomery Landing Site, Marine Eocene (Jackson) of Central Louisiana, Proceedings of a Symposium, 36th Annual GCAGS. Gulf Coast Association of Geological Societies, Baton Rouge, Louisiana, pp. 119-131.

———. 1990. The middle ear of the Archaeoceti. Journal of Vertebrate Paleontology, 10(1): 117-127.

LANG, T. G. and K. S. NORRIS. 1966. Swimming speed of a Pacific bottlenose porpoise. Science, 151: 588-590.

——— and K. PRYOR. 1966. Hydrodynamic performance of porpoises (*Stenella attenuata*). Science, 152: 531-533.

LAW, T. C. and R. W. BLAKE. 1994. Swimming behaviors and speeds of wild Dall's porpoises (*Phocoenoides dalli*). Marine Mammal Science, 10(2): 208-213.

LEGENDRE, S. 1986. Analysis of mammalian communities from the late Eocene and Oligocene of southern France. Paleovertebrata, Montpellier, 16(4): 191-212.

LEIDY, J. 1852. [Description of *Pontogeneus priscus*]. Proceedings of the Academy of Natural Sciences of Philadelphia, 6: 52.

LING, J. K. 1974. The integument of marine mammals. *In*: R. J. Harrison (ed.), Functional Anatomy of Marine Mammals, Academic Press, London, pp. 1-44.

LUO, Z. and E. R. EASTMAN. 1995. Petrosal and inner ear of a squalodontoid whale: implications for evolution of hearing in odontocetes. Journal of Vertebrate Paleontology, 15(2): 431-442.

——— and P. D. GINGERICH. 1999. Terrestrial Mesonychia to aquatic Cetacea: transformation of the basicranium and evolution of hearing in whales. University of Michigan Papers on Paleontology, 31: 1-98.

MADDISON, W. P. and D. R. MADDISON. 2000. MacClade: Analysis of Phylogeny and Character Evolution Version 4.0. Sinauer Associates, Inc., Sunderland, Massachusetts, 398 pp.

MARINO, L. 1995. Brain-behavior relationships in cetaceans and primates: Implications for the evolution of complex intelligence. Unpublished dissertation, State University of New York, University at Albany, Albany, New York, 488 pp.

———. 1998. A comparison of encephalization between odontocete cetaceans and anthropoid primates. Brain, Behavior and Evolution, 51: 230-238.

———, M. D. UHEN, B. FROHLICH, J. M. ALDAG, C. BLANE, D. BOHASKA, and F. C. WHITMORE JR. 2000. Endocranial volume of mid-late Eocene archaeocetes (Order: Cetacea) revealed by computed tomography: implications for cetacean brain evolution. Journal of Mammalian Evolution, 7(2): 81-94.

———, M. D. UHEN, N. D. PYENSON, and B. FROHLICH. 2003. Reconstructing Cetacean Brain Evolution Using Computed Tomography. The Anatomical Record (Part B: New Anat.), 272B: 107-117.

MARPLES, B. J. 1949. Two endocranial casts of cetaceans from the Oligocene of New Zealand. American Journal of Science, 247: 462-471.

MARTIN, R. D. 1981. Relative brain size and basal metabolic rate in terrestrial vertebrates. Nature, 293: 57-60.

MCFARLAND, W. L., M. S. JACOBS, and P. J. MORGANE. 1979. Blood supply to the brain of the dolphin, *Tursiops truncatus*, with comparative observations on special aspects of the cerebrovascular supply of other vertebrates. Neuroscience and Biobehavioral Reviews, 3(Supplement 1): 1-93.

MEAD, J. G. 1989. Bottlenose whales *Hyperoodon ampullatus* (Forster, 1770) and *Hyperoodon planifrons* Flower, 1882. *In*: Ridgway, S. H. and S. R. Harrison, (eds.), Handbook of Marine Mammal*s*. Academic Press, London, pp. 321-348.

MILLER, G. S. JR. 1923. The telescoping of the cetacean skull. Smithsonian Miscellaneous Collections, 76(5): 1-71.

MIMURA, T. 1939. Horoshitsu ni mirareru Seicho-sen no shuki. Kobyo-shi, 13: 454-455.

MORGANE, P. J. and M. S. JACOBS. 1972. Comparative anatomy of the cetacean nervous system. *In*: Harrison, R. J., (ed.), Functional Anatomy of Marine Mammals. Academic Press, London, pp. 117-244.

MOUSTAFA, Y. S. 1954. Additional information on the skull of *Prozeuglodon isis* and the morphological history of the Archaeoceti. Proceedings of the Egyptian Academy of Sciences, 9: 80-89.

MÜLLER, J. 1851. Neue Beiträge zur Kenntniss der Zeuglodonten. Bericht über die zur Bekanntmachung geeigneten Verhandlungen der Akademie der Wissenschaften, Berlin, 28: 236-246.

NISHIWAKI, M. and T. KAMIYA. 1958. A beaked whale *Mesoplodon* stranded at Oiso Beach, Japan. Scientific Reports of the Whales Research Institute, 13: 53-83.

——— and T. KASUYA. 1970. A Greenland right whale caught at Osaka Bay. Scientific Reports of the Whales Research Institute, 22: 45-62.

NORRIS, K. S. 1968. The evolution of acoustic mechanisms in odontocete cetaceans. *In*: E. T. Drake (ed.), Evolution and Environment, Yale University Press, New Haven, pp. 297-224.

———. 1980. Peripheral sound processing in odontocetes. *In*: R.-G. Busnel and J. F. Fish (eds.), Animal Sonar Systems, Plenum Press, New York, pp. 495-509.

——— and B. MØHL. 1983. Can odontocetes debilitate prey with sound? The American Naturalist, 122(1): 85-104.

NOVACEK, M. J. 1977. Aspects of the problem of variation, origin and evolution of the eutherian auditory bulla. Mammal Review, 7(3 and 4): 131-149.

OHSUMI, S. 1960. Relative growth of the fin whale, *Balaenoptera physalus* (Linn.). Scientific Reports of the Whales Research Institute, 15: 17-84.

OKADA, M. 1943. Hard tissues of animal body. The Shanghai Evening Post, Special Edition, Health Recreation and Medical Progress: pp.15-31.

O'LEARY, M. A. and J. H. GEISLER. 1999. The position of Cetacea within mammalia: Phylogenetic analysis of morphological data from extinct and extant taxa. Systematic Biology, 48(3): 455-490.

——— and M. D. UHEN. 1999. The time of origin of whales and the role of behavioral changes in the terrestrial-aquatic transition. Paleobiology, 25(4): 534-556.

OMURA, H. 1958. North Pacific right whale. Scientific Reports of the Whales Research Institute, 13: 1-52.

———. 1975. Osteological study of the Minke whale from the Antarctic. Scientific Reports of the Whales Research Institute, 27: 1-36.

———, T. KASUYA, H. KATO, and S. WADA. 1981. Osteological study of the Bryde's whale from the central south Pacific and eastern Indian Ocean. Scientific Reports of the Whales Research Institute, 33: 1-26.

OWEN, R. 1839. Geological Society. The Athenaeum, 585: 35-36.

———. 1842a. Observations on the *Basilosaurus* of Dr. Harlan (*Zeuglodon cetoides*, Owen). Transactions of the Geological Society of London, 6: 69-79.

———. 1842b. Observations on the teeth of the *Zeuglodon*, *Basilosaurus* of Dr. Harlan. Proceedings of the Geological Society of London, 3(60): 23-28.

PABST, D. A. 1990. Axial muscles and connective tissues of the bottlenose dolphin. *In*: S. Leatherwood and R. K. Reeves (eds.), The Bottlenose Dolphin, Academic Press, San Diego, pp. 51-67.

PATTERSON, C. 1982. Morphological characters and homology. *In*: K. A. Joysey and A. E. Friday (ed.), Problems of Phylogenetic Reconstruction, Academic Press, London, pp. 21-74.

PILLERI, G. 1985. Record of *Dorudon osiris* (Archaeoceti) from Wadi-el-Nutrun, lower Nile Valley. Investigations on Cetacea, 17: 35-37.

———. 1991. Betrachtugen über das gehirn der Archeoceti (Mammalia, Cetacea) aus dem Fayum Ägyptens. Investigations on Cetacea, 23: 193-211.

POMPECKJ, J. F. 1922. Das Ohrskelett von Zeuglodon. Senckenbergiana, 20(3/4): 41-100.

PROMISLOW, D. E. L. and P. H. HARVEY. 1990. Living fast and dying young: A comparative analysis of life-history variation among mammals. Journal of Zoology, London, 220: 417-437.

PURVES, P. E. 1966. Anatomy and physiology of the outer and middle ear in cetaceans. *In*: K. S. Norris (ed.), Whales, Dolphins, and Porpoises, University of California Press, Berkeley, pp. 320-380.

REICHENBACH, L. 1847. Systematisches. *In*: Carus, C. G., (Resultate geologischer, anatomischer und zoologischer untersuchungen über das unter den Namen *Hydrarchos* von Dr. A. C. Koch zuerst nach Europa gebrachte und in Dresden augestelte grofse fossile Skelett. Arnoldische Buchhandlung, Dresden, pp. 15.

REIDENBERG, J. S. and J. T. LAITMAN. 1994. Anatomy of the hyoid apparatus in Odontoceti (toothed whales): Specializations of their skeleton and musculature compared with those of terrestrial mammals. Anatomical Record, 240(4): 598-624.

REYSENBACH DE HAAN, F. W. 1957. Hearing in whales. Acta Oto-Laryngologica Supplementum, 134: 9-114.

———. 1960. Some aspects of mammalian hearing under water. Proceedings of the Royal Society of London, 152b: 54-62.

RIDEWOOD, W. G. 1923. Observations on the skull in foetal specimens of whales of the genera *Megaptera* and *Balaenoptera*. Transactions of the Royal Society of London, 211(5): 209-272.

RIDGWAY, S. H. 1990. The central nervous system of the bottlenose dolphin. *In*: S. Leatherwood and R. R. Reeves (eds.), The Bottlenose Dolphin, Academic Press, San Diego, pp. 69-97.

——— and R. HOWARD. 1979. Dolphin lung collapse and intramuscular circulation during free diving: evidence from nitrogen washout. Science, 206: 1182-1183.

ROMMEL, S. 1990. Osteology of the bottlenose dolphin. *In*: S. Leatherwood and R. K. Reeves (eds.), The Bottlenose Dolphin, Academic Press, San Diego, pp. 29-49.

SACHER, G. A. 1959. Relation of lifespan to brain weight and body weight in mammals. *In*: Wolstenholme, G. E. W. and M. O'Connor, (eds.), Ciba Foundation colloquia on ageing, Volume 5, The Lifespan of Animals. Ciba Foundation, New York, pp. 115-133.

SANDERS, A. E. 1974. A paleontological survey of the Cooper Marl and Santee Limestone near Harleyville, South Carolina, preliminary report. Geologic Notes, 18(1): 4-12.

SCHÄFER, W. 1972. Ecology and Palaeoecology of Marine Environments. The University of Chicago Press, Chicago, 568 pp.

SHANE, S. H., R. S. WELLS, and B. WÜRSIG. 1986. Ecology, behavior and social organization of the bottlenose dolphin: a review. Marine Mammal Science, 2(1): 34-63.

SILVA, M. and J. A. DOWNING. 1995. CRC Handbook of Mammalian Body Masses. CRC Press, Boca Raton, Florida, 359 pp.

SIMPSON, G. G. 1953. The Major Features of Evolution. Simon and Schuster, New York, 434 pp.

SLIJPER, E. J. 1936. Die Cetaceen. Capital Zoologica, 7: 1-590.

———. 1946. Comparative biologic-anatomical investigations on the vertebral column and spinal musculature of mammals. N. V. Noord-Holland sche Uitgevers Maatschappij, Amsterdam, 42(5): 1-128.

———. 1961. Locomotion and locomotory organs in whales and dolphins (Cetacea). Symposia of the Zoological Society of London, 5: 77-94.
———. 1962. Whales. Cornell University Press, Ithica, New York, 511 pp.
SMITH, B. H. 1989. Dental development as a measure of life history in primates. Evolution, 43(3): 683-688.
———. 1992. Life history and evolution of human maturation. Evolutionary Anthropology, 1(4): 134-142.
———, T. L. CRUMMETT, and K. L. BRANDT. 1994. Ages of eruption of primate teeth: a compendium for aging individuals and comparing life histories. Yearbook of Physical Anthropology, 37: 177-231.
STRICKLER, T. L. 1980. The axial musculature of *Pontoporia blainvillei*, with comments on the organization of this system and its effect on fluke-stroke dynamics in the Cetacea. American Journal of Anatomy, 157: 49-59.
STROMER, E. 1903. Zeuglodon-reste aus dem Oberen Mitteleocän des Fajum. Beiträge zur Paläontologie und Geologie Österreich-Ungarns und des Orients, 15: 65-100.
———. 1908. Die Archaeoceti des Ägyptischen Eozäns. Beiträge zur Paläontolgie und Geologie Östrerreich-Ungarns und des Orients, 21: 1-70.
SWIFT, C. C. and L. G. BARNES. 1996. Stomach contents of *Basilosaurus cetoides*: implications for the evolution of cetacean feeding behavior, and evidence for vertebrate fauna of epicontinental Eocene seas (abstract). Sixth North American Paleontological Convention Abstracts of Papers. Paleontological Society Special Publication, 8: 380.
SWOFFORD, D. L. 2002. PAUP* Phylogenetic Analysis Using Parsimony (*and Other Methods). Sinauer Associates, Sunderland, Massachusetts, Version 4.0b10 pp.
SZALAY, F. S. 1969. The Hapalodectinae and a phylogeny of the Mesonychidae (Mammalia, Condylarthra). American Museum Novitates, 2361: 1-26.
TAYLOR, M. A. 1993. Stomach stones for feeding or buoyancy? Philosophical Transactions of the Royal Society, London B, 341: 163-175.
THEWISSEN, J. G. M. and P. D. GINGERICH. 1989. Skull and endocranial cast of *Eoryctes melanus*, a new paleoryctid (Mammalia: Insectivora) from the early Eocene of western North America. Journal of Vertebrate Paleontology, 9(4): 459-470.
——— and S. T. HUSSAIN. 1993. Origin of underwater hearing in whales. Nature, 361: 444-445.
———, J. G. M., S. I. MADAR, and S. T. HUSSAIN. 1996. *Ambulocetus natans,* an Eocene cetacean (Mammalia) from Pakistan. Courier Forschungsinstitut Senckenberg, 191: 1-86.
———, E. M. WILLIAMS, L. J. ROE, and S. T. HUSSAIN. 2001. Skeletons of terrestrial cetaceans and the relationship of whales to artiodactyls. Nature, 413: 277-281.
TROFIMOV, B. A. and V. I. GROMOVA. 1968. Order Cetacea. *In*: V. I. Gromova (ed.), Fundamentals of Paleontology: Mammals. Israel Program for Scientific Translations, Jerusalem, pp. 225-241.
TRUE, F. W. 1908. The fossil cetacean, *Dorudon serratus* Gibbes. Bulletin of the Museum of Comparative Zoology, 52(4): 5-78.
TURNBULL, W. 1970. Mammalian masticatory apparatus. Fieldiana Geology, 18: 149-356.
TURNER, W. 1872. An account of the great finner whale (*Balaenoptera sibbaldii*) stranded at Longniddry. Part I. The soft parts. Transactions of the Royal Society of Edinburgh, 26: 197-251.
UHEN, M. D. 1991. Vertebral proportions as indicators of locomotor style in mammals (abstract). Journal of Vertebrate Paleontology, 11(3): 59A.
———. 1996. *Dorudon atrox* (Mammalia, Cetacea): Form, Function, and Phylogenetic Relationships of an Archaeocete from the Late Middle Eocene of Egypt. Ph.D. dissertation, University of Michigan, Ann Arbor, 608 pp.
———. 1997. What is *Pontogeneus brachyspondylus*? (abstract). Journal of Vertebrate Paleontology, 17(3): 82A.
———. 1998. Middle to late Eocene Basilosaurines and Dorudontines. *In*: J. G. M. Thewissen (ed.), The Emergence of Whales: Evolutionary Patterns in the Origin of Cetacea, Plenum Press, New York, pp. 29-61.
———. 2000. Replacement of deciduous first premolars and dental eruption in archaeocete whales. Journal of Mammalogy, 81(1): 123-133.
——— and P. D. GINGERICH. 2001. New genus of dorudontine archaeocete (Cetacea) from the middle-to-late Eocene of South Carolina. Marine Mammal Science, 17(1): 1-34.
URBÁN, J. R. and A. L. AGUAYO. 1987. Spatial and seasonal distribution of the humpback whale, *Megaptera novaeangliae*, in the Mexican Pacific. Marine Mammals Science, 3(4): 333-344.
VAN BENEDEN, P. J. and P. GERVAIS. 1880. Ostéographie des Cétacés Vivants et Fossiles. Arthus Bertrand, Paris, 634 pp.
WALL, W. P. 1983. The correlation between high limb-bone density and aquatic habits in recent mammals. Journal of Paleontology, 57(2): 197-207.
WATKINS, W. A., M. A. DAHER, K. M. FRISTRUP, T. J. HOWALD, and G. NOTARBARTOLO DI SCIARA. 1993. Sperm whales tagged with transponders and tracked underwater by sonar. Marine Mammal Science, 9(1): 55-67.
WEBB, P. W. 1975. Hydrodynamics and energetics of fish propulsion. Bulletin of the Fisheries Research Board of Canada, 190: 1-158.
WERTH, A. J. 1992. Anatomy and Evolution of Odontocete Suction Feeding. Ph.D. dissertation, Harvard University, Cambridge, Massachusetts, 313 pp.
WITMER, L. M. 1995. The extant phylogenetic bracket and the importance of reconstructing soft tissues in fossils. *In*: J. J. Thomason (ed.), Functional Morphology in Vertebrate Paleontology, Cambridge University Press, Cambridge, pp. 19-33.
WYSS, A. R. 1989. Flippers and pinniped phylogeny: has the problem of convergence been overrated? Marine Mammal Science, 5(4): 343-360.
YOSHIDA, H., M. SHIRAKIHARA, A. TAKEMURA, and K. SHIRAKIHARA. 1994. Development, sexual dimorphism, and individual variation in the skeleton of the finless porpoise, *Neophocaena phocaenoides*, in the coastal waters of western Kyushu, Japan. Marine Mammal Science, 10(3): 266-282.
ZULLO, V. A. and W. B. HARRIS. 1987. Sequence stratigraphy, biostratigraphy, and correlation of Eocene through lower Miocene strata in North Carolina. Cushman Foundation for Foraminiferal Research, Special Publication, 24: 197-214.

APPENDICES

Most of the data included in the following appendices are measurements of anatomical features of *Dorudon atrox* specimens. All measurements reported are in millimeters unless otherwise noted. The following conventions are used here:

□	A blank cell indicates that the measurement could not be taken because the structure was missing or extremely damaged.
—	Indicates that the measurement cannot be taken due to minor breakage or excessive wear on teeth.
†	Indicates that the measurement may be inaccurate due to wear.
E	Indicates that a tooth could not be measured because the tooth was erupting.
*	Indicates that the measurement was taken on one side of a bilaterally symmetrical structure and multiplied by two.
~	Indicates that the measurement is an approximation, probably based on a damaged specimen.
‡	Indicates that the measurement is the average of the right and left sides of an individual.

APPENDIX I: LIST OF SPECIMENS OF *DORUDON ATROX*.

Naturmuseum Senckenberg, Frankfurt au Main

1. NSFM 4451, relatively complete adult skull and left dentary. Skull has a red color, which suggests it came from the Gebel Mokattam Formation rather than the Birket Qarun Formation.
2. NSFM 7768, two caudal vertebrae from the Birket Qarun Formation, north of Birket Qarun. The two vertebrae are presumably from the same individual, but they are not adjacent in the vertebral column. The more anterior has articulations for chevrons, but no neural arch. It is probably around Ca13. The more posterior vertebra has no neural arch and no chevron articulations and the vertebrarterial canals are beginning to close, suggesting that it is around Ca 15.
3. NSFM M7866a-d, four vertebrae presumably from a single individual. Adhering sediment appears to indicate the specimen is from the Birket Qarun Formation rather than the Gebel Mokattam Formation. Stromer (1903) referred this specimen to *Zeuglodon* and indicated that it was juvenile. Presumably this is based on the small size of the vertebrae relative to vertebrae now referred to *Basilosaurus isis*. There are no indications that this individual is a juvenile. All epiphyses are fused to the vertebral bodies. The size and morphology of the vertebrae are fully consistent with their assignment to *Dorudon atrox*. M7866a is a caudal vertebra, around, Ca11-12. M7866b is a cervical vertebra, probably C5. M7866c is an anterior thoracic vertebra around T3-4. M7866d is a cervical vertebra, probably C7.

Cairo Geological Museum

1. CGM 9319, skull and right mandible. This is the type specimen of *Dorudon atrox*.
2. CGM 9230, Zeuglodon Valley (Andrews, 1906 p. 255), axis vertebra possibly associated with skull BMNH M 9266. Certainly associated with vertebrae CGM 9329 and 9332.
3. CGM 9329, Zeuglodon Valley (Andrews, 1906 p. 255), atlas vertebra possibly associated with skull BMNH M 9266. Certainly associated with vertebrae CGM 9230 and 9332.
4. CGM 9332, Zeuglodon Valley (Andrews, 1906 p. 255), third cervical vertebra possibly associated with skull BMNH M 9266. Certainly associated with vertebrae CGM 9230 and 9329.
5. CGM 42183, locality ZV-001. Skull, scapula, and nearly complete axial skeleton. A cast of the atlas and axis vertebrae have been given the University of Michigan specimen number UM 93229.
6. CGM 42184, locality ZV-186. Five vertebral bodies.
7. CGM 42185, locality ZV-188. Skull of a juvenile.
8. CGM 42186, locality ZV-199. Many vertebrae of a juvenile lacking epiphyses.
9. CGM 42187, locality ZV-225. Skull and partial skeleton of an adult individual.
10. CGM 42288, locality ZV-192. Lumbar and caudal vertebrae.

Natural History Museum, London

1. BMNH M 9265, artificial endocast of specimen BMNH M 9266.
2. BMNH M 9266, skull of a juvenile *Dorudon atrox*, Zeuglodon Valley (Andrews, 1906 p. 255). The specimen is relatively complete with alveoli for dI^{1}-dP^{2}, and dP^{3-4} present. The alveolus for the upper first molars are present, but both teeth are missing.
3. BMNH M 9266a, right dentary associated with specimen BMNH M 9266. dP_2-M_2 present.
4. BMNH M 9372a-c, casts of CGM 9329, 9230, and 9332 respectively. See the description above.
5. BMNH M 10173, type specimen of *Dorudon* (*Zeuglodon*) *intermedius* (Dart). The specimen consists of a skull with most of the teeth and the basicranium destroyed. In addition, an artificial endocast is included under the same specimen number. See the discussion of the synonomy of *Dorudon intermedius* with *Dorudon atrox* for a more detailed description of the specimen.
6. BMNH M 21896, cast of the type specimen of *Prozeuglodon atrox*, CGM 9319.
7. BMNH M 51755, posterior or anterior caudal vertebra from "the surface of Wadi Hof, near Helwan, Egypt," (letter with specimen from the collector John L. Gilbert, 1950).

Staatliches Museum für Naturkunde, Stuttgart

1. SMNS unnumbered specimen I, juvenile skull and right dentary. Left and right dP^{2-4} present but broken, $M^{1}{}_{1}$ erupted but both are missing, $M^{2}{}_{2}$ not yet erupted. Dentary contains dI_1 to dP_4, but P_1 is missing.
2. SMNS 11234, badly broken juvenile skull. Most of the rostrum, basicranium, and occiput are missing. Originally described by Stromer (1908) as *Prozeuglodon atrox*, specimen St 1. Collected from the Birket el Qarun Formation, Egypt.
3. SMNS 11417a, right dentary. Right P_2 to M_3 present, but P_4 is missing. Originally, the specimen number 11417a referred to Stromer's (1908) specimen "St 15", which consisted of an isolated humerus and a slightly crushed right ulna (Kellogg, 1936, p. 76). Kellogg referred this specimen to *Prozeuglodon isis*. This specimen is now missing (E. J. Heizmann, pers. com., 1994). The left and right dentaries bearing the specimen number SMNS 11417 are clearly different sizes although Kellogg did not note this, and put the specimen in *Dorudon osiris* (now *Saghacetus osiris*). The right dentary (now given the number 11417a) is clearly smaller than the left dentary (11417b), which is probably *Basilosaurus isis*. These were collected near Dimeh, Fayum Egypt by Markgraf in 1905.
4. SMNS 11951a, broken juvenile skull. The skull is in five large pieces including; the left maxilla with dP^{2}-dP^{3} and alveoli for dP^{4} (status of M^{1} is unclear), frontal, parietal and squamosal, supraoccipital, and the exoccipital and basioccipital sutured together. Collected from Wadi Rayan, Egypt by Markgraf in 1906 or 1907.
5. SMNS 13138, miscellaneous teeth from "Kasr Karun", Egypt.

University of Florence Paleontology Museum

1. UFPM IGF-1310, partial cranium including rostrum from dP^1-M^1, external nares, and part of the frontal area. This specimen was first reported by Pilleri (1985) as *Dorudon osiris*. Gingerich (1991) noted that the individual was more likely to be "*Prozeuglodon*"*atrox* based on its size, since "*Dorudon*" *osiris* (now *Saghacetus osiris*) is much smaller. He also concluded that it was also not likely to be from Wadi-el-Nutrûn, as indicated by the information with the specimen (Pilleri, 1985), but it was most likely from the Birket Qarun Formation of the Fayum region. Based on the size of the specimen and the confirmation of the nasals, it is probably a juvenile *Dorudon atrox*.

University of Michigan Museum of Paleontology

1. UM 83902, locality ZV-077, Gehannam Formation. Juvenile individual represented by left and right dentaries including the following teeth: left $dP_{1\text{-}4}$ (dP_3 crushed), and M_1 erupting, right $dP_{2\text{-}3}$ and M_1 erupting.
2. UM 93220, locality ZV-002, Birket Qarun Formation. Juvenile individual represented by a virtually complete skull and partial skeleton. The skull has the following teeth: left and right $dI^{1\text{-}2}$ roots (the tip of I^1 can be seen in the crypt) dI^3 (left, roots only on right side), dC^1 roots, P^1, $dP^{2\text{-}4}$, M^1, M^2 erupting. The weathered dentaries have the following teeth: left and right multiple dI_x, $dP_{2\text{-}4}$ (P_4 can be seen in the broken right dentary forming in the crypt), $M_{1\text{-}2}$. The specimen also includes stylohyoids, a virtually complete rib cage, the xiphisternum, cervical vertebrae 1 to 7 and thoracic vertebrae 1 to 17 in articulation.
3. UM 93232, locality ZV-071, Gehannam Formation. Juvenile individual represented by a badly crushed skull. The left periotic is rather well-preserved and the stapes is present as well.
4. UM 93234, locality ZV-206, Gehannam Formation. Cranial endocast of a juvenile. Specimen also preserves a cast of the cartilaginous plate between the basisphenoid and presphenoid.
5. UM 93253, locality Zeuglodon Valley. Cranial endocast of a juvenile.
6. UM 94786, locality ZV-036. Weathered cranial endocast of a juvenile.
7. UM 94794, locality ZV-004. Weathered cranial endocast with an internal cast of a dentary and a lower molar, probably M_1.
8. UM 94795, locality ZV-008, Birket Qarun Formation. Left dentary in a sandstone concretion with P_4-M_3. This specimen is a juvenile that shows P_4 in eruption. The specimen also includes a well-preserved cranial endocast.
9. UM 94796, locality ZV-010. Badly weathered skull of a juvenile with a well-preserved cranial endocast. Specimen also includes an internal cast of the posterior portions of the right and left dentaries.
10. UM 94797, locality ZV-018. Well-preserved cranial endocast with well-preserved cranial nerves and casts of the nares. Specimen also includes a left dentary with molds of left $dP_{3\text{-}4}$ and a poorly preserved right dentary with roots of $dP_{3\text{-}4}$ and M_1.
11. UM 94799, locality ZV-037. Badly weathered skull of a juvenile with a cranial endocast.
12. UM 84802, locality ZV-061. Poorly preserved cranial endocast of a juvenile.
13. UM 94804, locality ZV-024, Birket Qarun Formation. Extremely weathered fragments of a partial skeleton. Mainly thoracic vertebrae with fragments of scapula, humerus, and ulna.
14. UM 94807, locality ZV-056, Gehannam Formation. Juvenile individual represented by a weathered proximal humerus, a distal ulna with an unfused epiphysis, and a xiphisternum.
15. UM 94811, locality ZV-044, Gehannam Formation. Juvenile individual represented by a disarticulated skull including: premaxilla fragments, maxillae, frontals and the basicranium. Teeth present include $dP^{3\text{-}4}$ and the alveoli for M^1. Fragmentary anterior teeth and deciduous premolars are also present. The skull has unhealed bite marks on the frontal area.
16. UM 94814, locality ZV-041, Gehannam Formation. Juvenile individual represented by a weathered fragmentary skull, dentaries, and anterior skeleton. The skull includes the left premaxilla, maxillae, the left jugal, parietals, occiput, basicranium, and periotic. Upper teeth present include: I^x, left $dP^{3\text{-}4}$ roots, left M^1, right $dP^{3\text{-}4}$ roots and right M^1. Lower teeth present include: I_X, left P_1, left $dP_{2\&4}$, left M_1 with M_2 erupting, right M_1 . The anterior skeleton consists of cervical vertebrae 1 to six and left ribs 1 and 2.
17. UM 94819, locality ZV-069, Gehannam Formation. Right auditory bulla and periotic.
18. UM 94834, locality ZV-065. Juvenile individual represented by a cast of a skull and left dentary including: frontals, parietals, basicranium, periotic, left auditory bulla and the occiput. A single upper molar cast is present as well. The dentary includes part of dP_3, dP_4, and M_1.
19. UM 97506, locality ZV-072, Gehannam Formation. Left dentary and partial skeleton. The dentary includes$P_{2\text{-}4}$ and $M_{1\text{-}3}$. The partial skeleton includes some fragmentary thoracic and lumbar vertebrae, various ribs and rib fragments and a left forelimb including: a virtually complete scapula, crushed humerus, radius, and ulna and most of the carpus and manus. This is the only specimen known to have portions of the hind limb preserved. These include: a proximal femur, a complete patella, and a proximal astragalus.

20. UM 97509, locality ZV-088, Birket Qarun Formation. Shaft and distal end of a partly crushed humerus. A small fragment of the weathered head is also present.
21. UM 97511, locality ZV-098, Birket Qarun Formation. Juvenile individual represented by a very small scapula.
22. UM 97512, locality ZV-099, Birket Qarun Formation. Skull and partial skeleton. The skull is broken in pieces including: portions of the premaxillae and maxilla, frontals, parietals, basicranium, and left and right auditory bullae. Broken left and right dentaries are present with right teeth I_x and C_1-P_2. Much of the hyoid apparatus, most ribs, and the entire sternum are present. Cervical vertebrae 2 to 7 are present along with some thoracic vertebrae, a semi-articulated lumbar series and most of the caudal vertebrae. Most of the right forelimb including the scapula, humerus, radius, ulna, carpals, and the manus are all present.
23. UM 97516, locality ZV-120, Gehannam Formation. Badly weathered skull of a juvenile with cranial endocast. The endocast includes a cast of the cranial nerves that continues all the way anterior to the narial passages. The cast shows the distribution of the olfactory nerve into the narial passages and the optic nerve in the orbit.
24. UM 97517, locality ZV-122, Birket Qarun Formation. Isolated temporal portion of the squamosal.
25. UM 97519, locality ZV-127. Weathered skull with well-preserved cranial endocast and partial auditory region of a juvenile.
26. UM 97548, locality west end of Birket Qarun, Gehannam Formation. Isolated weathered lumbar vertebral body.
27. UM 100139, locality ZV-189, Gehannam Formation. Juvenile individual represented by a skull that includes disarticulated maxillae with left and right dP^{1-4}, and M^1 erupting. The posterior portion of the skull is virtually complete with the right periotic, auditory bulla and malleus in place.
28. UM 100142, locality ZV-183, Birket Qarun Formation. Juvenile individual represented by a disarticulated skull that includes the frontals, basicranium and periotics. The atlas is also present.
29. UM 100143, locality ZV-176, Birket Qarun Formation. Articulated thoracic vertebral column and ribs along with a posterior basicranium and mesosternal elements.
30. UM 100144, locality ZV-182, Birket Qarun Formation. Cranial endocast along with one weathered thoracic vertebra and four anterior caudal vertebra. Also includes a humeral head and a mold of a left dentary with P_4-M_3 included.
31. UM 100146, locality ZV-197, Gehannam Formation. Left mandible with P_1, P_4, and M_{1-3}. Miscellaneous vertebrae are present from throughout the column including some from the cervical , thoracic , lumbar, and caudal regions. Many fragmentary ribs are also present.
32. UM 100149, locality ZV-111, Birket Qarun Formation. Very weathered fragmentary skull and assorted vertebrae.
33. UM 100185, locality ZV-139, Gehannam Formation. Specimen consists of an articulated vertebral column in limestone plus other skeletal elements. The vertebral column was left in the field and a chevron and metacarpal V were collected.
34. UM 101215, locality ZV-210, Gehannam Formation. Disarticulated skull and skeleton. Skull includes broken pieces of frontals, parietals, occiput, basicranium, periotics and left and right auditory bullae. Assorted teeth including incisors, canines, premolars, and molars are present but not in place. Most vertebrae and ribs are present, along with some chevron bones and a complete sternum. Left and right forelimbs are complete to the wrist, with some carpals, metacarpals, and phalanges present.
35. UM 101222, locality ZV-224, Birket Qarun Formation. Articulated skull and partial skeleton. The skull is virtually complete with left P^{3-4} and M^{1-2} in place. A weathered right dentary is present with P_{1-4} and M_{1-3}. A partially articulated hyoid apparatus is present. Virtually complete left and right forelimbs are present with scapulae, humeri, radii, ulnae, carpals, metacarpals, and phalanges. The vertebral column is articulated from cervical vertebra 1 to thoracic vertebra 13. The posterior thoracic vertebrae, lumbar vertebrae, and anteriormost caudal vertebrae are badly weathered or missing. The caudal vertebrae are articulated from caudal vertebra 5 to the end of the series, caudal vertebra 21. Some articulated chevron bones are also present.
36. UM 101223, locality ZV-226, Gehannam Formation. Juvenile individual represented by a relatively complete, articulated skull with both auditory bullae, a periotic broken to show the cochlea and other middle ear structures along with the stapes. The skull includes left dI^3, left P^1, roots of left dP^{1-4} to M^1, right dI^3, right dC^1, and roots of right dP^{2-4} to M^1. In addition there is a left dentary with dP_{2-4} and isolated left and right dI_{1-3}, right M_{1-2} and other tooth fragments. The specimen also includes most of the ribs and some thoracic vertebrae.
37. UM 101230, locality ZV-179, Birket Qarun Formation. Isolated left P^4, weathered thoracic vertebra, and pieces of phalanges.

Additional destroyed specimens

1. Munich 1904 XII 135c, two single rooted teeth; Munich 1904 XII 135d, proximal end of a left humerus without the head and the anterior end of a right radius; Munich 1904 XII 135e, fragmentary sixth cervical vertebra, elongate thoracic or lumbar vertebra, three lumbar vertebrae, two caudal vertebrae, a two headed rib, and a posterior sternal element (destroyed). Stromer (1908) grouped all of these skeletal elements under a single reference number, his Mn. 16. Only the radius is figured in his plate VII(IV), figures three, four, and five. This radius appears to be the size of *Dorudon atrox*, but the elongated thoracic or lumbar vertebra is certainly from *Basilosaurus isis*. It is possible that Stromer's Mn. 16 is a mixture of both *Basilosaurus* and *Dorudon*.
2. Munich 1904 XII 135f, anterior end of a right dentary (destroyed). This specimen was not figured nor included in any tables of Stromer (1908). Without figures or measurements this specimen cannot be confidently assigned to a species.
3. Munich 1922 IX 7, several anterior ribs (destroyed). This specimen has not been figured nor have measurements been published, so it cannot be confidently assigned to a species.
4. Berlin, M-17, an imperfect axis (destroyed?). This specimen has not been figured nor have measurements been published, so it cannot be confidently assigned to a species.

APPENDIX II: DECIDUOUS TOOTH MEASUREMENTS

Appendix IIA: Upper Teeth

Measurements of deciduous teeth of *Dorudon atrox*, taken as shown in Figure 9. L in the column headings indicates a left, while R indicates a right tooth. In the rows, L is length, W is width, and H is breadth.

Tooth	Dim.	BMNH M 9266		BMNH 21896		SMNS UnI		SMNS 11951a		UM 93220		UM 94811		UM 94814		UM 100139		UM 101223	
		L	R	L	R	L	R	L	R	L	R	L	R	L	R	L	R	L	R
dI1	L	—	—	—	—	14.0	—	—	—	—	—	—	—	—	—	—	—	—	15.0
	W	—	—	—	—	12.0	—	—	—	—	—	—	—	—	—	—	—	—	10.3
	H	—	—	—	—	—	—	—	—	—	—	—	—	—	—	—	—	—	—
dI2	L	—	—	—	—	—	—	—	—	—	—	—	20.2	—	20.1	—	—	—	—
	W	—	—	—	—	13.0	—	—	—	—	—	—	12.6	—	—	—	—	—	—
	H	—	—	—	—	—	—	—	—	—	—	—	—	—	—	—	—	—	—
dI3	L	—	—	—	—	15.0	—	—	—	19.9	—	—	—	—	—	—	—	16.6	16.3
	W	—	—	—	—	11.0	—	—	—	15.6	—	—	—	—	—	—	—	9.9	9.5
	H	—	—	—	—	—	—	—	—	—	—	—	—	—	—	—	—	24.2	21.0†
dC1	L	—	—	—	—	—	—	—	—	—	—	—	—	—	26.0	—	—	—	21.4
	W	—	—	—	—	—	—	—	—	—	—	—	—	—	14.0	—	—	—	13.2
	H	—	—	—	—	—	—	—	—	—	—	—	—	—	—	—	—	—	—
dP1	L	—	—	—	—	E	E	—	—	31.7	—	—	—	—	—	E	E	—	—
	W	—	—	—	—	E	E	—	—	16.0	—	—	—	—	—	E	E	—	—
	H	—	—	—	—	E	E	—	—	—	—	—	—	—	—	E	E	—	—
dP2	L	—	—	—	46.4	44.9	45.0	44.1	—	—	—	43.0	—	—	—	48.2	48.1	—	—
	W	—	—	—	—	—	—	—	—	—	—	12.1	—	—	—	11.8	11.2	—	—
	H	—	—	—	—	—	—	—	—	—	—	26.0	23.9	—	—	—	—	—	—
dP3	L	48.3	—	—	45.5	49.0	48.0	45.0	—	46.0	—	—	42.0	48.5	—	47.1	47.4	—	—
	W	—	—	—	11.9	—	—	—	—	—	—	—	—	11.3	—	12.2	12.4	—	—
	H	—	—	—	—	—	—	—	—	—	—	—	—	—	—	24.3	—	—	—
dP4	L	44.8	43.0	—	40.1	43.0	—	42.0	—	42.2	—	—	—	43.1	—	45.8	43.3	—	—
	W	—	—	—	11.6	—	—	—	—	10.8	—	—	—	12.8	—	11.2	11.5	—	—
	H	—	—	—	—	—	—	—	—	—	—	—	—	18.3	—	17.5	18.1	—	—

Appendix IIB: Lower Teeth

Measurements of deciduous teeth of *Dorudon atrox*, taken as shown in Figure 9. L in the column headings indicates a left, while R indicates a right tooth. In the rows, L is length, W is width, and H is breadth.

Tooth	Dim.	BMNH M 9266		BMNH 21896		SMNS UnI		UM 83902		UM 93220		UM 94814		UM 100144		UM 101223		UM 101992	
		L	R	L	R	L	R	L	R	L	R	L	R	L	R	L	R	L	R
dI_1	L	—	—	—	—	—	—	—	—	17.0	—	—	—	—	—	9.5	9.5	—	—
	W	—	—	—	—	—	—	—	—	11.0	—	—	—	—	—	—	7.6	—	—
	H	—	—	—	—	—	—	—	—	—	—	—	—	—	—	14.9	—	—	—
dI_2	L	—	—	—	—	—	—	—	—	15.5	—	—	—	—	—	17.3	—	—	—
	W	—	—	—	—	—	—	—	—	10.6	—	—	—	—	—	10.8	—	—	—
	H	—	—	—	—	—	—	—	—	25.5	—	—	—	—	—	24.2	—	—	—
dI_3	L	—	—	—	—	—	—	—	—	—	—	—	—	—	—	17.7	17.0	—	—
	W	—	—	—	—	—	12.0	—	—	—	—	—	—	—	—	10.9	10.9	—	—
	H	—	—	—	—	—	—	—	—	—	—	—	—	—	—	25.6	—	—	—
dIC_1	L	—	—	—	—	—	—	—	—	—	—	—	—	—	—	—	20.3	—	—
	W	—	—	—	—	—	—	—	—	—	—	—	—	—	—	—	12.2	—	—
	H	—	—	—	—	—	—	—	—	—	—	—	—	—	—	—	30.9	—	—
dP_1	L	—	—	—	—	—	—	—	—	—	22.5	28.0	26.0	—	—	—	25.4	—	—
	W	—	—	—	—	—	—	—	—	—	12.7	—	11.4	—	—	—	12.9	—	—
	H	—	—	—	—	—	—	—	—	—	29.2	—	35.0	—	—	—	29.6	—	—
dP_2	L	—	37.3	—	33.3	—	35.9	38.7	—	41.2	—	43.5	—	—	—	36.5	38.3	—	—
	W	—	—	—	11.4	—	11.0	9.5	—	—	—	—	—	—	—	—	10.5	—	—
	H	—	—	—	22.7	—	—	21.5	—	—	—	—	—	—	—	—	—	—	—
dP_3	L	—	55.0	—	58.6	55.0	54.3	58.7	58.2	—	59.7	—	—	—	—	60.2	—	—	—
	W	—	—	—	—	—	—	11.4	11.3	11.8	—	—	—	—	—	—	—	—	—
	H	—	—	—	—	—	—	27.2	26.3	—	—	—	—	—	—	—	—	—	—
dP_4	L	—	61.0	—	54.0	54.0	59.0	—	56.3	56.0	—	56.1	—	—	53.0	60.2	—	—	—
	W	—	—	—	12.0	—	14.0	—	12.0	—	—	10.7	—	—	—	12.8	—	—	—
	H	—	—	—	—	—	—	—	—	—	—	27.0	—	—	34.0	28.2	—	—	—

APPENDIX III: PERMANENT TOOTH MEASUREMENTS

Appendix IIIA: Upper Teeth

Measurements of teeth of *Dorudon atrox*, taken as shown in Figure 9. L in the column headings indicates a left, while R indicates a right tooth. In the rows, L is length, W is width, and H is breadth.

Tooth	Dimension	BMNH 21896		NSFM 4451		SMNS 13138		UM 93220		UM 94814	
		L	R	L	R	L	R	L	R	L	R
I^1	L	—	—	21.5	22.0	—	—	—	—	—	—
	W	—	—	15.1	15.3	—	—	—	—	—	—
	H	—	—	—	—	—	—	—	—	—	—
I^2	L	—	—	—	22.9	—	—	—	—	—	—
	W	—	—	—	14.2	—	—	—	—	—	—
	H	—	—	—	30.2	—	—	—	—	—	—
I^3	L	—	—	25.3	25.7	—	—	—	—	—	—
	W	—	—	14.4	17.0	—	—	—	—	—	—
	H	—	—	36.6	36.9	—	—	—	—	—	—
C^1	L	—	—	29.8	28.6	—	—	—	—	—	—
	W	—	—	17.4	17.6	—	—	—	—	—	—
	H	—	—	34.5	36.5	—	—	—	—	—	—
P^1	L	—	—	21.7	22.1	—	—	—	—	—	—
	W	—	—	—	—	—	—	—	—	—	—
	H	—	—	—	9.3	—	—	—	—	—	—
P^2	L	—	—	51.7	51.7	—	—	—	—	—	—
	W	—	—	14.1	13.5	—	—	—	—	—	—
	H	—	—	32.5	27.7	—	—	—	—	—	—
P^3	L	—	—	42.6	47.9	—	—	—	—	—	—
	W	—	—	13.4	14.7	—	—	—	—	—	—
	H	—	—	—	11.8	—	—	—	—	—	—
P^4	L	—	—	43.0	43.3	—	—	—	—	—	—
	W	—	—	13.6	13.8	—	—	—	—	—	—
	H	—	—	26.4	24.7	—	—	—	—	—	—
M^1	L	—	30.2	30.0	29.7	—	—	34.0	32.0	32.5	32.5
	W	—	12.0	11.3	12.0	—	—	13.9	—	9.8	9.6
	H	—	—	12.3	11.0	—	—	18.7	—	16.8	15.4
M^2	L	—	—	—	—	25.7	—	E	E	—	—
	W	—	—	—	—	10.0	—	E	E	—	—
	H	—	—	—	—	12.0	—	E	E	—	—

Appendix IIIA: Upper Teeth (cont.)

Tooth	Dimension	UM 97512		UM 100139		UM 101215		UM 101222		UM 101230	
		L	R	L	R	L	R	L	R	L	R
I^1	L	—	—	—	—	—	—	—	—	—	—
	W	—	—	—	—	—	—	—	—	—	—
	H	—	—	—	—	—	—	—	—	—	—
I^2	L	—	—	—	—	—	—	—	—	—	—
	W	—	—	—	—	—	—	—	—	—	—
	H	—	—	—	—	—	—	—	—	—	—
I^3	L	—	—	—	—	—	—	—	—	—	—
	W	—	—	—	—	—	—	—	—	—	—
	H	—	—	—	—	—	—	—	—	—	—
C^1	L	—	32.3	—	—	—	—	33.2	—	—	—
	W	—	18.8	—	—	—	—	19.4	—	—	—
	H	—	39.1	—	—	—	—	—	—	—	—
P^1	L	—	—	—	—	—	—	27.0	—	—	—
	W	—	—	—	—	—	—	—	—	—	—
	H	—	—	—	—	—	—	—	—	—	—
P^2	L	—	—	—	—	—	—	56.2	—	—	—
	W	—	—	—	—	—	—	20.0	—	—	—
	H	—	—	—	—	—	—	—	—	—	—
P^3	L	—	—	—	—	—	—	53.6	—	52.1	—
	W	—	—	—	—	—	—	17.0	—	13.9	—
	H	—	—	—	—	—	—	31.6†	—	22.4†	—
P^4	L	—	—	—	—	54.6	—	48.2	—	—	—
	W	—	—	—	—	15.2	—	15.8	—	—	—
	H	—	—	—	—	27.6	—	28.0†	—	—	—
M^1	L	—	—	—	—	—	29.6	32.1	—	—	—
	W	—	—	—	—	—	—	11.0	—	—	—
	H	—	—	—	—	—	—	17.8†	—	—	—
M^2	L	—	—	—	—	—	29.0	30.2	—	—	—
	W	—	—	—	—	—	10.4	11.7	—	—	—
	H	—	—	—	—	—	14.7	—	—	—	—

Appendix IIIB: Lower Teeth

Measurements of teeth of *Dorudon atrox*, taken as shown in Figure 9. L in the column headings indicates a left, while R indicates a right tooth. In the rows, L is length, W is width, and H is breadth.

Tooth	Dimension	BMNH 9266(a)		NSFM 4451		SMNS UnI		SMNS 13138		SMNS 11417a		UM 93220	
		L	R	L	R	L	R	L	R	L	R	L	R
I_1	L	—	—	—	—	—	—	—	—	—	—	—	—
	W	—	—	—	—	—	—	—	—	—	—	—	—
	H	—	—	—	—	—	—	—	—	—	—	—	—
I_2	L	—	—	—	—	—	—	—	—	—	—	—	—
	W	—	—	—	—	—	—	—	—	—	—	—	—
	H	—	—	—	—	—	—	—	—	—	—	—	—
I_3	L	—	—	—	—	—	—	—	—	—	—	—	—
	W	—	—	—	—	—	—	—	—	—	—	—	—
	H	—	—	—	—	—	—	—	—	—	—	—	—
C_1	L	—	—	25.7	—	—	—	28.0	—	—	—	—	—
	W	—	—	15.4	—	—	—	13.7	—	—	—	—	—
	H	—	—	29.0	—	—	—	12.0	—	—	—	—	—
P_1	L	—	—	34.1	—	—	—	—	—	—	—	—	—
	W	—	—	12.7	—	—	—	—	—	—	—	—	—
	H	—	—	23.5	—	—	—	—	—	—	—	—	—
P_2	L	—	—	46.2	—	—	—	—	—	—	42.1	—	—
	W	—	—	14.4	—	—	—	—	—	—	16.2	—	—
	H	—	—	30.3	—	—	—	—	—	—	35.7	—	—
P_3	L	—	—	60.2	—	—	—	59.5	—	—	58.8	—	—
	W	—	—	15.5	—	—	—	14.4	—	—	—	—	—
	H	—	—	19.7	—	—	—	21.7	—	—	—	—	—
P_4	L	—	—	53.0	—	—	—	57.3	—	—	—	—	—
	W	—	—	15.3	—	—	—	13.0	—	—	—	—	—
	H	—	—	38.2	—	—	—	27.0	—	—	—	—	—
M_1	L	—	45.0	34.0	—	—	45.0	34.7	—	—	34.0	43.0	43.1
	W	—	—	11.7	—	—	16.0	13.2	—	—	13.4	15.1	14.7
	H	—	—	23.9	—	—	—	28.0	—	—	26.1	30.0	31.1
M_2	L	—	43.8	35.0	—	—	—	—	—	—	36.3	39.9	40.2
	W	—	—	11.7	—	—	—	—	—	—	15.0	13.5	15.4
	H	—	—	33.2	—	—	—	—	—	—	34.0	35.3	35.0
M_3	L	—	—	32.0	—	—	—	—	—	—	32.6	E	E
	W	—	—	9.7	—	—	—	—	—	—	11.2	E	E
	H	—	—	26.6	—	—	—	—	—	—	27.2	E	E

Appendix IIIB: Lower Teeth (cont.)

Tooth	Dimension	UM 94795		UM 94814		UM 94834		UM 97506		UM 97512		UM 100144	
		L	R	L	R	L	R	L	R	L	R	L	R
I_1	L	—	—	—	—	—	—	—	—	—	17.6	—	—
	W	—	—	—	—	—	—	—	—	—	12.2	—	—
	H	—	—	—	—	—	—	—	—	—	—	—	—
I_2	L	—	—	—	—	—	—	—	—	21.3	—	—	—
	W	—	—	—	—	—	—	—	—	15.2	—	—	—
	H	—	—	—	—	—	—	—	—	—	—	—	—
I_3	L	—	—	—	—	—	—	—	—	—	26.4	—	—
	W	—	—	—	—	—	—	—	—	—	16.4	—	—
	H	—	—	—	—	—	—	—	—	—	—	—	—
C_1	L	—	—	—	—	—	—	—	—	26.6	26.3	—	—
	W	—	—	—	—	—	—	—	—	18.0	—	—	—
	H	—	—	—	—	—	—	—	—	28.5†	—	—	—
P_1	L	—	—	—	—	—	—	—	—	—	34.5	—	—
	W	—	—	—	—	—	—	—	—	—	14.4	—	—
	H	—	—	—	—	—	—	—	—	—	24.1	—	—
P_2	L	—	—	—	—	—	—	—	—	—	—	—	—
	W	—	—	—	—	—	—	—	—	—	—	—	—
	H	—	—	—	—	—	—	—	—	—	—	—	—
P_3	L	—	—	—	—	—	—	60.2	—	—	—	—	—
	W	—	—	—	—	—	—	18.8	—	—	—	—	—
	H	—	—	—	—	—	—	—	—	—	—	—	—
P_4	L	—	—	—	—	—	—	56.0	—	—	—	—	—
	W	—	—	—	—	—	—	18.6	—	—	—	—	—
	H	—	—	—	—	—	—	36.0	—	—	—	—	—
M_1	L	—	—	42.5	42.2	40.9	—	39.0	—	—	—	37.0	—
	W	—	—	—	13.7	—	—	15.2	—	—	—	—	—
	H	—	—	—	31.6	29.9	—	27.0†	—	—	—	—	—
M_2	L	—	—	—	—	—	—	35.0	—	—	—	35.0	—
	W	—	—	—	—	—	—	15.0	—	—	—	—	—
	H	—	—	—	—	—	—	—	—	—	—	30.0	—
M_3	L	—	—	—	—	—	—	33.9	—	—	—	35.8	—
	W	—	—	—	—	—	—	13.9	—	—	—	—	—
	H	—	—	—	—	—	—	29.0	—	—	—	30.0	—

Appendix IIIB: Lower Teeth (cont.)

Tooth	Dimension	UM 100146		UM 101215		UM 101222		UM 101223	
		L	R	L	R	L	R	L	R
I_1	L	—	—	—	—	—	—	—	—
	W	—	—	—	—	—	—	—	—
	H	—	—	—	—	—	—	—	—
I_2	L	—	—	—	—	—	—	—	—
	W	—	—	—	—	—	—	—	—
	H	—	—	—	—	—	—	—	—
I_3	L	—	—	—	—	—	—	—	—
	W	—	—	—	—	—	—	—	—
	H	—	—	—	—	—	—	—	—
C_1	L	—	—	—	—	—	30.0	—	—
	W	—	—	—	—	—	—	—	—
	H	—	—	—	—	—	—	—	—
P_1	L	31.7	—	—	34.0	—	38.0	—	—
	W	11.5	—	—	13.1	—	—	—	—
	H	26.2	—	—	25.2	—	—	—	—
P_2	L	—	—	—	48.9	—	—	—	—
	W	—	—	—	13.8	—	13.7	—	—
	H	—	—	—	18.0†	—	15.4†	—	—
P_3	L	—	—	—	61.9	—	63.9	—	—
	W	—	—	—	14.5	—	17.5	—	—
	H	—	—	—	34.5†	—	38.2†	—	—
P_4	L	58.0	—	—	53.6	—	61.4	—	—
	W	13.9	—	—	14.6	—	—	—	—
	H	36.4†	—	—	29.1†	—	—	—	—
M_1	L	36.0	—	—	35.0†	—	—	—	45.9
	W	12.3	—	—	13.8	—	17.0	—	—
	H	22.7†	—	—	24.6†	—	31.0	—	—
M_2	L	34.0	—	—	—	—	—	—	40.6
	W	10.3	—	—	—	—	15.0†	14.9	13.4
	H	27.5	—	—	—	—	36.0	38.0	36.2
M_3	L	32.2	—	36.4	—	—	40.0	—	—
	W	10.3	—	11.6	—	—	—	—	—
	H	25.8	—	26.8	—	—	30.0	—	—

APPENDIX IV: CRANIAL AND MANDIBULAR MEASUREMENTS

Appendix IVA: Cranial Measurements, Dorsal View

Measurements taken on the skulls of *Dorudon atrox*, as shown in Figure 22. CBL is condylobasal length. RBI^1 is the rostrum breadth at I^1. RBC^1 is rostrum breadth at C^1. DPL is dorsal premaxilla length. NL is the length of the narial opening. NB is the breadth of the narial opening. NSL is the length of the nasal bone. FNP is length of the projection of the frontal between the posterior nasals. FSB is frontal shield breadth. MFL is the maximum frontal length. CSB is the central skull breadth at the frontal/parietal suture.

Specimen	CBL	RBI^1	RBC^1	DPL	NL	NB	NSL	FNP	FSB	MFL	CSB
BMNH M 9266	—	40.3	80.1	—	—	—	—	—	246.0*	—	50.6
BMNH M 10173	~777.0	—	79.8	—	~140.0	55.4	~202.0‡	76.1‡	282.0	164.0	~61.0
BMNH M 21896	652.0	40.1	82.0	~279.0	~105.0	~34.0	—	—	260.0*	~140.0	~45.0
CGM 42183	940.0	—	—	—	—	—	—	—	—	—	—
NSFM 4451	~944.0	53.9	91.8	~503.0	—	51.7	240.5‡	~87.0	~355.0	~195.0	—
SMNS 11951a	—	—	—	—	—	—	—	—	~230.0*	—	—
UM 93220	~780.0	—	89.5	337.0	213.0	~50.0	190.0‡	—	288.2	—	—
UM 94814	—	—	—	—	—	—	—	—	224.0‡	—	43.8
UM 97512	—	45.8	—	—	—	—	—	—	—	—	—
UM 100139	—	—	—	—	—	—	—	—	252.0	—	44.8
UM 100142	—	—	—	—	—	—	—	—	232.0	—	45.7
UM 101215	—	—	—	—	—	—	—	—	356.0	—	57.3
UM 101222	~940.0	46.1	82.0	~487.0‡	126.8	55.8	240.0‡	76.3	342.0	179.8	50.0
UM 101223	770.0	64.0	87.3	—	—	—	—	—	—	—	—

Appendix IVB: Cranial Measurements, Ventral and Posterior Views

Measurements taken on the skulls of *Dorudon atrox* as shown in Figure 22. VPL is ventral premaxilla length. ABL is auditory bulla length. ABB is auditory bulla breadth. NCB is nuchal crest breadth. NCH is nuchal crest height. FMH is foramen magnum height. FMB is foramen magnum breadth. CB is condylar breadth. OB is occipital breadth. ZSB is breadth of the skull across the zygomatic arches.

Specimen	VPL	PL	ABL	ABB	NCB	NCH	FMH	FMB	CB	OB	ZSB
BMNH M 9266	~235.0	—	—	—	~132.0	113.0	~35.0	~59.0	~107.0	215.0	—
BMNH M 10173	—	—	—	—	111.3	155.0	~38.0	53.8	111.8	~268*	—
BMNH M 21896	~134.0	—	—	—	—	—	—	—	—	—	—
CGM 42183	—	—	83.0	~53.0	—	—	—	—	121.0	~300.0	~500.0
NSFM 4451	353.0	—	—	—	115.0	~144.0	~35.0	—	—	304.0	~416.0
SMNS 11951a	—	—	—	—	—	—	~31.0	~55.0	—	~195.0*	—
UM 93220	276.3	~217.0	77.7‡	57.1‡	—	~149.0	~44.0	~61.0	~105.0	236.0	—
UM 94814	—	—	77.0	50.5‡	105.1	~102.0	—	48.0	—	204.0	282.0
UM 97512	—	—	86.1	~56.0	139.5	—	—	—	—	—	—
UM 100139	—	~104.0	80.5	58.6	—	—	—	—	—	—	—
UM 100142	—	—	—	—	113.5	104.9	—	—	~116.0	210.0	—
UM 101215	—	—	79.9‡	59.1‡	—	—	—	—	121.6	~353.0	—
UM 101222	362.0	—	—	—	152.1	184.0	—	~46.0	126.0*	310.0*	—
UM 101223	—	—	—	—	—	—	—	—	—	—	—

Appendix IVC: Mandibular and Hyoid Measurements

Measurements of the mandible as shown in Figure 23. Those of the hyoid are shown in Figure 79. DL is dentary length. MDI_1 is the mandible depth posterior to I_1. MDC_1 is the mandible depth posterior to C_1. MDP_4 is the mandible depth posterior to P_4. CH is the coronoid height. BHB is basihyoid breadth. BHML is basihyoid midline length. BHDL is basihyoid distal length. SHPB is stylohyoid proximal breadth. THPB is thyrohyoid proximal breadth.

Specimen	DL	MDI_1	MDC_1	MDP_4	CH	BHB	BHML	BHDL	SHPB	THPB
BMNH M 9266a	—	—	48.7	68.7	—	—	—	—	—	—
BMNH M 21896	—	—	—	72.7	168.0	—	—	—	—	—
CGM 42183	850.0	—	53.0	89.0	—	—	—	—	—	—
NSFM 4451	~810.0	—	68.8	92.5	218.0	—	—	—	—	—
SMNS UnI	—	39.2	44.5	—	—	—	—	—	—	—
SMNS 11417a	—	—	~69.0	~113.0	—	—	—	—	—	—
UM 83902	—	—	—	—	—	—	—	—	—	—
UM 93220	—	—	—	—	—	—	—	—	11.9	18.3‡
UM 94795	—	—	—	—	—	—	—	—	—	—
UM 94814	—	—	37.7	58.7	—	—	—	—	—	—
UM 97512	—	32.7	59.8	—	—	66.7	32.5	45.6‡	13.9	39.7‡
UM 100146	—	—	58.7	79.3	—	—	—	—	—	—
UM 101215	—	—	53.3	80.8	~258.0	—	—	—	—	—
UM 101222	—	—	~60.0	—	—	66.2	32.5	48.1	17.7‡	38.1
UM 101223	—	—	49.2	62.9	—	—	—	—	—	—

APPENDIX V: VERTEBRAL MEASUREMENTS

Measurements of the vertebrae as shown in Figure 52. L is centrum length, W is centrum width on the anterior face, and H is the centrum height on the anterior face.

Vertebral	CGM 42813			NSFM M7866			UM 97512			UM 100146			UM 101215			UM 101222		
dimension	L	W	H	L	W	H	L	W	H	L	W	H	L	W	H	L	W	H
C1	—	—	—	—	—	—	—	—	—	—	—	—	40.9	~116.0	22.9	—	~136.0	—
C2	—	—	—	—	—	—	39.6	—	—	—	—	—	34.6	~110.0	32.9	—	—	33.4
C3	25.0	—	—	—	—	—	26.9	66.7	61.6	—	—	—	—	—	—	—	—	—
C4	28.0	—	—	—	—	—	24.7	65.2	57	26.0	56.7	56.3	23.4	61.9	59.0	—	—	—
C5	30.0	—	—	—	—	—	24.2	69.2	56.4	23.0	59.2	57.6	23.3	64.0	62.3	~27.0	—	—
C6	34.0	—	—	—	—	—	—	—	—	28.0	61.0	61.0	24.6	71.1	61.5	~31.0	—	—
C7	30.0	73.0	—	—	—	—	27.0	—	—	—	—	—	25.7	67.9	58.7	~31.0	—	—
T1	41.0	—	—	—	—	—	37.0	—	—	38.8	68.1	49.8	38.6	75.2	55.9	41.8	~73.0	57.1
T2	49.0	—	—	—	—	—	—	—	—	45.0	70.0	45.1	—	—	—	46.1	—	—
T3	49.0	59.0	50.0	—	—	—	—	—	—	—	—	—	46.8	66.9	52.2	52.8	73.3	52.9
T4	54.0	—	—	—	—	—	—	—	—	—	—	—	49.8	72.3	52.7	56.1	69.5	—
T5	51.0	—	—	—	—	—	48.0	74.0	—	—	—	—	49.5	69.7	52.5	57.6	70.5	53.5
T6	50.0	—	—	—	—	—	49.0	—	—	—	—	—	49.0	68.4	52.3	57.7	70.1	53.9
T7	—	—	—	—	—	—	51.2	76.0	62.0	—	—	—	—	—	—	58.1	71.0	55.2
T8	56.0	—	45.0	—	—	—	52.2	74.5	53.2	—	—	—	53.6	68.3	53.4	60.2	74.4	56.9
T9	59.0	—	—	—	—	—	—	—	—	—	—	—	56.3	69.2	54.3	63.8	80.3	57.2
T10	—	—	—	—	—	—	57.0	—	56.1	—	—	—	58.7	77.2	56.7	65.0	80.9	61.2
T11	57.0	83.0	59.0	—	—	—	—	—	—	—	—	—	62.6	82.1	63.4	68.7	89.1	65.7
T12	62.0	—	63.0	—	—	—	—	—	—	68.5	79.9	57.1	64.0	85.2	63.5	70.6	~91.0	65.3
T13	64.0	—	66.0	—	—	—	—	—	—	—	—	—	65.8	85.0	63.8	~71.0	~94.0	~68.0
T14	68.0	84.0	69.0	—	—	—	—	—	—	—	—	—	68.3	93.0	68.6	—	—	—
T15	62.0	—	—	—	—	—	—	83.0	66.1	66.0	75.1	61.5	68.9	93.7	68.1	—	—	—
T16	73.0	80.0	67.0	—	—	—	—	—	—	70.5	77.6	62.7	71.3	90.1	73.2	—	—	—
T17	—	—	—	—	—	—	—	—	—	—	—	—	—	—	—	—	—	—
L1	69.0	74.0	70.0	—	—	—	62.0	83.4	71.4	—	—	—	70.4	89.5	73.7	—	—	—
L2	71.0	68.0	69.0	—	—	—	63.0	—	—	—	—	—	72.1	93.1	77.9	—	—	—
L3	73.0	72.0	70.0	—	—	—	64.7	84.1	71.9	—	—	—	70.7	94.4	81.8	—	—	—
L4	74.0	75.0	—	—	—	—	65.6	83.7	72.3	—	—	—	72.3	91.1	76.7	—	—	—
L5	—	—	71.0	—	—	—	68.8	88.8	80.1	—	—	—	71.7	92.5	77.6	—	—	—
L6	72.0	—	68.0	—	—	—	73.0	86.9	81.0	—	—	—	72.7	95.2	80.6	—	—	—
L7	71.0	70.0	67.0	—	—	—	66.7	—	—	—	—	—	74.1	97.6	84.0	—	—	—
L8	73.0	—	—	—	—	—	—	92.5	—	—	—	—	73.2	92.3	88.2	—	—	—
L9	78.0	—	—	—	—	—	65.1	—	—	—	—	—	76.8	98.5	83.6	—	—	—
L10	77.0	—	—	—	—	—	—	—	—	—	—	—	75.1	96.9	86.1	—	—	—
L11	80.0	77.0	73.0	—	—	—	66.2	92.0	—	—	—	—	73.9	95.8	84.4	—	—	—
L12	75.0	—	—	—	—	—	64.0	—	—	—	—	—	71.9	94.6	84.8	—	—	—
L13	76.0	—	78.0	—	—	—	70.0	—	—	—	—	—	71.7	96.7	81.2	—	—	—
L14	76.0	—	77.0	—	—	—	—	—	—	—	—	—	73.1	95.9	82.8	—	—	—
L15	78.0	80.0	75.0	—	—	—	64.5	—	—	—	—	—	77.2	94.0	85.7	—	—	—
L16	78.0	—	78.0	—	—	—	—	—	—	—	—	—	74.6	96.3	86.7	—	—	—
L17	78.0	—	76.0	—	—	—	65.0	—	—	—	—	—	77.4	92.4	82.2	—	—	—
L18	78.0	78.0	76.0	—	—	—	64.4	—	—	—	—	—	77.2	90.0	83.0	—	—	—
L19	78.0	76.0	75.0	—	—	—	71.0	—	—	—	—	—	—	—	—	—	—	—
L20	77.0	80.0	79.0	—	—	—	70.0	—	—	—	—	—	78.0	92.9	87.6	—	—	—
Ca1	78.0	81.0	81.0	—	—	—	70.9	—	—	—	—	—	75.8	89.1	87.6	—	—	—
Ca2	80.0	83.0	81.0	—	—	—	68.6	94.6	—	—	—	—	76.2	89.9	87.3	—	—	—
Ca3	78.0	—	77.0	—	—	—	70.6	—	—	—	—	—	75.7	85.8	84.6	—	—	—
Ca4	78.0	85.0	75.0	—	—	—	67.5	95.9	—	—	—	—	76.6	87.5	85.7	—	—	—

Appendix V: Vertebral Measurements (cont.)

Ca5	79.0	89.0	76.0	—	—	—	72.1	90.5	—	—	—	—	75.0	93.0	82.0	—	—	—
Ca6	77.0	85.0	77.0	—	—	—	73.5	95.3	75.4	—	—	—	76.6	93.8	81.5	~85.0	—	—
Ca7	75.0	81.0	72.0	—	—	—	68.0	92.6	—	83.0	84.1	77.0	78.1	92.9	80.6	~85.0	—	—
Ca8	77.0	—	—	—	—	—	70.0	90.8	75.3	—	—	—	73.8	92.5	82.4	~81.0	87.9	—
Ca9	77.0	—	—	—	—	—	66.5	86.7	74.7	—	—	—	—	—	—	80.9	88.6	~75.0
Ca10	71.0	84.0	—	—	—	—	63.2	83.9	76.7	—	—	—	—	—	—	79.5	88.4	79.0
Ca11	65.0	80.0	—	—	—	—	61.9	83.7	74.3	—	—	—	—	—	—	75.0	87.2	79.4
Ca12	51.0	—	—	—	—	—	57.0	82.4	74.8	—	—	—	57.0	78.8	81.0	63.2	85.0	79.4
Ca13	39.0	68.0	—	—	—	—	50.0	—	—	54.5	79.4	72.3	—	—	—	47.7	76.6	70.1
Ca14	34.0	65.0	51.0	—	—	—	38.2	72.8	—	—	—	—	41.1	67.5	67.5	39.1	64.6	57.7
Ca15	30.0	51.0	—	—	—	—	31.0	53.8	67.2	30.6	59.2	54.8	31.0	60.4	55.7	28.0	53.7	48.3
Ca16	28.0	37.0	—	—	—	—	27.2	46.1	59.3	28.0	48.1	47.3	28.8	47.5	46.1	29.5	45.5	37.4
Ca17	26.0	—	—	—	—	—	22.7	—	—	—	—	—	—	—	—	29.7	38.1	33.2
Ca18	21.0	—	—	—	—	—	15.5	—	—	—	—	—	—	—	—	26.7	34.0	28.5
Ca19	—	—	—	—	—	—	—	—	—	—	—	—	—	—	—	19.8	27.4	22.3
Ca20	—	—	—	—	—	—	—	—	—	—	—	—	—	—	—	13.3	24.6	13.0
Ca21	—	—	—	—	—	—	—	—	—	—	—	—	—	—	—	11.0	14.3	9.8

APPENDIX VI: RIB AND STERNUM MEASUREMENTS

Appendix VIA: Rib Measurements

Measurements of the ribs as shown in Figure 79. A-P breadth is anterior-posterior breadth of the body at the angle and M-L breadth is the medial-lateral breadth of the body at the angle.

Rib	Measurement	UM 93220		UM 101215		UM 101222	
		L	R	L	R	L	R
Rib 1	Length	37.6	34.6	—	—	—	49.8
	Cord Length	15.9	14.7	—	—	—	23.3
	Cord Area	56.1	52.4	—	—	—	81.8
	A-P Breadth	10.8	10.6	—	—	—	16.7
	M-L Breadth	32.5	30.6	—	—	—	38.9
Rib 2	Length	—	—	58.1	69.2	65.7	67.1
	Cord Length	—	22.7	28.4	27.0	—	29.1
	Cord Area	—	121.8	188.2	186.7	—	188.7
	A-P Breadth	10.8	10.4	13.6	11.7	14.0	13.8
	M-L Breadth	32.5	25.3	37.2	34.7	33.0	36.6
Rib 3	Length	66.9	—	84.5	—	—	89.2
	Cord Length	27.4	—	33.9	—	—	38.5
	Cord Area	208.7	—	319.7	—	—	300.0
	A-P Breadth	11.1	11.3	11.5	—	16.4	15.0
	M-L Breadth	21.2	19.6	26.3	—	29.8	32.0
Rib 4	Length	78.8	—	—	—	—	104.3
	Cord Length	31.5	—	—	—	—	45.3
	Cord Area	272.2	—	—	—	—	387.4
	A-P Breadth	10.3	—	—	11.5	15.5	15.7
	M-L Breadth	20.9	—	—	25.8	29.0	29.3
Rib 5	Length	82.6	—	107.7	—	—	109.8
	Cord Length	33.5	—	42.2	—	—	47.8
	Cord Area	310.0	—	514.2	—	—	456.9
	A-P Breadth	10.3	—	17.0	—	13.7	14.4
	M-L Breadth	20.9	—	25.4	—	30.0	30.3
Rib 6	Length	81.8	83.7	—	—	—	113.9
	Cord Length	34.0	35.8	—	—	—	49.6
	Cord Area	307.8	266.8	—	—	—	464.4
	A-P Breadth	9.9	10.7	11.1	—	15.5	17.3
	M-L Breadth	21.5	22.0	23.2	—	27.7	31.7
Rib 7	Length	—	—	—	—	107.6	—
	Cord Length	—	—	—	—	—	46.8
	Cord Area	—	—	—	—	—	451.1
	A-P Breadth	10.0	10.0	—	—	16.4	16.7
	M-L Breadth	21.8	19.4	—	—	30.8	31.7
Rib 8	Length	78.0	—	—	—	97.2	—
	Cord Length	—	34.5	—	—	—	42.0
	Cord Area	—	230.0	—	—	—	364.6
	A-P Breadth	9.1	9.4	11.7	11.6	16.2	15.4
	M-L Breadth	20.6	21.3	29.4	29.6	32.7	33.1

Appendix VIA: Rib Measurements (cont.)

Rib 9	Length	76.7	—	—	—	—	88.5
	Cord Length	32.7	—	—	—	—	40.2
	Cord Area	201.0	—	—	—	—	270.0
	A-P Breadth	10.4	10.2	10.4	—	15.4	15.8
	M-L Breadth	21.1	21.2	25.9	—	31.6	30.4
Rib 10	Length	75.3	74.3	—	—	—	87.3
	Cord Length	34.9	33.7	—	—	—	40.6
	Cord Area	170.5	181.0	—	—	—	236.4
	A-P Breadth	10.1	10.3	—	12.4	13.5	13.7
	M-L Breadth	19.4	20.3	—	35.3	33.7	32.0
Rib 11	Length	69.5	—	85.7	—	—	89.7
	Cord Length	32.5	—	40.3	—	—	42.1
	Cord Area	136.5	—	211.0	—	—	236.3
	A-P Breadth	10.1	9.5	14.6	—	13.6	13.2
	M-L Breadth	20.7	21.5	27.7	—	32.0	34.0
Rib 12	Length	—	—	—	—	81.3	—
	Cord Length	—	—	—	—	—	38.2
	Cord Area	—	—	—	—	—	163.9
	A-P Breadth	—	9.4	12.1	13.2	12.3	12.8
	M-L Breadth	—	21.8	27.8	25.9	29.2	29.8
Rib 13	Length	62.7	—	87.6	—	77.7	—
	Cord Length	—	29.1	—	38.8	—	37.6
	Cord Area	—	106.4	—	197.6	—	124.6
	A-P Breadth	9.0	8.4	—	14.3	—	13.0
	M-L Breadth	18.0	17.7	—	23.7	—	24.5
Rib 14	Length	—	—	—	—	—	—
	Cord Length	—	—	—	—	—	—
	Cord Area	—	—	—	—	—	—
	A-P Breadth	8.7	8.4	11.4	12.4	—	—
	M-L Breadth	16.1	17.2	22.0	23.6	—	—
Rib 15	Length	52.7	—	—	—	—	—
	Cord Length	25.1	—	—	—	—	—
	Cord Area	68.7	—	—	—	—	—
	A-P Breadth	9.5	9.6	—	13.7	—	—
	M-L Breadth	13.5	15.0	—	22.4	—	—
Rib 16	Length	—	68.6	—	—	—	—
	Cord Length	—	—	33.1	—	—	—
	Cord Area	—	—	90.9	—	—	—
	A-P Breadth	8.1	9.1	10.1	—	—	—
	M-L Breadth	13.6	13.6	18.0	—	—	—
Rib 17	Length	—	—	—	—	—	—
	Cord Length	—	—	—	—	—	—
	Cord Area	—	—	—	—	—	—
	A-P Breadth	8.1	8.2	—	9.4	—	—
	M-L Breadth	10.0	10.6	—	16.9	—	—

Appendix VIB: Sternum Measurements

Measurements of the sternebrae as shown in Figure 70. PB is proximal breadth. DB is distal breadth. MB is maximum breadth. L is craniocaudal length. PD is proximal depth. DD is distal depth.

Specimen	Manubrium					Sternebra 2			Sternebra 3			Sternebra 4			Xiphisternum				
	PB	DB	L	PD	DD	MB	L	MD	MB	L	MD	MB	L	MD	PB	DB	L	PD	DD
UM 97512	81.1	70.8	112.8	31.9	42.4	68.0	76.9	33.0	67.0	84.7	34.4	75.9	78.1	28.5	51.3	—	96.5	25.0	7.8
UM 100146	—	—	—	—	—	—	78.0	39.6	—	—	—	75.8	74.0	35.1	—	—	—	—	—
UM 101215	98.8	83.1	118.8	44.7	47.8	79.3	80.3	45.0	82.5	74.6	39.2	72.8	67.8	33.8	61.4	53.9	113.1	25.2	4.0
UM 101222	97.5	83.8	108.9	32.1	49.0	80.1	81.6	39.4	80.7	79.5	37.3	78.0	68.9	34.4	50.8	47.0	157.0	36.7	2.5

APPENDIX VII: FORELIMB MEASUREMENTS

Appendix VIIA: Scapula Measurements

Measurements of the scapula as shown in Figure 99. SCH is scapula height. SCL is scapula length. ACL is acromion process length. ACH is acromion process height. CPH is coracoid process height. CPL is coracoid process length. GCL is glenoid cavity length. SPSFA is supraspinous fossa area. ISFA is infraspinous fossa area. TFA is teres fossa area.

Specimen	Side	SCH	SCL	ACL	ACH	CPH	CPL	GCL	SPSF (cm^2)	ISFA (cm^2)	TFA (cm^2)
CGM 42183	R	250.2	261.0	—	—	—	—	—	59.5	298.6	7.5
UM 97506	R	300.0	249.0	25.4	96.8	20.0	50.1	55.5	87.0	344.0	12.0
UM 97509	L	—	—	—	—	—	—	—	—	—	—
UM 97512	R	240.0	230.0	—	—	19.5	57.4	52.7	66.4	247.2	5.2
UM 101215	L	274.0	255.0	31.6	87.7	19.1	61.3	54.0	92.0	311.0	28.0
UM 101215	R	255.0	254.0	—	—	18.6	59.1	53.5	101.0	318.0	22.0
UM 101222	L	—	—	—	—	19.7	55.4	52.8	—	—	10.4
UM 101222	R	311.0	282.0	30.5	105.8	16.1	48.0	54.4	99.0	343.0	14.0

Appendix VIIB: Humerus Measurements

Measurements of the humerus as shown in Figure 101. HL is humerus length. HMSD is humeral mid-shaft diameter. HMB is humeral shaft mid breadth. DCB is deltopectoral crest breadth. HDB is humeral distal breadth. PDHHD is proximal-distal humeral head diameter. APHHD is anterior-posterior humeral head diameter. HDAB is humeral distal articular breadth.

Specimen	Side	HL	HMSD	HMB	DCB	HDB	PDHHD	APHHD	HDAB
UM 97509	L	—	—	—	—	44.0	—	—	32.5
UM 97512	R	230.0	35.3	67.0	86.6	42.7	53.1	60.3	31.8
UM 101215	L	224.0	35.3	69.0	90.0	46.0	53.4	62.4	34.3
UM 101215	R	230.0	35.4	—	87.2	42.7	52.4	—	33.7
UM 101222	L	250.0	29.9	67.4	91.0	46.0	—	64.9	35.0
UM 101222	R	253.0	30.5	66.3	87.8	47.8	60.0	67.0	34.7

Appendix VIIC: Ulna and Radius Measurements

Measurements of the ulna (top) and radius (bottom) as shown in Figure 103. UGL is ulna greatest length. USL is ulna shaft length. UL is ulna length. OL is olecranon length. OB is olecranon breadth. UMB is ulna mid-shaft breadth. UDB is ulna distal breadth. RGL is radius greatest breadth. RSL is radius shaft length. RL is radius length. RPB is radius proximal breadth. RMB is radius mid-shaft breadth. RDB is radius distal breadth.

Specimen	Side	UGL	USL	UL	OL	OB	UMB	UDB
UM 94807	R	—	—	—	—	—	—	55.5
UM 97506	R	—	—	—	78.2	—	47.1	52.7
UM 97512	R	218.0	153.0	169.0	66.7	94.3	43.2	56.6
UM 101215	L	214.0	143.0	152.0	80.6	93.4	48.2	57.8
UM 101215	R	214.0	140.0	156.0	79.5	100.4	48.1	58.8
UM 101222	L	214.0	139.0	159.0	71.5	100.4	49.3	66.3
UM 101222	R	216.0	142.0	160.0	76.1	100.2	48.6	61.4

Specimen	Side	RGL	RSL	RL	RPB	RMB	RDB
UM 97506	R	—	—	—	—	50.0	—
UM 97512	R	—	—	—	—	40.6	42.0
UM 101215	L	165.0	144.3	161.0	34.1	46.7	46.4
UM 101215	R	164.0	145.0	157.0	30.1	45.6	45.5
UM 101222	L	167.0	140.0	156.0	35.5	41.8	41.9
UM 101222	R	166.0	142.0	156.0	34.5	42.6	43.6

Appendix VIID: Metacarpal Measurements

Measurements of the metacarpals (top) and phalanges (bottom) as shown in Figure 103. L is length. PB is proximal breadth. DB is distal breadth.

		MC I			MC II			MC III			MC IV			MC V		
Specimen	Side	L	PB	DB	L	PB	DB	L	PB	DB	L	PB	DB	L	PB	DB
UM 97506	L	—	—	—	—	—	—	—	—	—	65.8	19.2	—	—	24.3	—
UM 97506	R	—	—	—	—	—	15.8	—	—	—	—	—	—	—	—	—
UM 97512	R	—	—	—	56.1	18.2	16.9	—	—	—	61.8	19.6	18.4	46.7	21.1	18.5
UM 100185	L	—	—	—	—	—	—	—	—	—	—	—	—	48.2	23.0	18.9
UM 101215	L	—	—	—	—	22.0	—	71.6	24.5	18.6	62.1	18.2	15.1	46.8	24.2	18.2
UM 101222	L	—	11.3	—	59.6	21.3	16.5	69.4	24.3	20.2	62.4	19.7	18.8	47.0	22.2	19.3
UM 101222	R	44.3	11.0	5.2	57.9	20.8	16.3	68.7	24.6	20.0	63.3	18.9	19.5	45.1	22.3	18.7

Appendix VIIE: Proximal Phalanx Measurements

		Ph I-1			Ph II-1			Ph III-1			Ph IV-1			Ph V-1		
Specimen	Side	L	PB	DB	L	PB	DB	L	PB	DB	L	PB	DB	L	PB	DB
UM 97506	L	—	—	—	—	16.0	—	90.8	18.3	12.6	—	—	—	—	—	—
UM 97506	R	—	—	—	—	—	—	90.6	—	14.5	—	—	—	—	—	—
UM 97512	R	—	—	—	—	—	—	93.2	18.9	15.0	90.4	18.5	15.9	71.9	19.2	15.0
UM 101222	L	—	—	—	—	—	—	84.3	19.3	16.2	79.5	17.6	14.3	67.4	18.9	14.2
UM 101222	R	*	*	*	64.4	15.4	12.2	—	19.3	—	79.1	17.2	14.2	63.3	18.8	12.9
UM 101230	L	—	—	—	—	14.1	—	—	—	—	—	—	—	—	—	—

Appendix VIII: Additional Taxa Included in Phylogenetic analysis

		Bos	Hippopotamus	Qaisracetus	Artiocetus	Rodhocetus
1.	Frontal shield size rel to CB	>2.5	>2.5	< 2	>2< 2.5	>2< 2.5
2.	Posterior frontal border	?	?	straight	straight	straight
3.	Rostrum breadth	moderate	very broad	moderate	moderate	moderate
4.	Skull length relative to CB	< 7	< 7	< 7	>8	7- 8
5.	Embrasure pits	absent	absent	present	present	present
6.	Orbit height rel to CB	>0.3	>0.3	>0.3	>0.3	>0.3
7.	Orbit position	low	high	low	low	low
8.	Palate narrows at	post to M3	?	M2	M2	M2
9.	Palate shape	flat	flat	flat	flat	flat
10.	Falcate process of BO	absent	absent	large	large	large
11.	Vomer covers BO/BS suture	no	no	?	?	?
12.	Pachyosteosclerotic bulla	absent	absent	present	present	present
13.	Medial bulla articulation	?	?	?	?	absent
14.	Pt sinus depth	?	?	absent	absent	absent
15.	Lateral wall of pt sinus	?	?	absent	absent	absent
16.	Sigmoid process	?	?	large	large	large
17.	Hypoglossal foramen in jugular	no	?	?	?	yes
18.	Anterior palatine foramen	present	present	absent	absent	absent
19.	Nuchal crest orientation	vertical	vertical	angled back	slightly angled back	slightly angled back
20.	Exoccipital shape	?	?	?	?	squared
21.	Position of posterior nares	C1	C1	C1	C1	C1
22.	Posterior nasal breadth	narrow	broad	moderate	moderate	?
23.	Posterior medial max contacts	nasal	nasal	nasal	nasal	nasal
24.	Mandibular foramen	small	small	large	large	large
25.	Mandibular symphysis position	anterior to P1	anterior to P1	?	P2	P2
26.	Mandibular symphysis fused	no	yes	no	no	no
27.	Incisors in tooth row	no	no	yes	yes	yes
28.	Cheek teeth with many denticles	no	no	no	no	no
29.	Number P1/ roots	?	one	one	one	?
30.	Number of upper molars	three	three	three	three	three
31.	#M1/ roots	?	?	three	three	three
32.	#M2/ roots	?	?	three	three	three
33.	#M3/ roots	?	?	three	?	three
34.	Tooth replacement	diphyodont	diphyodont	?	?	?
35.	Number of P/1 roots	?	one	?	?	two
36.	Reentrant groove on lower molar	absent	absent	?	?	present
37.	Cervical vertebrae compressed	none	none	moderate	moderate	moderate
38.	Number of thoracics	10-15	10-15	10-15	?	10-15
39.	Number of lumbars	<10	<10	<10	?	<10
40.	Lumbars elongated	no	no	no	?	no
41.	Lumbar zygapophyses	revolute	revolute	curved	?	curved
42.	# sacrals solidly ankylosed	5	three	two	?	none
43.	# sacrals loosely joined	0	0	two	?	four
44.	# sacrals articulate with pelvis	two	two	one	?	one
45.	Posterior caudals d-v compressed	no	no	?	?	?
46.	Anterior caudals elongate	no	no	yes	?	no
47.	Posterior caudals elongate	no	no	?	?	?
48.	Infraspinous fossa on scapula	small	small	?	?	?
49.	Coracoid process oriented anteriorly	yes	yes	?	?	?
50.	Acromion process oriented anteriorly	no	no	?	?	?
51.	Humeral shaft a/p thick	no	no	?	?	?
52.	Deltopectoral crest position	proximal	proximal	?	?	?
53.	Distal humeral articulation div	yes	yes	?	?	?
54.	Radius and ulna flat	no	no	?	?	?
55.	Broad olecranon process	no	no	?	?	yes
56.	Distal ulna	pointed	pointed	?	?	?
57.	Saddle-shaped carpal arts	yes	yes	?	?	yes

Appendix VIII: Additional Taxa Included in Phylogenetic analysis (cont.)

		Bos	Hippopotamus	Qaisracetus	Artiocetus	Rodhocetus
58.	Trapezoid and magnum	fused	fused	?	?	separate
59.	Carpals in alternating rows	no	no	?	?	yes
60.	Pisiform	big and flat	big and flat	?	?	long and narrow
61.	Hyperphalangy	not present	not present	?	?	not present
62.	Pelvis	large	large	large	large	large
63.	Pelvis rotation	no	no	no	no	no
64.	Femur	large	large	?	?	moderate
65.	Tarsals	fused	fused	?	?	separate
66.	Tibia/fibula	fused	fused	?	?	separate
67.	Sternum form	flat and light	flat and light	?	?	big and heavy
68.	Body size	large	very large	moderate	moderate	moderate
69.	Stratigraphic position	post Priabonian	post Priabonian	late Lutetian	early Lutetian	early Lutetian